

TECHNICAL REPORT STANDARD TITLE PAGE

1. Report No. FHWA/TX-92/1170-1F		2. Government Accession No.		3. Recipient's Catalog No.	
4. Title and Subtitle Improved ACP Mixture Design: Development and Verification				5. Report Date March 1992	
				6. Performing Organization Code	
7. Author(s) Dallas N. Little and Hisham Youssef				8. Performing Organization Report No. Research Report 1170	
9. Performing Organization Name and Address Texas Transportation Institute Highway Materials Division Texas A&M University College Station, Texas 77843-3136				10. Work Unit No.	
				11. Contract or Grant No. Study No. 2-9-88-1170-1F	
12. Sponsoring Agency Name and Address Texas Department of Transportation 125 East 11th Street Austin, Texas 78701				13. Type of Report and Period Covered Final - March 1988 March 1992	
				14. Sponsoring Agency Code	
15. Supplementary Notes Research performed in cooperation with DOT and FHWA. Research study title "Improved ACP Mixture Design: Development and Verification"					
16. Abstract <p>This report describes the testing methodologies and evaluation procedures and criteria for the evaluation of uniaxial compressive creep data to determine the susceptibility of asphalt concrete mixtures to permanently deform or rut. The methodology described and the supporting figures and tables allows the user to perform uniaxial creep testing in accordance with the procedure explained in the Asphalt Aggregate Mixture Analysis System (AAMAS) under a stress state that realistically duplicates the in situ condition for the specific pavement and traffic condition to which the asphalt mixture will be subjected. Furthermore, the procedure provides creep strain, creep curve slope and creep stiffness criteria by which to evaluate the potential of the mixture to deform in specific conditions of pavement structure and traffic. The procedure was developed with the intent of integration into the AAMAS procedure.</p> <p>The reports explains the use of a method to analyze triaxial shear test data in order to determine the susceptibility of asphalt concrete mixtures to deform under specific conditions of loading and in specific pavement structural situations. This procedure is based on the evaluation of the ratio of induced octahedral shear stress to the octahedral shear strength of the asphalt concrete under the specific conditions of stress actually induced in the pavement structure.</p>					
17. Key Words Mix design, asphalt concrete, creep modulus, creep stiffness, triaxial strength, shear stress ratio, mixture analysis, octahedral stresses.			18. Distribution Statement No Restrictions. This document is available through NIF, 5285 Port Royal Road, Springfield, Virginia 22161		
19. Security Classif. (of this report) Unclassified		20. Security Classif. (of this page) Unclassified		21. No. of Pages 340	22. Price

**IMPROVED ACP MIXTURE DESIGN: DEVELOPMENT AND VERIFICATION**

by

Dallas N. Little  
and  
Hisham A. Youssef

Research Study No. 2-9-88-1170

Sponsored by

Texas Department of Transportation

in cooperation with

The U.S. Department of Transportation  
Federal Highway Administration

March 1992

Texas Transportation Institute  
Texas A&M University  
College Station, Texas 77843

# METRIC (SI\*) CONVERSION FACTORS

## APPROXIMATE CONVERSIONS TO SI UNITS

Symbol	When You Know	Multiply By	To Find	Symbol
<b>LENGTH</b>				
in	inches	2.54	millimetres	mm
ft	feet	0.3048	metres	m
yd	yards	0.914	metres	m
mi	miles	1.61	kilometres	km

Symbol	When You Know	Multiply By	To Find	Symbol
<b>AREA</b>				
in <sup>2</sup>	square inches	645.2	millimetres squared	mm <sup>2</sup>
ft <sup>2</sup>	square feet	0.0929	metres squared	m <sup>2</sup>
yd <sup>2</sup>	square yards	0.836	metres squared	m <sup>2</sup>
mi <sup>2</sup>	square miles	2.59	kilometres squared	km <sup>2</sup>
ac	acres	0.395	hectares	ha

Symbol	When You Know	Multiply By	To Find	Symbol
<b>MASS (weight)</b>				
oz	ounces	28.35	grams	g
lb	pounds	0.454	kilograms	kg
T	short tons (2000 lb)	0.907	megagrams	Mg

Symbol	When You Know	Multiply By	To Find	Symbol
<b>VOLUME</b>				
fl oz	fluid ounces	29.57	millilitres	mL
gal	gallons	3.785	litres	L
ft <sup>3</sup>	cubic feet	0.0328	metres cubed	m <sup>3</sup>
yd <sup>3</sup>	cubic yards	0.0765	metres cubed	m <sup>3</sup>

NOTE: Volumes greater than 1000 L shall be shown in m<sup>3</sup>.

## TEMPERATURE (exact)

°F	Fahrenheit temperature	5/9 (after subtracting 32)	Celsius temperature	°C
----	------------------------	----------------------------	---------------------	----

## APPROXIMATE CONVERSIONS TO SI UNITS

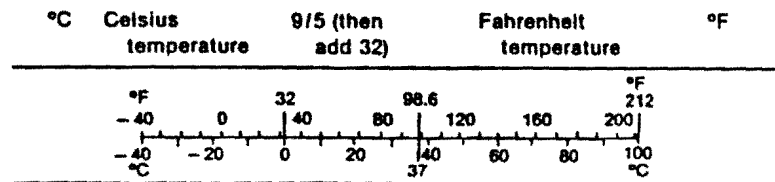
Symbol	When You Know	Multiply By	To Find	Symbol
<b>LENGTH</b>				
mm	millimetres	0.039	inches	in
m	metres	3.28	feet	ft
m	metres	1.09	yards	yd
km	kilometres	0.621	miles	mi

Symbol	When You Know	Multiply By	To Find	Symbol
<b>AREA</b>				
mm <sup>2</sup>	millimetres squared	0.0016	square inches	in <sup>2</sup>
m <sup>2</sup>	metres squared	10.764	square feet	ft <sup>2</sup>
km <sup>2</sup>	kilometres squared	0.39	square miles	mi <sup>2</sup>
ha	hectares (10 000 m <sup>2</sup> )	2.53	acres	ac

Symbol	When You Know	Multiply By	To Find	Symbol
<b>MASS (weight)</b>				
g	grams	0.0353	ounces	oz
kg	kilograms	2.205	pounds	lb
Mg	megagrams (1 000 kg)	1.103	short tons	T

Symbol	When You Know	Multiply By	To Find	Symbol
<b>VOLUME</b>				
mL	millilitres	0.034	fluid ounces	fl oz
L	litres	0.264	gallons	gal
m <sup>3</sup>	metres cubed	35.315	cubic feet	ft <sup>3</sup>
m <sup>3</sup>	metres cubed	1.308	cubic yards	yd <sup>3</sup>

## TEMPERATURE (exact)



These factors conform to the requirement of FHWA Order 5190.1A.

\* SI is the symbol for the International System of Measurements



## IMPLEMENTATION STATEMENT

The Asphalt Aggregate Mixture Analysis System (AAMAS) was developed through contract with the National Cooperative Highway Research Program (NCHRP). This procedure provides an improved mix-design methodology for asphalt concrete which should optimize the selection, proportioning and processing of asphalt binders and aggregate materials to produce pavements uniformly resistant to all forms of distress such as fatigue cracking, thermal cracking, permanent deformation, moisture damage and age hardening.

Five laboratory tests are recommended for use in the AAMAS procedure: the diametral resilient modulus test, the indirect tensile strength test, the gyratory shear strength test and the indirect tensile and uniaxial compressive creep tests. All of these tests except the gyratory shear strength test performed with the Corps of Engineers Gyratory Testing Machine (GTM) can be readily integrated into the Texas mixture design methodology.

The AAMAS procedure for the design and analysis of asphalt concrete mixtures presents methodologies by which to simply and effectively evaluate the potential of mixtures to resist the major modes of distress: permanent deformation, fatigue cracking, low temperature cracking and disintegration. It is important that these methodologies be used in Texas as quickly as the applicability of these models to Texas conditions is verified.

Based on the developments in AAMAS and the evolution of mixture design and analysis as influenced by the massive Strategic Highway Research Program (SHRP), Project 1170 attempted to develop protocols and methodologies which effectively complement the AAMAS philosophy and approach. In this study, specific attention was given to the development of an improved procedure by which to evaluate permanent deformation or rutting potential of asphalt concrete mixtures in specific pavement and traffic categories in the State of Texas. This work does not replace the AAMAS procedures and protocols but complements them. The methodology and criteria presented in this report for the evaluation of uniaxial compressive creep data are compatible with the AAMAS procedure for specimen fabrication and specimen testing. The only change suggested is the way in which the parameters obtained from the uniaxial compressive creep test are evaluated. This report suggests that the slope of the steady state creep curve, the strain at one-hour of loading,

the total resilient strain from uniaxial compressive resilient modulus testing and strain at failure from unconfined compressive testing to failure be used to evaluate rutting potential. A table of evaluation criterias is provided in Chapter 3 of the report. The study also suggests that the creep test be performed under realistic conditions of loading which are defined based on the pavement structure and traffic conditions to which the pavement in which the mixture will be used will be subjected.

The procedure for the performance of the uniaxial compressive creep testing and for the evaluation of the uniaxial compressive creep data is ready for implementation into the general AAMAS approach for the State of Texas.

A testing procedure and evaluation methodology was developed based on the confined triaxial shear strength test. This methodology is not to be applied to routine mixture design but is to be used in specific conditions to evaluate the potential of specific asphalt concrete mixtures to function in specialized pavement and traffic environments. This procedure provides considerable insight into the potential of the mixture to effectively perform in a specific pavement and traffic environment. This procedure is ready for implementation and should complement the AAMAS design and analysis procedure as modified for use in the State of Texas.

#### **DISCLAIMER**

The contents of this report reflect the view of the authors who are responsible for the opinions, findings, and conclusions presented herein. The contents do not necessarily reflect the official view or policies of the Federal Highway Administration. This report does not constitute a standard, specifications, or regulations.

There is no invention or discovery conceived or first actually reduced to practice in the course of or under this contract, including any art, method, process, machine, manufacture, design or composition of matter, or any new and useful improvement thereof, or any variety of plant which is or may be patentable under the patent law of the United States of America or any foreign country. This report is not intended for construction, bidding or permit purposes.

## TABLE OF CONTENTS

	Page
Implementation Statement . . . . .	iv
Disclaimer . . . . .	v
Chapter 1 - Introduction . . . . .	1
Study Objectives . . . . .	1
Evolution of the Study . . . . .	1
Revised Objectives of the 1170 Study . . . . .	2
Organization of this Report . . . . .	5
Chapter 2 - Suggestions Revisions to the AAMAS Procedure	
Based on the Research of Project 1170 . . . . .	6
General . . . . .	6
Recommendations for Use of AAMAS Procedure . . . . .	10
Modifications to AAMAS Criteria for Mixture Evaluation . . . . .	14
The AAMAS Procedure for the Evaluation of Fatigue	
Cracking . . . . .	15
The AAMAS Procedure for the Evaluation of the Appropriate	
Range of Diametral Resilient Modulus as a Function	
of Testing Temperature . . . . .	19
The AAMAS Procedure for the Evaluation of Low Temperature	
Cracking Potential . . . . .	23
The Selection of the Gyrotory Method of Mixture	
Compaction . . . . .	24
Chapter 3 - Development of the Creep Test for Analyzing the	
Resistance of Mixture to Permanent Deformation . . . . .	28
Background and Theory . . . . .	28
Basic Concepts . . . . .	28
Differences between the Creep Test and Other	
Rutting Tests . . . . .	34
Relationship between the Creep Test and Actual	
Rutting . . . . .	37
Modifications to the Shell Predictive Rutting	
Approach in Project 2474 . . . . .	38

## TABLE OF CONTENTS (Continued)

	Page
Modified Shell Equation . . . . .	40
Development of Permanent Deformation Criteria . . . . .	47
Development of the AAMAS Rutting Charts . . . . .	51
Comparison of AAMAS Rutting Chart Criteria with Creep Modulus Criteria Developed by Other Agencies . . . . .	57
Development of TTI Rutting Evaluation Procedure . . . . .	70
Establish Critical Values of Slope of Creep strain Versus Time of Loading Curve and Strain at One-Hour Loading . . . . .	70
Determination of Appropriate Testing Temperature . . . . .	87
Determine Appropriate Level of Axial Stress in Unconfined Compression Creep Test . . . . .	90
Creep Recovery Criteria for Permanent Deformation Evaluation . . . . .	106
Criteria for the Evaluation of Uniaxial Compressive Creep Test Data . . . . .	110
Examples of Use of the Rutting Criteria . . . . .	115
Guidelines for Evaluation of Rutting Potential Based on Creep Data . . . . .	120
Special Considerations . . . . .	121
Chapter 4 - Evaluation of Permanent Preformation By Shear Strength Analysis . . . . .	124
Background and Theory . . . . .	124
Nijboer Analysis . . . . .	124
Other Analyses of Triaxial Test Data . . . . .	129
Development of Testing Procedure Based on Historical Background . . . . .	133
Octahedral Analysis of Triaxial Test Data . . . . .	134
Theoretical Aspects . . . . .	135
Example Cases . . . . .	137
Laboratory Experiment to Evaluate Sensitivity of Triaxial Test to Variation in Asphalt Mixture Components . . . . .	156

**TABLE OF CONTENTS (Continued)**

	Page
Details of Laboratory Test Matrix . . . . .	157
Procedure for the Evaluation of Triaxial Shear	
Strength Data . . . . .	161
Sensitivity of the OSSR Analysis to Mixture	
Variables . . . . .	172
Chapter 5 - Summary of the Approach for Performing Uniaxial	
Creep Test and Evaluating Data to Determine	
Rutting Susceptibility . . . . .	186
Chapter 6 - Summary of Design Parameters Which Influence	
Permanent Deformation . . . . .	188
General . . . . .	188
Aggregate Gradation . . . . .	188
Air Void Content . . . . .	189
VMA . . . . .	189
Temperature . . . . .	190
Other Considerations . . . . .	191
Chapter 7 - Conclusions and Recommendations . . . . .	192
Conclusions . . . . .	192
Recommendations . . . . .	196
References . . . . .	197
Appendix A . . . . .	A-1
Appendix B . . . . .	B-1
Appendix C . . . . .	C-1
Appendix D . . . . .	D-1

## LIST OF TABLES

Table	Page
2.1. Summary of the Approximate Time Requirements for the Laboratory Compaction, Conditioning and Testing of Asphalt Concrete Mixtures Using AAMAS. (After Von Quintus, et al (1991)) . . . . .	9
3.1. Values of $C_m$ for Various Types of Mixtures . . . . .	38
3.2. Simple Power Law Exponent as Reported by Different Researchers . . . . .	44
3.3. Rutting Severity Classification . . . . .	48
3.4. Comparison of Extreme Slope Values of the Steady State Portion of the Creep Curve and Permanent Strain at One-Hour Loading for Gyrotory Compacted Samples . . . . .	66
3.5. Comparison of Extreme Values of Slope of Steady State Creep Versus Time of Loading Plot and Permanent Strain at One-Hour Loading for Gyrotory Prepared Samples. (Analysis of Data from Sousa, et al. (1991)) . . . . .	69
3.6. Comparison of Steady State Slopes Prior to Tertiary Creep in Unconfined Mixtures . . . . .	72
3.7. Comparison of Steady State Creep Slopes and Permanent Strain at One-Hour Time of Creep Loading . . . . .	72
3.8. Comparison of Uniaxial Creep ( $\sigma^1 = 60$ psi) Data from Ten Selected Mixtures. (Each Value is the Average of Data Points) . . . . .	73
3.9. Design Pavement Temperature for Permanent Deformation Analysis Derived from Pavement Temperature Profile Analysis. (After Mahboub and Little (1987)) . . . . .	90
3.10. Temperature Distribution of 2 in. Asphalt Overlay (Dallas Area). (After Li, et al. (1987)) . . . . .	91
3.11. Temperature Distribution of 3 in. Asphalt Overlay (Dallas Area). (After Li, et. al. (1987)) . . . . .	91
3.12. Winter Temperature Distribution of 2 in. Asphalt Overlay (Dallas Area). (After Li, et at. (1987)) . . . . .	92
3.13. Winter Temperature Distribution of 3 in. Asphalt Overlay (Dallas Area). (After Li, et al. (1987)) . . . . .	92
3.14. Stresses to be Applied to Laboratory Samples (Triaxial and Uniaxial) to Represent Field Conditions of a Hot Climate, Free Rolling Tires and Full Bond Between AC Overlay and AC Base . . . . .	95
3.15. Stresses to be Applied to Laboratory Samples (Triaxial and Uniaxial) to Represent Field Conditions of a Hot Climate, Free Rolling Wheel and Full Bond Between AC Overlay and PCC Base . . . . .	96

LIST OF TABLES (Continued)

Table	Page
3.16. Stresses to be Applied to Laboratory Samples (Triaxial and Uniaxial) to Represent Field Conditions of a Hot Climate, Free Rolling Wheel and Full Bond Between AC Overlay and Flexible Base . . . . .	97
3.17. Stresses to be Applied to Laboratory Samples (Triaxial and Uniaxial) to Represent Field Conditions of a Hot Climate, Braking Wheel and Full Bond Between AC Overlay and AC Base . . . . .	98
3.18. Stresses to be Applied to Laboratory Samples (Triaxial and Uniaxial) to Represent Field Conditions of a Hot Climate, Braking Wheel and Full Bond Between AC Overlay and PCC Base . . . . .	99
3.19. Stresses to be Applied to Laboratory Samples (Triaxial and Uniaxial) to Represent Field Conditions of a Hot Climate, Braking Wheel and Full Bond Between AC Overlay and Flexible Base . . . . .	100
3.20. Stresses to be Applied to Laboratory Samples (Triaxial and Uniaxial) to Represent Field Conditions of a Hot Climate, Braking Wheel and Partial Loss of Bond Between AC Overlay and AC Base . . . . .	101
3.21. Stresses to be Applied to Laboratory Samples (Triaxial and Uniaxial) to Represent Field Conditions of a Hot Climate, Braking Wheel and Partial Loss of Bond Between AC Overlay and PCC Base . . . . .	102
3.22. Stresses to be Applied to Laboratory Samples (Triaxial and Uniaxial) to Represent Field Conditions of a Hot Climate, Heavy Wheel Load, Free Rolling Wheel and Full Bond Between AC Overlay and Base . . . . .	103
3.23. Stresses to be Applied to Laboratory Samples (Triaxial and Uniaxial) to Represent Field Conditions of a Hot Climate, Heavy Wheel Load, Braking Wheel and Full Bond Between AC Overlay and Base . . . . .	104
3.24. Strain at One-Hour Creep Loading and Slope of Steady State Creep Curve Required to Reduce Rutting Potential to Very Low Level . . . . .	111
3.25. Creep Stiffness Criteria at One-Hour Creep Loading . . . . .	111
4.1. Temperature Distribution of 4 in. Asphalt Overlay (Dallas Area). (After Li, et al. (1986)) . . . . .	139
4.2. Temperature Distribution of 3 in. Asphalt Overlay (Dallas Area). (After Li, et al. (1986)) . . . . .	139

**LIST OF TABLES (Continued)**

Table	Page
4.3 Summary of C and $\phi$ Values for Various Limestone and River Gravel Mixtures with and without Polymer Modification. (After Little (1992)) . . . . .	149
4.4. Summary of Shear Strength Parameters from Triaxial Testing for Three Mixtures Types . . . . .	159
4.5. Summary of Strain at Failure Data from Triaxial Testing on Three Mixture Types . . . . .	160

## LIST OF FIGURES

Figure	Page
2.1. Conceptual Flow Chart Illustrating the AAMAS Procedure. (After Von Quintus, et al. (1991)) . . . . .	6
2.2. Flow Chart for the Design of Dense-Graded Asphalt Concrete Mixtures. (Von Quintus, et al. (1991)) . . . . .	7
2.3. Flow Chart for the AAMAS Mixture Evaluation Procedure. (After Von Quintus, et al. (1991)) . . . . .	8
2.4. Flow chart for the Design of Dense-Graded Asphalt Mixtures Employing the Texas Hveem Stabilimeter for Evaluation of Mixture Stability in Lieu of the GTM. (Modified from Von Quintus, et al. (1991)) . . . . .	11
2.5. Relationship Between Indirect Tensile Strains and Resilient Modulus Using Two Different Fatigue Relationships. (After Von Quintus (1991)) . . . . .	16
2.6. Chart for Total Resilient Modulus Versus Temperature Using Indirect Tensile Loading Conditions. (After Von Quintus, et al. (1991)) . . . . .	20
2.7. Estimation of the Fatigue Factor to Determine an Equivalent Annual Resilient Modulus . . . . .	21
2.8. Chart for Estimating Structural Layer Coefficient of Dense-Graded Asphaltic Concrete Based on the Elastic (Resilient Modulus). (After the Asphalt Institute, 1981) . .	22
3.1. Influence of Creep Stress Intensity on Creep Rate. (After Mitchell (1976)) . . . . .	29
3.2. Stages of Creep (After Mitchell (1976)) . . . . .	30
3.3. Comparison of Creep Curves Calculated on the Basis of Hill's Model with Measured Values for Various Mixes. (After Hills (1973)) . . . . .	32
3.4. Log-linear Relationship Between the Applied Stress and the Accumulated Permanent Deformation Per Cycle (Averaged Over the First 100 Cycles of Stable Hysteresis). (After Mahboub and Little (1987)) . . . . .	43
3.5. Asphaltic Concrete Mixture Rutting Potential for Layers Placed Over Rigid Pavements or Rigid Base Materials. (After Von Quintus, et al. (1991)) . . . . .	52
3.6. Asphaltic Concrete Mixture Rutting Potential for the Lower Layers of Full-Depth Asphalt Pavements. (After Von Quintus, et al. (1991)) . . . . .	53
3.7. Asphaltic Concrete Mixture Rutting Potential for Intermediate Layers in Thick or Full-Depth Asphalt Pavements. (After Von Quintus, et al. (1991)) . . . . .	54

## LIST OF FIGURES (Continued)

Figure	Page
3.8. Asphaltic Concrete Mixture Rutting Potential for Surface Layers of Asphaltic Concrete Pavements. (After Von Quintus, et al. (1991)) . . . . .	55
3.9. Viscoplastic Stiffness (Creep Stiffness) Versus Time of Loading for ACP over PEC for a Specific Structural Category. (After Mahboub and Little (1991)) . . . . .	56
3.10. Combined Effects of Compaction and Asphalt Type on Compressive Creep Modulus, AAK-1 [B] and AAG-1 [V]. (After Sousa, et al. (1991)) . . . . .	60
3.11. Combined Effects of Compaction and Asphalt Content on Compressive Creep Modulus, Optimum Asphalt [0] and High Asphalt [1]. (After Sousa, et al. (1991)) . . . . .	61
3.12. Combined Effects of Compaction and Aggregate Type on Compressive Creep Modulus, RL Chert [T] and RB Granite [W] (1 psi = 6.89 kPa). (After Sousa, et al. (1991)) . . . . .	62
3.13. Combined Efforts of Compaction and Air-Void Content on Compressive Creep Modulus, Low Voids [0] and High Voids [1]. (After Sousa, et al. (1991)) . . . . .	63
3.14. Combined Effects of Compaction and Temperature on Compressive Creep Modulus, 104°F (40°C) [0] and 140°F (60°C) [1]. (After Sousa, et al. (1991)) . . . . .	64
3.15. Combined Effects of Compaction and Stress Level on Compressive Creep Modulus, 14.5 psi [0] and 29.0 psi [1]. (After Sousa, et al. (1991)) . . . . .	65
3.16. Constancy of Collapse Strain for a Number of Randomly Selected Tests Under Compressive Creep. (After Sousa, et al. (1991)) . . . . .	67
3.17. Arithmetic Plot of Creep Strain Versus Time of Loading for 100 Percent Crushed Limestone Mixture 1 . . . . .	74
3.18. Arithmetic Plot of Creep Strain Versus Time of Loading for 100 Percent Crushed Limestone Mixture 2 . . . . .	75
3.19. Arithmetic Plot of Creep Strain Versus Time of Loading for 100 Percent Crushed Limestone Mixture 3 . . . . .	76
3.20. Arithmetic Plot of Creep Strain Versus Time of Loading for 100 Percent Crushed Limestone Mixture 4 . . . . .	77
3.21. Arithmetic Plot of Creep Strain Versus Time of Loading for 10 Percent Natural Sand--90 Percent Crushed Limestone Mixture 1 . . . . .	78

## LIST OF FIGURES (Continued)

Figure	Page
3.22. Arithmetic Plot of Creep Strain Versus Time of Loading for 10 Percent Natural Sand--90 Percent Crushed Limestone Mixture 2 . . . . .	79
3.23. Arithmetic Plot of Creep Strain Versus Time of Loading for 10 Percent Natural Sand--90 Percent Crushed Limestone Mixture 3 . . . . .	80
3.24. Arithmetic Plot of Creep Strain Versus Time of Loading for 10 Percent Natural Sand--90 Percent Crushed Limestone Mixture 4 . . . . .	81
3.25. Arithmetic Plot of Creep Strain Versus Time of Loading for 20 Percent Natural Sand--80 Percent Crushed Limestone Mixture 1 . . . . .	82
3.26. Arithmetic Plot of Creep Strain Versus Time of Loading 20 Percent Natural Sand--80 Percent Crushed Limestone Mixture 2 . . . . .	83
3.27. Arithmetic Plot of Creep Strain Versus Time of Loading 20 Percent Natural Sand--80 Percent Crushed Limestone Mixture 3 . . . . .	84
3.28. Arithmetic Plot of Creep Strain Versus Time of Loading 20 Percent Natural Sand--80 Percent Crushed Limestone Mixture 4 . . . . .	85
3.29. Relationship Between Slope of the Steady State Creep Curve and Time of Loading to 0.8 Percent Strain or Greater . . . . .	87
3.30. Regional Map of Texas. (After Mahboub and Little (1987)) . . . . .	89
3.31. Linear Representation of Typical Creep and Recovery Behavior of a 40 Percent Natural Sand Mix at High Air Void Contents. (After Perdomo (1990)) . . . . .	108
3.32. Triaxial Test Data Demonstrating the Departure from Linearity at About $0.5 \epsilon_{qu}$ for 20 Percent Natural Sand and 80 Percent Crushed Limestone Mixture Loaded at a Stroke Rate of 2 Inches Per Minute . . . . .	114
3.33. Creep Strain Versus Time of Loading Plots for a River Gravel and Limestone Screening Mixture with Various Level of LDPE Modification . . . . .	117
3.34. Creep Strain Versus Time of Loading Plots for Crushed Limestone and Natural Sand (Field Sand) with Varying Percentages of Natural Sand . . . . .	118

## LIST OF FIGURES (Continued)

Figure	Page
3.35. Example of the Effects of Polymer Modification on the Response of Strain at Failure of Mixture in Triaxial Compression Testing ( $\sigma_3 = 0$ , 104°F, 0.5 in/min. Loading Rate) . . . . .	122
4.1. Representation of $\eta_m \frac{d\varepsilon}{dt} = \frac{2\cos \phi}{3-\sin \phi} \left[ \frac{\sigma_1-\sigma_3}{2\cos \phi} - \frac{\sigma_1 + \sigma_3}{2} \text{tg } \phi - \tau_e \right]$ by Mohr circle . . . . .	125
4.2. Influence of the particle size of coarse aggregate on the viscosity of the mass. (After Nijboer (1948)) . . . . .	126
4.3. Relation Between the Initial Resistance $\tau_e$ and the Bituminous Initial Resistance $\tau_b$ with varying concentration of the coarse aggregate $C_v$ . (After Nijboer (1948)) . . . . .	127
4.4. Relation Between the Viscosity of the Mass $\eta_m$ , and the Concentration of Coarse Aggregate, $C_r$ , and Concentration of Sand and Coarse Aggregate, $C_r^1$ . (After Nijboer (1948)) . . . . .	129
4.5. Asphalt Concrete Mixture Stability Curves for Static Pressures. (After Finn, et al. (1967)) . . . . .	131
4.6. Illustrating Stability Curves for a Given Vertical Load for Bituminous Paving Mixtures Subject to Braking Stresses. (After McLeod (1950)) . . . . .	132
4.7. Traditional Pavement Structure. (After Perdomo (1991)) . . . . .	140
4.8. Asphalt Treated Base Pavement Structure. (After Perdomo (1991)) . . . . .	140
4.9. Octahedral Normal Stress Contours for 40 Percent Natural Sand Mix Surface Layer in Traditional Pavement Structure Under Single Tire Loading and for Hottest Season (Season 1). (After Perdomo (1991)) . . . . .	141
4.10. Octahedral Shear Stress Contours for 40 Percent Natural Sand Mix Surface Layer in Traditional Pavement Structure Under Single Tire Loading and for Hottest Season (Season 1). (After Perdomo (1991)) . . . . .	142
4.11. Octahedral Shear Strength Contours for 40 Percent Natural Sand Mix Surface Layer in Traditional Pavement Structure Under Single Tire Loading and for Hottest Season (Season 1). (After Perdomo (1991)) . . . . .	143

LIST OF FIGURES (Continued)

Figure	Page
4.12. Octahedral Shear Stress Ratio Contours for 40 Percent Natural Sand Mix Surface Layer in Traditional Pavement Structure Under Single Tire Loading, and for Hottest Season (Season 1). (After Perdomo (1991)) . . . . .	144
4.13. Maximum OSSR Versus Resilient Modulus for First Two Inches of Surface Layering Traditional Pavement Structure Under Single Tire Loading. (After Perdomo (1991)) . . . . .	145
4.14. Maximum OSSR Versus Resilient Modulus for First Two Inches of Surface Layer in Traditional pavement Structure Under DUAL Tire Loading. (After Perdomo (1991)) . . . . .	145
4.15. Maximum OSSR Versus Resilient Modulus for First Two Inches of Surface Layer in Asphalt Treated Base Pavement Structure Under Single Tire Loading. (After Perdomo (1991)) . . . . .	146
4.16. Maximum OSSR Versus Resilient Modulus for First Two Inches of Surface Layer in Asphalt Treated Base Pavement Structure Under DUAL Tire Loading. (After Perdomo (1991)) . . . . .	146
4.17. Contours of Equal (a) Octahedral Shear Stress, (b) Octahedral Normal Stress, (c) Octahedral Shear Strength and (d) Octahedral Shear Stress to Shear Strength Ratios (OSSRs) for River Gravel and AC-20 Mixtures. (After Little, et al. (1992)) . . . . .	151
4.18. Contours of Equal (a) Octahedral Shear Stress, (b) Octahedral Normal Stress, (c) Octahedral Shear Strength and (d) Octahedral Shear Stress to Shear Strength Ratios (OSSRs) for Mixtures of River Gravel and AC-20 Modified with 5 Percent LDPE. (After Little, et al. (1992)) . . . . .	152
4.19. Contours of Equal Octahedral Shear Stress Ratios for River Gravel Mixtures (a) with AC-20 and (b) AC-20 Modified with 5 Percent LDPE for 4-Inch Asphalt Concrete Pavement Over 10-Inch Aggregate Base. (After Little, et al. (1992)) . . . . .	153
4.20. Loci of Maximum OSSRs at Depth of 0.5 Inches Below the Surface for Mixtures of River Gravel and AC-20 and Mixtures of River Gravel and AC-20 Modified with 5 Percent LDPE. (After Little, et al. (1992)) . . . . .	155
4.21. Loci of Maximum OSSRs at Depth of 1.5 Inches Below the Surface for Mixtures of River Gravel and AC-20 and Mixtures of River Gravel and AC-20 Modified with 5 Percent LDPE. (After Little, et al. (1992)) . . . . .	155

## LIST OF FIGURES (Continued)

Figure	Page
4.22. Contours of Octahedral Shear Stress in 2 Inch ACP Overlay Over PCC Base for a Free Rolling Wheel with Full Bending Between ACP and PCC Layers (Hot Season) Values on Contours are in psi . . . . .	163
4.23. Contours of Normal Octahedral Stress in 2 Inch ACP Over PCC Base for a Free Rolling Wheel with Face Bonding Between ACP and PC Layers (Hot Season) Values on Contours are in psi . . . . .	164
4.24. Contours of the Ratio of Normal Octahedral Stress to Octahedral Shear Stress (NTSR) in 2 Inch ACP Over PCC Base for a Free Rolling Wheel with Full Bond Between ACP and PCC Layers (Hot Season) . . . . .	165
4.25. Octahedral Shear Stress Ratio (OSSR) Contours Within 2 Inch ACP Overlay Over PCC Base for Free Rolling Wheel With Full Bond Between Layers . . . . .	166
4.26. Normal Octahedral Stress Contours for 2 Inch ACP Over PCC Base for Braking Wheel with Partial Slippage Between Layers (Hot Season) Values on Contours are in psi . . . . .	167
4.27. NTSR Contours in 2 Inch ACP Over PCC Base for Braking Wheel With Partial Slippage Between Layers (Hot Season) . . . . .	168
4.28. Mohr-Coulomb Failure Envelope Developed From Triaxial Testing at Confining Pressures of 0, 30, 60 and 90 psi . . . . .	170
4.29. OSSR Contours for 4 Inches of ACP Over PCC, 100 Percent Crushed Limestone Mixture, Optimum Asphalt Content, Low Air Voids, Free Rolling Wheel and Full Bond Between Layers (ADT Season) . . . . .	174
4.30. OSSR Contours for 4 Inches of ACP Over PCC, 100 Percent Crushed Limestone Mixture, Optimum Asphalt Content, High Air Voids, Free Rolling Wheel and Full Bond Between Layers (ADT Season) . . . . .	175
4.31. OSSR Contours for 4 Inches of ACP Over PCC, 100 Percent Crushed Limestone Mixture, Optimum Asphalt Content, Binder-Rich Mixture, High Air Voids, Free Rolling Wheel and Full Bond Between Layers (ADT Season) . . . . .	176
4.32. OSSR Contours for 4 Inches of ACP Over PCC, 80 Percent Crushed Limestone - 20 Percent Natural Sand, Optimum Asphalt Content, Low Air Voids, Free Rolling Wheel and Full Bond Between Layers (Hot Season) . . . . .	177

## LIST OF FIGURES (Continued)

Figure	Page
4.33. OSSR Contours for 4 Inches of ACP Over PCC, 80 Percent Crushed Limestone - 20 Percent Natural Sand, Optimum Asphalt Content, High Air Voids, Free Rolling Wheel and Full Bond Between Layers (Hot Season) . . . . .	178
4.34. OSSR Contours for 4 Inch of ACP Over PCC, 80 Percent Crushed Limestone - 20 Percent Natural Sand, Optimum Asphalt Content, Binder Rich Mixture, High Air Voids, Free Rolling Wheel and Full Bond Between Layers (Hot Season) . . . . .	179
4.35. OSSR Contours for 4 Inch ACP Over PCC, 100 Percent Crushed Limestone, Optimum Binder Content, Low Air Voids, Braking Induced Surface Stresses, Full Bond Between Layers (Hot Season) . . . . .	180
4.36. OSSR Contours for 4 Inch ACP Over PCC, 100 Percent Crushed Limestone, Optimum Binder Content, High Air Voids, Braking Induced Surface Stresses, Full Bond Between Layers (Hot Season) . . . . .	181
4.37. OSSR Contours for 4 Inch ACP Over PCC, 100 Percent Crushed Limestone, Binder Rich Mixture, High Air Voids, Braking Induced Surface Stresses, Full Bond Between Layers (Hot Season) . . . . .	182
4.38. OSSR Contour for 4 Inches of ACP Over PCC, 80 Percent Crushed Limestone - 20 Percent Natural Sand, Optimum Asphalt Content, Low Air Voids, Braking Induced Surface Shearing Stresses, Full Bond . . . . .	183
4.39. OSSR Contour for 4 Inches of ACP Over PCC, 80 Percent Crushed Limestone - 20 Percent Natural Sand, Optimum Asphalt Content, High Air Voids, Braking Induced Surface Shearing Stresses, Full Bond . . . . .	184
4.40. OSSR Contour for 4 Inches of ACP Over PCC, 80 Percent Crushed Limestone - 20 Percent Natural Sand, Binder-Rich Mixture, High Air Voids, Braking Induced Surface Shearing Stresses, Full Bond . . . . .	185



## CHAPTER 1

### INTRODUCTION

#### STUDY OBJECTIVES

The objectives of this study were to develop methodologies which can be used to improve mixture design and analysis. Originally, the objectives were to:

1. Develop a methodology to employ the indirect tensile creep test for use in the evaluation of low temperature cracking potential.
2. Develop the methodology by which to determine Mohr-Coulomb failure envelopes for asphalt concrete paving mixtures and to use the triaxial shear test as a test by which to evaluate the potential of asphalt concrete mixtures to rut or permanently deform due to low stability.
3. Develop an improved creep test and compressive creep analysis procedure.
4. Develop and refine mixture fabrication procedures.
5. Evaluate the use of the repeated load indirect tensile test as a methodology by which to evaluate flexural, load-related fatigue potential of asphalt concrete mixtures.
6. Verify the methodologies developed through mixture testing and a field verification program.
7. Implement findings.

#### EVOLUTION OF THE STUDY

This study began in 1987 prior to the beginning of SHRP and at the beginning of the Asphalt Aggregate Mixture Analysis Program (AAMAS) sponsored by the National Highway Research Program (NCHRP). The AAMAS program was charged to develop a comprehensive and integrated mixture design and analysis system. This system was to address all phases of mixture design and analysis including the major distress modes of fatigue cracking potential, rutting potential (due to both densification and instability), low temperature or thermal cracking and disintegration due to moisture

damage.

Shortly after the advent of the AAMAS program the Strategic Highway Research Program (SHRP) was initiated. This massive effort is divided into six major research programs in the area of asphalt technology including a \$9,000,000 study dedicated to mixture design and analysis. Thus, two major programs have overlapped the 1170 project during the last four years. The impact of these major national programs cannot be ignored as they will influence the methodology of mixture design and analysis for the foreseeable future.

With the realization of the great impact of AAMAS and SHRP, the approach to Project 1170 was redirected in certain aspects in order that the research in Project 1170 would not be redundant and that it would complement in every way possible the work performed in AAMAS and SHRP.

Fortunately, Texas A&M Researchers have been heavily involved in both the AAMAS program and in the SHRP program. This involvement has enabled the researchers to maintain a close contact with the AAMAS and SHRP procedures as they evolve and has allowed input from Texas Transportation Institute (TTI) researchers into the SHRP and AAMAS programs.

It is a well documented fact that the research performed in the preceding study to 1170, Research Study 2474, provided considerable input to the AAMAS procedures ultimately adopted and presented in the NCHRP Report 338 which documents the AAMAS procedure.

#### **REVISED OBJECTIVES OF THE 1170 STUDY**

As a consequence of AAMAS and SHRP the objectives of Study 1170 changed moderately to avoid duplication of effort and to take full advantage of the complementary research efforts. This approach was particularly meaningful as the researchers involved in Study 1170 at TTI were also heavily involved in the NCHRP 9-6(1), AAMAS study.

The AAMAS study directed considerable effort to the development of a methodology to fabricate asphalt mixtures in the laboratory to simulate field plant mix and compaction efforts as closely as possible. Furthermore, the AAMAS study developed very effective protocols and procedures to evaluate the potential of asphalt concrete mixtures to resist fatigue

cracking, resist low temperature fracture and to evaluate moisture damage and disintegration potential. Researchers involved in Project 1170 and also involved in the AAMAS study felt that the methodologies developed in the AAMAS study for the evaluation of fatigue cracking potential, low temperature cracking potential and disintegration potential were superior models and excellently suited for routine mixture design and/or analysis. Consequently, the original 1170 study objective of the development of an improved procedure of fatigue testing using the indirect tensile test was amended as it was found that the AAMAS procedure of evaluating fatigue potential on the basis of the simple-to-obtain parameters of indirect tensile strain at failure and indirect tensile resilient modulus is a superior approach. In fact, this AAMAS approach is very similar to the approach suggested by Little and Richey (1983) in which the results of indirect tensile resilient modulus and indirect tensile strain at failure were used in the form of a failure envelope to evaluate the fatigue potential of asphalt concrete mixtures.

Similar to the development of the methodology and protocol for the evaluation of fatigue potential, AAMAS researchers developed a methodology by which to evaluate low temperature fracture potential of asphalt concrete mixtures. This methodology was considered by 1170 researchers to be an excellent method and a realistic method for the evaluation of the potential of asphalt concrete mixtures to fracture due to thermal fluctuations.

Although the AAMAS procedure for the evaluation of rutting potential is a well documented and excellent procedure, it was determined that the most effective effort in Study 1170 would be to concentrate on improving the methodology for the evaluation of rutting potential of asphalt concrete mixtures in typical Texas environments. The AAMAS procedure employs two approaches to evaluate deformation potential: the gyratory testing machine and the uniaxial compressive creep test. The gyratory testing machine is a specialty piece of equipment which is not presently available in Texas. Whether or not the equipment is deemed valuable enough to warrant purchase in the future is to a large degree dependent on recommendations coming from the SHRP program. The second approach to the routine evaluation of rutting potential in the AAMAS program is based on the uniaxial compressive creep test. The results of the uniaxial compressive creep test are typically

evaluated based on a minimum required level of creep modulus. This procedure for evaluation of the adequacy of the mixture based on a minimum value of creep modulus has been considered as inadequate, mainly because of the lack of uniformity among creep testing procedures and the wide range of creep modulus criteria used to evaluate creep test data.

Based on a careful evaluation of the state of the knowledge in the area of mixture design and analysis and based on the insight of 1170 researcher into the developments in the AAMAS and SHRP methodologies and protocol, it was considered that the most beneficial and effective objectives of the 1170 study would be to:

1. Develop an improved testing methodology for uniaxial creep testing and one that is compatible with the existing AAMAS procedures and one that can accommodate the testing of field cores which typically have height to diameter ratios which make them unsuitable for most uniaxial compressive modes of testing.
2. Develop improved criteria by which to evaluate the uniaxial compressive creep test data as this data will be the most important data by which the potential of the mixture to resist permanent deformation will be judged.
3. Develop a procedure to evaluate the stability and resistance to permanent deformation of asphalt concrete mixtures under well defined and reproducible stress states using a shear strength criterion such as the Mohr-Coulomb failure criteria.
4. Develop as necessary improved equipment and testing protocols for indirect tensile resilient modulus and strength and strain at failure testing.
5. Evaluate the sensitivity of the procedures and protocols developed through extensive laboratory testing of carefully controlled factorial type mixture studies and through the testing of representative field cores and loose mixtures from field projects.
6. Maintain a commitment to development of evaluation criteria, equipment and procedures that will complement and be compatible with the AAMAS procedure and specifically its use in Texas.

## **ORGANIZATION OF THIS REPORT**

This report is organized into four chapters. The first chapter is this introduction. The second chapter discusses how the procedures developed in this study interact with the AAMAS approach described in detail in NCHRP Report 338 (Von Quintus, et al. (1991)). The third chapter is a detailed discussion of the methodology by which to evaluate compressive uniaxial creep test data. The fourth chapter is an extensive discussion of the methodology for performing and evaluating confined triaxial shear strength testing.



## CHAPTER 2

### SUGGESTIONS REVISIONS TO THE AAMAS PROCEDURE BASED ON THE RESEARCH OF PROJECT 1170

#### GENERAL

The Asphalt Aggregate Mixture Analysis System (AAMAS) is a system developed to measure engineering properties of mixtures and then to judge the potential of these mixtures to function in pavement layers based on the best available and most appropriate failure criteria for each test mode. Figure 2.1 is a flow chart that conceptualizes the different steps in the AAMAS procedure.

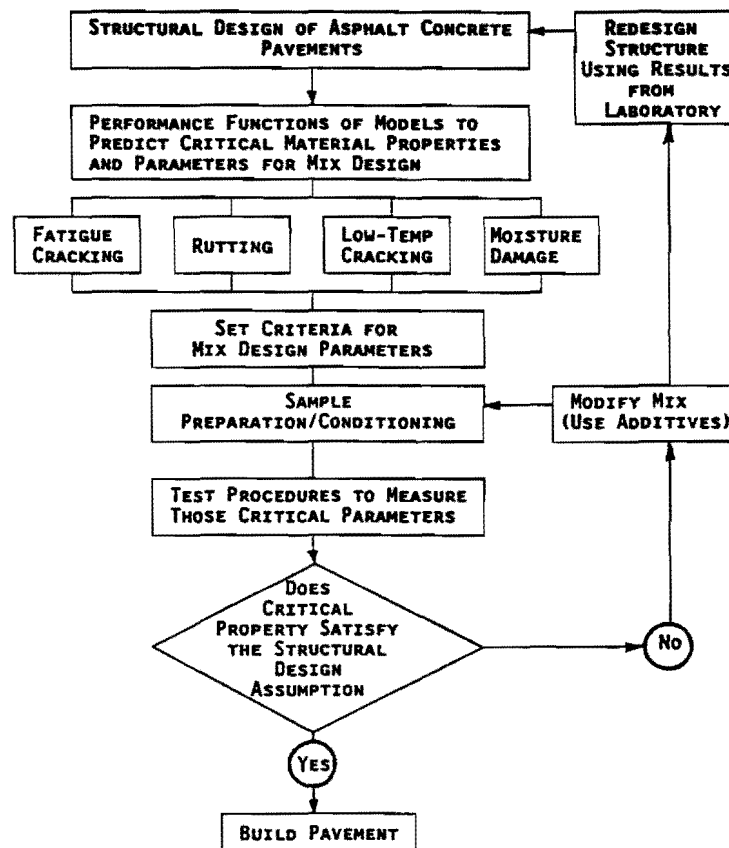


Figure 2.1. Conceptual Flow Chart Illustrating the AAMAS Procedure. (After Von Quintus, et al. (1991)).

Four distress mechanisms were selected for incorporation in AAMAS. These were rutting, fatigue cracking, low temperature cracking and moisture damage. Secondary consideration was given to disintegration caused by raveling and loss of skid resistance.

Five tests were selected as tools for mixture evaluation in AAMAS because they measure the mixture properties required by the structural models. These tests were the diametral resilient modulus test, indirect tensile strength test, gyratory shear strength test and the indirect tensile and uniaxial compression creep test.

Figure 2.2 summarizes the mixture design procedure in flow chart form, and Figure 2.3 summarizes the general AAMAS mixture evaluation procedure in flow chart form, identifying the four sections of the AAMAS analysis. Table 2.1 summarizes the appropriate time requirements for the laboratory compaction, conditioning and testing of asphalt concrete mixtures.

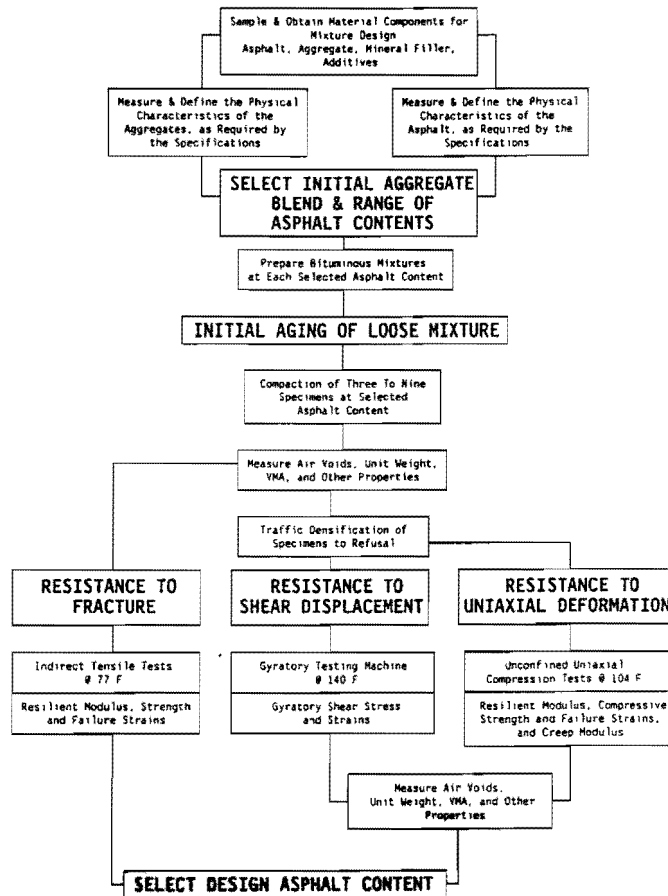


Figure 2.2. Flow Chart for the Design of Dense-Graded Asphalt Concrete Mixtures (Von Quintus, et al. (1991)).

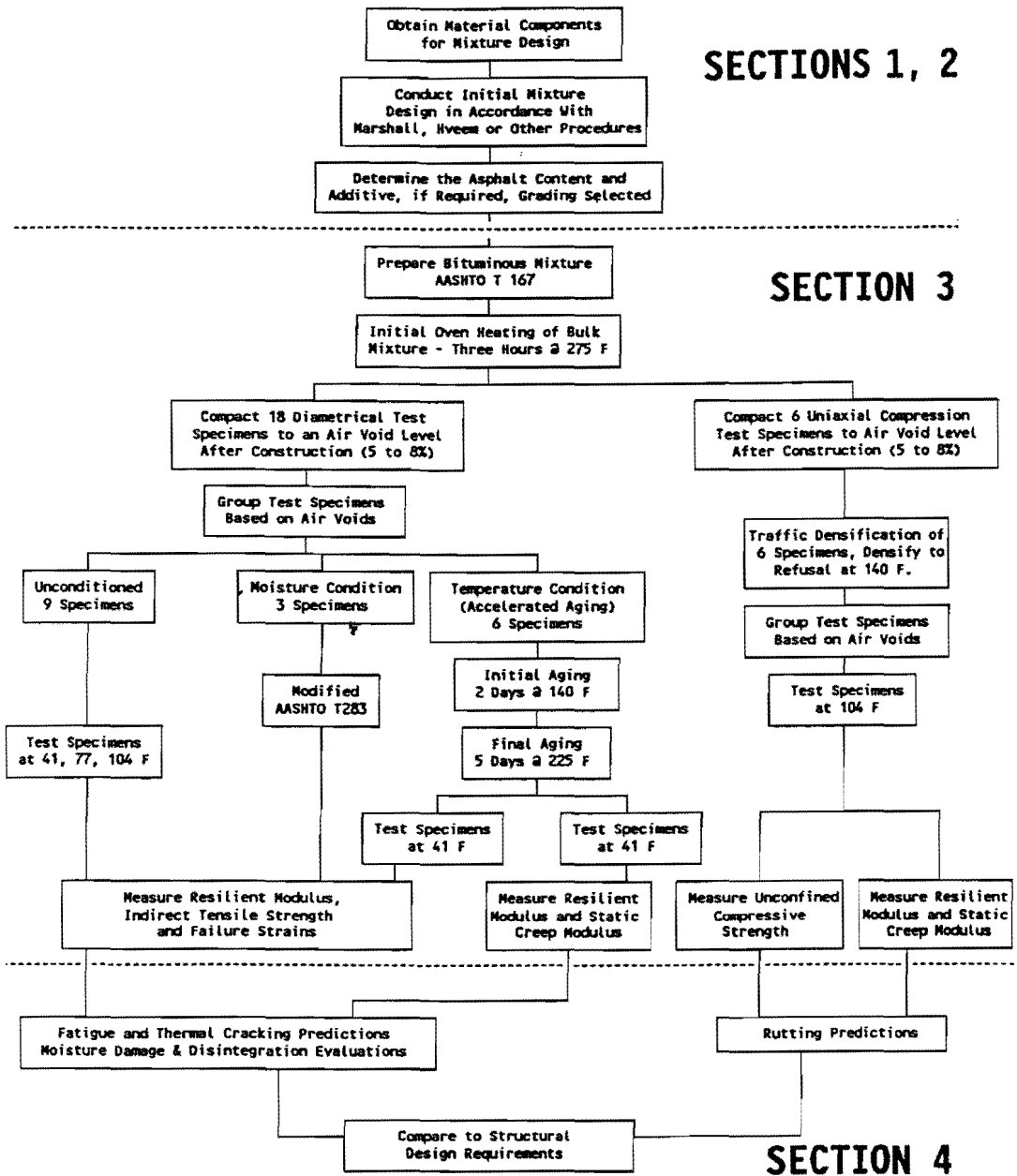


Figure 2.3. Flow Chart for the AAMAS Mixture Evaluation Procedure (After Von Quintus, et al. (1991)).

Table 2.1. Summary of the Approximate Time Requirements for the Laboratory Compaction, Conditioning and Testing of Asphalt Concrete Mixtures Using AAMAS (After Von Quintus, et al. (1991)).

Laboratory Steps	Time in Days										
	1	2	3	4	5	6	7	8	9	10	11
1. Prepare & Mix Materials											
2. Initial Heat Conditioning of Loose Mix	12	12									
3. Specimen Compaction - Unconditioned	9										
Moisture Conditioned	3										
Temperature Conditioned		6									
Traffic Densified		6									
4. Measure Air Voids & Sort Into Subsets			24								
5. Moisture Condition Samples			3								
6. Heat Conditioning			6								
7. Traffic Densification			6								
8. Test Unconditioned Specimens			3 @ 41F	3 @ 77F	3 @ 104F						
9. Test Heat Conditioned Specimens											6 @ 104F
10. Test Moisture Conditioned Specimens						3 @ 77F					
11. Test Traffic Densified Specified						6 @ 104F					

Numbers in blocks represent the number of specimens and/or test temperature. The total time frame to complete the entire AAMAS process is less than 2 weeks. The times shown above are in relation to the time needed to run the Marshall and Hveem mix design methods.

As was discussed in Chapter 1, this study has evolved based on the work done in the extensive AAMAS study and based on the work now being done in the SHRP study. The intention of this report is to provide the information to supplement and improve the AAMAS procedure for use in Texas. The main emphasis has been placed on the performance of static creep testing and the evaluation of static creep data.

Since the AAMAS report is available as NCHRP Report 338 no attempt is made in this report to recapitulate the AAMAS procedure nor the procedure for performing testing. This chapter will, however, explain how the findings of this report will interact and supplement those of the AAMAS study.

It is recommended that the procedure for evaluation of fracture fatigue and low temperature fracture be followed precisely as defined in the AAMAS procedure. This recommendation is based on extensive testing at Texas A&M University on laboratory developed mixtures which represent controlled variations in mixture components and upon testing of mixtures from field sites around the nation.

#### **RECOMMENDATIONS FOR USE OF AAMAS PROCEDURE**

The AAMAS procedure should be used for mixture design evaluation as summarized in Figures 2.1 through 2.3. It is recommended that the gyratory testing machine be included in the mixture design as indicated in Figure 2.2. However, since this device is not normally available to TxDOT laboratories at the present time, a reasonable mixture design can be performed by replacing the evaluation of resistance to shear displacement by means of the gyratory testing machine (GTM) with the evaluation of mixture stability based on the use of the Hveem stabilometer as traditionally used in Texas (Texas Test Method 204F). Thus the revised flow chart for mixture design will be that shown in Figure 2.4.

Since the GTM is not normally available in Texas, all compaction of mixture will be in accordance with Texas Test Method 206F.

The evaluation of the test data developed from testing defined in Figure 2.4 will be in accordance with the appropriate guidelines in the NCHRP 338 Report. However, the criteria for the evaluation of compressive

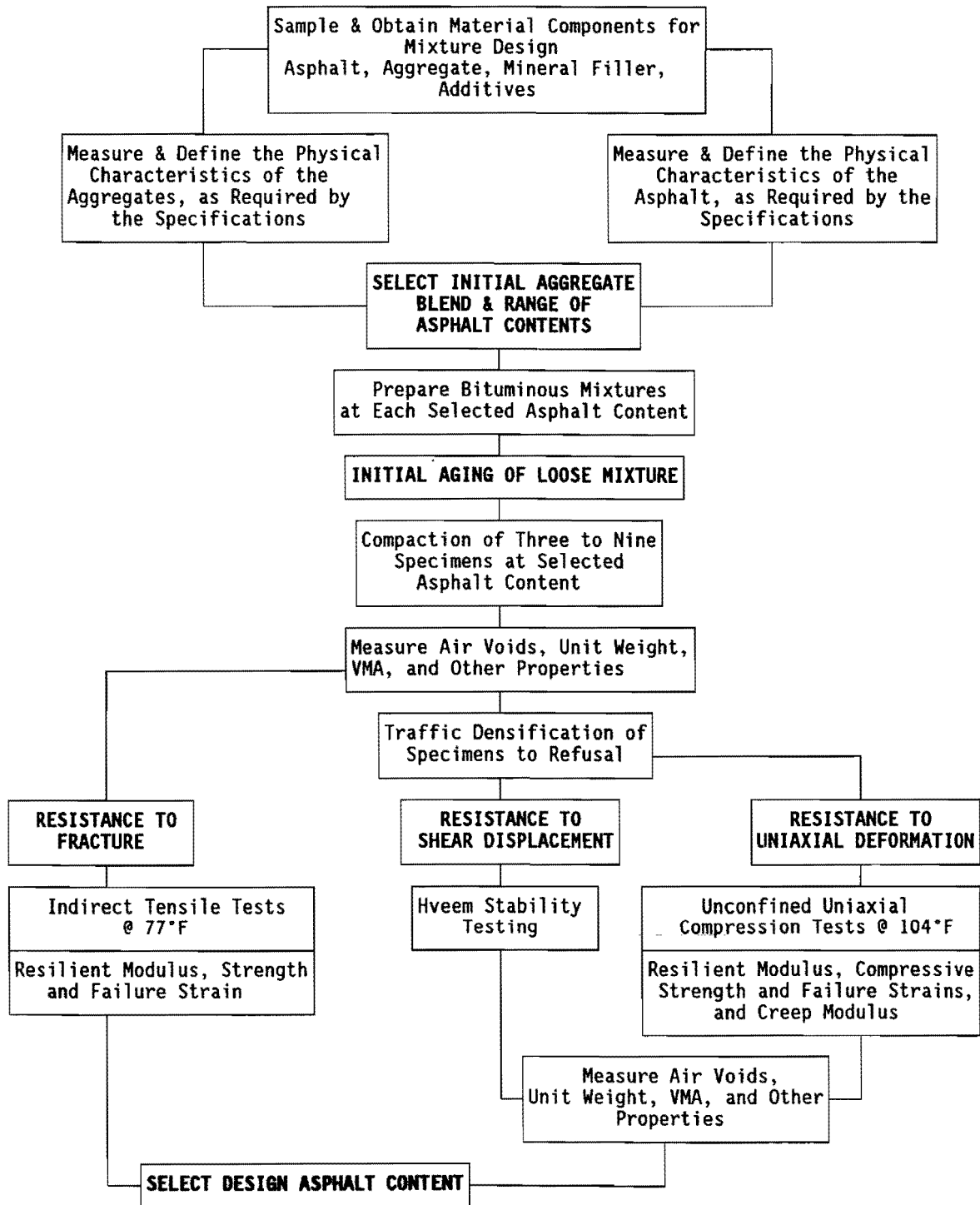


Figure 2.4. Flow Chart for the Design of Dense-Graded Asphalt Mixtures Employing the Texas Hveem Stabilometer for Evaluation of Mixture Stability in Lieu of the GTM. (Modified from Von Quintus, et al. (1991)).

creep data will be replaced by the guidelines developed in this Report. These guidelines will be summarized in the section of this chapter entitled **Guidelines for the Evaluation of Asphalt Concrete Mixtures.**

It is recommended that the procedure described in Figure 2.3 be followed except that the Texas gyratory compaction device should be used in lieu of the GTM and that the samples prepared for uniaxial compressive creep testing be prepared to refusal densification, as defined in the AAMAS report, prior to static creep testing in lieu of initially compacting the specimens to 5 to 7 percent air voids and then densifying to refusal at 140°F using the GTM. The GTM approach is, however, the preferred approach. Therefore, if and when the GTM apparatus becomes available, the procedure as defined in Figure 2.3 should be used without modification.

It is recommended that the mixture design approach in Section 2 of the NCHRP 338 Report be followed. Section two of the AAMAS report describes the required testing equipment (paragraph 2.5) and preparation of mixtures (paragraph 2.6). The discussion of methods of testing are in subsequent paragraphs of the same section: resistance to fracture (paragraph 2.7), resistance to shear displacement using the GTM (paragraph 2.8) and resistance to uniaxial deformations (paragraph 2.9). Finally, paragraph 2.10 provides detailed guidance and protocol for the interpretation of data collected in the mixture design methodology.

It is important to note that the very critical preconditioning procedures are described in the referenced paragraphs for each phase of testing. These procedures must be followed explicitly.

Section 3 of the AAMAS Report explains in detail the testing and data evaluation procedures required for the analysis of asphalt concrete mixtures. The procedures discussed in Sections 2 and 3 of the AAMAS report were developed through extensive testing of mixtures from throughout the United States. This work was performed in labs at Texas A&M University, the University of Florida and the University of Texas. All research was under the direction of Brent Rauhut Engineers (BRE), Inc. of Austin, Texas. Since many procedural methods evolved in the AAMAS study based on the extensive laboratory testing and development work accomplished in this study and in the 2474 study (Mahmoud and Little (1987)), it is recommended that the testing procedures discussed in Sections 2 and 3 of the AAMAS report be

followed. Specifically, Section 3 of the AAMAS Report addresses the following pertinent topics:

- Preparation of Test Specimen - Paragraph 3.6
- Grouping of Test Specimen - Paragraph 3.7
- Preconditioning of Test Specimen - Paragraph 3.8
- Testing Procedure - Paragraph 3.10
- Calculations - Paragraph 3.10
- Report - Paragraph 3.11

Addendum A of Section 3 discusses in detail Test Methods for Indirect Tensile Strength of Bituminous Mixture and Addendum B discusses in detail Test Methods for Creep Modulus Testing of Bituminous Mixtures. Work on test development of AAMAS at Texas A&M and work on TxDOT Studies 1177 (Little, et al. (1991)) and 1170 has resulted in the development of new test apparatus for axial tests such as uniaxial creep and indirect tensile testing such as diametral resilient modulus testing, diametral creep and diametral resilient modulus. Both a generalized indirect resilient modulus test device and a test device for rapid indirect tensile resilient modulus testing were developed.

These devices are fully compatible with the AAMAS procedure (Von Quintus, et al. (1991)) and are fully compatible with the 1986 AASHTO Design Guide for Flexible Pavement Design. Details behind the development of the three testing apparatus along with machine drawings are presented in Little, et al. (1991).

The purpose of the development of the indirect tensile apparatus was to provide a set up for more precise generalized and rapid methods to measure indirect tensile creep, strength and resilient modulus. These procedure samples and equipment were to be fully compatible with both AAMAS and 1986 AASHTO Design Guide methodologies.

The purpose of the development of an axial compressive testing apparatus was to provide more complete instrumentation coverage of the specimen, provide instrumentation for measurement of Poisson's ratio/dilatation and to suggest an approach to solve the problem of axial loading of short pavement cores. For example, most cores which must be

analyzed are overlays and are consequently thin (less than 4 inches). Therefore, it is impossible to achieve the desired height to diameter ratio of at least unity as required by AAMAS. This problem is addressed by the procedures developed as a joint effort among studies 1170 and 1177.

As discussed the axial test protocol and test configuration also provides a method for measuring dilatation ratio or Poisson's ratio. This is important as this ratio is used to some extent in current pavement design methodologies and in AAMAS. Based on recent SHRP research, it is apparent that future analysis techniques will utilize the dilatation ratio in design/analysis to a greater and greater extent.

The devices are described in Appendix A (development of testing procedures). The devices provide the necessary capability for current design procedure and NDT evaluation procedures. They should also maintain their utility for the foreseeable future as new design and evaluation tools are developed (i.e., SHRP).

Detailed procedure for testing with these devices is presented in Appendix B of the 1177-1F report (Little, et al. (1991)).

#### **MODIFICATIONS TO AAMAS CRITERIA FOR MIXTURE EVALUATION**

The evaluation procedures discussed in the NCHRP 338 Report should be followed for the evaluation of the resistance to fatigue cracking and low temperature fracture as discussed in detail in Sections 2, 3 and 4 of the AAMAS Report. However, changes in the procedure for the evaluation of uniaxial static creep testing data are recommended. These changes are discussed in detail in Chapter 3 of this report and are summarized as follows:

1. The one hour creep test should be performed at 104°F as described in the AAMAS Report and at a stress state that represents as closely as possible the stress state induced within the asphalt concrete mixture in the pavement section and under the traffic and temperature in the field. In order to insure a realistic stress state, Tables 3.14 through 3.23 are presented in Chapter 3. These tables should be entered with the appropriate pavement structural

identification in order to select the appropriate uniaxial compressive stress to be used in laboratory testing.

2. The values of creep strain are to be plotted against time of loading on an arithmetic plot. The purpose of the arithmetic plot is so that the stages of creep are readily apparent: i.e., primary, secondary and tertiary.
3. The criteria for evaluation of the compressive creep data are: strain at the end of one-hour of creep testing under the appropriate level of stress, log-log slope of the steady state portion creep strain versus time of loading curve and the creep stiffness at the end of one hour of loading. The steady state slope of the creep curve is generally calculated between about 1,000 seconds and 3,000 to 3,600 seconds. The slope of the steady state portion of the creep curve can be calculated as:

$$\frac{\log \epsilon_{pt_1} - \log \epsilon_{pt_2}}{\log t_1 - \log t_2} \quad (2.1)$$

where  $\epsilon_{pt}$  is the total creep strain at times  $t_1$  and  $t_2$ .

4. The final criterion for evaluation of deformation potential is based on the total resilient strain,  $\epsilon_{rt}$ , calculated from the dynamic resilient modulus test, ASTM D 3497, and the strain at failure in the unconfined compressive strength test, AASHTO T 167,  $\epsilon_{qu}$ . The requirement is that the sum of the total resilient strain and the total creep strain,  $\epsilon_p$ , are less than  $0.5\epsilon_{qu}$ :

$$\epsilon_p + \epsilon_{rt} = 0.5\epsilon_{qu} \quad (2.2)$$

#### THE AAMAS PROCEDURE FOR THE EVALUATION OF FATIGUE CRACKING

Figure 2.5 presents the evaluation criteria by which fatigue potential is evaluated in AAMAS based on the mixture properties of indirect tensile strain at failure and diametrical resilient modulus. The relationship

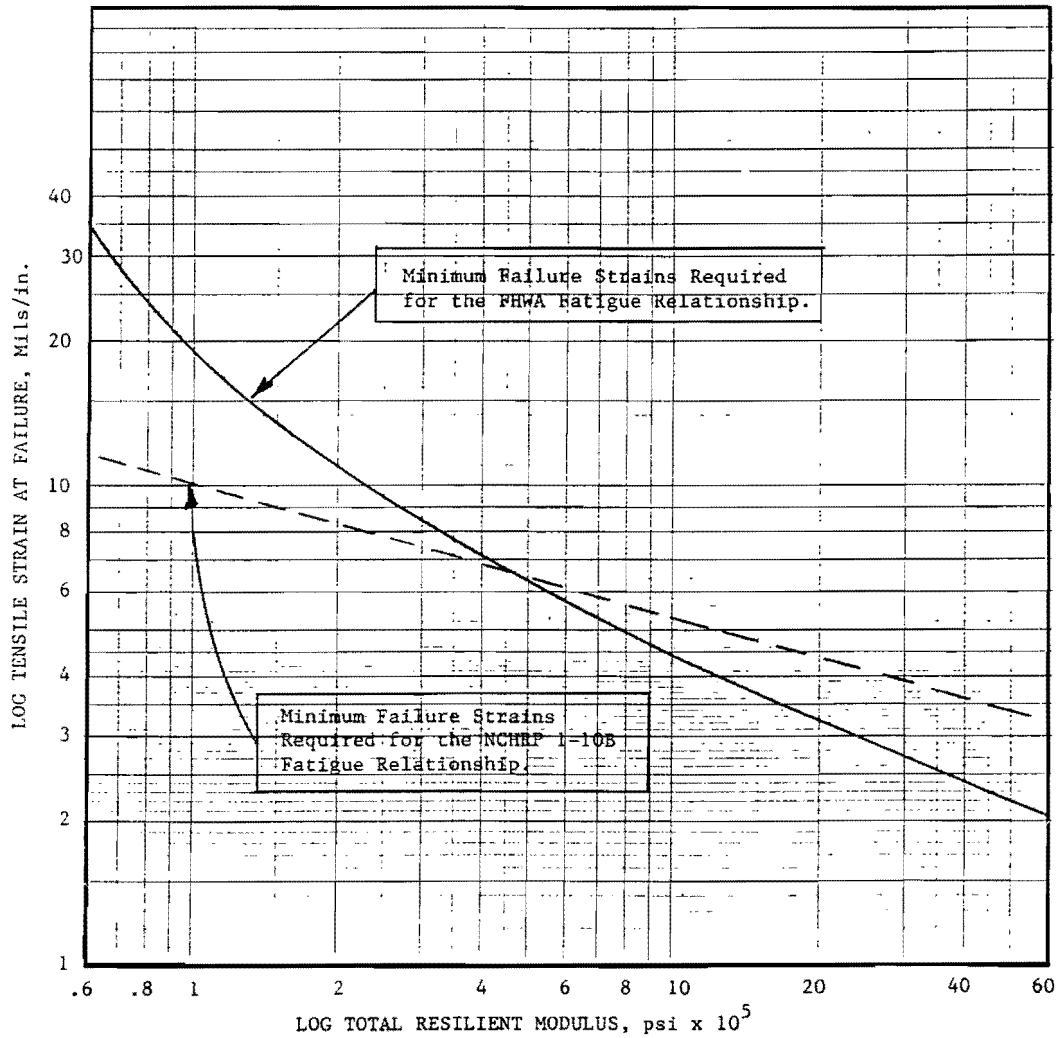


Figure 2.5. Relationship Between Indirect Tensile Strains and Resilient Modulus Using Two Different Fatigue Relationships. (After Von Quintus (1991)).

between indirect tensile strain at failure and diametrical resilient modulus in Figure 2.5 is derived based on the generalized fatigue relationship:

$$N = K_1(\epsilon_t)^{-n} \quad (2.3)$$

where  $N$  is the number of loading applications or cycles,  $\epsilon_t$  is the tensile strain at the bottom of the asphalt concrete pavement layer and  $K_1$  and  $n$  are

fatigue regression constants. Von Quintus, et al. (1991) present methods for determining the value of  $K_1$  and  $n$  for different mixtures and for different temperatures. However, determination of  $K_1$  and  $n$  for various mixtures is not a portion of the basic mixture design procedure of AAMAS as this determination is impractical for routine mixture design/analysis procedures. Basically two methods can be used for evaluation of the potential of asphalt concrete mixtures to fatigue crack. The first is to ensure that the mixture meets or exceeds the fatigue resistance of a "standard" material (which is assumed in the structural design), and the second is to ensure that the mixture has the required fatigue resistance for the specific environment and pavement cross section. This second method requires that the fatigue properties of the mixture be measured from laboratory fatigue tests or estimated from other mixture properties.

AAMAS selected the standard mixture to be the dense-graded asphalt concrete placed at the AASHTO Road Test. The fatigue curves from this mixture have been widely studied and are included in NCHRP 1-10B (1977). This basic fatigue relationship for this "standard" mixture is one of the most widely accepted and used. The NCHRP 1-10B fatigue relationship is as follows:

$$\log N = C_f - 3.291 \log \epsilon_t - 0.854 \log E_R \quad (2.4)$$

where  $C_f$  is the fatigue coefficient or transformation factor to field conditions and is dependent on the level or amount of fatigue cracks:  $C_f = 14.820$  for crack initiation or laboratory conditions,  $C_f = 15.947$  for 10 percent fatigue cracks and  $C_f = 16.086$  for 45 percent fatigue cracks.

Using the NCHRP 10-1B fatigue curve as a base line, the tensile strain at  $N = 1$ , or one loading repetition can be calculated. This represents a very fast indirect tensile test, i.e., at a stroke rate of 2 inches per minute. Thus it is assumed that the tensile strain calculated from equation 2.4 (for crack initiation) would be the same failure strain measured from an indirect tensile strength test at the same temperature. It should be noted that even though the tensile strength recorded in the indirect tensile test is highly dependent on rate of loading, the tensile strain at failure at temperatures below 77°F is not much less dependent. Therefore, the

loading rate of 2 inches per minute is used for all indirect tensile testing in AAMAS.

Using this approach, the tensile strain at failure ( $N = 1$ ) can be calculated for the different stiffnesses using the following equation:

$$\log \epsilon_f = 4.503 - 0.2595 \log E_R \quad (2.5).$$

An FHWA cost allocation study (Rauhut, et al. (1984)) adjusted equation 2.4 to account for the variation in the slope of the fatigue curve that occurs when fatigue tests are performed at different temperatures. Thus two base fatigue relationships (relationships between the indirect tensile strain at failure and the resilient modulus at the temperature in question) were available for use: the NCHRP 10-1B model and the Rauhut model. The Rauhut model was selected by AAMAS, and it is the model that appears in Figure 2.5.

Thus, if the total resilient modulus and indirect tensile strains at failure for a particular mixture plot above the standard mixture in Figure 2.5, it is assumed that the mixture has better fatigue resistance than the standard mixture. On the other hand, if the locus of the indirect tensile strain at failure and the resilient modulus at a selected temperature are below the standard curve, the mixture is more fatigue susceptible than the standard mixture.

Von Quintus, et al. (1991) present a method by which to approximate fatigue constants for non-standard mixtures. This is a valuable approach. However, the approach is time consuming and requires numerous computations and requires solving simultaneous equations. Thus, AAMAS recommends that indirect tensile strain and resilient modulus test results be compared to the standard mixture for the evaluation of fatigue resistance.

If layered elastic design is used to design the appropriate pavement thickness, the standard mixture (as defined in terms of fatigue life by equation 2.4) should be used. If equation 2.4 is used in thickness design and the actual design mixture meets the requirements set forth in Figure 2.5, then the mixture is considered as adequately resistant to fatigue if the NCHRP 10-18 criteria are used (Figure 2.5). If the FHWA (Rauhut) criteria are used for mixture fatigue evaluation and equation 2.4 is used in thickness design, then the results will be highly conservative at lower

temperature (below about 70°F) and unconservative at temperatures about 70°F. Thus, the best approach is to use the FHWA (Rauhut) procedure both in pavement thickness design and in fatigue potential evaluation (Figure 2.5).

Considerable work was done in this study to determine whether the basic fatigue regression constants in equation 2.3 could be approximated from simple tests. It was determined that the best method to approximate  $n$  in equation 2.3 is based on the slope of the indirect tensile creep curve. A lab matrix and field cores were tested in indirect tensile fatigue and indirect tensile creep to verify that a relationship does exist, as is supported by theory, between the slope of the indirect tensile creep curve and  $n$ . This testing demonstrated that the relationship is that the slope  $n$  of the fatigue curve is approximately equal to the slope of the indirect tensile creep curve,  $n_t$ , divided by two.

Although the use of the indirect tensile creep test can be effectively used to predict fatigue performance at this time, it is recommended that the AAMAS approach be followed. It is, however, recommended that if one wishes to approximate the fatigue life of a mixture, the indirect tensile creep test be performed in accordance with the AAMAS protocol (Section 3 - Addendum A) at three temperatures (41, 77 and 104°F) and that the value  $n$  be approximated as  $\frac{n_t}{2}$ . The value of  $K_1$  can then be approximated from the relationship:

$$n = 1.75 - 0.252 \log K_1 \quad (2.6).$$

#### **THE AAMAS PROCEDURE FOR THE EVALUATION OF THE APPROPRIATE RANGE OF DIAMETRICAL RESILIENT MODULUS AS A FUNCTION OF TESTING TEMPERATURE**

Figure 2.6 presents the AAMAS recommendations for the relationship between diametrical resilient modulus and temperature. Note that the relationship is required to fall within a band of values in order to insure that the mixture is not too stiff or too soft. If the mixture is too stiff, then thermal cracking or fatigue problems may occur. If, on the other hand, the mixture is too soft, the asphalt concrete layer will not satisfactorily perform its function of protecting the underlying layers. The result could

be the development of excessive stresses and deformation in the lower, more deformation susceptible layers. This approach is very similar to and is derived from the approach presented by Mahboub and Little (1987).

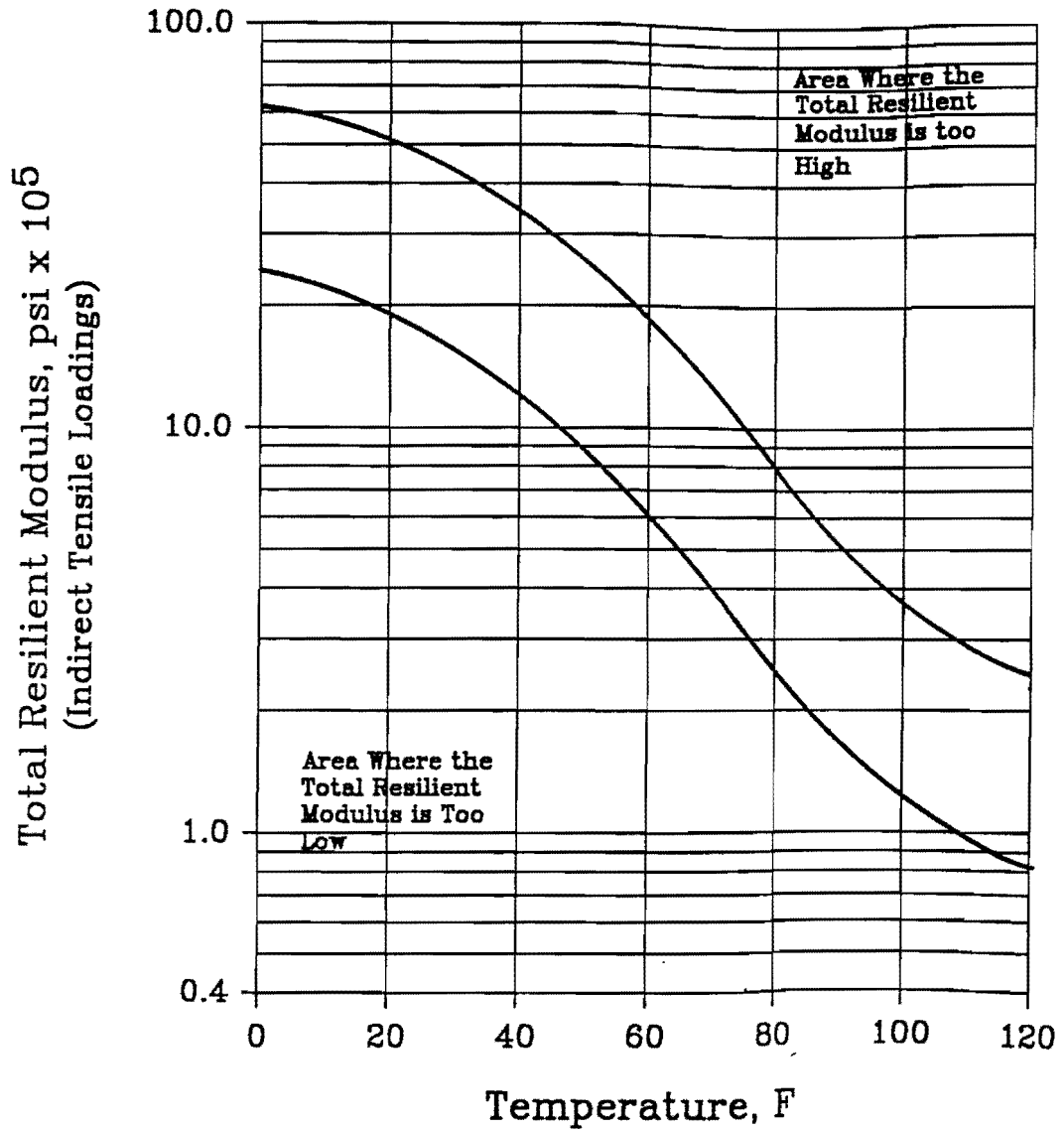


Figure 2.6. Chart for Total Resilient Modulus Versus Temperature Using Indirect Tensile Loading Conditions. (After Von Quintus, et al. (1991)).

In addition to the required range within which the resilient modulus versus temperature relationship must fall, a weighted AASHTO structural layer coefficient is calculated in the AAMAS procedure (paragraph 4.4 of the NCHRP Report 338). This approach considers seasonal fatigue damage and their effects on the structural layer coefficient. The seasonal resilient moduli are used to calculate seasonal fatigue damage, and the seasonal fatigue damage is summed to determine annual damage. From the annual damage, an equivalent asphaltic concrete resilient modulus is calculated as follows:

$$E_{RE} = \Sigma \frac{E_{Rt}(i) \times FF(i)}{\Sigma FF} \quad (2.7)$$

where  $E_{RE}$  is the equivalent resilient modulus based on a fatigue damage approach;  $E_{Rt}$  is the total resilient modulus as measured by ASTM D 4123 at the average pavement temperature for season  $i$ ; and  $FF$  is the fatigue factors obtained from Figure 2.7.

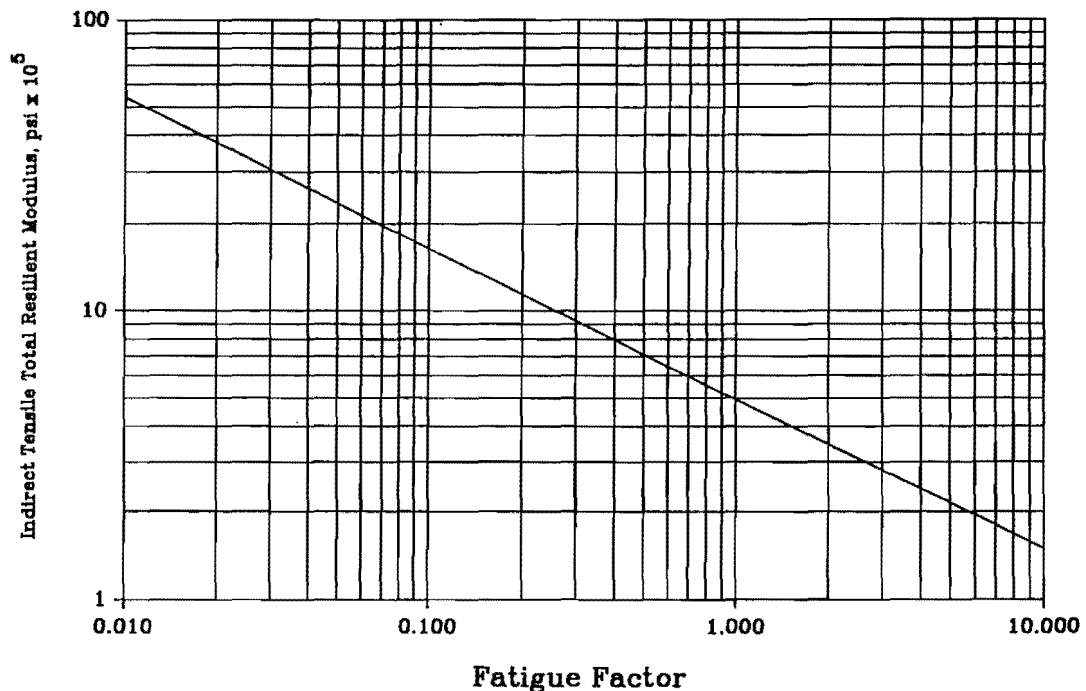


Figure 2.7. Estimation of the Fatigue Factor to Determine an Equivalent Annual Resilient Modulus.

The following is the AAMAS step-by-step procedure that is used to ensure that the asphalt concrete mixture meets or exceeds the layer coefficient assumed during structural design:

1. Obtain the seasonal average pavement temperature for each season.
2. Determine the total resilient modulus at each seasonal temperature.
3. Obtain the fatigue factor for each seasonal resilient modulus for Figure 2.7.
4. Calculate the equivalent resilient modulus from equation 2.7.

The relationship between the structural layer coefficient and fatigue cracking is obviously limited and it does not consider any damage caused by permanent deformation and disintegration. However, it does allow seasonal and environmental effects to be used in estimating the AASHTO structural layer coefficient.

Figure 2.8 is used in the 1986 AASHTO Design Guide to compute the AASHTO structural layer coefficient based on the total resilient modulus at 68°F.

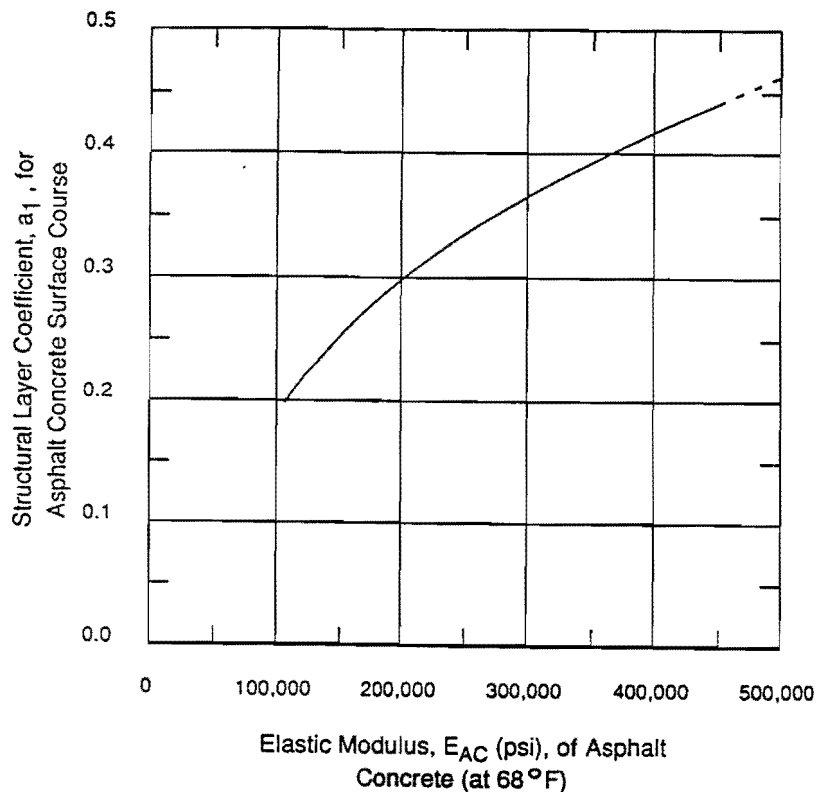


Figure 2.8. Chart for Estimating Structural Layer Coefficient of Dense-Graded Asphaltic Concrete Based on the Elastic (Resilient Modulus). (After the Asphalt Institute, 1981).

## THE AAMAS PROCEDURE FOR THE EVALUATION OF LOW TEMPERATURE CRACKING POTENTIAL

The AAMAS procedure in NCHRP Report 338 presents a procedure to predict the critical temperature change at which cracking will occur. This critical change in temperature can be estimated using the following equation:

$$\Delta T = \left[ \frac{E_{ct}(T_i)}{E_o} \right]^{1/n_r} \cdot \frac{t_r^{n_c}}{\alpha_A E_o(T_i)} \quad (2.8)$$

where  $E_{ct}(T_i)$  is the indirect tensile creep modulus measured at temperature  $T_i$ ,  $E_o$  is a regression constant developed from lab test data, and  $n_r$  is the slope of the relationship between indirect tensile strength and resilient modulus of the mixtures measured at temperatures of 41, 77 and 104°F. The relationship between indirect tensile strength and resilient modulus developed over a range of temperatures is mathematically stated as:

$$\log E_{ct}(T_i) = \log E_o + n_r \log S_t(T_i) \quad (2.9)$$

where  $S_t(T_i)$  is the indirect tensile strength measured at temperature  $T_i$  in psi. The term  $t_r$  in equation 2.9 is time of relaxation and is usually 3,600 seconds,  $\alpha_A$  is the thermal coefficient of volume change (typically not measured but assumed to be between  $1.0 \times 10^{-5}$  to  $1.8 \times 10^{-5}$  in./in./°F.), and  $n_c$  is the slope of the indirect tensile creep curve.

Therefore the following procedure is required to determine the critical temperature change at which cracking occurs:

1. Develop the relationship between indirect tensile strength and indirect tensile creep modulus as defined in equation 2.8 (at temperatures of 41, 77 and 104°F). Tests should be performed in accordance with Addendum A and Addendum B of the NCHRP 338 Report.
2. From step 1, identify  $n_r$ , the slope of the relationship between creep modulus and indirect tensile strength and  $E_o$ .
3. Determine the critical temperature drop at the two test temperatures of 41 and 77°F using equation 2.8.

The evaluation of  $\Delta T$  is not typical of routine mixture design. The variables which influence  $\Delta T$  are predominately those that influence the rheology of the mastic (binder, dust and fine sand). These include binder source, binder grade and mineralogy and physical nature of the fines (i.e., minus 200 sieve size material including lime or other additives). Therefore, if the mixture is deemed to be susceptible to thermal fracture an adjustment of mastic rheology, as discussed above, should be achieved, and the influence of this adjustment on  $\Delta T$  should be evaluated.

### **THE SELECTION OF THE GYRATORY METHOD OF MIXTURE COMPACTION**

Three studies have been performed in the last three years regarding the appropriate method of laboratory compaction. The first was part of the AAMAS study. This study compared the Texas gyratory compactor with four other compaction devices: the traditional Marshall drop hammer (ASTM D 1559), the California kneading compactor (ASTM D 1560), the Arizona kneading-vibratory compactor and the mobile steel wheel simulator.

The Marshall drop hammer compacts the asphalt concrete sample through an impact load. The California kneading compactor induces a kneading action as the pressure is increased and the decreased in the form of a haversine wave on a compactor foot that has a contact surface area of approximately 25 percent of the surface area of the compaction sample. This kneading action is very different from the drop hammer and induces a concentrated stress at large aggregate points of contact. The Arizona kneading-vibratory compactor simultaneously kneads and vibrates the sample in an effort to simulate the action produced by a rolling vibratory roller. Finally, the mobile steel wheel roller actually simulates the rolling action of a steel wheel roller as a box containing asphalt mix translates back and forth under the rocker action of a hinged steel wheel arc.

The AAMAS study compared these compaction devices based on mixture properties from field cores and from laboratory compacted loose mix from construction projects from Colorado, Virginia, Michigan, Wyoming and Texas. The mixture properties evaluated were: indirect tensile resilient modulus at three temperatures, indirect tensile strength and indirect tensile creep. These tests were selected primarily because the sample size required for

these tests is appropriate for field cores on relatively thin pavement overlays as many of these pavements were.

All test results were sorted and analyzed on the basis of project, type of test and temperature using the PC version of the Statistical Analysis System (SAS). Mixture properties evaluated using the SAS program included: indirect tensile strength at 41, 77 and 104°F, creep load strains at 77 and 104°F for a time of loading of 300 seconds and slopes of the creep curve at 77 and 104°F. The data analyzed is summarized below for the MSE comparisons:

<u>Lab Compaction Method</u>	<u>Average MSE Ranking by Mixture</u>		
	<u>Project</u>	<u>Property</u>	<u>Temperature</u>
Arizona V-K	5.0	4.8	4.7
California K	2.0	2.0	2.0
Marshall	4.0	3.5	3.3
Mobile steel	1.7	2.8	2.0
Texas gyratory	1.0	1.5	1.3

No single laboratory compaction method always provided the best match to the results from field compaction. However, based on the MSE calculations (least MSE meaning best correlation between lab fabricated specimens and field cores), the Texas gyratory compaction device ranks first in terms of close correlation with field compaction based on mixture properties. The following is an overall summary of the number of cells by compaction device, which were closer to the target value or field cores using all available data:

<u>Compaction Device</u>	<u>Percentage of Cells with a No. 1 Rating, %</u>	<u>Percentage of Cells with a No. 1 or 2 Rating, %</u>
Marshall Hammer	7	30
Arizona V-K	7	24
California K	23	48
Mobile Steel Wheel	25	55
Gyratory Shear (Texas)	45	72

In addition to calculating mean squared error, each data set was evaluated to determine if two adjacent cells were significantly different or indifferent based on the mean and variation using a confidence level of 95 percent. The following provides an overall summary of the percentage of cells for each compaction device that were indifferent when comparing field cores to laboratory compacted specimens:

<u>Compaction Device</u>	<u>Percentage of Cells Indifferent from Target Value, %</u>
Marshall Hammer	35
Arizona K-V	41
California K	52
Mobile Steel Wheel	49
Texas Gyrotory Shear	63

Based on this statistical summary of findings, it is apparent that the Texas gyrotory compactor produces mixtures with properties most similar to those from field cores.

A comprehensive study as part of the Strategic Highway Research Program (SHRP) was performed at the University of California at Berkeley (Sousa, et al. (1990)). This study was performed on laboratory mixtures only and evaluated the magnitude and nature of the difference among mixtures prepared with different types of laboratory compaction devices: kneading, rolling wheel and gyrotory. The Berkeley study resulted in the general conclusions that the method of compaction does affect the performance of mixtures. For example, gyrotory compaction produces mixtures which are more susceptible to permanent deformation as the gyrotory compaction device produces a hydrostatic effect which is more sensitive to the grade and amount of asphalt cement binder in the mixture than are the kneading or rolling wheel methods of compaction. The kneading compactor produces mixtures which are the most resistant to permanent deformation presumably because of the high level of aggregate to aggregate contact developed under the action of the kneading compactor which produces a high concentration of stress at the aggregate contact surfaces. The overall conclusion of the Berkeley study was that the rolling wheel compactor produces the "best" intermediate level of mixture based on resistance to permanent deformation and fatigue

cracking. The limitation of the Berkeley study was that it did not compare mixtures to field compaction.

Finally, Texas A&M performed a study for the Strategic Highway Research Program (SHRP) in which a modified version of the Marshall hammer (with a rotating and beveled base), the Texas gyratory and the EXXON rolling wheel compactor were compared to field compaction based on the mixture properties produced in mixtures fabricated by using each device. The mixture properties evaluated include indirect tensile resilient modulus, indirect tensile strength and strain at failure and compressive creep. In addition, fractal analysis was used to evaluate the influence of the various compaction procedures on the orientation of aggregate particles. In this study great care was taken to insure that a wide range of air void contents were considered during the evaluation of each mixture considered. Four construction sites were evaluated.

The Texas A&M study (1992) concluded that the differences between mixture properties of the field cores and the laboratory compacted samples are not statistically significant when the differences are compared for the three compaction devices. Thus one could use the Texas gyratory or the modified Marshall hammer and produce mixtures as similar to those produced in situ as if the expensive rolling wheel type compactor were used.

Although the different studies provide different information and somewhat different pieces of the entire puzzle, the consensus must be, at this point, that use of the Texas gyratory compactor for the preparation of laboratory mixtures for the purpose of mixture design and analysis is sufficient. Although it can be argued that the gyratory compaction device may produce mixtures which are more susceptible to binder rheology and content than are mixtures produced with the rolling wheel or kneading compactor, proof does not exist that the laboratory version of the rolling wheel produces mixtures which are more statistically similar to field compacted mixtures. Furthermore, the AAMAS compaction study demonstrates that there is no significant difference statistically between gyratory prepared samples and steel wheel simulated compaction based on comparing mixture properties from lab compacted samples and field compacted samples.

Based on these studies, it is recommended that mixture fabrication be accomplished using the Texas gyratory compactor (Texas Test Method 206F).

## CHAPTER 3

### DEVELOPMENT OF THE CREEP TEST FOR ANALYZING THE RESISTANCE OF MIXTURES TO PERMANENT DEFORMATION

#### BACKGROUND AND THEORY

##### Basic Concepts

The process of creep in soils and other particulate media has, on occasion, been explained as a rate process. The basis of the rate process theory is that atoms, molecules and particles participating in a time dependent flow process are constrained from movement relative to adjacent equilibrium positions. The displacement of flow units to new positions requires the introduction of activation energy of sufficient magnitude to surmount the barrier. Mitchell (1976) explains that the rate of shear in a particulate media, such as soil, is influenced by a number of factors as explained by the equation:

$$\epsilon = 2X \frac{kT}{h} \exp \left[ - \frac{\Delta F}{RT} \right] \sinh \left[ \frac{f\lambda}{2kT} \right] \quad (3.1)$$

where  $\Delta F$  is activation energy,  $T$  is absolute temperature ( $^{\circ}K$ ),  $k$  is the Boltzman constant,  $h$  is Planck's constant,  $f$  is force,  $\lambda$  represents the distance between successive equilibrium positions,  $X$  represents the proportion of successful barrier crossings and  $R$  is the universal gas constant.

Equation 3.1 represents the direct effect of temperature on the rate of strain: as temperature increases, the rate process increases. If, in equation 3.1, the term  $(f\lambda/2kT)$  is  $< 1$ , then the rate is directly proportional to the force,  $f$ . This is the case for an ordinary Newtonian fluid. Equation 3.1 is a reasonable first approximation of the rate process which explains the creep of asphalt concrete mixtures. One would expect this deformation process to be a rate process.

A schematic representation of the influence of creep stress intensity on creep rate at some selected time after stress application is presented in Figure 3.1. At low stresses, creep rates are small and of little

practical importance. The curve shape in this region is compatible with the hyperbolic sine function predicted by the rate process equation 3.1. In the midrange of stresses, a nearly linear relationship is found between the log of stress rate and stress. This is also predicted by equation 3.1 when the argument of the hyperbolic sine is greater than 1. At stresses approaching the strength of the material, the strain rates become very large and represent the onset of failure. From Figure 1 and equation 3.1, it is apparent that the creep response of any particulate material, such as asphalt concrete, is not necessarily linear. If the stress state in the field (creep stress intensity) is one that pushes the log strain rate into the region near failure (beyond the steady state region) then assumptions of linearity are most certainly not appropriate. This point is a very important one because in the past linear viscoelastic response of asphalt mixtures under field loading conditions has been assumed. This has largely been because such an assumption is convenient, and creep data from laboratory tests at relatively low stress levels are simply shifted to higher stress states in the field by employing principles of linear viscoelastic superposition. Such an approach is clearly incorrect in the highly non-linear region of Figure 3.1. The importance of selecting a realistic stress state for laboratory testing is then essential.

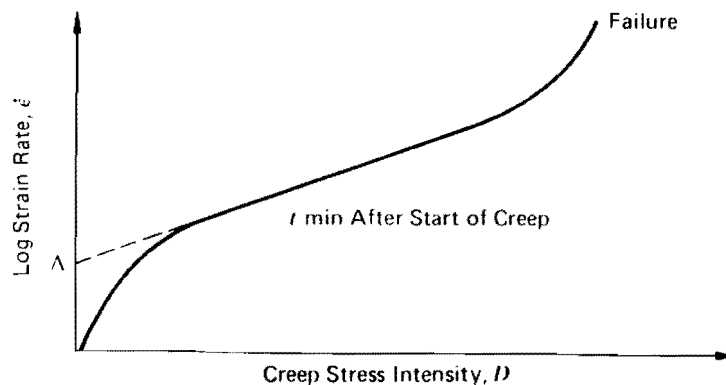


Figure 3.1. Influence of Creep Stress Intensity on Creep Rate (After Mitchell (1976)).

Another popular generalized form used to illustrate the various stages of creep is illustrated in Figure 3.2. In this figure creep strain, for a given stress level, is plotted versus time, and the creep strain is divided into three stage. In the first or primary stage the rate of deformation increases rapidly. In the second or "steady state" region, the deformation rate is constant as is the angle of slope, rate of deformation. The third region is the failure stage, in which the deformation again increases rapidly.

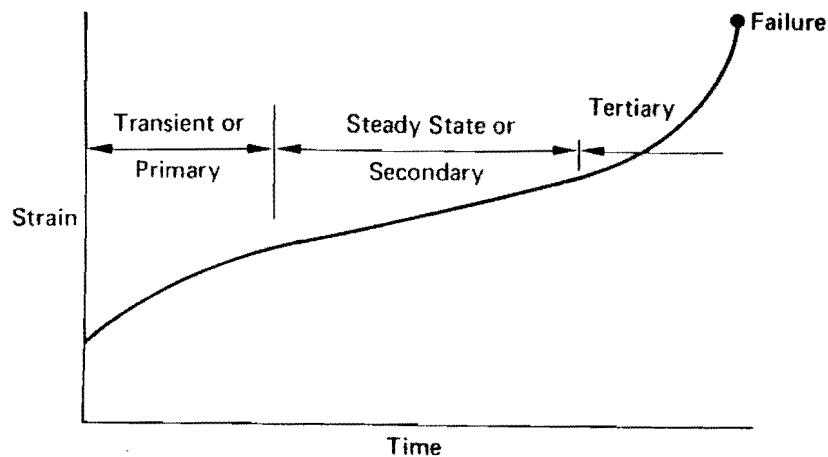


Figure 3.2. Stages of Creep (After Mitchell (1976)).

The relationship between creep strain and logarithm of time may actually be linear, concave upward or concave downward. A linear relationship is often assumed for engineering applications because of its simplicity in analysis. However, there is no fundamental "law" of behavior to dictate one form or another.

Use of the uniaxial creep test to define the stability and rut susceptibility of asphalt concrete mixtures has long been a popular approach because of its relative simplicity and because of the logical ties between the creep test and permanent deformation in asphalt concrete pavements. The major difficulty in developing criteria associated with the creep test by which to evaluate the rutting potential of asphalt concrete mixtures is in

relating this criteria to field performance. This is true for all types of lab testing which must be correlated to field results. However, even without the benefit of correlations between lab creep tests and field results, it is evident that a stable and rut resistant mixture should not demonstrate tertiary creep if tested under stresses and at temperatures in the laboratory which simulate actual field conditions.

Hills (1973) presented a pseudo-theoretical physical model with the aid of which the creep behavior of an asphalt mix can be described mathematically. This model attempts to explain, on a microscopic scale under the influence of an external load, the relative displacement (shear) of a pair of adjacent mineral aggregate particles in a viscoelastic matrix. The mechanism is thus one in which the film of binder between the mineral particles gradually becomes thinner and the overall area of "dry" mineral contacts increases. Hills assumes (1) a thin binder film and no hydrostatic effects in the binder, (2) deformation is solely due to shear in the binder and volume change is regarded as negligible and (3) under the influence of a constant stress, the rate of relative displacement of a pair of adjacent mineral particles is determined by the decreasing thickness of the binder film and by the viscosity of the binder.

Based on his assumptions, Hills was able to characterize the deformation of asphalt mixtures during the creep test with the basic equation:

$$\frac{\epsilon_{mix}}{F_y} = 2^q \left[ \left( 1 + \frac{\sigma t}{3\eta F_x} \right)^{\frac{1}{2q}} - 1 \right] \quad (3.2)$$

where  $1/F_y$ ,  $1/F_x$  = factors which are constant for one particular creep test and are dependent on the internal structure of the asphalt mix at the start of the test,  $q$  = an integer  $> 1$  corresponding to the number of "Chinese boxes" used in the model (this number is determined by the gradation of the aggregate) and  $\sigma t/3\eta$  is the viscous component of strain.

Hills used this equation to help present mixture creep data in terms of creep or stiffness data of the bitumen. This relationship is illustrated

in Figure 3.3. The shape and position of the creep curve, presented in the form of  $S_{mix}$  as a function of  $S_{bit}$ , is determined by the composition and internal structure of the mix at the stage of the test. During the creep test the internal structure of the mixture undergoes a change, which is, therefore, taken into account in the model.

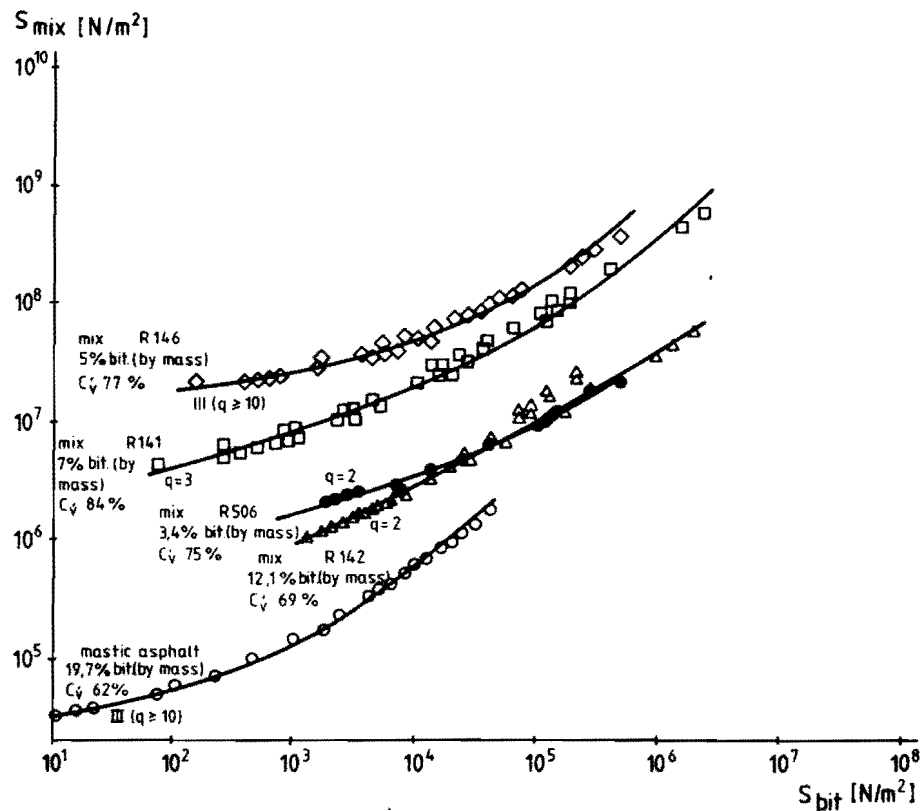


Figure 3.3. Comparison of Creep Curves Calculated on the Basis of Hills's Model with Measured Values for Various Mixes (After Hills (1973)).

The creep behavior of an asphalt concrete mixture can be pretty well explained by considering the total strain during the creep test, the reversible strain, the irreversible strain, the rates of irreversible strain and reversible strain and the strain ratio or Poisson's ratio. In fact a good evaluation of creep test data can be made based on an analysis of these properties.

The total strain at failure after a period of loading, such as 3,600 seconds, has often been used to define an acceptable mixture response in the creep test. This strain is divided into the constant stress applied to the specimen to calculate the creep modulus. This approach is used in AAMAS to define a minimum creep modulus after 3,600 seconds of loading.

It would seem more proper to use only the irrecoverable strain (viscoplastic strain) in the computation of the creep modulus used to evaluate the suitability of a mix. This is because only the irrecoverable portion of the strain is important when one considers rutting potential. In actuality the total creep modulus at the long loading time of 3,600 seconds is dominated by the viscous response (irrecoverable) of the binder. The elastic portion of binder stiffness at this long loading time and the relatively high test temperatures at which the creep test is typically performed is practically non-existent and the viscous portion of the stiffness dominates over the delayed elastic portion. Thus, when one considers the binder only, the creep modulus calculated based on total strain is essentially as appropriate as using the creep modulus based on irrecoverable modulus only.

This is not necessarily the case, however, when the effects of the aggregate are considered. The resilience offered by the aggregate matrix should be considered if practicable in order to evaluate the effect of the aggregate matrix on the permanent deformation potential of the mixture. Probably the most direct and simplest way to account for the effects of the aggregate matrix on the resilience or "recoverability" of the mixture is by performing a recovery test immediately following the creep test. This allows one to judge the effects of the resilience or "recoverability" of the aggregate matrix on the performance of the entire mixture.

In addition to the ultimate level of strain or the ultimate creep modulus following a given time of loading and the knowledge of what percentage of the creep is recoverable at the end of the test period, it is important to define the rate of creep. Creep trends in tests of soils and asphalt mixtures have demonstrated that the rate of creep and the shape of the creep curve is difficult to predict. However, a general trend is usually observed. This trend is that both total strain and irrecoverable strain are functions of time of loading, temperature, stress state, mix type and other parameters, such as the manner of loading and reloading

conditions. With increasing consolidation, more asphalt cement binder is squeezed into the voids and stress is gradually transferred to the mineral particle contacts. The strain rate decreases as this occurs. Therefore, a constant positive strain rate indicates an unstable state between the external force and the internal resistance of the material. This type response will result in failure at some point in time. During failure, the strain rate rapidly increases and the curve becomes concave upward.

Finally, an important factor in the complete analysis of uniaxial creep data is the strain ratio. This strain ratio is defined as the ratio of radial strain to axial strain and is called the dilation ratio to differentiate it from Poisson's Ratio. Poisson's Ratio is the ratio of lateral to axial strain for an elastic material in the linear elastic region. Since the creep test is not conducted in the linear elastic region on the composite material of asphalt concrete, the dilation ratio often exceeds 0.5 and may reach as high as 2.0. Obviously, a value of Poisson's ratio in excess of 0.5 is impossible according to elastic theory.

The values of dilation ratio in excess of 0.5 are indicative of why certain asphalt concrete mixtures perform better in the field than would be expected based on uniaxial lab creep or uniaxial resilient modulus testing. The radial dilation of the mixture produces an effective confining stress which can actually enhance the deformation resistance and resilient properties of the asphalt concrete mixture. This property has been seen in stone mastic (SMA) type mixtures which demonstrate a higher than usual dilation potential, possible due to the unique coarse aggregate matrix developed within these mixtures.

A methodology has been developed at Texas Transportation Institute in Project 1170 and in conjunction with Project 1177 (Little and Crockford, 1991) to measure all pertinent uniaxial creep parameters. This test methodology and testing equipment will be discussed in detail in Appendix A of this report and in Report 1177-1F.

#### Differences between the Creep Test and Other Rutting Tests

Several approaches currently exist by which to evaluate the rutting potential of asphalt concrete. Among these are the uniaxial creep test,

repeated load uniaxial tests, confined or triaxial creep and confined repeated load deformation tests, repeated load shear tests (with or without confinement), triaxial type strength tests and laboratory simulations of actual wheel loading tests. Of these tests, the laboratory simulation of wheel loading is generally considered the most reliable as it is believed to most closely simulate the stress conditions that occur in the pavement. The obvious difficulty with this test is that the equipment is expensive, specimen preparation (e.g., compaction) is time consuming and intricate and routine testing time is far too long for routine mixture design and/or analysis.

Of the remaining tests, which are performed on "laboratory-sized" samples, the simplest is the uniaxial creep test. This test was selected for mixture design (and routine mixture analysis) because of its simplicity, reproducibility and speed of testing. All repeated load tests require more intricate equipment to apply the repeated load and considerably longer testing time than is required for the creep test. Generally, the uniaxial creep test is sufficient to prioritize the different mixtures in terms of relative resistance to permanent deformation. However, recent testing on stone mastic and open graded porous course mixtures demonstrates that in certain cases a realistic comparison of stone mastic type mixtures requires application of a confining pressure to more closely simulate the actual field condition. This concept will be discussed latter and doubtlessly has to do with the coarse fraction grain-to-grain nature of the stone mastic type mixture which distributes the load among the coarse aggregate fraction. It has become apparent through extensive testing of stone mastic type mixtures that for the grain-to-grain matrix to function effectively, it is necessary to "hold" the matrix in place with a mastic of strong internal cohesive strength. It has become clear that even though the uniaxial creep test is effective in ranking the relative resistance of these stone mastic type mixtures to deformation, at least a minimum level of confinement is required to realistically evaluate the grain-to-grain matrix interaction.

The primary difference between a repeated load test and a static test is the plastic deformation that occurs between loading applications. Bolk (1981) explains that the difference between static and repeated load testing can be much better understood by considering static load tests versus

repeated load tests on aggregate systems without binder. Creep tests on these systems reveal that deformation is virtually independent of loading times. However, deformation is highly dependent on number of cycles. This difference is due to the plastic deformation that occurs at particle-to-particle dry contacts. This plastic deformation or relative movement among particles is most effectively produced under dynamic loading conditions as the dynamic effect of each repetition produces some level of relative movement. It is obviously extremely difficult to quantify the difference between dynamic and static deformation in an aggregate system whether or not that aggregate system is dry or contains asphalt binder. Because of this difficulty, the only practical way to relate the two is through empirical correction factors such as the  $C_m$  factor introduced by Shell researchers (Bolk, 1981). This factor ranges between 1 and 2, depending on the nature or the aggregate fraction and the type of mixture.

The major difference between the static creep test and a repeated load permanent deformation test is that the uniaxial creep test is highly dependent on the cohesion of the binder and the mastic portion of the mixture. In the case of a true triaxial test, mineral interlock plays an important role in deformation resistance. Therefore, the deformation behavior in the pavement or in a realistic triaxial test is much more dependent on mineral interlock than in the creep test. The only way to improve the creep test to better account for mineral interlock is through applying confinement. Or, perhaps another way to approach the analysis of mixtures is to use the creep test as a means to evaluate the role of the binder and the mastic in deformation resistance and to couple this test with a simple shear strength test, such as a simple triaxial test or Hveem stability test to evaluate the mineral aggregate internal friction.

The uniaxial repeated load permanent deformation test still suffers from the inability of the test to fully evaluate mineral aggregate interaction and internal friction due to lack of confinement. The repeated loading effect does perhaps provide some insight into the mixture that the uniaxial creep test does not provide due to the ability to evaluate the effect of repeated loading on plastic deformation among aggregate particles. Thus, the most complete laboratory evaluation of permanent deformation, short of

a simulated wheel rutting test, would be one which incorporates confinement and cyclic loading.

### Relationship between the Creep Test and Actual Rutting

Shell researchers have related the measured results of rutting tests to results of laboratory creep tests by calculating the rutting in a pavement layer from the creep test and comparing these results to the measured results.

In order to account for the effects of time of loading and temperature, Shell researchers have used the classic relationship between the mixture stiffness and the bitumen stiffness, Figure 3.3. In this figure the  $S_{bit}$  decreases with increasing time of loading and/or increasing temperature. A concomitant decrease in  $S_{mix}$  results. However, a flattening of the curve results due to the effects of changes in the mineral aggregate structure due to consolidation and shifts in the aggregate matrix.

In order to be theoretically correct in the prediction of rutting using the Shell approach, it is necessary to calculate the viscous portion of the stiffness of the bitumen,  $S_{bit,visc.}$ , as this is the portion that is irrecoverable and hence causes permanent deformation to develop. However, from a practical standpoint it is not necessary to calculate the  $S_{bit,visc.}$  at long times of loading (such as 3,600 seconds for the creep test) as the values of  $S_{bit,visc.}$  and  $S_{bit}$  are nearly equal at this long loading time. In fact, this is, for practical purposes, true when  $S_{bit}$  is  $10^5$  N/m<sup>2</sup> or less. Thus by entering the plot of  $S_{bit}$  versus  $S_{mix}$  with values of  $S_{bit}$  associated with creep testing, a corresponding creep stiffness value of  $S_{mix}$  can be determined. This mixture stiffness value is appropriate for use in the Shell rutting prediction equation, which is as follows:

$$\Delta H = H \cdot \frac{\sigma_{tire}}{S_{mix}} \cdot C_m \cdot Z \quad (3.3)$$

where H is the thickness of the asphalt pavement in question,  $\Delta H$  is the change in height of the layer, rutting,  $\sigma_{tire}$  is the average value of compressive vertical stress within the hot mix asphalt concrete (HMAC)

layer,  $C_m$  is the correction factor for dynamic versus static deformation and  $Z$  is a stress distribution correction factor.

Values commonly used for  $C_m$  are based on the mixture type as shown in Table 3.1.

Table 3.1. Values of  $C_m$  for Various Types of Mixtures.

Mix Type		$C_m$
OPEN	Sand sheet and lean sand mixes Lean open asphaltic concrete	1.6-2.0
	Lean bitumen macadam	1.5-1.8
	Asphaltic concrete Gravel sand asphalt Dense bitumen macadam	1.2-1.6
	DENSE	
	Mastic types Gus-asphalt Hot rolled asphalt	1.0-1.3

#### Modifications to the Shell Predictive Rutting Approach in Project 2474

Several modifications have been made to the Shell approach for use in the methodology for the prediction for rutting and mixture stability in an improved mixture design method for the Texas Department of Transportation (TxDOT). These modifications are discussed in the following paragraphs.

There are practical limitations for mixture design/analysis associated with the original Shell equation:

1. The stiffness parameter,  $S_{mix}$ , is a pseudo-elastic parameter, and it is used in a Hooke's Law format:

$$Strain = \frac{Stress (Z\sigma_{tire})}{Stiffness (S_{mix})} \quad (3.4).$$

It is extremely important to remember that the above format only holds true for elastic (recoverable) deformations. As a result, using the total stiffness parameter,  $S_{mix}$ , which represents the combination of elastic, plastic, viscoelastic, and viscoplastic

responses in a Hooke's Law format for rutting prediction is not valid.

2. The original Shell equation accounts for the field dynamic effects through the  $C_m$  factor. This factor magnifies the rutting predictions by 30 to 100 percent (Table 3.1). Normally in viscoelastic materials, dynamic loading causes less deformation than does static creep loading. This phenomenon was thoroughly explained by Kinder (1986). Kinder's data suggest that static loads have a more deleterious effect on asphalt concrete than do dynamic and cyclic loads. According to these observations, the  $C_m$  factor should be a reduction factor (less than one) rather than its present form as reported by Shell researchers (ranging from 1.3 to 2.0) (Table 3.1). It is clear that Shell researchers have incorporated this factor into their rutting equation based on discrepancies that they had observed between their rutting predictions and the actual observed rutting in the field (Van de Loo, 1974 and 1978). The source of these discrepancies may lie in the fact that simple linear extrapolation of laboratory-measured deformation trends to field conditions is not adequate. It may be necessary for the laboratory-to-field transformation to be more elaborate than a simple shift constant and to account for a range of mixture, climate and structural variables.
3. Another serious consequence of using a Hookian constitutive relationship for permanent deformation characterization is the assumption of linearity. According to Khedr (1986) and Texas Transportation Institute's investigations (Mahboub and Little, 1987), accumulation of permanent strains is not linearly proportional to stress level. In fact, the relationship between the independent variable (stress) and the dependent variable (permanent strain) is of a log-linear form. The slope of this log-linear relationship is approximately 1.61 according to Mahboub and Little (1987). The "intercepts" of this log-linear relationship are a function of mixture type. Softer mixes cause a shift in the intercept while the slope remains almost constant. Similar results

were reported by Perl, Uzan, and Sides (1984) who suggest that log-linear slope should be 1.45. This led to the conclusion that the logarithmic rate at which permanent strains are accumulated as a function of applied stress is relatively constant.

These practical limitations point out above all else the necessity to test at stress states in the lab which are as realistic as possible. It is important to mention that the stress dependency of permanent deformations, as defined in item c), was derived under conditions of equilibrium, i.e., accumulation of irrecoverable deformations become asymptotic, using a repeated-load compression test. It is, however, conceivable that under a large number of load repetitions, permanent deformations may accumulate at a faster rate which results in deformation beyond the equilibrium conditions. This may cause a "rebound" from the assumed asymptotic conditions.

Shell researchers (Van der Loo, 1974 and 1978), who pioneered the use of the static creep test, have developed their creep and rutting criteria based on the static compressive creep. Others have presented their rutting prediction models based on the repetitive load creep test. The VESYS model (Kenis, 1978) and the Modified ILLIPAVE model (Tseng and Lytton, 1986) are two examples of predictive models which require repetitive load testing. Researchers at the Australian Road Research Board (ARRB) investigated both the static creep and the repetitive creep tests (Kinder, 1986). They showed that although the magnitude of plastic deformation will be different depending on the type of the creep test, the irrecoverable deformation trends are similar. This conclusion is in agreement with the one made by Van der Poel (1954) describing the dynamic and static responses of bitumens.

The above discussion suggests that perhaps no single method fully simulates field rutting behavior. Nevertheless, for qualitative comparisons, static creep data seem to be very effective and can reasonably quantify deformation potential.

#### Modified Shell Equation

Alterations were made to the Shell rutting prediction model based on research performed in TxDOT research Project 2474 (Mahmoud and Little,

1987). The analysis of any rutting prediction model requires an advanced knowledge of plasticity and viscoelasticity. The static creep test was the major material characterization tool in this study by which the viscous and plastic characteristics of asphaltic concrete mixtures were established for further use in the modified Shell equation.

The laboratory-measured viscoplastic characteristics are normalized in the modified Shell method to accommodate the stress levels at which they are developed. This allows transformation of laboratory-measured parameters to the field conditions where higher stresses are often encountered. As a result of this process, a parameter called the "viscoplastic component of mixture stiffness" was developed.

The original Shell method for rutting prediction assumes a linear relationship between the stress and the accumulated plastic strain. As previously discussed, the relationship is usually not linear. For example, doubling the stress level from  $\sigma$  to  $2\sigma$  may lead to an increase in accumulated viscoplastic strains of well over 300 percent. These observations led to the development of a refined version of the Shell rutting equation which does not depend on empirical correction factors. This modified Shell equation accounts for plasticity trends and nonlinearity of such deformations in the following format:

$$h = H \cdot \left[ \frac{Z \sigma_{tire}}{\sigma_{lab}} \right]^{1.61} \epsilon_{VP} (t) \quad (3.5)$$

where:  $h$  = calculated rut depth (inches),  
 $H$  = asphaltic layer thickness (inches),  
 $Z$  = vertical stress distribution factor (derived from layered elastic solutions),  
 $\sigma_{tire}$  = average contact pressure (psi),  
 $\sigma_{lab}$  = stress level at which the creep test is conducted (psi), and  
 $\epsilon_{vp}(t)$  = viscoplastic trend of the mixture measured by the creep test (in/in).

In radial tires, the average contact pressure is approximately the same as the tire inflation pressure. Due to the simplicity of the modified Shell equation, the assumption of radial tires was necessary. For bias-ply tires, studies indicate that the contact pressure is not uniform and peak values are often higher than the inflation pressure (Roberts, et al., 1986). Therefore, average of contact pressure should be used in the case of bias-ply tires.

The ratio of  $Z\sigma_{\text{tire}}$  to  $\sigma_{\text{lab}}$  is raised to the 1.61 power in order to account for the non-linearities involved in the accumulation of viscoplastic deformations. This exponent was derived from work performed in TxDOT Project 2474 (Mahboub and Little, 1987). This work is summarized in Figure 3.4, and the justification is outlined below along with the constitutive plasticity law that was used in this study.

Most of the information in the literature suggests that the accumulation of permanent deformation as a function of time or number of load cycles (for static or cyclic creep, respectively) can be approximated by a simple power relationship (Findley, et al., 1976). It is the form of the power law, however, which is the subject of dispute among researchers.

The VESYS model for permanent deformation (Kenis, 1978) was developed based on the following form of power law which characterizes rutting as a strain hardening process (i.e., the exponent of the power relationship is less than one).

$$\epsilon_{vp} = at^b \quad (3.6)$$

where:  $\epsilon_{vp}$  = viscoplastic strain;  
 $t$  = time; and  
 $a, b$  = regression constants.

This basic concept has been employed by many analysts around the world, particularly in Australia (Yandell, 1971 and Kinder, 1986).

Lai and Anderson (1973) also suggest a power law format of a strain hardening nature with a stress dependent term,  $a(\sigma)$ :

$$\epsilon_{vp} = a(\sigma)t^b \quad (3.7)$$

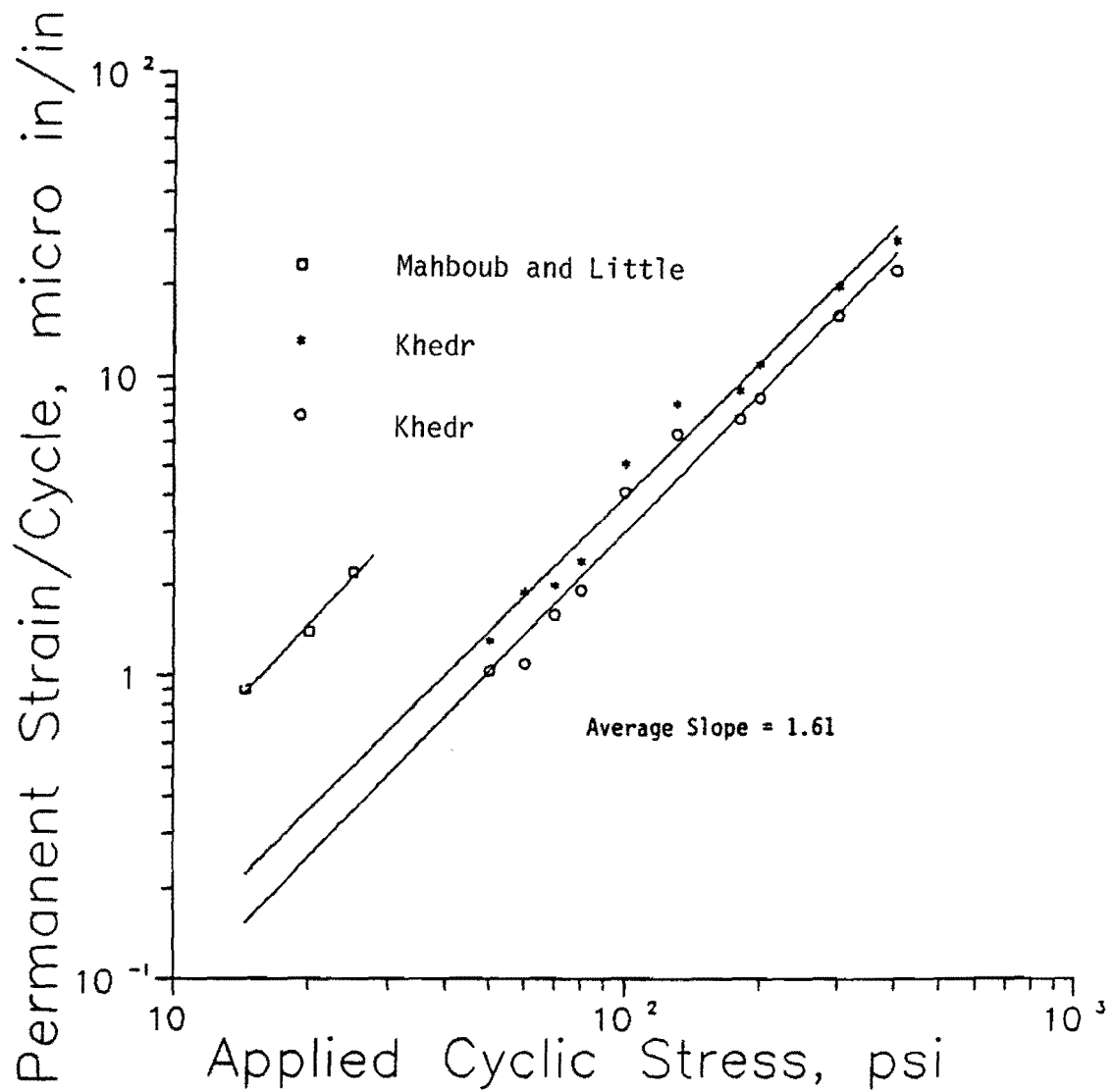


Figure 3.4. Log-linear Relationship Between the Applied Stress and the Accumulated Permanent Deformation Per Cycle (Averaged Over the First 100 Cycles of Stable Hysteresis). (After Mahboub and Little (1987)).

where:  $\epsilon_{vp}$  = viscoplastic strain,  
 $t$  = time,  
 $a(\sigma)$  =  $b_1\sigma + b_2\sigma^2$ ,  
 $\sigma$  = creep stress, and  
 $b, b_1, b_2$  = regression constants.

Perl, Uzan, and Sides (1984) have reported power relationships similar to Lai and Anderson's for both compressive and tensile modes of creep.

Studies show that the a-coefficient in a simple power law format is a function of creep stress and mixture stiffness (Perl, et al., 1984 and Lai and Anderson, 1973). The b-exponent, however, represents the rate at which permanent deformation is accumulated in a constant stress creep test as a function of time. For asphalt concrete, this exponent appears to be relatively constant. Table 3.2 summarizes the results which have been reported by different researchers.

Table 3.2. Simple Power Law Exponent as Reported by Different Researchers.

Reference	b-exponent
Kinder (1954)	0.25
Perl, Uzan and Sides (1986)	0.22
Lai and Anderson (1976)	0.25
Mahboub and Little (1987)	0.17, 0.22, 0.25 (average: 0.21)

Tseng and Lytton (1986) have proposed a 3-parameter power law for describing the permanent deformation under cyclic loading. Constants used in this model are generated from a nonlinear regression process. This model is of the following form:

$$\epsilon_a = \epsilon_o \cdot EXP - \left[ \frac{\rho}{n} \right]^B \quad (3.8)$$

where:  $\epsilon_a$  = permanent strain,  
N = load cycle, and  
 $\epsilon_0, B, \rho$  = regression constants

The above provides a better fit for the permanent deformation data and justifications for the form of the equation are based on activation energy concepts (Lytton, 1987). Although this relationship provides a powerful tool for permanent deformation data analysis, it requires repeated load testing rather than static creep testing, which has been selected for mixture design/analysis in this study because of its expedience. The three parameters in the Tseng-Lytton model, referred to as "material properties," are highly interdependent and are determined by nonlinear regression techniques. In the simple power law (Equation 3.6), the slope and intercept are treated as pseudo material properties.

The 2474 research study (Mahboub and Little, 1987) has produced a modified version of the Shell equation which:

- a) Utilizes a simple power law constitutive relationship for permanent deformation characterization.
- b) Accounts for the nonlinearity and stress dependency within the plasticity laws.

This was derived through a series of steps based on a series of cyclic permanent deformation tests over a range of stresses. A power relationship was used to relate the plastic or irrecoverable strain to the stress magnitude as:

$$\frac{\epsilon_{vp}}{N} = a\sigma^b \quad (3.9)$$

Where:

$\frac{\epsilon_{vp}}{N}$  = accumulated, viscoplastic deformation per cycle,  
 $\sigma$  = peak cyclic stress, and  
 $a, b$  = regression parameters.

The parameter  $\epsilon_{vp}/N$  was averaged over the last 10 cycles of about 100 cycles of the first stable hysteresis trend. Figure 3.4 illustrates the data from two independent sources which suggest that asphalt mixtures of different stiffness have different "a-parameters". The "b-parameter", however, is relatively constant and is equal to approximately 1.61. Consequently, one can rewrite Equation 3.9 for the two stress levels, one representing the field and the other representing the laboratory conditions:

$$\left[ \frac{\epsilon_{vp}}{N} \right]_{field} = a_{field} \cdot [\sigma_{field}]^{1.61} \quad (3.10).$$

and likewise:

$$\left[ \frac{\epsilon_{vp}}{N} \right]_{lab} = a_{lab} \cdot [\sigma_{lab}]^{1.61} \quad (3.11).$$

Therefore:

$$\frac{\left[ \frac{\epsilon_{vp}}{N} \right]_{field}}{\left[ \frac{\epsilon_{vp}}{N} \right]_{lab}} = \frac{a_{field}}{a_{lab}} \cdot \left[ \frac{\sigma_{field}}{\sigma_{lab}} \right]^{1.61} \quad (3.12).$$

Assuming that the laboratory-manufactured specimen has identical properties to the field-constructed mix, one can assume  $a_{field}$  and  $a_{lab}$  to be equal. Equation 3.12 then becomes

$$\frac{\left[ \frac{\epsilon_{vp}}{N} \right]_{field}}{\left[ \frac{\epsilon_{vp}}{N} \right]_{lab}} = \left[ \frac{\sigma_{field}}{\sigma_{lab}} \right]^{1.61} \quad (3.13).$$

The above equation illustrates the nonlinear nature of permanent deformation accumulation. Any laboratory to field projection of rutting showed account for the non-linear transition from the stress applied in the lab to that actually occurring in the field. Indeed, rutting criteria charts that are included in the 2474 study were developed using the nonlinear nature of permanent deformation accumulation.

#### Development of Permanent Deformation Criteria

In the development of any rutting criteria, the question which must be addressed is: how much rutting is excessive rutting? Therefore, it is necessary to define some limiting values or levels of severity for rutting. In this study, the limiting values for rutting were obtained from the Federal Highway Administration, Highway Pavement Distress Identification Manual (1979), which classified rutting in severity levels of high, medium and low. For safety considerations, a new class of rutting below the low severity level was developed to account for hydroplaning potential. The development of the limiting value for the hydroplaning class of rutting was based on:

- a) A roadway cross-slope of one percent.
- b) Vehicle speed of 55 miles per hour.
- c) Average pavement surface texture depth of 0.04 inches.
- d) Tire tread of 1/16 inches.
- e) Accumulation of 0.08 inches of water in the wheel path.

The above conditions were considered to be representative of Texas roads (Gallaway and Rose, 1970 and Hays and Brown, 1974). Rutting limiting values are summarized in Table 3.3 from which a series of rutting criteria charts were developed.

Table 3.3. Rutting Severity Classification.

Severity	Mean Rut Depth Criteria
Hydroplaning	0.20 - 0.25 in.
Low	>0.25 - 0.50 in.
Medium	>0.50 - 1.00 in.
High	>1.00 in.

These charts are used as acceptance or rejection guides in the improved mix design/analysis procedure. The process by which these charts were developed is summarized in the following paragraphs.

Researchers at the Australian Road Research Board (ARRB) (Kinder, 1986) have indicated that viscoplastic strains, measured from a simple static creep test, when normalized for the stress level under which they are accumulated, exhibit the following form of relationship:

$$\frac{\epsilon_{vp}}{\sigma} = 0.47 t^{0.25} \quad (3.14)$$

where:  $\epsilon_{vp}$  = viscoplastic strain; and  
 $t$  = time.

The above expression is in the form of compliance. In the inverted form, a parameter which will be referred to as viscoplastic stiffness is developed:

$$\frac{\sigma}{\epsilon_{vp}} = \left( \frac{1}{0.47} \right) t^{-0.25} \quad (3.15).$$

Equation 3.15 suggests that the viscoplastic stiffness is a decreasing function of time with the decay rate of -0.25 on a log-log scale. Perl, Uzan, and Sides studies suggest a decay rate of -0.22 for the viscoplastic stiffness parameter (1984). These observations were verified in the 2474

study by laboratory measurements which reflected decay rate values ranging from -0.17 to -0.25 (Table 3.2). These findings were incorporated into the development of rutting evaluation charts presented in Appendix C of the 2474-1F report (Mahboub and Little (1987)).

The VESYS viscoelastic computer model uses two parameters by which to identify and evaluate the permanent deformation potential of asphalt concrete mixtures: alpha ( $\alpha$ ) and gnu ( $\mu$ ). The parameter  $\alpha$  is equal to unity minus the slope of q the log-log plot of the accumulated permanent strain,  $\epsilon_p$ , versus member of leading cycles;

$$\log \epsilon_p = \log I + S \log N \quad (3.16)$$

where I is the intercept and N is the member of lead application.

Rauhut, et al. (1979) performed extensive testing of asphalt concrete mixtures and performed an extensive evaluation of test data. The Rauhut data concluded that S values for asphalt concrete are high sensitive to the temperature of testing and the level of stress applied during testing. Rauhut, et al. attempted to define regions of alpha and gnu which differentiate rut-susceptible mixtures from rut-resistant mixtures. Rauhut's work illustrated that good quality mixtures usually possesses slopes in the range of 0.10 to 0.35 with the vast majority of the data falling between 0.15 and 0.30. The mixtures with slopes in excess of 0.35 were generally determined to represent highly rut-susceptible mixtures.

Although the slope of the repeated load permanent deformation plot is not exactly the same as the slope of the static creep plot, a relationship does exist as defined by Von Quintus, et al. (1991). In this relationship the slope,  $m_R$ , of the repeated load test is calculated from the static creep data from the equation;

$$m_R = \frac{\log a + 3.5563 m + \log (1-x) - \log [a (0.1)^m - \epsilon_{rt}]}{4.5563} \quad (3.17)$$

where m is the slope of the static creep curve, x is the percent recoverable creep, a is the intercept of the static creep test, and  $\epsilon_{rt}$  is the resilient strain as recorded from a repeated load resilient modulus test prior to

creep testing. The value of  $m_R$  is typically larger than  $m$  by about 20 to 40 percent. This would mean that the slope values (log-log from static creep testing) which differentiate between rut-susceptible and rut resistant mixtures should fall below about 0.25.

It is remarkable that so many separate and totally independent studies arrive at a slope of the log-log steady static creep curve of 0.25 as being significant in its relationship to rutting potential. However, it is equally remarkable to review the considerable data that show rut-resistant mixtures with relatively high slope values (about 0.25 and even about 0.35). This apparent anomaly is probably explained by the wide differences in the aggregate structural interaction for various mixtures.

The viscoplastic stiffness rate of decay as a function of time was utilized in the development of boundary curves in the 2474. This was done by the following stepwise procedures:

- a) The viscoplastic stiffness necessary to yield a certain level of rutting (e.g., low severity rutting) after one million passes of standard 18 kip axles was back-calculated using the modified Shell equation. This established an end-point in the rutting criteria chart representing the final rutting stage in the hot mix asphalt concrete (HMAC) layer.
- b) Based on this back-calculated terminal value (the end-point) and the rate of viscoplastic stiffness decay (the slope), the trend of this parameter was established as a function of time.

The rutting criteria charts were developed accounting for the following variables:

- a) Levels of subgrade strength (3 levels).
- b) Types of pavement structures (4 types).
- c) Range of HMAC layer moduli (3 moduli).

These charts are presented in Appendix B of the 2474 report. Upon the completion of the rutting criteria charts, it was decided that it is

necessary to be able to evaluate a wider range of the above variables (a through c) in order to better approximate the actual field conditions. It was, therefore, decided that an extended analysis procedure should be developed which addresses the following variables:

- a) Broader range of layer moduli.
- b) Traffic levels other than one million 18 kip axle load.
- c) Variations in temperature profiles and traffic distributions.

This was accomplished through the extension of the same analytical procedures which were used in the development of rutting criteria charts. The results are presented in a series of nomographs in Appendix C of the 2474 report. The nomographs provide ample flexibility for the specific needs of the bituminous design engineer. However, mixture design does not require a prediction of the amount of rutting but a prioritization or identification of rutting potential.

#### Development of the AAMAS Rutting Charts

AAMAS uses the same type of chart that was developed in Project 2474 for the evaluation of rutting potential. In fact, the four creep modulus versus time of loading charts used for rutting evaluation in AAMAS were developed from the 36 charts developed in Project 2474 and presented in Appendix B of report 2474-1F.

To illustrate this point Figures 3.5 through 3.8 are the four charts used for rutting potential evaluation in AAMAS Report 338 (1990). Figure 3.9 is a chart from Appendix B of report 2474-1F (1987) from which Figure 3.5, Asphalt Concrete Mixture Rutting Potential for Layers Placed over Rigid Pavements or Rigid Base Materials, was derived. Notice that the upper bound for the concomitant AAMAS chart was selected as the boundary for incipient hydroplaning in Figure 3.5, and the lower bound in the concomitant AAMAS chart was selected as the medium severity line in Figure 3.5. Note also that the slopes of the upper boundary and lower boundary in both charts (Figures 3.5 and 3.9) are approximately 0.17 and 0.21, respectively.

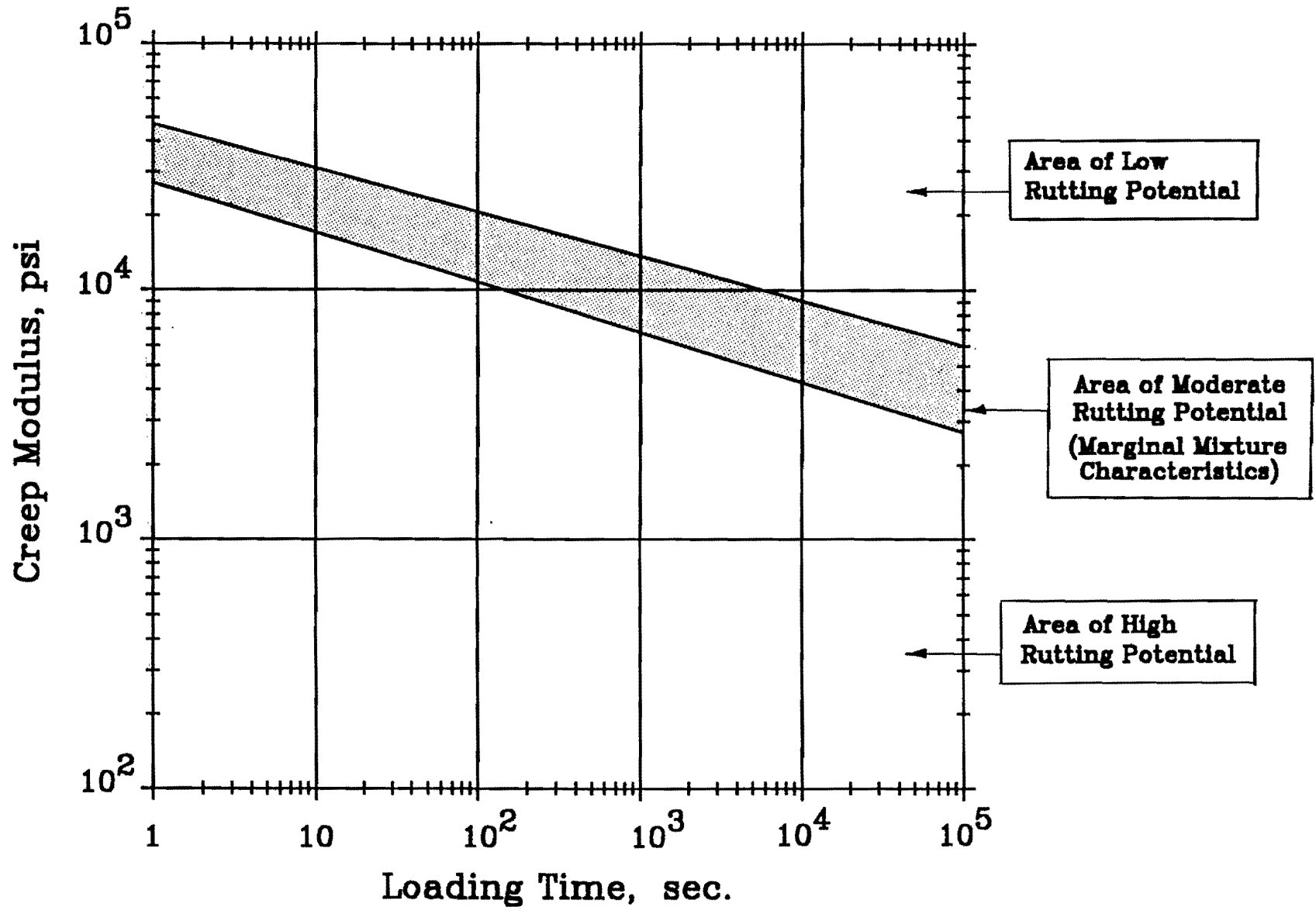


Figure 3.5. Asphaltic Concrete Mixture Rutting Potential for Layers Placed Over Rigid Pavements or Rigid Base Materials (After Von Quintus, et al. (1991)).

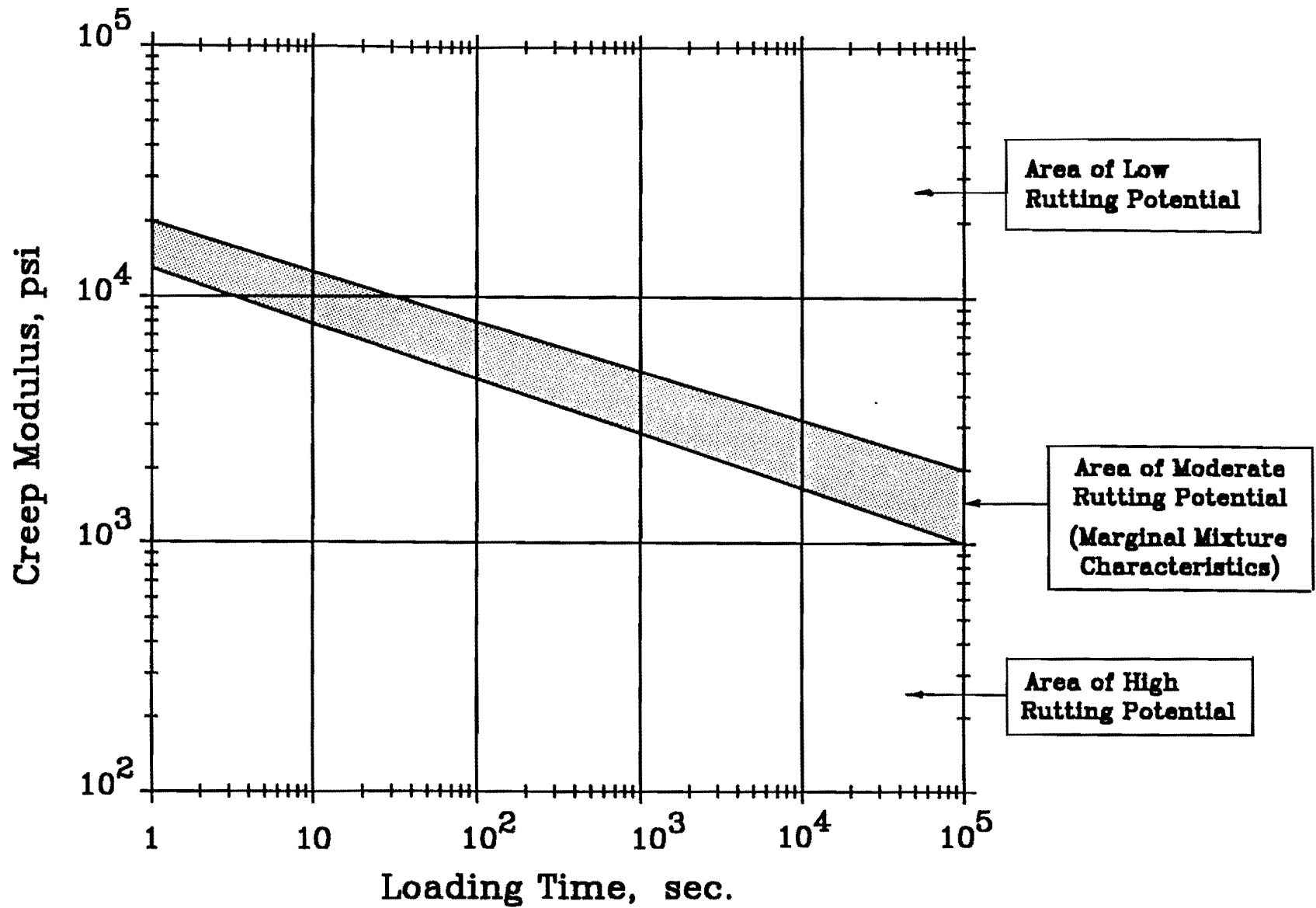


Figure 3.6. Asphaltic Concrete Mixture Rutting Potential for the Lower Layers of Full-Depth Asphalt Pavements. (After Von Quintus, et al. (1991)).

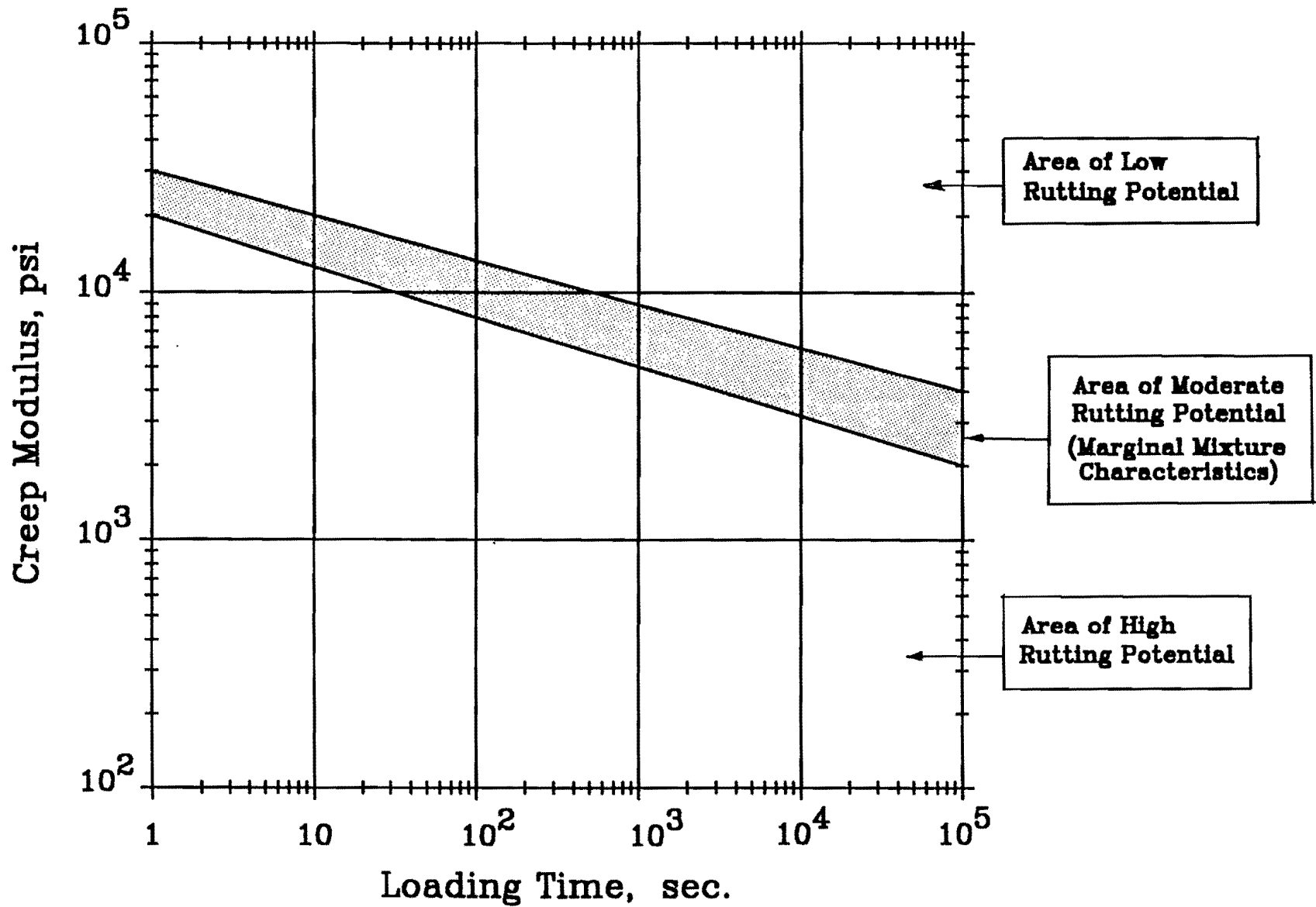


Figure 3.7. Asphaltic Concrete Mixture Rutting Potential for Intermediate Layers in Thick or Full-Depth Asphalt Pavements. (After Von Quintus, et al. (1991)).

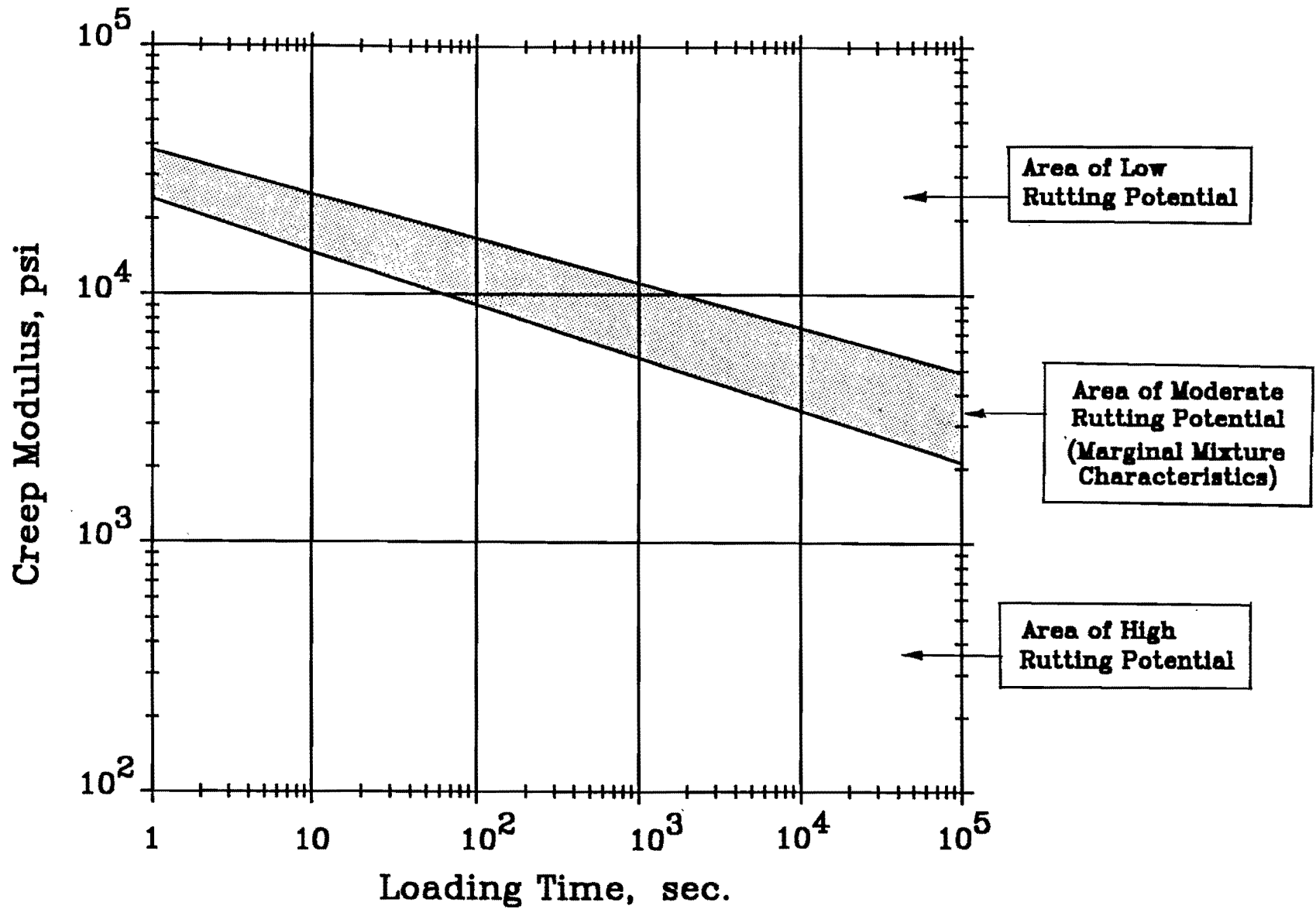


Figure 3.8. Asphaltic Concrete Mixture Rutting Potential for Surface Layers of Asphaltic Concrete Pavements. (After Von Quintus, et al. (1991)).

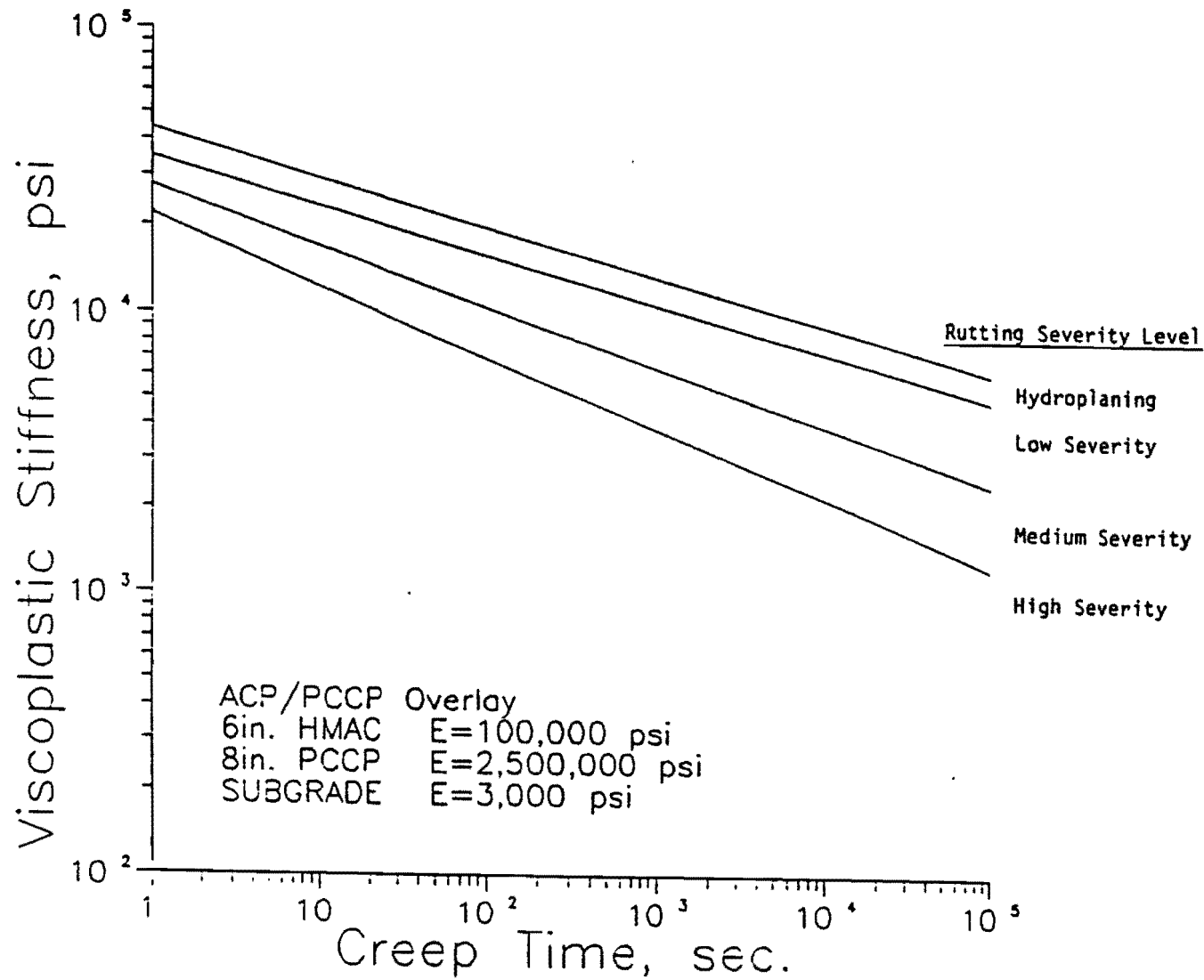


Figure 3.9. Viscoplastic Stiffness (Creep Stiffness) Versus Time of Loading for ACP over PEC for a Specific Structural Category (After Mahboub and Little (1991)).

Therefore, both the position and the slope of the creep stiffness plots are used as indicators of rutting susceptibility. In order to meet the highest standards of rut resistance the creep stiffness must maintain a high stiffness and a shallow enough slope not to penetrate into the regions indicative of higher rutting potential.

**COMPARISON OF AAMAS RUTTING CHART CRITERIA WITH CREEP MODULUS CRITERIA DEVELOPED BY OTHER AGENCIES**

It is interesting to compare the creep modulus criteria of the AAMAS creep modulus charts (and hence the creep modulus charts developed in TxDOT Project 2474) creep modulus criteria developed by other agencies. The creep test in AAMAS is performed for 3,600 seconds as is the creep test developed in Project 2474. Both tests also include a 3,600 second recovery period. The one-hour creep test period is a popular test period. Perhaps, it is popular because it is long enough to be applicable to the loading conditions during which rutting occurs in the pavement yet short enough to be a practicable testing period.

If one computes the minimum required creep modulus at 3,600 seconds of loading from the creep modulus charts developed in Project 2474 or from the AAMAS charts (Figures 3.5 through 3.8), the minimum values of creep modulus are:

<u>Pavement Category</u>	<u>Minimum Creep Modulus, psi</u>
Asphalt concrete over rigid base	10,000 - low rut potential 5,000 - moderate rut potential
Full depth asphalt concrete (intermediate layers)	8,000 - low rut potential 3,000 - moderate rut potential
Full depth asphalt concrete (lower layers)	4,000 - low rut potential 2,500 - moderate rut potential

Surface asphalt concrete

layers

8,000 - low rut potential

4,000 - moderate rut potential

Of course all of these criteria are for testing for 3,600 seconds or 60 minutes at a test temperature of 104°F and at a stress level which approximates a realistic average vertical compressive stress within the pavement layer.

Other researchers have developed similar criteria from the creep test. Viljoen, et al. (1981) says that the minimum creep modulus to prevent rutting is 12,000 psi after 100 minutes of loading at 104°F at a stress level of 30 psi. Finn, et al. (1983) says that the minimum creep modulus after 60 minutes of testing at a stress level of 30 psi at 104°F should be at least 20,000 psi. Kronfuss, et al. (1983) suggests the following set of criteria at a stress level of 15 psi, a test temperature of 104°F and a time of testing of 60 minutes:

<u>Traffic Level</u>	<u>Acceptable Creep Modulus Value of Range, psi</u>
Low intensity traffic	3,000 psi or above
Moderate intensity traffic	3,000 psi to 4,500 psi
High intensity traffic	4,500 psi to 6,570 psi

Kronfuss, et al. (1983) also established an upper limit of stiffness at 6,750 psi. Kronfuss, et al. (1983) felt that stiffnesses above this level were too high and subject to cracking due to load induced fatigue or thermal effects. However, this upper limit was established for cooler European climates where low temperature fracture effects must be considered in a different level of significance than they are in Texas.

One of the most comprehensive and recent studies of the effects of mixture variable on the compressive creep characteristics of asphalt concrete mixtures is documented in a report prepared by Sousa, et al. (1991) for the Strategic Highway Research Program (SHRP). The primary goal of this study was to evaluate the influence of different types of laboratory compaction equipment on selected asphalt concrete mixture properties.

However, the extensive compressive creep testing performed in the study makes this study an excellent source of creep testing information. Figures 3.10 through 3.15 present the influence of asphalt cement type, asphalt content, aggregate type, air void content, compaction temperature and stress level on the results of compressive creep testing.

A careful review of these figures reveals that the compressive creep test is sensitive to all mixture variables and would appear to be a reasonable, reliable and expedient routine test to evaluate the potential of various mixtures to perform satisfactorily in a pavement system.

The Sousa, et al. (1991) study compared several compaction devices. However, only the results for specimens prepared using the gyratory compactor are presented as this device is the compaction device of preference in the mixture design/analysis procedure recommended by this report. The comparison of various laboratory compaction devices is discussed separately in Chapter 2 of this report. After looking at the compressive creep data report by Sousa, et al. (1991) for samples prepared using the gyratory compactor, it is apparent that the several parameters derived from the creep versus temperature plot when presented on a log-log scale are acceptable and reasonable parameters by which to evaluate deformation potential. These parameters include: the value of the creep modulus or strain (permanent) following a specific period of loading, time to reach a critical level of strain (time of rupture) and slope of the creep curve in a designated region, such as the steady state region. Based on the results reported by Sousa, et al. (1991) these potential parameters by which to evaluate permanent deformation potential will be discussed.

First of all, if one considers the slope of the log-log creep modulus versus time of loading curve, the most deformation resistant mixture for each category of evaluation possess a slope of between 0.2 and 0.35, Table 3.4. with most of the "deformation resistant" mixtures yielding a slope of between 0.22 and 0.30. This is higher than the slopes found in the TTI 2474 study and in previously documented studies but not substantially higher. Although it is difficult to define the slope of the steady state region of the creep modulus versus time of loading relationship which differentiates a deformation resistant mixture from a deformation susceptible mixture, the data presented by Sousa indicate that the critical value of slope is in the

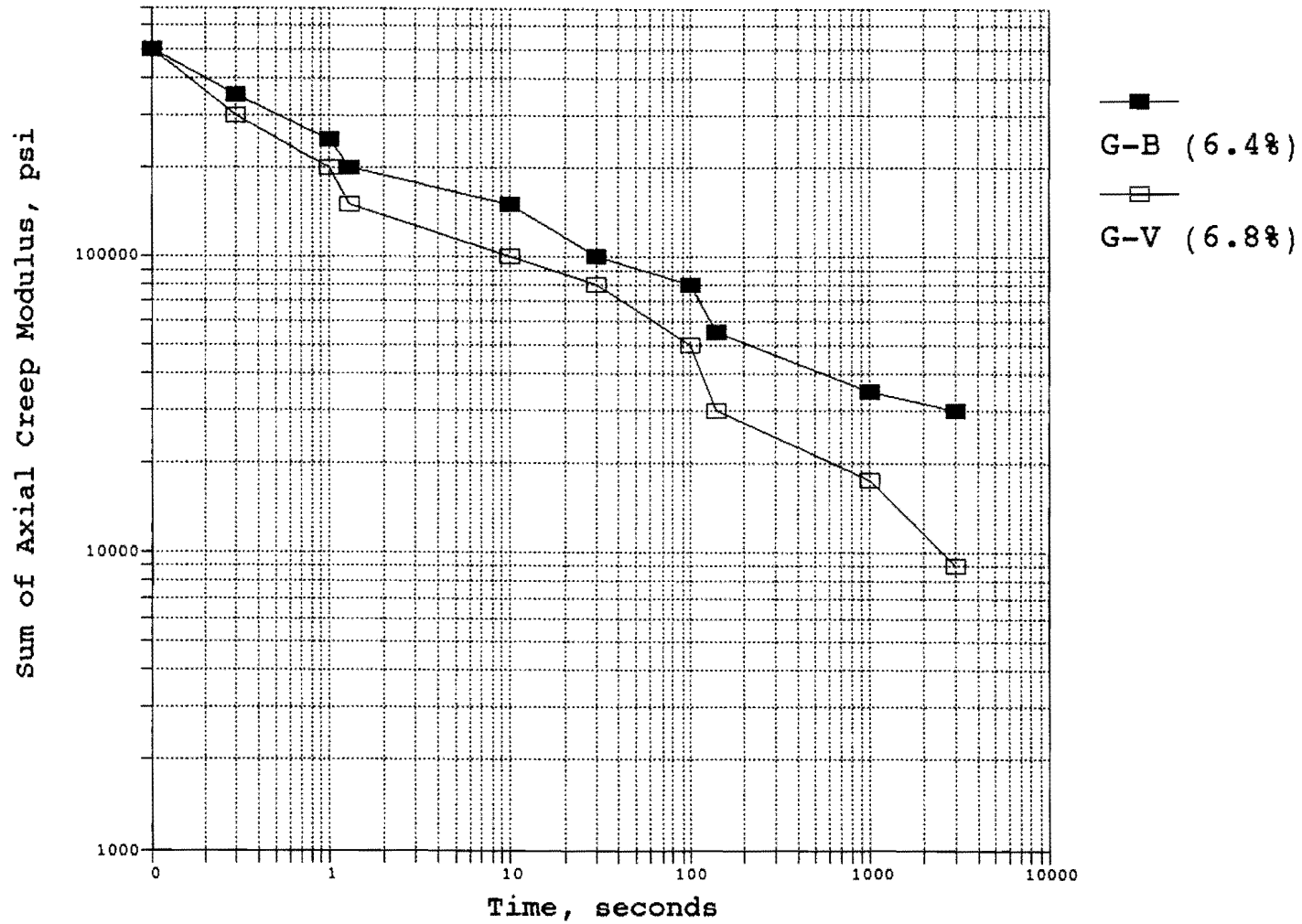


Figure 3.10. Combined Effects of Compaction and Asphalt Type on Compressive Creep Modulus, AAK-1 [B] and AAG-1 [V]. (After Sousa, et al. (1991)).

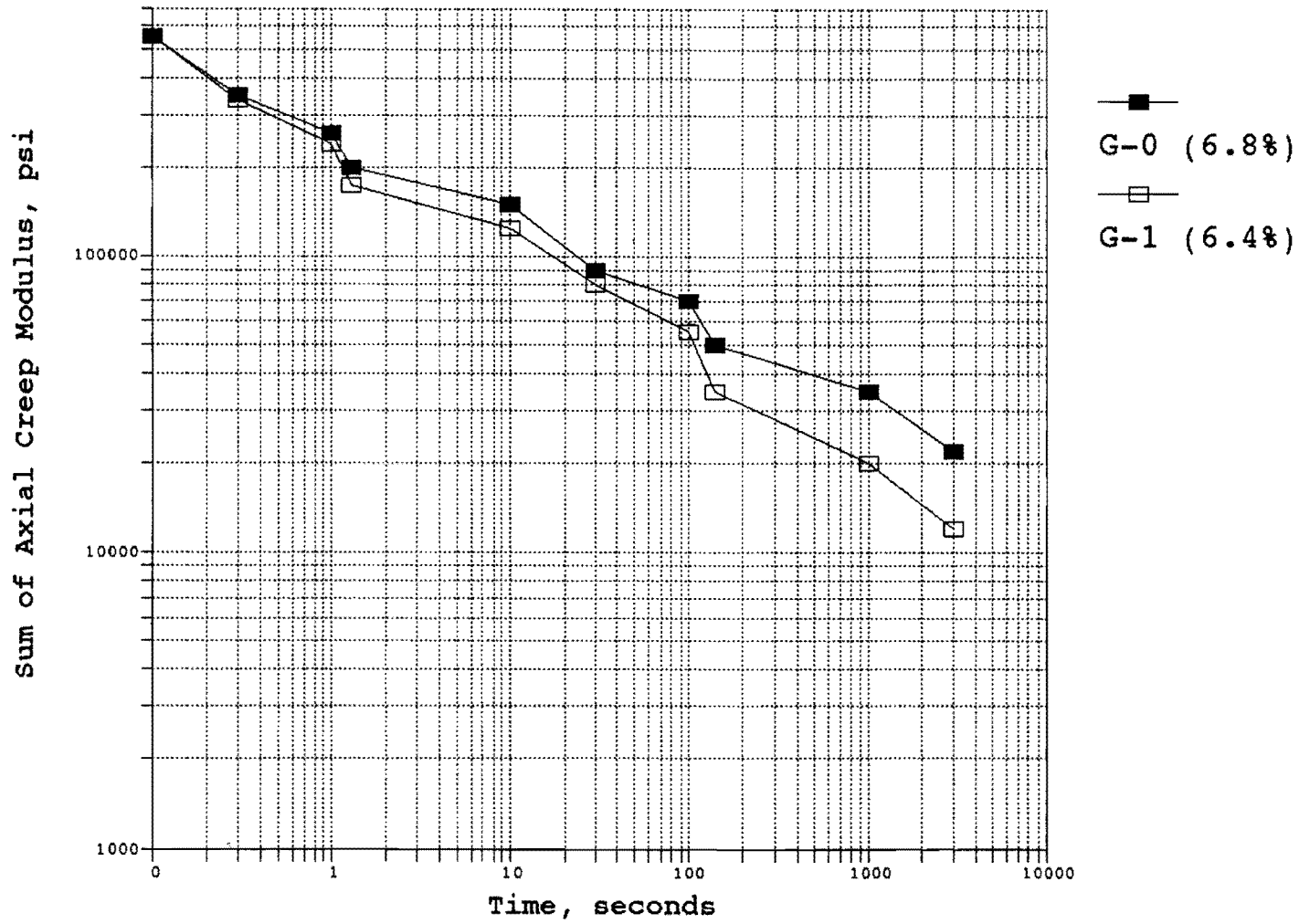


Figure 3.11. Combined Effects of Compaction and Asphalt Content on Compressive Creep Modulus, Optimum Asphalt [0] and High Asphalt [1]. (After Sousa, et al. (1991)).

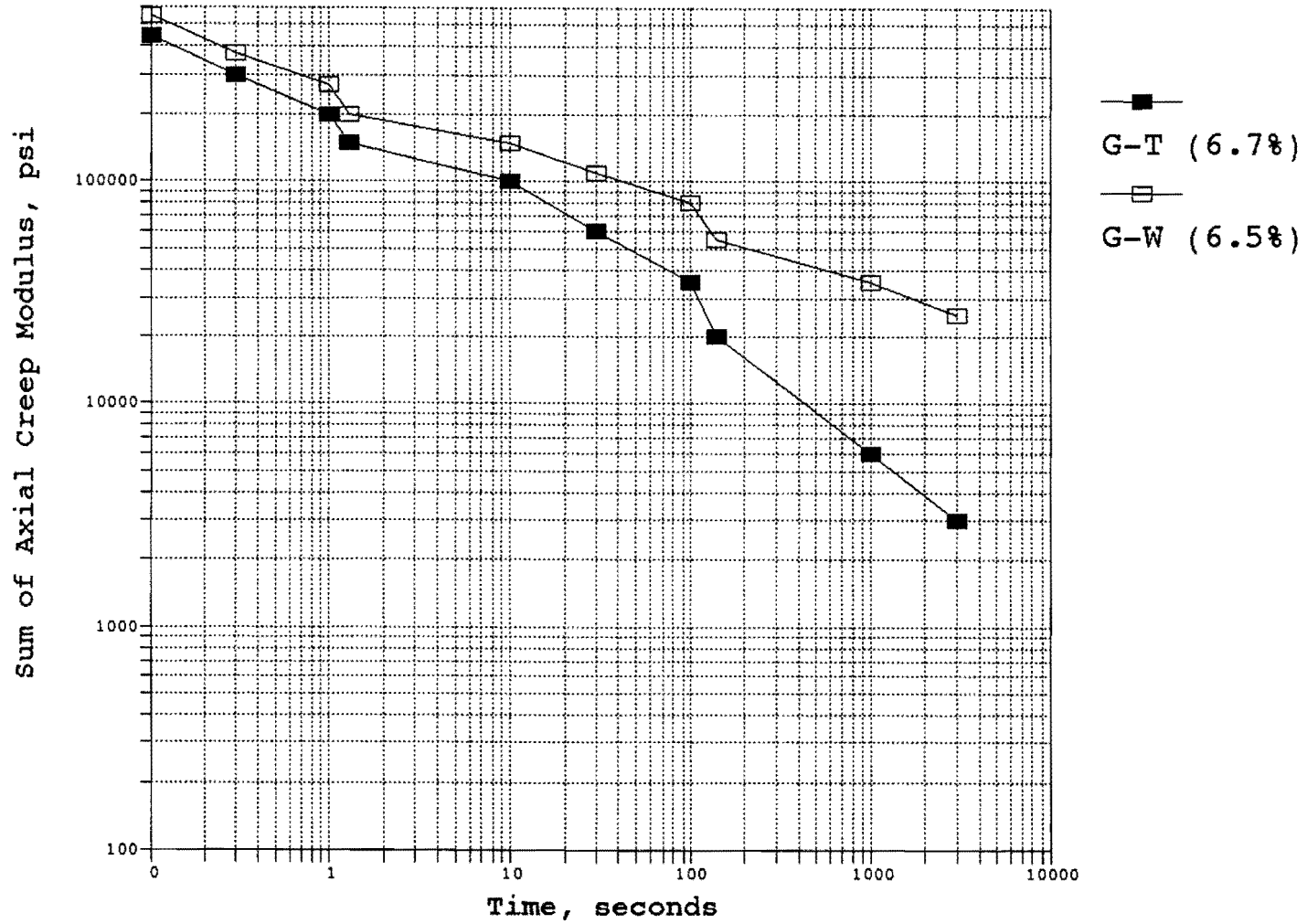


Figure 3.12. Combined Effects of Compaction and Aggregate Type on Compressive Creep Modulus, RL Chert [T] and RB Granite [W] (1 psi = 6.89 kPa). (After Sousa, et al. (1991)).

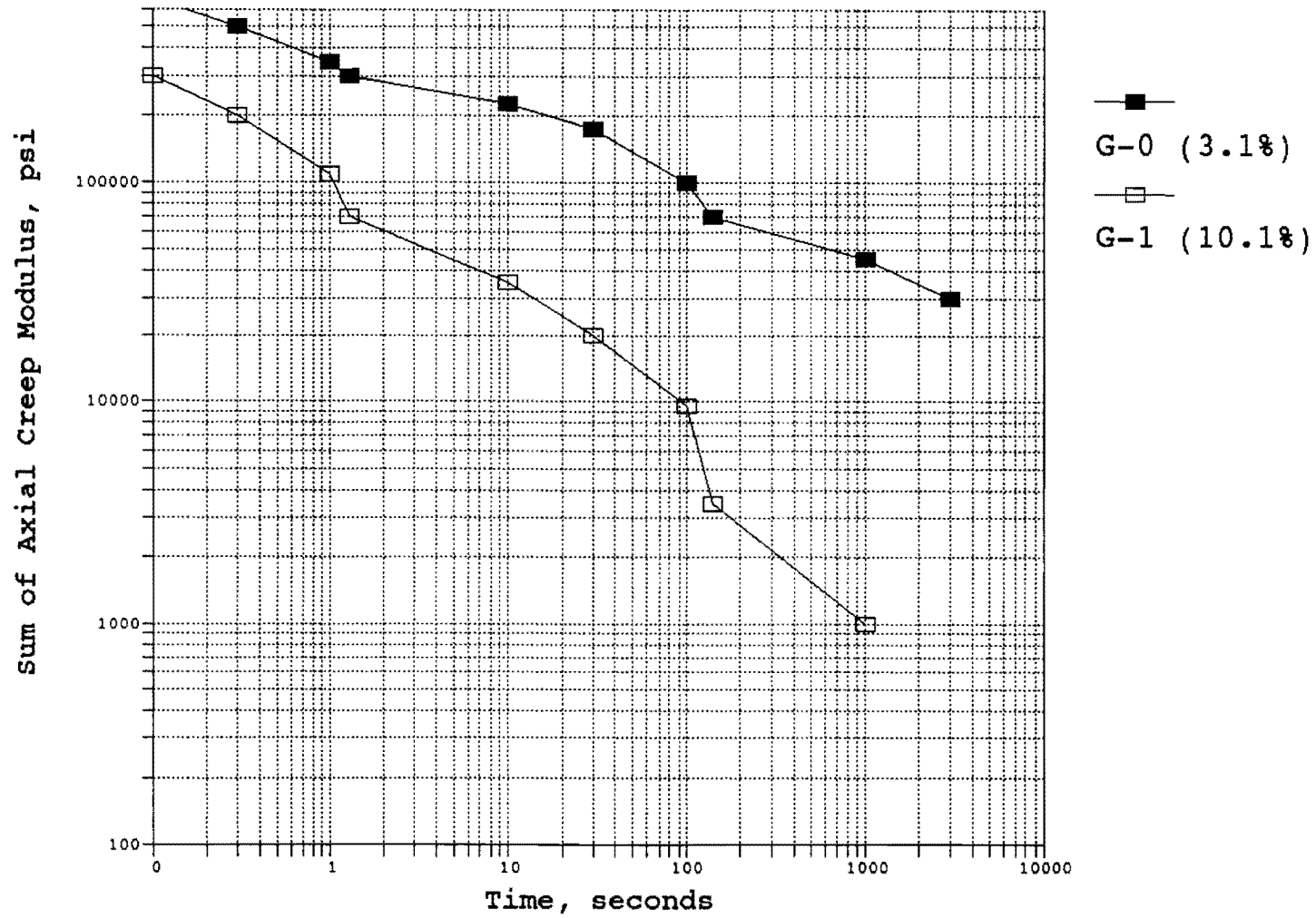


Figure 3.13. Combined Efforts of Compaction and Air-Void Content on Compressive Creep Modulus, Low Voids [0] and High Voids [1]. (After Sousa, et al. (1991)).

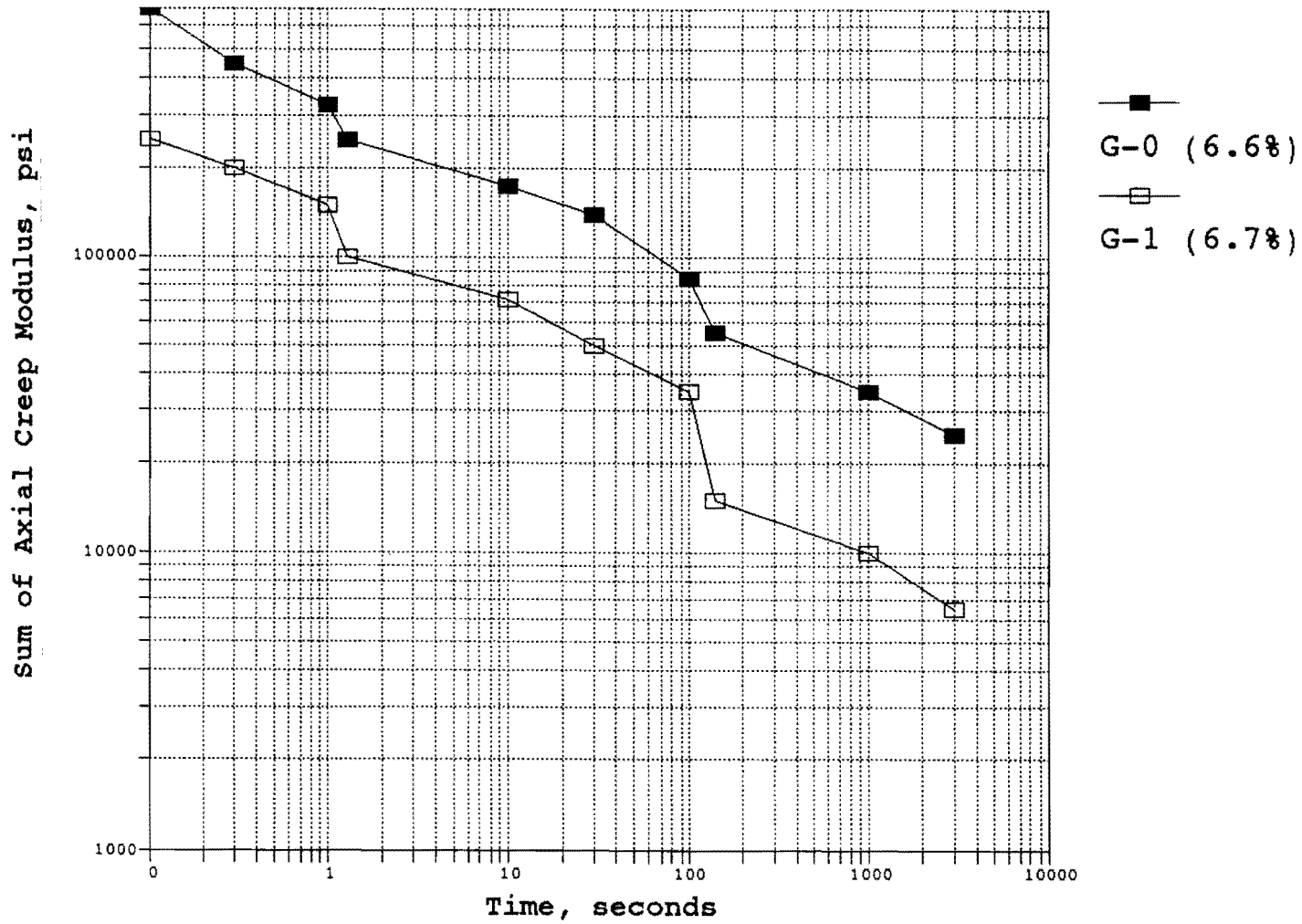


Figure 3.14. Combined Effects of Compaction and Temperature on Compressive Creep Modulus, 104°F (40°C) [0] and 140°F (60°C) [1]. (After Sousa, et al. (1991)).

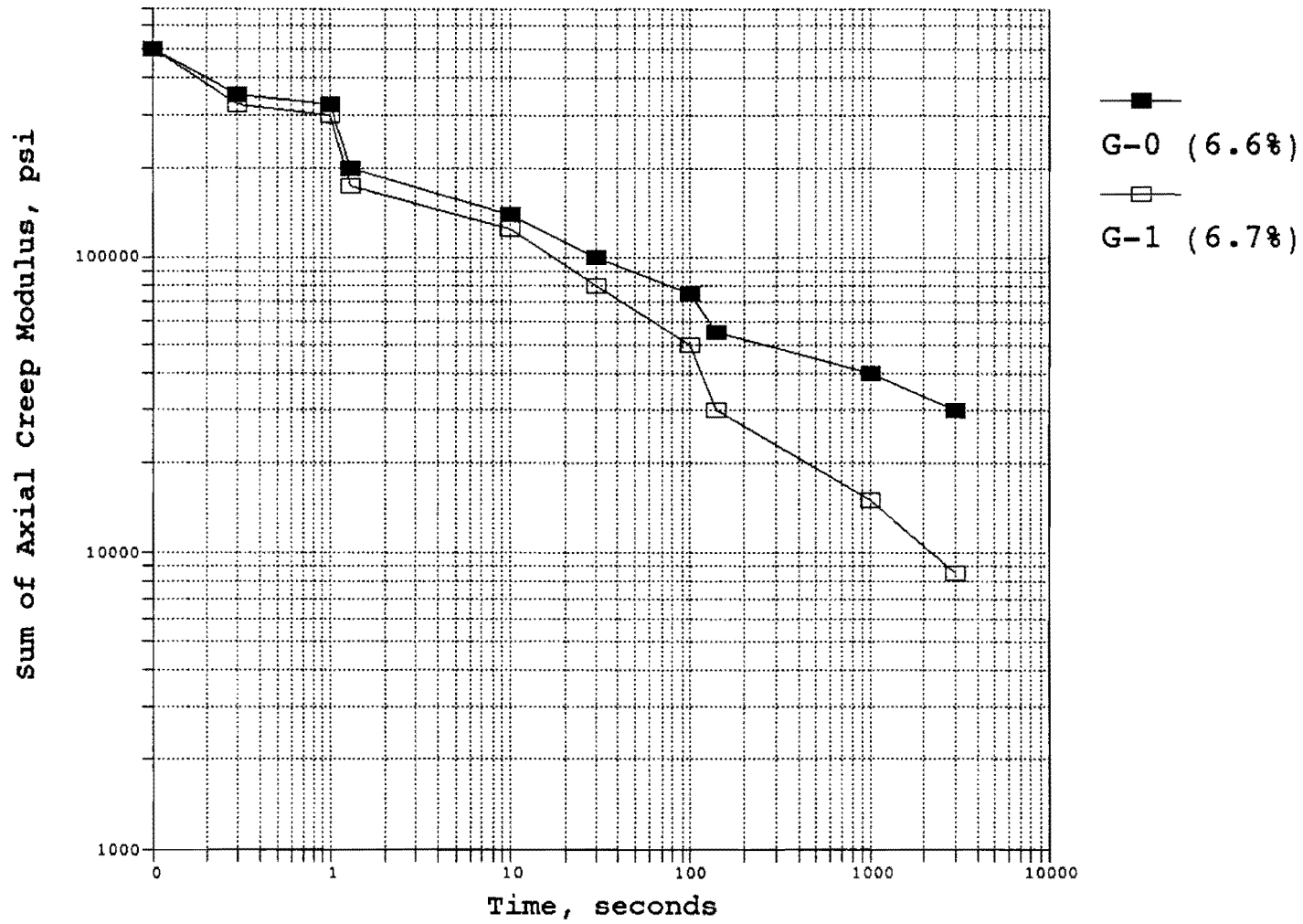


Figure 3.15. Combined Effects of Compaction and Stress Level on Compressive Creep Modulus, 14.5 psi [0] and 29.0 psi [1]. (After Sousa, et al. (1991)).

neighborhood of 0.35 to 0.40. Slopes of the steady state curve which are greater than this value seem to result in tertiary creep at or near the one-hour loading time and or in creep moduli below the levels generally deemed too low for successful field performance.

Table 3.4. Comparison of Extreme Slope Values of the Steady State Portion of the Creep Curve and Permanent Strain at One-Hour Loading for Gyratory Compacted Samples.

Variable Considered	Maximum Value		Minimum Value		Change in Value	
	Slope	Strain, %	Slope	Strain, %	Slope	Strain, %
AC Type	0.41	0.43	0.32	0.20	0.09	0.23
AC, %	0.35	0.30	0.30	0.20	0.05	0.10
Aggr. Type	0.45	1.20	0.25	0.20	0.20	1.00
Air Void, %	0.50	3.00	0.30	0.30	0.20	2.70
Temperature	0.40	0.50	0.30	0.15	0.10	0.35
Stress Level	0.40	0.50	0.30	0.09	0.10	0.41

Further results presented by Sousa, et al. (1991) are summarized in Figure 3.16. These data clearly demonstrate that a critical strain level does indeed seem to exist in the compressive creep test. This critical strain level is, based on the Sousa, et al. data, in the range of approximately 0.8 percent. The mixtures that do not reach the 0.8 percent strain before or at the 3,600 second time of loading have a creep modulus or at least 3,750 psi and a slope of less than approximately 0.35. These same data trends are supported by evaluation of data in Figures 3.10 through 3.15.

Based on analysis of the Sousa, et al. data, the following suggestions are in order concerning a mixtures rut resistance based on compressive creep data:

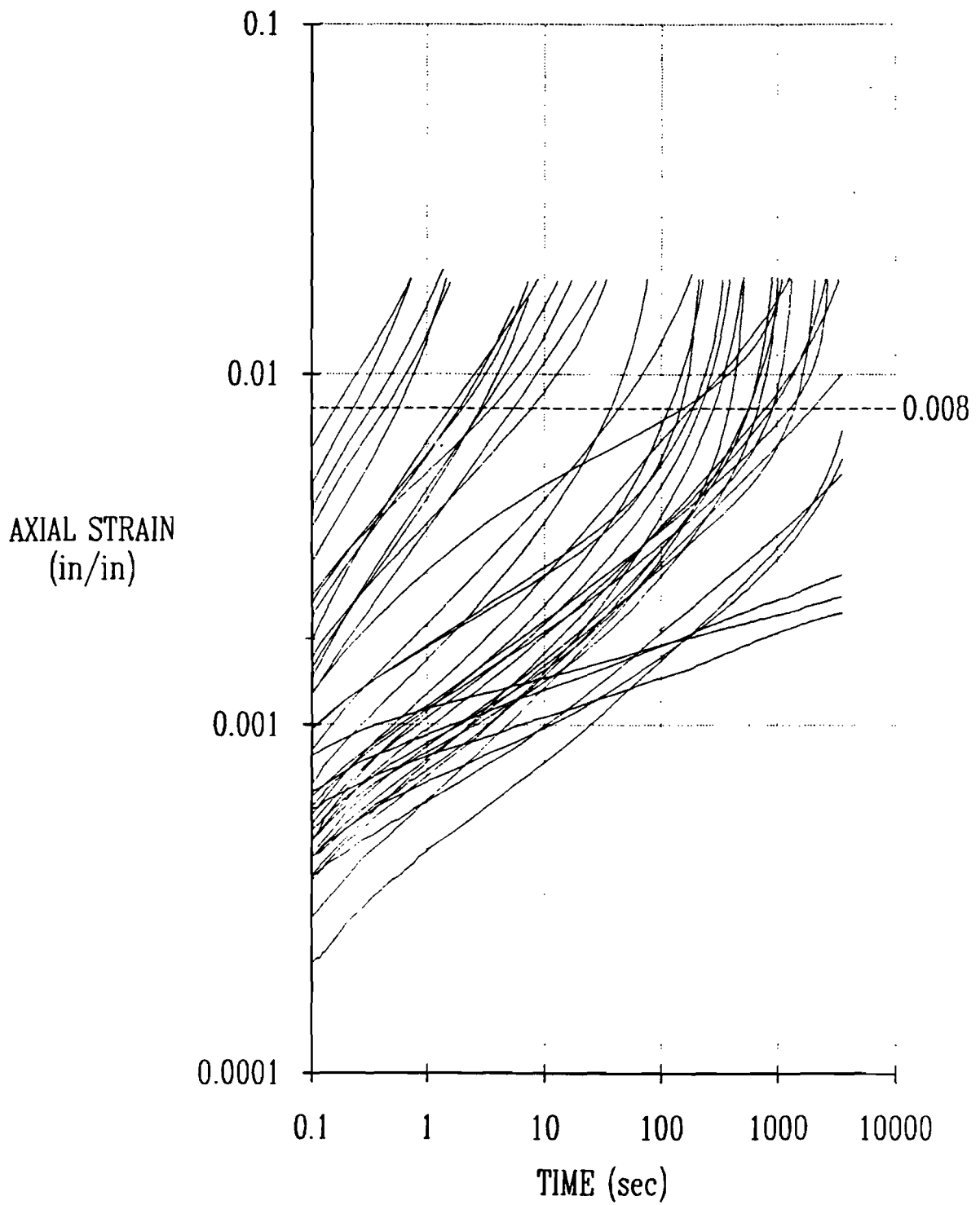


Figure 3.16. Constancy of Collapse Strain for a Number of Randomly Selected Tests Under Compressive Creep. (After Sousa, et al. (1991)).

<u>Slope of steady state creep curve</u>	<u>Creep Modulus, psi</u>
Very Low to Low Rutting Potential less than 0.25	greater than 10,000 psi for 30 psi constant stress
Low to Moderate Rutting Potential between 0.25 and 0.35	between 6,000 psi and 10,000 psi for 30 psi constant stress
Moderate to High Rutting Potential between 0.35 and 0.40	between 3,750 psi and 6,000 psi for 30 psi constant stress
High rutting Potential greater than 0.40	less than 3,750 psi for 30 psi constant stress

In addition to the establishment of these criteria for the evaluation of compressive creep data, the Sousa, et al. (1991) report defines the sensitivity to the variables discussed as summarized in Table 3.5. These levels of sensitivity as documented in this table are proof of the applicability of the compressive creep test for prioritization of asphalt concrete mixtures. From the data summarized in Table 3.5, the following information is gleaned:

1. Both the slope of the steady state creep portion of the creep versus time of loading plot and the strain at a specified time of loading are sensitive to changes in mixture variables and thus a relationship between slope of the steady state creep curve and strain at a specified time of loading (or the associated creep modulus) must exist.

Table 3.5. Comparison of Extreme Values of Slope of Steady State Creep Versus Time of Loading Plot and Permanent Strain at One-Hour Loading for Gyrotory Prepared Samples. (Analysis of Data from Sousa, et al. (1991)).

Variable Considered	Slope of Steady State Creep Curve			Permanent Strain at One-Hour Loading, %		
	Maximum	Minimum	Change	Maximum	Minimum	Change
AC Type	0.41	0.32	0.09	0.43 (7000)	0.20 *(15,000)	0.23
AC Content	0.35	0.30	0.05	0.30 (9100)	0.20 *(15,000)	0.10
Aggregate Type	0.45	0.25	0.20	1.20 (2500)	0.20 *(15,000)	1.00
Air Void Content	0.50	0.30	0.20	3.00 (1000)	0.30 *(10,000)	2.70
Temperature	0.40	0.30	0.10	0.50 (1000)	0.15 *(20,000)	0.35
Stress Level	0.40	0.30	0.10	0.50 (6000)	0.09 *(33,000)	0.41

\* Values in parentheses are creep modulus at one-hour loading for 30 psi constant stress level.

- The most influential mixture variables in terms of their effect on the slope of the steady state creep curve and on the permanent strain at one-hour loading are, in order of influence--most influential to least influential: air void content of the mixture, aggregate type, stress level, temperature, asphalt cement type and asphalt cement content.
- Values of creep modulus were calculated for the permanent strains measured at one-hour of loading under the constant stress level of 30 psi used in testing. A substantial, very large, difference in creep modulus exists when one compares the levels of each variable. Note that the creep modulus for the maximum level of each variable (most deleterious level) ranges from 9,100 psi to 1,000 psi whereas the range for the minimum level of each variable (least deleterious) ranges from 33,000 psi to 10,000 psi.

Analysis of these data is further evidence that a creep modulus after a specified period of loading, comparable with that expected in the field, of greater than 10,000 psi is indicative of very low sensitivity to rutting. On the other hand, critical creep moduli, representing moderate to high levels of sensitivity to rutting, are in the 6,000 psi to 1,000 psi range. It is more difficult to assign a critical value of slope which differentiates mixtures based on rutting susceptibility.

## **DEVELOPMENT OF TTI RUTTING EVALUATION PROCEDURE**

### Establish Critical Values of Slope of Creep Strain Versus Time of Loading Curve and Strain at One-Hour Loading

An extended evaluation of over 100 mixtures was conducted in order to ascertain the critical values of slope of the steady state portion of the creep versus time of loading curve and the permanent strain after a one hour loading period. The variables addressed in the parametric study included the following: asphalt content, asphalt type and grade, aggregate type and gradation, temperature, air voids, polymer modification and stress level.

Basically the experimental designs for these studies consisted of a partial factorial experiment with the following factors and levels of factors.

#### Aggregate type:

- 100 percent crushed limestone (CLS)
- 98 percent CLS + 10 percent natural sand (field sand)
- 80 percent CLS + 20 percent natural sand
- 60 percent CLS + 40 percent natural sand

#### Asphalt:

- AC-20
- AC-10
- AC-20 + low density polyethylene modification at three levels (4.3, 5.0 and 6.0 LDPE)

Asphalt Content:

Optimum

Optimum - 0.8 percent

Optimum + 0.4 percent

Optimum + 0.8 percent

Creep curves from a number of miscellaneous mixtures (not a part of the factorial study) will be used to supplement findings from the factorial study.

Tables 3.6, 3.7 and 3.8 present selected, representative data from the extensive parametric study. Table 3.6 is a summary of uniaxial compression data from a parametric study where aggregate in a 100 percent crushed limestone mixture was replaced in 10 percent increments with natural field sand of a rounded to sub-rounded nature. These data are also presented graphically in Figures 3.17 through 3.28. From this information the following conclusions are drawn:

1. A basic relationship between slope of the steady state creep versus time of loading curve and time to tertiary creep exists. However, the relationship is capricious and often poorly defined. However, it is apparent that basic guidelines can be developed by which to prioritize the potential of mixtures to deform permanently or by which to broadly categorize rutting potential in a mixture design/analysis system.
2. The slope of the creep curve in Figures 3.17 through 3.28 and in Table 3.6 progresses in a logical manner. The slope increases with the increase in natural, rounded sand content of the mixture. This can also be said of the time to tertiary creep (defined as a rapid upward slope change) as the time to rupture is progressively smaller with an increase in the percentage of natural field sand.
3. Based on these data it is apparent that a log-log slope of the creep versus time of loading curve of less than 0.25 is indicative of a mixture which will not become unstable (reach tertiary creep) within the testing period of 3,600 seconds.

Table 3.6. Comparisons of Steady State Slopes Prior to Tertiary Creep in Unconfined Mixtures.

Mixture Identification	Slope of Steady State Creep Prior to Tertiary Creep	Time to Tertiary Creep, Sec	Strain at 3,600 seconds, Percent
100% Crushed Stone, $\sigma_3=0$ psi, $\sigma_1 = 60$ psi, 3.2% Air Voids	0.23	7,000	0.55
100% Crushed Stone, $\sigma_3=0$ psi, $\sigma_1=60$ psi, 6.3% Air Voids	0.42	1,700	>3.0
10% Natural Sand, $\sigma_3=0$ psi, $\sigma_1= 60$ psi, 3.6% Air Voids	0.32	3,200	0.9
10% Natural Sand $\sigma_3=0$ psi, $\sigma_1=60$ psi, 5.9% Air Voids	0.54	800	Failed
20% Natural Sand, $\sigma_3=0$ psi $\sigma_1 = 60$ psi, 3.3% Air Voids	0.42	2,800	2.0
20% Natural Sand, $\sigma_3 = 0$ psi, $\sigma_1 = 60$ psi, 5.2% Air Voids	0.34	400	Failed

Table 3.7. Comparison of Steady State Creep Slopes and Permanent Strain at One-Hour Time of Creep Loading.

Mixture Identification	$\sigma_3$ , psi	Air Voids, Percent	Slope of Steady State Creep Curve	Permanent Strain at One-Hour Loading, Percent
100% Crushed Stone	15	4.0	0.17	0.36
	30	4.2	0.15	0.28
10% Natural Sand	15	4.5	0.22	0.56
	30	3.9	0.10	0.40
20% Natural Sand	15	4.0	0.25	0.68
	30	3.6	0.18	0.48

Table 3.8. Comparison of Uniaxial Creep ( $\sigma_1=60$  psi) Data from Ten Selected Mixtures. (Each Value is the Average of Data Points).

Aggregate	Binder	Air Voids, Percent	Slope of Steady State Creep Curve	Time to Tertiary Creep, Seconds
100% Crushed	AC-10	3.2	0.23	7,000
	AC-10+ 4.3% LDPE	3.7	0.17	> 10,000
	AC-10+ 6.0% LDPE	3.4	0.15	> 10,000
90% Crushed 10% Natural Sand	AC-10	3.8	0.32	3,200
	AC-10+ 5% LDPE	4.2	0.25	6,000
80% Crushed 20% Natural Sand	AC-10	3.3	0.42	2,800
	AC-10+ 5% LDPE	3.4	0.22	5,500
100% Rounded River Gravel (RG)	AC-20	4.2	0.40	2,000
80% RG+ 20% Crushed	AC-20	4.4	0.30	3,000
80% RG 20% Crushed	AC-20 +5% LDPE	3.9	0.24	5,900
100% Crushed Granite	AC-20	5.1	0.30	4,000
	AC-20 +5% LDPE	5.0	0.17	20,000
Stone Mastic Mixture (SMA)	AC-30	3.0	0.35	2,000
0.3% Fiber (Georgia Granite)	AC-30 +5% LDPE	3.0	0.20	> 3,600
SMA with Crushed Gravel (Colorado) 0.3% Fiber	AC-10	2.8	0.29	3,600
	AC-10+ LDPE	3.0	0.20	> 3,600

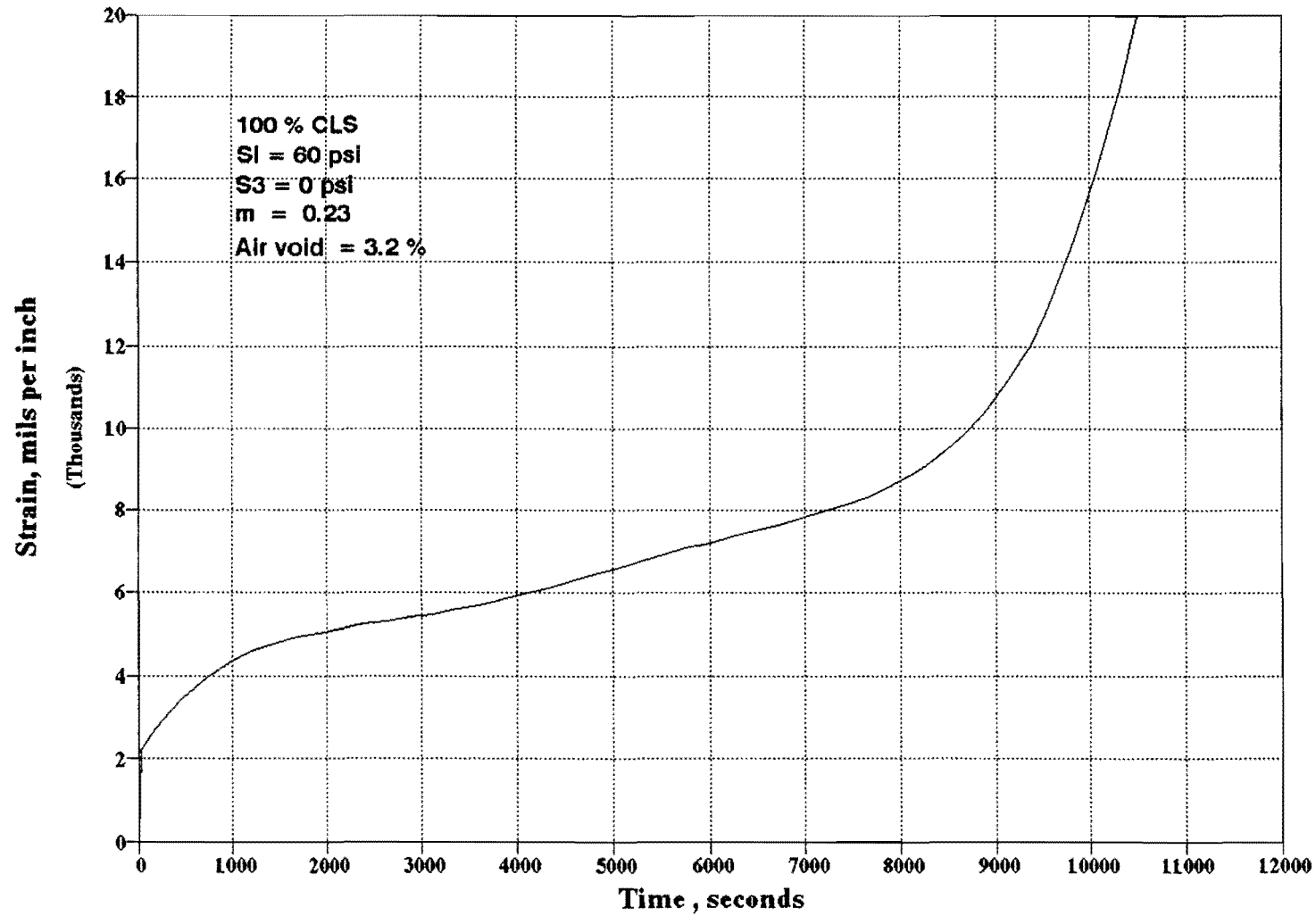


Figure 3.17. Arithmetic Plot of Creep Strain Versus Time of Loading for 100 Percent Crushed Limestone Mixture 1.

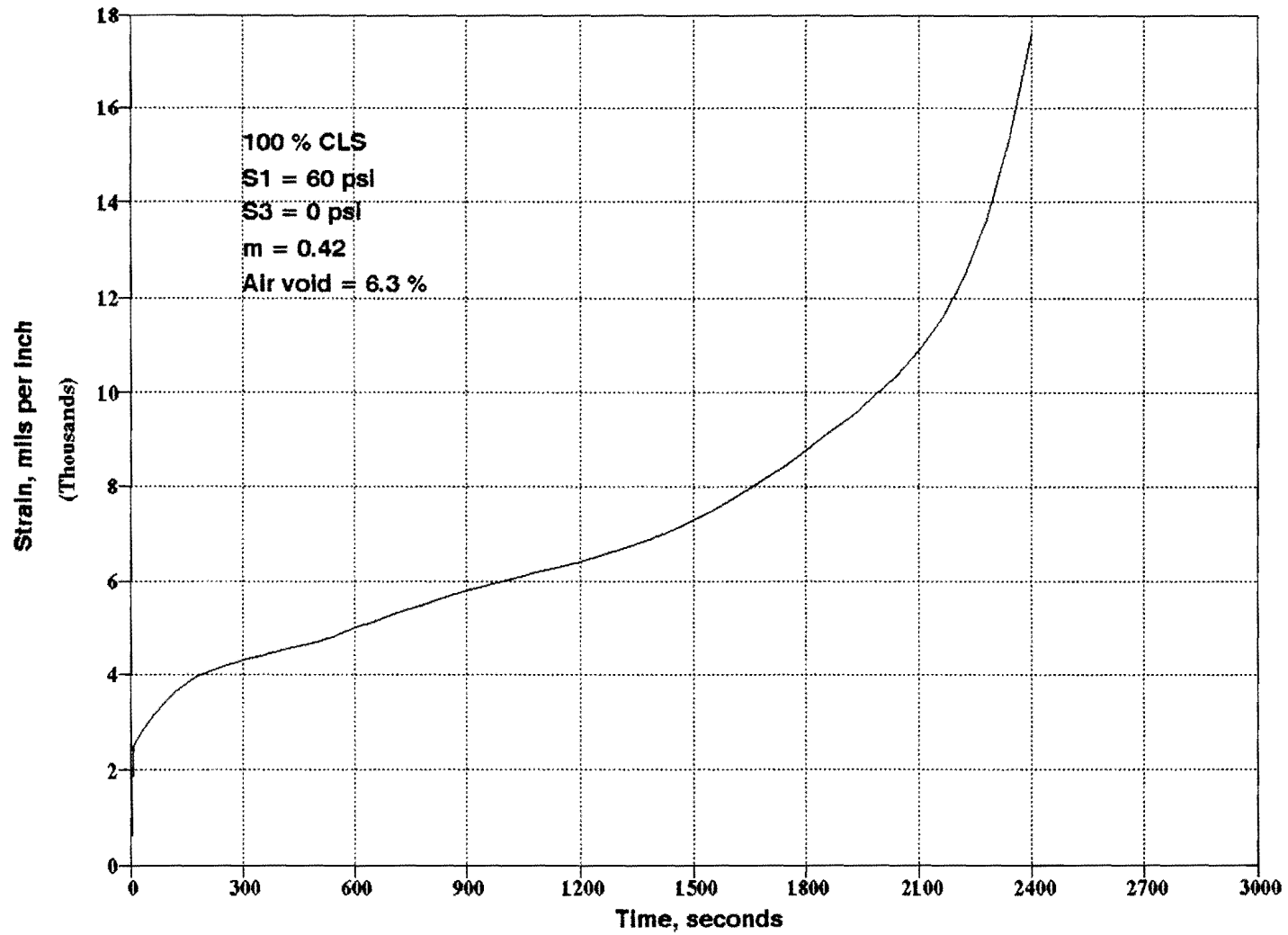


Figure 3.18. Arithmetic Plot of Creep Strain Versus Time of Loading for 100 Percent Crushed Limestone Mixture 2.

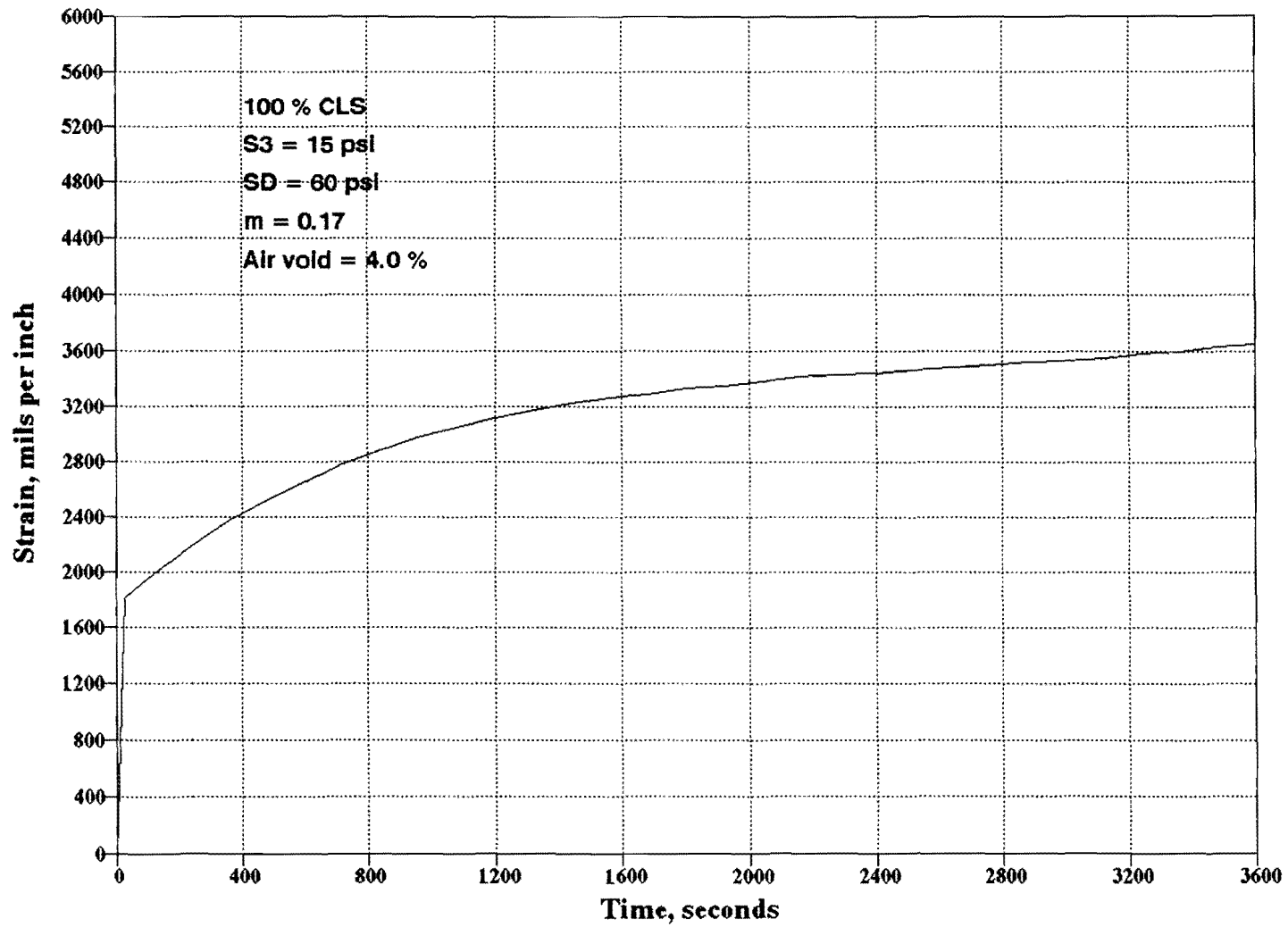


Figure 3.19. Arithmetic Plot of Creep Strain Versus Time of Loading for 100 Percent Crushed Limestone Mixture 3.

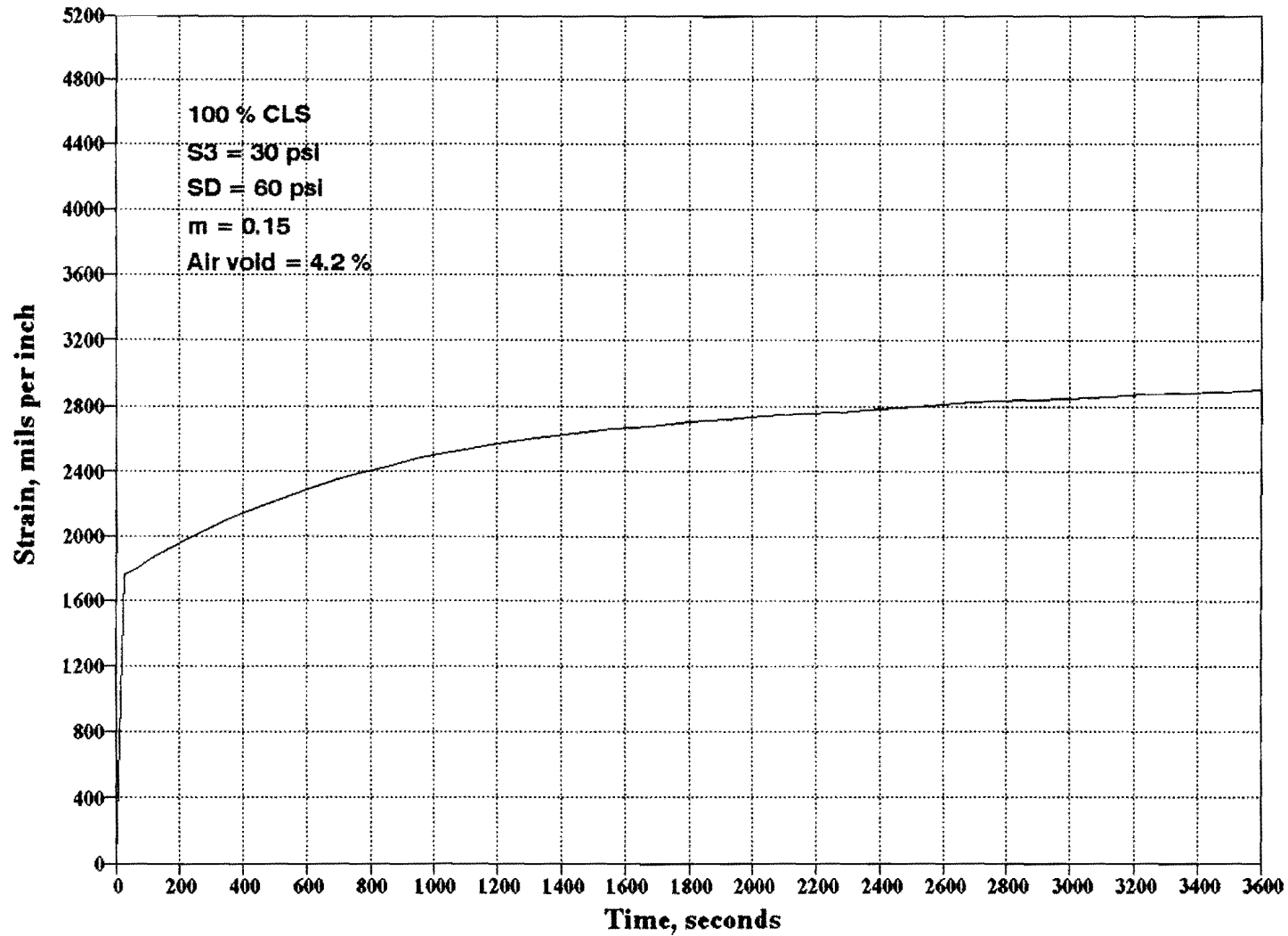


Figure 3.20. Arithmetic Plot of Creep Strain Versus Time of Loading for 100 Percent Crushed Limestone Mixture 4.

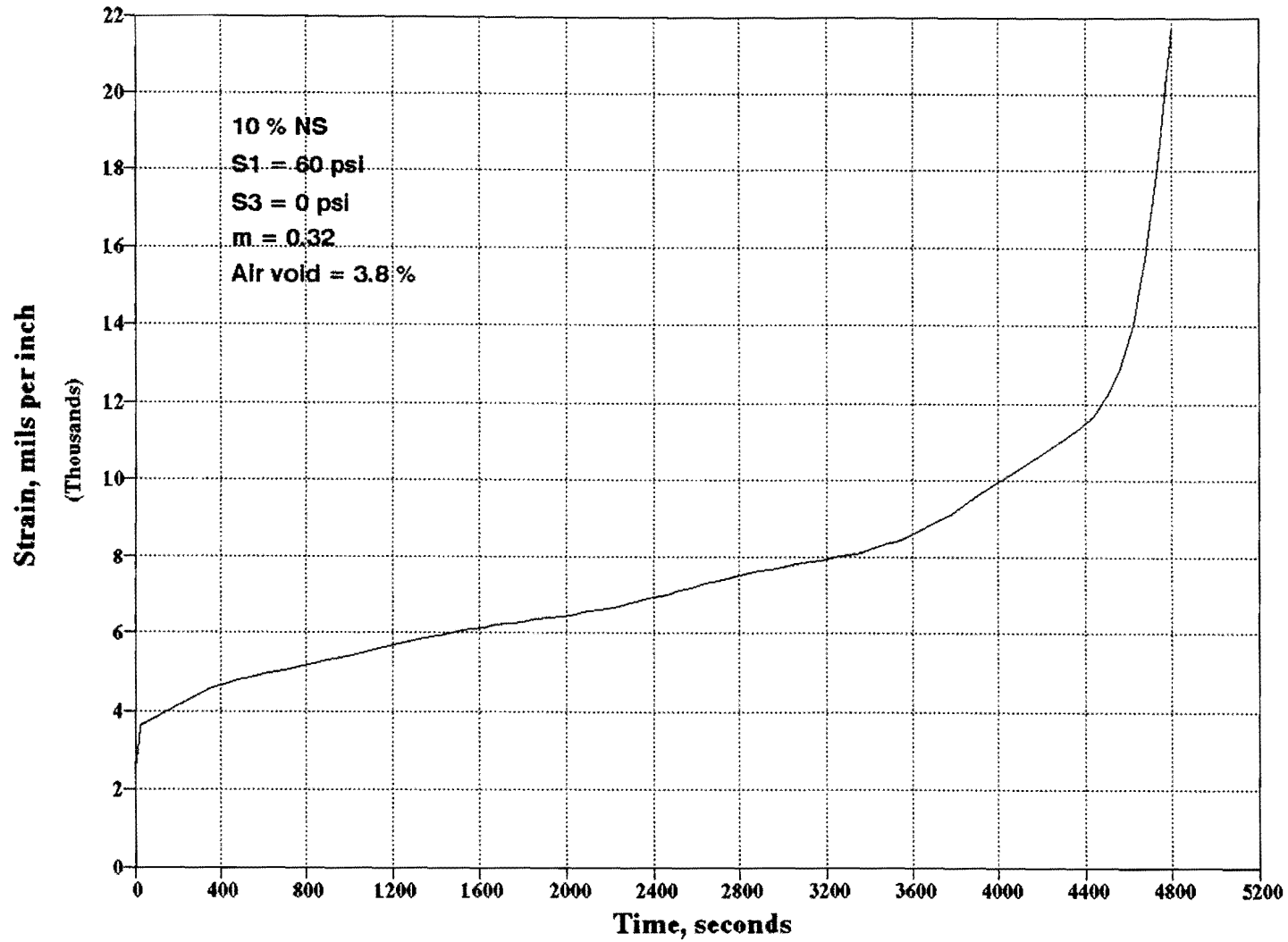


Figure 3.21. Arithmetic Plot of Creep Strain Versus Time of Loading for 10 Percent Natural Sand--90 Percent Crushed Limestone Mixture 1.

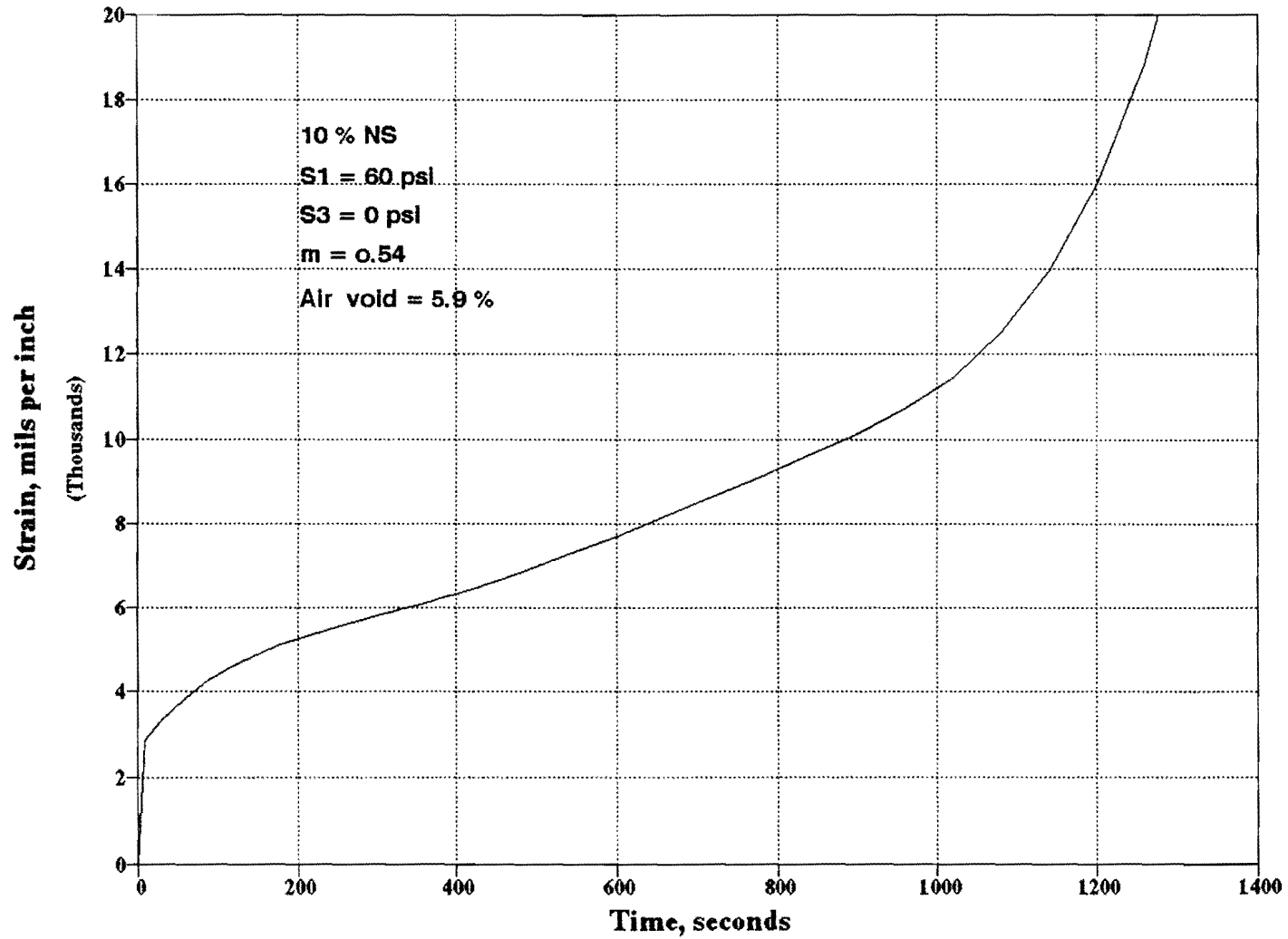


Figure 3.22. Arithmetic Plot of Creep Strain Versus Time of Loading for 10 Percent Natural Sand--90 Percent Crushed Limestone Mixture 2.

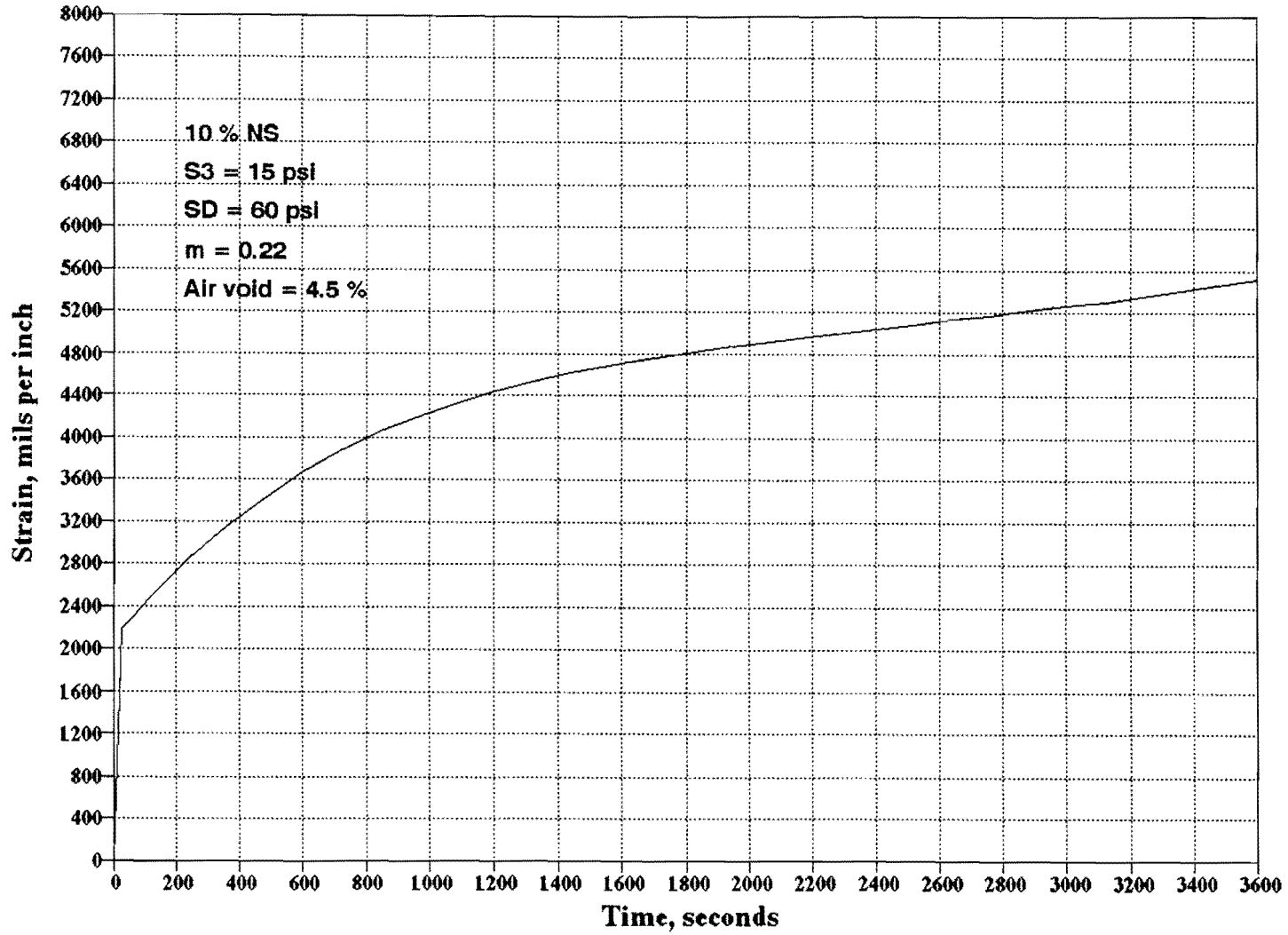


Figure 3.23. Arithmetic Plot of Creep Strain Versus Time of Loading for 10 Percent Natural Sand--90 Percent Crushed Limestone Mixture 3.

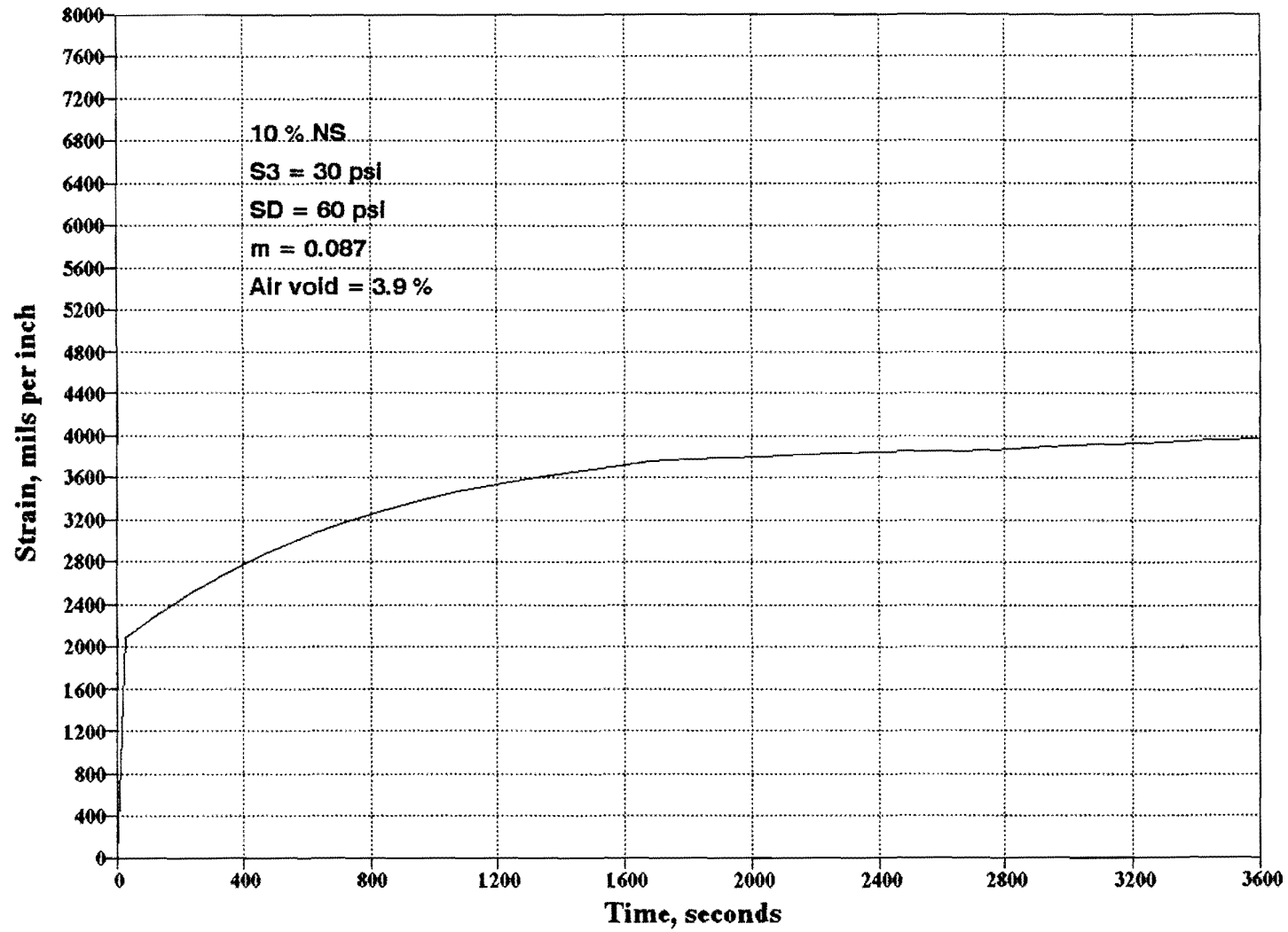


Figure 3.24. Arithmetic Plot of Creep Strain Versus Time of Loading for 10 Percent Natural Sand--90 Percent Crushed Limestone Mixture 4.

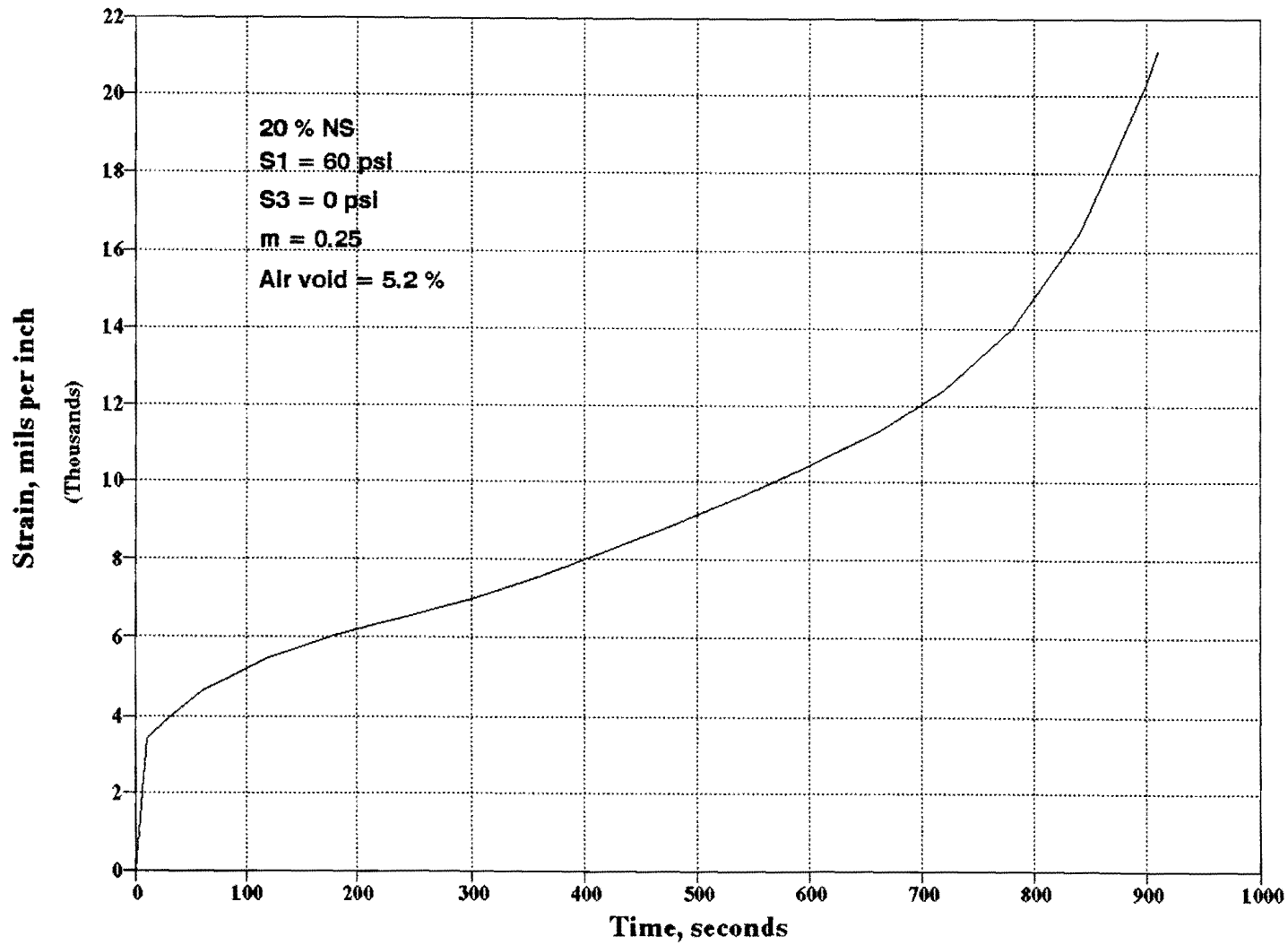


Figure 3.25. Arithmetic Plot of Creep Strain Versus Time of Loading for 20 Percent Natural Sand--80 Percent Crushed Limestone Mixture 1.

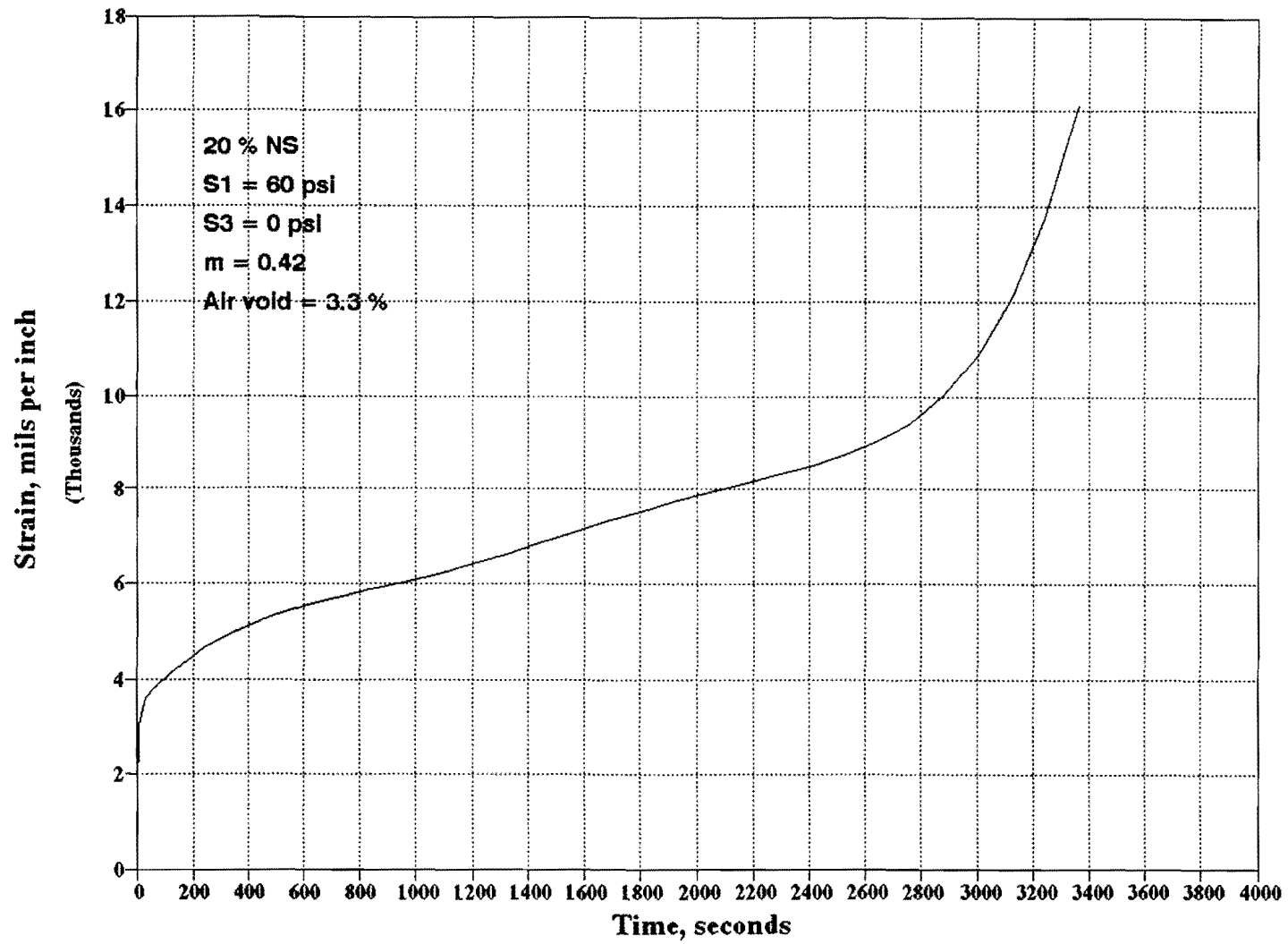


Figure 3.26. Arithmetic Plot of Creep Strain Versus Time of Loading 20 Percent Natural Sand--80 Percent Crushed Limestone Mixture 2.

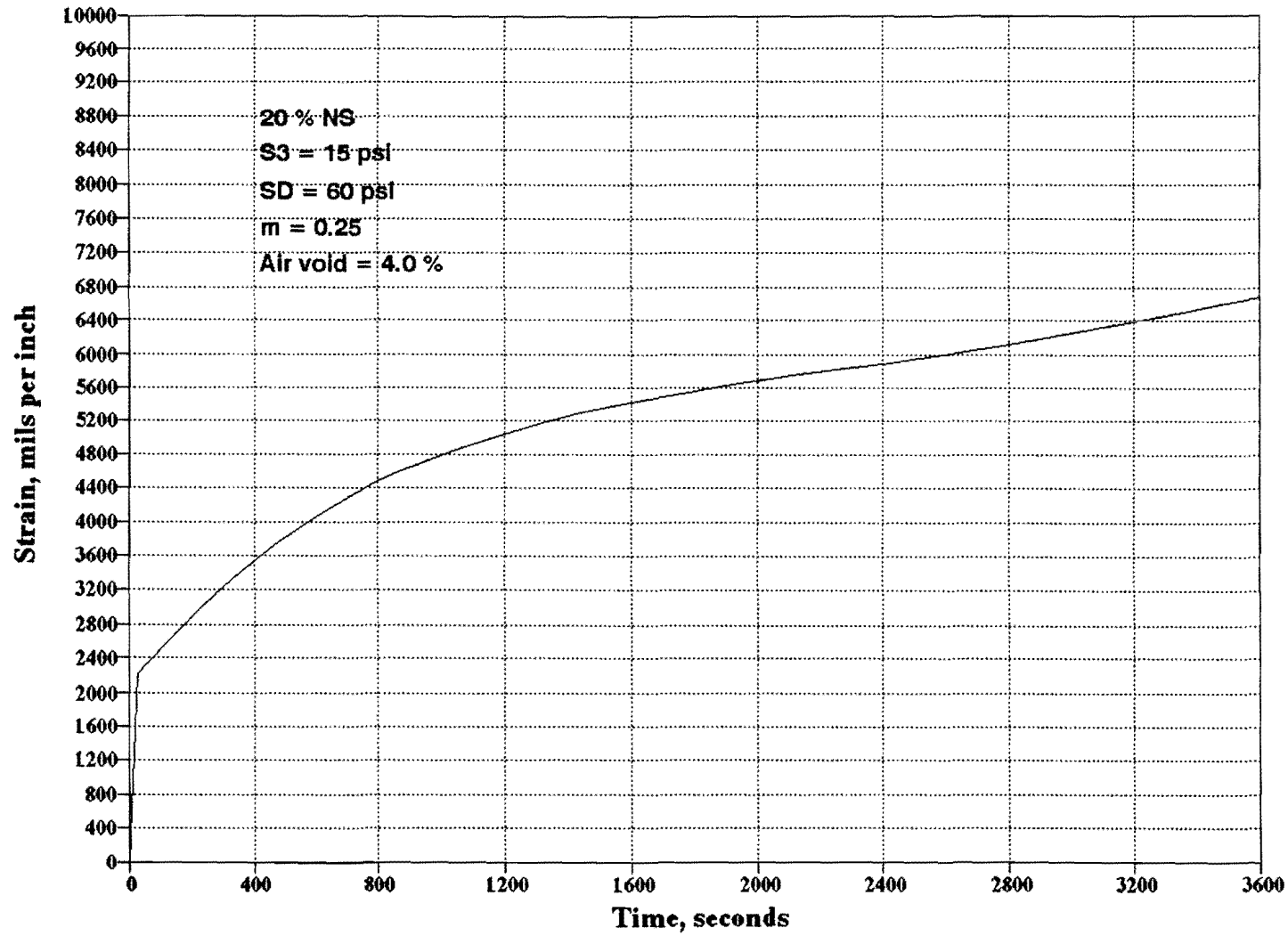


Figure 3.27. Arithmetic Plot of Creep Strain Versus Time of Loading 20 Percent Natural Sand--80 Percent Crushed Limestone Mixture 3.

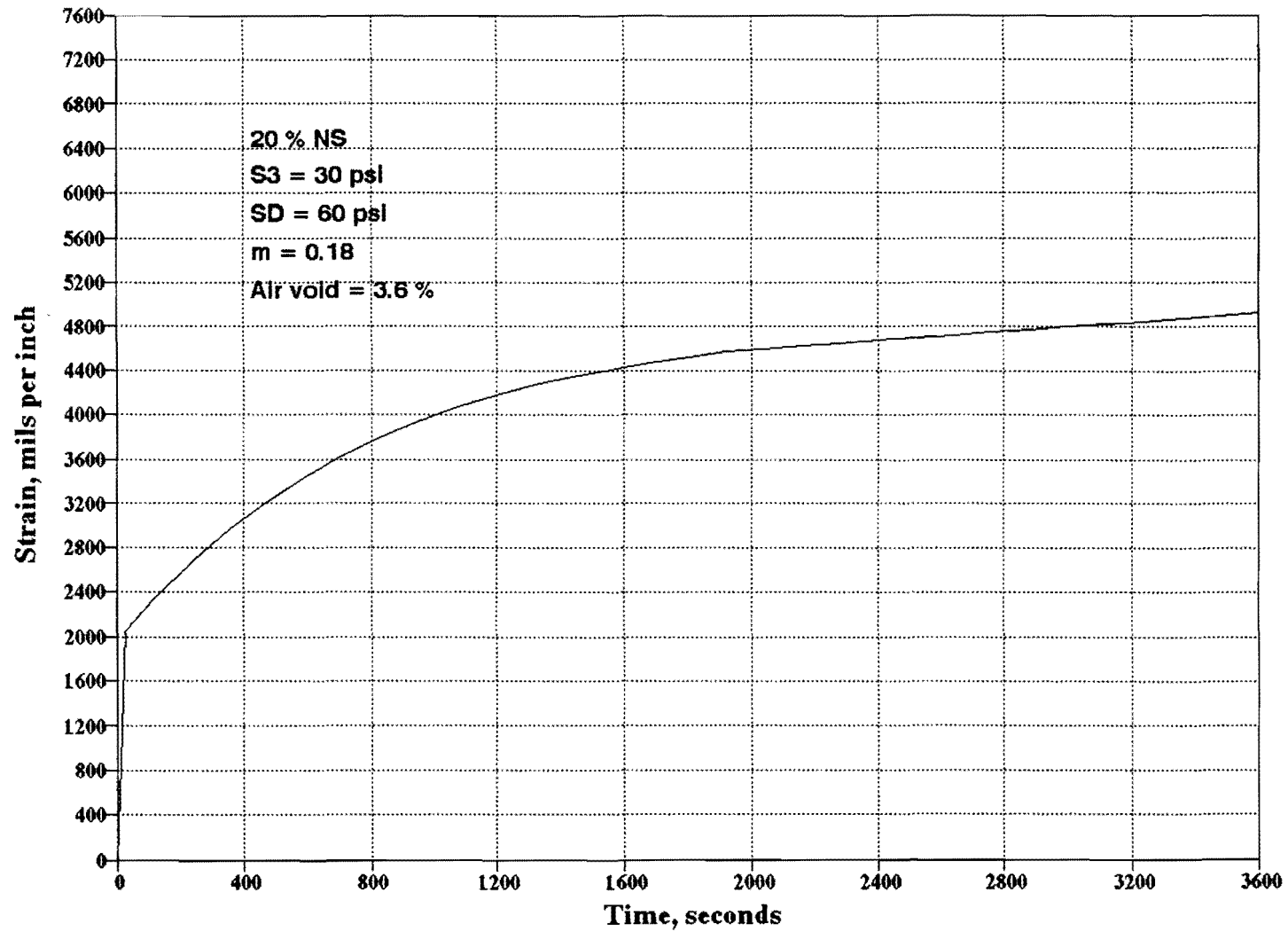


Figure 3.28. Arithmetic Plot of Creep Strain Versus Time of Loading 20 Percent Natural Sand--80 Percent Crushed Limestone Mixture 4.

4. The trends demonstrated in Table 3.6 and in the concomitant figures substantiate the findings of other researchers such as Sousa et al. (1991).

Table 3.7 summarizes the data for the same crushed limestone mixtures with replacement of varying percentages of the aggregate portion with natural field sand but with confining pressures of either 15 or 30 psi. These data demonstrate that the application of confinement substantially and predictably reduces the slope of the steady state portion of the creep curve and reduces the magnitude of permanent strain at the one-hour loading time. Note in Table 3.7 that as the confining pressure is increased from 15 to 30 psi, in each case, the slope is reduced and the strain at one-hour loading is significantly reduced. This is important as it points out the influence of state of stress on the results of the creep test and the importance of trying to mimic the state of stress induced in the actual pavement as closely as possible during laboratory creep testing for mixture design/analysis.

Data in Tables 3.6 and 3.7 are presented graphically in Figures 3.17 through 3.28. These figures when viewed together with Figures 3.10 through 3.16 demonstrate the presence of the tertiary creep region at a strain of approximately 0.8 to 1.0 percent for all unconfined mixtures. The time at which this tertiary creep region begins is obviously dependent on mixture variables. The tertiary creep region is reached in uniaxial creep testing for all mixtures except the low air void 100 percent crushed mixture, Figure 3.17. However, upon the application of confinement, the tertiary creep region is not reached within the one-hour loading period.

Figure 3.29 presents a regression relationship between the slope of the steady state region of the creep deformation versus time of loading curve to a strain of 0.8 percent or more for many of the mixture groups tested. Although this figure demonstrates the substantial variance associated with this relationship, it does demonstrate that a relationship exists and should be a valuable tool in investigating mixture performance based on creep test data.

Table 3.8 presents a summary of extended mixture creep data for mixtures with other aggregate types and with different binders including polymer-

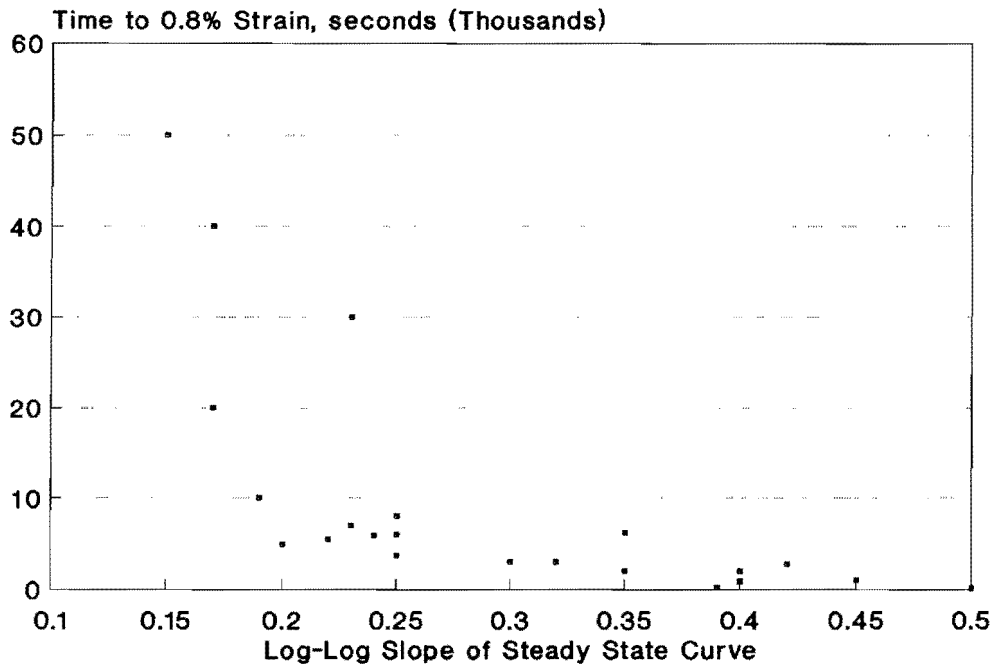


Figure 3.29. Relationship Between Slope of the Steady State Creep Curve and Time of Loading to 0.8 Percent Strain or Greater.

modified binders. These data further substantiate the information presented in Table 3.7 for a wide variety of mixtures.

Results summarized in Tables 3.6 through 3.8 and results from previous research were used to establish criteria for evaluation of creep test data as a diagnostic test. Test criteria will be discussed at the end of this section.

#### Determination of Appropriate Testing Temperature

A testing temperature of 104°F was selected for creep testing. This temperature was selected because of the history of use of this temperature for creep testing, because of the selection of this test temperature by AAMAS and because the use of this testing temperature makes sense when one considers temperature profiles in pavements under Texas climatic conditions.

TTI developed a regression model in Research Report 452-2 (1989) based on an extensive volume of weather data which predicts air temperature at any locality within Texas at any time during the year. The model then translates the predicted air temperature into pavement temperature profiles which are expressed as a function of depth for any category of pavement.

The regression model, which has been developed based on the 180 hottest days of an average year within the 30 years of weather data studied, is divided into two important periods: one representing the daytime and another representing the nighttime. The representative  $R^2$  values for these regression models for HMAC varying from 2 to 5 inches are all above 0.98. The general forms of the models are:

$$T = a_0 + a_1x + a_2y + a_3z + a_4yz + a_5x^2 + a_6y^2 + a_7y^2z + a_8y^3 \quad (3.18)$$

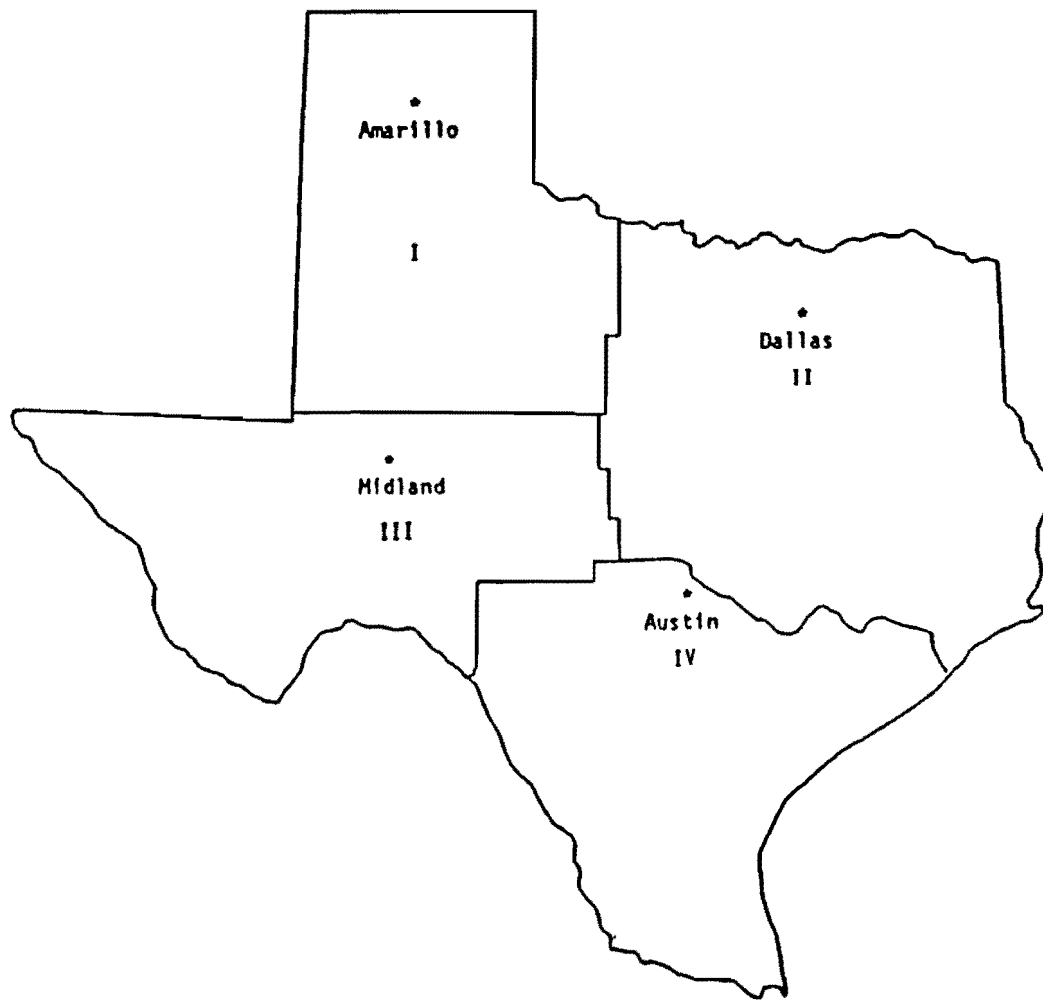
where: T is temperature at the center of each sublayer, x is the period of the year (1 through 36), y is the hour of the day ( $y > 7$  and  $y < 19$ ), z is the sublayer and a's are regression constants and

$$T = b_0 + b_1x + b_2y + b_3z + b_4xz + b_5yz^2 + b_6y^3 + b_7y^4 \quad (3.19)$$

where: b's are regression constants.

In the temperature analysis by climatic categories, the State of Texas was divided into four relatively distinct geographical regions, Figure 3.30. A study by Li (1989) verified that these four regions are statistically distinct. Temperature profiles for all four categories of pavement structure were generated for each climatic region. These temperature profiles were generated using the techniques developed and presented by Claessen, et al. (1977).

From the average hottest temperature profile data, based on the work of Li, Olsen and Little (1989), for the four climatic regions of Texas the average pavement temperatures are presented in Table 3.9. These profiles are similar to those developed by Morris, et al. (1974).



I --- Amarillo	(93) 91 - 98 <sup>0</sup> F	
II -- Dallas	(96) 90 - 99 <sup>0</sup> F	(88 - 90 <sup>0</sup> F in small area)
III - Midland	(95) 92 - 102 <sup>0</sup> F	(83 - 92 <sup>0</sup> F in small area)
IV -- Austin	(95) 90 - 100 <sup>0</sup> F	(88 - 90 <sup>0</sup> F in small area)

Figure 3.30. Regional Map of Texas. (After Mahboub and Little (1987)).

Table 3.9. Design Pavement Temperatures for Permanent Deformation Analysis Derived from Pavement Temperature Profile Analysis. (After Mahboub and Little (1987)).

Pavement Structural Category				
Climatic Region	Thin Flexible	Intermediate	Thick Flexible	HMAC/PCCP Overlay
I	94*	95	90	92
II	110	106	102	104
III	107	105	100	102
IV	110	106	102	104

\* Temperatures are in degrees Fahrenheit.

In order to further illustrate typical temperature profiles in Texas, Tables 3.10 through 3.13 present the average hottest temperature profiles in a thin overlay (2-inches--an extreme condition) for Region II for both summer (hottest 180 days) and winter (coolest 180 days) conditions. In these tables, column 1 identifies the profile, column 2 is the temperature range in the top sublayer, columns 3 and 4 are the sub-layer temperatures and column 5 is the percent of time the profile occurs during the period addressed. These data indicate that the average temperature within the 2-inch overlay exceeds 104°F only about 19 percent of the time in the hottest 180 days of the year or only about 9 percent of the time based on the full 365 days of the year. Obviously, in certain areas where traffic is concentrated in this time zone of profile 6, the pavement would be stressed for a significant period of time or by a significant number of loading applications at a substantially higher temperature than the 104°F test temperature. However, for most traffic profiles, the 104°F test temperature as an approximation of a nominal high pavement layer temperature seems acceptable.

#### Determine Appropriate Level of Axial Stress in Unconfined Compression Creep Test

The literature is filled with creep test data where low stress states are applied in the laboratory creep test. For example, in the VESYS

Table 3.10. Temperature Distribution of 2 in. Asphalt Overlay (Dallas Area)  
(After Li, et al. (1987)).

Profile Number	Temperature (°F)	Sub-layer Temperature (°F)		Percent Time
		1	2	
1	< 75	68	70	25.69
2	75-85	79	81	25.69
3	85-95	90	89	14.93
4	95-105	100	97	14.47
5	105-115	110	105	12.38
6	115-125	118	112	6.84
TOTAL				100

Table 3.11. Temperature Distribution of 3 in. Asphalt Overlay (Dallas Area).  
(After Li, et al. (1987)).

Profile Number	Temperature (°F)	Sub-layer Temperature (°F)			Percent Time
		1	2	3	
1	< 75	68	70	72	25.69
2	75-85	79	81	82	25.69
3	85-95	90	89	88	14.93
4	95-105	100	97	94	14.70
5	105-115	110	105	101	12.15
6	115-125	118	112	107	6.84
TOTAL				100	

Table 3.12. Winter Temperature Distribution of 2 in. Asphalt Overlay (Dallas Area) (After Li, et al. (1987)).

Profile Number	Temperature (°F)	Sub-layer Temperature (°F)		Percent Time
		1	2	
1	< 45	41	43	18.69
2	45-55	50	51	26.80
3	55-65	60	60	25.00
4	65-75	70	68	14.86
5	75-85	80	76	8.56
6	85-95	90	85	4.62
7	> 95	97	92	1.46
TOTAL				100

Table 3.13. Winter Temperature Distribution of 3 in. Asphalt Overlay (Dallas Area). (After Li, et al. (1987)).

Profile Number	Temperature (°F)	Sub-layer Temperature (°F)			Percent Time
		1	2	3	
1	< 45	41	43	44	18.69
2	45-55	50	51	53	26.80
3	55-65	60	60	51	25.00
4	65-75	70	68	66	14.86
5	75-85	80	77	74	8.67
6	85-95	90	85	81	4.50
7	> 95	97	92	87	1.46
TOTAL				100	

procedure (1976) a uniaxial stress of 20 psi or less is recommended. If the strain during a preconditioning period exceeds 2500 micro inches of strain (0.25 percent) then the stress level is to be reduced until the strain falls below the 2500 micro inch strain level. This often results in a uniaxial stress of as low as 5 psi. The major reason for maintaining a stress level within these prescribed bounds is to stay within the linear viscoelastic region so that the pavement can be analyzed using linear viscoelastic theory. However, stress levels between 5 and 20 psi are usually much too low to simulate actual field stress conditions. This is not a problem for linear viscoelastic theory as the difference between the stress induced in the pavement and the test in the lab can be easily handled by linear viscoelastic superposition. However, the asphalt concrete does not respond in a linear viscoelastic manner up to the point of failure. The response is often highly non-linear and, therefore, a laboratory mixture evaluation test must account for this non-linearity by testing at the appropriate stress level.

Mahboub and Little (1987) developed Z-factors similar to those developed by Shell researchers which demonstrate that vertical compressive stress within the asphalt concrete pavements layer generally range between 65 and 86 percent of the average contact stress between the tire and the pavement surface. Since today's truck tires are often inflated to as high as 150 psi, this can mean average vertical compressive stresses of as much as five times those prescribed by methods such as VESYS.

Von Quintus, et al. (1991) used linear elastic theory to calculate the distribution of vertical compressive stresses within the asphalt concrete layer. In an example showing how to use the AAMAS method they suggested using 65 psi in the uniaxial static creep test (104°) to simulate the stress in an asphalt concrete surface layer (full depth) subjected to a tire pressure of 130 psi which varied from 115 psi at the top of the layer to 20 psi at the bottom. The 65 psi compressive stress was used as it is the point at which the horizontal stresses are approximately 0. This would represent a critical stress condition for the uniaxial test.

Tielking (1986) demonstrated that the conditions of stress under actual loading may be much more severe than is demonstrated by layered elastic approximation because layered elastic approximation does not account for the

non-uniformity of loading across the tire carcass nor the horizontal shearing stresses induced by braking and/or cornering.

In order to more realistically evaluate the stress level to which the uniaxial creep sample should be subjected, various pavements structural sections were modeled with the modified Illi-pave structural model. Realistic tire contact pressures, stress distributions and shearing stresses were introduced for each specific condition. From the calculated stress conditions octahedral normal and shear stresses were calculated and contours of equal normal stress and shear stresses were plotted using a computer graphic program.

The Mohr-Coulomb failure theory is a realistic simple approximation of the failure stress level in an asphalt mixture at high pavements temperatures:

$$\tau_{(oct) failure} = c + \sigma_{(oct) normal} \tan \phi \quad (3.20)$$

where  $c$  is the cohesive strength and  $\sigma_{(oct)n} \tan \phi$  is the strength mobilized through frictional interaction among the aggregate particles (see Chapter 4 for further discussion of triaxial test data). Based on the Mohr-Coulomb failure law, it is apparent that the critical stress state within the asphalt concrete pavement layer should exist where the stress state is such that the frictional component of shear strength has the lowest potential to develop and where the induced shear stress is greatest. This would occur where the ratio of octahedral normal stress to octahedral shear stress (NTSR) is a minimum based on this hypothesis. Contours of NTSR for 6 important pavement structural and environmental condition are defined in Tables 3.14 through 3.23. In these tables the first column describes the pavement environment and loading condition. A hot climate was used with an average asphalt concrete modulus representative of a hot mix layer with an average temperature of 104°. The term rolling in the column refers to a free rolling wheel. A representative surface shear was used in the calculation of the stresses. The term braking replaces rolling where severe surface shear is modeled in the analysis such as at intersections or on high truck traffic downhill grades. The term bond means a 100 percent or full bond is developed between the asphalt concrete overlay and the base.

Table 3.14. Stresses to be Applied to Laboratory Samples (Triaxial and Uniaxial) to Represent Field Conditions of a Hot Climate, Free Rolling Tires and Full Bond Between AC Overlay and AC Base.

<u>Environment</u>	<u>Condition of Surface Shear</u>	<u>Condition of Bonding</u>	Surface Course	Depth in Asphalt Concrete, inches	Normal Octahedral Stress, psi	NTSR	Stress, in Lab Test									
							Axial Stress, psi	Confining Stress, psi	Uniaxial Stress, psi	Average Uniaxial Stress, psi						
Hot Season/ Rolling/ Full Bond	2" AC AC Base	0 1 2	36 38 45	2.46 1.95 1.48	56 65 88	25 24 23	47 54 70	57								
									4" AC AC Base	0 2 4	35 34 29	1.98 1.23 1.22	59 73 62	22 14 12	50 63 56	56

Table 3.15. Stresses to be Applied to Laboratory Samples (Triaxial and Uniaxial) to Represent Field Conditions of a Hot Climate, Free Rolling Wheel and Full Bond Between AC Overlay and PCC Base.

<u>Environment</u>	<u>Condition of Surface Shear</u>	<u>Condition of Bonding</u>	Surface Course	Depth in Asphalt Concrete, inches	Normal Octahedral Stress, psi	NTSR	Stress, in Lab Test			
							Axial Stress, psi	Confining Stress, psi	Uniaxial Stress, psi	Average Uniaxial Stress, psi
Hot Season/ Rolling/ Full Bond	2" AC PCC Base	0	30	1.70	53	18	47	55		
		1	32	1.64	59	18	51			
		2	42	1.46	82	21	67			
	4" AC PCC Base	0	30	1.37	60	14	54	57		
		2	32	1.2	69	13	61			
		4	31	1.35	63	14	56			
	6" AC PCC Base	0	31	1.42	61	15	54	54		
		3	27	0.98	65	7	61			
		6	25	1.49	48	13	44			

Table 3.16. Stresses to be Applied to Laboratory Samples (Triaxial and Uniaxial) to Represent Field Conditions of a Hot Climate, Free Rolling Wheel and Full Bond Between AC Overlay and Flexible Base.

<u>Environment</u>	<u>Condition of Surface Shear</u>	<u>Condition of Bonding</u>	Surface Course	Depth in Asphalt Concrete, inches	Normal Octahedral Stress, psi	NTSR	Stress, in Lab Test			
							Axial Stress, psi	Confining Stress, psi	Uniaxial Stress, psi	Average Uniaxial Stress, psi
Hot Season/ Rolling/ Full Bond	2" AC Flex Base	0	45	2.32	72	31	56	67		
		1	37	1.35	75	17	64			
		2	30	0.77	85	2	82			
	4" AC Flex Base	0	48	2.5	75	34	57	67		
		2	33	0.86	87	5	81			
		4	7		ERR	ERR	ERR			
	6" AC Flex Base	0	48	2.87	71	36	54	62		
		3	25	0.78	70	2	68			
		6			ERR	ERR	ERR			

Table 3.17. Stresses to be Applied to Laboratory Samples (Triaxial and Uniaxial) to Represent Field Conditions of a Hot Climate, Braking Wheel and Full Bond Between AC Overlay and AC Base.

<u>Environment</u>	<u>Condition of Surface Shear</u>	<u>Condition of Bonding</u>	Surface Course	Depth in Asphalt Concrete, inches	Normal Octahedral Stress, psi	NTSR	Stress, in Lab Test			
							Axial Stress, psi	Confining Stress, psi	Uniaxial Stress, psi	Average Uniaxial Stress, psi
Hot Season/ Braking/ Full Bond	2" AC AC Base		0	0	44	0.95	109	11	93	87
			1	1	51	1.5	99	26	75	
			2	2	72	1.43	143	36	93	
4" AC AC Base			0	0	49	0.98	119	13	98	93
			2	2	61	1.2	132	25	96	
			4	4	47	1.16	104	18	84	
6" AC AC Base			0	0	40		ERR	ERR	ERR	87
			3	3	46	0.9	118	9.8	102	
			6	6	39	1.19	85	15	72	

Table 3.18. Stresses to be Applied to Laboratory Samples (Triaxial and Uniaxial) to Represent Field Conditions of a Hot Climate, Braking Wheel and Full Bond Between AC Overlay and PCC Base.

<u>Environment</u>	<u>Condition of Surface Shear</u>	<u>Condition of Bonding</u>	Surface Course	Depth in Asphalt Concrete, inches	Normal Octahedral Stress, psi	NTSR	Stress, in Lab Test			
							Axial Stress, psi	Confining Stress, psi	Uniaxial Stress, psi	Average Uniaxial Stress, psi
Hot Season/ Braking/ Full Bond	2" AC PCC Base	0	40	1.22	ERR	ERR	ERR	85		
		1	48		103	20	82			
		2	77		144	43	89			
	4" AC PCC Base	0	45	0.8	124	5	113	96		
		2	60		130	24	95			
		4	53		107	25	81			
	6" AC PCC Base	0	45	0.91	ERR	ERR	ERR	80		
		3	47		120	10	102			
		6	37		70	20	59			

Table 3.19. Stresses to be Applied to Laboratory Samples (Triaxial and Uniaxial) to Represent Field Conditions of a Hot Climate, Braking Wheel and Full Bond Between AC Overlay and Flexible Base.

<u>Environment</u>	<u>Condition of Surface Shear</u>	<u>Condition of Bonding</u>	Surface Course	Depth in Asphalt Concrete, inches	Normal Octahedral Stress, psi	NTSR	Stress, in Lab Test			
							Axial Stress, psi	Confining Stress, psi	Uniaxial Stress, psi	Average Uniaxial Stress, psi
Hot Season/ Braking/ Full Bond	2" AC	Flex	0	68	1.92	118	42	77	103	
		Base	1	56	1.16	124	21	94		
		Base	2	48	0.72	142	0	139		
	4" AC	Flex	0	82	2.3	132	56	78	103	
		Base	2	60	0.87	157	11	128		
		Base	4	4		ERR	ERR	ERR		
	6" AC	Flex	0	55	1.08	127	18	98	104	
		Base	3	40	0.75	115	2	111		
		Base	6			ERR	ERR	ERR		

Table 3.20. Stresses to be Applied to Laboratory Samples (Triaxial and Uniaxial) to Represent Field Conditions of a Hot Climate, Braking Wheel and Partial Loss of Bond Between AC Overlay and AC Base.

<u>Environment</u>	<u>Condition of Surface Shear</u>	<u>Condition of Bonding</u>	Surface Course	Depth in Asphalt Concrete, inches	Normal Octahedral Stress, psi	NTSR	Stress, in Lab Test			
							Axial Stress, psi	Confining Stress, psi	Uniaxial Stress, psi	Average Uniaxial Stress, psi
Hot Season/ Braking/ Slip	2" AC AC Base	0 1 2	0	50	1	120	14	98	93	
			1	32		ERR	ERR	ERR		
			2	67	1.4	134	33	91		
	2" AC AC Base	0 2 4	0	55	1.18	120	22	91	100	
			2	52	0.93	131	12	108		
			4	26		ERR	ERR	ERR		
	6" AC AC Base	0 3 6	0	48	0.72	142	0	139	95	
			3	40	0.78	112	3.7	105		
			6	30	3.2	43	23	37		

Table 3.21. Stresses to be Applied to Laboratory Samples (Triaxial and Uniaxial) to Represent Field Conditions of a Hot Climate, Braking Wheel and Partial Loss of Bond Between AC Overlay and PCC Base.

<u>Environment</u>	<u>Condition of Surface Shear</u>	<u>Condition of Bonding</u>	Surface Course	Depth in Asphalt Concrete, inches	Normal Octahedral Stress, psi	NTSR	Stress, in Lab Test			
							Axial Stress, psi	Confining Stress, psi	Uniaxial Stress, psi	Average Uniaxial Stress, psi
Hot Season/ Braking/ Slip	2" AC PCC Base	0	45	0.85	119	7	106	90		
		1	30		ERR	ERR	ERR			
		2	68	1.35	139	32	94			
	4" AC PCC Base	0	47	0.9	120	10	103	93		
		2	52	1	125	15	101			
		4	45	1.3	93	20	75			
	6" AC PCC Base	0	45		ERR	ERR	ERR	75		
		3	40	0.83	108	5	99			
		6	42	3.28	60	32	48			

Table 3.22. Stresses to be Applied to Laboratory Samples (Triaxial and Uniaxial) to Represent Field Conditions of a Hot Climate, Heavy Wheel Load, Free Rolling Wheel and Full Bond Between AC Overlay and Base.

<u>Environment</u>	<u>Condition of Surface Shear</u>	<u>Condition of Bonding</u>	Surface Course	Depth in Asphalt Concrete, inches	Normal Octahedral Stress, psi	NTSR	Stress, in Lab Test			
							Axial Stress, psi	Confining Stress, psi	Uniaxial Stress, psi	Average Uniaxial Stress, psi
Hot Season/ Heavy Axle/ Rolling/ Full Bond	4" AC AC Base	0	37	1.94	63	23	53	66		
		2	46	1.26	97	20	78			
		4	41	1.2	89	16	74			
	4" AC PCC Base	0	32	1.08	73	11	66	72		
		2	43	1.2	93	17	77			
		4	43	1.33	88	20	72			
	4" AC Flex Base	0	53	2.6	81	38	60	80		
		2	44	0.88	114	8	100			
		4			ERR	ERR	ERR			

Table 3.23. Stresses to be Applied to Laboratory Samples (Triaxial and Uniaxial) to Represent Field Conditions of a Hot Climate, Heavy Wheel Load, Braking Wheel and Full Bond Between AC Overlay and Base.

<u>Environment</u>	<u>Condition of Surface Shear</u>	<u>Condition of Bonding</u>	Surface Course	Depth in Asphalt Concrete, inches	Normal Octahedral Stress, psi	NTSR	Stress, in Lab Test			
							Axial Stress, psi	Confining Stress, psi	Uniaxial Stress, psi	Average Uniaxial Stress, psi
Hot Season/ Heavy Axle/ Braking/ Full Bond	4" AC AC Base	0	50	0.9	128	10	108	102		
		2	80	1.32	165	37	103			
		4	64	1.28	134	28	94			
	4" AC PCC Base	0			ERR	ERR	ERR	102		
		2	77	1.21	167	32	108			
		4	68	1.32	140.85	31	95			
	4" AC Flex Base	0	80	1.9	139	50	84	98		
		2	75	0.88	195	14	146			
		4	32	1.13	72	11	64			

Extensive research by Ameri-Gaznon and Little (1987) demonstrated that slight slippage between the asphalt concrete layer in question and the supporting layer can result in greatly magnified levels of shearing stress and a far higher potential to rut. The tables were developed for a 4,500 percent dual tire, 18,000 percent single axle load and a 125 psi tire content pressure.

Column 6, 7 and 8 presents the stresses that should be applied to laboratory samples to duplicate (to a reasonable degree) the actual stress state induced in the field. This critical stress level was calculated based on a minimum NTSR. Thus, the axial and confining stress in the triaxial test (columns 6 and 7) are designed to produce a critical NTSR ratio in the triaxial specimen. The uniaxial stress in column 8 is calculated to produce this critical NTSR in the uniaxial creep test sample.

The triaxial loading conditions are found from the NTSR relationship using the following simple relationship derived from Mohr-Coulomb failures theory:

$$\sigma_1 \text{ (axial stress) } = \sigma_{oct \text{ critical}} + \frac{\sqrt{2}}{2} \tau_{oct \text{ critical}} \quad (3.21)$$

$$\sigma_3 \text{ (confining stress) } = \sigma_{oct \text{ critical}} - \frac{\sqrt{2}}{2} \tau_{oct \text{ critical}} \quad (3.22)$$

where  $\sigma_{oct}$  is the normal octahedral stress on the critical plane and  $\tau_{oct}$  is the octahedral shear stress induced by the load in the field on the critical plane.  $\sigma_1$  and  $\sigma_3$  are determined from the critical NTSR and the value of the normal stress at the point of critical NTSR for a specific pavement category. It is then a simple matter to approximate  $\sigma_1$  when  $\sigma_3 = 0$  based on typical values of  $c$  and  $\phi$  and the Mohr-Coulomb equation. The  $\sigma_1$  value for uniaxial loading is an averaged value for approximate  $c$  and  $\phi$  values for typical asphalt concrete mixture.

Contour plots of normal octahedral stress and NTSRs are presented in Appendix B.

Tables 3.14 through 3.23 demonstrate that in most overlay cases, the uniaxial stress should be between 40 and 80 psi. In these cases the asphalt concrete overlay rests over either an existing asphalt concrete base (AC)

or a portland cement concrete base (PCC). These cases are represented in Table 3.14 and 3.15. Case 3 is for an asphalt concrete layer over a flexible base, Table 3.16.

Since uniaxial creep samples that will be tested will be either 4 inches or 6 inches in height, it is recommended that the average of the three uniaxial stresses (over the pavement depth) be used (column 9). It is apparent from a review of Tables 3.14 and 3.15 that a uniaxial stress of approximately 55 to 60 psi is reasonable for cases 1 and 2 which represents the vast majority of mixture designs. A reasonable uniaxial stress for case 3 is approximately 70 psi.

Case 4 through 6, Tables 3.17 through 3.19, are special cases of braking and cases 7 and 8, Tables 3.20 and 3.21, deal with braking on asphalt concrete overlays on asphalt concrete or portland cement concrete where a slight level of slip exists between the overlay and the base. Finally cases 9 and 10, Tables 3.22 and 3.23, represent data for typical pavement structural sections subjected to very heavy wheel loads.

#### Creep Recovery Criteria for Permanent Deformation Evaluation

Perdomo (1990) used derivations developed by Lytton (1990) to model creep and creep recovery curves for various mixtures of crushed limestone and field sand. Lytton had shown (1990) that the creep and recovery curves could be modeled by hyperbolic functions. For the creep portion of the curve the time dependent creep compliance can be modeled as:

$$D(t) = \frac{D_o + D_m at^m}{1 + at^m} \quad (3.23)$$

where  $D_o$  is initial creep compliance,  $D_m$  is maximum creep compliance,  $a$  is a regression constant,  $t$  is time and  $m$  is the slope factor. For the recovery portion of the curve, the time dependent recovery is modeled by a very similar equation as follows:

$$R(t) = \frac{R_o - R_m bt^{mp}}{1 + bt^{mp}} \quad (3.24)$$

where  $R_m$  is maximum recovery compliance,  $b$  is a regression constant,  $t$  is time and  $p$  is a slope factor modifier. The two hyperbolic equations for creep and recovery are of the same form and differ only in the  $p$ -value which modifies the slope factor of the recovery portion from the slope of the creep curve. This  $p$ -value serves as a tool by which to characterize the influence of the aggregate on the resilience and loading recovery of the mixture following creep testing.

Lytton (1990) demonstrated how the hyperbolic equations for creep and recovery could be used to develop a permanent deformation model to be used in an updated version of the Texas Flexible Pavement System (Perdomo, 1991). This relationship is based on the VESYS approach (1976) which defines rutting susceptibility of the mixture based on the two parameters alpha and gnu. Alpha is defined as unity minus the slope of the steady state creep compliance (1-m). The general VESYS permanent deformation model is then defined as:

$$\frac{\delta \epsilon_p}{\delta N} = \epsilon_r \cdot \mu \cdot N^{-\alpha} \quad (3.25)$$

where  $\mu$  is gnu and  $\alpha$  is alpha and  $N$  is number of loading cycles. Lytton further defines gnu as a function of the  $p$ -value.

Figure 3.31 demonstrates the ability of the hyperbolic functions to match the creep and recovery curves. The match between the experimental data and the hyperbolic curve is almost exact. Perdomo (1990) developed hyperbolic creep and recovery curves to match experimental test data for creep and recovery periods of 1000 seconds each and for a loading stress level of 14.5 psi. Lytton (1992) has suggested that the  $p$ -value, or the ratio of the slope of the recovery to slope of the creep curve, should be relatively high for high quality mixtures. This high  $p$ -value indicates good recovery potential. A low  $p$ -value indicates a mixture which does not recover well and hence is more susceptible to permanent deformation. Lytton suggested that a  $p$ -value of unity or greater is required for mixtures subjected to high levels of traffic. Values of the ratio of recovery slope to creep slope of less than unity indicate lower quality, more rut-sensitive mixtures.

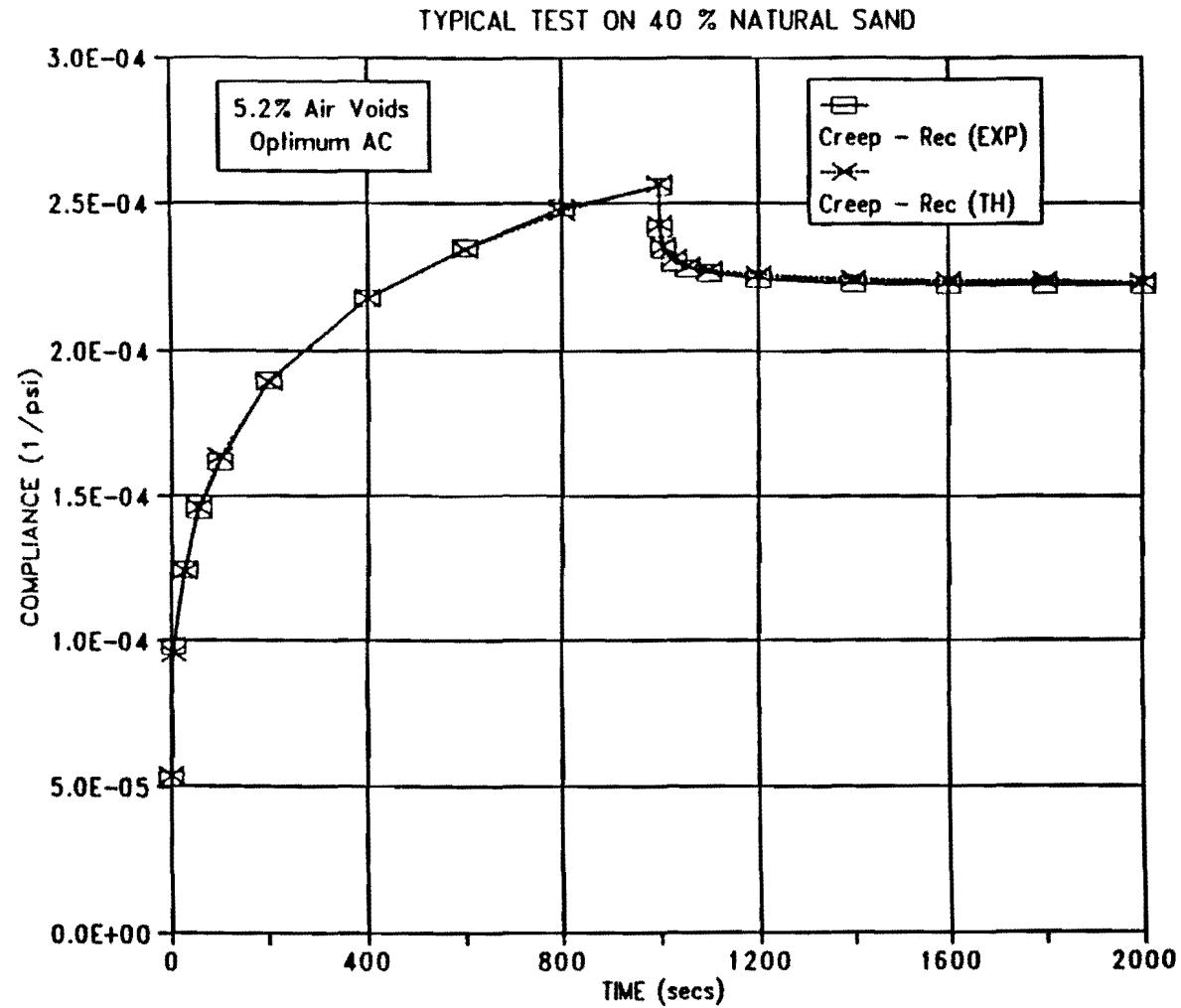


Figure 3.31. Linear Representation of Typical Creep and Recovery Behavior of a 40 Percent Natural Sand Mix at High Air Void Contents. (After Perdomo (1990)).

Perdomo (1990) was able to differentiate mixtures with various types of aggregates based on the p-value response which was significantly different among the various types of mixtures. However, the p-value was found to be highly sensitive to test temperature and stress level.

Von Quintus (1991) suggested a recovery efficiency factor to be applied to creep and recovery data. This efficiency factor could be calculated as unity minus the ratio of the strain at the end of the recovery period to the strain at the end of the creep period. Von Quintus (1992) suggested that high quality mixtures should possess inelastic recovery coefficients of in excess of 70 percent.

It seems to be a logical approach to incorporate the recovery factor into determination of rutting potential either in terms of the p-value or the recovery coefficient. At this point in time, too little data exist upon which to establish a criterion for recovery. This is particularly true of the p-value which is very highly dependent on the conditions of the test: temperature and stress state applied during the test. At this point is prudent to continue the investigation of creep recovery and to try to develop realistic criteria for creep recovery that can be used in mixture design and analysis together with creep at the end of a specified period of loading and the slope of the steady state portion of the creep curve.

Probably the most realistic approach at this point is to measure resilience by means of a relatively short loading and recovery period (about 10 seconds each). This testing should occur at relatively low stress levels perhaps 15 to 20 psi. This evaluation of resilience should occur in the pre-conditioning period prior to the creep test.

A considerable amount of short term creep and recovery data was collected on a variety of mixtures. Based on the performance of these mixtures in the creep test, the percent recovery after a cycle of 10 seconds creep followed by 10 seconds recovery should be approximately:

<u>Rutting Potential</u>	<u>Percent Inelastic Recovery</u>
Very Low	80% or above
Low	70% or above
Moderate	50% or above
Substantial	Below 50%

Although the percent recovery is an attractive approach, not enough data are currently available to support its use.

#### Criteria for the Evaluation of Uniaxial Compressive Creep Test Data

Tables 3.24 and 3.25 present the summary of criteria suggested for use in the evaluation of compressive creep test data. Table 3.24 presents the characteristics or parameter values of the compressive creep curve required to provide rut-resistant mixtures. These values were developed from a careful review and study of the data presented in Tables 3.5 through 3.7 and of the data from other researchers.

The basis for the development of these criteria is the understanding of the nature of the creep response as explained earlier in this section. Most importantly, instability in the creep curve occurs at strains above approximately 0.008 in./in. Thus the general approach was to insure that for a loading condition representing field conditions as closely as possible, the strain at a time of loading representing the traffic intensity and accumulation in the field does not exceed 0.008 in./in. The traffic intensity in these tables is defined by the number of standard axle equivalents to which the pavement will be subjected. This calculation was based on the assumption that a 4,500 pound wheel with 100 psi contact pressure applies a haversine-type stress function to the pavement over a period of approximately 0.01 seconds. Thus, a 3,600 second creep period is representative of approximately 360,000 applications of a standard axle equivalent (ESAL). For traffic intensities of greater than 360,000, the total strain at 3,600 seconds was calculated which would result in a total strain at the end of the appropriate period that does not exceed approximately 0.008 in./in. This calculation was made taking into account the slope of the steady state creep curve of various mixtures.

It should be noted that the approximation of performance of mixtures which are to perform in high traffic areas (greater than about 360,000 ESALs) is difficult because of the often erratic changes in the nature and slope of the creep curve between strains of about 0.5 and 1 percent. Hence, a better way is to test the specimen in creep for the appropriate period of creep loading. This can be approximated for fast moving traffic, i.e., highway

Table 3.24. Strain at One-Hour Creep Loading and Slope of Steady State Creep Curve Required to Reduce Rutting Potential to Very Low Level.

Total Strain at One-Hour of Loading, %	Slope of Steady State Creep Curve					
	< 0.17	< 0.20	< 0.25	< 0.30	< 0.35	< 0.40
< 0.25	IV <sup>2</sup>	IV <sup>2</sup>	IV <sup>2</sup>	IV <sup>2</sup>	IV <sup>2</sup>	III
< 0.40	IV <sup>2</sup>	IV <sup>2</sup>	IV <sup>2</sup>	III <sup>2</sup>	III <sup>2</sup>	III <sup>2</sup>
< 0.50	IV <sup>2</sup>	IV <sup>2</sup>	III <sup>2</sup>	III <sup>2</sup>	III <sup>2</sup>	II
< 0.80	III <sup>2</sup>	III <sup>2</sup>	II	II	II	II
< 1.0	I	I	I	I	I <sup>1</sup>	
< 1.2	I <sup>1</sup>	I <sup>1</sup>	I <sup>1</sup>			

Notes:

- I - Low traffic intensity: < 10<sup>5</sup> ESALs
- II - Moderate traffic intensity: Between 10<sup>5</sup> and 5 x 10<sup>5</sup> ESALs
- III - Heavy traffic intensity: Between 5 x 10<sup>5</sup> and 10<sup>6</sup> ESALs
- IV - Very heavy traffic intensity: >10<sup>6</sup> ESALs

1. Must also have  $\epsilon_p < 0.8\%$  at 1,800 seconds of creep loading
2. Should also meet the following criteria:  $\epsilon_{rt} + \epsilon_p < 0.5 \epsilon_{qu}$

Table 3.25. Creep Stiffness Criteria at One-Hour Creep Loading.

Level of Rut Resistance	Traffic Intensity Level	Required Minimum Creep Stiffness, psi, for Test Constant Stress Level of:		
		30 psi	50 psi	70 psi
Highly Rut Resistant	IV	15,000	17,500	22,500
	III	7,000	10,000	14,000
	II	5,000	6,500	8,750
	I	3,000	4,000	6,000
Moderately Rut Resistant	IV	7,500	10,000	14,000
	III	5,000	7,250	10,000
	II	3,500	6,000	7,500
	I	2,500	3,000	4,000

traffic, by multiplying the traffic expected during the hottest 180 of the year by the 0.01 seconds per load application. Thus the appropriate time of loading for various traffic intensities are as follows:

<u>Traffic Level, ESALs</u>	<u>Appropriate Time of Creep Loading, seconds</u>
100,000 or less	one hour
500,000	1.5 hours
1,000,000	3 hours
10,000,000	30 hours

For purposes of mixture design, it is generally not acceptable to perform tests for extended periods of time: greater than about one-hour. For this reason, an approximation of performance after one-hour of creep testing is necessary. Table 3.24 summarizes the criteria of acceptability after one-hour of creep loading at 104°F at the appropriate stress level.

To use Table 3.24, enter the table with the creep strain at the end of one-hour of loading on the left-hand set of rows. Enter with the appropriate slope at the top. The box at the intersection identifies the traffic intensity level which is acceptable for the creep results identified. The value in the box is the most intense traffic level which can be supported by the mixture tested. All lower traffic levels could also be supported. For example, if a creep curve has a slope of the steady state portion of 0.25 and a creep strain at the end of one-hour of 0.005 in./in., Table 3.24 indicates that this mixture can support type III, type II or type I traffic intensity levels with very high resistance to rutting.

Table 3.25 presents the approximate creep stiffness values at the end of one-hour of creep testing at the appropriate stress level used in testing to duplicate actual field stress conditions. This table is not necessary for evaluation of creep data but is presented for guidance as the creep stiffness at the end of one-hour loading is a popular method of quick evaluation of creep test data.

Footnote 2 in Table 3.24 identifies an additional criterion which must be met in order to meet all requirements. This criterion is based on the AAMAS procedure (Von Quintus, et al. (1991)) which suggests that the

permanent strain at the end of a one-hour period of creep loading should be compared to the trace of the stress versus strain results of the unconfined compression test. Accordingly, the sum of the permanent strain,  $\epsilon_p$ , at the end of the 3,600 second loading period of the creep test and the total resilient strain,  $\epsilon_{rt}$ , measured during the uniaxial resilient modulus test, should not exceed approximately 50 percent of the strain determined during the unconfined compression test,  $\epsilon_{qu}$ , ASTM T 167. The total strain recovered,  $\epsilon_{rt}$ , is measured at a loading frequency of 1 cps (0.1-sec. load duration and 0.9-sec. rest period). In equation form this reads:

$$\epsilon_p + \epsilon_{rt} < 0.5\epsilon_{qu} \quad (3.26).$$

This relationship attempts to insure that the permanent strain developed in the creep test is limited so that strain softening does not develop in the mixture. Strain softening was generally thought to occur at approximately one-half the value of the strain at peak load during the unconfined compressive test. This is verified by a substantial amount of data recorded in this study, see for example, Figure 3.32. In this figure, it is clear that for mixtures the non-linearity marking the beginning of strain softening occurs at approximately  $0.5\epsilon_{qu}$ . Data in Appendix C shows the consistency of strain softening (non-linearity) beginning at approximately  $0.5 \epsilon_{qu}$ .

It is suggested at this point to limit the sum of the total resilient strain,  $\epsilon_{rt}$ , and the permanent strain from the creep test,  $\epsilon_p$ , to  $0.5\epsilon_{qu}$ . This specification should be a part of the criteria for creep evaluation. This evaluation is then a practical substitute for the resilient recovery factor until more complete and specific testing is performed.

Three parameters are used to evaluate the creep data: slope of the steady state creep curve, strain at one-hour of loading and the sum of the total resilient strain and total strain at the end of one-hour of creep loading at 104°F under realistic loading conditions.

When one considers the contact surface of a typical standard wheel load and the stress function it simulates when passing over a point on the pavement surface, approximately a haversine wave function; the dwell time of loading is approximately 0.01 seconds for fast moving traffic, approximately

NS(20%), CLS(80%), Temp=104F, AV=(3-4%)  
AC% (opt.), Load Rate= (2in./min.)

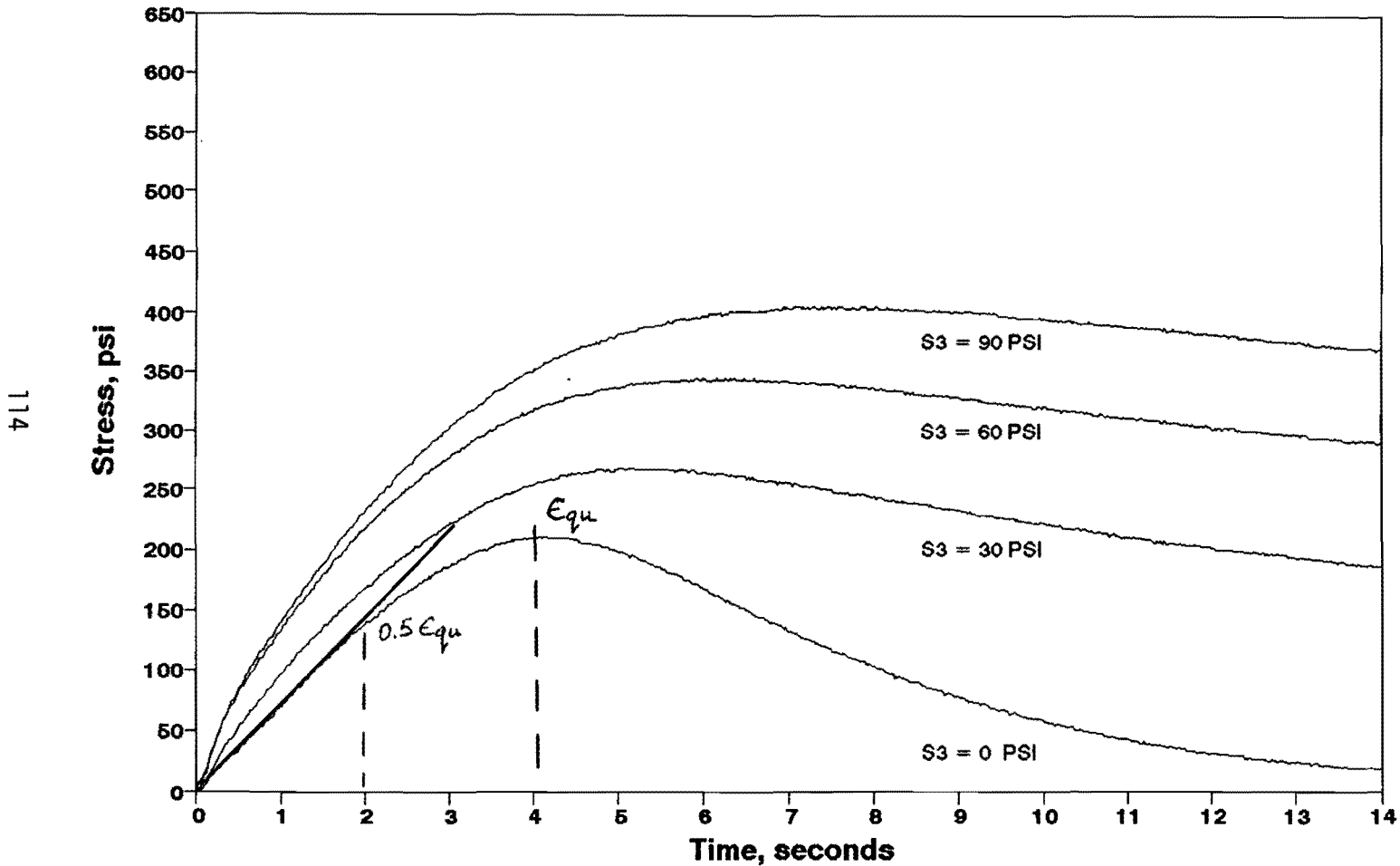


Figure 3.32. Triaxial Test Data Demonstrating the Departure from Linearity at About  $0.5 \epsilon_{qu}$  for 20 Percent Natural Sand and 80 Percent Crushed Limestone Mixture Loaded at a Stroke Rate of 2 Inches Per Minute.

60 mile per hour, and approximately 0.06 seconds for traffic moving at a speed of 10 miles per hour.

If one considers that the strain in a pavement (with a modulus of approximately 200,000 psi) under a contact stress of approximately 100 psi can be calculated by dividing 100 psi by the 200,000 psi pavement stiffness, the calculated strain is 0.0005 in./in. If this strain is divided by the dwell time of the contact pressure, the strain rate or stroke rate for unconfined or triaxial testing can be calculated. The appropriate value of strain rate to simulate the 60 mph traffic is thus 0.0005 in./in. divided by 0.01 seconds or 0.05 in./in. per second, and the appropriate rate to simulate the slow moving traffic is 0.0083 in./in. per second. The corresponding stroke rate to simulate slow moving traffic, a critical condition, for samples 4 inches, 6 inches and 8 inches in height is as follows:

<u>Sample Height, in.</u>	<u>Appropriate Stroke Rate, in./min.</u>
4	2 (10 mph), 0.24 (1 mph)
6	3 (10 mph), 0.36 (1 mph)
8	4 (10 mph), 0.48 (1 mph)

Since a slow speed or rate of loading is appropriate to simulate the most deleterious field conditions, it is recommended that the unconfined compression test be performed at a stroke rate of between 2 and 0.25 inches per minute on 4 inch high samples. AASHTO T 164 recommends a loading rate of 0.15 inches per inch of specimen height per minute. Since this is within the calculated range (4 inch sample X 0.15 inches/inch of sample height = 0.6 inches per minute), this approach should be followed. Resilient strain,  $\epsilon_{rt}$ , should be calculated in accordance with the AAMAS procedure and ASTM D3497. The creep strain at the end of one-hour of testing under appropriate stress conditions plus the resilient strain should not exceed one-half of the strain at which the maximum load in the unconfined compression test occurs.

#### EXAMPLES OF USE OF THE RUTTING CRITERIA

Consider the mixture of crushed limestone aggregate (90 percent) and field sand (10 percent) with an optimum binder content of 5.2 percent (AC-10). The mixture has an air void content of 3.8 percent and a VMA of 14

percent.

Creep data for a representative sample of the mixture are presented (in terms of an arithmetic plot--as recommended) in Figure 3.33. From this figure the important creep parameters are:

$\epsilon_p$  at one-hour--0.0085 in./in.

$m$  of the steady-state creep curve--0.32

This mixture is to be used as an overlay (2 inches) for an existing pavement (over existing asphalt concrete). From Table 3.14 the uniaxial stress to be applied to the sample to mimic field stresses is 57 psi.

The compressive resilient modulus performed in accordance with the AAMAS procedure (Von Quintus, et al. (1991)) and ASTM D 3497 produced a total resilient strain under the 57 psi stress of 0.0005 in./in. The strain at maximum load from the uniaxial compression test at a loading rate of 0.6 inches per minute was 0.018 in./in. Thus the sum of the strain at a one-hour time of creep loading and total resilient strain is:

$$\epsilon_p + \epsilon_{rt} = 0.0085 + 0.0005 = 0.0090: \quad \text{and } 0.5\epsilon_{qu} = (0.5)0.018 = 0.0090.$$

Thus the mixture is acceptable and the total of resilient and creep strain is within the region prescribed to prevent strain softening.

For this particular mixture (Figure 3.33) the arithmetic plot of creep data illustrates that a region of instability is reached beyond the one-hour loading. Obviously, on this basis the mixture is borderline and should be limited to type I use, or it should be realized that the risk of permanent deformation problems are substantially increased if the mixture is used in type II traffic. If this mixture is to be used in type II traffic, it should be limited to use where the traffic level is to the lower end of the suggested traffic range.

This mixture does meet the maximum  $\epsilon_p$  level of 0.008 following a creep loading of 1,800 seconds, Figure 3.33.

As a second example, consider the data in Figure 3.34 for the mixture of AC-20 binder, river gravel with limestone screenings and modified with 5 percent low density polyethylene (LDPE). Based on the steady state slope ( $m$

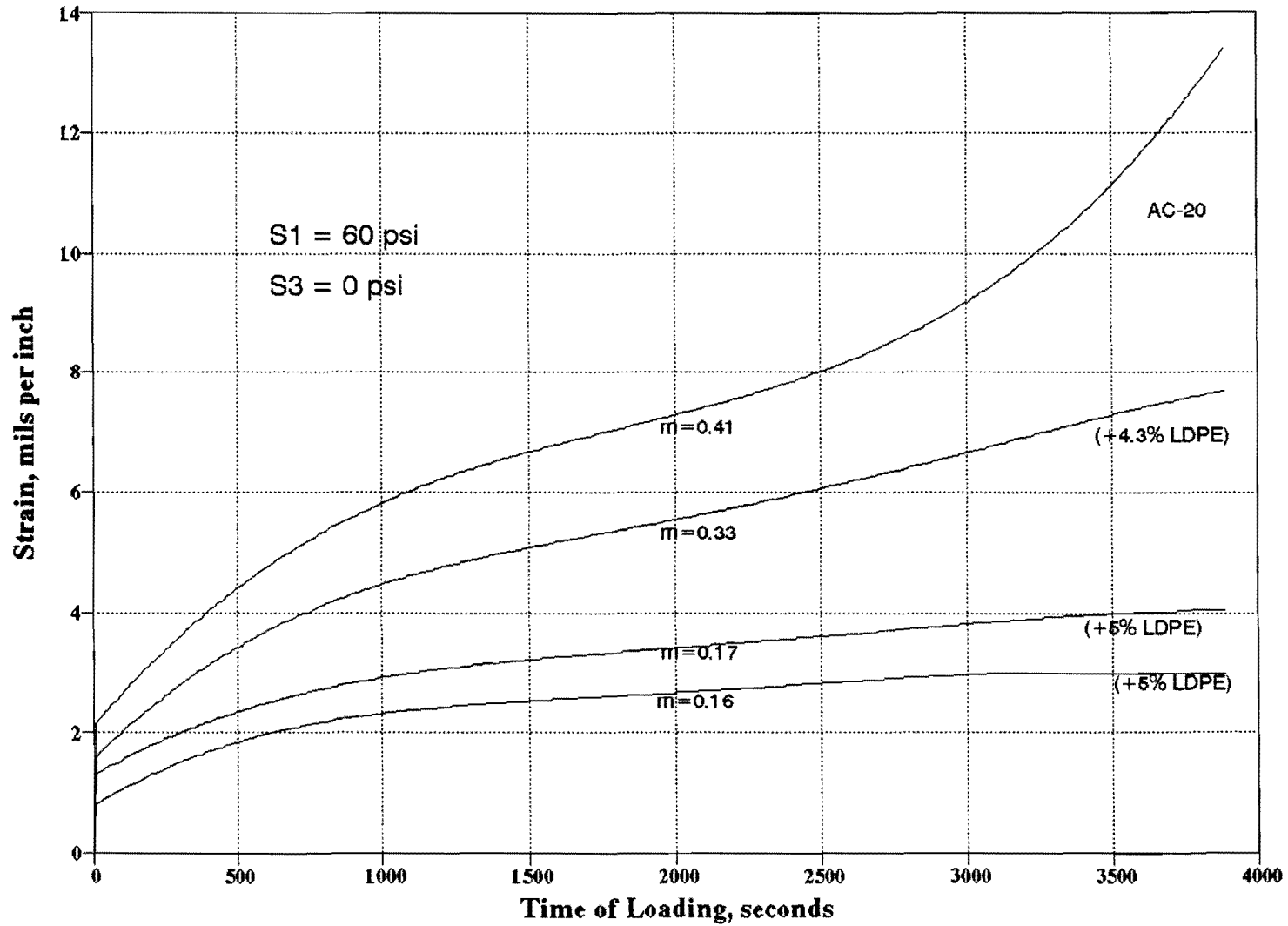


Figure 3.33. Creep Strain Versus Time of Loading Plots for a River Gravel and Limestone Screenings Mixture with Various Levels of LDPE Modification.

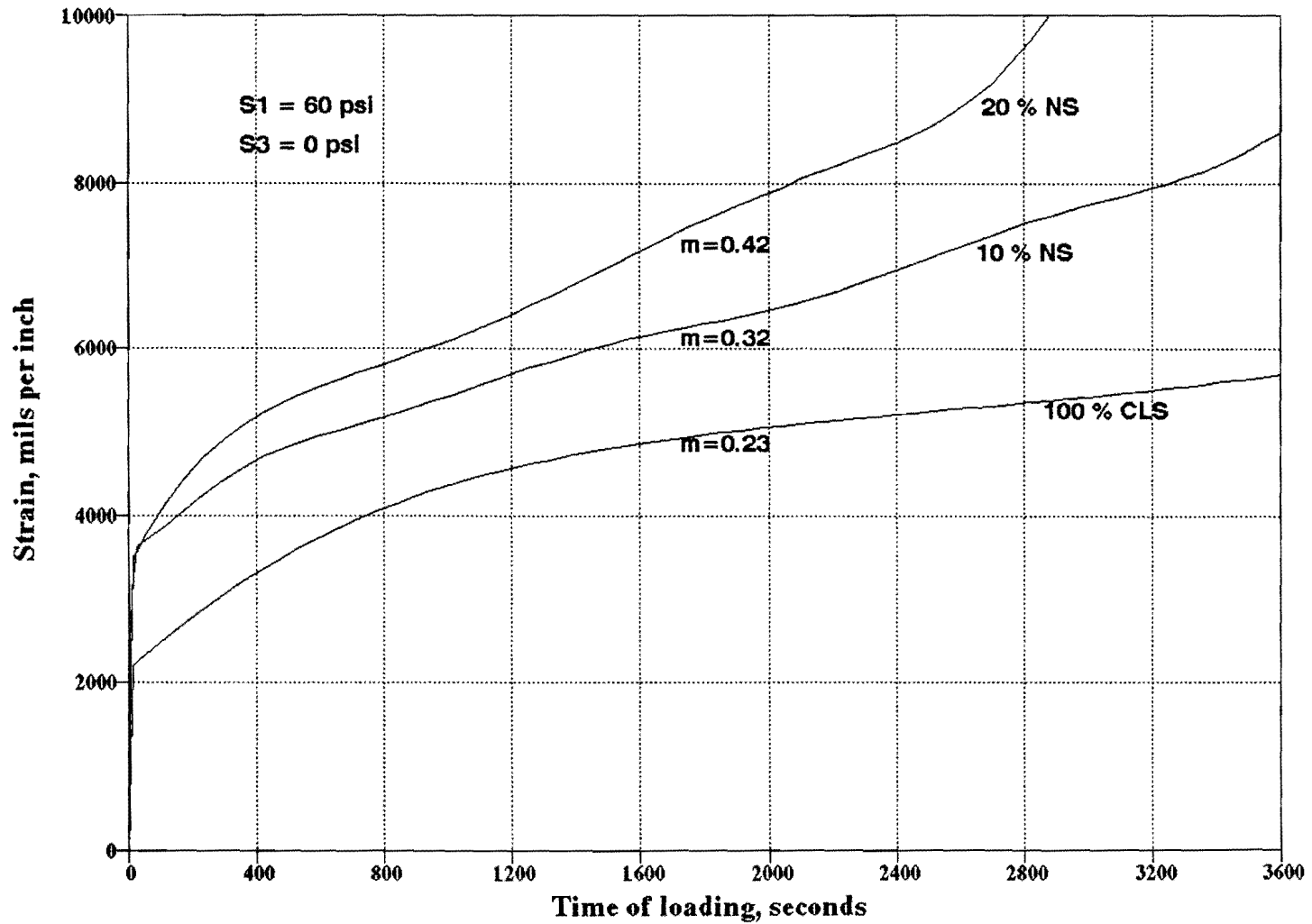


Figure 3.34. Creep Strain Versus Time of Loading Plots for Crushed Limestone and Natural Sand (Field Sand) with Varying Percentages of Natural Sand.

= 0.17) and  $\epsilon_p$  at 3,600 seconds (0.38 percent), the mixture is highly rut resistant to type III traffic. The same mixture with 6 percent LDPE is, based on Table 3.24, highly rut resistant when used as in type IV traffic.

The unmodified mixture graphically presented in Figure 3.34 is comprised of a river gravel aggregate with approximately 15 percent of limestone screenings and an AC-20 asphalt cement binder. Under a constant uniaxial stress of 60 psi, this mixture creeps to a strain level of 1 percent at the end of one-hour of loading at a temperature of 104°F. The slope of the mixture in the steady state region just before the onset of tertiary creep is 0.41 (log-log slope). According to Table 3.24 the unmodified mixture is not suitable for use as a pavement material with a low to very low susceptibility to rutting. However, as discussed above the addition of a polymer, in this case LDPE, has substantially improved the mixture in terms of reduction of rutting potential.

Figure 3.33 shows how the improvement of the mixture through the reduction of natural sand has a similar effect to the addition of polymer on the reduction of rutting potential. The mixture of 80 percent crushed limestone and 20 percent natural sand is not suitable based on Table 3.24 because of the high strain at one-hour of loading and because of the high slope of the creep curve. This mixture is upgraded to a mixture suitable for use in type III traffic by reducing the natural sand content from 20 to zero percent. The creep stiffness at one-hour loading of the river gravel - limestone screening mixture is increased upon the addition of LDPE as follows:

<u>Mixture Identification</u>	<u>Creep Stiffness, psi</u>
River gravel, screenings AC-20	6,000
River gravel, screenings AC-20 + 4.3% LDPE	9,375
River gravel, screenings AC-20 + 5.0% LDPE	15,789
River gravel, screenings AC-20 + 6.0% LDPE	20,000

Based on these results and the criteria in Table 3.25 for moderate rut susceptibility, the unmodified mix is suitable only for type I traffic, the mixture modified with 4.3 percent LDPE is suitable for type III traffic, the mixture modified with 5 percent LDPE is suitable for type IV traffic (type III traffic with high rut resistance) and the mixture modified with 6 percent LDPE is suitable for use in type IV traffic with a high level of rut susceptibility.

Reduction in the percentage of natural sand in the crushed limestone mixture from 20 to 10 to zero increases the creep stiffness from 3,000 psi to 6,667 psi to 10,526 psi, respectively.

#### **GUIDELINES FOR EVALUATION OF RUTTING POTENTIAL BASED ON CREEP DATA**

The rutting potential of asphalt concrete mixture in this procedure is based on the one-hour creep test at a test temperature of 104°F. The following steps are required for evaluation of rutting potential:

1. Determine the traffic intensity of the roadway where the mixture is to be used. Traffic intensity is defined as the number of ESALs predicted during the 180 hottest days of the year. This is a conservative approach. Determine the pavement structure where the mixture is to be used.
2. Enter the appropriate table for the pavement structure in question and determine the uniaxial stress level to be applied during the one-hour creep test at 104°F.
3. Perform the creep test and record creep data in accordance with Figure 14 (of the NCHRP Report 338).
4. Obtain a continuous read-out over the 3,600 second test period (at least one data point every 100 seconds) and plot the creep data on an arithmetic plot as shown in Figures 3.17 through 3.28. The purpose of this plot is to identify tertiary creep if it exists during the one-hour creep loading period.
5. Calculate the steady-state portion of the creep curve between approximately 1,000 seconds and 3,600 seconds.
6. Enter table with the slope,  $m$ , and the strain at one-hour loading,  $\epsilon_p$ ,

and determine for which levels of traffic the mixture is acceptable. If the mixture is not acceptable for the traffic level intended, alter the mixture through changes in the aggregate gradation, mineral aggregate selection, binder selection or binder modification.

7. From results of the resilient modulus test performed prior to the one-hour creep test (ASTM D 3497 and paragraph 2.9 of NCHRP Report 338 (Von Quintus, et al. (1991)) and from the uniaxial compressive creep test (AASHTO T 167 and NCHRP Report 338, paragraph 2.9) insure that the following requirements are met:

$$\epsilon_{rt} + \epsilon_p < 0.5\epsilon_{qu}$$

This is applicable for the mixtures identified in Table 3.24.

8. As a verification of the rutting potential the amount of rutting can be approximated by the procedure discussed in paragraph 4.5.2 of the NCHRP 338 Report.

### **SPECIAL CONSIDERATIONS**

Asphalt mixtures which are modified with certain polymer additives sometimes behave differently from traditional mixtures. For example, extensive testing was performed on three mixtures. Mixture A is a densely graded mixture with unmodified asphalt cement. Mixture B is the same mixture but modified with a high percentage of styrene-butadiene-styrene (SBS) copolymer. Mix C is the same densely graded mixture but modified with approximately 5 percent low density polyethylene (LDPE).

A full complement of triaxial testing and static creep testing was performed on all mixtures. The results of unconfined compressive creep testing are presented in Figure 3.35. The result of the testing revealed the following important trends:

1. The high percentage of SBS modification produced mixtures of relatively low shear strength and thus relatively low  $c$  and  $\phi$  shear strength parameters.
2. The mixture modified with a high percentage of SBS exhibited unique

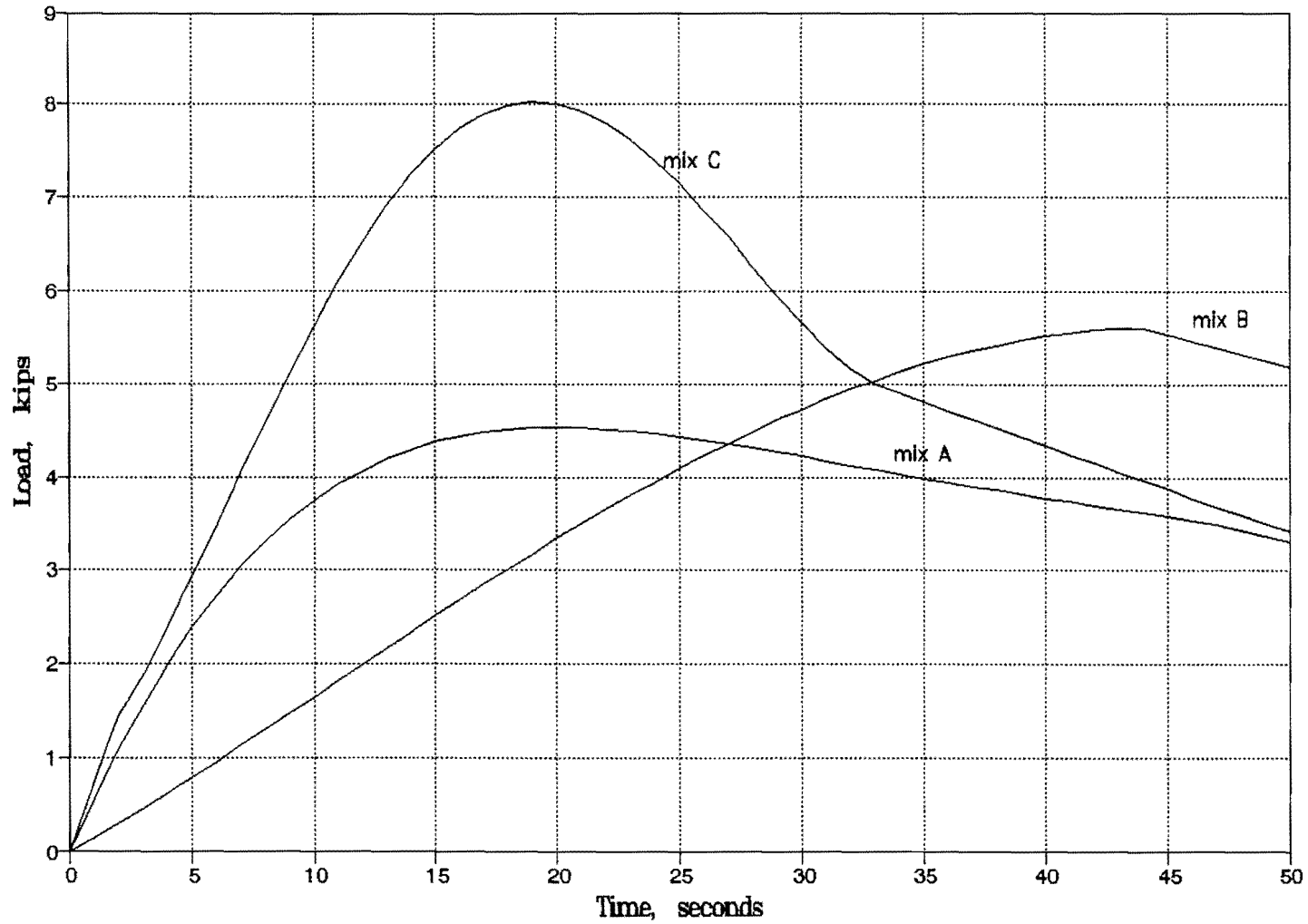


Figure 3.35. Example of the Effects of Polymer Modification on the Response of Strain at Failure of Mixtures in Triaxial Compression Testing ( $\sigma_3=0$ , 104°F, 0.5 in/min. Loading Rate).

properties in triaxial and static creep testing. Specifically, the strain at one-hour of creep testing was quite high, well in excess of one percent; yet tertiary creep apparently had not begun based on the evaluation of the arithmetic creep plot.

3. Review of the unconfined triaxial strength test results revealed that the strain at failure of Mix B is approximately three times that of either Mix A or Mix C.

Based on these observations, it is clear that certain polymer modified mixtures may have to be treated differently from conventional mixtures in terms of evaluation of the creep data based on a "critical" strain of approximately 0.8 percent and on a creep stiffness at the end of one-hour of creep loading.

In this example, Mix A possesses a creep stiffness at 104°F, 60 psi loading stress, of 3,000 psi. The creep curve was still apparently in the secondary creep region with no definite signs of tertiary creep. However the rate of creep as denoted by the slope of the creep curve was significantly higher than for Mixes B and C. With a creep strain at the end of 3,600 seconds of loading of 0.019 in./in. and a total resilient strain (ASTM D 3497) of 0.0012 in./in., the sum of  $\epsilon_p$  and  $\epsilon_r$  is 0.0202 in./in., which is only about 40 percent of the strain at failure in unconfined compression (AASHTO T 167). This indicates that despite the high level of creep strain, Mix B may not have reached the non-linear or strain softening region. Consequently, the mixture modified with a high percentage of the elastomeric additive apparently responds noticeably differently from the traditional mixtures.

Even though the mixture apparently does not enter the strain softening region, the strain at one-hour of loading is quite high and creep recovery of the elastomer-modified sample was greater, but not substantially greater, than for mixtures A and C. Thus the low creep stiffness at the one-hour point of loading is certainly indicative, in itself, of high deformation under load and potentially high levels of permanent deformation. More research is required to determine whether or not the evaluation criteria discussed in this report is applicable for specialty mixtures such as Mix B which is modified with a high percentage of SBS elastomer.

CHAPTER 4  
EVALUATION OF PERMANENT PREFORMATION  
BY SHEAR STRENGTH ANALYSIS

BACKGROUND AND THEORY

Nijboer Analysis

Triaxial type shear strength tests have long and widely been used to evaluate stability of aggregate and bituminous-aggregate systems. One of the most interesting, ingenious and oldest of procedures used to evaluate triaxial data was presented by Nijboer (1948).

Nijboer cleverly developed an equation for the viscous resistance to shearing in a triaxially loaded asphalt concrete mixture:

$$\eta_m \frac{d\varepsilon}{dt} = \frac{2\cos \phi}{3-\sin \phi} \left[ \frac{\sigma_1 - \sigma_3}{2\cos \phi} - \frac{\sigma_1 + \sigma_3}{2} \operatorname{tg} \phi - \tau_e \right] \quad (4.1)$$

where  $\eta_m$  is viscosity of the mass,  $d\varepsilon/dt$  is the rate of deformation,  $\phi$  is the angle of internal friction of the mixture,  $\operatorname{tg}$  is friction on this shearing plane,  $\tau_e$  is initial frictional resistance and  $\sigma_1$  and  $\sigma_3$  are major and minor principal stresses, respectively. The part of equation (4.1) in parenthesis can be plotted graphically using Mohr circle graphical techniques, Figure 4.1. This graphical representation is very important as it illustrates how shear strength can be separated into three components: viscous shearing resistance, NT, initial resistance TR and frictional resistance RM.

It is possible to separate shear strength into component parts by performing triaxial tests at different rates by loading ( $d\varepsilon/dt$ ). The intersection of a tangent line to the Mohr circle (failure) envelope and the  $\tau$ -axis gives the sum of initial and viscous resistance at a rate of deformation ( $d\varepsilon/dt = 0$ ). This sum is called apparent initial resistance,  $\tau_{app}$ . The viscous component should be proportional to rate of deformation. Thus,  $\tau_e = \tau_{app}$  for  $d\varepsilon/dt = 0$ . A graphical approach can be used to determine a  $\tau_{app} / d\varepsilon/dt$  diagram that should show a straight line

(therefore, only two loading rates are required). The slope of this line is  $\eta_m$ .

In this way it is possible to analyze resistance to plastic deformation of a material by separating it into a part characterized by the angle of internal friction (RM), a part defined by the differential viscosity of the mass,  $\eta_m$  (poises), viscous shearing resistance ( $\eta_m d\epsilon/dt - NT$ ) and  $\tau_e$  (initial resistance).

Thus, it is theoretically possible to identify mastic and aggregate matrix contributions to mechanical shear strength by performing a triaxial shear test at multiple confining pressures and at least two different rates of loading. This ability can be extremely valuable if one wishes to diagnose the reason for mixture rutting susceptibility. Is it the coarse aggregate matrix structure (RM) or the mass viscosity of the mastic that is lacking in terms of their contribution to mixture stability?

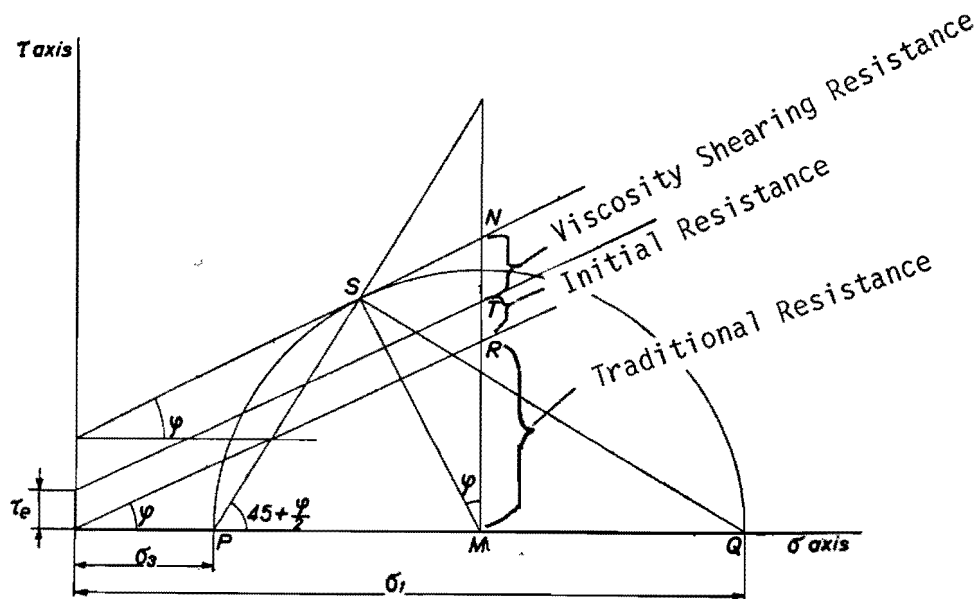


Figure 4.1. Representation of  $\eta_m \frac{d\epsilon}{dt} = \frac{2\cos \phi}{3-\sin \phi} \left[ \frac{\sigma_1 - \sigma_3}{2\cos \phi} - \frac{\sigma_1 + \sigma_3}{2} \tan \phi - \tau_e \right]$   
by Mohr circle.

The ability to separate out the contribution of the coarse aggregate matrix was vividly illustrated by Nijboer (1948), Figures 4.2 and 4.3. These figures illustrate the influence of volume concentration of aggregate on  $\tau_e$ , initial resistance of the mix, and  $\eta_m$ , mass viscosity of the mix. A relationship of the type shown in Figure 4.2 may help to illustrate why stone mastic type mixtures are rut resistant due to the initial resistance to shear developed by a large coarse aggregate fraction. Figure 4.3 illustrates the influence of fine aggregate concentration on mass viscosity of the mix.

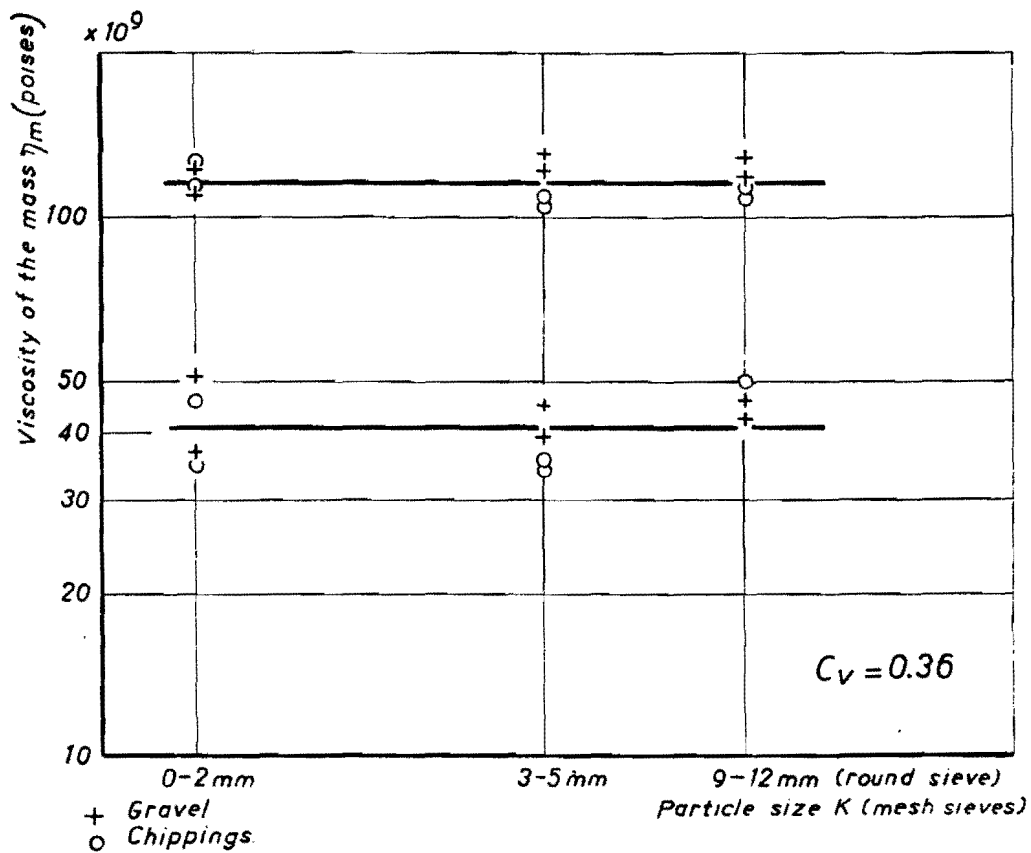


Figure 4.2. Influence of the particle size of coarse aggregate on the viscosity of the mass. (After Nijboer (1948)).

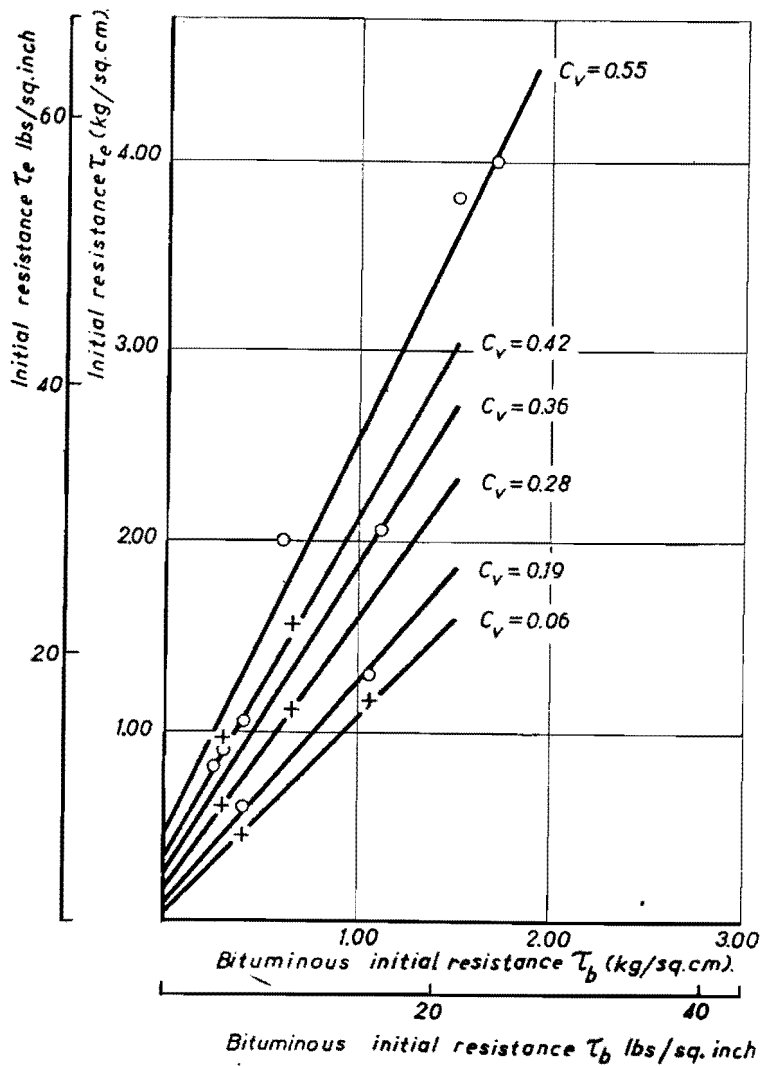


Figure 4.3. Relation Between the Initial Resistance  $\tau_e$  and the Bituminous Initial Resistance  $\tau_b$  with varying concentration of the coarse aggregate  $C_v$ . (After Nijboer (1948)).

It does not require a great deal of imagination to realize how such a methodology could be applied as a diagnostic tool or for evaluation of the relative benefits of asphalt cement modification, which should show up in  $\eta_m$  effects, or in aggregate gradation - shape/texture modification, which should show up in the friction resistance (RM) or  $\tau_e$  components. Knowledge as to whether the RM or  $\tau_e$  component is most highly influenced by mixture component changes would further identify the probable nature and type of pavement failure or distortion.

Later in this chapter the separation of triaxial data into components will be illustrated for various mixtures evaluated in a partial factorial

matrix which compared various aggregates and binders. Nijboer (1948) illustrated the power of triaxial test data to identify the contributions of mixture components to stability.

Nijboer (1948) evaluated the influence of coarse aggregate on mixture stability. In his analysis he divided the resistance to plastic deformation into the three components previously discussed: (a) angle of internal friction, (b) initial resistance,  $\tau_e$ , and (c) viscosity of the mass,  $\eta_m$ . In his coarse aggregate evaluation, Nijboer more specifically evaluated the influence of aggregate size and quantity of coarse aggregate.

Nijboer used the component analysis to show that the coarse aggregate size has very little (no significant) influence on the angle of internal friction, a significant influence on initial resistance and no noticeable influence on viscosity of the mass. Nijboer demonstrated that the influence of the quantity of coarse aggregate is much more important and significant than is the influence of the size of coarse aggregate. Figure 4.2 illustrates the pronounced influence of coarse aggregate concentration on the initial resistance,  $\tau_e$ . Two important and timely points can be gleaned from this figure. First an increase in coarse aggregate concentration  $C_v$ , substantially increases  $\tau_e$ . This may help explain why stone mastic or SMA mixtures tend to be more resistant to permanent deformation. The ability to increase  $\tau_e$  and to substantially increase internal friction (as Nijboer also demonstrated) by an increase in  $C_v$  illustrates how the component analysis of triaxial data may well prove useful as a diagnostic and/or analytical tool for mixture design/evaluation.

Figure 4.4 illustrates the influence of concentration of coarse aggregate and sand on the viscosity of the mass. This increase in mass viscosity indicates that in mixtures containing small quantities of coarse aggregate, these particles act as solids moving in a liquid formed by bitumen and the fine mineral aggregate. At high concentrations of the coarse aggregate, stearic hinderance in the mixture occurs which influences mass viscosity. This demonstration of the influence of aggregate concentration on mass viscosity is a further indication of how this tool could be used to help explain the influence of filler, fiber, aggregate and polymer in mixtures.

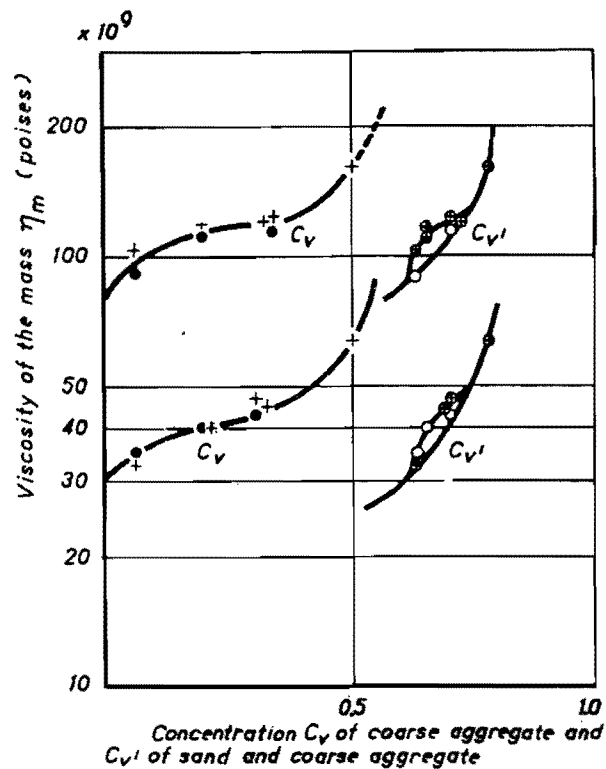


Figure 4.4. Relation Between the Viscosity of the Mass  $\eta_m$ , and the Concentration of Coarse Aggregate,  $C_r$ , and Concentration of Sand and Coarse Aggregate,  $C_r^1$ . (After Nijboer (1948)).

#### Other Analyses of Triaxial Test Data

Besides Nijboer, Barber (1962), Hewitt (1965), McLeod (1950) and Smith (1949) have presented analyses and recommendations concerning triaxial data. McLeod developed a relationship defining the allowable vertical pressure in terms of angle of friction, cohesion and lateral support provided by the pavement adjacent to the loaded area. Ameri-Gaznon and Little (1987) performed an extensive analysis of McLeod's work.

Although the analysis procedures prescribed by various researchers of triaxial data have been substantially different, they have all been based on the Mohr-Coulomb shear strength theory. The major difference concerning

the actual triaxial testing has been based on the temperature of testing and the rate of loading during testing. The vast majority of work in this area has been to use triaxial data as a method to evaluate the shear strength of the asphalt concrete mixture under very slow moving loads or under static loads. Smith (1949) used a static load for testing. Nijboer (1948) essentially promoted the same approach as he used a very slow loading rate of 0.005 inches per minute. McLeod followed suit using loading rates in the range of from 0 (equilibrium) to 0.4 inches per minute. As a result the measurements of  $c$  and  $\phi$  during triaxial testing were fairly consistent among the researchers. Figure 4.5 presents mixture stability curves for static pressures as shown. Figure 4.6 presents stability curves for a given vertical load for bituminous paving mixtures subject to braking stresses.

Generally, the reason for the use of static or near static loading is because it is rather simple to apply and because it, in effect, eliminates the problem of having to account for the influence of pavement temperature.

Figure 4.6 from McLeod's work demonstrates the influence of the surface shear caused by braking stresses at the tire-pavement interface. This figure demonstrates that the requirements on the mixture are substantially increased when a surface shearing action is applied.

Ameri-Gaznon and Little (1987) proposed that the rate of loading on a triaxial test must be substantially higher than those rates used by previous researchers to mimic the effects of moving wheel loads. To this end Ameri-Gaznon and Little suggested loading rates in the range of 2 inches to 4 inches per minute. This is similar to suggestions made by Freeman and Carpenter (1986). This is also in relatively close agreement with conventional testing procedures. For example, the Marshall test is performed at a temperature of 140°F and at a loading rate of 2 inches per minute on samples 4 inches high. This corresponds to a rate of loading of 4 inches per minute on samples 8 inches in height such as the triaxial samples tested in this study. The rate of loading in the Hveem stabilometer test is approximately 0.05 inches per minute for specimens 2.5 inches in height, approximately 0.06 inches per minute for specimens 2 inches high and would equate to a required loading rate of approximately 0.2 inches per minute if the same test were performed on samples 8 inches in height. Thus the range of loading rates suggested by Ameri-Gaznon and Little is

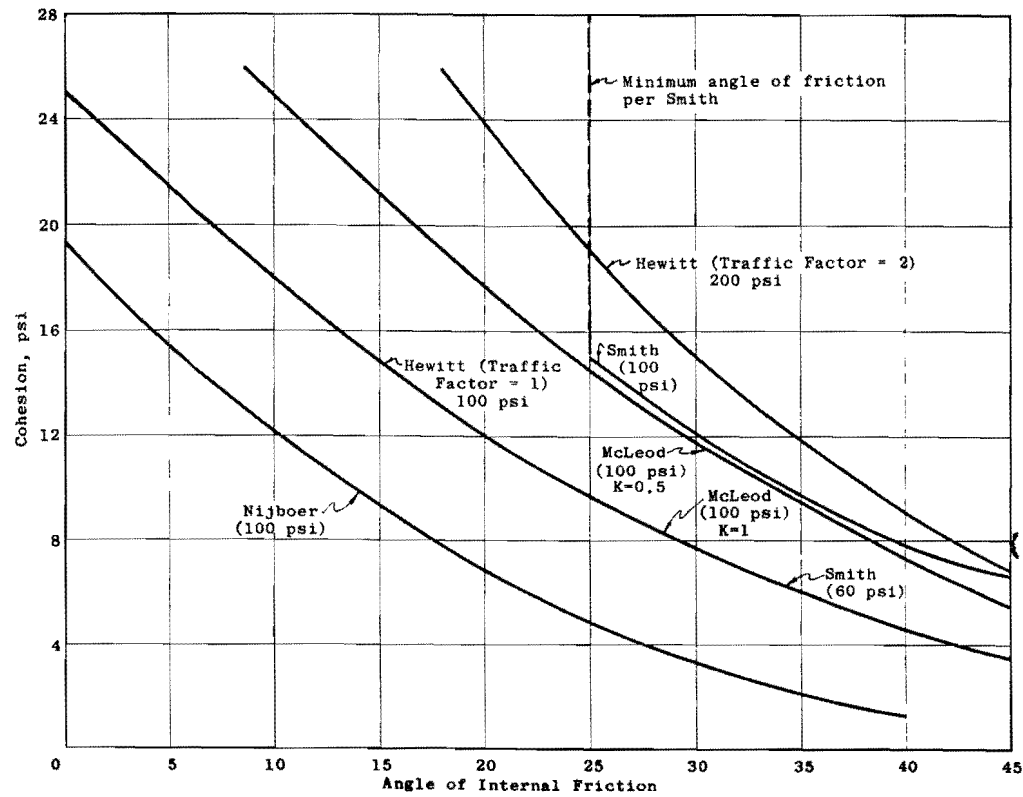


Figure 4.5. Asphalt Concrete Mixture Stability Curves for Static Pressures. (After Finn, et al. (1967)).

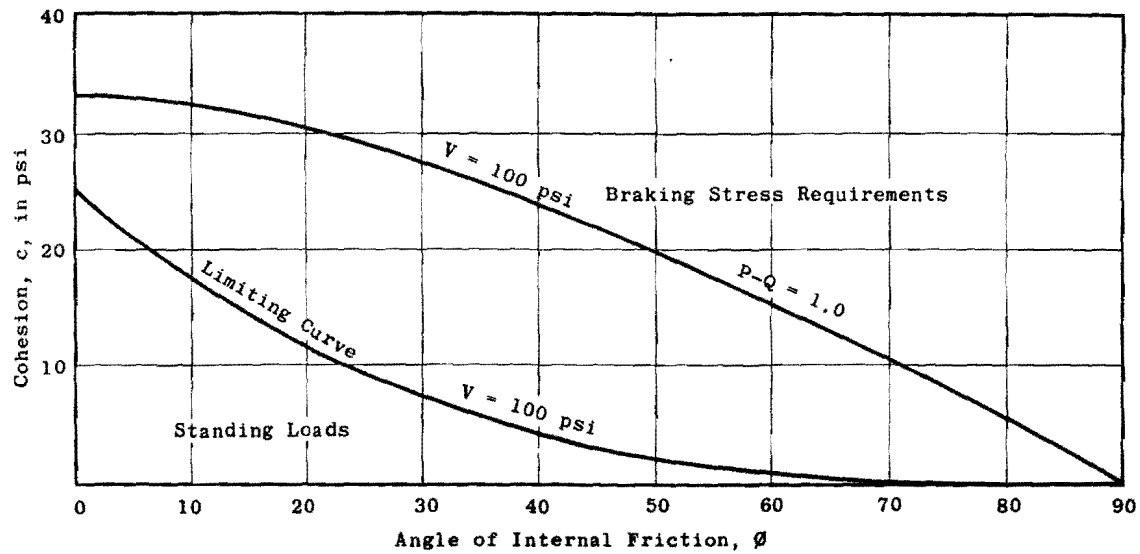


Figure 4.6. Illustrating Stability Curves for a Given Vertical Load for Bituminous Paving Mixtures Subject to Braking Stresses. (After McLeod (1950)).

reasonable when compared to traditionally used stability tests when specimen size is taken into consideration.

Since the rate of loading has a pronounced effect on the cohesive component of the shear stress, values of  $c$  and  $\phi$  must be determined at realistic loading rates. In this study triaxial testing was performed at loading rates of between 0.5 and 2 inches per minute on samples 8 inches high. This corresponds to loading rates of from 0.38 to 1.5 inches per minute for 6 inch high samples, from 0.25 to 1 inches per minute for 4 inch high samples and 0.12 to 0.5 inches per minute for samples 2 inches high.

#### **DEVELOPMENT OF TESTING PROCEDURE BASED ON HISTORICAL BACKGROUND**

Most of the testing in this report was performed on samples which are 4 inches in diameter and 8 inches in height. These samples were prepared using kneading type compaction. However, in accordance with the AAMAS guidelines of using gyratory compaction, a decision was made to perform triaxial testing on samples prepared with the large gyratory compactor in accordance with the procedures discussed in NCHRP report 338 (Von Quintus et al. (1991)). The compaction procedure is discussed in Sections 2 and 3 of the AAMAS Report. The suggested sample size using the large gyratory compactor is a 4 inch diameter sample which is at least 6 inches in height. Fabrication of this type of sample will require coring the larger sample produced using the large gyratory compactor.

The selected test temperature for the triaxial test is 104°F as is the case for the uniaxial creep test. This temperature has been shown to be a reasonable nominal high temperature for Texas climatic conditions.

The rate of loading suggested for the triaxial test is from 0.5 to 2 inches per minute for 4 inch diameter and 8 inch high samples and from 0.5 to 1.5 inches per minute for 4 inch diameter and 6 inch high samples. These rates of loading are reasonable for traffic ranging from relatively slow moving traffic to traffic moving at regular highway speeds. If it is expected that the pavement will be subjected to relatively high speed traffic, the 1.5 to 2.0 inch per minute loading rate should be used. If it is expected that traffic will be moving at slow to moderate rates, then the 0.5 inch per minute rate of loading should be employed. These suggested

loading rates are reasonable based on the suggestions of previous researchers including McLeod (1950), Smith (1949), Freeman and Carpenter (1986) and Ameri-Gaznon and Little (1987). In addition, these loading rates are compatible with loading rates in traditional stability tests such as Marshall and Hveem. However, the suggested loading rates are not theoretically based nor explicitly determined. The relationship between rate of loading and temperature of testing is confounded based on the non-linear viscoelastic properties of the asphalt concrete.

For details of sample fabrication techniques follow the guidelines for fabricating in paragraph 2.9 of the AAMAS procedure from the NCHRP 338 Report (Von Quintus et al. (1991)).

#### Octahedral Analysis Of Triaxial Test Data

Freeman and Carpenter (1986) used octahedral shear stress theory to analyze premature deformation in asphalt concrete overlays over Portland cement concrete pavements. They found that the octahedral shear stress in a pavement can indicate how close to failure a mixture is when loaded. This indication of incipient failure was given by the ratio of actual octahedral shear stress in the pavement to the failure octahedral shear stress predicted by theory.

Ameri-Gaznon and Little (1987) followed Freeman and Carpenter's work and thoroughly developed the octahedral shear stress theory for a series of typical pavement sections found across Texas. Their work is considered of great value and importance in the field of mechanistic analysis of pavement structures.

Perdomo (1991) used octahedral shear stress theory and the approach developed by Ameri-Gaznon and Little (1987) to analyze the potential for rutting of the two most widely different mixes: a 100 percent crushed limestone mix (low rut susceptibility) and a crushed limestone mix with 40 percent natural sand mix (high rut susceptibility). Their results will be presented as an example of the power of their technique following a brief discussion of the theoretical aspects.

### Theoretical Aspects

In general, the octahedral shear stress is a scalar parameter that defines the influence of nine stresses at a specific point. It is defined in a general form as:

$$\tau_{oct} = \frac{1}{3} \left[ (\sigma_x - \sigma_y)^2 + (\sigma_y - \sigma_z)^2 + (\sigma_z - \sigma_x)^2 + (\tau_{xy}^2 + \tau_{yx}^2 + \tau_{zx}^2) \right]^{\frac{1}{2}} \quad (4.2)$$

where

$$\begin{aligned} \sigma_x, \sigma_y, \sigma_z &= \text{normal stresses,} \\ \tau_{xy}, \tau_{yz}, \tau_{zx} &= \text{shearing stresses, and} \\ \tau_{oct} &= \text{octahedral shear stress (invariant).} \end{aligned}$$

Equation (4.1) in terms of principal stresses on a plane will reduce to:

$$\tau_{oct} = \frac{1}{3} \left[ (\sigma_1 - \sigma_2)^2 + (\sigma_2 - \sigma_3)^2 + (\sigma_1 - \sigma_3)^2 \right]^{\frac{1}{2}} \quad (4.3)$$

where

$$\begin{aligned} \sigma_1 &= \text{major principal stress,} \\ \sigma_2 &= \text{intermediate principal stress, and} \\ \sigma_3 &= \text{minor principal stress.} \end{aligned}$$

From Mohr-Coulomb failure theory, the equation that represents the relationship between major and minor principal stresses at failure is given by:

$$\sigma_1 = \sigma_3 \left[ \frac{1 + \sin\phi}{1 - \sin\phi} \right] + 2c \left[ \frac{1 + \sin\phi}{1 - \sin\phi} \right]^{\frac{1}{2}} \quad (4.4)$$

where

$$\sigma_1, \sigma_3 = \text{major and minor principal stresses,}$$

$\phi$  = angle of internal friction, and  
 $c$  = cohesion.

On the other hand, the octahedral normal stress is defined as:

$$\sigma_{oct} = \frac{1}{3} [\sigma_x + \sigma_y + \sigma_z] \quad (4.5).$$

Equation (4.5) in terms of principal stresses on a plane reduces to:

$$\sigma_{oct} = \frac{1}{3} [\sigma_1 + \sigma_2 + \sigma_3] \quad (4.6).$$

If one considers the octahedral shear strength to be obtained from triaxial compression tests ( $\sigma_2 = \sigma_3$ ) at a specific temperature and rate of loading, Equations 4.3 and 4.6 and can be combined with Equation 4.4 to obtain general equation for octahedral shear strength:

$$\tau_{oct\ strength} = \frac{2\sqrt{2}}{3 - \sin \phi} [\sigma_{oct} \cdot \sin \phi + c \cdot \cos \phi] \quad (4.7)$$

where

$\sigma_{oct}$  = octahedral normal stress,  
 $\eta$  = angle of internal friction, and  
 $c$  = cohesion.

Using an appropriate computer program such as modified ILLIPAVE (1968) where the pavement is modeled three-dimensionally by using a two-dimensional halfspace of a finite solid of revolution, one can obtain reasonably good information by which to evaluate the stress state within the pavement structure under any loading and pavement boundary conditions.

An indication of potential for rutting can be assessed by means of evaluating and analyzing the octahedral shear stress ratio, which is the ratio of the critical induced octahedral shear stress in the pavement layer,

to the octahedral shear strength of the material, as defined by equation. A procedure for calculating this octahedral shear stress ratio can be summarized in the following steps:

1. Find  $\tau_{oct}$  from the modified ILLIPAVE computer program using equation.
2. Find  $\sigma_{oct}$  from the modified ILLIPAVE computer program using equation.
3. Use values of the  $\sigma_{oct}$ , found in step 2, and appropriate  $\phi$  and  $c$  values, obtained from triaxial compression testing, in equation (4.7) order to obtain  $\tau_{oct \text{ strength}}$  for all  $\sigma_{oct}$  stresses.
4. Calculate octahedral shear stress ratios by dividing  $\tau_{oct}$  from step 1 by  $\tau_{oct \text{ strength}}$  from step 3, and draw contour lines for the different values obtained. Contours of octahedral shear stress ratios will give a complete picture of the distribution of failure potential within a pavement structure.

### Example Cases

This section presents two independent comparisons of hypothetical pavements analyzed by Perdomo (1991).

1. Two HMAC surface layers, one with the 100 percent crushed limestone and the other with the 60 percent crushed limestone and 40 percent natural sand mix, both in a traditional pavement structure, are compared.
2. Two HMAC overlays, one with the zero percent natural sand mix and the other with the 40 percent natural sand mix, both placed on an asphalt treated base are compared.

Perdomo (1991) performed the Octahedral shear stress analysis based on the following pavement boundary conditions and general assumptions:

1. A tire pressure of 115 psi was used with a 6,000-pound circular wheel load in order to represent high stress conditions. The

Tielking tire model (1986) was used to determine the contact vertical pressure distribution and the shear stress distribution to be used in the modified ILLIPAVE computer program.

2. The surface layers in both cases were subdivided into 1-inch thick sublayers in order to incorporate the temperature gradient models derived by Li, et al. (1986). The Dallas, Texas, region environment was selected as the model for this particular analysis. The temperature distributions, used in cases 1 and 2, are shown in Tables (4.1) and (4.2), respectively. Only the last four profiles from each table were used in the ILLIPAVE program because they were considered to be the most critical profiles for rutting performance (the highest temperature distributions). The highest temperature profile was labeled season 1 and subsequent profiles were labeled in order of decreasing temperature. Different modulus values were then assigned according to the temperature in each sublayer.
3. A Mohr Coulomb failure envelope was obtained for both the zero percent and 40 percent natural sand mixes at a temperature of 104°F. The values for cohesion and friction calculated from the envelopes were then used to compute octahedral shear strengths at this temperature. For the other temperatures within the pavement structure, the octahedral shear strengths were adjusted according to the ratio of moduli, which is considered to be a conservation approach.
4. Both pavement structures (Figures 4.7 and 4.8) were analyzed under two loading conditions: single and dual tire loading.

Perdomo (1991) developed a series of charts showing the variation of the octahedral shear stress ratio for the different mixes and cases analyzed under both single and dual tire loading conditions. Figures 4.9 through 4.12 present typical results for octahedral normal stress, octahedral shear stress, octahedral shear strength, and octahedral shear stress ratio for the pavement structure corresponding to case 1 and having a 40 percent natural sand mix as a surface layer. The figures are presented (for the single wheel load only) in order to illustrate the steps outlined in the procedure to calculate octahedral shear stress ratio.

Table 4.1. Temperature Distribution of 4 in. Asphalt Overlay (Dallas Area).  
(After Li, et al. (1986)).

Profile Number	Season Label*	Temp. (°F)	Sub-layer Temp. (°F)				% Time
			1	2	3	4	
1		< 75	68	70	72	73	25.58
2		75- 85	79	81	82	84	25.58
3	4	85- 95	90	89	88	87	15.05
4	3	95-105	100	97	94	91	14.58
5	2	105-115	110	105	101	97	12.15
6	1	115-125	118	112	107	103	6.83

\* Season labels used in ILLIPAVE analysis.

Table 4.2. Temperature Distribution of 3 in. Asphalt Overlay (Dallas Area).  
(After Li, et al. (1986)).

Profile Number	Season Label*	Temp. (°F)	Sub-layer Temp. (°F)			% Time
			1	2	3	
1		< 75	68	70	72	25.69
2		75- 85	79	81	82	25.69
3	4	85- 95	90	89	88	14.93
4	3	95-105	100	97	94	14.70
5	2	105-115	110	105	111	12.15
6	1	115-125	118	112	107	6.84

\* Season labels used in ILLIPAVE analysis.

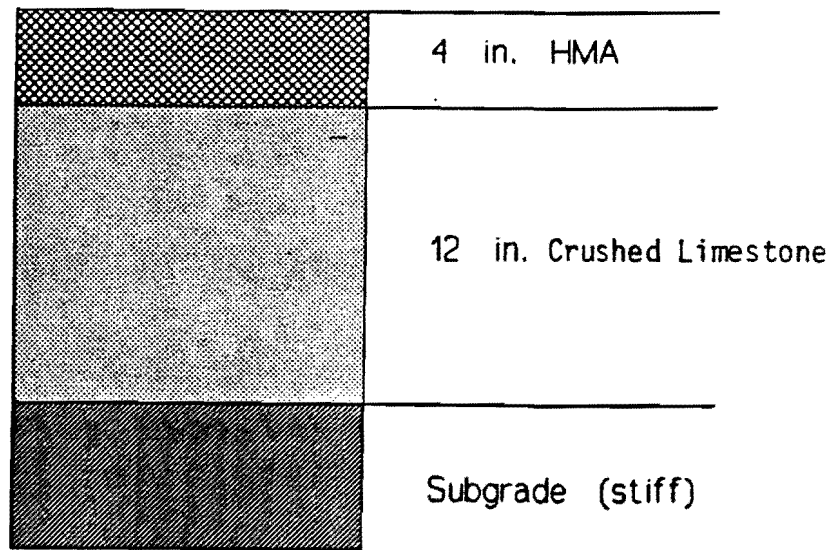


Figure 4.7. Traditional Pavement Structure. (After Perdomo (1991)).

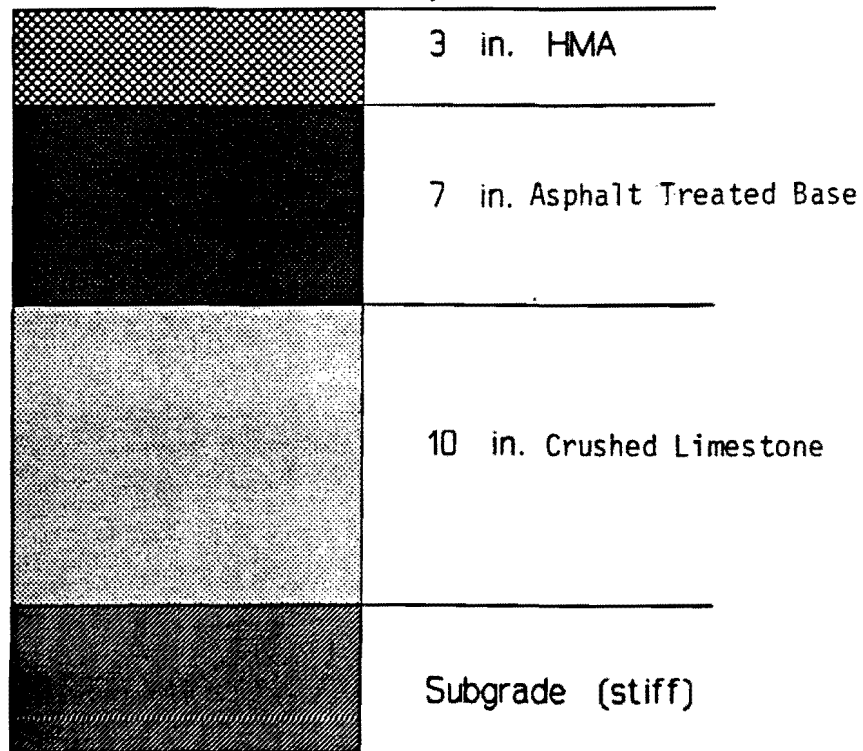


Figure 4.8. Asphalt Treated Base Pavement Structure. (After Perdomo (1991)).

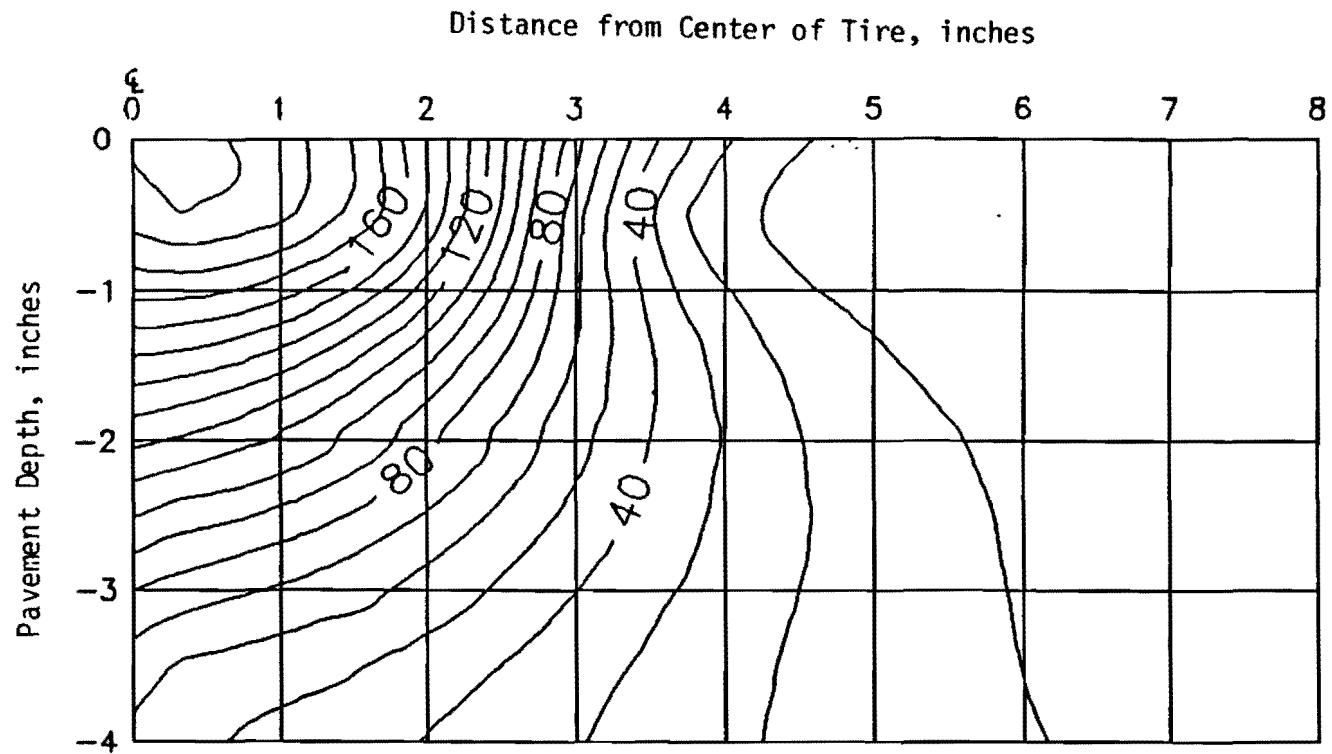


Figure 4.9 Octahedral Normal Stress Contours for 40 Percent Natural Sand Mix Surface Layer in Traditional Pavement Structure Under Single Tire Loading, and for Hottest Season (Season 1). (After Perdomo (1991)).

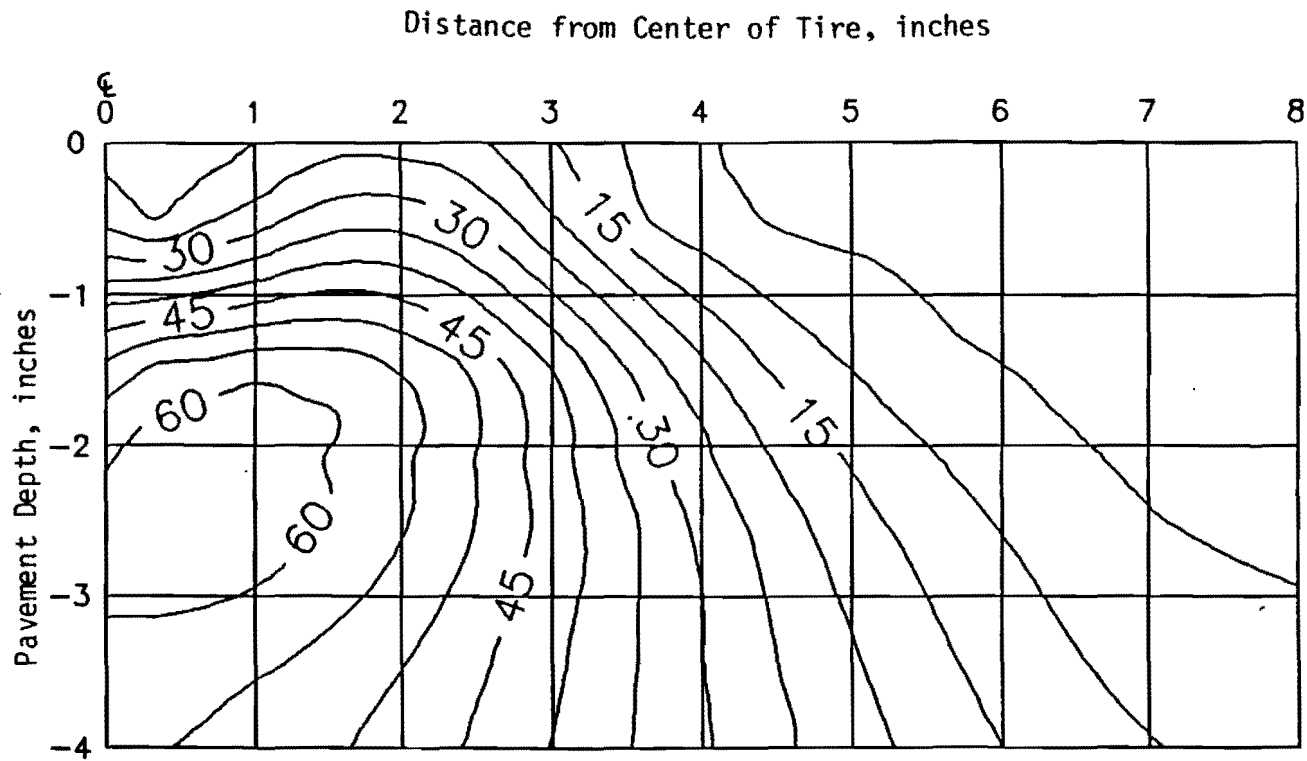


Figure 4.10. Octahedral Shear Stress Contours for 40 Percent Natural Sand Mix Surface Layer in Traditional Pavement Structure Under Single Tire Loading, and for Hottest Season (Season 1). (After Perdomo (1991)).

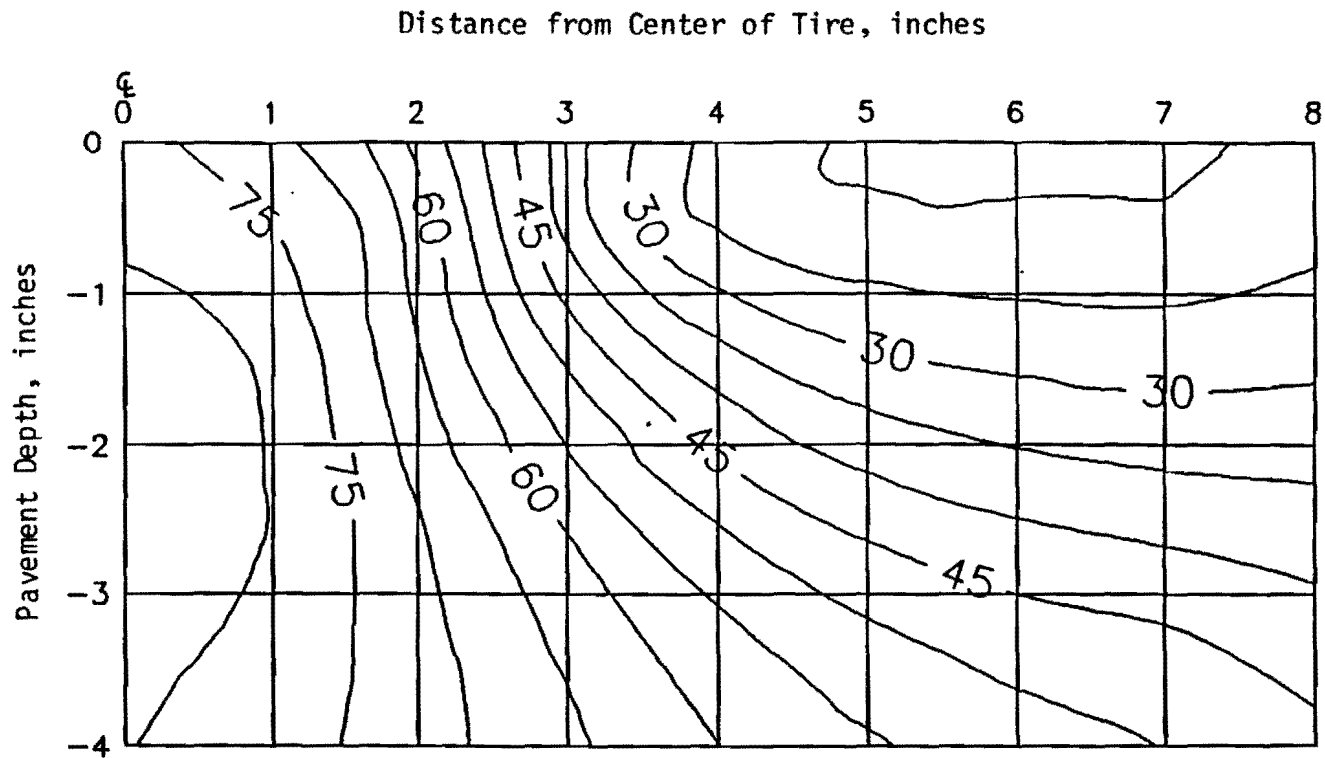


Figure 4.11. Octahedral Shear Strength Contours for 40 Percent Natural Sand Mix Surface Layer in Traditional Pavement Structure Under Single Tire Loading, and for Hottest Season (Season 1). (After Perdomo (1991)).

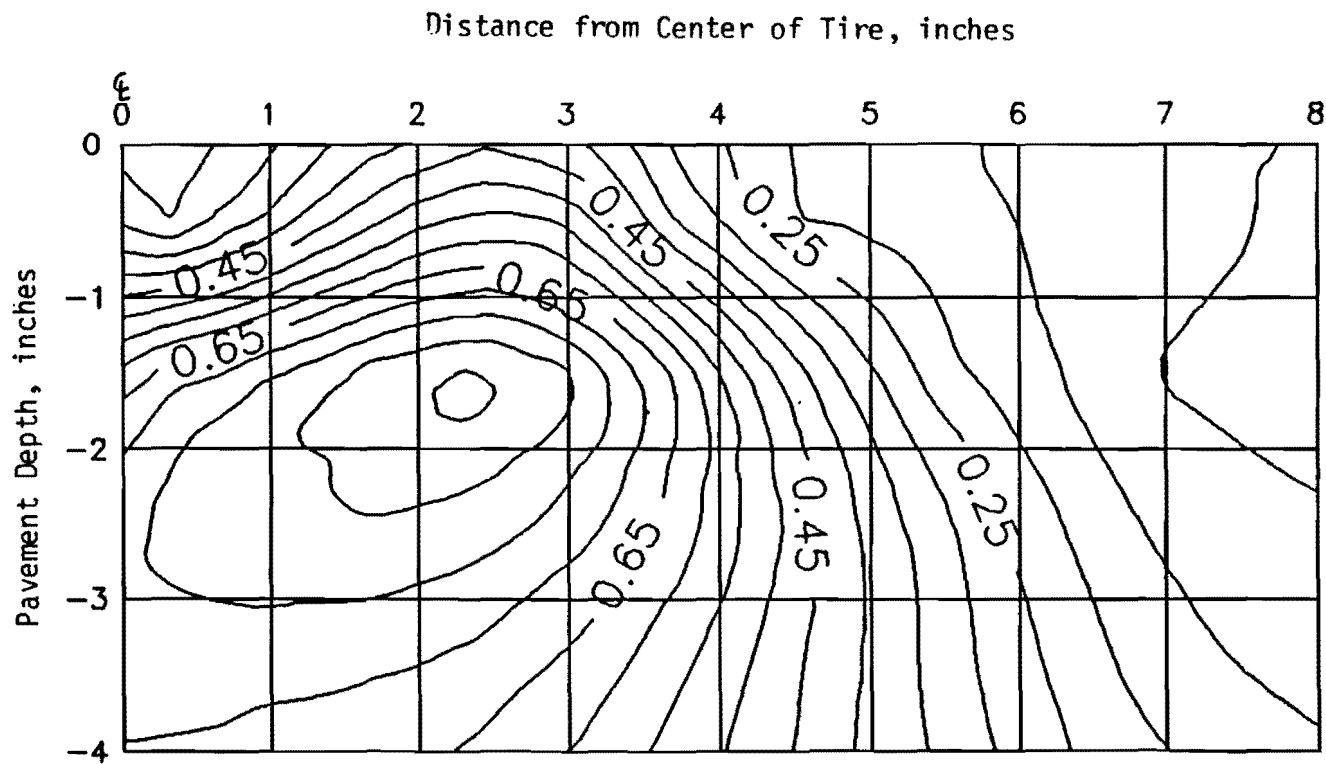


Figure 4.12. Octahedral Shear Stress Ratio Contours for 40 Percent Natural Sand Mix Surface Layer in Traditional Pavement Structure Under Single Tire Loading, and for Hottest Season (Season 1). (After Perdomo (1991)).

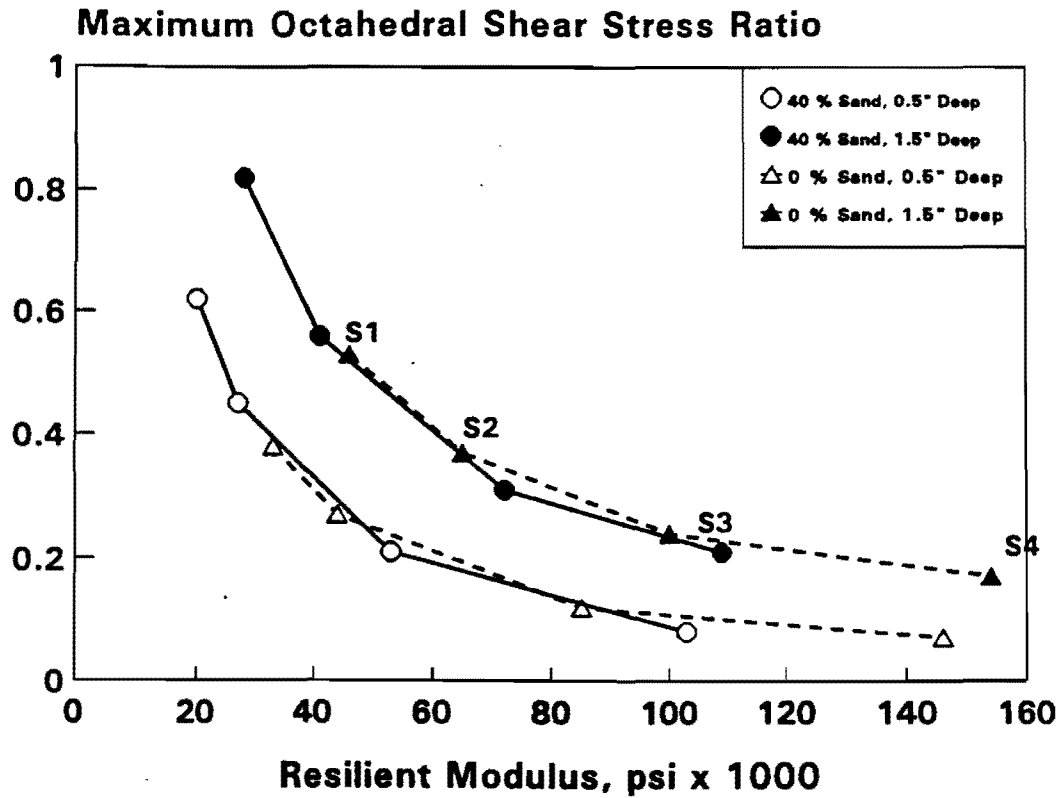


Figure 4.13. Maximum OSSR Versus Resilient Modulus for First Two Inches of Surface Layering Traditional Pavement Structure Under Single Tire Loading. (After Perdomo (1991)).

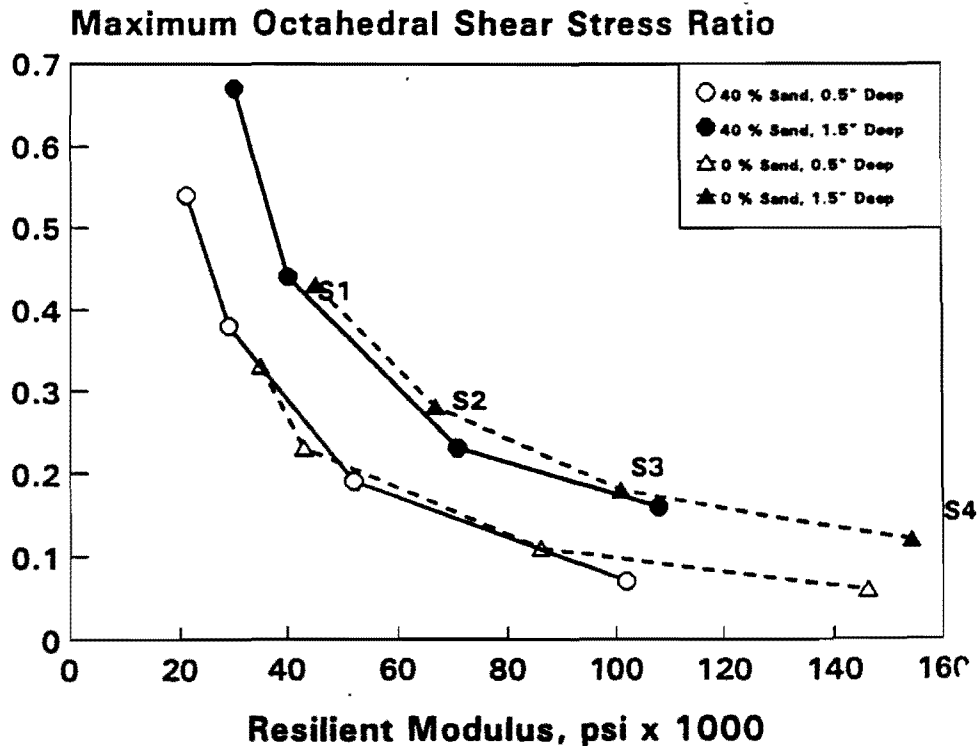


Figure 4.14. Maximum OSSR Versus Resilient Modulus for First Two Inches of Surface Layer in Traditional pavement Structure Under DUAL Tire Loading. (After Perdomo (1991)).

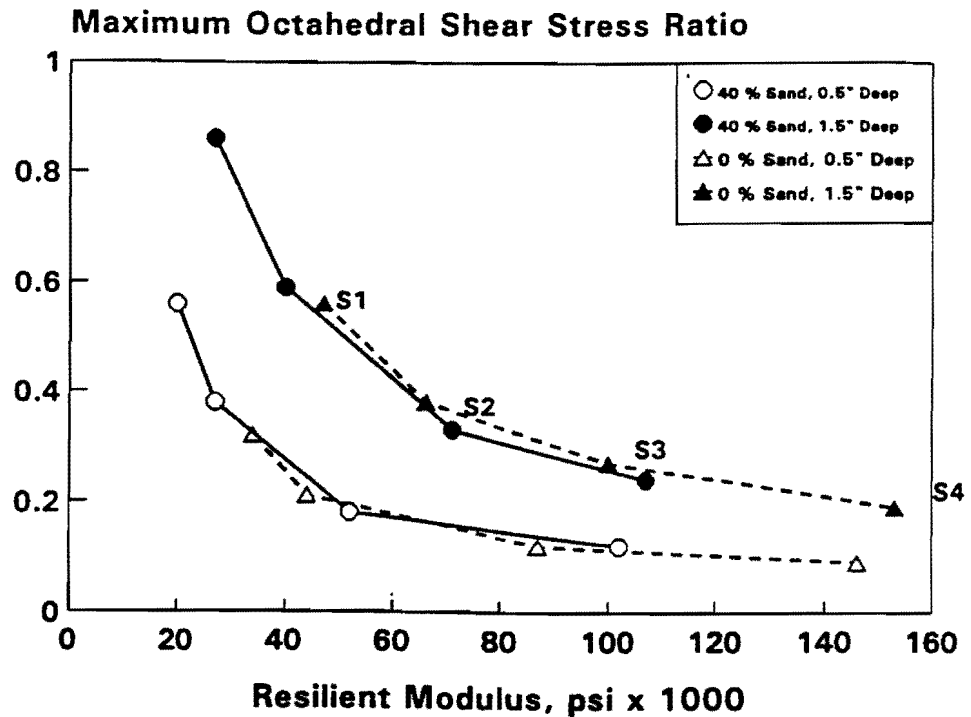


Figure 4.15. Maximum OSSR Versus Resilient Modulus for First Two Inches of Surface Layer in Asphalt Treated Base Pavement Structure Under Single Tire Loading. (After Perdomo (1991)).

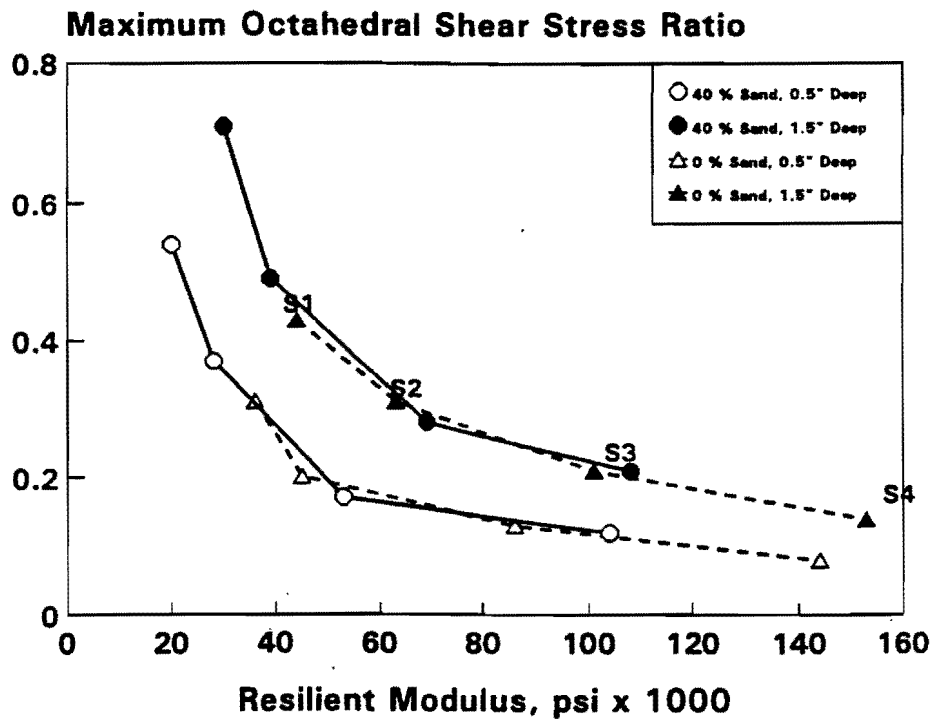


Figure 4.16. Maximum OSSR Versus Resilient Modulus for First Two Inches of Surface Layer in Asphalt Treated Base Pavement Structure Under DUAL Tire Loading. (After Perdomo (1991)).

Perdomo (1991) stated that the octahedral shear stress ratio contours "illustrate a novel way" of representing failure potential within a particular pavement structure (Figures 4.9 and 4.12). Furthermore, Figure 4.13 through 4.16 contribute considerably to the overall analysis of the potential for rutting in a particular asphalt concrete mixture. The maximum octahedral shear stress ratios are plotted against resilient modulus for the first two sublayers of the asphalt concrete surface layer. The four seasons analyzed are plotted as points on the curves (S1 through S4), with a season convention given for only one of the curves (first point on the left corresponds to season 1). For the hottest season (season 1), it is observed that the potential for failure in the first inch of the surface layer is 1.6 to 1.8 times higher for a 40 percent natural sand mix than it is for a zero percent natural sand mix.

Figure 4.13 through 4.16 summarize the results obtained from the octahedral shear stress analysis. Perdomo (1991) conducted the following from the figures:

1. For both pavement structures (cases 1 and 2), under both single and dual tire loading conditions, there seems to be a critical modulus value. Above this critical value, variations in the mix characteristics have no major influence on the maximum octahedral shear stress ratio values for the first inch of the pavement structure. This fact may indicate that octahedral shear stress theory should be limited to the analysis of shear strength data collected at relatively high temperatures due to the overpowering influence (on shear strength) of the cohesive strength of the asphalt at low temperatures. Furthermore, it is well known that 80 percent (and more) of the permanent deformation in an asphalt concrete mixture occurs during the hottest periods of the year (modulus values are easily below 100,0000 psi in the first sublayer). Permanent deformation and creep analysis can be considered complementary tools when using octahedral shear stress theory to analyze rutting potential.
2. If one concentrates solely on analyzing the first inch of the pavement structure, based on the fact that most of the rutting occurs in this first sublayer, one can tell from the figures that

in all cases the potential for rutting, during the two hottest seasons (season 1 and 2), is 1.6 to 1.8 times greater for the 40 percent sand mix than it is for the 100 percent limestone mix.

3. Finally, the octahedral shear stress analysis results emphasize the fact that a mixture containing high percentages of natural sand is much more susceptible to rutting than a mixture that does not contain any natural sand (other variables being constant).

Little (1992) performed an analyses using the OSSR similar to that performed by Perdomo.

In Little's analysis (1992) a modified version of the Illipave computer program (1968) was used to calculate octahedral normal and shear stresses. The non-uniform distribution of contact stresses and surface shearing stresses he used were based on a finite element analysis of the effects of the tire carcass on contact stress distribution. This analysis was preformed by Tielking (1986). In this analysis, the wheel load model was a dual load of 6,000 pounds per tire with an inflation pressure of 125 psi. Based on the Tielking model, contact pressures are non-uniform and vary across the contact area between the tire and the pavement surface from 0 to 240 psi. Surface shear stresses induced by tire deformation and rolling of the tire vary non-uniformly across the contact surface from 0 to 70 psi.

The pavement modeled in the OSSR analyses consisted of a 3-inch overlay over an existing asphalt concrete pavement which is 7-inches thick. This, in turn, rests on 10-inches of aggregate base course and a native, highly plastic clay subgrade.

A computer program was written to plot contours of equal  $\sigma_{oct}$ ,  $\tau_{oct}$ ,  $T_{oct}$ , and OSSR for the pavement and loading conditions summarized above. Each plot was prepared for each of four seasons representing conditions in the Dallas, Texas, area.

In this analysis a mixture of AC-20 grade asphalt cement and river gravel aggregate was used as the 3-inch asphalt concrete surface. Tests were performed on mixtures with and with LDPE modification (5 percent). The addition of LDPE substantially improved shear strength and shear strength parameters  $C$  and  $5.\phi$  It also substantially increased the resilient moduli (ASTM D4123) of the mixture at the higher test temperatures. The river

gravel aggregate used in the mixture was a densely graded Brazos Valley river gravel with 20 percent limestone screenings to improve stability. The mixture had an optimum binder content of 5 percent, a VMA of 13 percent and a design air void content of 4 percent.

Parameters C and  $\phi$  are presented in Table 4.3 for the river gravel mixture used in the analysis along with C and  $\phi$  values for a limestone mixture (85 percent crushed limestone and 15 percent field sand) with two different AC-20 grade asphalts: with and without LDPE modification.

Table 4.3. Summary of C and  $\phi$  Values for Various Limestone and River Gravel Mixtures with and without Polymer Modification. (After Little (1992)).

Mixture Identification			Shear Strength Parameters	
Binder	Binder Content	Aggregates	$\phi$ degrees	C, psi
AC-20	opt.	crushed limestone (CLS)	35	40
AC-20	opt. + 0.4%	CLS	25	50
AC-20 - 4.3% LDPE	opt. + 0.4%	CLS	35	85
AC-20 - 6.0% LDPE	opt.	CLS	30	100
AC-20 + 6.0% LDPE	opt. + 0.4%	CLS	35	120
AC-20	opt.	River Gravel (RG)	28	25
AC-20 + 5.0% LDPE	opt.	RG	40	80

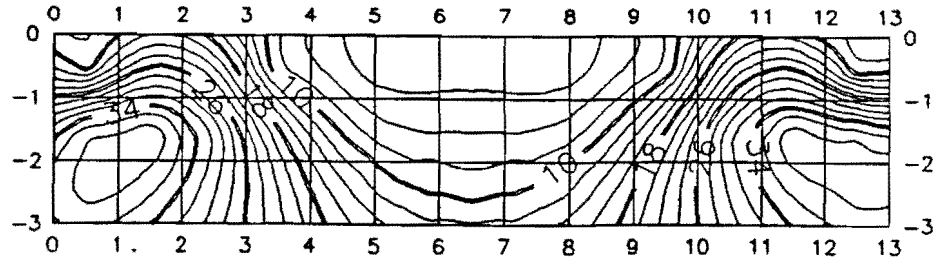
In the analysis the asphalt pavement was divided into sublayers which were assigned stiffness moduli and  $\phi$  and C strength parameters based on mean temperatures within each sublayer. The distribution of temperature with the asphalt surface was calculated by using a model developed by Li, Olsen and Little (1987) based on 30 years of climatic data in the Dallas, Texas, area. The value of stiffness assigned to each sublayer was based on the climatic data and resilient moduli (ASTM D 4123) measured as a function of

temperature. Values of  $c$  were adjusted in direct proportion to resilient moduli values as a function of the temperature in the pavement sublayer to accommodate variations in sublayer shear strength as a function of temperature. This procedure was verified in this study where the ratio of change in shear strength with temperature was demonstrated to be virtually equal to the change in stiffness ratio with temperature.

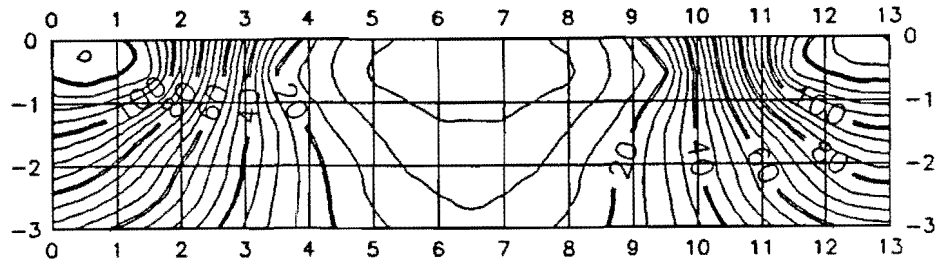
Results of the analyses are presented in Figures 4.17 through 4.19. Figure 4.17 presents induced octahedral shear stresses, octahedral normal stresses, octahedral shear strength and octahedral shear stress to shear strength ratios for the river gravel and AC-20 mixture. The numbers running horizontally across the top of Figures 4.17 through 4.19 represent radial offsets in inches (1-inch = 25.4-mm). The horizontal center of each figure is midway between the dual wheel loads in Figures 4.17 and 4.18. In Figure 4-19 the center of the single tire is designed as the point of zero radial offset. The numbers running vertically in Figures 4.17 through 4.19 are depths below the surface. The surface of the asphalt concrete is designated as zero with depths below the surface designated by negative numbers in inches. Figure 4.18 represents data for an identical mixture as in Figure 4.17 but modified with 5 percent LDPE. Figures 4.17 and 4.18 are only for season 1 which is the critical season for rutting. The relative differences in OSSRs between the two mixtures over the other three seasons were essentially the same as for the critical season.

From these data the following conclusions are drawn:

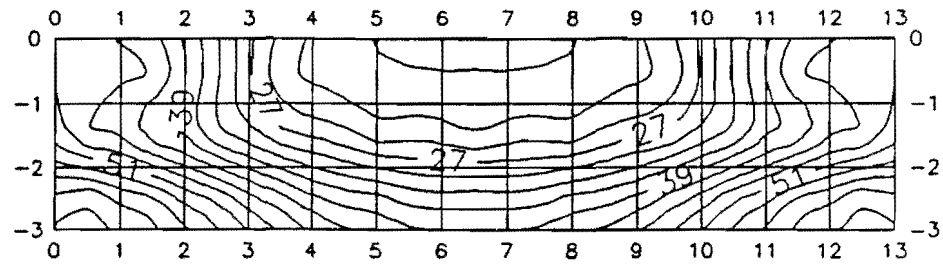
- (1) For season 2 (and for the other three seasons), the induced normal and shearing stresses in the 3-inch overlay are very nearly the same.
- (2) Mobilized shear strength, as represented by shear strength contours are substantially higher in the LDPE-modified asphalt layer than for the unmodified layer. Consequently, maximum OSSRs in the modified layer are approximately 50 percent lower than in the unmodified layer.
- (3) OSSRs for the LDPE-modified overlay are lower than for the unmodified layer by from 50 to 67 percent for seasons 2, 3 and 4.



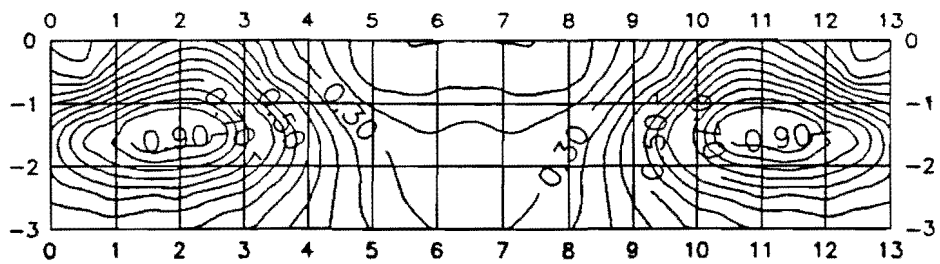
**a**



**b**

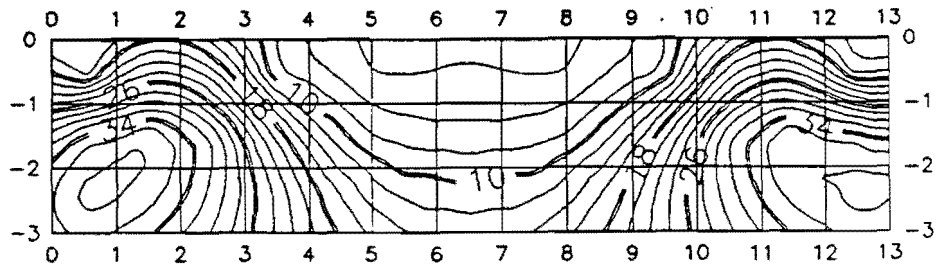


**c**

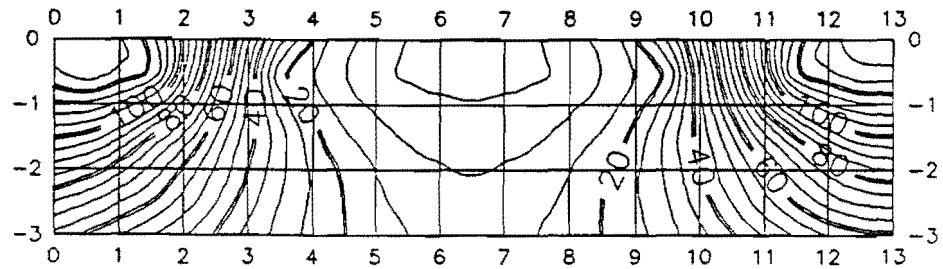


**d**

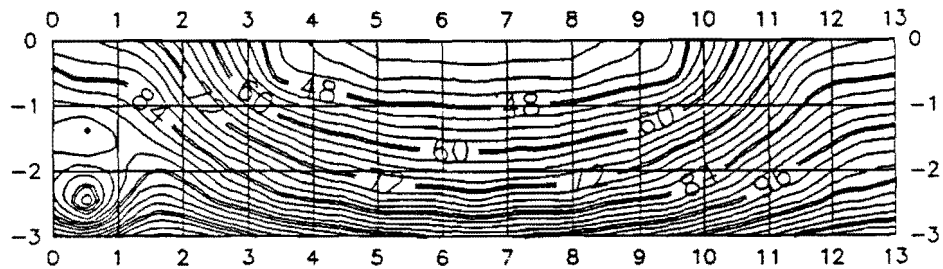
Figure 4.17. Contours of Equal (a) Octahedral Shear Stress, (b) Octahedral Normal Stress, (c) Octahedral Shear Strength and (d) Octahedral Shear Stress to Shear Strength Ratios (OSSRs) for River Gravel and AC-20 Mixtures. (After Little, et al. (1992)).



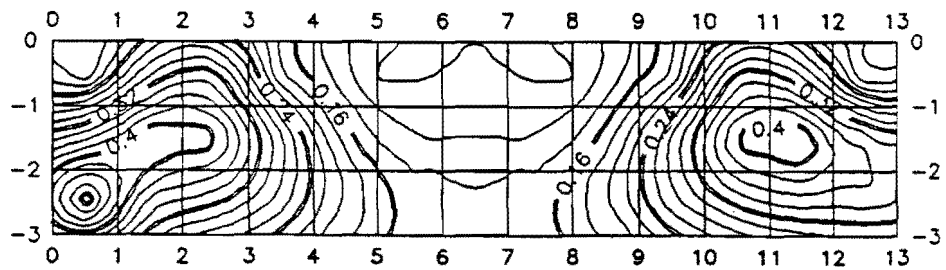
**a**



**b**

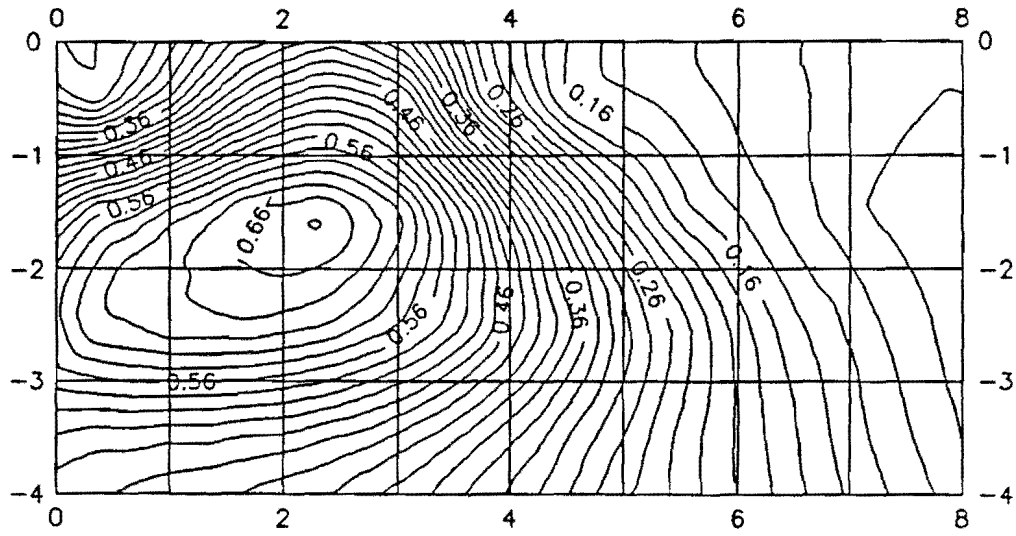


**c**

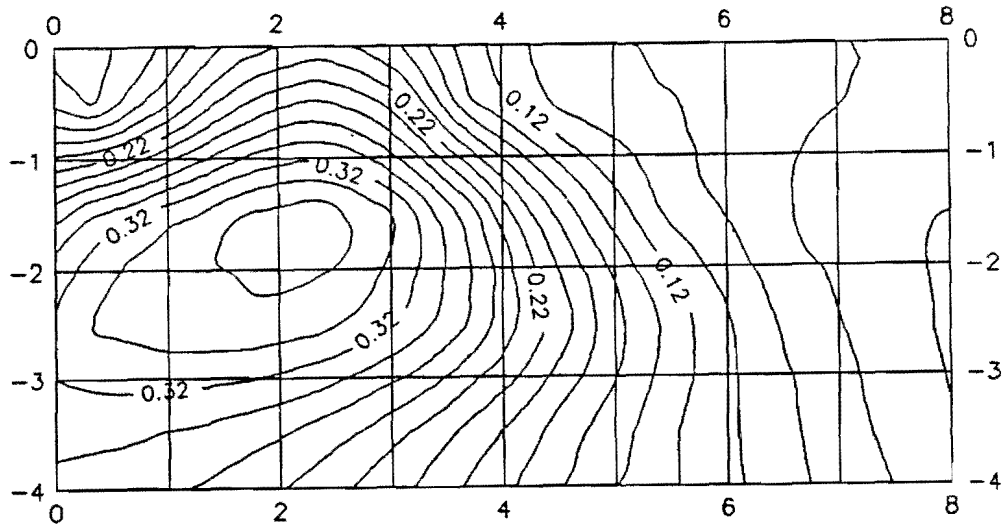


**d**

Figure 4.18. Contours of Equal (a) Octahedral Shear Stress, (b) Octahedral Normal Stress, (c) Octahedral Shear Strength and (d) Octahedral Shear Stress to Shear Strength Ratios (OSSRs) for Mixtures of River Gravel and AC-20 Modified with 5 Percent LDPE. (After Little, et al. (1992)).



**a**



**b**

Figure 4.19. Contours of Equal Octahedral Shear Stress Ratios for River Gravel Mixtures (a) with AC-20 and (b) AC-20 Modified with 5 Percent LDPE for 4-inch Asphalt Concrete Pavement Over 10-inch Aggregate Base. (After Little, et al. (1992)).

Figures 4.19 compares OSSRs for the same mixtures but for a single - 6,000 pound, 125 psi inflation pressure wheel load and a different pavement structure. As in the dual wheel analysis, the normal and shear contact stresses were modeled as non-uniform according to the Tielking model. This pavement structure is a 4-inch asphalt concrete pavement over 12 inches of densely graded aggregate base. The results are, once again, substantially lower maximum OSSRs (approximately 50 percent lower, 0.32 versus 0.68) in the LDPE-modified pavement. This may be interpreted as a 100 percent increase in the factor of safety against shear failure for the LDPE-modified pavement mixture. In this analysis, the maximum OSSR occurs at a depth of about 1.7 inches.

Similar analysis were performed with the crushed limestone mixture (Little, 1992). These analyses demonstrated much higher resistance to shear failure (lower OSSRs for both modified and unmodified mixtures than did the gravel mixtures). The ratios of OSSRs were, as with the river gravel mixture, much lower (approximately 40 to 55 percent lower) for the LDPE-modified mixtures.

Figures 4.20 and 4.21 present the loci of resilient modulus and maximum OSSR, for the four seasons, computed at a given depth ( $z$ ) within the pavement layer. These data are for the 3-inch (75-mm) asphalt overlay over the existing 7-inch (178-mm) existing asphalt pavement. Figure 4.20 compares loci for the four seasons a depth of 0.5 inches (12-mm) below the surface for the river gravel and AC-20 mixtures with and without LDPE. Figure 4.21 compares loci for the four seasons at a depth of 1.5 inches (38-mm) below the surface for the AC-20 river gravel mixture with and without LDPE and for a AC-20 - crushed limestone mixture.

By comparing the loci of resilient modulus and maximum OSSR for each season (seasons 1 through 4 are represented by the points on each curve reading sequentially from left to right for seasons 1, 2, 3 and 4) in Figure 4.21, it is apparent that LDPE modification substantially reduces OSSR (approximately 50 percent) and a significant increase in resilient modulus.

Figure 4.21 presents the same results at  $z = 1.5$  inches (38-mm) below the surface. In this figure the reduction in maximum OSSR and the increase in resilient modulus are similar when the control mixture (AC-20 plus river gravel) is modified with 6.0 percent LDPE or when the aggregate is changed

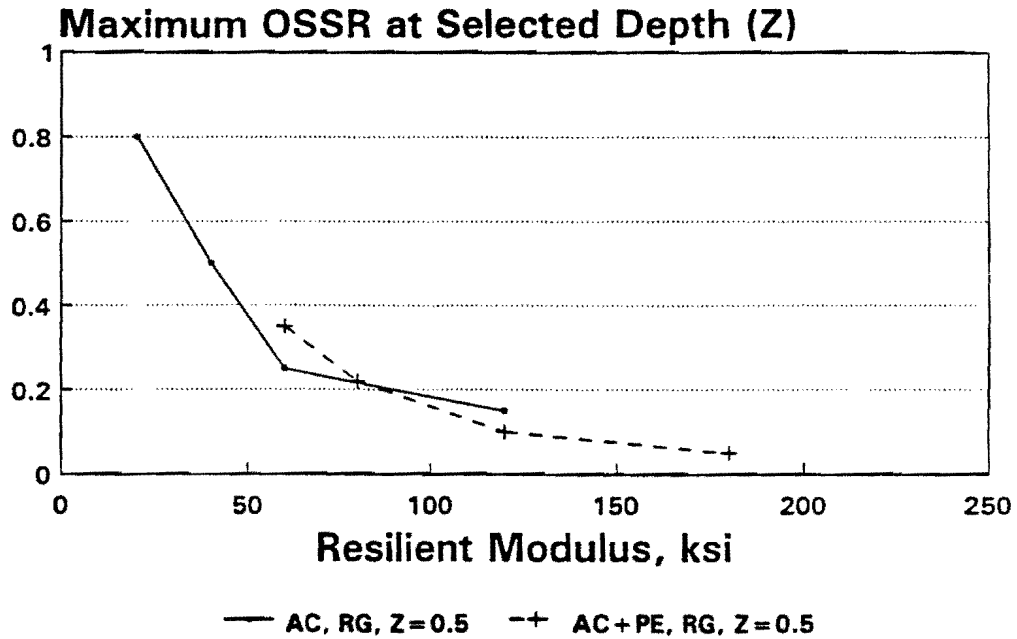


Figure 4.20. Loci of Maximum OSSRs at Depth of 0.5 Inches Below the Surface for Mixtures of River Gravel and AC-20 and Mixtures of River Gravel and AC-20 Modified with 5 Percent LDPE. (After Little, et al. (1992)).

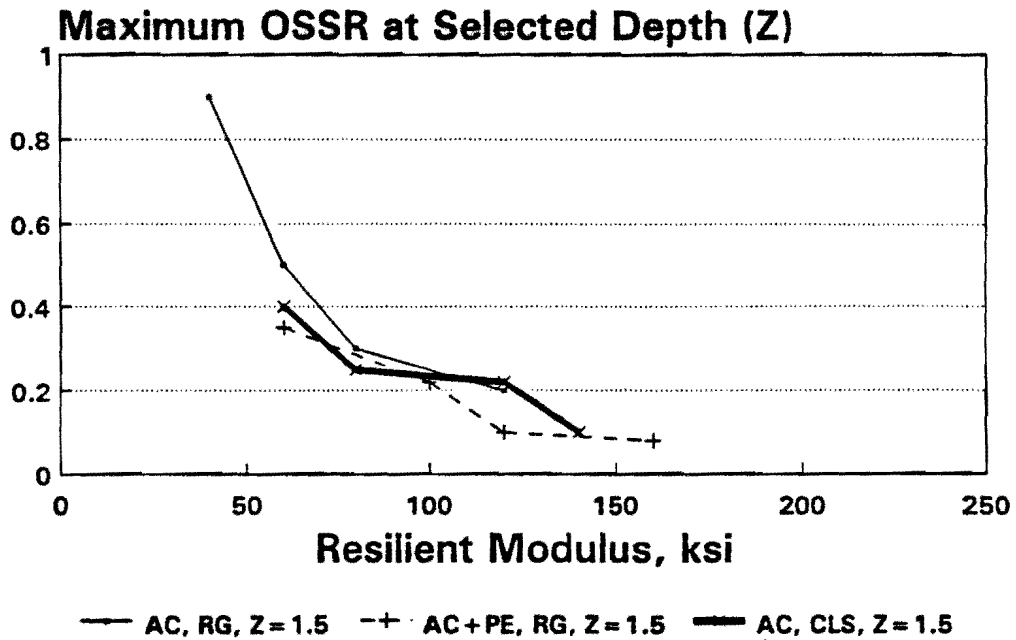


Figure 4.21. Loci of Maximum OSSRs at Depth of 1.5 Inches Below the Surface for Mixtures of River Gravel and AC-20 and Mixtures of River Gravel and AC-20 Modified with 5 Percent LDPE. (After Little, et al. (1992)).

from the rut susceptible river gravel with 20 percent limestone screenings to the more rut resistant crushed limestone with 15 percent field sand. The OSSR analysis has established that LDPE modification of asphalt concrete mixtures can and does substantially increase shear strength in a manner similar to mixture modification through aggregate manipulation. This is probably partly due to the fact that discrete "bundles" of LDPE dispersed in the asphalt thin films act, to a degree, as a reinforcing aggregate within the asphalt film. The result is a higher mass viscosity (high C) and greater internal friction (high  $\phi$ ).

#### **LABORATORY EXPERIMENT TO EVALUATE SENSITIVITY OF TRIAXIAL TEST TO VARIATION IN ASPHALT MIXTURE COMPONENTS**

The same basic test matrix used for evaluation of sensitivity of the uniaxial creep test was used to evaluate sensitivity of the triaxial test. This basic test matrix is defined as follows.

##### **Aggregate Variations:**

- 100% Crushed limestone (CLS) (densely graded)
- 90% CLS + 10% Natural sand (same gradation)
- 80% CLS + 20% Natural sand (same gradation)

##### **Asphalt Cement:**

AC-20

##### **Asphalt Content:**

- Optimum for each mixtures
- Optimum + 0.8 percent
- Optimum - 0.8 percent

##### **Air Voids:**

- 3-5 percent
- 5-7 percent

For each of these 18 combinations of mixture variations triaxial tests

were performed at 0, 30, 60 and 90 psi. This is a total of 68 samples. A loading rates of 2 inches per minute was applied to the 68 basic sample matrix samples prepared at optimum binder content. Twenty-four (24 samples) were also tested at a loading rate or stroke rate of 0.5 inches per minute. The two loading rates allows one to estimate mass viscosity of the mixture and therefore to separate the mixture shear strength into the three components as previous discussed.

In addition to the basic test matrix, triaxial tests performed by Little, (1992) on crushed limestone and river gravel with and without polymer (LDPE) modification provides additional data for evaluation as does work by Perdomo (1990) on mixtures with the same aggregate gradation and same binder as discussed for the primary test matrix except that 40 percent of the crushed limestone was replaced by field sand (natural sand).

The objective of testing samples from these test mixtures are to: (1) evaluate the sensitivity of shear strength (octahedral) parameters  $c$  and  $\phi$  to mixture variables, (2) evaluate the applicability of employing Nijboer's procedure of separating the shear strength into the components of mass viscosity, internal friction and initial resistance, (3) evaluate the potential to use the triaxial test in conjunction with uniaxial creep as a procedure for mixture design and analysis, specifically for specialty pavement conditions and situations. The results of this testing and how these results the above stated objectives will be presented and addressed in the following sections.

#### Details of Laboratory Test Matrix

The same laboratory test matrix which was evaluated in the laboratory creep study was evaluated in the triaxial test sensitivity analysis. The test mixture is comprised of crushed limestone (densely graded) with AC-20 asphalt used as a binder. Samples were varied by replacing portions of the crushed limestone aggregate with field sand--a rounded natural sand. Mixtures were prepared at high (5-7 percent) and low (3-4 percent) air voids. Mixtures were prepared at optimum binder content, binder-rich (optimum plus 0.8 percent) and binder-poor (optimum minus 0.8 percent). Two different loading rates were used (2 inches per minute and 0.5 inches per minute).

The triaxial tests were performed at confining pressures of 0, 30, 60 and 90 psi for each sample. The results of this testing are presented in Appendix C.

From the results summarized in Tables 4.4 and 4.5, the following trends are identified:

1. When compared with creep data, a very definite trend exists between the slope and total strain at one-hour loading, and the results of the triaxial tests. For example, the decrease in  $\phi$  values associated with a change from the 100 percent crushed limestone mixture to the crushed limestone mixtures containing 10 and 20 percent natural sand is from an average value (for all treatments) of approximately 41 degrees to 37 degrees to 33 degrees, respectively. The corresponding drop in the average c value is from 56 to 44 to 39 psi, respectively. The corresponding increase in creep slope values are from 0.32 to 0.42 to 0.42, respectively. The corresponding increase in percent strain at one-hour of loading in the creep test is from 0.58 to 0.90 to failure, respectively.
2. The increase in natural sand in the mixture causes a logical decrease in shear strength as measured by  $\phi$  and c. The increase in sand content in 10 percent increments is readily identified by the triaxial test as reflected in the c and  $\phi$  values.
3. The effect of change in asphalt binder content within a given mixture is not as well defined as is the change in aggregate type. However, a well defined and logical trend does exist as the binder content increases for binder-poor to binder-rich, the c value increases (from 47 to 50 to 56 as a pooled average) and the  $\phi$  values decreased (from 41 to 38 to 33 degrees--as a pooled average). This effect is seen consistently in every mixture.
4. The air void content, generally, has a dramatic influence on  $\phi$  and c values. The stronger mix is almost always the mixture with the lower air void content.
5. The rate of loading influences the cohesive strength, c, of the mixture but has essentially no influence on the mixture internal friction,  $\phi$ . This is as expected and as predicted by Nijboer.

Table 4.4. Summary of Shear Strength Parameters from Triaxial Testing for Three Mixture Types.

Mixture Property	Mixture Identification (AC Content/Air Void Level/Loading Rate)							
	Opt. % AC High-AV 2 in.	Opt. % AC Low-AV 2 in.	Opt. % AC High-AV 2 in.	High % AC Low-AV 2 in.	Low % AC High-AV 2 in.	Opt. % AC Low-AV 2 in.	Opt. % AC High-AV 0.5 in.	Opt. % AC Low-AV 0.5 in.
<u>100% CLS</u>								
$\phi$ , Degrees	40.36	38.42	36.28	33.39	45.73	42.68	40.83	38.83
C, psi	42.48	78.22	44.9	83.81	41.66	73.85	29.2	54.4
$\tau_e$ , psi	24.77	46.46	26.18	49.78	24.3	43.86	24.77	46.46
$\tau_{visc}$ , psi	18.29	31.76	18.72	34.03	17.36	29.99	4.43	7.94
<u>80% CLS - 10% NS</u>								
$\phi$	38.64	37.86	33.89	31.41	40.13	40.28	37.72	35.18
C	36.24	65.11	38.82	72.55	33.34	57.94	23.38	44.94
$\tau_e$	19.09	38.22	20.45	42.62	17.57	34.01	19.09	38.22
$\tau_{visc}$ , psi	17.15	26.89	18.37	29.93	15.77	23.93	4.29	6.72
<u>80% CLS - 20% NS</u>								
$\phi$	35.47	32.22	27.35	24.82	39.87	37.14	33.89	32.68
C	29.6	56.07	33.81	64.58	28.04	46.81	18.78	38.73
$\tau_e$	15.17	32.95	17.33	37.95	14.37	27.5	15.17	32.95
$\tau_{visc}$ , psi	14.43	23.12	16.48	26.63	13.67	19.31	3.61	5.78

Table 4.5. Summary of Strain at Failure Data from Triaxial Testing on Three Mixture Types.

Mixture Property	Mixture Identification (AC Content/Air Void Level/Loading Rates)							
	Opt. % AC High-AV 2 in.	Opt. % AC Low-AV 2 in.	Opt. % AC High-AV 2 in.	High % AC Low-AV 2 in.	Low % AC High-AV 2 in.	Opt. % AC Low-AV 2 in.	Opt. % AC High-AV 0.5 in.	Opt. % AC Low-AV 0.5 in.
<u>100% CLS</u>								
$\sigma_3=0$	1.37	1.71	1.48	1.87	1.79	1.23	1.19	1.04
$\sigma_3=30$	2.21	2.16	2.50	2.08	2.13	2.03	2.70	2.43
$\sigma_3=60$	3.63	2.98	3.99	2.84	2.82	4.14	3.73	3.33
$\sigma_3=90$	4.60	3.70	5.03	3.76	3.76		5.51	5.17
<u>80% CLS - 10% NS</u>								
$\sigma_3=0$	1.58	1.47	1.93	1.75	1.38	1.68	1.30	1.17
$\sigma_3=30$	1.90	1.60	2.22	1.78	1.56	2.19	2.79	2.52
$\sigma_3=60$	2.69	3.05	3.41	2.27	2.17	2.92	3.60	3.28
$\sigma_3=90$	5.11	3.51	5.75		3.09		4.15	
<u>80% CLS - 20% NS</u>								
$\sigma_3=0$	1.08	1.58	1.52	1.30	0.97	1.14	1.10	1.24
$\sigma_3=30$	2.30	1.98	2.11	2.58	1.89	1.76	2.29	2.22
$\sigma_3=60$	3.31	2.75	3.04	3.79	2.76	2.82	3.34	3.27
$\sigma_3=90$	4.27	2.99	3.67	4.87	3.83			

6. The value of mass viscosity,  $\eta_m$ , is influenced by air void content where  $\eta_m$  is significantly increased as air void content goes down. Mass viscosity is not significantly influenced by a change in aggregate.
7. The initial resistance of the mixture,  $\tau_o$ , is sensitive to both air void content and aggregate. The value of  $\tau_o$  is significantly involved as air voids decrease and as the content of natural sand in the mixture decreases.

The  $\tau_{visc}$  (viscous component of shear) and  $\tau_o$  and  $\phi$  sensitivity analysis indicates that a component breakdown of triaxial shear strength (Mohr-Coulomb) data is a reasonable and revealing way to analyze mixtures. The analysis requires performing triaxial tests over a range of confining stresses and at least two loading ratio (i.e., 2 inches per minute and 0.5 inches per minute).

The  $\tau_{visc}$  is much lower for slow loading rates (0.5 in./min.) than for fast loading rates (2.0 in./min.). This is as would be expected. The analysis points out how promising this approach is. More work on a wide variety of mixture types (including more work on polymer-modified mixtures is recommended).

Based on this study, the triaxial test is a sensitive and promising test by which to evaluate shear strength and ultimately deformation potential of asphalt concrete mixtures.

#### Procedure for the Evaluation of Triaxial Shear Strength Data

The state of stress induced in the pavement layer being analyzed is of critical importance in the evaluation of pavement failure potential due to the development of high shearing stresses. The approach used in Chapter 3 to evaluate the critical stress condition within the pavement layer was to select the lowest value of the ratio of normal to shear stress (NTSR) within the layer. This is the point at which the pavement should be the most susceptible to shearing failure based on the Mohr-Coulomb failure concept:

$$\tau_{oct} = C + \sigma_{oct} \cdot \tan \phi \quad (4.8).$$

Thus, when the octahedral normal stress,  $\sigma_{oct}$ , is low, the development of frictional shearing strength is diminished and the resultant octahedral shearing strength,  $\tau_{oct}$ , is diminished. This concept was followed in the evaluation of data from confined triaxial shear strength testing.

Figures 4.22 through 4.27 present representative stress contours (octahedral shearing stress, octahedral normal stress, NTSR and octahedral shear stress ratio, OSSR) for a pavement consisting of a 2 inch asphalt concrete overlay over 8 inches of portland cement concrete pavement. The pavement is subjected to a rolling wheel which induces some surface shear due to the rolling action of the tire. The stresses presented in these figures are induced in a hot season in a typical Texas locality where the average pavement temperature is 104°F. The Tielking (1986) tire model used to calculate these stresses is based on a bias tire where the distribution of normal stresses is not uniform. The highest stresses (both normal and shearing) in such a tire carcass are near the edge of the tire. It is clear from Figure 4.22 that the octahedral shearing stresses developed within the 2 inch overlay are, on the average, highest at or near the edge of the tire (approximately 2.25 inches from the centerline of the tire). Figure 4.22 confirms that the NTSR is, on average, lower at or near the edge of the tire than near the center of the loaded area. Consequently, in Tables 3.14 through 3.23, the critical NTSR was calculated by averaging the NTSRs over the pavement overlay depth or depth of the asphalt layer at or near the edge of the tire.

Data from triaxial shear strength testing can be used as a powerful analytical tool by evaluating the data in comparison with realistic stress information which occurs within the pavement section in question. This can be done by using the information in Appendix C. The following is a procedure for evaluation of confined triaxial shear strength data:

1. Locate the set of normal octahedral and NTSR contours applicable to the pavement section being evaluated in Appendix C.
2. Calculate the average normal octahedral shear stress and the average NTSR at or near the edge of the tire (approximately 2.5 to 3.2 inches from the centerline for rolling tires--and 2.0 to 2.5 for braking tires).

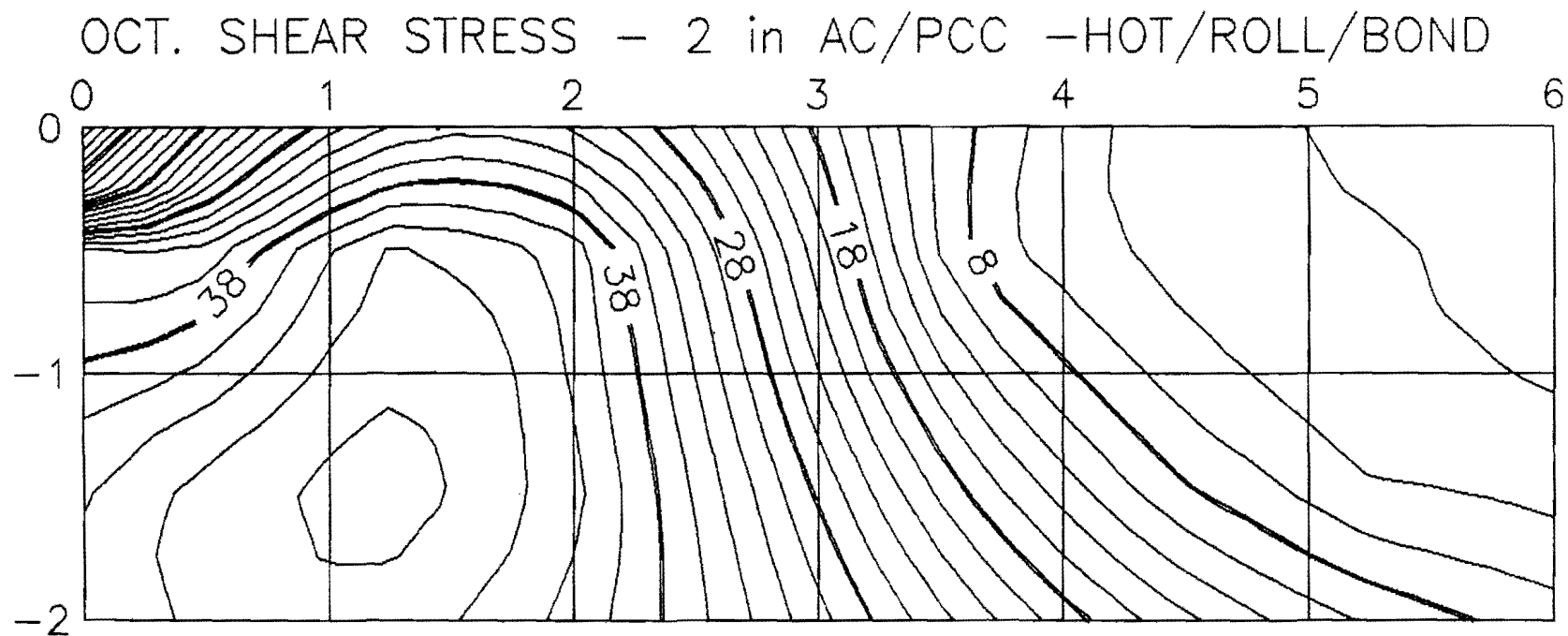


Figure 4.22. Contours of Octahedral Shear Stress in 2 inch AC/PCC Overlay Over PCC Base for a Free Rolling Wheel with Full Bending Between AC/PCC and PCC Layers (Hot Season). Values on Contours are in psi.

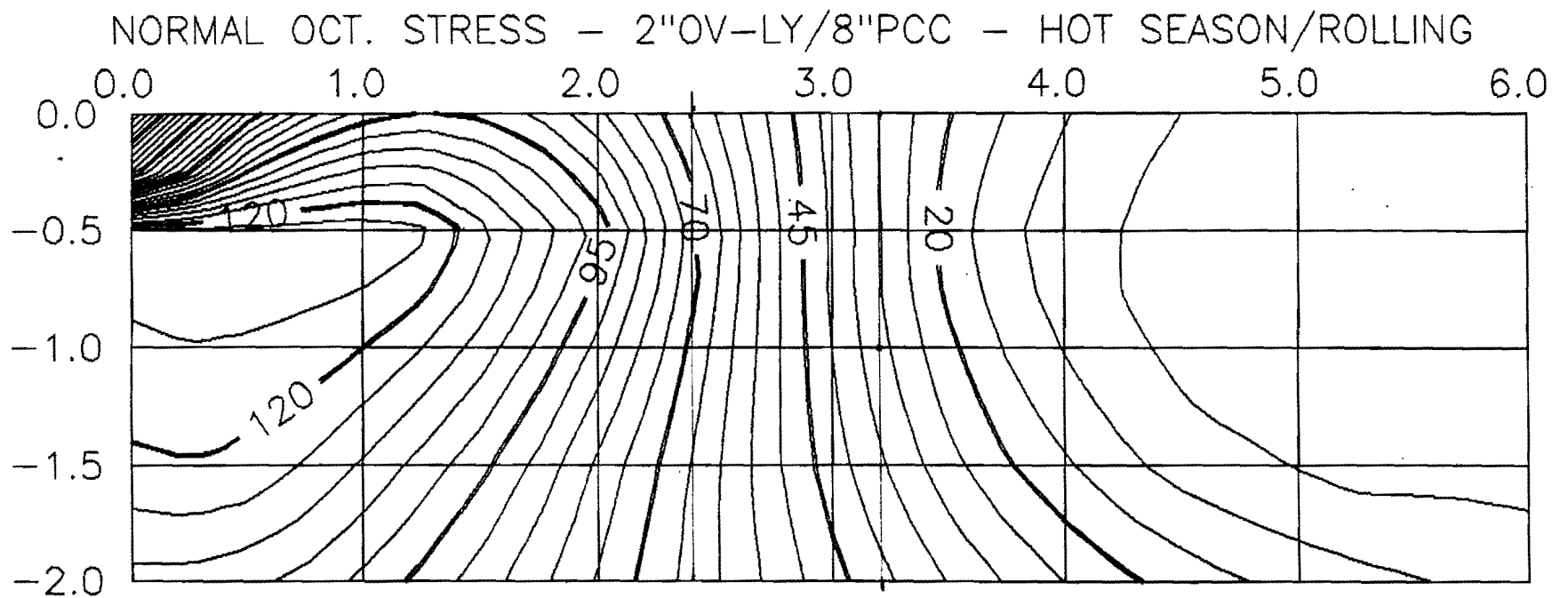


Figure 4.23. Contours of Normal Octahedral Stress in 2 Inch ACP Over PCC Base for a Free Rolling Wheel with Face Bonding Between ACP and PC Layers (Hot Season). Values on Contours are in psi.

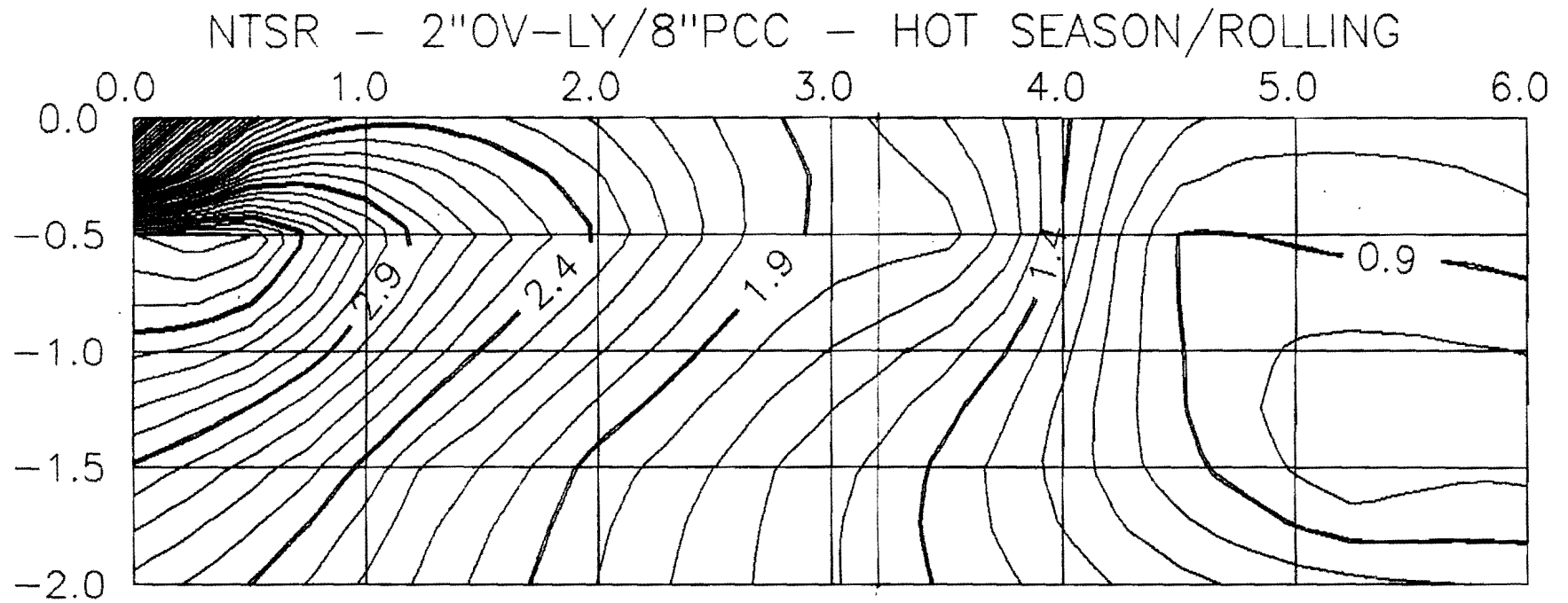


Figure 4.24. Contours of the Ratio of Normal Octahedral Stress to Octahedral Shear Stress (NTSR) in 2 Inch ACP Over PCC Base for a Free Rolling Wheel with Full Bond Between ACP and PCC Layers (Hot Season).

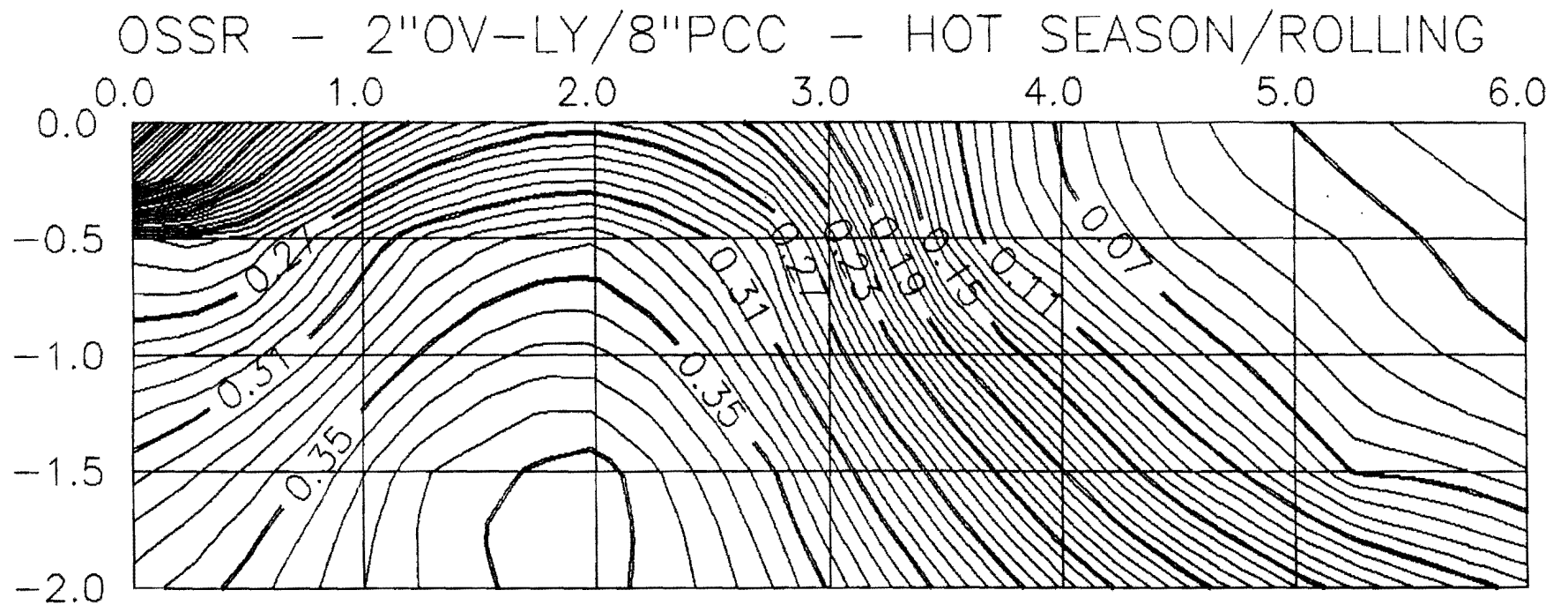


Figure 4.25. Octahedral Shear Stress Ratio (OSSR) Contours Within 2 Inch ACP Overlay Over PCC Base for Free Rolling Wheel With Full Bond Between Layers.

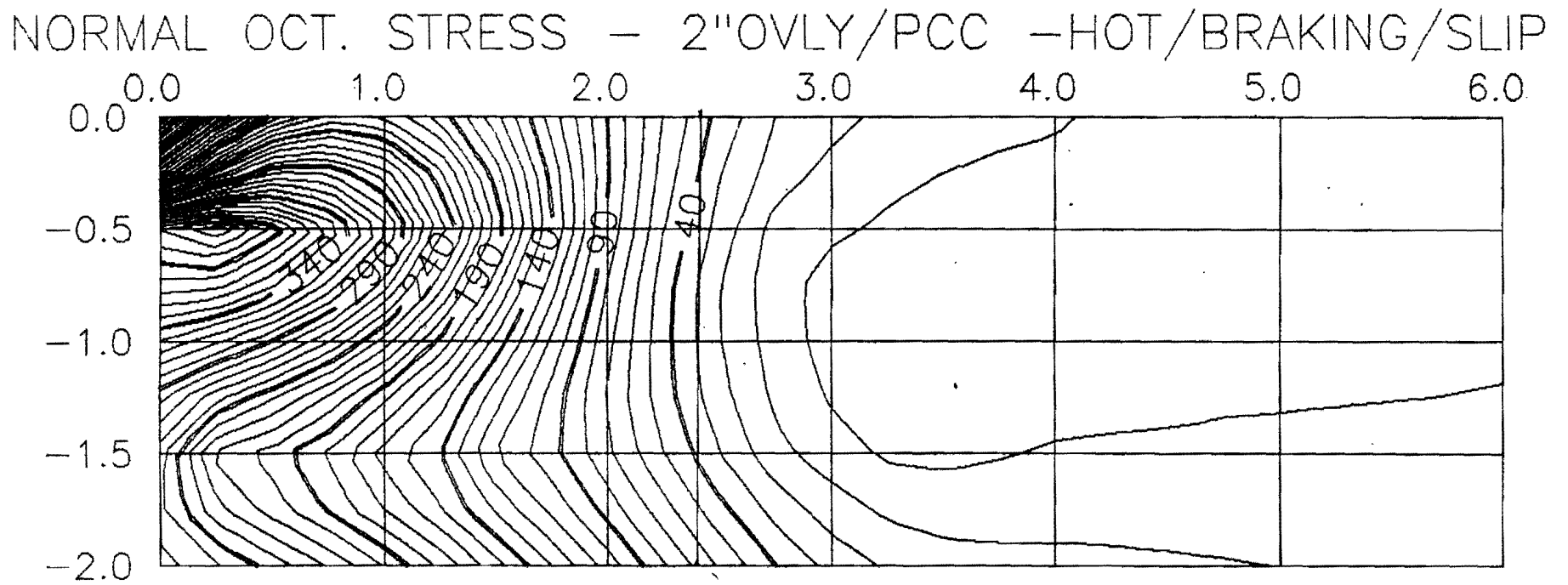


Figure 4.26. Normal Octahedral Stress Contours for 2 Inch ACP Over PCC Base for Braking Wheel with Partial Slippage Between Layers (Hot Season) Values on Contours are in psi.

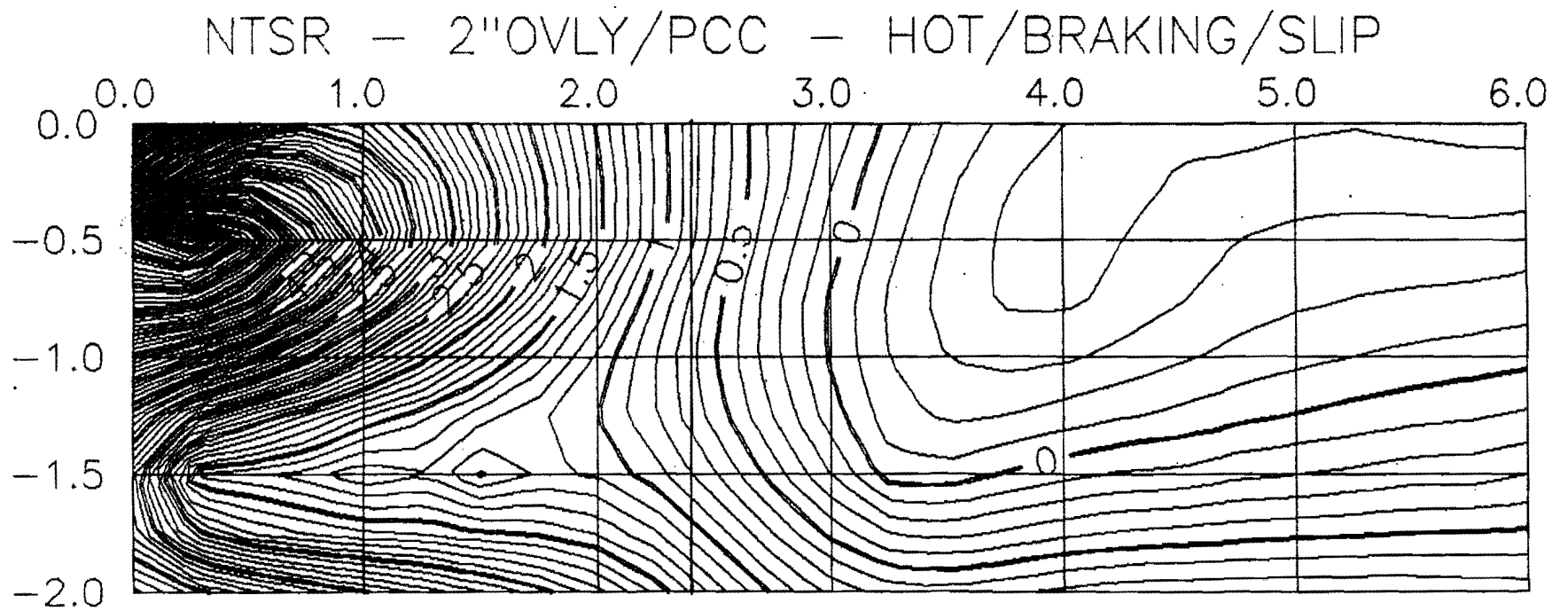


Figure 4.27. NTSR Contours in 2 Inch ACP Over PCC Base for Braking Wheel With Partial Slippage Between Layers (Hot Season).

3. Calculate the average shear stress induced at the critical NTSR (near the edge of the tire) by multiplying the average normal octahedral stress by the average NTSR.
4. Construct a Mohr-Coulomb failure envelop by plotting the Mohr circles representative of the stress conditions of the four tests used to evaluate shear strength (i.e., at 0, 30 60 and 90 psi confining pressures). A representative plot is shown in Figure 4.28. This plot is used to determine the strength parameters of  $c$  and  $\phi$ .
5. Calculate the octahedral shear strength,  $\tau_{oct\ strength}$  associated with the critical stress state identified in the pavement by entering  $c$ ,  $\phi$  and the critical value of  $\sigma_{oct}$  into equation 4.7:

$$\tau_{oct\ strength} = \frac{2.83}{3 - \sin \phi} [\sigma_{oct} \cdot \sin \phi + c \cdot \cos \phi] \quad (4.7).$$

6. Calculate the ratio of induced octahedral shear, as computed in step 3 to octahedral shear strength, as calculated in step 5. This is the octahedral shear strength ratio, OSSR. This value should be as low as possible, generally below about 0.7, in order to resist permanent deformation, shoving and general instability.

Obviously, this procedure is too complex for routine mixture design and/or analysis. However, it can be a valuable and powerful tool by which to evaluate special cases such as thin overlays where heavy braking is expected to occur or where it is suspected that some level of debonding may exist between the surface layer and the underlayer. These cases represent severe stress conditions in the overlay, and this type analysis can provide an evaluation of the relative potential of various mixtures to resist failure in these specific situations caused by severe stress conditions.

As an example of this procedure consider the relatively routine case of a 2 inch overlay over an 8 inch PCC slab as represented in Figures 4.22 through 4.25. The traffic is generally free rolling wheels without severe braking action. Following the procedure discussed above, the average critical NTSR is about 1.9. The average octahedral normal stress at this

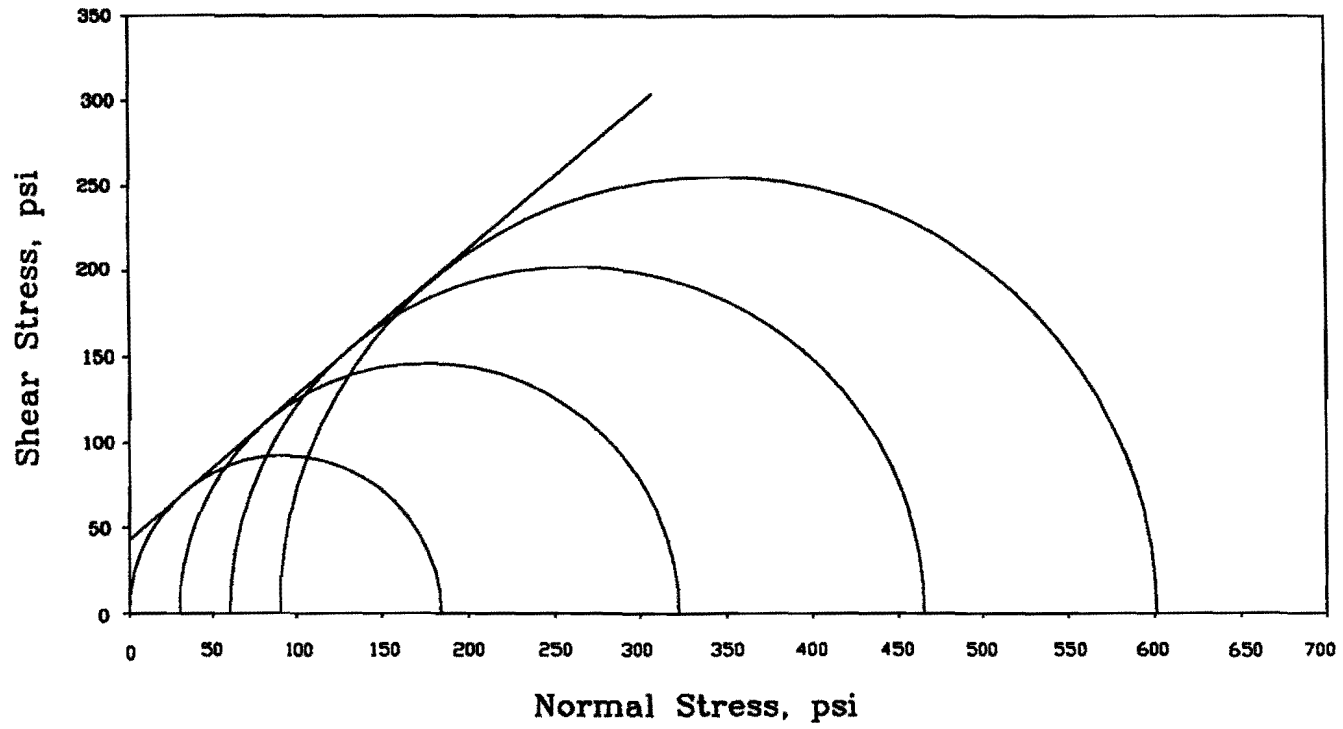


Figure 4.28. Mohr-Coulomb Failure Envelope Developed From Triaxial Testing at Confining Pressures of 0, 30, 60 and 90 psi.

point is approximately 70 psi. The calculated octahedral shearing stress is  $70 \text{ psi} / 1.9 = 36.8 \text{ psi}$ . The  $c$  and  $\phi$  values for the mixture to be used in this environment are 18 psi and 34 degrees, respectively. This is representative of the 20 percent natural sand mixture tested at a loading rate of 0.5 inches per minute. The calculated octahedral shear strength for this mixture at a normal octahedral stress of 70 psi using equation 4.7 is 62 psi. Therefore, the OSSR is  $36.8/62$  or approximately 0.6, which is relatively close to the suggested upper limit of 0.70 but is reasonably resistant to shear. If a change is made to a 40 percent natural sand mixture with  $c$  and  $\phi$  values of 15 psi and 28 degrees, respectively, the calculated OSSR is 0.72, which exceeds the recommended limit of 0.70. If, on the other hand, the 100 percent crushed limestone mixture is used, the OSSR is reduced to 0.41, representing a much more resistant mixture to instability for the stress conditions of this particular pavement structure.

Next, consider a severe environment where the pavements surface is subjected to high braking stresses, such as the pavement at the bottom of an hill where trucks are required to brake quickly. In addition, there is concern for this pavement that some slippage may occur at the interface between the asphalt concrete surface and the PCC base under the braking action of the truck tires because of the use of a fabric interlayer impregnated with asphalt. Slippage is defined as a very small movement between the layers and not full debonding. Consider once again the same pavement structure: 2 inch asphalt concrete overlay over 8 inch PCC base. Close scrutiny of Figures 4.26 and 4.27 reveals that the critical NTSR and octahedral normal stress are approximately 0.6 and 30 psi, respectively. Note that these values do not occur exactly at the edge of the tire contact area, but their position is evident upon evaluation of Figures 4.26 and 4.27. The calculated induced shear stress at this point is  $30/0.6 = 50 \text{ psi}$ . If the 40 percent natural mixture is used, the developed octahedral shear strength is 28 psi. Therefore, this mixture will certainly fail under these demanding stresses since the calculated OSSR is  $50/28 = 1.78$ . If the 100 percent crushed limestone mixture is substituted for the 40 percent natural sand and 60 percent crushed limestone mixture ( $c$  and  $\phi$  values of 29 psi and 40 degrees, respectively), the mobilized shear strength under the induced stress state is 65.2 psi. The calculated OSSR is thus  $50/65.2 = 0.76$ . This

value indicates that the mixture is still in jeopardy of deformation, but the change of aggregate results in an OSSR decrease of from 1.76 to 0.76 or 59 percent). It should also be considered that the reciprocal of the OSSR is a measure of the factor of safety against shear failure. This is by changing from the 40 percent natural sand mixture to the mixture with 100 percent crushed material, the factor of safety is increased from 0.56 to 1.32.

To reduce the OSSR below the 0.65 value considered safe, it would probably be necessary to use a modifier in the mixture. When 5 percent of a polyolefin additive is added to the 100 percent crushed limestone mixture, the triaxial parameters of  $c$  and  $\phi$  are increased to 80 psi and 40 degrees, respectively (Little, 1992). Based on the shear strength parameters, the calculated value of shear strength under the stress conditions induced in the 2 inch overlay over PCC under braking stress and interlayer slippage is 97 psi. The concomitant calculated OSSR is  $50/97 = 0.52$  which is well below the suggested safe value of 0.65.

The critical OSSR value of 0.65 in lieu of 1.00 was developed after considering the performance of pavement sections from IH-20 (Sweetwater), IH-45 (Fairfield), IH-45 (Centerville), IH-20 (Tyler), US 59 (Lufkin) and US 287 (Damas) and from tests on pavement cores from these sections as well as loose mixtures representative of these pavements. The reduced level of critical OSSR from 1.00 to 0.65 represents a correction factor much like that developed by Shell between rutting predictions based laboratory creep data and actual field measurements of rutting. This correction factor,  $c_m$ , was in the range of 1.5 to 2.0 (see Table 3.1). The reciprocal of 0.65 is 1.54 which also falls within this range.

#### Sensitivity of the OSSR Analysis to Mixture Variables

To assess the sensitivity of the OSSR analysis to mixture variables, the following mixtures were evaluated:

Mixture type: 100 percent crushed limestone  
80 percent crushed limestone--20 percent natural sand

Binder content: Optimum and binder-rich (optimum + 0.8%)

Air Void Content: High and low

These mixtures were evaluated based on the OSSR calculated for two pavement types: 4 inches of asphalt concrete over existing asphalt concrete base under free rolling wheels in a hot climatic period and 4 inches of asphalt concrete over existing asphalt concrete base subject to braking stresses in a hot climatic season.

The results of the analyses are presented in Figures 4.29 through 4.40. In these figures the number across the top are the radial offsets in inches from the centerline of the tire, and the numbers listed vertically are the depth in inches below the top of the pavement.

As can be seen from these results, the OSSR analysis is sensitive to mixture component variation. Note that as the percentage of natural sand increases from zero to 20 percent for both free rolling and braking conditions, the OSSR's increase. If Figure 4.29 is compared to Figure 4.34, it is apparent that the mixture with 100 percent crushed limestone, optimum binder content and low air voids (3 to 5 percent), Figure 4.29, is much more resistant to shear induced deformation than the 80 percent crushed limestone and 20 percent natural sand mixture with high binder content and high air voids (5 to 7 percent), Figure 4.34, based on the value calculated for OSSR. This comparison is much more evident when one compares Figure 4.29 and 4.36 for the same mixtures and pavement structures but with the addition of the action of braking stresses. It should also be noted that the influence of mixture component variation is more evident under the action of surface braking stresses as illustrated in Figures 4.35 through 4.40. Note that the influence of the mixture variables is predictable with higher OSSRs in mixtures with higher air void contents (5 to 7 percent in lieu of 3 to 5 percent), binder contents in excess of optimum and in mixtures with higher contents of natural sand (20 in lieu of zero percent).

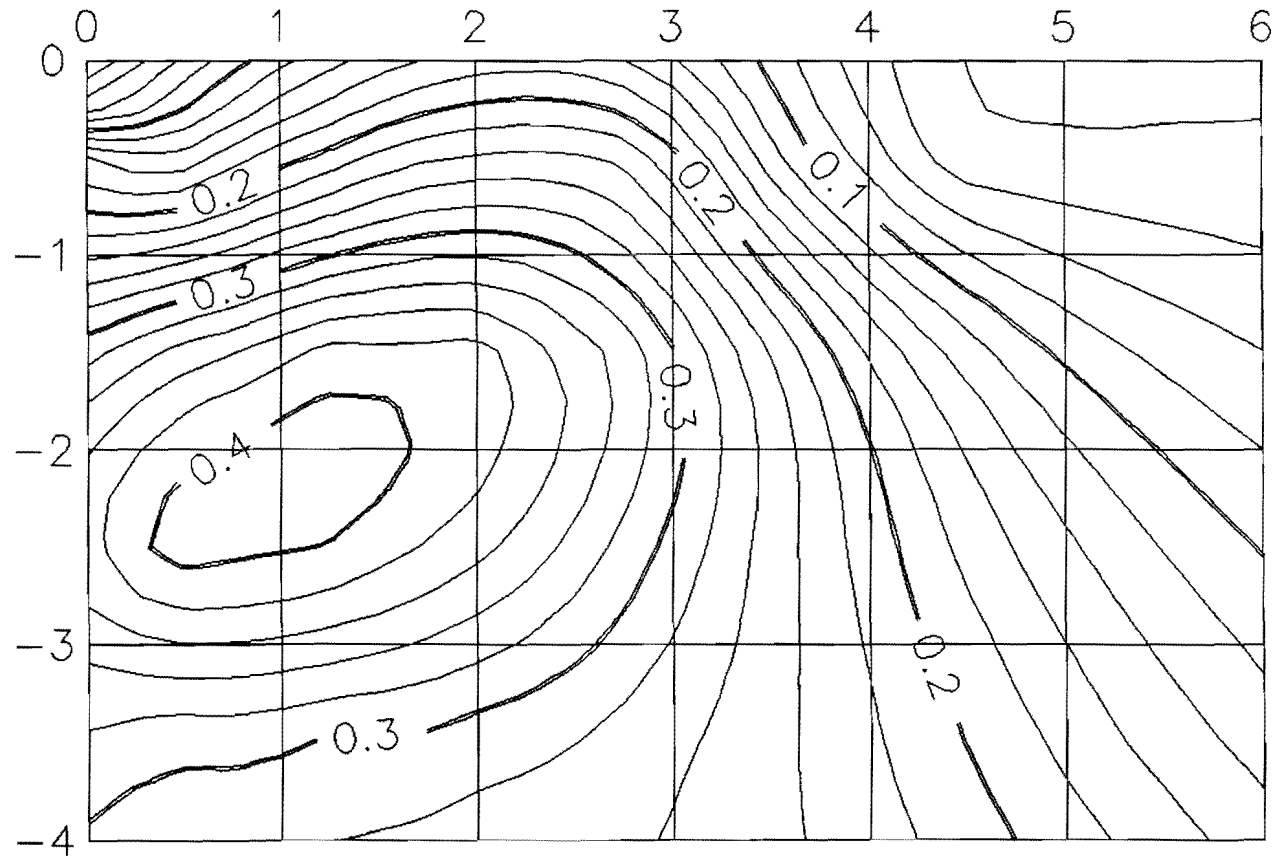


Figure 4.29. OSSR Contours for 4 Inches of ACP Over PCC, 100 Percent Crushed Limestone Mixture, Optimum Asphalt Content, Low Air Voids, Free Rolling Wheel and Full Bond Between Layers (ADT Season).

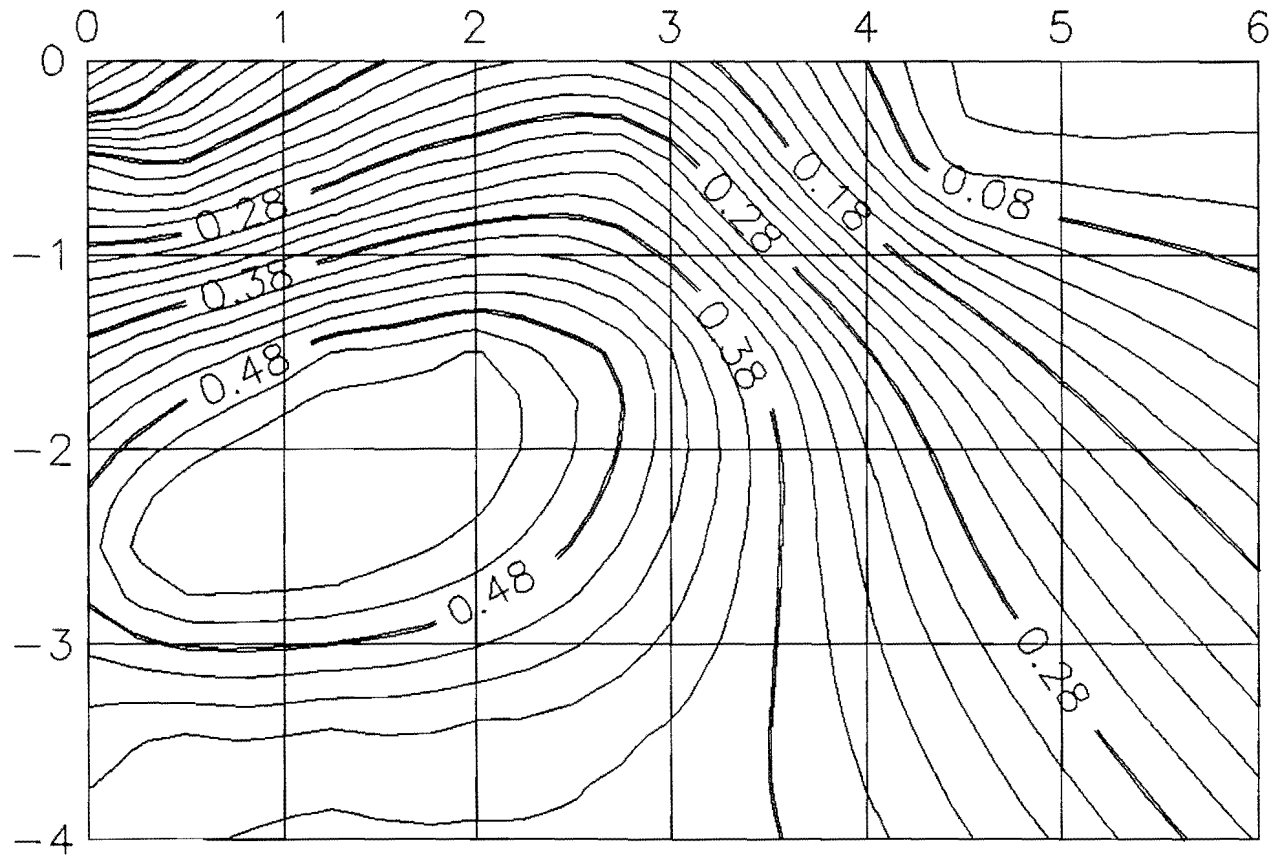


Figure 4.30. OSSR Contours for 4 Inches of ACP Over PCC, 100 Percent Crushed Limestone Mixture, Optimum Asphalt Content, High Air Voids, Free Rolling Wheel and Full Bond Between Layers (ADT Season).

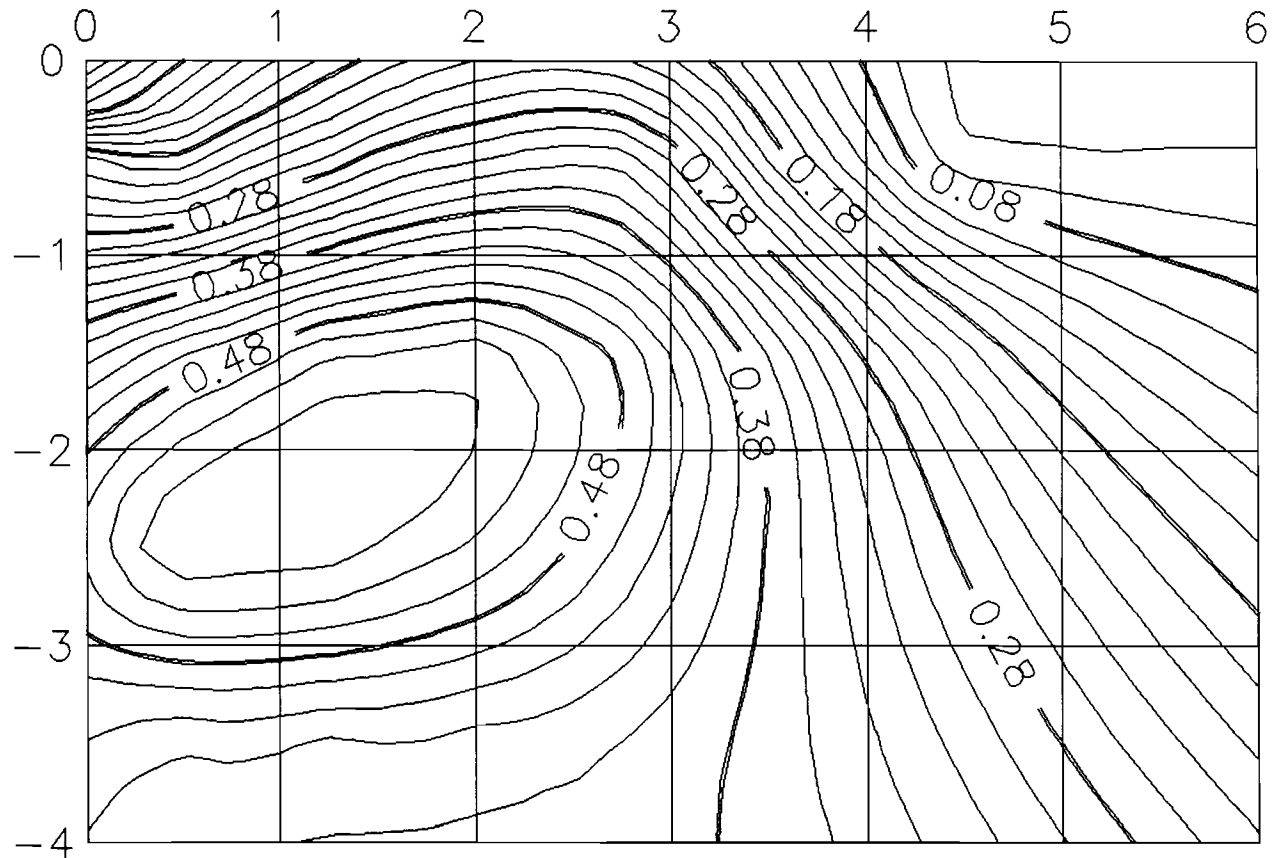


Figure 4.31. OSSR Contours for 4 Inches of ACP Over PCC, 100 Percent Crushed Limestone Mixture, Optimum Asphalt Content, Binder-Rich Mixture, High Air Voids, Free Rolling Wheel and Full Bond Between Layers (ADT Season).

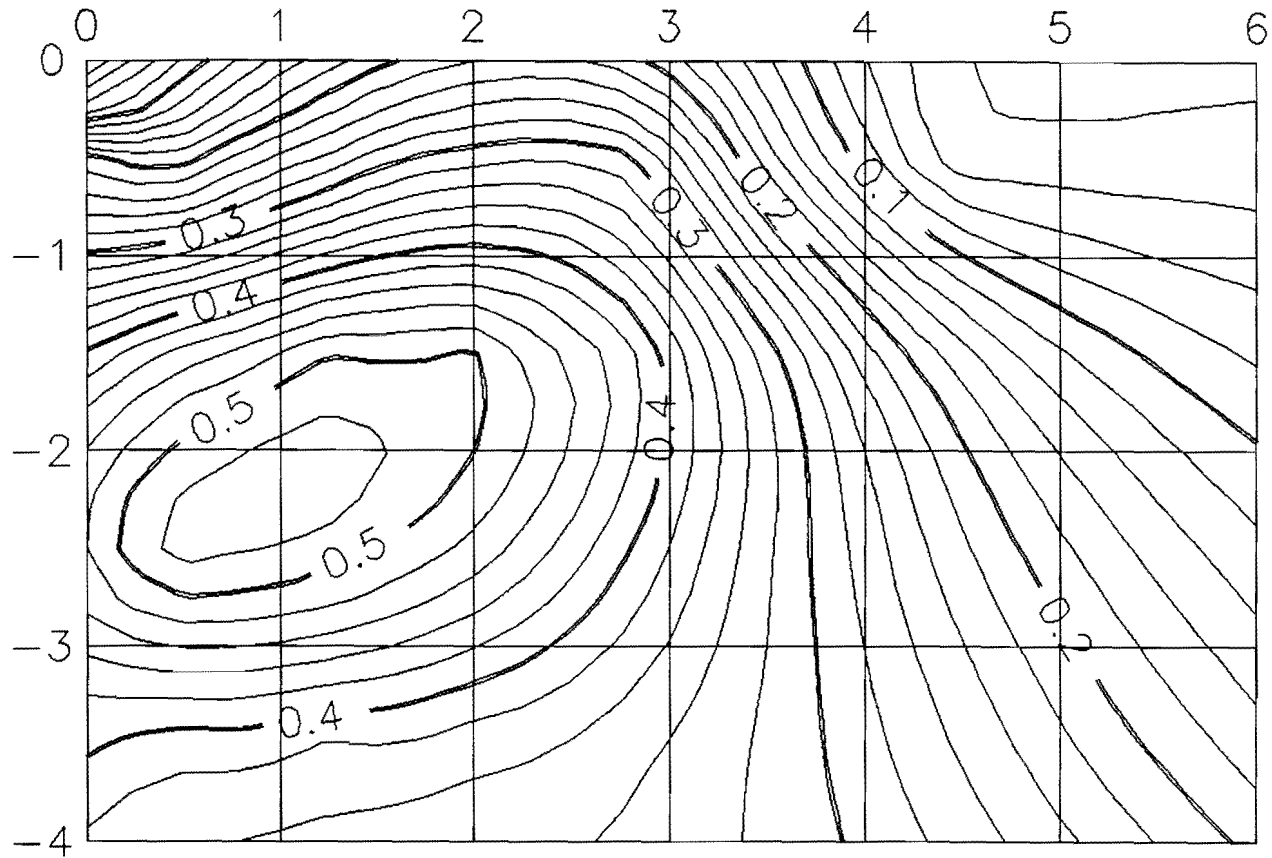


Figure 4.32. OSSR Contours for 4 Inches of ACP Over PCC, 80 Percent Crushed Limestone - 20 Percent Natural Sand, Optimum Asphalt Content, Low Air Voids, Free Rolling Wheel and Full Bond Between Layers (Hot Season).

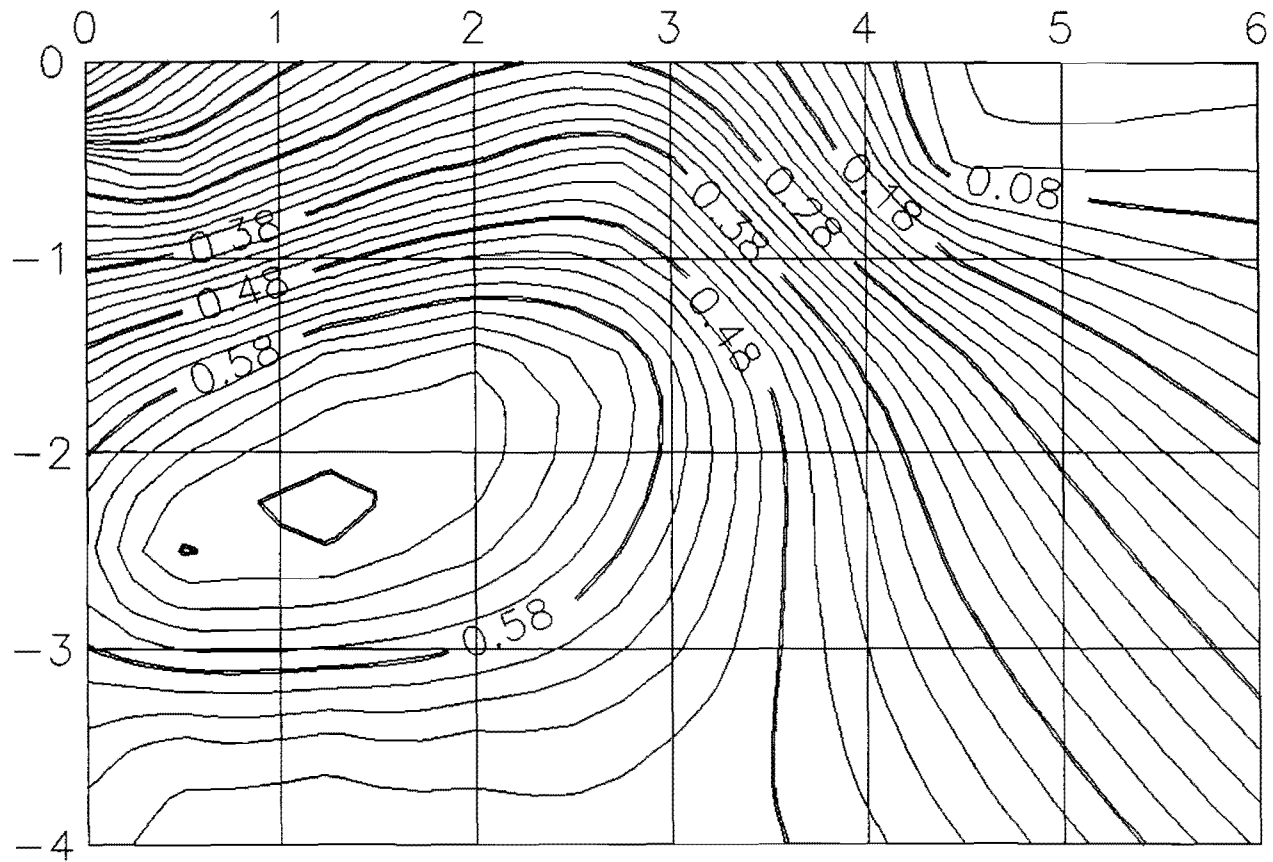


Figure 4.33. OSSR Contours for 4 Inches of ACP Over PCC, 80 Percent Crushed Limestone - 20 Percent Natural Sand, Optimum Asphalt Content, High Air Voids, Free Rolling Wheel and Full Bond Between Layers (Hot Season).

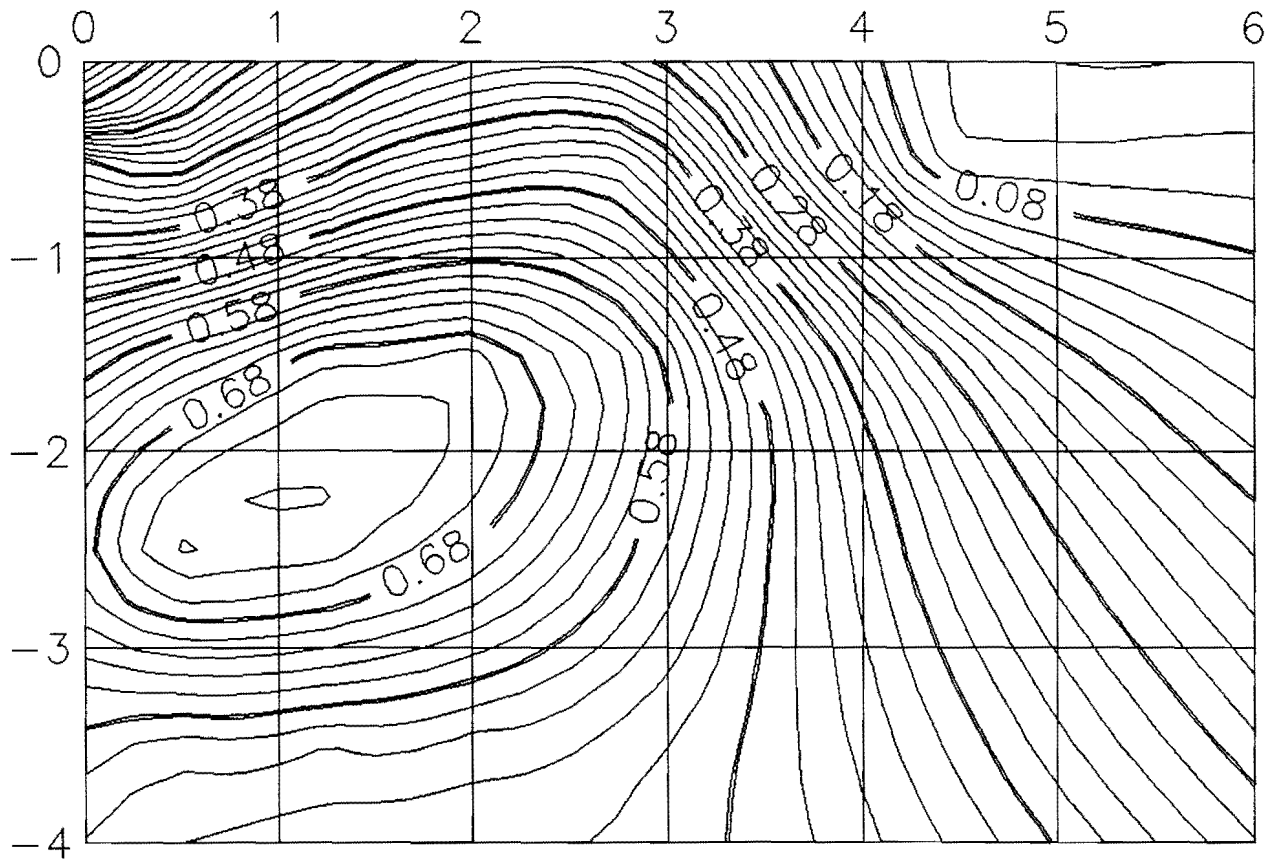


Figure 4.34. OSSR Contours for 4 Inch of ACP Over PCC, 80 Percent Crushed Limestone - 20 Percent Natural Sand, Optimum Asphalt Content, Binder Rich Mixture, High Air Voids, Free Rolling Wheel and Full Bond Between Layers (Hot Season).

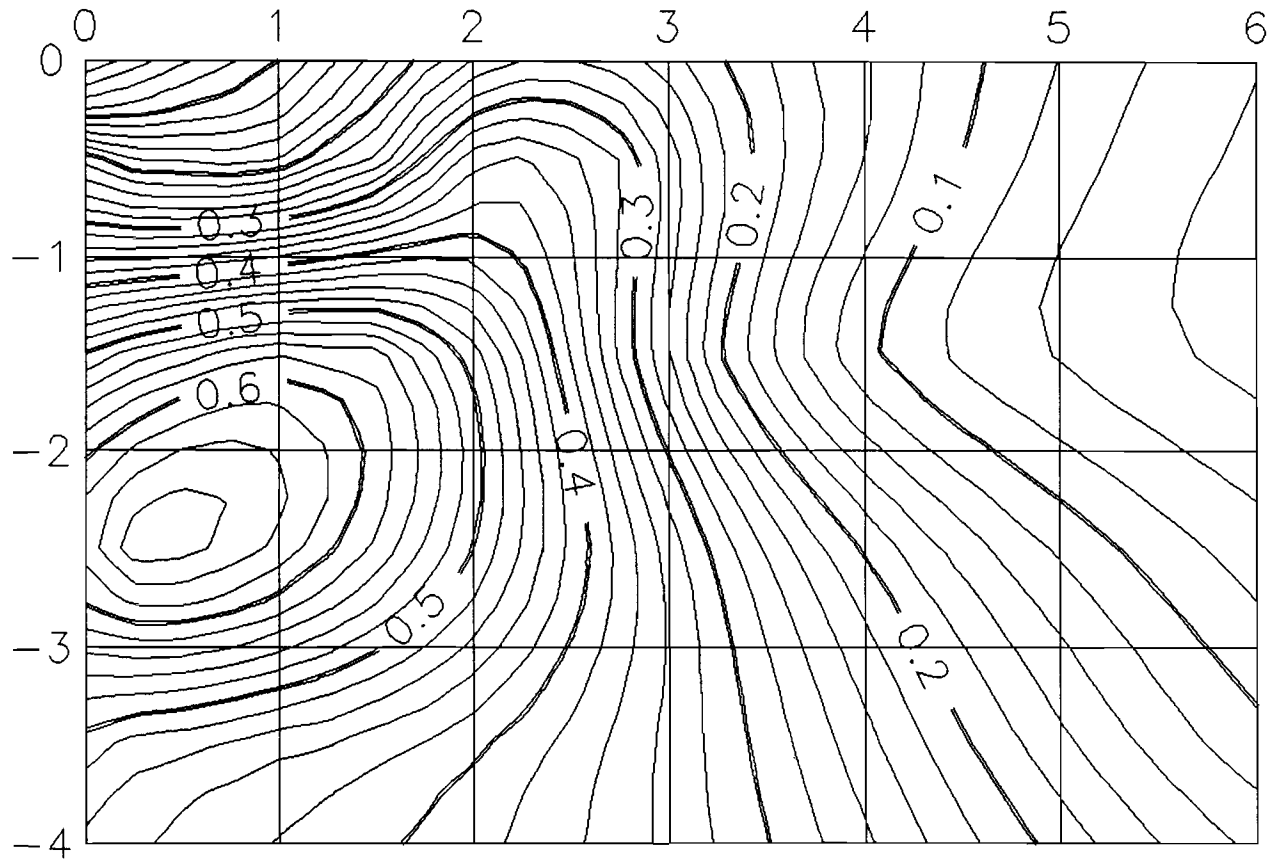


Figure 4.35. OSSR Contours for 4 Inch ACP Over PCC, 100 Percent Crushed Limestone, Optimum Binder Content, Low Air Voids, Braking Induced Surface Stresses, Full Bond Between Layers (Hot Season).

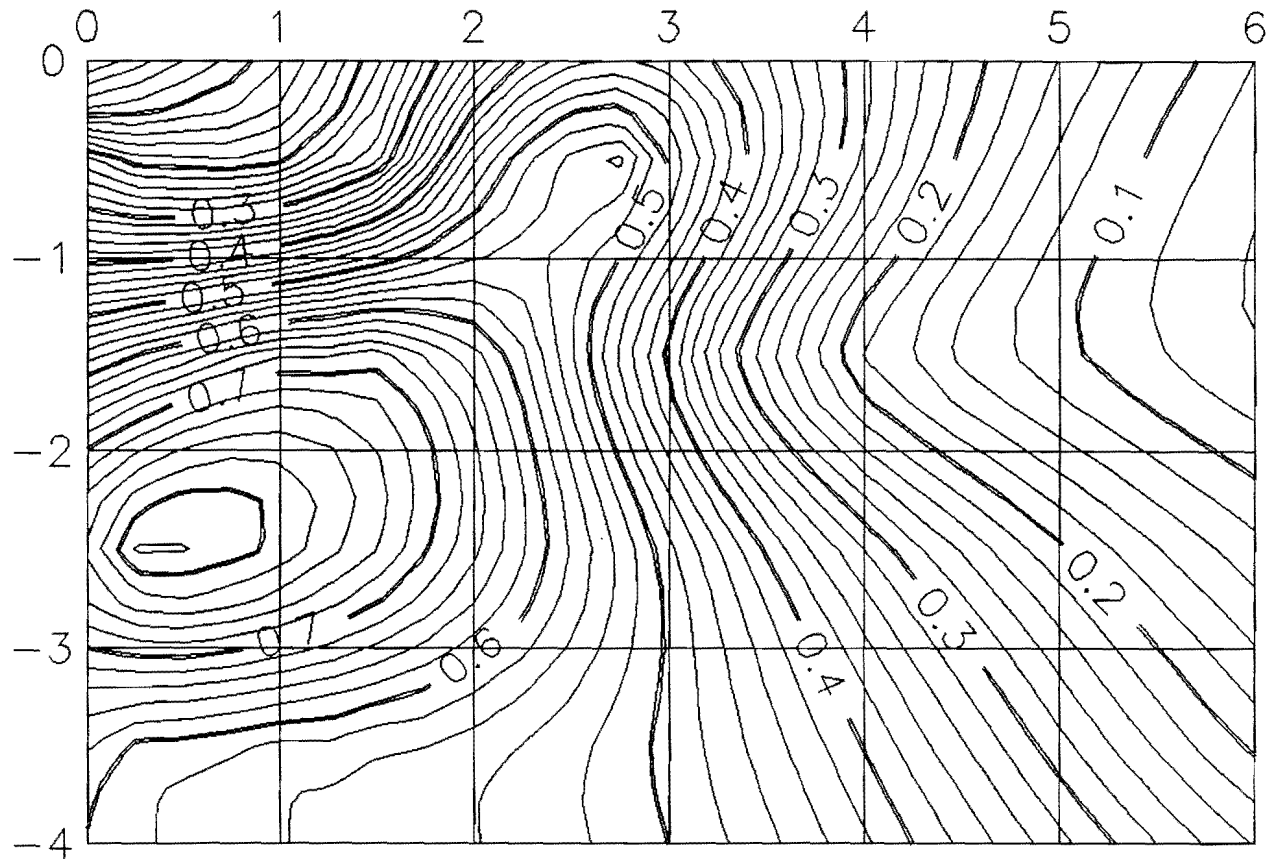


Figure 4.36. OSSR Contours for 4 Inch ACP Over PCC, 100 Percent Crushed Limestone, Optimum Binder Content, High Air Voids, Braking Induced Surface Stresses, Full Bond Between Layers (Hot Season).

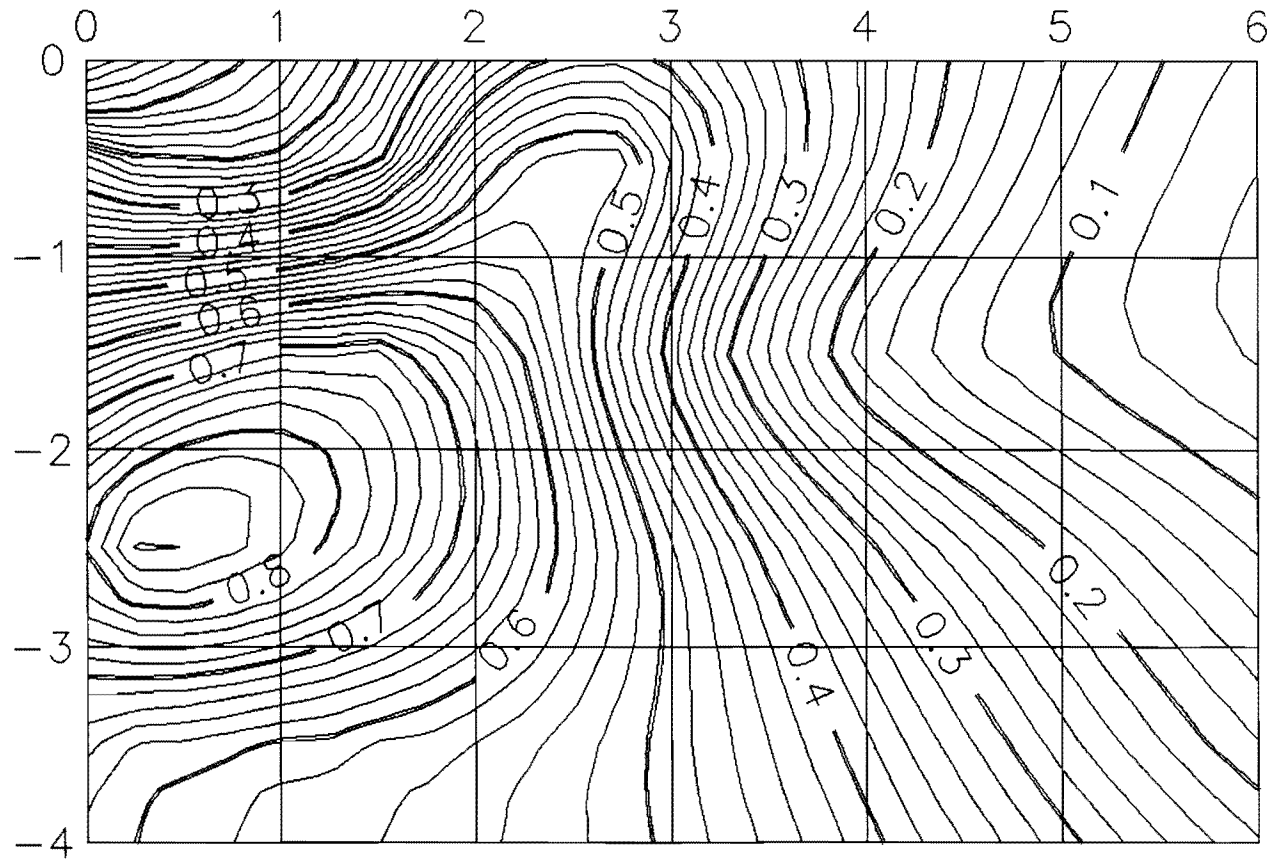


Figure 4.37. OSSR Contours for 4 Inch ACP Over PCC, 100 Percent Crushed Limestone, Binder Rich Mixture, High Air Voids, Braking Induced Surface Stresses, Full Bond Between Layers (Hot Season).

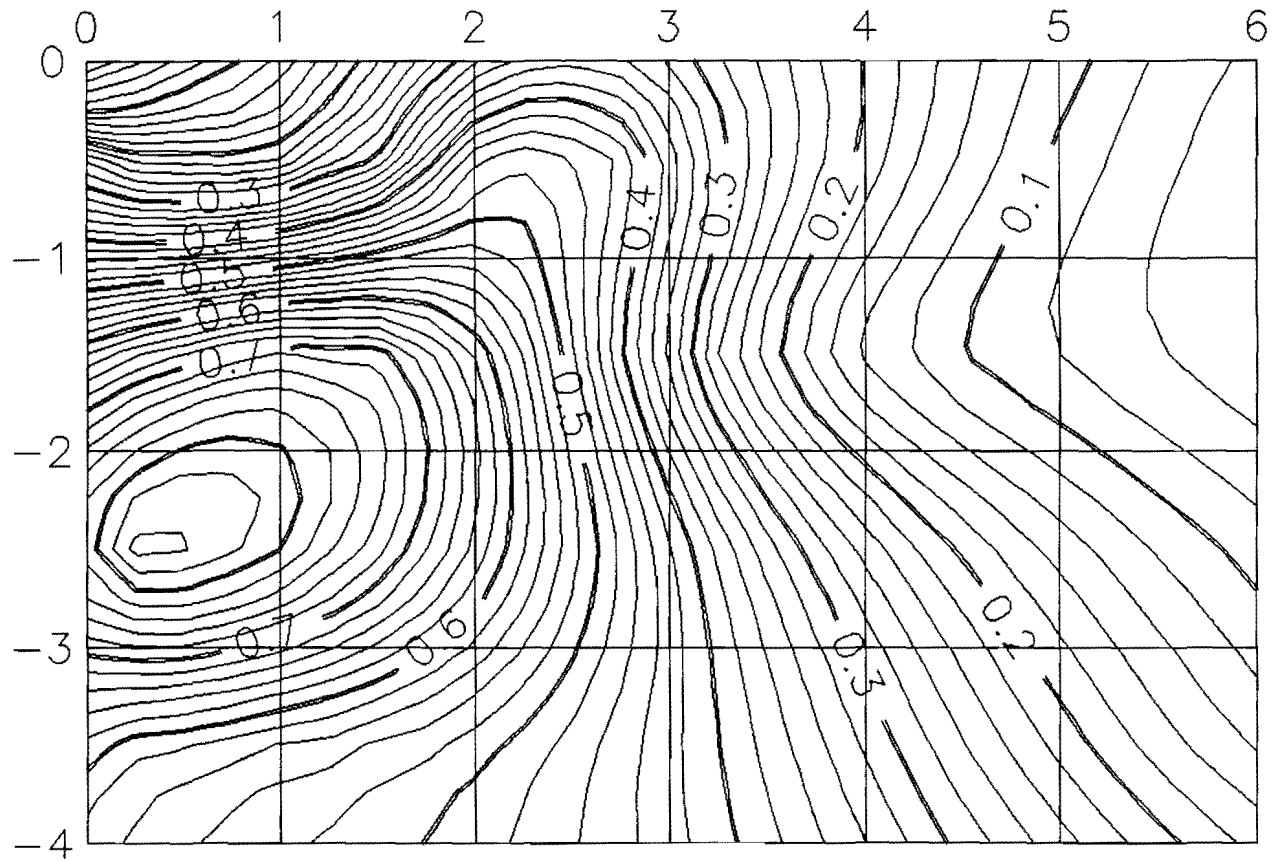


Figure 4.38. OSSR Contour for 4 Inches of ACP Over PCC, 80 Percent Crushed Limestone - 20 Percent Natural Sand, Optimum Asphalt Content, Low Air Voids, Braking Induced Surface Shearing Stresses, Full Bond.

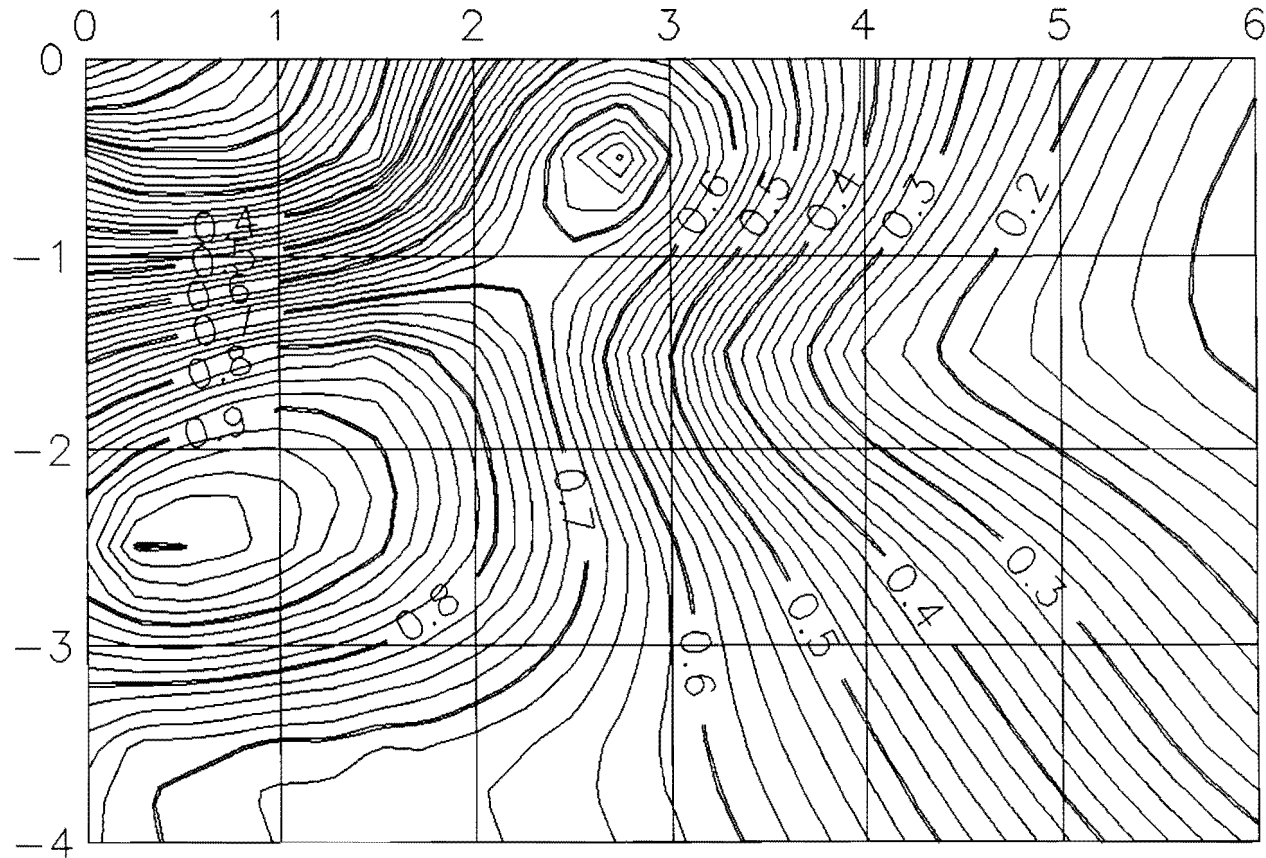


Figure 4.39. OSSR Contour for 4 Inches of ACP Over PCC, 80 Percent Crushed Limestone - 20 Percent Natural Sand, Optimum Asphalt Content, High Air Voids, Braking Induced Surface Shearing Stresses, Full Bond.

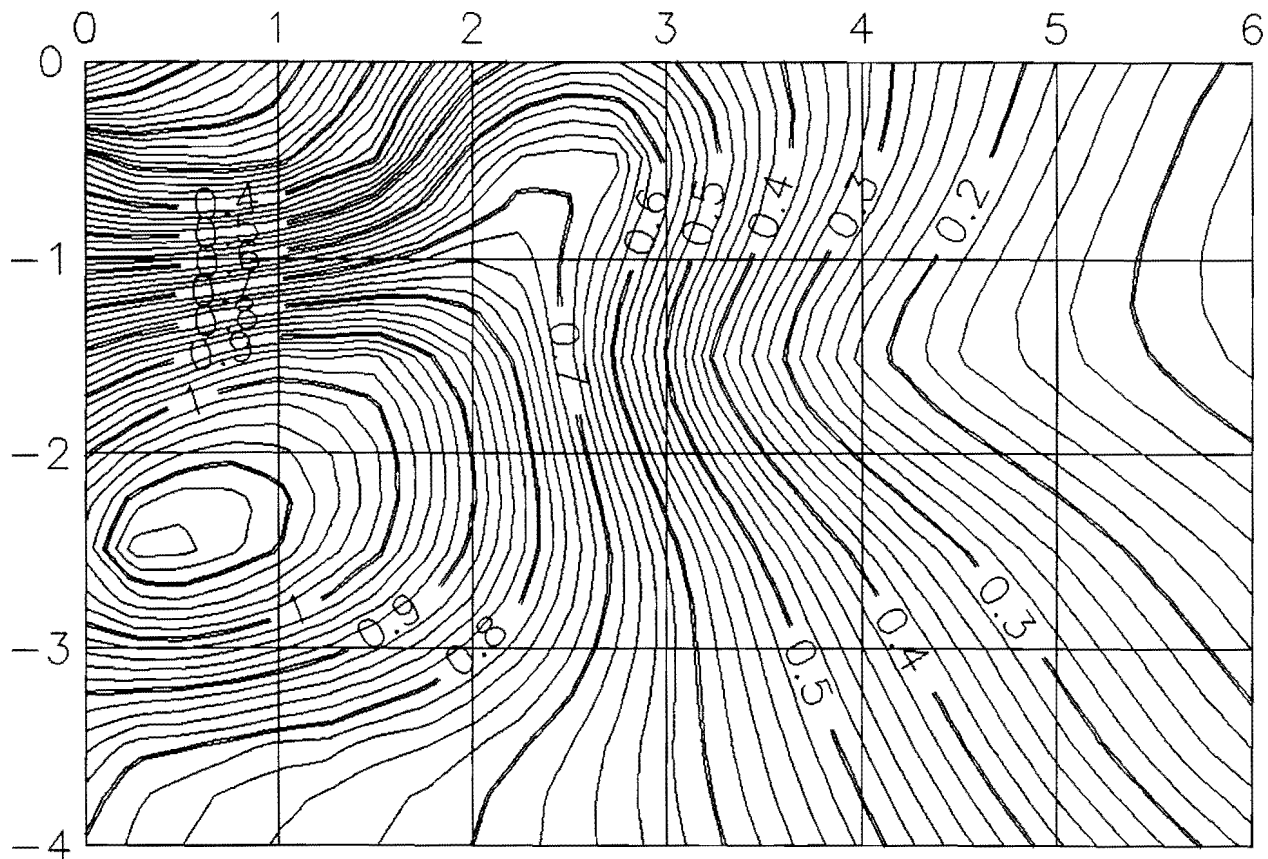


Figure 4.40. OSSR Contour for 4 Inches of ACP Over PCC, 80 Percent Crushed Limestone - 20 Percent Natural Sand, Binder-Rich Mixture, High Air Voids, Braking Induced Surface Shearing Stresses, Full Bond.

**CHAPTER 5**  
**SUMMARY OF THE APPROACH FOR PERFORMING UNIAXIAL**  
**CREEP TEST AND EVALUATING DATA TO DETERMINE RUTTING SUSCEPTIBILITY**

1. Fabricate samples for uniaxial creep testing in accordance with section 2.9 of NCHRP Report 338 using either the GTM (ASTM D 3387) or gyratory compactor (TEX 206-F).

2. Perform the unconfined creep test in accordance with the procedure described in section 2.9, paragraph 2.9.3.4. with the exception that the stress level applied to the sample should be determined based on the approach described on page 90 of the report under the heading "Determine Appropriate Level of Axial Stress in Unconfined Compression Creep Test."

3. Visually evaluate the arithmetic plot of creep strain versus time of loading data and try to visually differentiate among the primary, secondary and tertiary regions of the creep curve. This plot should be obtained from the data acquisition system used to perform the creep test. This test should be performed on a servo-hydraulic system such as MTS. This involves the following steps:

- a. Reduce the digital data file using a spread sheet such as Quattro or Lotus 123. This converts the numerical format data to a visual X v. Y graphical plot.
- b. While in the spread sheet, average separate channel data and initial starting points set as zero. The spread sheet also allows for plotting small sections of each data set.

The instrumentation used for measuring vertical deformation is discussed in Appendix A and in TxDOT Research Report 1177-1F.

4. Determine the strain at the end of one-hour of creep testing and, using this value of strain, compute the creep stiffness at the end of one-hour of creep testing.

5. Calculate the slope of the steady state region of the creep strain versus time of loading curve by one of two methods:

- a. Visually identify the secondary or steady state creep region from the plot of data (steps 3a and 3b), and calculate the steady state region log-log slope as follows:

$$m = \frac{\log \epsilon_{t_1} - \log \epsilon_{t_2}}{\log t_1 - \log t_2}$$

where  $\epsilon_{t_1}$  is the creep strain at 3,600 seconds or at the end of the steady state region,  $\epsilon_{t_2}$  is the creep strain at 1,000 seconds or at the beginning of the steady state creep region and  $t_1$  and  $t_2$  are the times corresponding to the end and beginning of the steady state creep regions, respectively.

b. Calculate the slope of the steady state region using the software developed by TTI. This program accepts the creep data in an ASCII format. The program calculates the instantaneous slope and identifies regions where the instantaneous slope does not significantly change (less than a 10 percent change in the instantaneous slope within the region). The regions with a constant slope are then identified and compared to select the largest region (in terms of time) which can be identified as steady state.

6. Enter Tables 3.24 and 3.25 with the values of  $\epsilon_p$  and  $m$  and creep stiffness and determine whether or not this mix will meet the creep parameter requirements for the pavement category in question.

7. Calculate the total resilient strain,  $\epsilon_{rt}$ , and unconfined compressive strain at failure,  $\epsilon_{qu}$ , in accordance with the procedures explained in section 2.9, paragraphs 2.9.3.3 and 2.9.3.4, respectively in NCHRP Report 338.

8. Using the values of  $\epsilon_{rt}$  and  $\epsilon_{qu}$  determined in step 7, and the value of  $\epsilon_p$  determined in step 4, determine whether or not the mixture is susceptible to enter a region of strain softening as predicted by the following relationship:

$$\epsilon_p + \epsilon_{rt} < 0.5\epsilon_{qu}$$

If this equation is true, then the mixture should be resistant to strain softening.

9. If the criteria in steps 7 and 8 are both met, then the mixture is resistant to rutting. If the criteria are not met, then the mixture requires redesign.

**CHAPTER 6**  
**SUMMARY OF DESIGN PARAMETERS WHICH**  
**INFLUENCE PERMANENT DEFORMATION**

**GENERAL**

There is general agreement in the literature that the permanent deformation potential of asphalt concrete mixtures is influenced by: aggregates, binder, mixture properties and field conditions. Sousa, Craus and Monismith (1991) summarized the factors which influence rutting and the direction of this influence, see Table 5.1.

Most of the factors and changes in the factors are self-explanatory or self-evident and more complete discussions exist elsewhere in the literature, i.e., Sousa, Craus and Monismith. However, the effect of the laboratory compaction effort and methodology is not self-evident to the general reader. The effects of different types of laboratory compaction devices on the compressive creep test and other tests geared to evaluate permanent deformation potential have been discussed in Chapter 2 of this report. The "bottom line" is that the type of lab compaction device does indeed significantly influence the sensitivity of the mixture to compaction. Thus, it is important to select a lab compaction device which simulates the field compaction effort as closely as possible. AAMAS research as well as research in this study and by SHRP (Button, Little, Pendelton and Jagadam, 1992) supports the use of the Texas gyratory compaction device as a lab compaction device that satisfactorily simulates the compaction that occurs in the field. The AAMAS research demonstrates that the kneading compactor can be used in lieu of a gyratory compactor without significantly (statistically) affecting engineering properties of the mixture.

Although most of the parameters presented in Table 5.1 are not controversial in terms of the effect in a change in the respective parameter on the permanent deformation potential of the mixture, it is worthwhile to address specific factors which may require some additional discussion. These factors include: aggregate gradation, air void content, VMA and temperature.

**AGGREGATE GRADATION**

The change from a gap-graded to a continuous gradation results in an

increase to rutting resistance in most cases. However, new types of mixtures have emerged on the scene during the last several years. Among these are the European Stone Mastic Mixes (SMA's). These mixes derive their resistance to deformation from a "stone-to-stone" contact that is promoted in the coarse aggregate fraction. This contact matrix is promoted by the gradation of the binder which tends to be more gap graded than most traditional mixes. In fact in this mix the percentage of stones larger than 2 mm is increased from the 40 and 70 percent that would occur in a traditional densely graded mix to from 70 to 80 percent in the SMA mix. The SMA mix is a mastic-rich mix and is also binder rich. The mastic is designed to fill the voids between the gap graded coarse aggregate fraction.

Thus, although Table 5.1 is generally correct in the fact that a change from a gap to a more continuous gradation reduces rutting potential in a traditional densely graded mix, this does not necessarily apply to special mixtures, such as the SMA mixtures.

#### **AIR VOID CONTENT**

Although Table 5.1 indicates that a reduction in air voids results in an increase in resistance of the mixture to rut, the caveat must be applied that the air void content must never drop below a level that will result in plastic flow. The general guideline for this is that the air voids in the mix should not be less than 3.0 percent.

#### **VMA**

In 1984 the Illinois Department of Transportation (Miller, et al.) developed an interstate highway specification addressed at reducing rutting. The top item of the list was to increase the specified VMA from 11-13 percent to a 15 percent minimum. On the other hand, Cooper, Brown and Pooley (1985) concluded that good resistance to permanent deformation requires low voids in the mineral aggregate (VMA) and that the desirable grading for minimum VMA can be determined using dry aggregate tests. However, they cautioned that the lowest theoretical VMA could be undesirable as it may not allow sufficient voids in the aggregate for enough binder to ensure satisfactory compaction without the mixture becoming overfilled.

Foster (1990) prepared a report for the National Asphalt Paving

Association in which he reviewed literature from 9 different sources in an effort to determine the important levels of VMA as so far as rutting resistance is concerned. In three of the sources he found that all pavement performed satisfactorily regardless of VMA, in two the performance of all pavements was unsatisfactory regardless of VMA. The data from the first five sources proved no support for a minimum or maximum VMA.

In the other four articles studied by Foster both satisfactory and unsatisfactory performances were reported. However, in none of the four cases could a VMA be selected that would separate the pavements showing satisfactory performance (in terms of rutting) from those showing unsatisfactory performance.

Foster (1990) concludes that if a minimum VMA is really needed, it is something less than 12 percent. However, he reiterates that the field data do not support a minimum VMA requirement despite the compelling argument for a minimum VMA (i.e., that enough space in the aggregate voids is necessary to facilitate both the air voids to resist rutting and the binder needed for durability).

## TEMPERATURE

Temperature certainly has a significant effect on rutting. Hofstra and Klomp (1972) determined that when test track temperatures increased from 68°F to 140°F, the rutting increased by a factor of 250 to 350 percent. Linden and Van der Heide (1987) reported significant increase in rutting in Europe due to the very hot summers of 1975 and 1976.

The importance of the test temperature has caused some researchers to test within the high temperature range of those encountered in the field. Bonnot (1986) selected a test temperature of 140°F for surface courses and 115°F for binder courses. These conditions were selected to represent the most unfavorable conditions in France.

In the 2474 and 1170 study the hottest pavement profile was selected to represent critical conditions in Texas. Other assumptions about the accumulation of permanent deformation in Texas included that permanent deformation occurs daily over the time interval from 7:30 a.m. to 5:30 p.m., significant permanent deformation occurs only in the period of from April to October and permanent deformation can be ignored at temperature below 50°F.

Performing rutting tests; whether they be uniaxial creep, triaxial, repeated load or wheel tracking tests; at higher temperatures will result in a greater rutting potential than if the test were performed at a lower temperature. However, in terms of the uniaxial creep test, which was selected as the test of choice in this study, the test temperature must be tempered with the considerations of the limitations of the testing methodology. In uniaxial tests, a test temperature above about 104°F is often impractical. Secondly, the temperature of 104°F is a realistic high nominal profile temperature for the hottest months of the year in Texas. Although it is a fact that significant periods of the year exist when near surface temperatures are significantly higher than 104°F, the average nominal temperature profile over the thickness of the hot mix layer does not often substantially exceed 104°F (only about 6 percent of the time).

Although testing thin surface mixes at temperatures above 104°F may be appropriate for specific situations, the authors believe that in an unconfined, uniaxial compressive mode of testing, the 104°F test is an appropriate test to evaluate rutting sensitivity of candidate mixtures.

#### **OTHER CONSIDERATIONS**

An excellent review of the causes of rutting is presented by Button and Perdomo (1989). Among the factors discussed which are in addition to those already discussed in this chapter are the effects of:

1. Drum plants operated at relatively low temperatures,
2. Excessive permissible moisture in the mix,
3. Elimination of multiple stockpile requirements,
4. Excessive fines (sand-size particles) allowed in the mix,
5. Use of control strip density requirements rather than reference type density requirements,
6. Temperature susceptible asphalt cement,
7. Rounded aggregates or insufficient crushed particles,
8. Excessive asphalt content and
9. Cold weather paving which leads to low density.

## CHAPTER 7 CONCLUSIONS AND RECOMMENDATIONS

### CONCLUSIONS

1. The uniaxial compressive creep test is an effective test by which to evaluate the resistance of asphalt concrete mixtures to permanent deformation. Although a confined, repeated load test provides a superior method by which to test for rutting sensitivity, the creep test can be effectively used in mixture design to differentiate among candidate mixtures and to differentiate between acceptable and unacceptable mixtures.

2. Three parameters from creep tests should be used to evaluate permanent deformation sensitivity: the strain at the end of 3,600 seconds of loading,  $\epsilon_p$ ; the slope of the steady state portion of the creep curve,  $m$ ; and the stiffness at 3,600 seconds of loading. All testing should be at 104°F, except for special conditions, and at realistic stress conditions. This stress condition should simulate field stress states.

3. In addition to the three creep test parameters, the relationship between the sum of the total resilient modulus (from the dynamic modulus test, ASTM D 3497),  $\epsilon_{rt}$ , and  $\epsilon_p$  and the strain at failure in the unconfined compressive strength test,  $\epsilon_{qu}$ , is a good indicator of resistance to permanent deformation. This relationship expressed mathematically, is:

$$\epsilon_p + \epsilon_{rt} < 0.5\epsilon_{qu}$$

Thus by insuring that the sum of  $\epsilon_p$  and  $\epsilon_{rt}$  remains less than one-half of the value of  $\epsilon_{qu}$  the strain soften region should not be entered.

4. The slope of the uniaxial creep curve should, theoretically, be a good indicator of the rate of rutting and the sensitivity of the mixture to rutting. A strong relationship was established in this study between the slope of the steady state uniaxial compressive creep curve and the creep strain at 3,600 seconds of loading. The major difficulty in the identification of the slope of the creep curve is in deciding which slope to use. In this study the log-log slope of the visually identified steady state portion of the creep curve was selected. In most cases where a stable mixture is being tested (one in which tertiary creep will not occur during

the testing period - one-hour), the log-log slope of the steady state portion of the creep curve remains relatively constant between 1,000 and 3,600 seconds. This slope should be calculated as follows:

---

$$m = \frac{\log \epsilon_{p,3,600\text{sec.}} - \epsilon_{p,1,000\text{sec.}}}{0.56}$$

If it is visually evident that the steady state region is not reached prior to 1,000 seconds, then the value of  $m$  should be calculated between the range of 3,600 seconds and the time at which the steady state portion is reached.

$$m = \frac{\log \epsilon_{t_1} - \log \epsilon_{t_2}}{\log t_1 - \log t_2}$$

where  $t_1$  and  $t_2$  are the times in seconds that represent the end and beginning of the visually identified steady state portion of the creep strain versus time of loading curve, respectively.

5. A better approach is to develop software that calculates the slope of the steady state creep curve at any point. Based on this study, software has been developed that computes the instantaneous slope of creep strain versus time of loading data. The software (available from TTI) accepts creep strain versus time of loading data in an ASCII format. The program calculates the instantaneous slope and identifies regions where the instantaneous slope does not significantly change (less than 10 percent change). The regions with a constant slope are then identified and compared to select the largest region which can be identified a steady state. These data are being studied and will be reported. However, at the present time, and until this can be fully verified, the approach summarized in conclusion four is recommended. The approach in conclusion four is a valid approach because, in almost all cases, the steady state region is readily identifiable and the slope in this region is relatively constant, unless tertiary creep is reached.

6. Mixture volume calculations such as air voids, voids in the mineral aggregate (VMA), voids filled with asphalt, etc., are indispensable parts

of the mixture design process. In this study a clear and strong influence of the air voids content was established. The general trend of the influence of air voids was in accordance with what would be expected, i.e., high air void contents, above about five percent lead to higher levels of rutting and very low air voids (lower than about two percent) produce more rut sensitive mixtures. However, no clear relationship was established between rutting susceptibility as identified by the uniaxial creep test and/or the triaxial shear test and VMA. These findings are generally supported by the work of Foster (1989). However, the data obtained in this study fully support the established philosophy that a minimum VMA is required to provide sufficient room in the mix for asphalt binder (durability) and air voids (stability). There is no evidence of a minimum VMA based on the criterion of permanent deformation (from creep or triaxial test data).

7. The conditions of stress state during testing and the temperature at which the test is performed are of critical importance. This procedure offers a rational evaluation of the required stress state at which to perform uniaxial (unconfined) creep testing. The concomitant temperature for all creep testing was selected as 104°F. Although surface pavement layers are subjected to substantially higher surface pavement temperatures, the researchers feel that the procedure suggested in this report is appropriate for evaluating rutting potential. The stress state represents a critical stress state and the 104°F temperature represents a temperature profile temperature average that is exceeded only about 6 percent of the time. In addition testing at higher temperatures in an unconfined test require more evaluation.

8. The Gyrotory Test Machine (GTM) is the preferred method of compaction as it allows one to compact 4-inch diameter specimens that are at least 4-inches high. GTM compaction procedures are explained in ASTM D 3387. In addition to the ability to fabricate specimens that meet requirements for uniaxial compression testing, the GTM provides the ability to further density compacted specimens and to evaluate gyrotory shear stress and strain in accordance with AAMAS procedures as defined in NCHRP Report 338, Von Quintus, et al. (1991).

9. NCHRP Report 338 indicates that the Texas gyrotory (ASTM D 4013, Texas Test Method TEX 206-F) compactor can be used in lieu of the GTM. The

procedure calls for the specimen to be compacted prior to creep testing in accordance with TEX 206-F with the following exceptions:

- a. Mixture compaction temperature shall be in accordance with AASHTO T 246.
- b. The pre-gyration stress shall be 90 psi.
- c. Compactive effort is applied to these specimens to the refusal air void level. For most mixtures, 45 revolutions (or 15 sets of three revolutions each) of the gyratory molding press is sufficient to determine the final air void content.

TTI was able to modify the Texas gyratory compactor to fabricate samples approximately 3.5-inches high. This is still one-half inch short of the minimum required value of 4-inches high required by NCHRP Report 338.

10. A proven alternative to use of the standard gyratory (TEX Method 206-F) is to use the large gyratory press as explained in test method Tex 126-E. This press produces a 6-inch diameter and 8-inch high specimen which can be tested as is for larger stone mixtures (maximum aggregate size larger than 1-inch) or can be cored to a 4-inch diameter and cut to a 4-inch height to meet AAMAS requirements for mixtures with maximum aggregate sizes of less than 1-inch. If the large gyratory compactor is used, the general procedure explained in Tex 126-E (steps 11 through 15 or part II) should be used with the exception that the number of gyrations applied in step 13 should be increased until the specimen reaches a minimum air voids content, refusal.

11. The criteria for evaluating creep data in this report were developed on samples that were 4-inches in diameter and 8-inches high, samples that were 4-inches in diameter and 4-inches high and samples that were 4-inches in diameter and 3.5 inches high. The criteria presented in this report is valid for all sets of samples. However, it is important to note that the majority of testing was performed on 4-inch high and 4-inch diameter samples prepared using the kneading compaction device (ASTM D1561).

12. Research at the University of California at Berkeley Sousa, et al. (1991) demonstrates that mixtures prepared using the kneading compactor are generally more resistant to deformation than are mixtures prepared using the gyratory compactor. The reinforcing effect of short specimens (shorter than

4-inches high) reduces deformation potential. The net effect of testing 3.5-inch gyratory samples is that they show approximately the same sensitivity to deformation as do the 4-inch high samples prepared by kneading compaction.

13. The criteria presented in Tables 3.24 and 3.25 are provided for the purpose of ascertaining the sensitivity of a mixture to rutting for moderately to highly trafficked pavements for mixture design and analysis purposes. Neither the creep test nor the criteria in these tables are meant to be used for approximating actual rut depths. However, a procedure for extending the analysis to very highly trafficked pavements is presented in Chapter 3.

14. The criteria for the evaluation of permanent deformation potential established in this study represents a significant improvement over the method used in NCHRP Report 338. When using Table 3.24, the stiffness at the end of one-hour of creep loading and the creep strain at the end of one hour should be used as the primary criteria for evaluation of permanent deformation sensitivity with the log-log slope of the steady state creep region as the secondary criterion.

15. The creep criteria presented in this report should be used together as a part of the AAMAS procedure as explained in NCHRP Report 338.

## **RECOMMENDATIONS**

1. The permanent deformation evaluation criteria established in this report should be used in conjunction with the NCHRP 338 Report and in lieu of the creep evaluation criteria presented in the 338 Report.

2. NCHRP Report 338 procedures and criteria for the evaluation of low temperature cracking, load-induced fatigue, moisture damage, aging and disintegration should be followed as presented in the 338 Report.

3. The uniaxial creep test, as discussed in this report, should be supplemented by a confined (triaxial test) performed at a higher temperature to evaluate special cases of rutting potential. These special conditions may include intersections and near surface, i.e., upper 1-inch, distortion.

## REFERENCES

Ameri-Gaznon, M. and Little, D. N., "Permanent Deformation Potential in Asphalt Concrete Overlays Over PCC Pavements," Research Report No. 452-3F, Texas Transportation Institute, Texas A&M University, November 1988.

Barber, W. R. and Brabston, W. N., "Development of a Structural Design Procedure for Flexible Airport Pavements," FAA Report No. FAA-RD-74-199, 1975.

Bolk, H. J. N. A., The Creep Test, SCW Record 5, Study Centre for Road Construction, The Netherlands, 1981.

Bonnot, J., "Assessing the Properties of Materials for the Structural Design of Pavements," Proceedings, Third International Conference on the Structural Design of Asphalt Pavements, Vol. 1, September, 1972.

Button, J. W. and Little, D. N., "Evaluation of Laboratory Compaction Devices and Their Ability to Duplicate Field Compaction," Strategic Highway Research Program (SHRP) Report, 1992.

Button, J. W., Little, D. N., Pendleton, O. and Jagadam, S., "Comparison of Rolling Wheel Compactor, Gyrotory Compactor, Rotating Base Marshall Compactor and Elf Rolling Wheel Compactor to Field Compaction," Report Prepared for the Strategic Highway Research Program (SHRP), 1992.

Claessen, A. I. M., Edwards, J. M., Sommer, P. and Uge, P., "Asphalt Pavement Design-The Shell Method," Proceeds, Fourth International Conference on the Structural Design of Asphalt Pavements, University of Michigan, 1977.

Cooper, K. E., Brown, S. F. and Pooley, G. R., "The Design of Aggregate Gradings for Asphalt Base Courses," Vol 54, Proceedings, Association of Asphalt Paving Technologists, 1985.

Finn, F., "Factors Involved in the Design of Asphaltic Pavement Surfaces," NCHRP Report 39, 1967.

Finn, F., Saraf, C., Kuldarni, R., Nair, K., Smith, W. and Abdulla, A., "The Use of Distress Prediction Subsystems for the Design of Pavement Structures," Proceeding, Fourth International Conference on the Structural Design of Asphalt Pavements, 1977.

Finn, F., Monismith, C. L. and Markevich, N. J., "Pavement Performance and Asphalt Concrete Mix Design," Proceedings, AAPT, Vol. 52, 1983.

Foster, C., "VMA Versus Pavement Performance," National Asphalt Paving Association, 1986.

Freeman, T. J. and Carpenter, S. H., "Characterizing Permanent Deformation in Asphalt Concrete Placed Over Portland Cement Concrete Pavements," TRR 1070, 1986.

Gallaway, B. M. and Rose, J. G., "Macro-Texture, Friction, Cross Slope and Wheel Track Depression Measurements on 41 Typical Highway Pavements," Research Report 138-2, Texas Transportation Institute, 1970.

---

Hays, D. F. and Brown, A. L., The Physics of Tire Traction, Theory and Experiment, General Motors Research Laboratories, Plenum Press, New York, 1974.

Hewitt, W. L., "Analysis of Stresses in Flexible Pavements and Development of a Structural Design Procedure," HRB Bulletin 269, 1960.

Highway Pavement Distress Identification Manual for Highway Conditions and Quality of Highway Construction Survey, DOT-FHWA-11-9175/NCHRP 1-19, 1979.

Hills, J. F., "The Creep of Asphalt Mixes," Journal of the Institute of Petroleum, Vol. 59, 1973.

Hofstra, A. and A. J. G. Klomp, "Permanent Deformation of Flexible Pavements Under Simulated Road Traffic Conditions", Proceedings, Third International Conference on the Structural Design of Asphalt Pavements, 1972, Vol. 1, London, pp 613-621.

Kenis, W. J., "Predictive Design Procedures - VESYS User's Manual," FHWA, 1978.

Kenis, W. J., "Predictive Design Procedures - A Design Method for Flexible Pavements Using the VESYS Structural Subsystem," Proceedings, Fourth International Conference on the Structural Design of Asphalt Pavements, 1977.

Khedr, S. A., "Deformation Mechanism in Asphaltic Concrete," Journal of Transportation, ASCE, Vol. 112, 1986.

Kinder, D. F., "A Study of Both the Viscoelastic and Permanent Deformation Properties of a New South Wales Asphalt," 13th Australian Road Research Board, New South Wales, Australia, 1986.

Kronfuss, R., Krzemien, R., Nievelt, G. and Putz, P., "Verformungsfestigkeit von Asphalten Ermittlung in Kriechtest, Bundesministerium fur Bauten and Technik, Strassenforschung," Heft 240, Wien, Australia, 1984.

Lai, J. S. and Anderson, D. A., "Irrecoverable and Recoverable Non-Linear Viscoelastic Properties of Asphalt Concrete," Transportation Research Record 468, 1973.

Li, J., "Use of Climatic Data for the Prediction of Permanent Deformation in Flexible Pavements," Master of Engineering Report, Texas A&M University, 1987.

Linden, F. and J. Van der Heide, "Some Aspects of the Compaction of Asphalt Mixes and Its Influence on Mix Properties, Proceedings, The Association of Asphalt Paving Technologists, 1987, Vol 56, pp 408-426.

---

Little, D. N. and Crockford, W. W., "Resilient Modulus of Asphalt Concrete," Research Report 1177-1F, Texas Transportation Institute, 1991.

Little, D. N. and Richey, B. L., "A Mixture Design Procedure Based on the Failure Envelope Concept," Proceedings, AAPT, Vol. 52, 1983.

Little, D. N., "Analysis of the Influence of Low Density Polyethylene Modification (Novophalt) on Asphalt Concrete Mixture Shear Strength and Creep Deformation Potential," ASTM Special Technical Publication 1108, 1992.

Lytton, R. L. Personal correspondence, 1992.

Mahboub, K. and Little, D. N., "Improve Asphalt Concrete Mixture Design," Research Report 2474-1F, Texas Transportation Institute, 1988.

McLeod, N. W., "Rational Design of Bituminous Paving Mixtures with Curved Mohr Envelopes," Proceedings of AAPT, Vol. 21, 1952.

Miller, J., Monroney, H. and Traylor, M., "Illinois Develops Stable Mixes," Engineering and Research Division, Illinois Asphalt Pavement Association, Springfield, Illinois, 1987.

Mitchell, J. K., Fundamental of Soil Behavior, John Wiley and Sons, 1976.

Morris, J., Haas, R. C. G., Reilly, P. and Higrell, E. T., "Permanent Deformation in Asphalt Concrete Pavements Can Be Predicted," Proceedings, AAPT, Vol. 43, 1974.

Nijboer, L. W., Plasticity as a Factor in the Design of Bituminous Road Carpets, Elsevier, 1948.

Perdomo, D., "Identifying and Correcting Rut Susceptible Mixtures," Ph.D. Dissertation, Texas A&M University, 1991.

Perl, M. J., Uzan, J. and Sides, A., "Viscoelastic Constitutive Law for a Bituminous Mixture Under Repeated Loading," TRR 911, 1984.

Rauhut, J. B., Roberts, F. L. and Kennedy, T. W., "Models and Significant Material Properties for Predicting Distresses in Zero-Maintenance Pavements," Report No. FHWA-RD-78-84, 1978.

Rauhut, J. B., Lytton, R. L. and Darter, M. I., "Pavement Damage Functions for Cost Allocation - Volume 1, Damage Functions and Load Equivalence Factors," Report No. FHWA/RD-84/018, 1984.

Roberts, F. L., Tielking, J. T., Middleton, D., Lytton, R. L. and Tseng, K. H., "Effects of Tire Pressure on Flexible Pavements," Report No. 372-1F, Texas Transportation Institute, 1986, pp. 223-235.

Smith, V. R., "Triaxial Stability Method for Flexible Pavement Design," Proceedings of AAPT, Vol. 18, 1949.

---

Sousa, J. B., Harvey, J., Painter, L., Deacon, J. A. and Monismith, C. L., "Evaluation of Laboratory Procedures for Compacting Asphalt Aggregate Mixtures," Institute of Transportation Studies, University of California, 1991.

Tseng, K. H. and Lytton, R. L., "Prediction of Permanent Deformation in Flexible Pavement Materials," Presented at ASTM Symposium on Implication of Aggregate in the Design, Construction and Performance of Flexible Pavements, New Orleans, Louisiana, 1986.

Van de Loo, P. J., "Creep Testing, A Simple Tool to Judge Asphalt Mix Stability," Proceedings, AAPT, Vol. 43, 1974.

Van de Loo, P. J., "The Creep Test: A Key Tool in Asphalt Mix Evaluation and in Prediction of Rutting," Proceedings of AAPT, 1978, pp. 522-557.

Viljoen, A. W. and Meadows, K. "The Creep Test - A Mix Design Tool to Rank Asphalt Mixes in Terms of Their Resistance to Permanent Deformation Under Heavy Traffic," National Institute of Road Research, Pretoria, South Africa, 1981.

Von Quintus, H. L., Scherocman, J. A., Hughes, C. S. and Kennedy, T. W., "Asphalt Aggregate Mixture Analysis System (AAMAS)," NCHRP Report 338, March 1991.

Yandell, W. O., "The Prediction of the Behavior or Elastoplastic Roads During Repeated Rolling Using the Mechano-Lattice Analog," HRR 374, 1971.



APPENDIX A  
APPARATUS DEVELOPMENT: IDT AND  
AXIALLY LOADED TESTING EQUIPMENT

---

Three new devices were designed and fabricated during the course of this study. Machine drawings for the critical components of the devices can be found in Appendix D of Report 1177-1F. The use of the three devices is described in Part II of the suggested test procedure presented in Appendix B of Report 1177-1F. Two of the devices that were developed are indirect tension test devices and the remaining device is for axial loading. The primary objectives in the design of the axial loading device were to obtain more complete instrumentation coverage of the specimen, provide instrumentation for measurement of Poisson's ratio/dilatation, and suggest some approaches for solving the problem of axial loading of short pavement cores. The goals of the development of the diametral resilient modulus apparatus were to overcome problems associated with mounting sensors and specimen alignment with respect to the loading axis. A capability for measurement of Poisson's ratio was desired while maintaining the maximum speed and simplicity possible. Overall, the common goal of the development of the devices and test procedures was to provide the Department of Transportation with laboratory test procedures that can be used in conjunction with the 1986 AASHTO Guide and nondestructive testing to improve design and evaluation. Although the devices provide the necessary capability for current design procedures and NDT evaluation procedures, they should also maintain their utility for the foreseeable future as new design and evaluation tools are developed.

#### Axial Loading Apparatus

The axial loading apparatus is a simple modification of existing equipment. The emphasis in the development was put on on-sample measurements. This approach was required because remotely mounted sensors are usually inadequate if the specimen translates during loading or if there is considerable slack in the loading system. Specimens cored from an in-service pavement will almost always have ends that are not parallel. These ends are very difficult to saw parallel, so capping compounds must be used. This technique is acceptable for length to diameter ratios greater than two, but the practice restricts the movement of the ends on shorter cores. For this reason, short cores are not capped and load application almost always results in some specimen translation.

To ensure that a reasonable average of vertical displacements is available,

three vertical Linear Variable Differential Transformers (LVDTs) are glued to the surface of the specimen using small mounting fixtures. A simple positioning jig is used to make sure the fixtures are placed every 120° around the diameter and at a specified gauge length (usually 2-4 inches for an 8 inch tall specimen, 1.5 inches for a 3 inch specimen). To ensure that a reasonable integrated picture of the radial strain is available, a circumference measurement device is positioned around the specimen at mid-height between the vertical sensor gauge points. Both the non-contact, externally mounted sensor system and the circumferential measurement device are illustrated in the figure below.

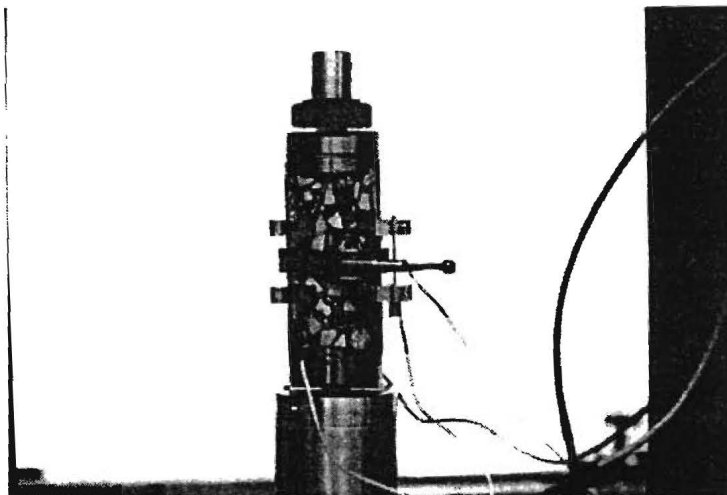
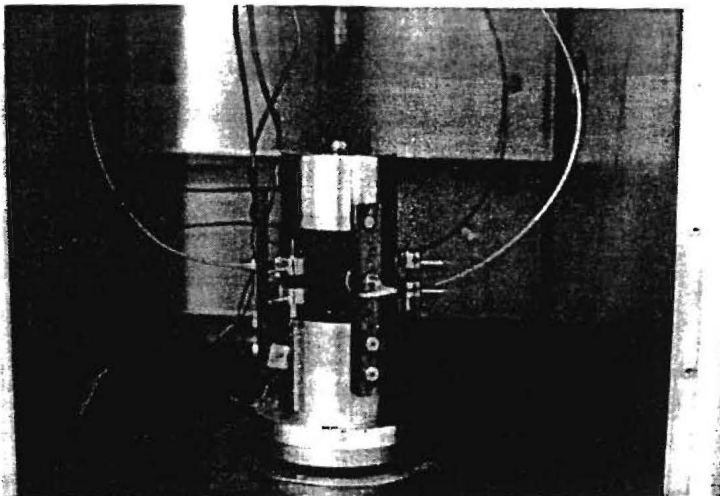


Figure A.1. Axial Measurement Devices: (top) Contact Vertical LVDTs and Remotely Mounted Noncontact Radial Transducers, (lower) Contact Sensors All Directions.

The axial configuration can be used with confining pressure to extend the range of stress states that can be applied. For relatively low confining pressures and fast cycle times, a membrane is not used. For slower rates and higher confinement, the specimen should be placed in an impermeable membrane. Generally, the specimen in this test configuration is loaded with a sine wave frequency spectrum to obtain the "dynamic" modulus. As will be shown later in the report, the results from loading at a frequency equal to that applied in the indirect tensile configuration will generate results that are not statistically different from one procedure to the other.

### Indirect Tension (Diametral) Devices

Two devices were developed. The first device allows the measurement of Poisson's ratio. The second device was developed for speed only and does not include a capability for measuring Poisson's ratio at this time. Both devices use a universal loading head that incorporates a removable loading strip. The loading head is illustrated below.

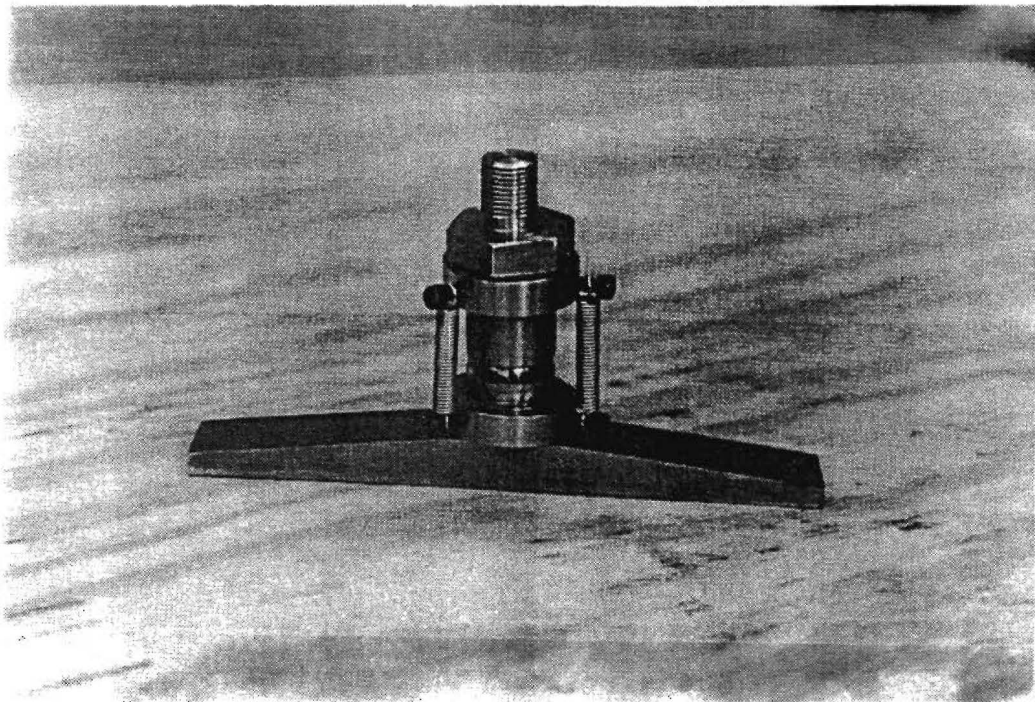


Figure A.2. Universal Loading Head for Diametral Test.

### Generalized Indirect Tension Device

The measurement of Poisson's ratio in the diametral test has been met with mixed reviews. Many of the reviews are not complimentary. The reason for this

is that, unless the applied load levels are very small and/or the temperatures very low, a plastic zone develops in the vicinity of the loading strip where it contacts the specimen. The development of this plastic zone can cause erroneous vertical deformation readings. This is especially true if the loading strips are not aligned with each other along the diameter of the specimen.

---

In the new device, the loading strips are glued to the specimen in an alignment frame as shown below. This frame insures that the strips are located on the diameter and that the specimen will be loaded through the center. The glue stiffness should be reasonably well matched to the specimen stiffness. A hot glue appears to work reasonably well for this application as long as the testing is conducted at a sufficiently low temperature and the glue film thickness is kept to a minimum.

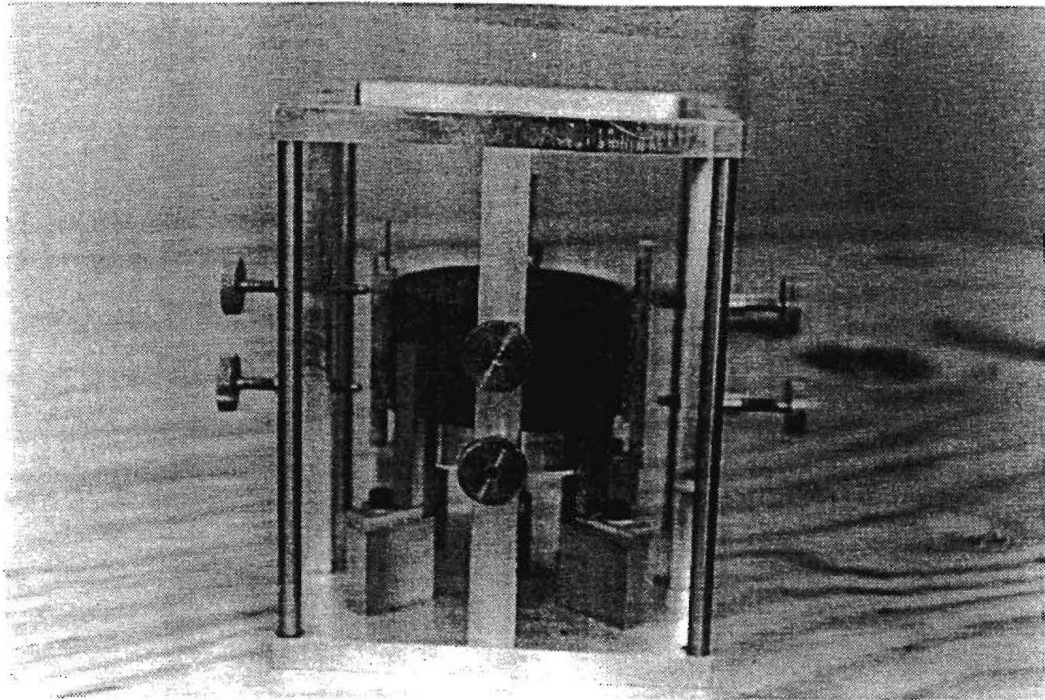


Figure A.3. Gluing Fixture for Diametral Loading Strips.

The device illustrated above allows control both vertical and horizontal alignment of the diametral resilient modulus specimen. After the strips have been glued to the specimen, the assembly is as shown below.

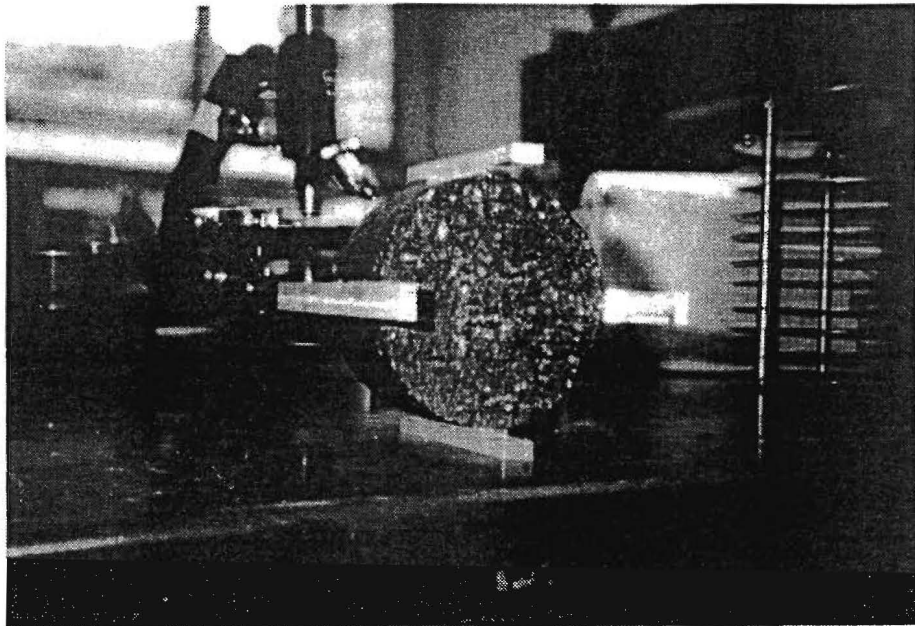


Figure A.4. Specimen with Loading/Gauging Strips Mounted.

The dual purpose loading/gauging strips have been designed to accommodate four spring loaded sensors. The four loading strips are positioned perpendicular to the face of the specimen and  $90^\circ$  apart from each other. Two sensors are positioned on each side of the specimen such that they can measure both vertical and horizontal displacements. The surface of the strip glued to the specimen is machined to the nominal specimen radius.

Schlumberger/Sangamo AGZ0.5 spring loaded gauging transducers have been used to measure the horizontal and vertical displacements. Selected features of these spring loaded sensors include:

- a. a linear stroke of 0.5 mm,
- b. an acceptable temperature range of  $-40^\circ\text{C}$  to  $100^\circ\text{C}$ ,

- c. AC powered and perform very well when there is vibration or wide temperature variations, and
  - d. accurate linear movement of the shaft is assured by a linear bearing and antirotation guide.
- 

Two important properties of these "gage head" type LVDTs must be recognized. The first is that the standard spring may be too strong for this application at high temperature if the hot glue begins to soften. The standard spring can be removed quite easily and replaced with a weaker spring if desired. The second property is that the core of the LVDT is not free to move completely through the body of the device. Therefore the vertical LVDTs should be carefully set and monitored throughout the test so that they are not damaged by a compressive load. External signal conditioning for these LVDTs is provided by a CAH series carrier card. The original cards contained some inferior chips which were replaced after results from a portion of the testing revealed inconsistent and significant noise problems.

#### **Rapid Diametral Testing Device**

The Texas Department of Transportation reviewed the generalized indirect tension testing device and determined that a method having a shorter setup time was needed. Several devices were studied to determine their acceptability. The disadvantages of existing devices were that many of the devices had large sensor support structures mounted on the specimen or mounted on a rigid base that did not move with the specimen as it moved under loading. Some of the devices have a yoke that is held to the specimen by four screws. This concept was extended to the design of the accelerated testing device. Instead of using screws to hold and instrumentation support structure; spring loaded, grooved, linear bearing shafts were used to mount a yoke system to the specimen. The pressure points were then used as the gauge points for displacement measurements. The difference between the approaches is shown below. The spring pressure should be adjusted if necessary as a function of the temperature to make up for the changing stiffness of the specimen. Since the horizontal displacement measurement is not taken across the full diameter, an integration must be performed to determine the formula for the horizontal strain. This derivation is carried out in Appendix A. The reader can easily demonstrate that the formula reduces to the more familiar form when the gauge length is made equal to the diameter and substituted into the final equation.

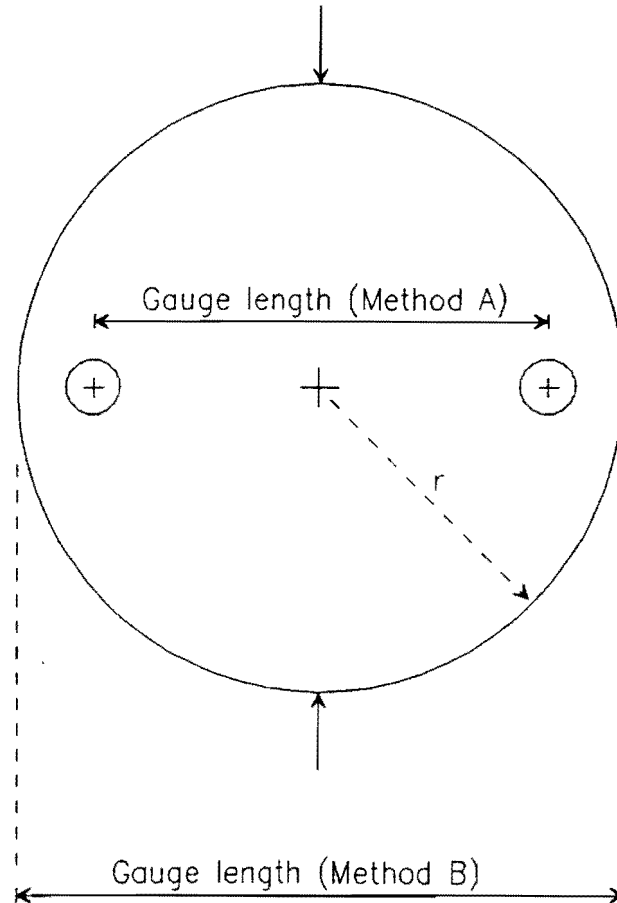


Figure A.5. Comparison of Horizontal Deflection Measurements in the Diametral Test.

The yoke system was designed to be light, yet stiff. The weight of the yokes acts through the contact points parallel to the gravity vector. The springs are removed from the LVDTs in this application. The entire system comprises a specimen centering and loading strip aligning device, and the yoke system. In the following series of figures, the components of this device are illustrated.

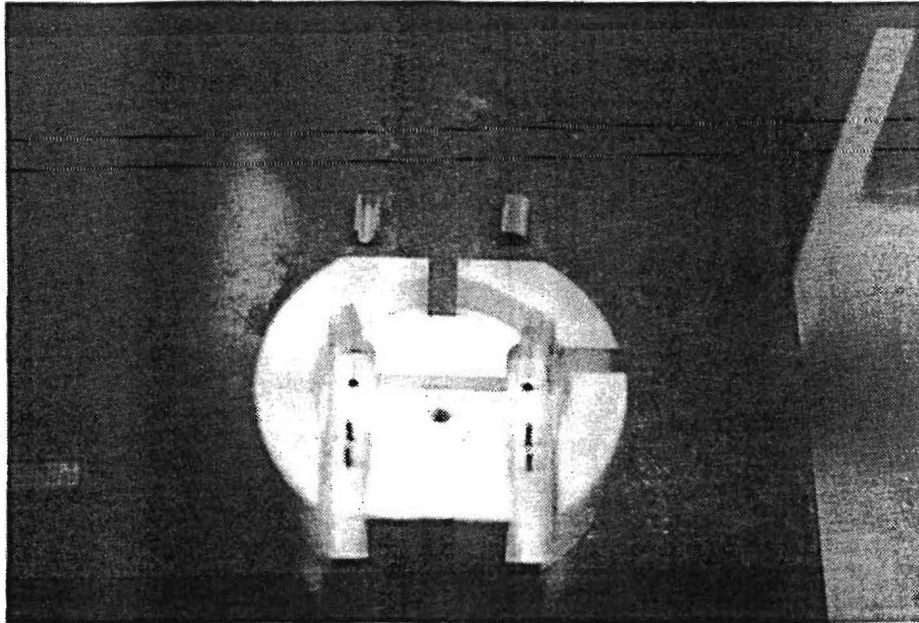


Figure A.6. Specimen Centering and Loading Strip Alignment Device.

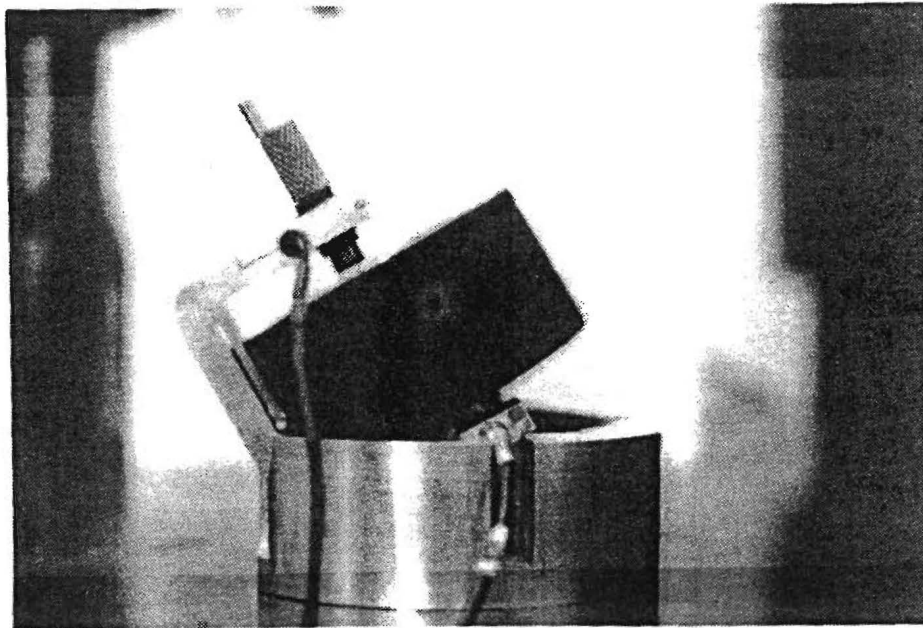


Figure A.7. Installing Specimen in Yoke/Centering Device Assembly.

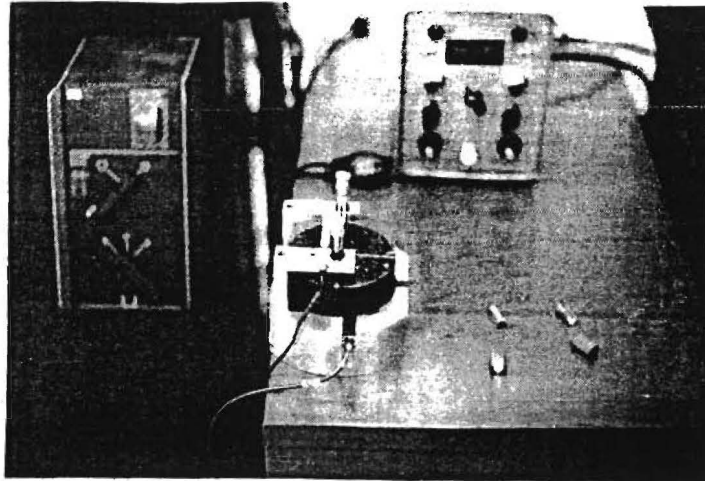


Figure A.8. Centering Device with Yokes and Specimen in Place.

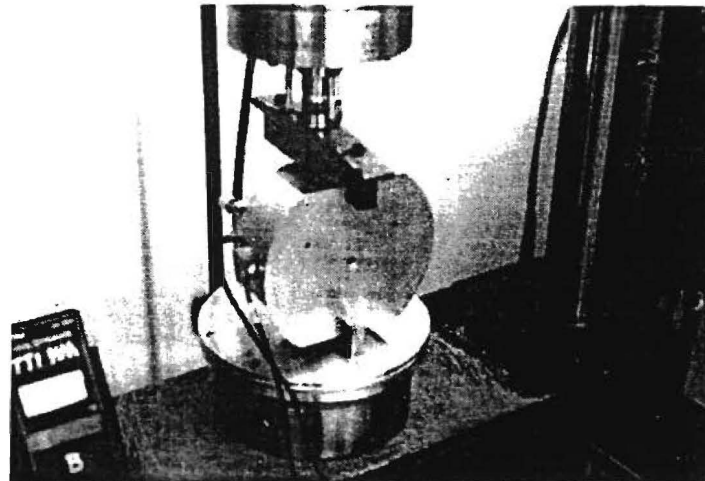


Figure A.9. Complete Assembly of Previous Figure in Testing Machine with Static Seating Load Applied.

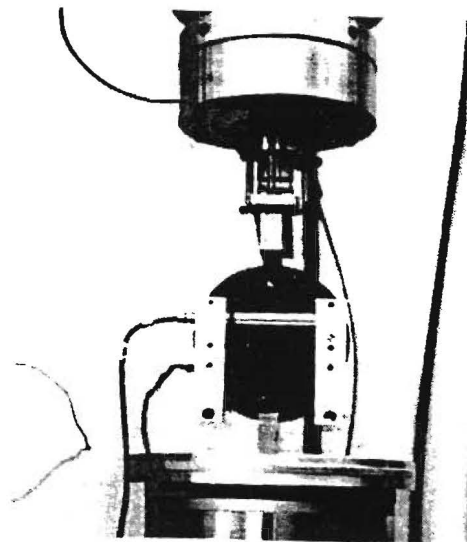


Figure A.10. Centering Device Removed and Specimen and Yoke Assembly Ready for Testing.



APPENDIX B

NORMAL OCTAHEDRAL STRESS AND NTSR CONTOURS  
FOR VARIOUS PAVEMENT STRUCTURAL CATEGORIES

Normal Wheel Loads

<u>Seasons</u>	<u>Base Type</u>	<u>ACP Thickness, in.</u>	<u>Condition of Surface Shear</u>	<u>Interlayer Bending</u>	<u>Parameter</u>	<u>Page</u>	
Moderate	ACP	2	Rolling	Bond	NOS	B-4	
					4	NTSR	B-5
						NOS	B-6
						NTSR	B-7
					6	NOS	B-8
						NTSR	B-9
	PCC	2			NOS	B-10	
					4	NTSR	B-11
						NOS	B-12
						NTSR	B-13
					6	NOS	B-14
						NTSR	B-15
	CLS	2			NOS	B-16	
					4	NTSR	B-17
						NOS	B-18
						NTSR	B-19
					6	NOS	B-20
						NTSR	B-21
Hot	ACP	2	Rolling	Bond	NOS	B-22	
					4	NTSR	B-23
						NOS	B-24
						NTSR	B-25
					6	NOS	B-26
						NTSR	B-27
	PCC	2			NOS	B-28	
					4	NTSR	B-29
						NOS	B-30
						NTSR	B-31
					6	NOS	B-32
						NTSR	B-33
	CLS	2			NOS	B-34	
					4	NTSR	B-35
						NOS	B-36
						NTSR	B-37
					6	NOS	B-38
						NTSR	B-39

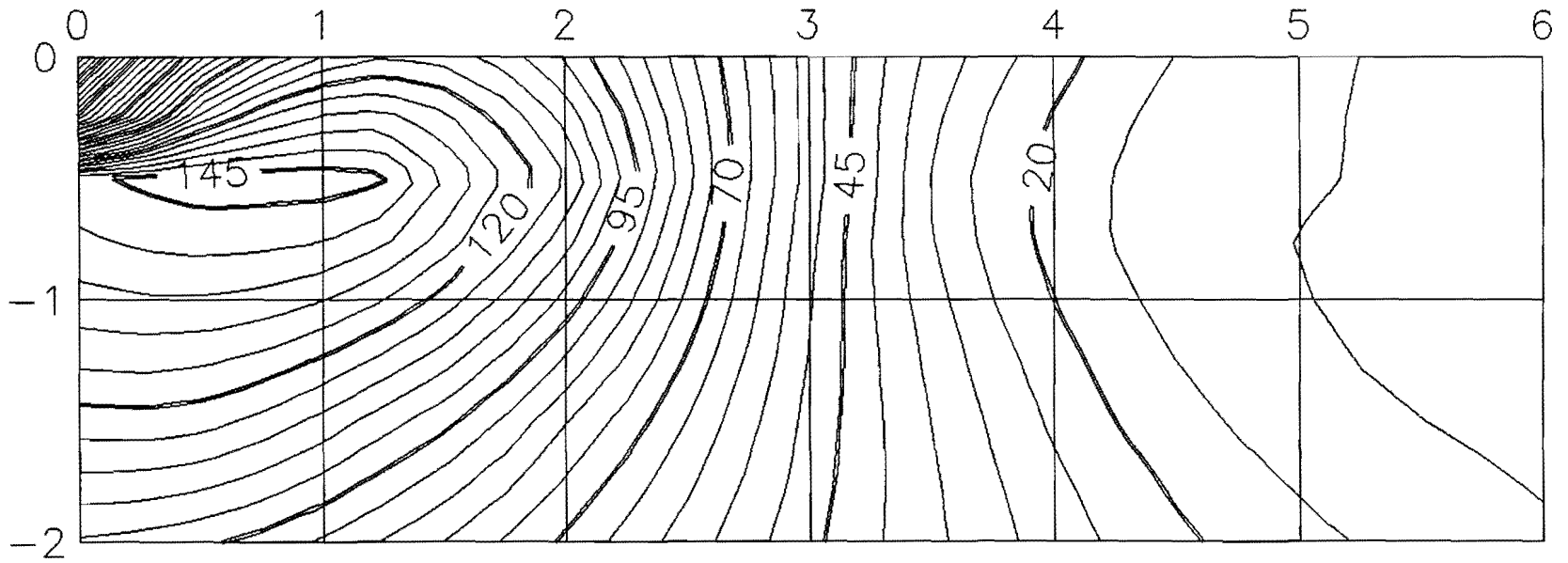
Normal Wheel Loads

<u>Seasons</u>	<u>Base Type</u>	<u>ACP Thickness, in.</u>	<u>Condition of Surface Shear</u>	<u>Interlayer Bending</u>	<u>Parameter</u>	<u>Page</u>	
Hot	ACP	2	Braking	Bond	NOS	B-40	
					NTSR	B-41	
		4			NOS	B-42	
					NTSR	B-43	
		6			NOS	B-44	
					NTSR	B-45	
		PCC			2	NOS	B-46
						NTSR	B-47
					4	NOS	B-48
		NTSR	B-49				
		6	NOS	B-50			
		NTSR	B-51				
	CLS	2	NOS	B-52			
			NTSR	B-53			
		4	NOS	B-54			
			NTSR	B-55			
		6	NOS	B-56			
			NTSR	B-57			
Hot	ACP	2	Braking	Slip	NOS	B-58	
					NTSR	B-59	
		4			NOS	B-60	
					NTSR	B-61	
		6			NOS	B-62	
					NTSR	B-63	
		PCC			2	NOS	B-64
						NTSR	B-65
					4	NOS	B-66
		NTSR	B-67				
		6	NOS	B-68			
		NTSR	B-69				
	CLS	2	NOS	B-70			
			NTSR	B-71			
		4	NOS	B-72			
			NTSR	B-73			
		6	NOS	B-74			
			NTSR	B-75			

Heavy Wheel Loads

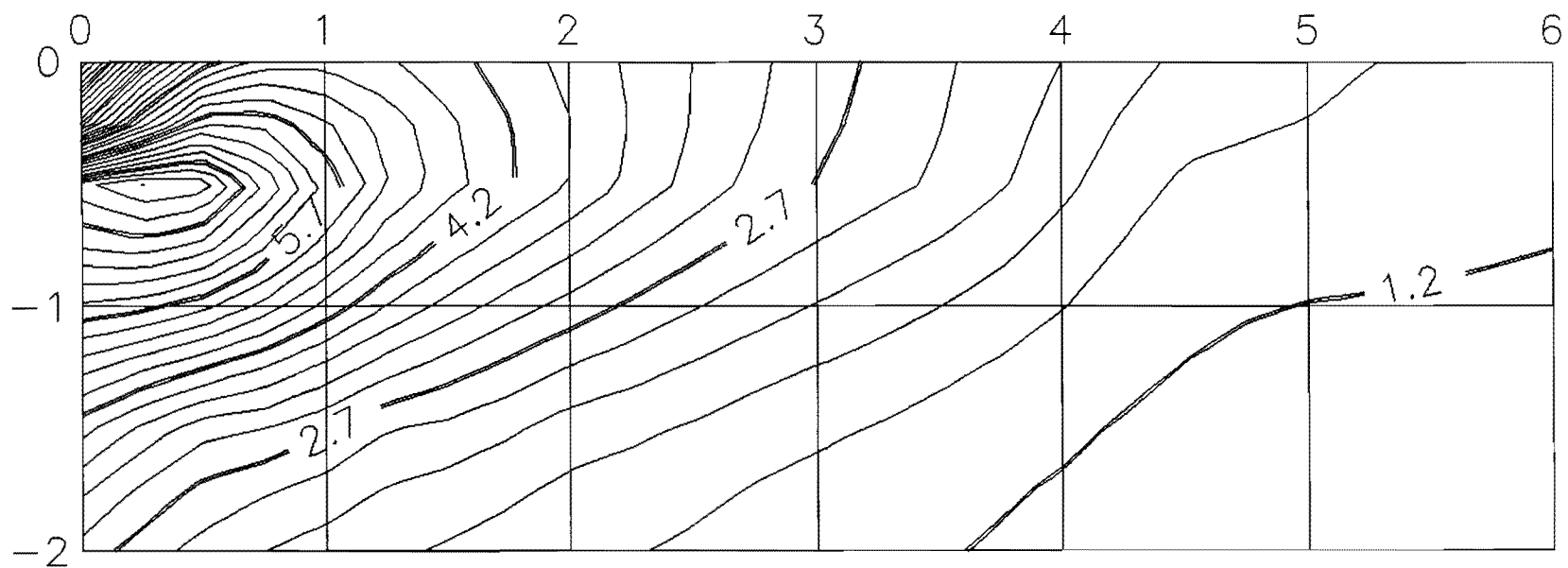
<u>Seasons</u>	<u>Base Type</u>	<u>ACP Thickness, in.</u>	<u>Condition of Surface Shear</u>	<u>Interlayer Bending</u>	<u>Parameter</u>	<u>Page</u>		
Hot	ACP	4	Hvy. Rlg.	Bond	NOS	B-76		
							NTSR	B-77
	PCC	4					NOS	B-78
							NTSR	B-79
	CLS	4					NOS	B-80
							NTSR	B-81
	ACP	4	Hvy. Brkg.		NOS	B-82		
							NTSR	B-83
	PCC	4					NOS	B-84
							NTSR	B-85
	CLS	4					NOS	B-86
							NTSR	B-87

Nor. Oct. Stress (psi) - 2 in. AC/AC Base - Mod. Season - Rolling Wheel - Bond



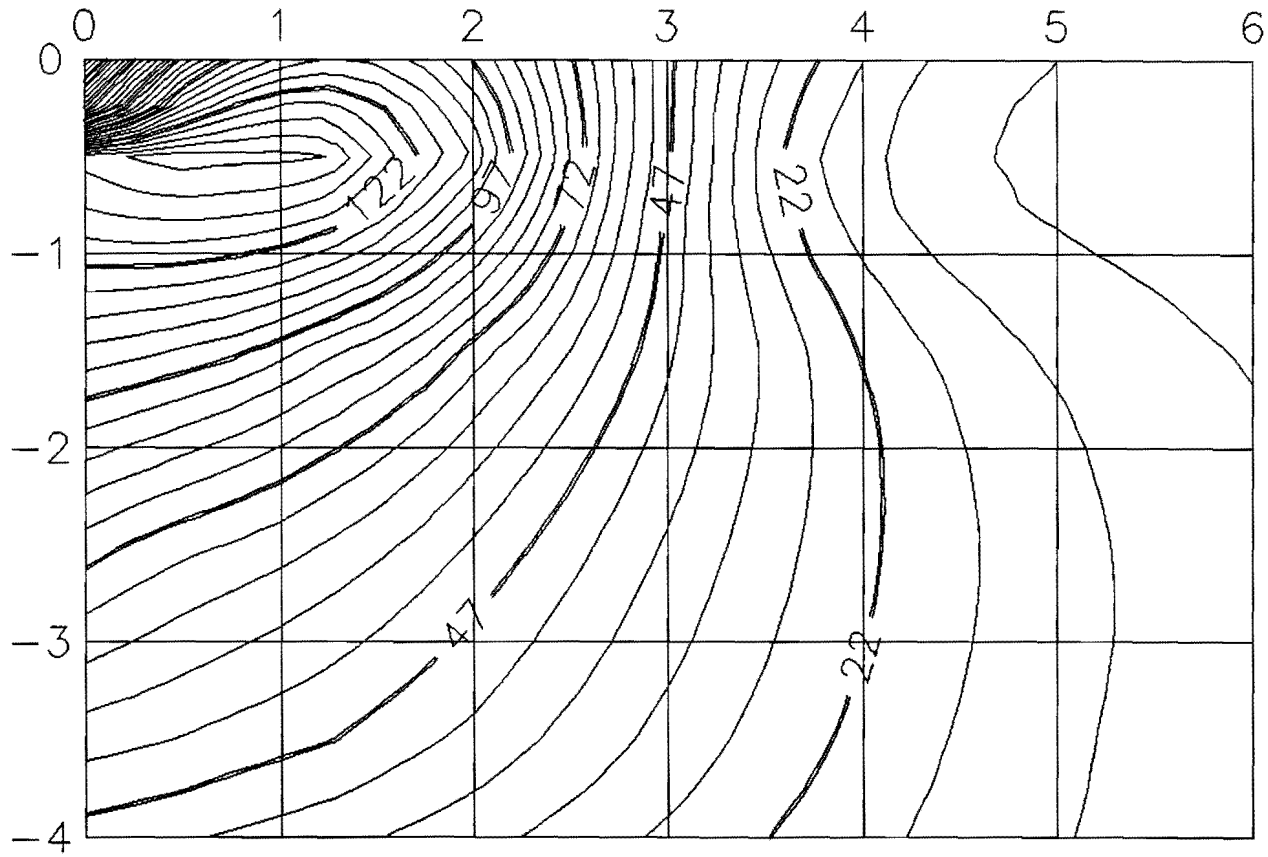
B-4

NTSR - 2 in. AC/AC Base - Moderate Season - Rolling Wheel - Bond

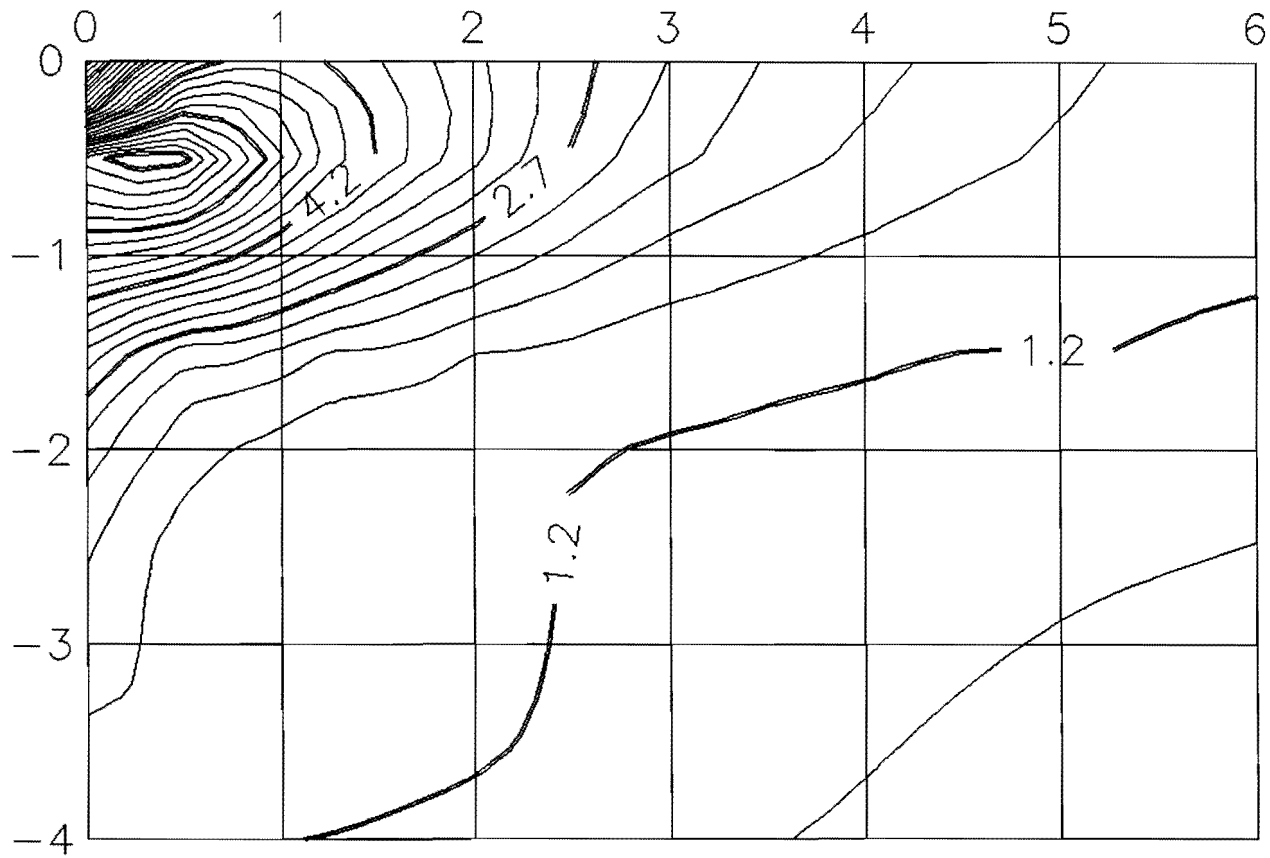


B-5

Nor. Oct. Stress (psi) - 4 in. AC/AC Base - Mod. Season - Rolling Wheel - Bond

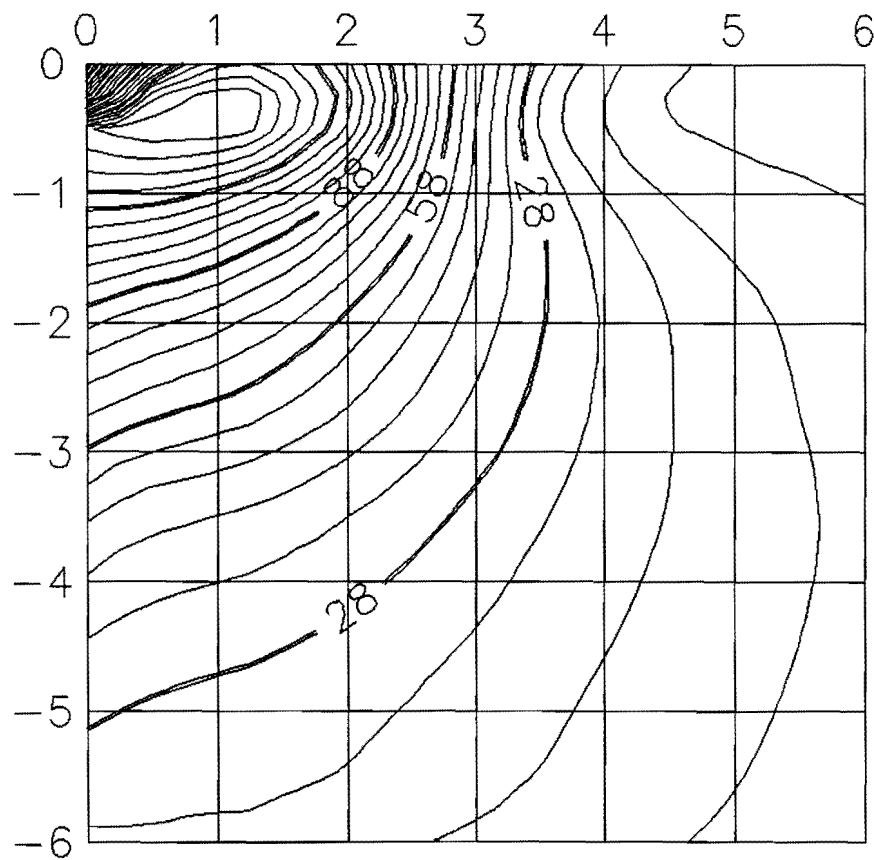


NTSR - 4 in. AC/AC Base - Moderate Season - Rolling Wheel - Bond



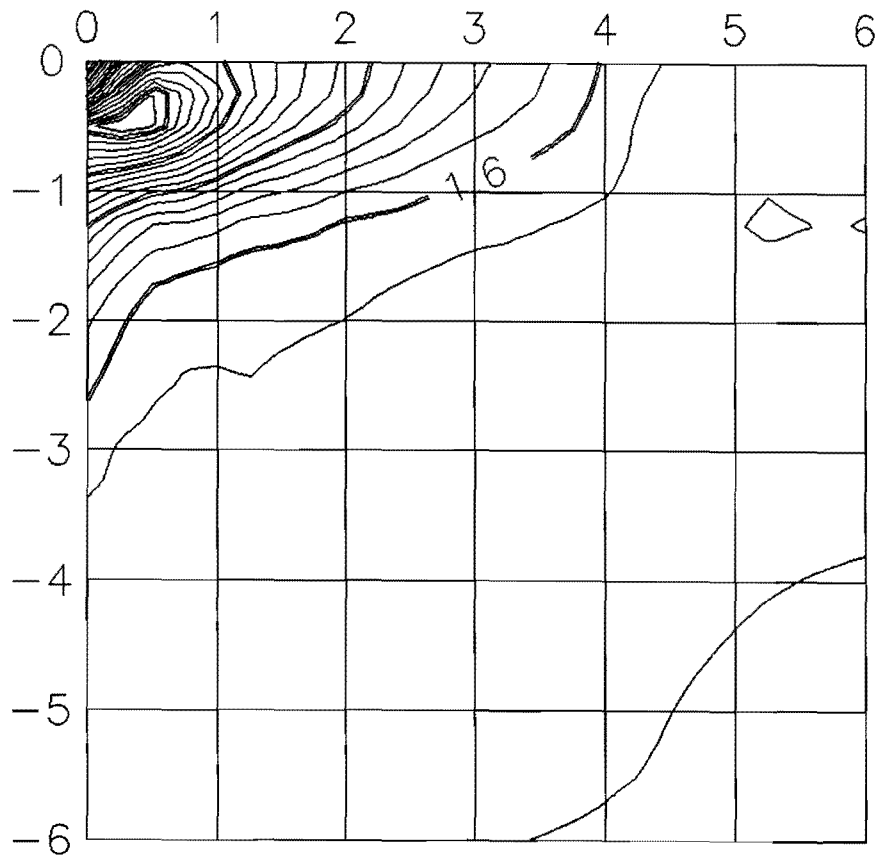
B-7

Nor. Oct. Stress (psi) - 6 in. AC/AC Base - Mod. Season - Rolling Wheel - Bond



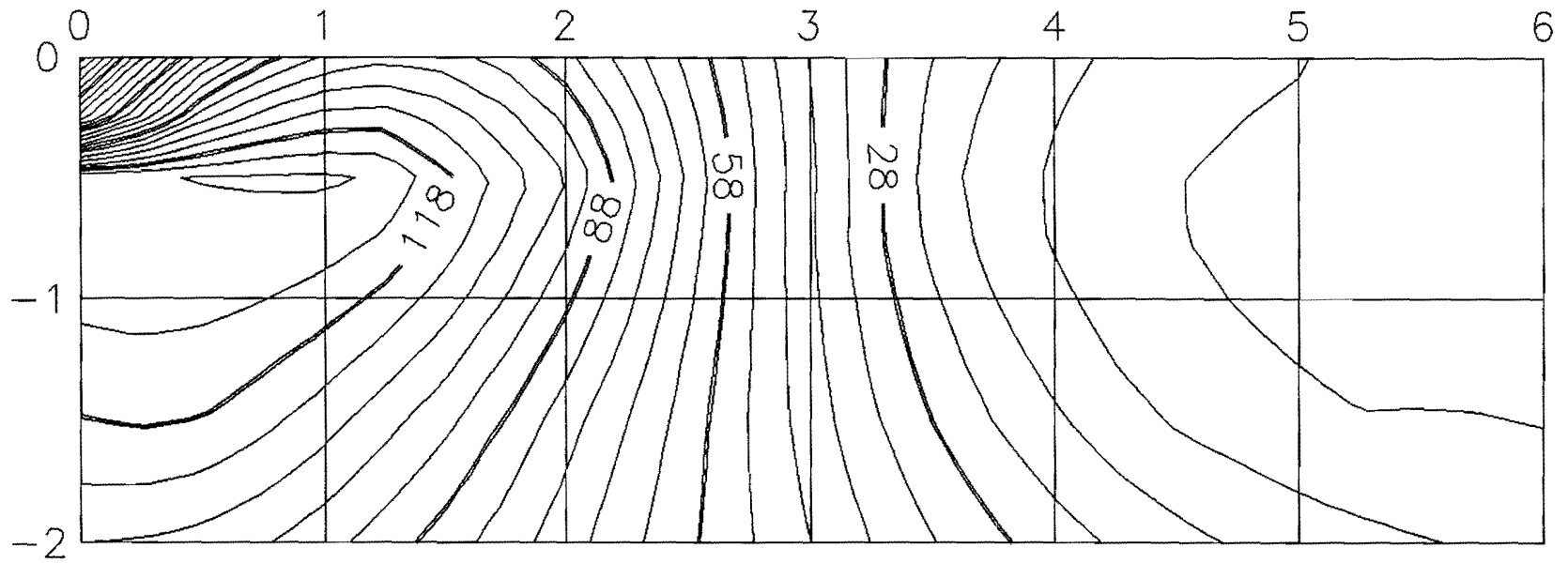
B-8

NTSR - 6 in. AC/AC Base - Moderate Season - Rolling Wheel - Bond



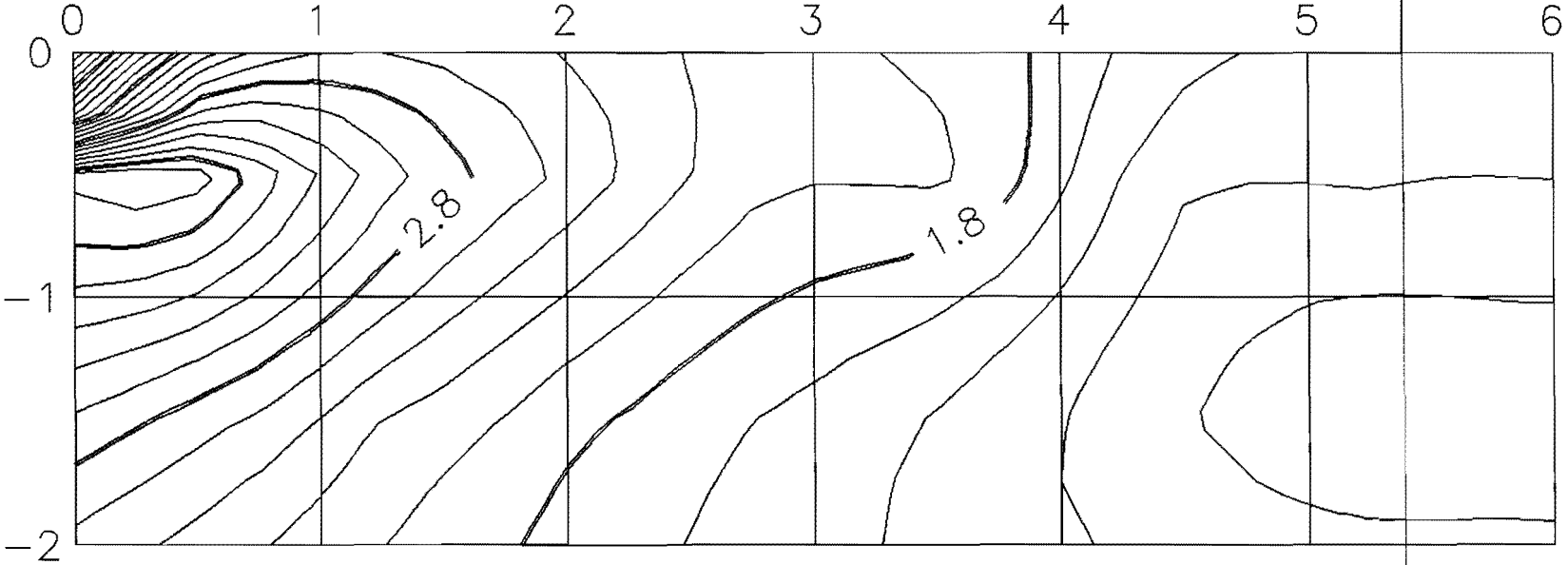
B-9

Nor. Oct. Stress (psi) - 2 in. AC/PCC Base - Mod. Season - Rolling Wheel - Bond



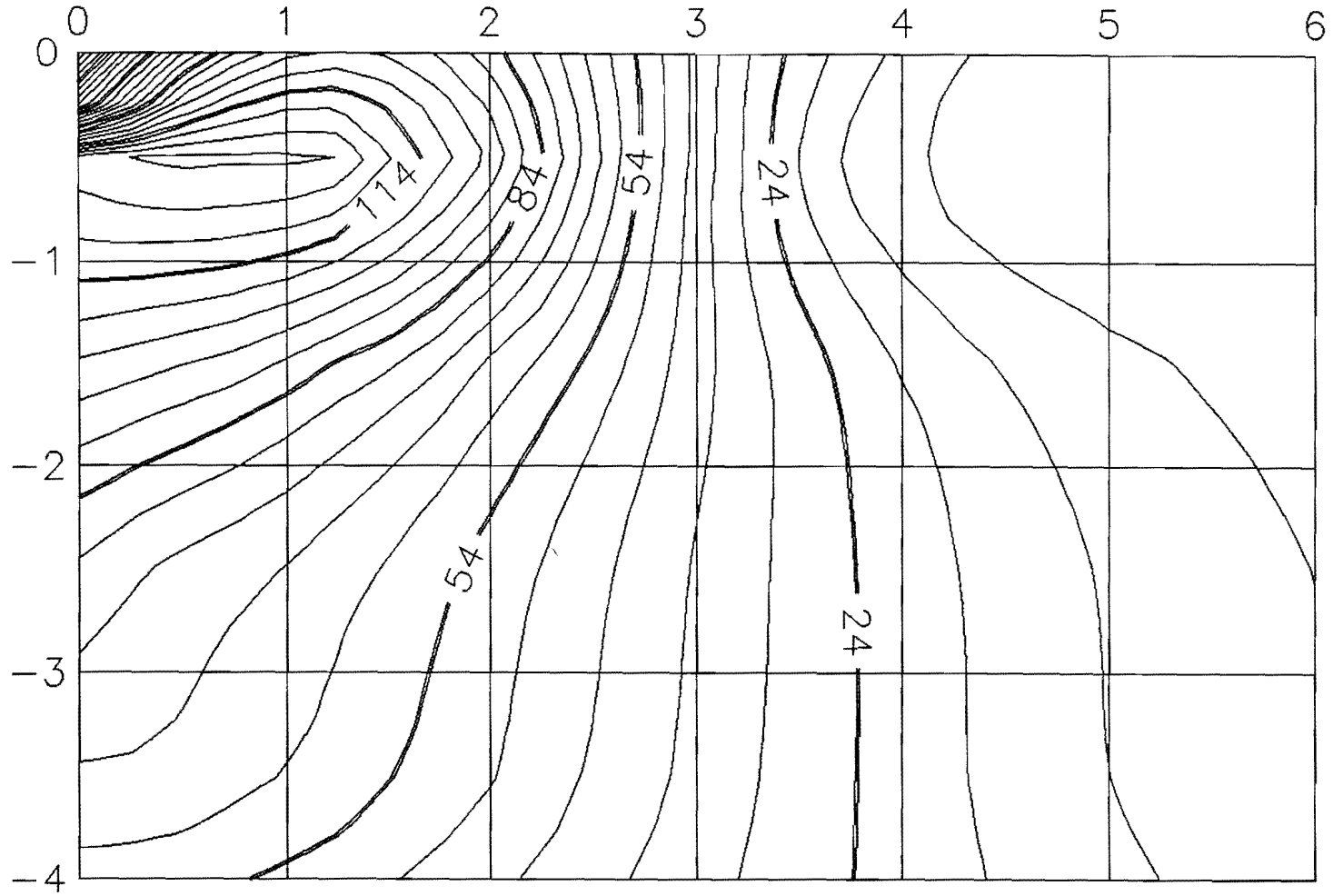
B-10

NTSR - 2 in. AC/PCC Base - Moderate Season - Rolling Wheel - Bond



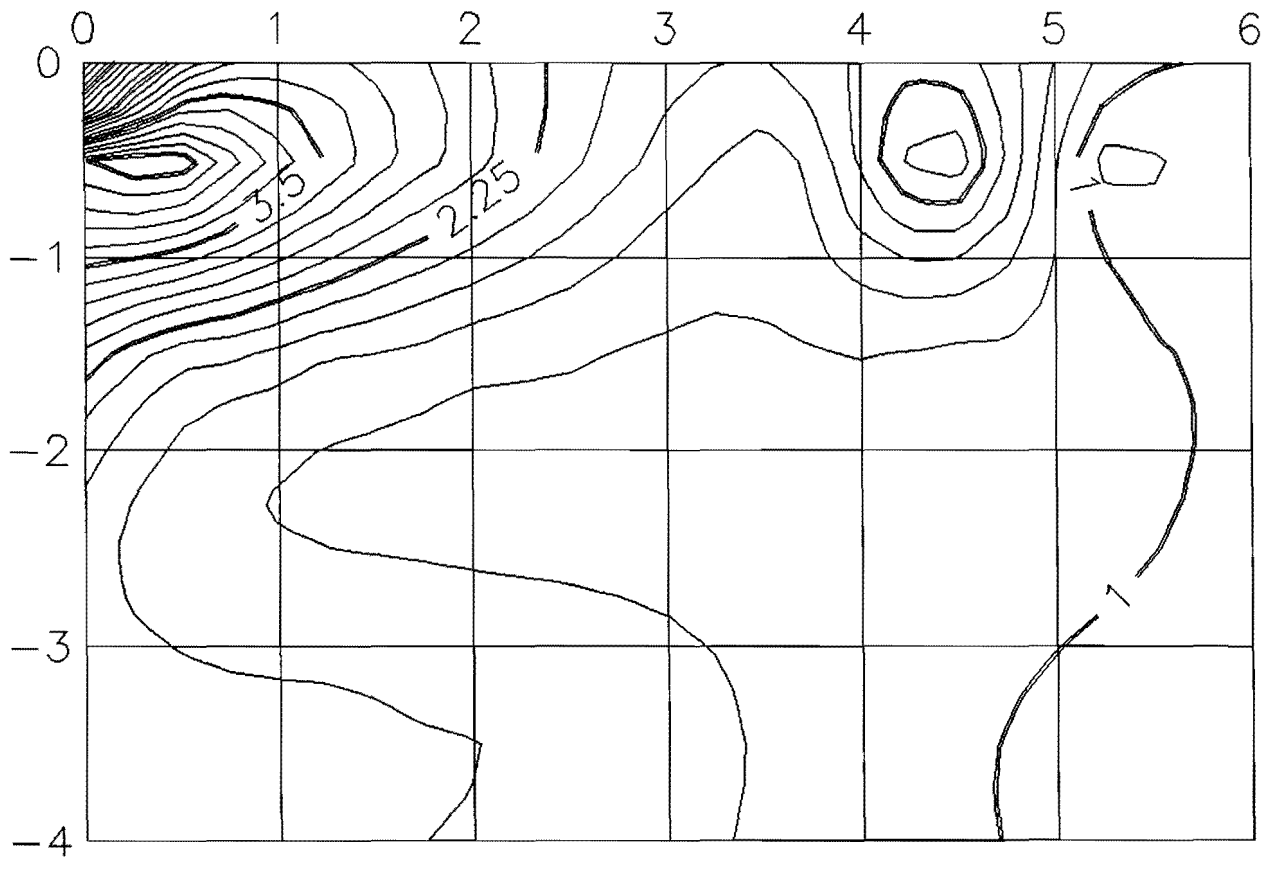
B-11

Nor. Oct. Stress (psi) - 4 in. AC/PCC Base - Mod. Season - Rolling Wheel - Bond



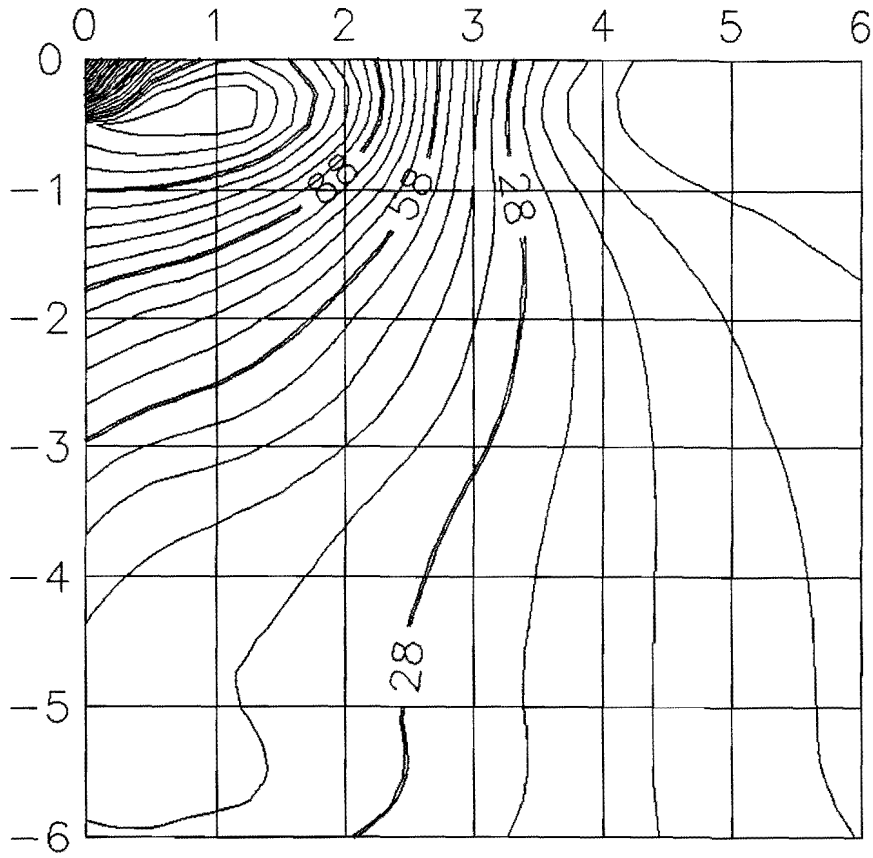
B-12

NTSR - 4 in. AC/PCC Base - Moderate Season - Rolling Wheel - Bond

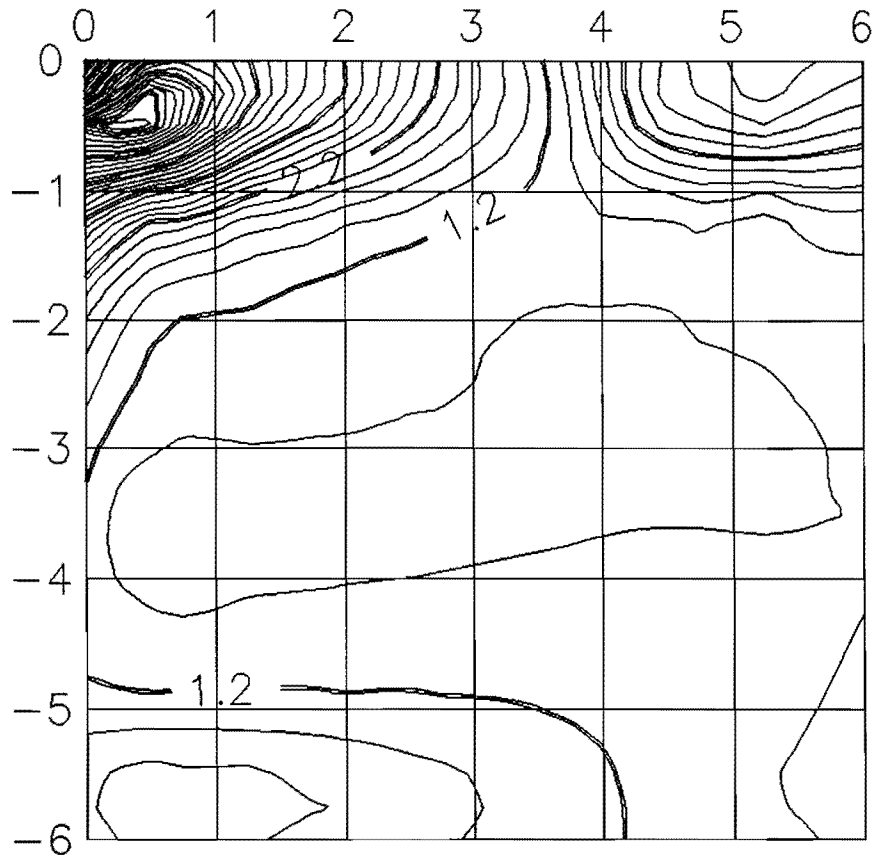


B-13

Nor. Oct. Stress (psi) - 6 in. AC/PCC Base - Mod. Season - Rolling Wheel - Bond

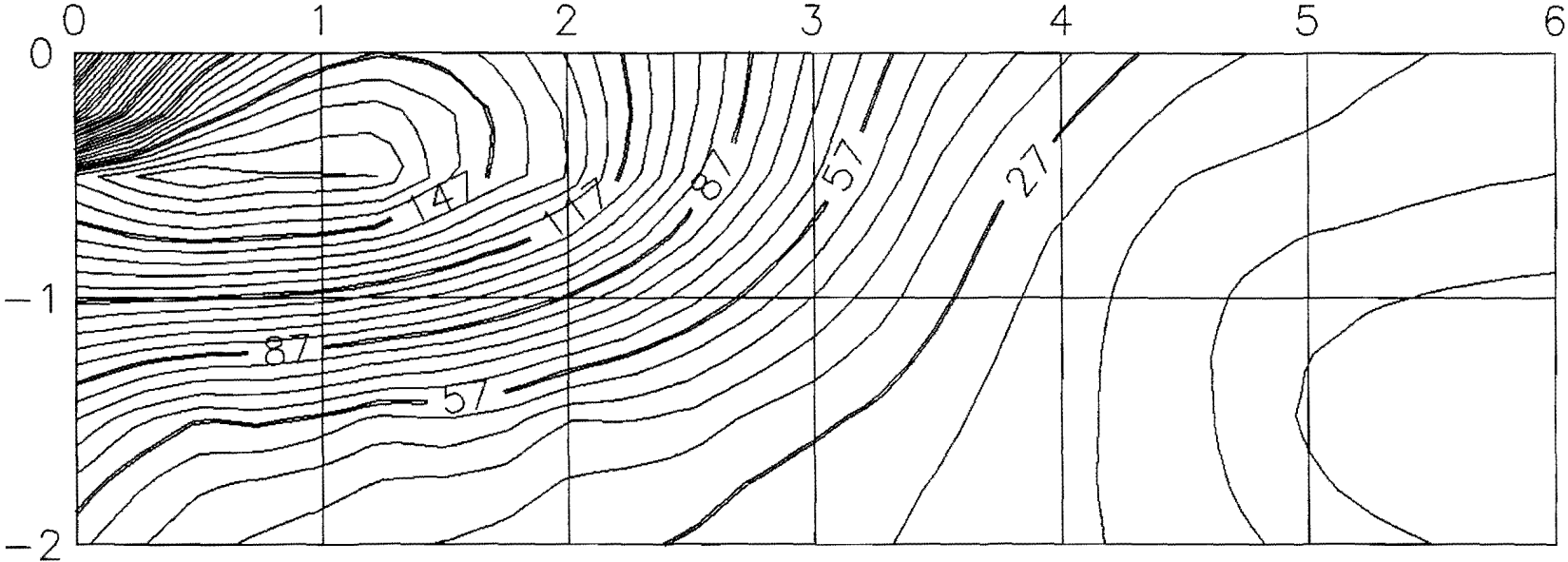


NTSR - 6 in. AC/PCC Base - Moderate Season - Rolling Wheel - Bond



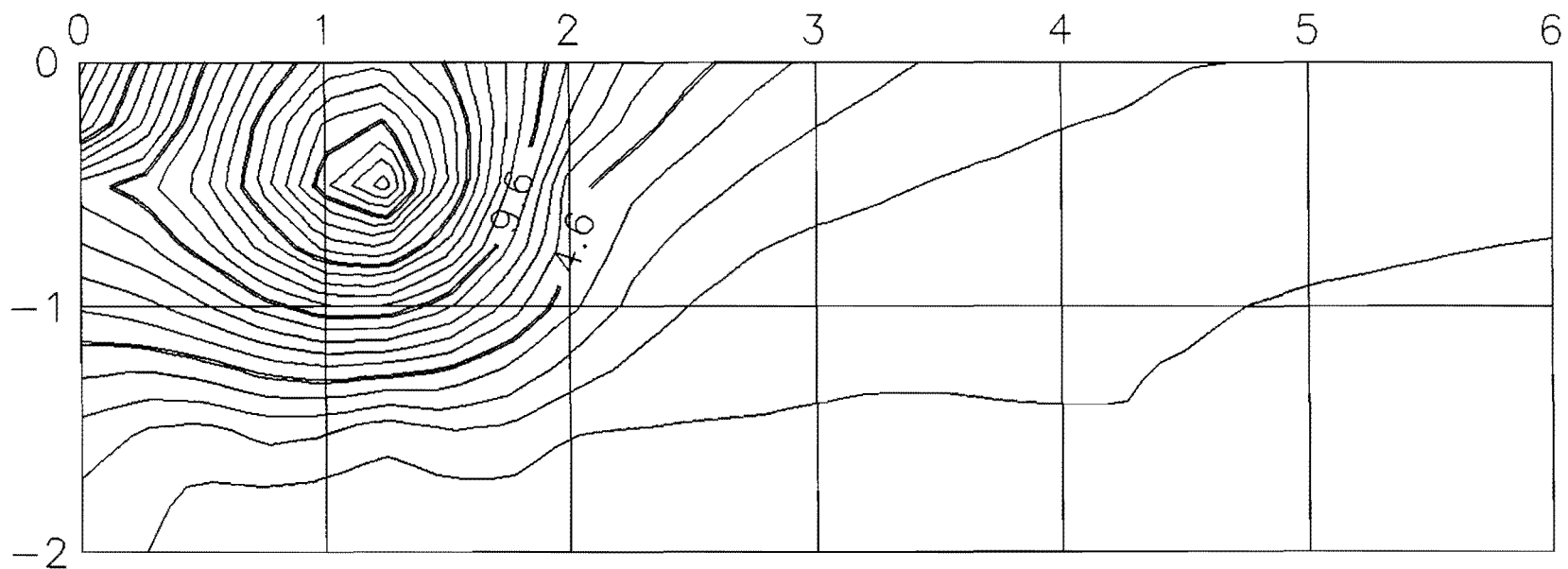
B-15

Nor. Oct. Stress (psi) - 2 in. AC/CLS Base - Mod. Season - Rolling Wheel - Bond



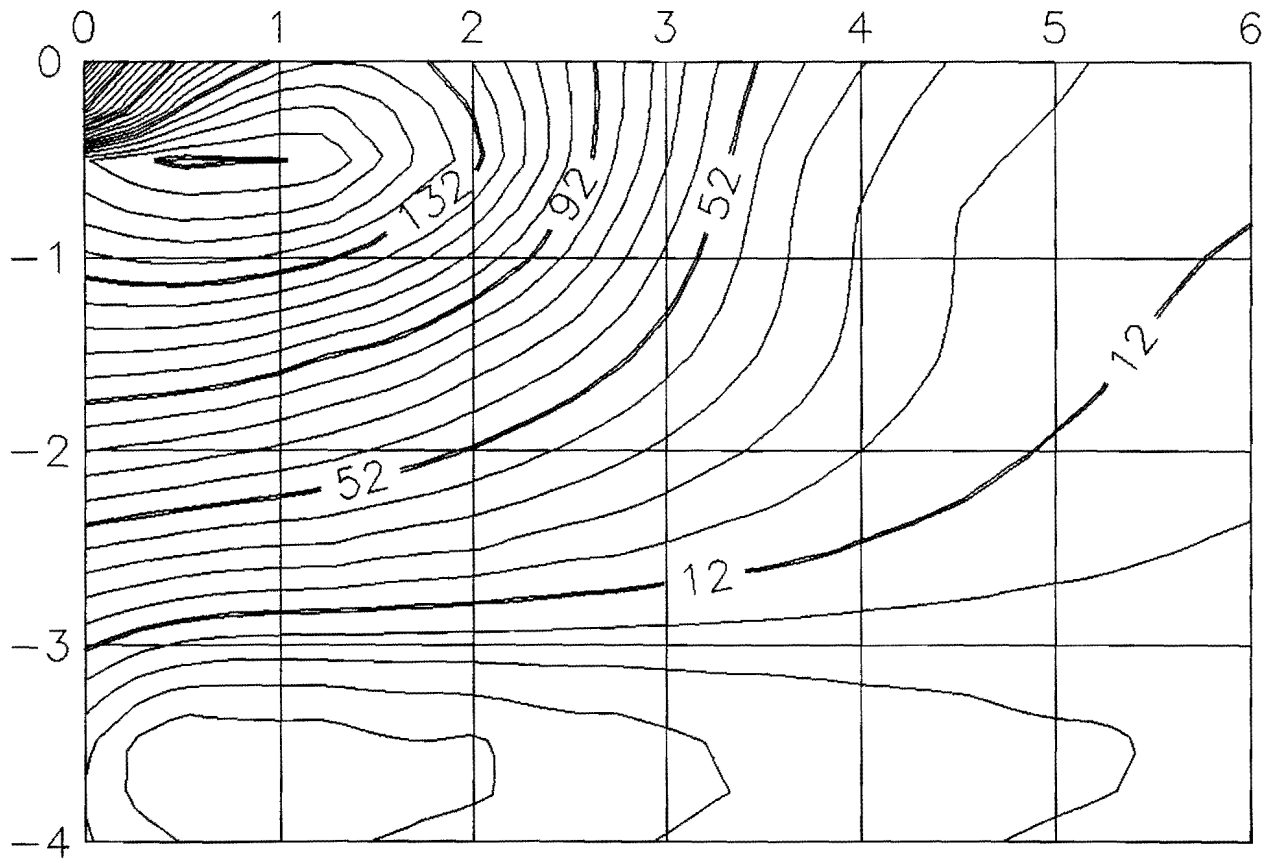
B-16

NTSR - 2 in. AC/CLS Base - Moderate Season - Rolling Wheel - Bond



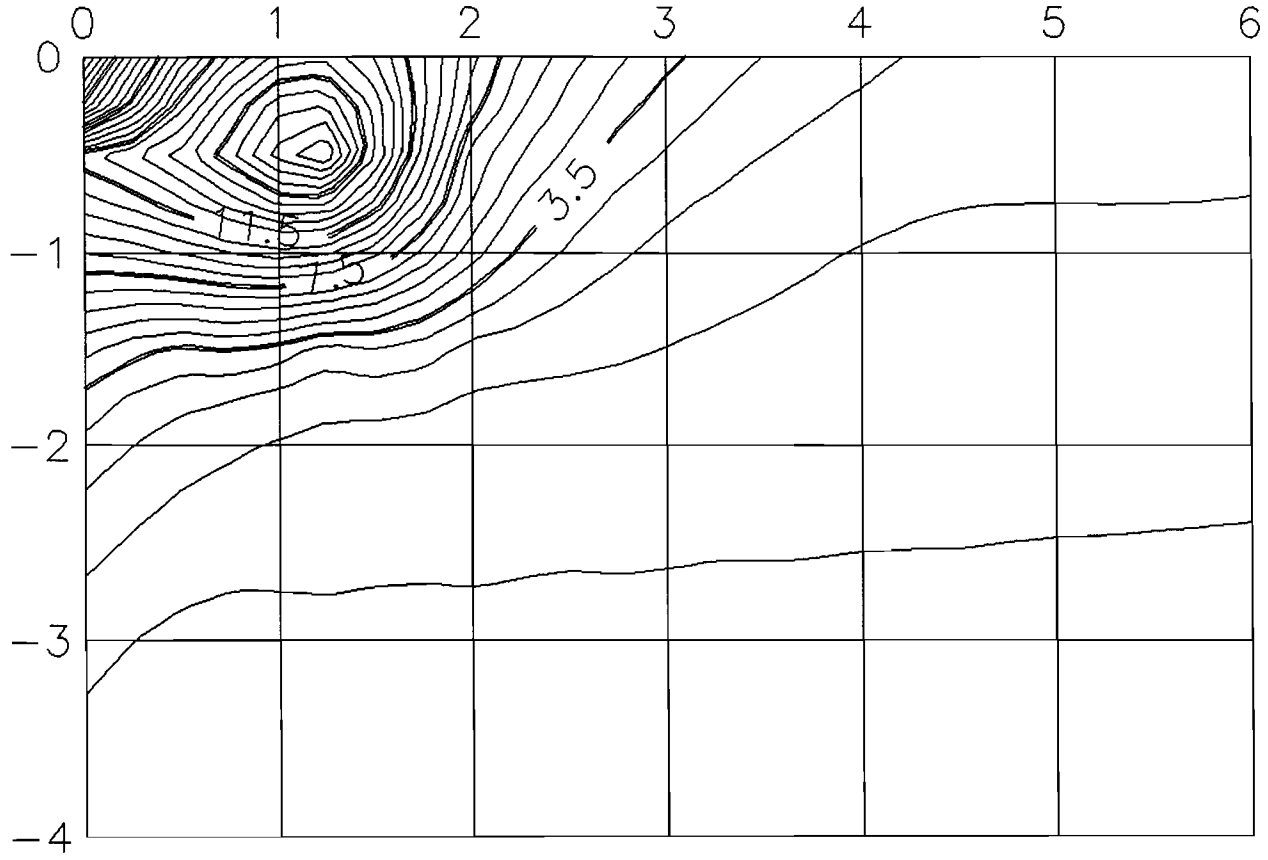
B-17

Nor. Oct. Stress (psi) - 4 in. AC/CLS Base - Mod. Season - Rolling Wheel - Bond



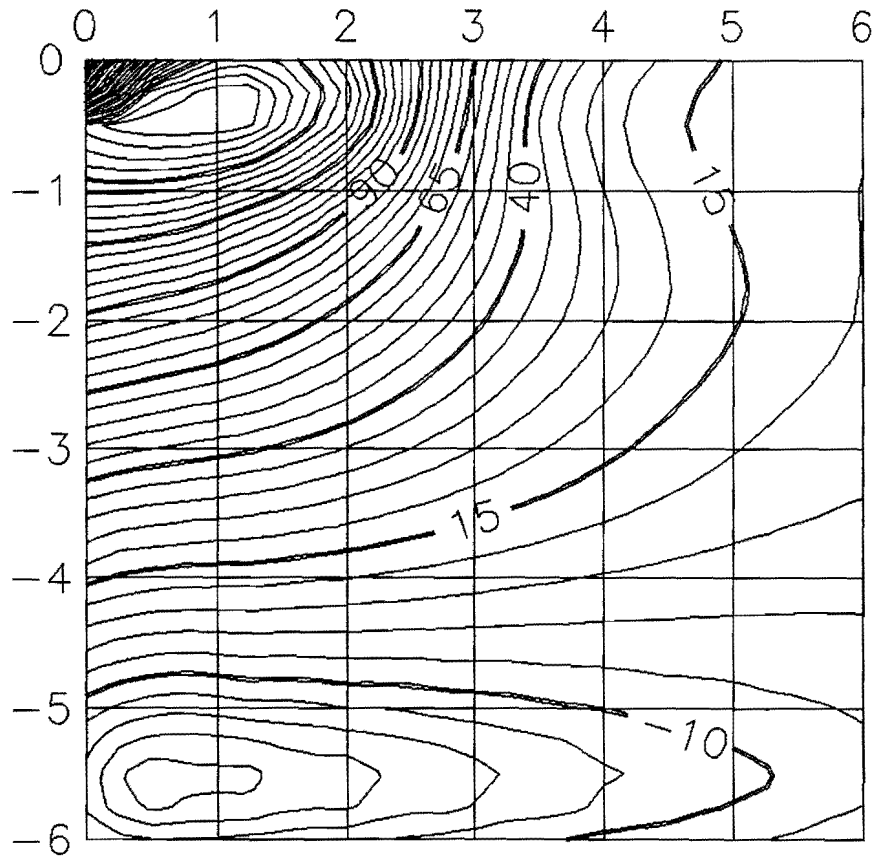
B-18

NTSR - 4 in. AC/CLS Base - Moderate Season - Rolling Wheel - Bond



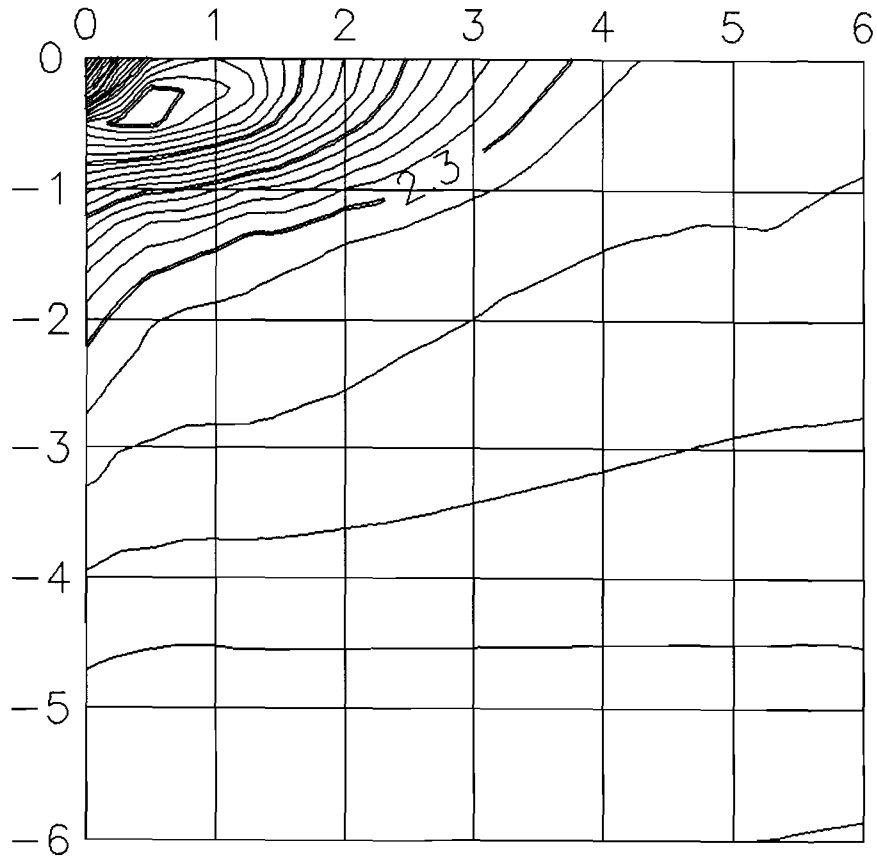
B-19

Nor. Oct. Stress (psi) - 6 in. AC/CLS Base - Mod. Season - Rolling Wheel - Bond

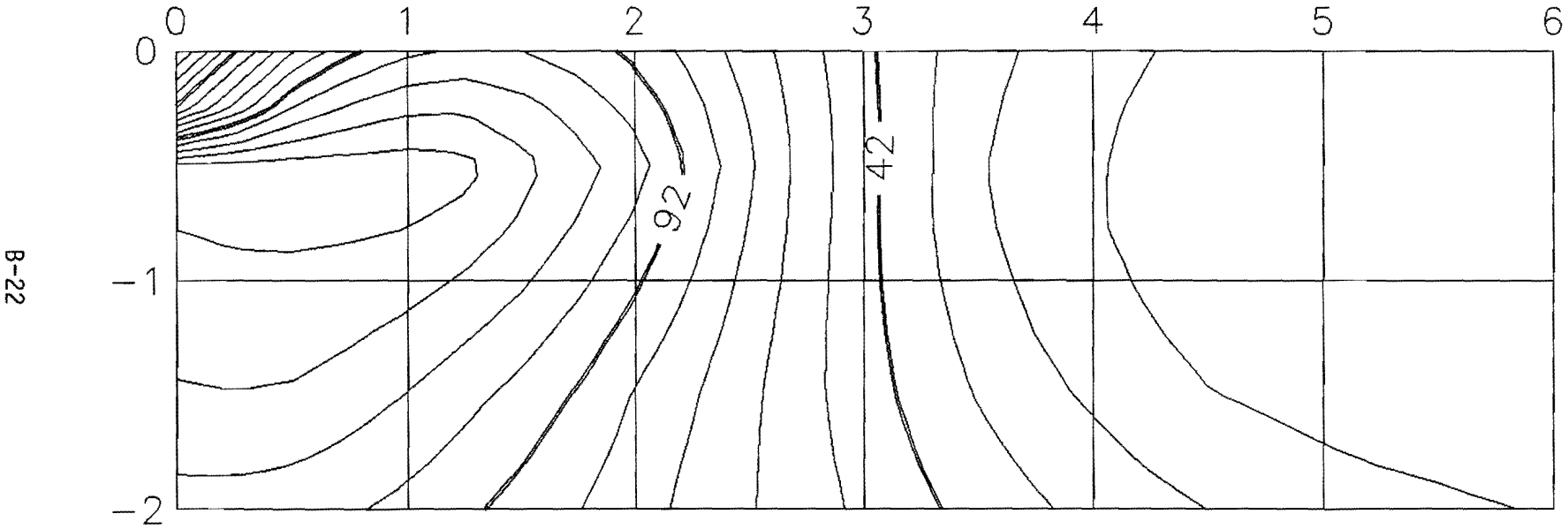


B-20

NTSR - 6 in. AC/CLS Base - Moderate Season - Rolling Wheel - Bond

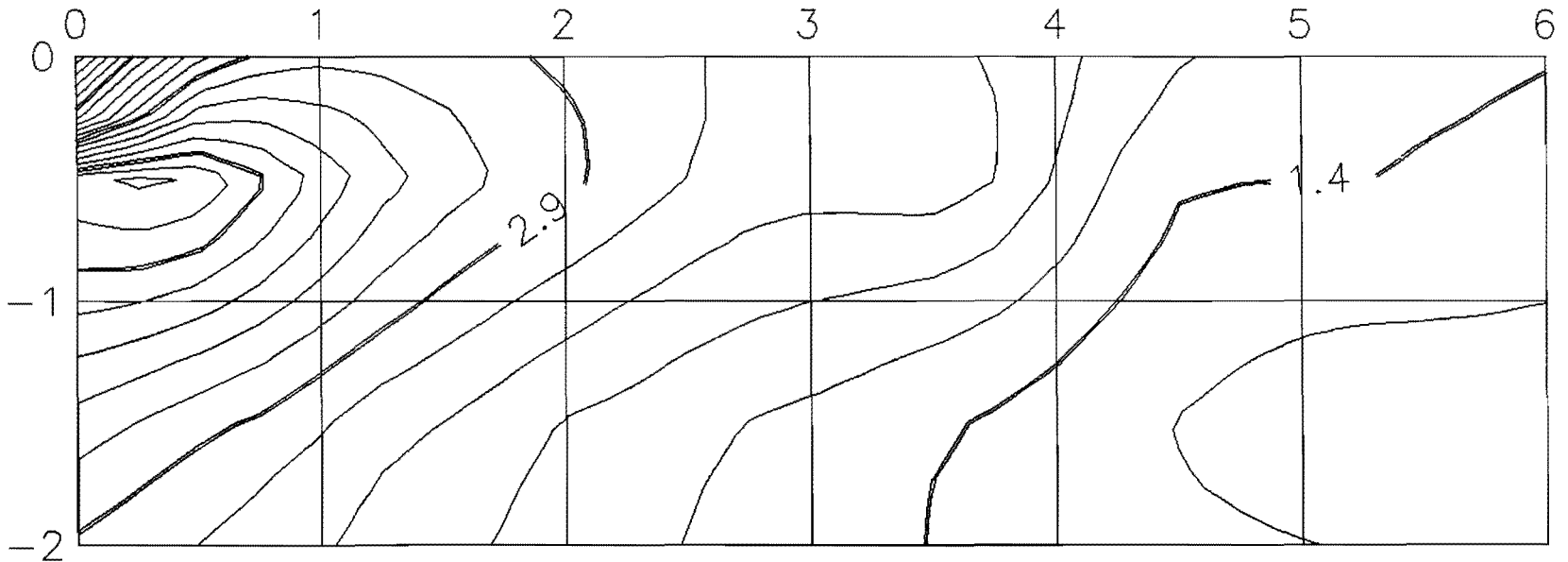


Nor. Oct. Stress (psi) - 2 in. AC/AC Base - Hot Season - Rolling Wheel - Bond



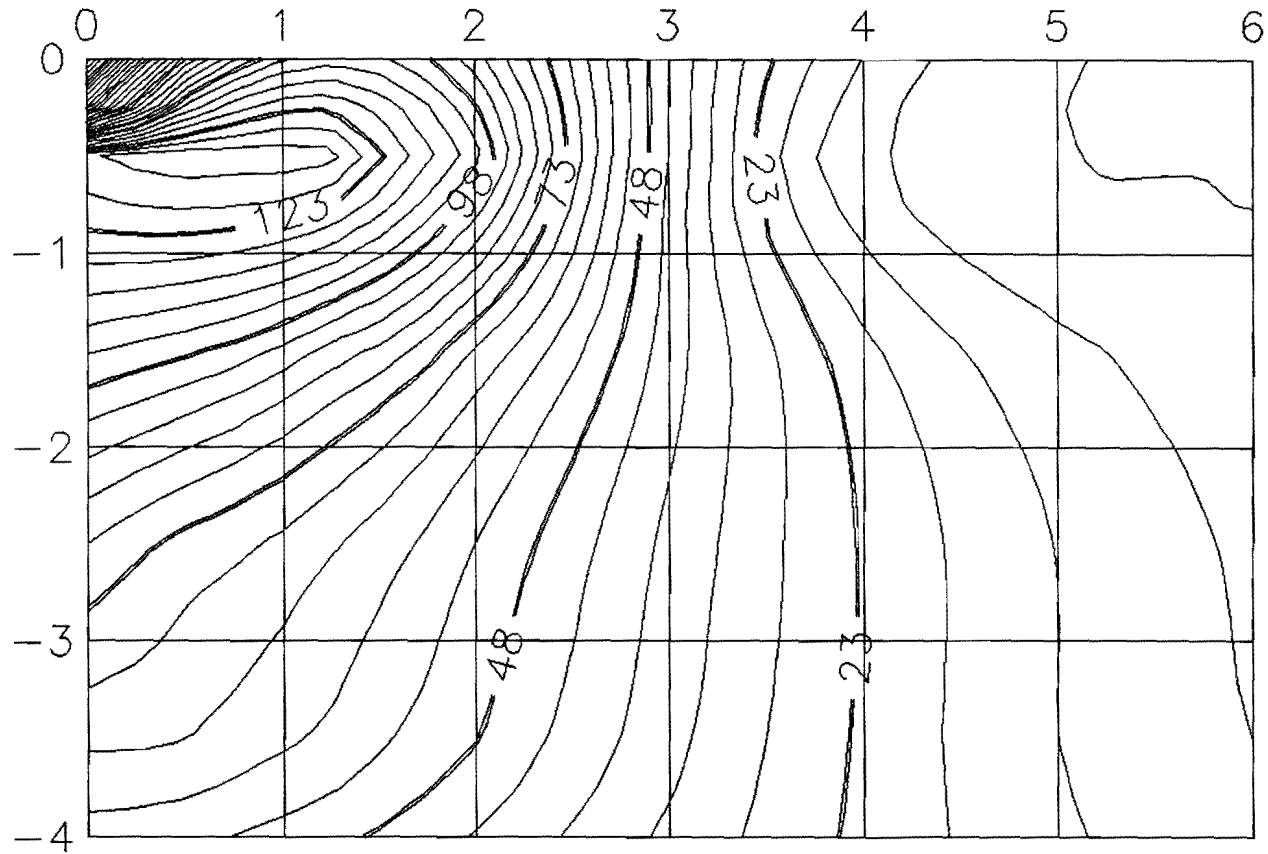
B-22

NTSR - 2 in. AC/AC Base - Hot Season - Rolling Wheel - Bond



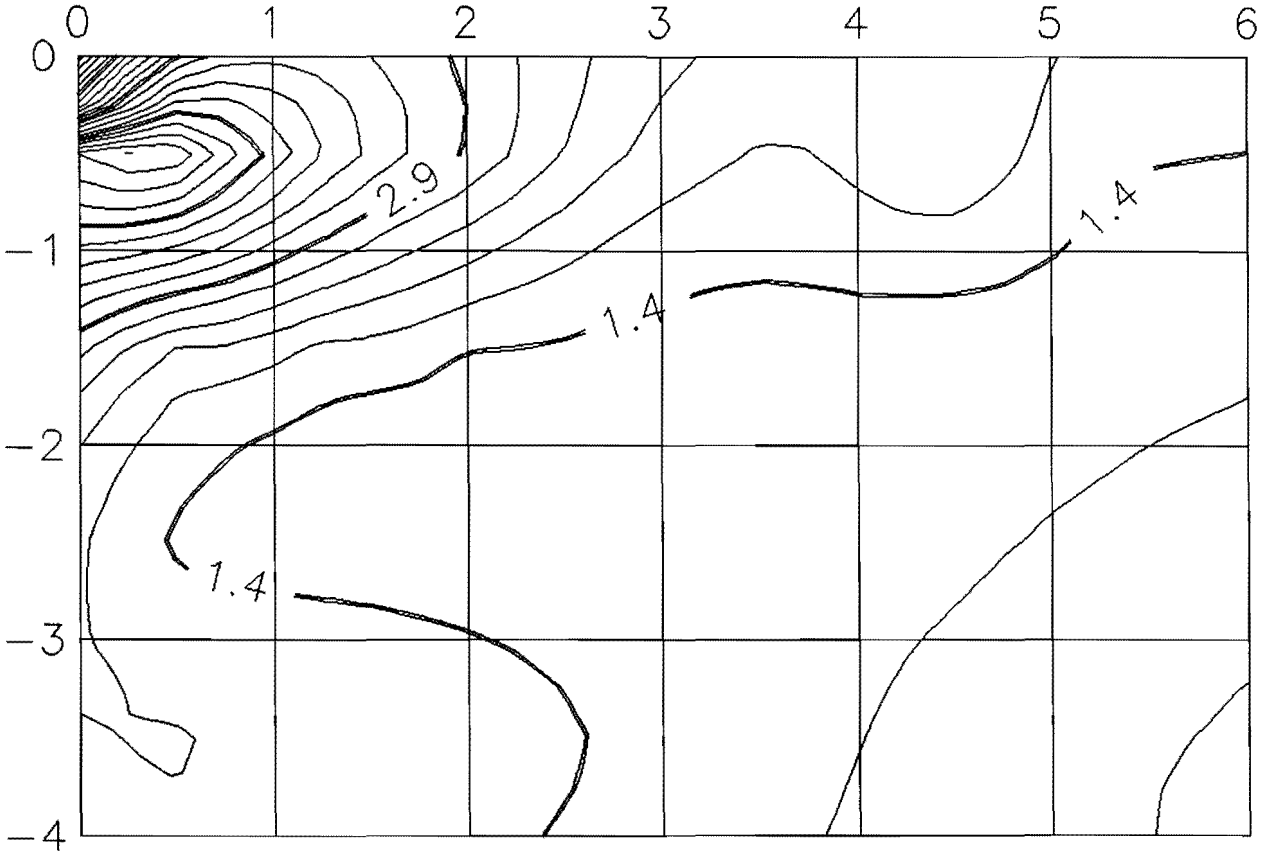
B-23

Nor. Oct. Stress (psi) - 4 in. AC/AC Base - Hot Season - Rolling Wheel - Bond



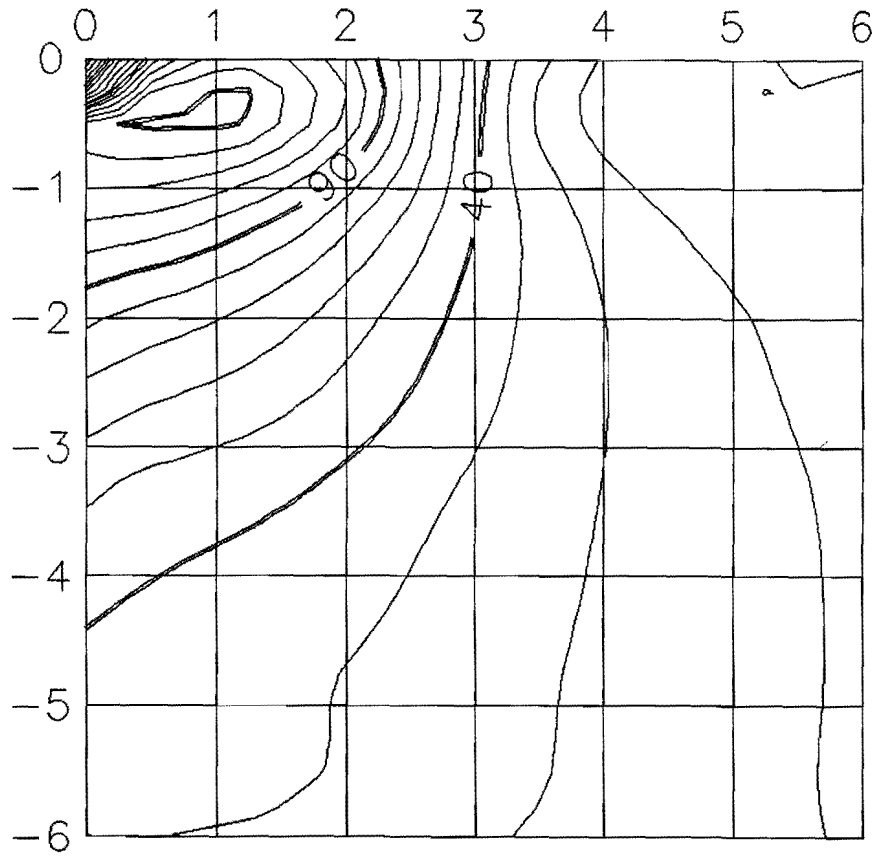
B-24

NTSR - 4 in. AC/AC Base - Hot Season - Rolling Wheel - Bond

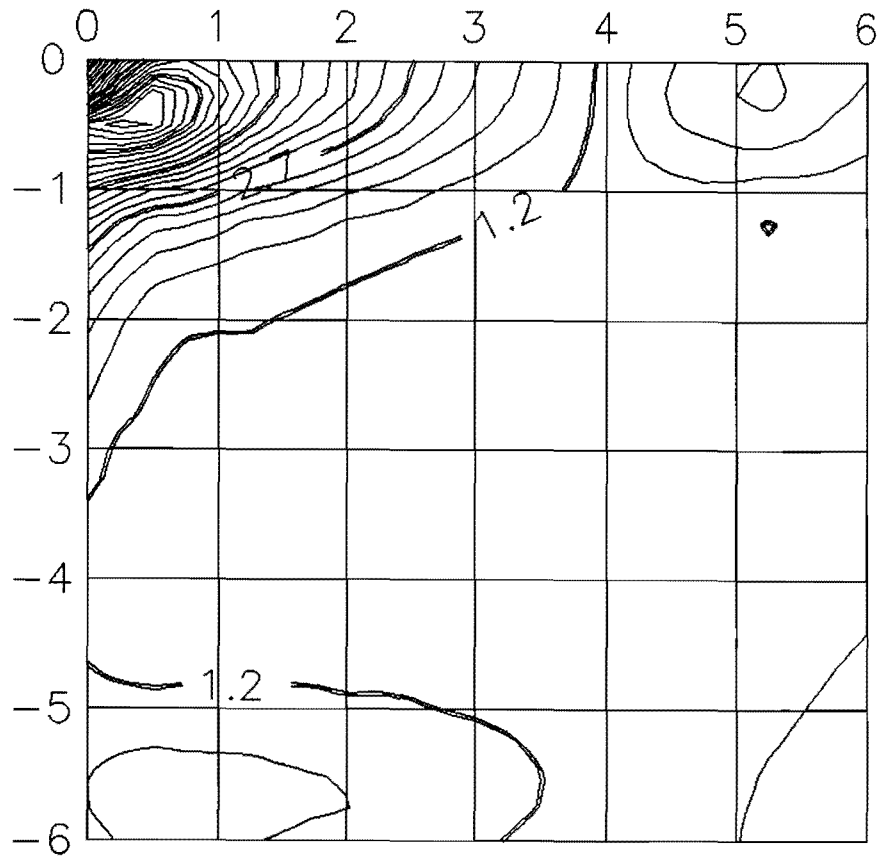


B-25

Nor. Oct. Stress (psi) - 6 in. AC/AC Base - Hot Season - Rolling Wheel - Bond

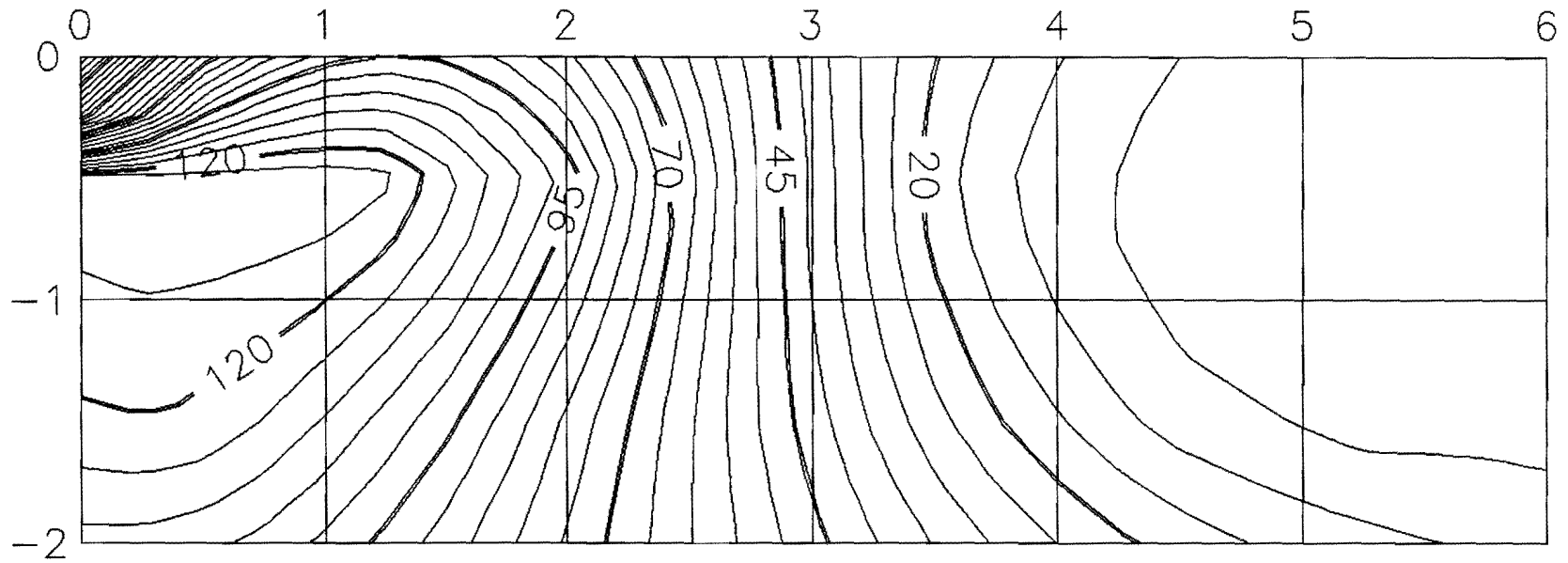


NTSR - 6 in. AC/AC Base - Hot Season - Rolling Wheel - Bond

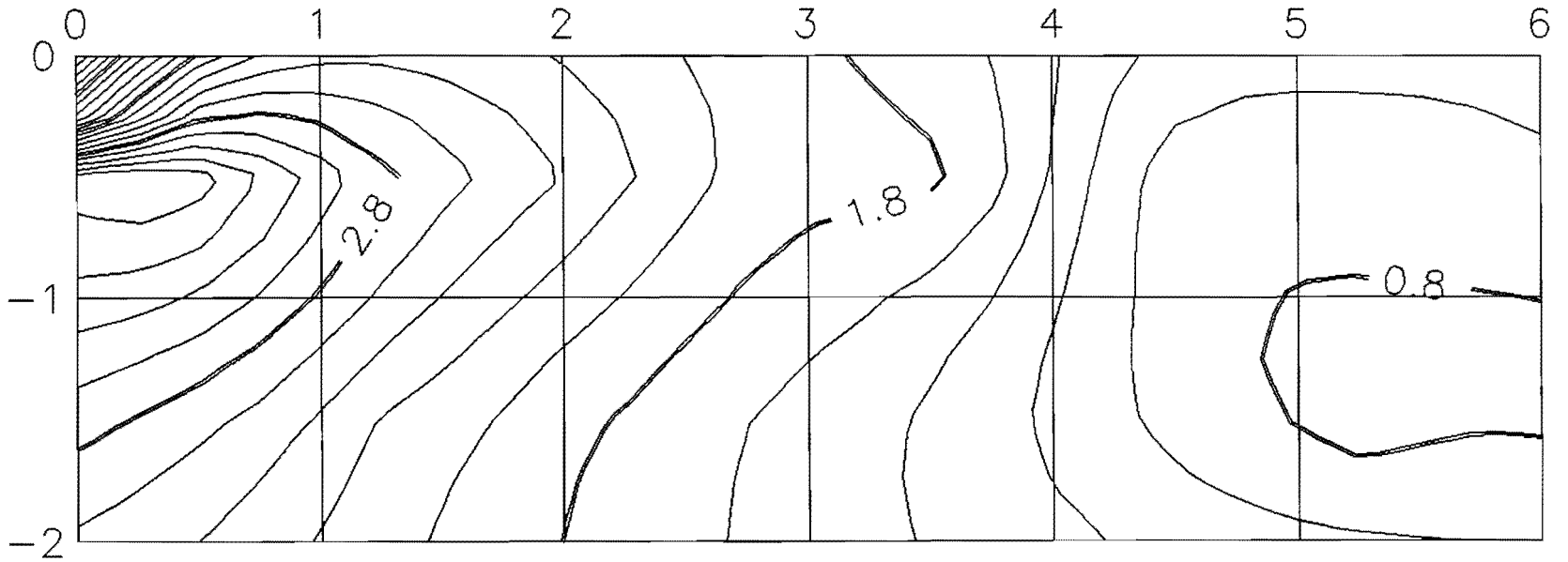


B-27

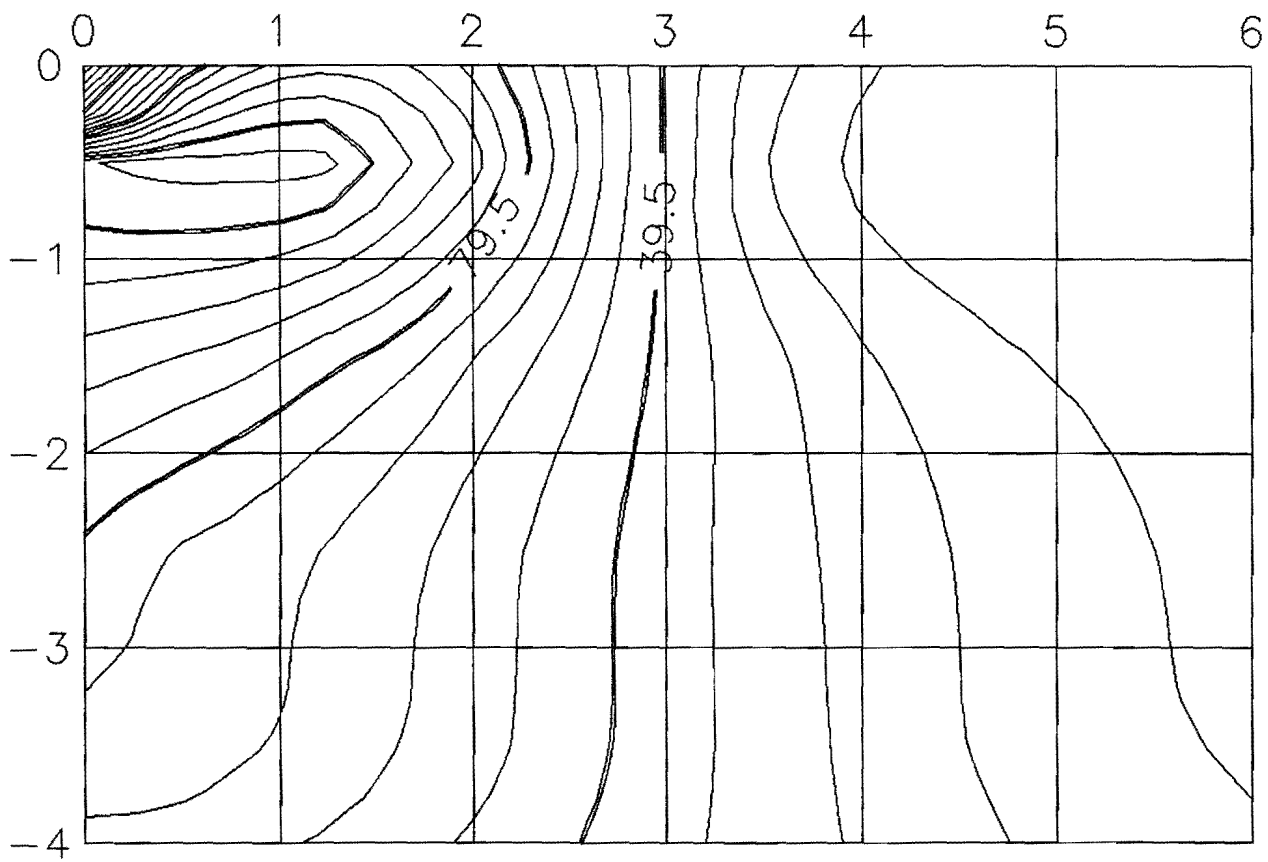
Nor. Oct. Stress (psi) - 2 in. AC/PCC Base - Hot Season - Rolling Wheel - Bond



NTSR - 2 in. AC/PCC Base - Hot Season - Rolling Wheel - Bond

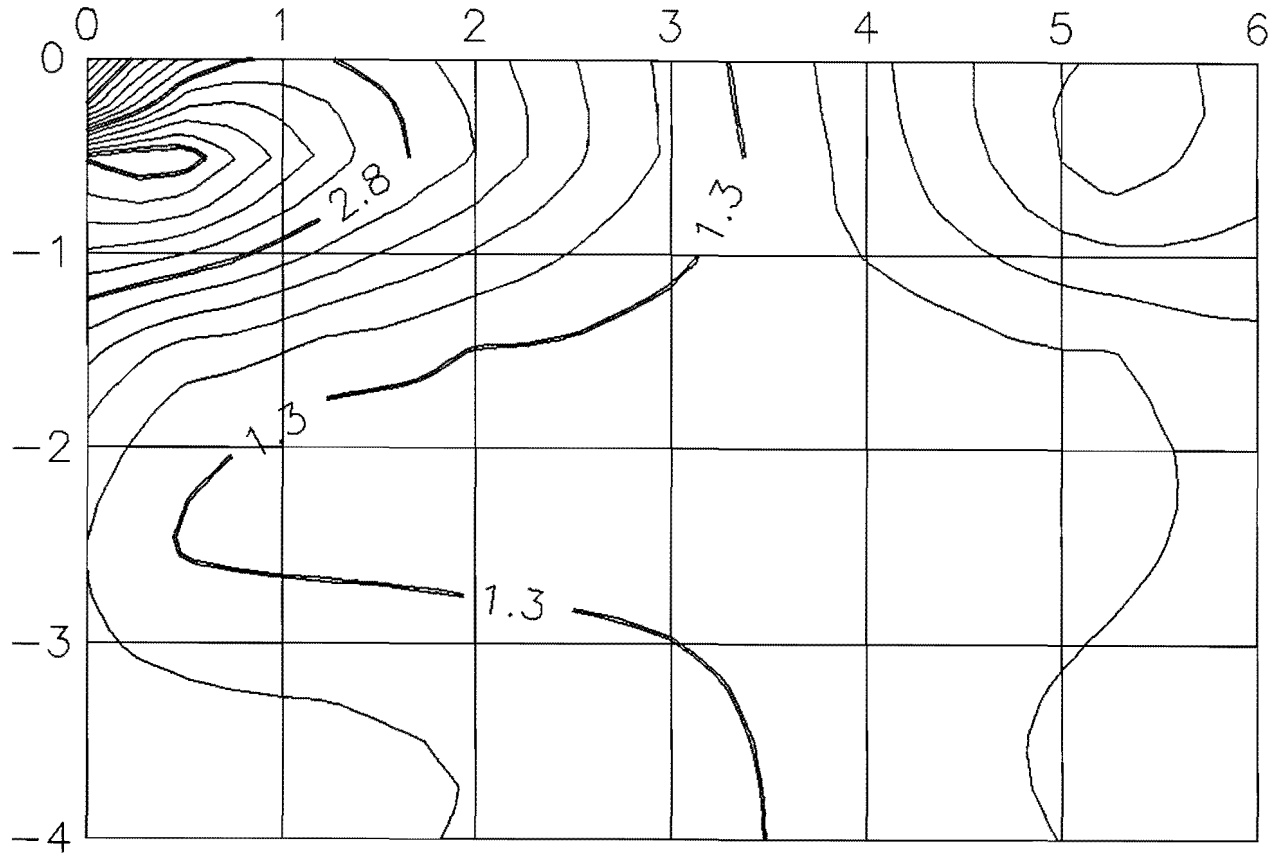


Nor. Oct. Stress (psi) - 4 in. AC/PCC Base - Hot Season - Rolling Wheel - Bond



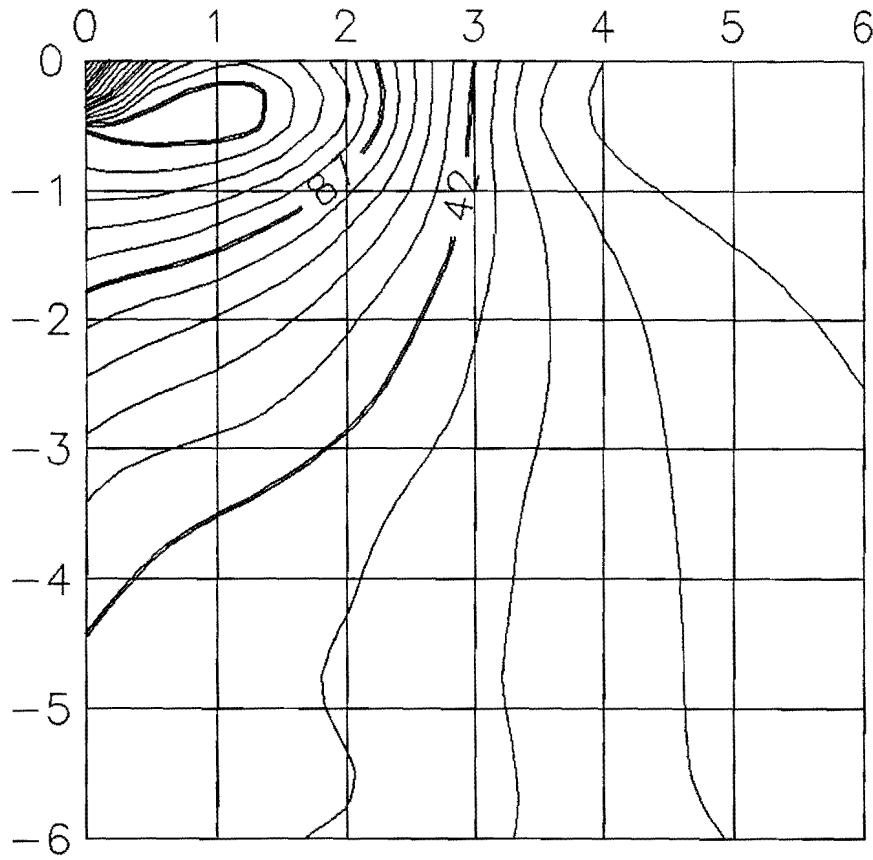
B-30

NTSR - 4 in. AC/PCC Base - Hot Season - Rolling Wheel - Bond

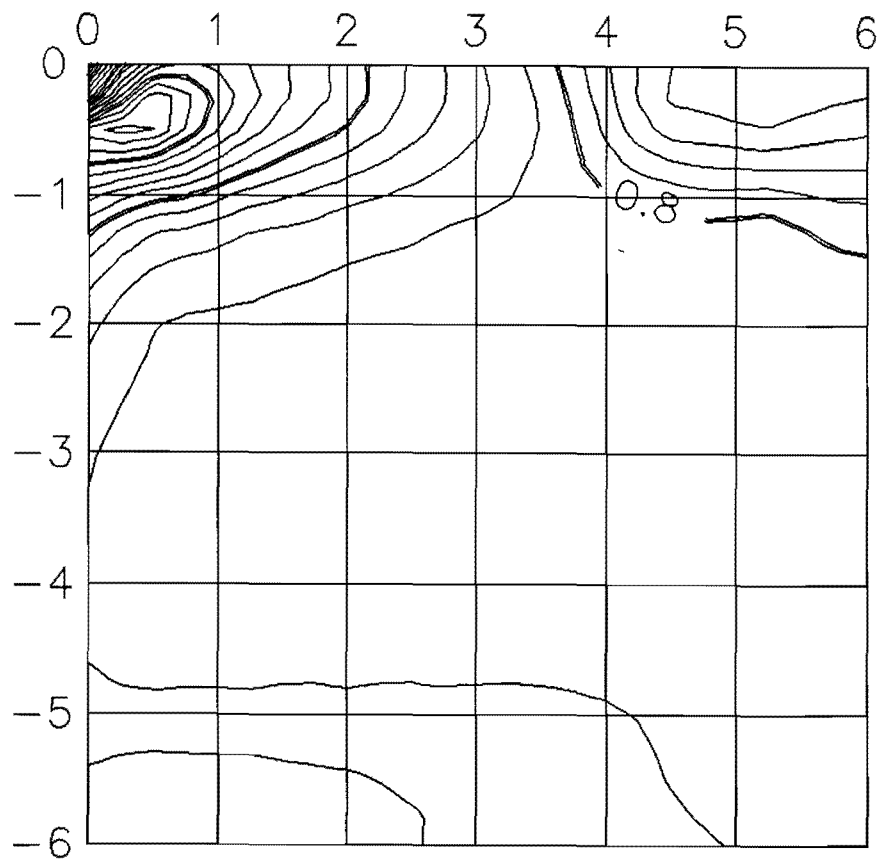


B-31

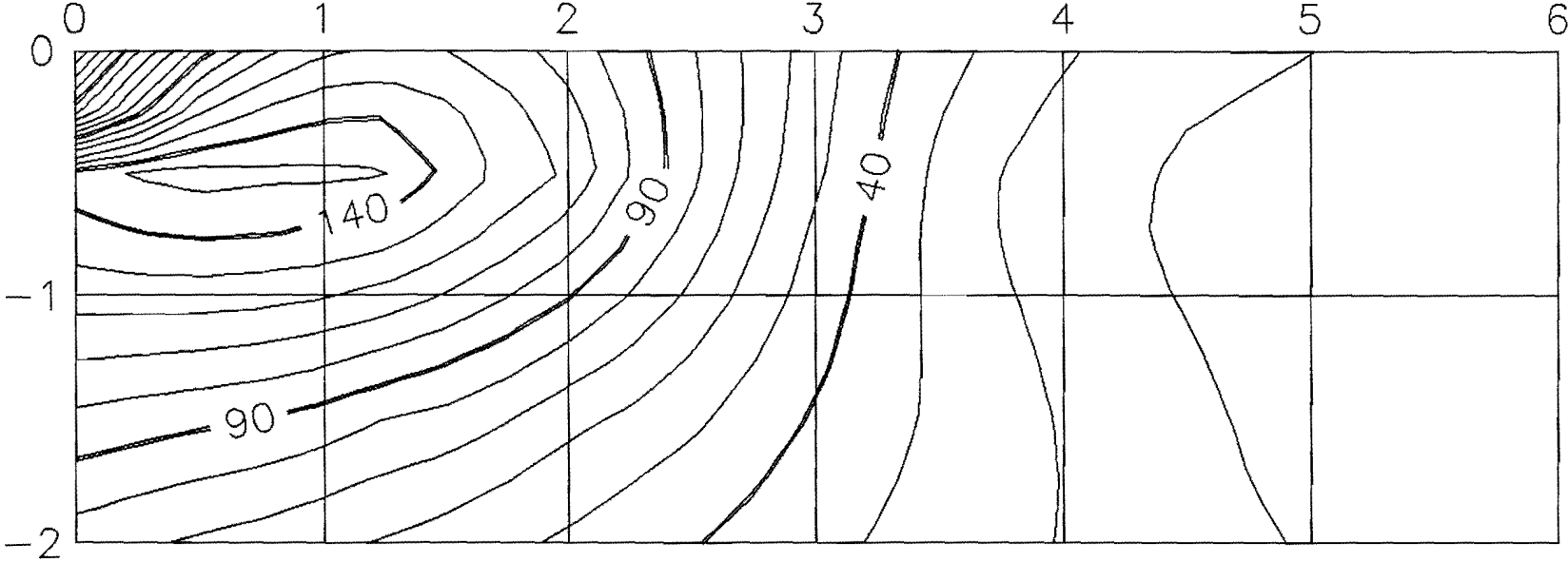
Nor. Oct. Stress (psi) - 6 in. AC/PCC Base - Hot Season - Rolling Wheel - Bond



NTSR - 6 in. AC/PCC Base - Hot Season - Rolling Wheel - Bond

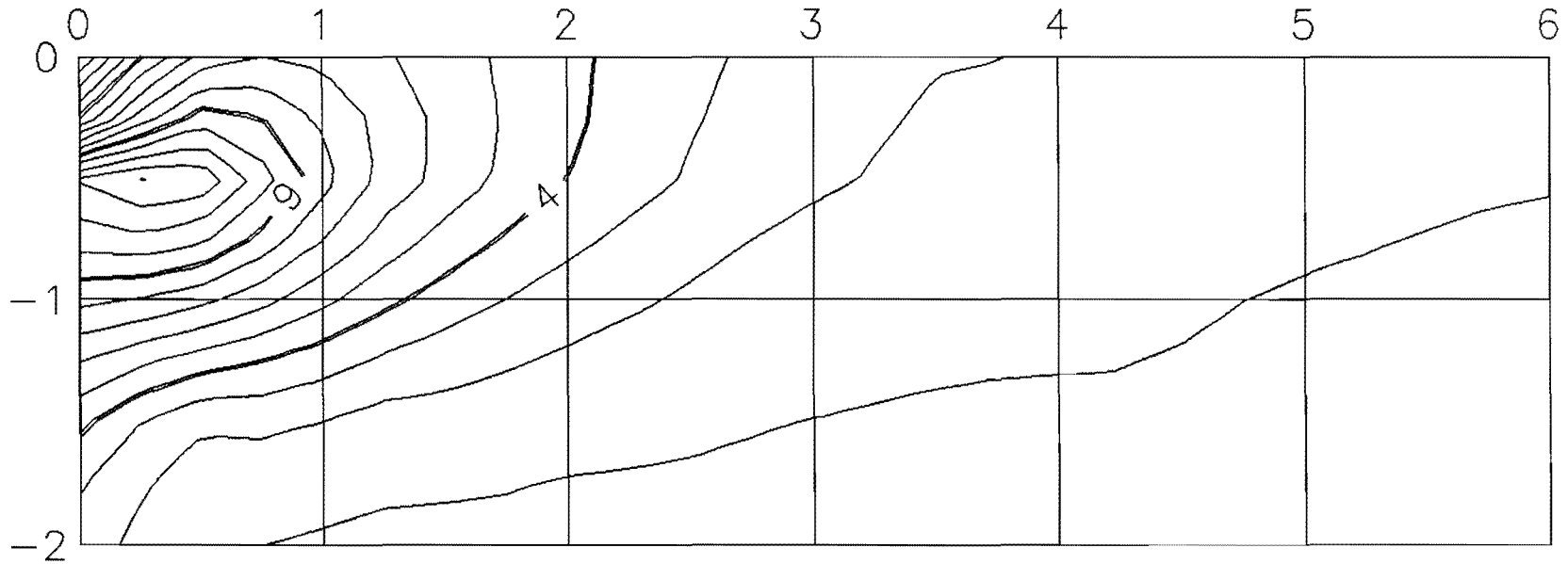


Nor. Oct. Stress (psi) - 2 in. AC/CLS Base - Hot Season - Rolling Wheel - Bond



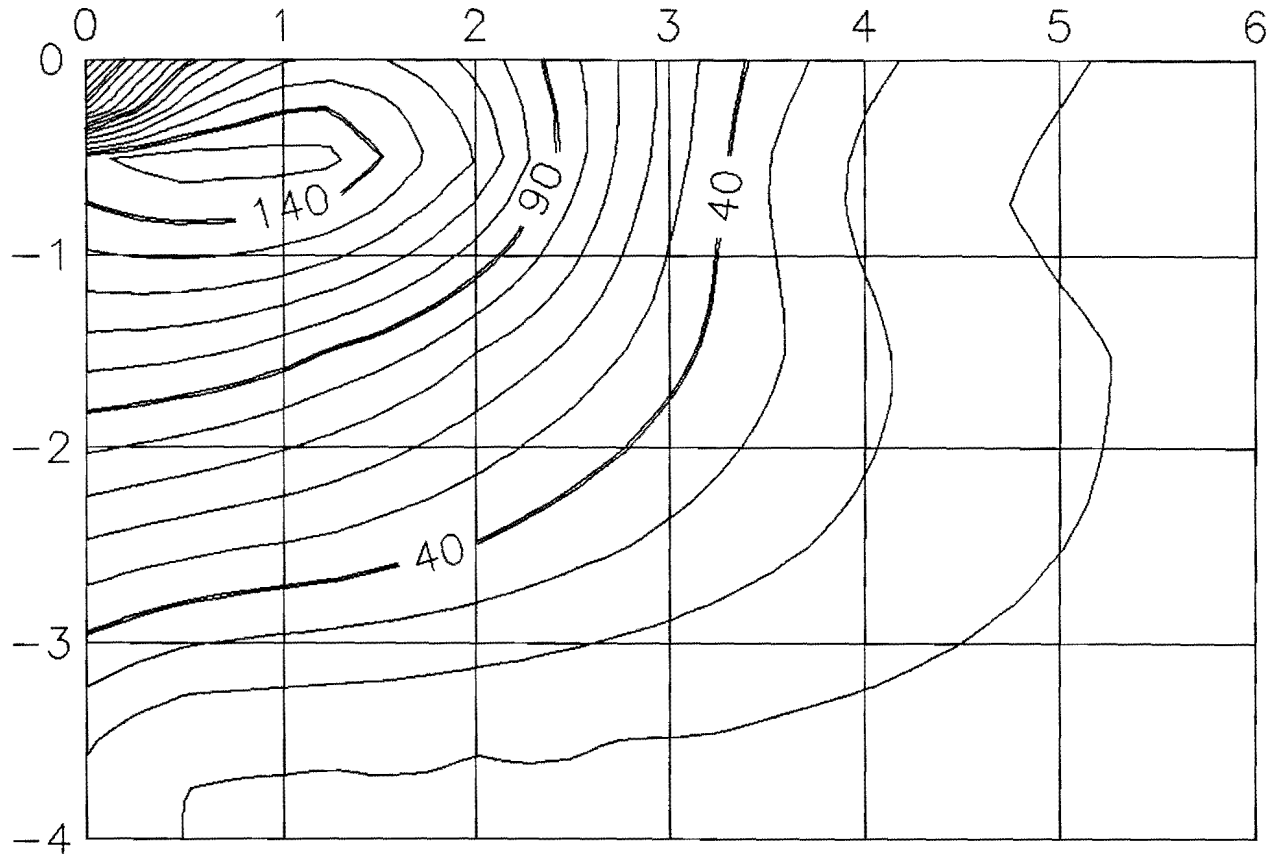
B-34

NTSR - 2 in. AC/CLS Base - Hot Season - Rolling Wheel - Bond

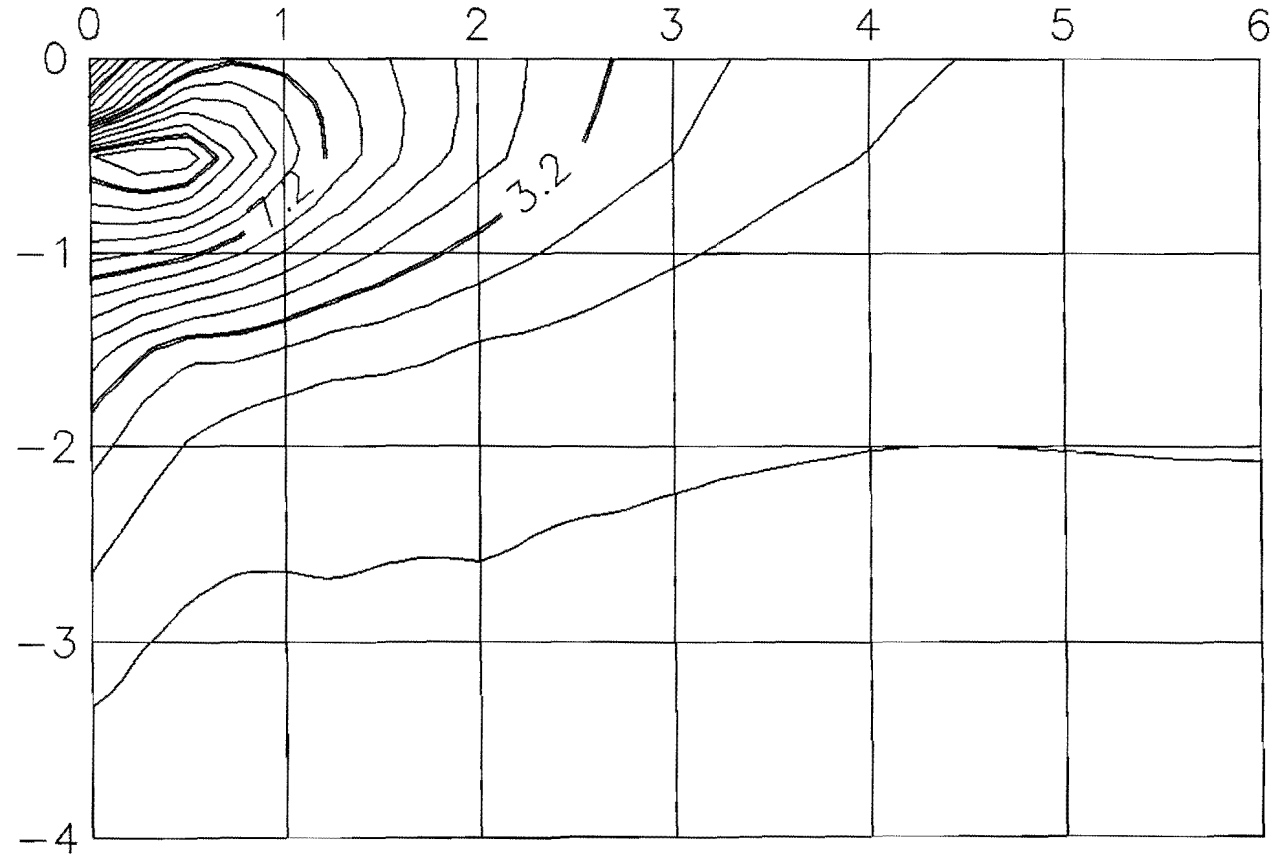


B-35

Nor. Oct. Stress (psi) - 4 in. AC/CLS Base - Hot Season - Rolling Wheel - Bond

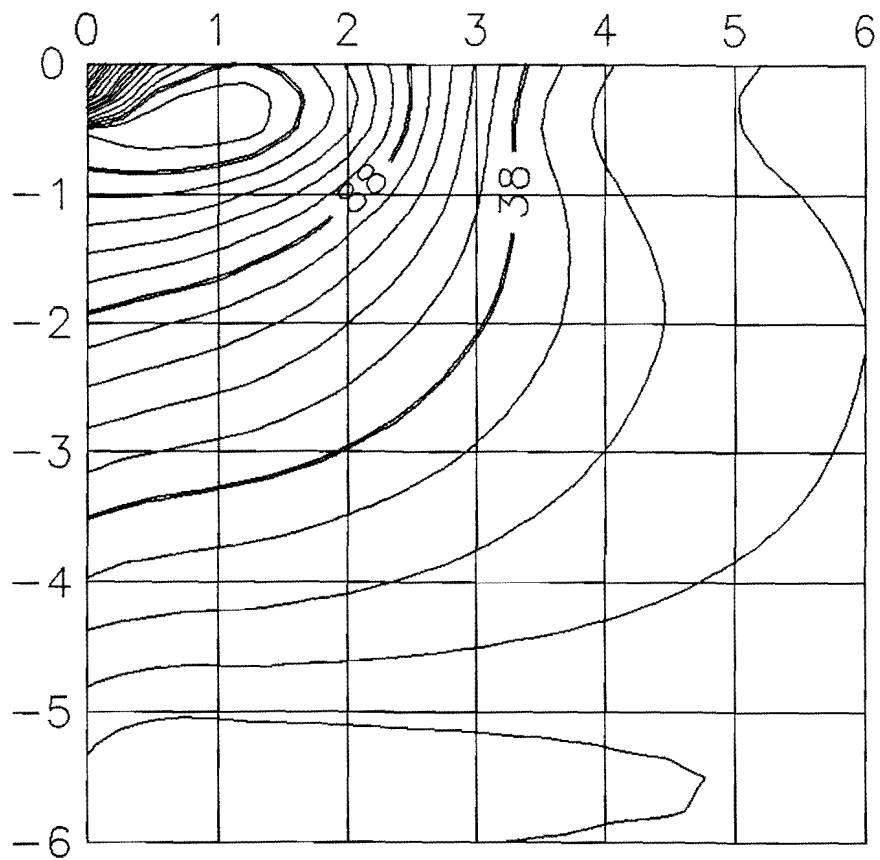


NTSR - 4 in. AC/CLS Base - Hot Season - Rolling Wheel - Bond

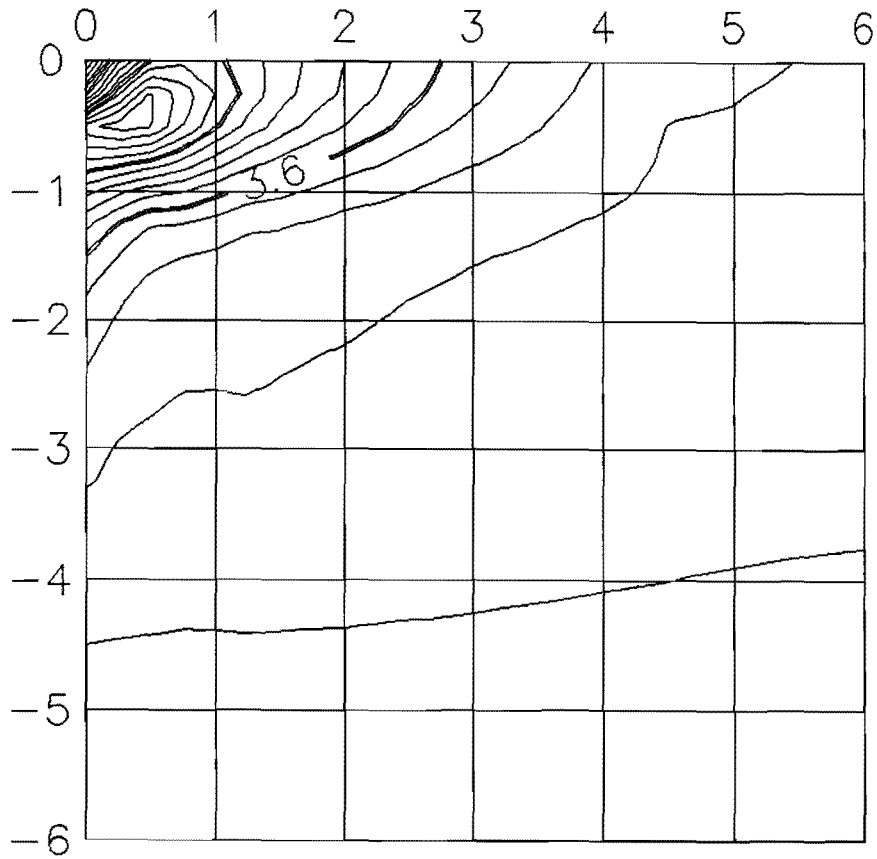


B-37

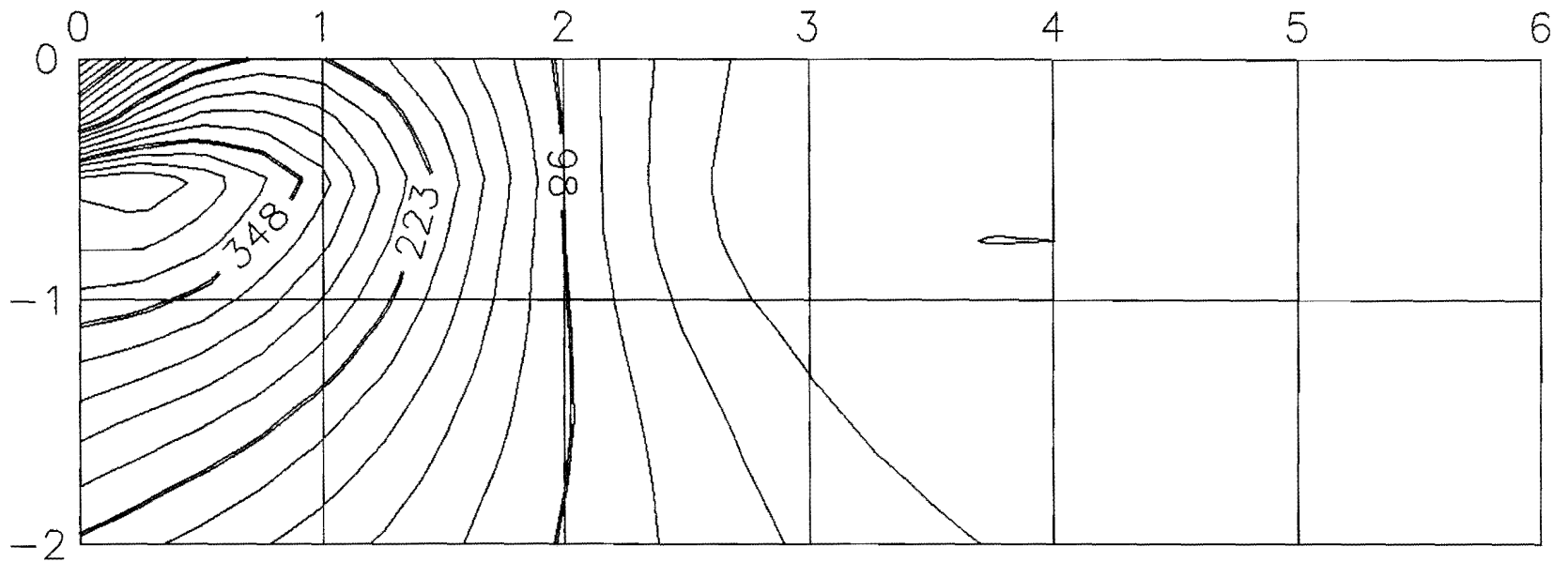
Nor. Oct. Stress (psi) - 6 in. AC/CLS Base - Hot Season - Rolling Wheel - Bond



NTSR - 6 in. AC/CLS Base - Hot Season - Rolling Wheel - Bond

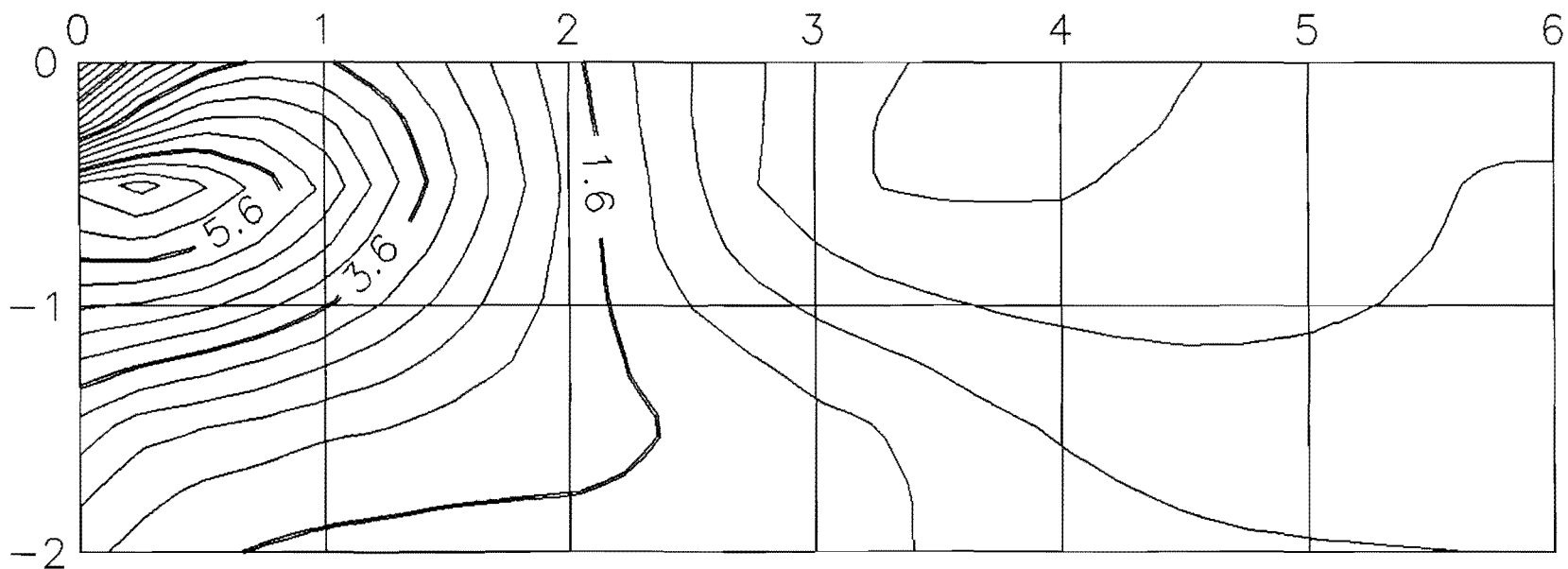


Nor. Oct. Stress (psi) - 2 in. AC/AC Base - Hot Season - Braking wheel - Bond

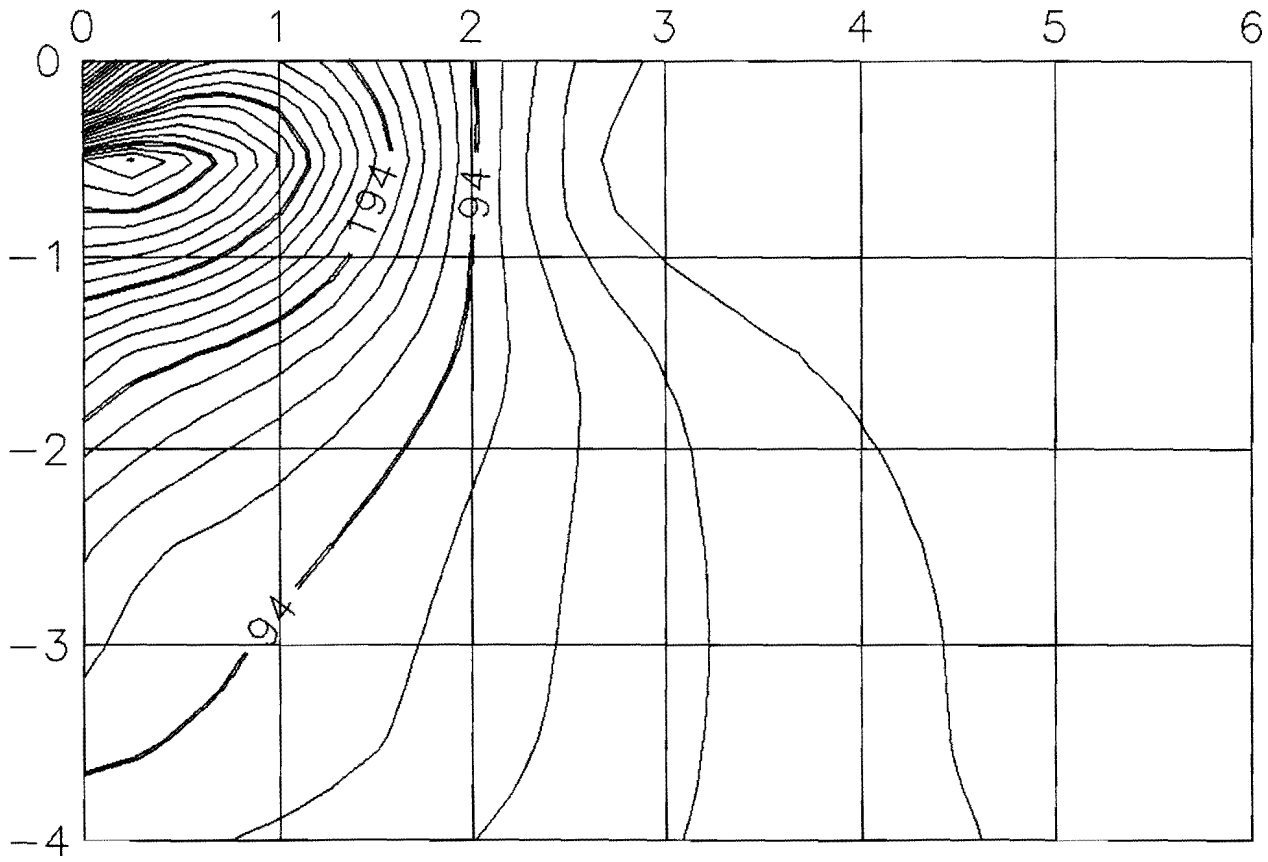


B-40

NTSR - 2 in. AC/AC Base - Hot Season - Braking Wheel - Bond

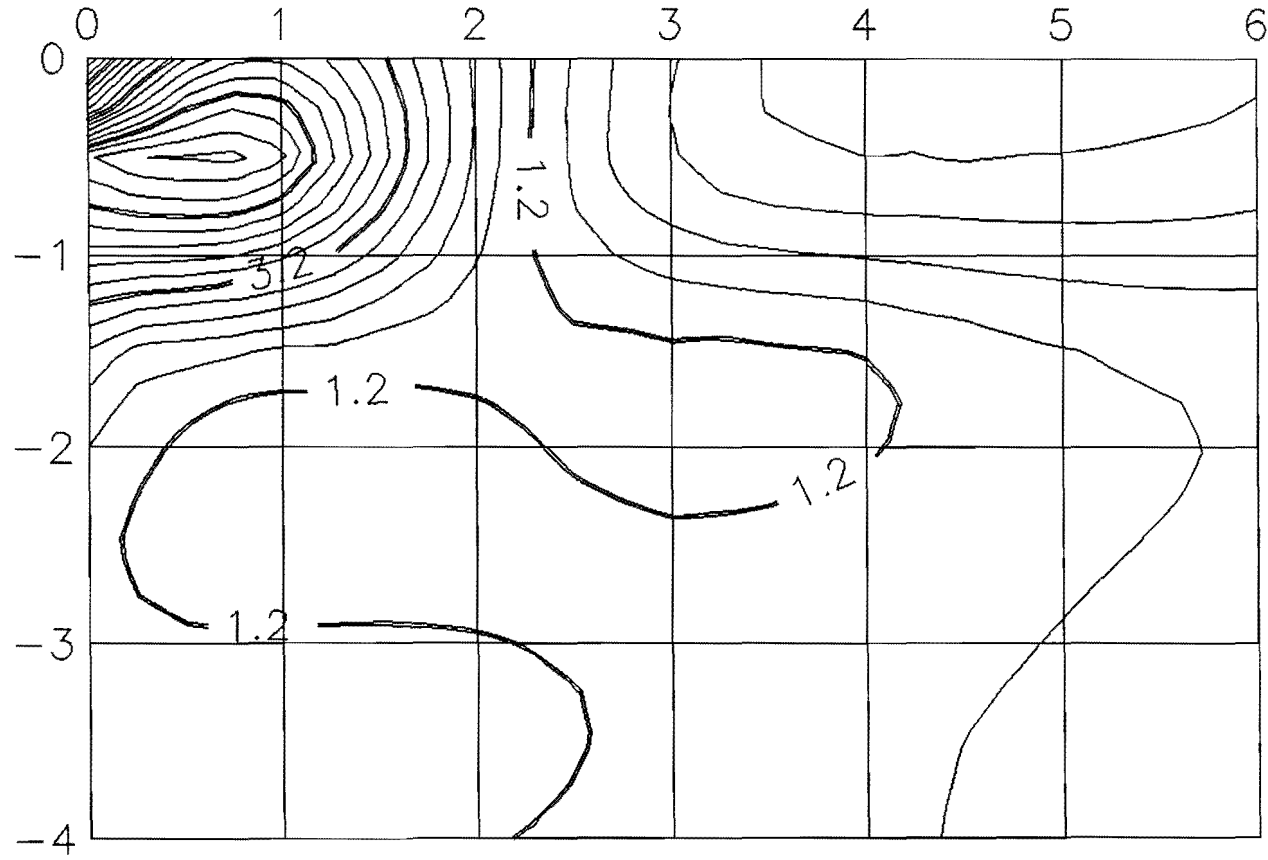


Nor. Oct. Stress (psi) - 4 in. AC/AC Base - Hot Season - Braking Wheel - Bond



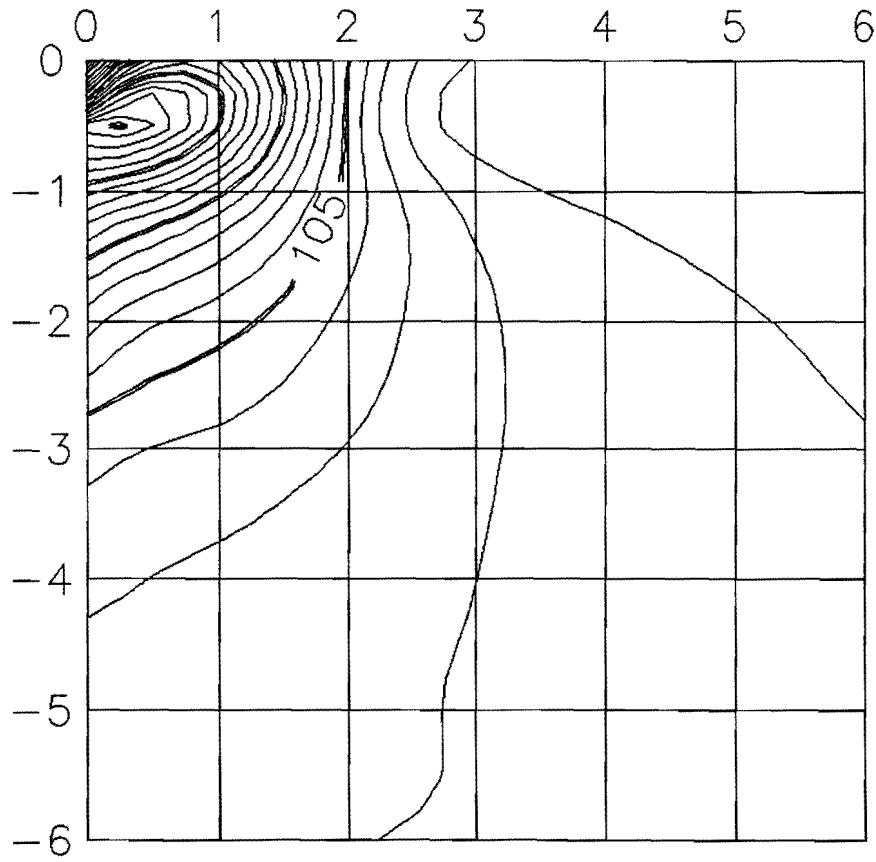
B-42

NTSR - 4 in. AC/AC Base - Hot Season - Braking wheel - Bond



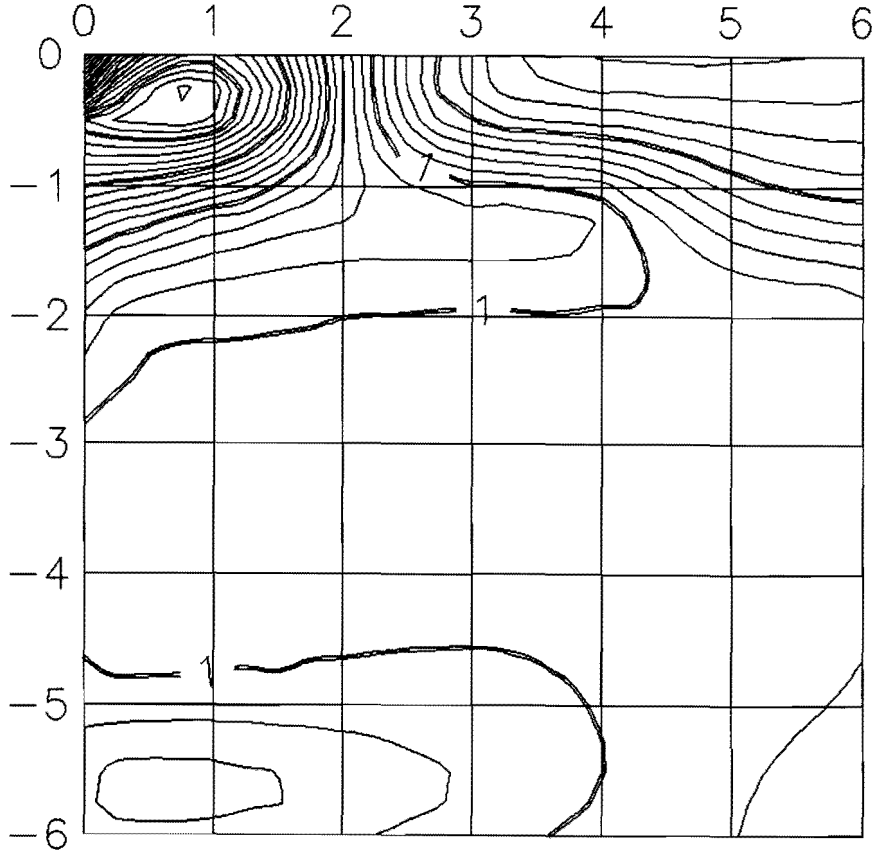
B-43

Nor. Oct. Stress (psi) - 6 in. AC/AC Base - Hot Season - Braking Wheel - Bond



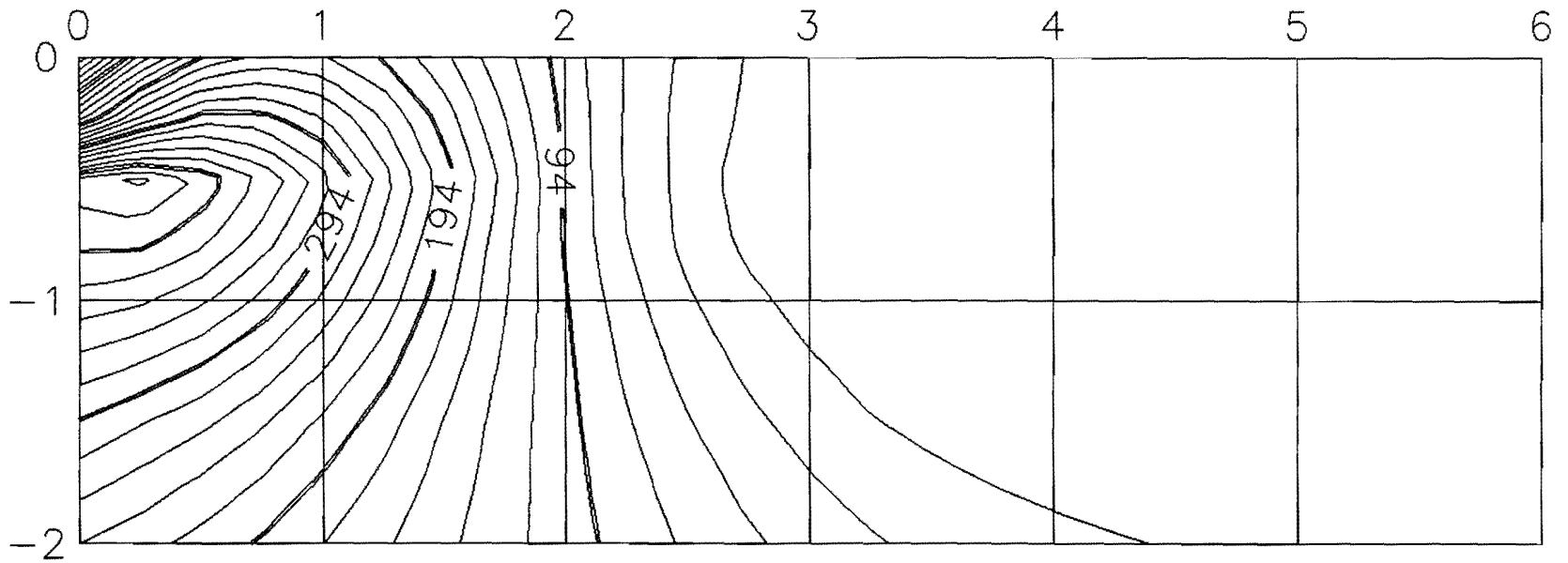
B-44

NTSR - 6 in AC/AC Base - Hot Season - Braking Wheel - Bond

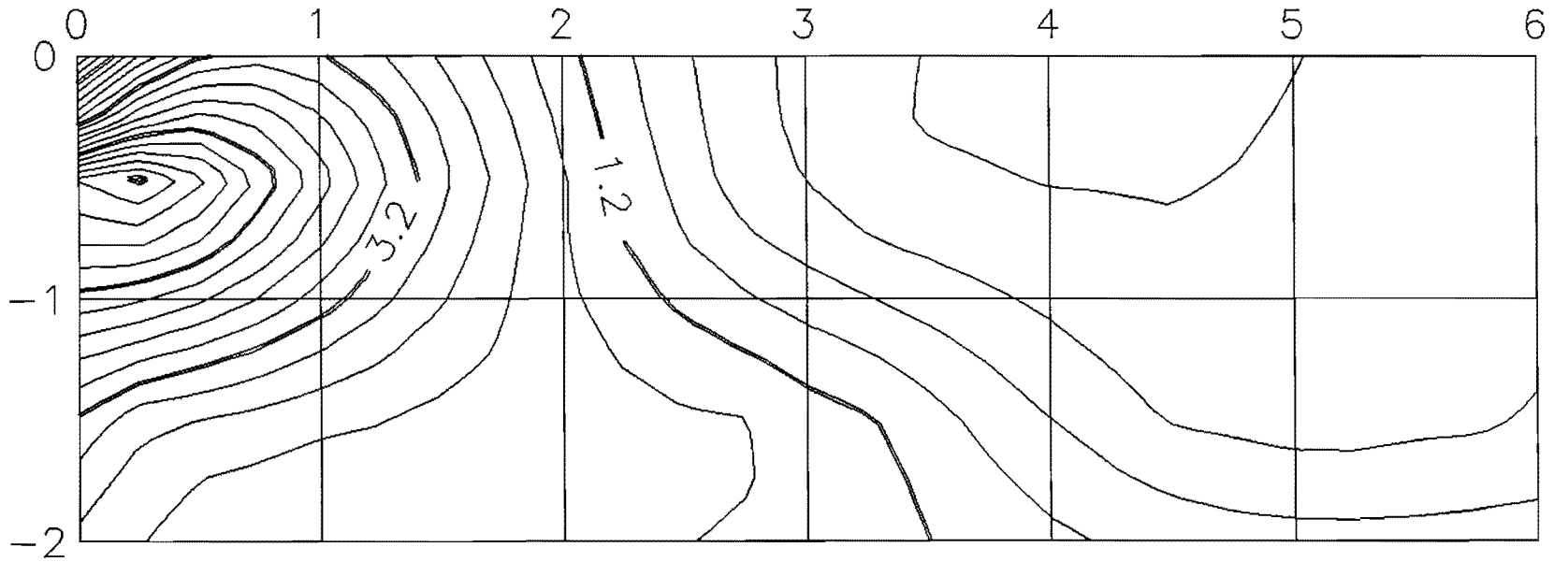


B-45

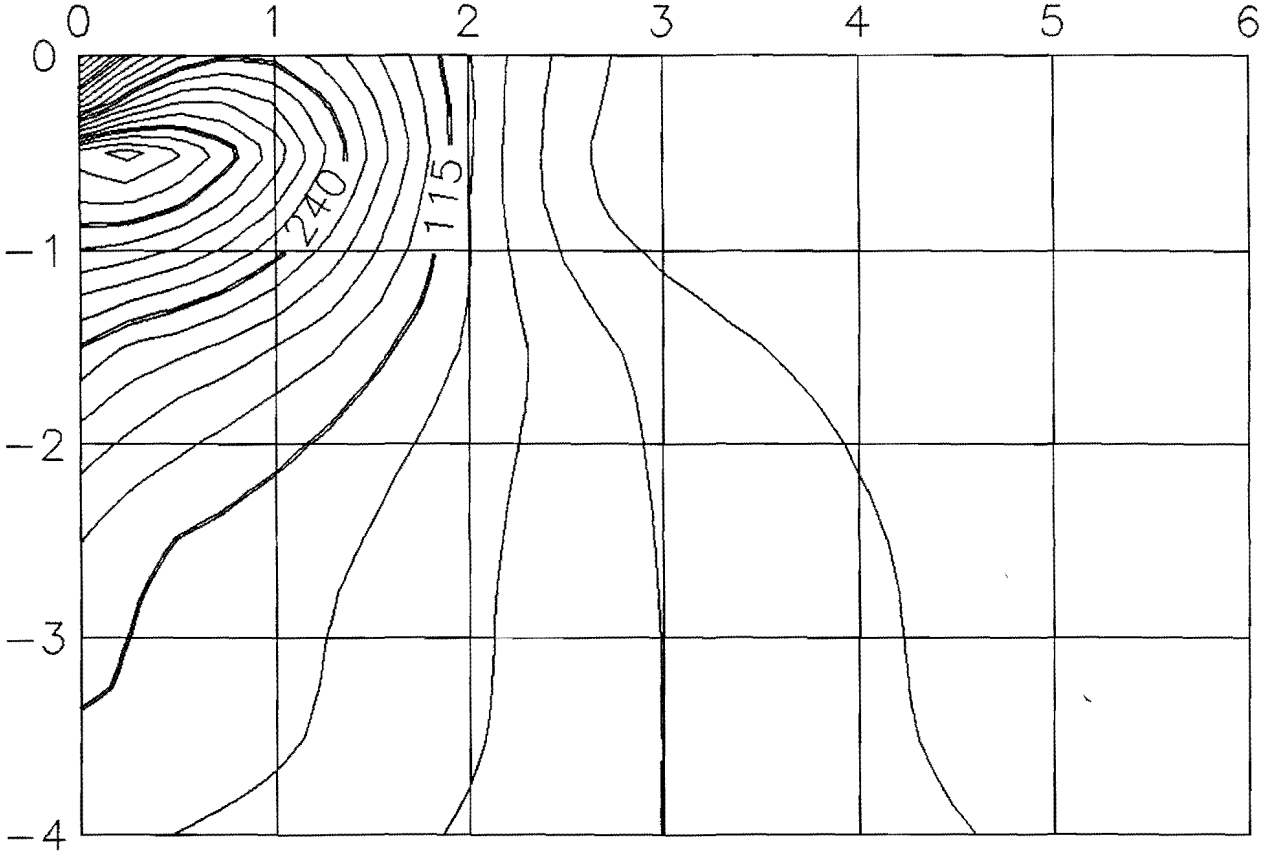
Nor. Oct. Stress (psi) - 2 in. AC/PCC Base - Hot Season - Braking Wheel - Bond



NTSR - 2 in. AC/PCC Base - Hot Season - Braking Wheel - Bond

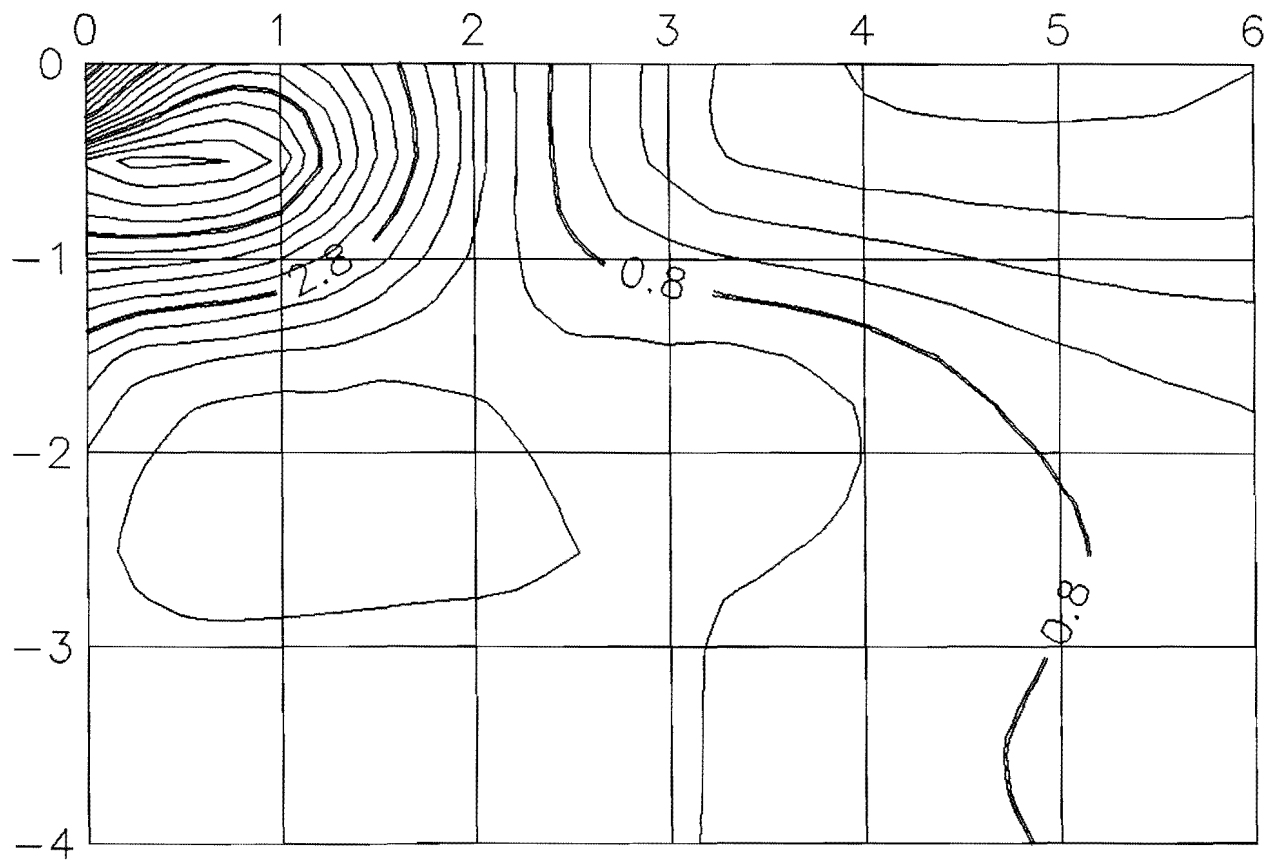


Nor. Oct. Stress (psi) - 4 in. AC/PCC Base - Hot Season - Braking Wheel - Bond

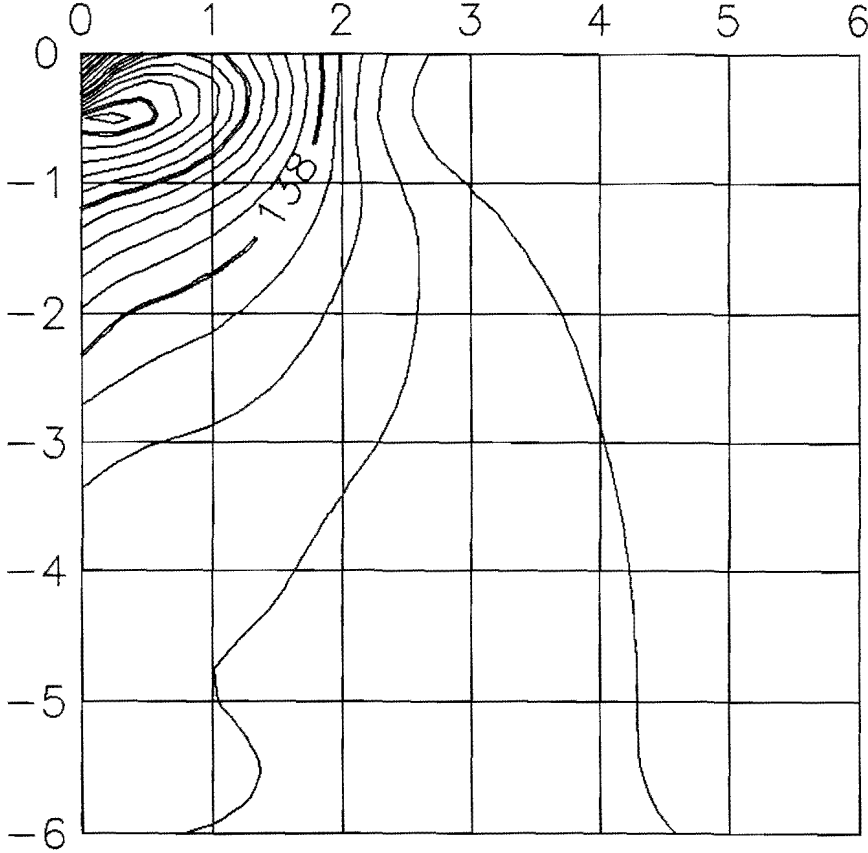


B-48

NTSR - 4 in. AC/PCC Base - Hot Season - Braking Wheel - Bond

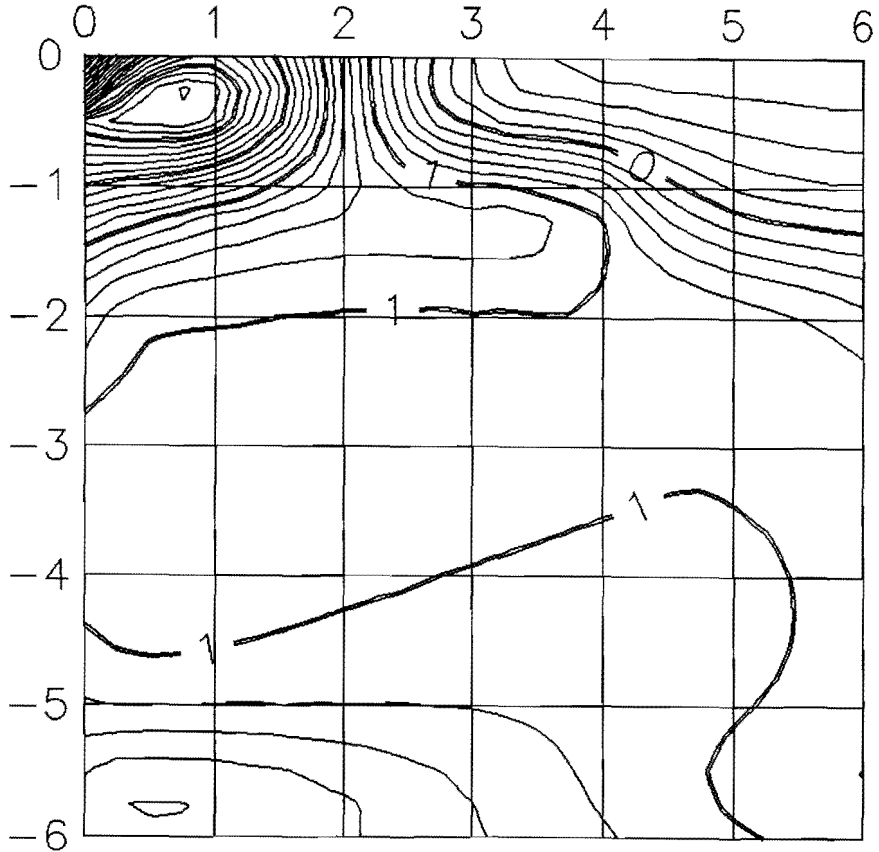


Nor. Oct. Stress (psi) - 6 in. AC/PCC Base - Hot Season - Braking Wheel - Bond



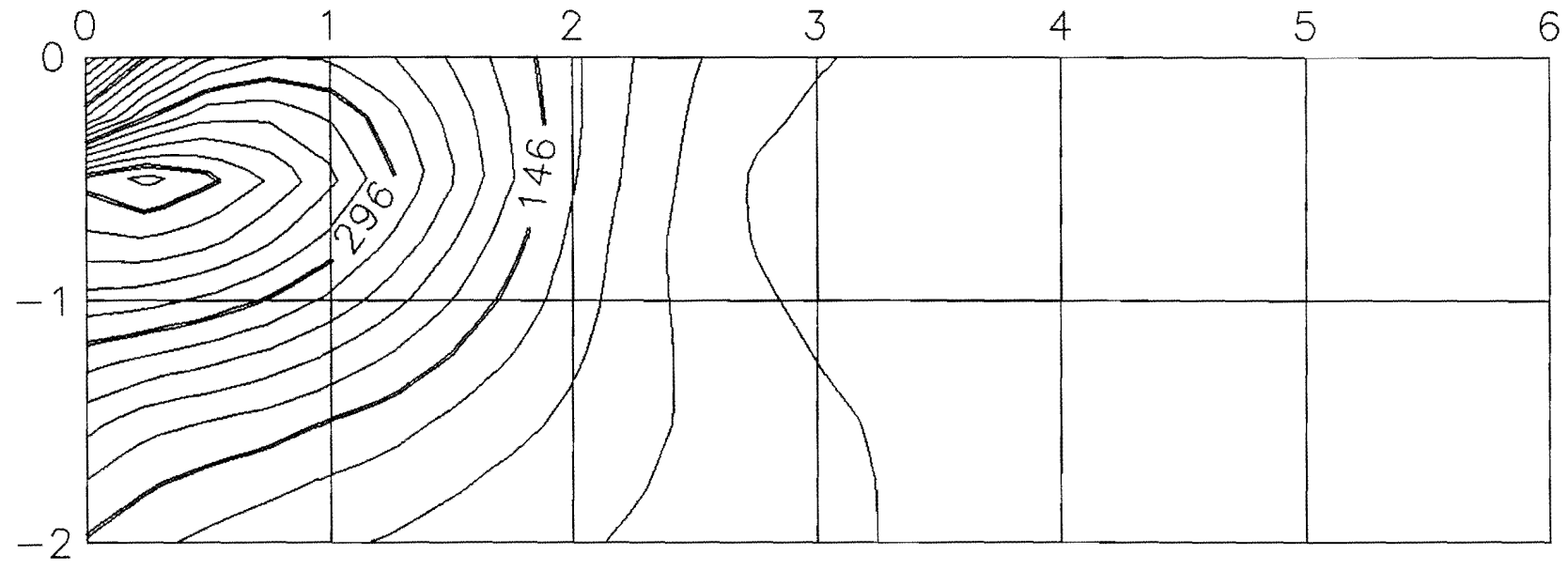
B-50

NTSR - 6 in. AC/PCC Base - Hot Season - Braking Wheel - Bond



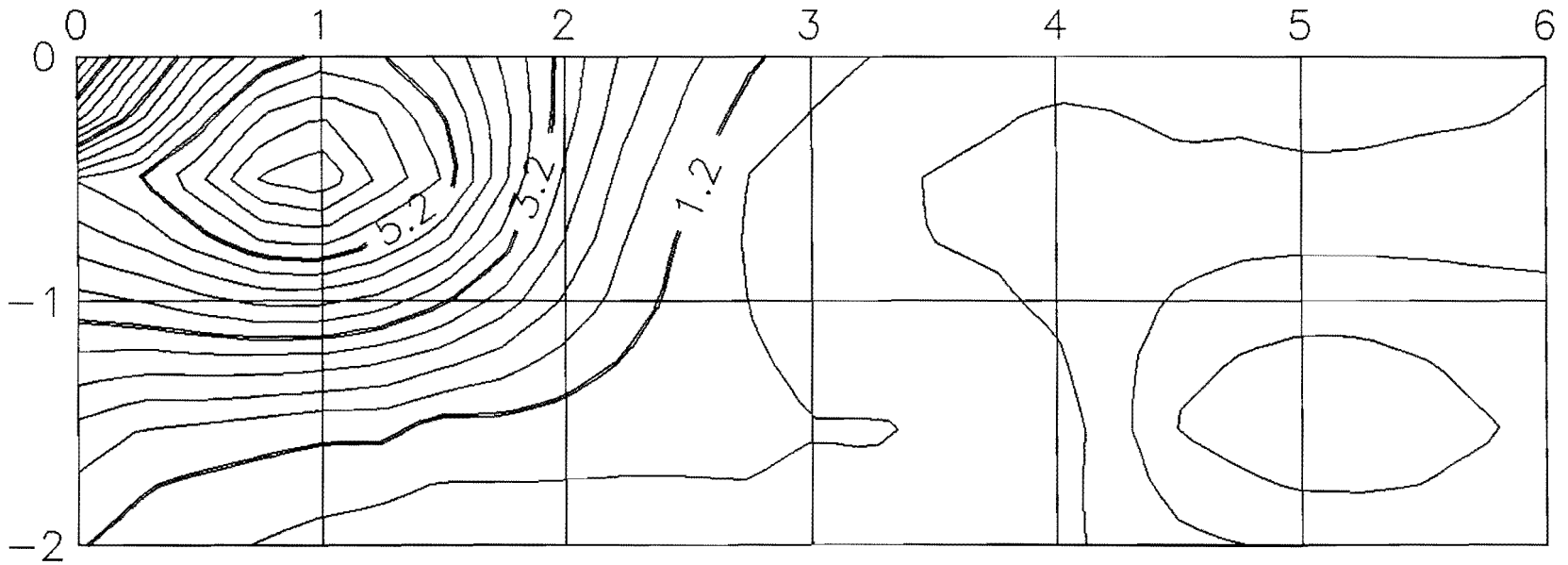
B-51

Nor. Oct. Stress (psi) - 2 in. AC/CLS Base - Hot Season - Braking Wheel - Bond



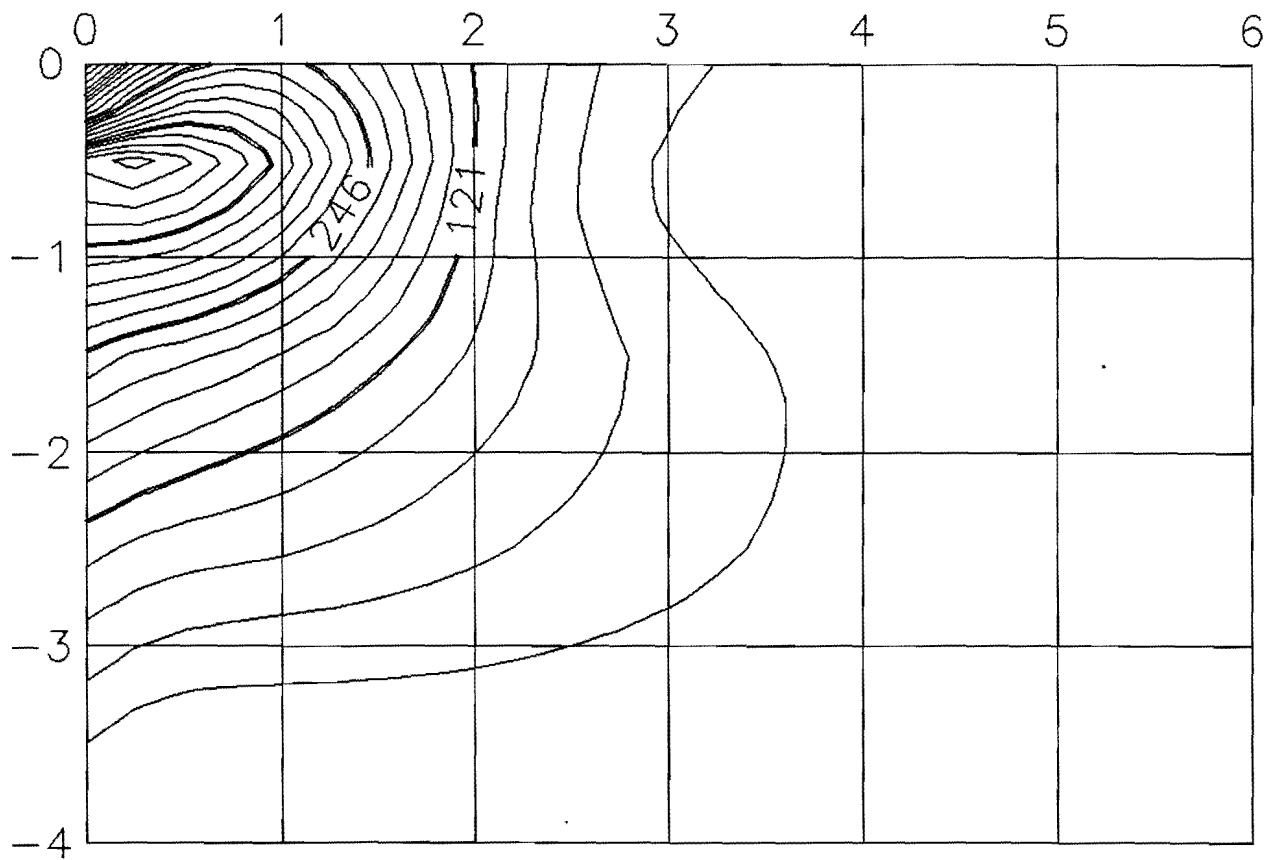
B-52

NTSR - 2 in. AC/PCC Base - Hot Season - Braking Wheel - Bond



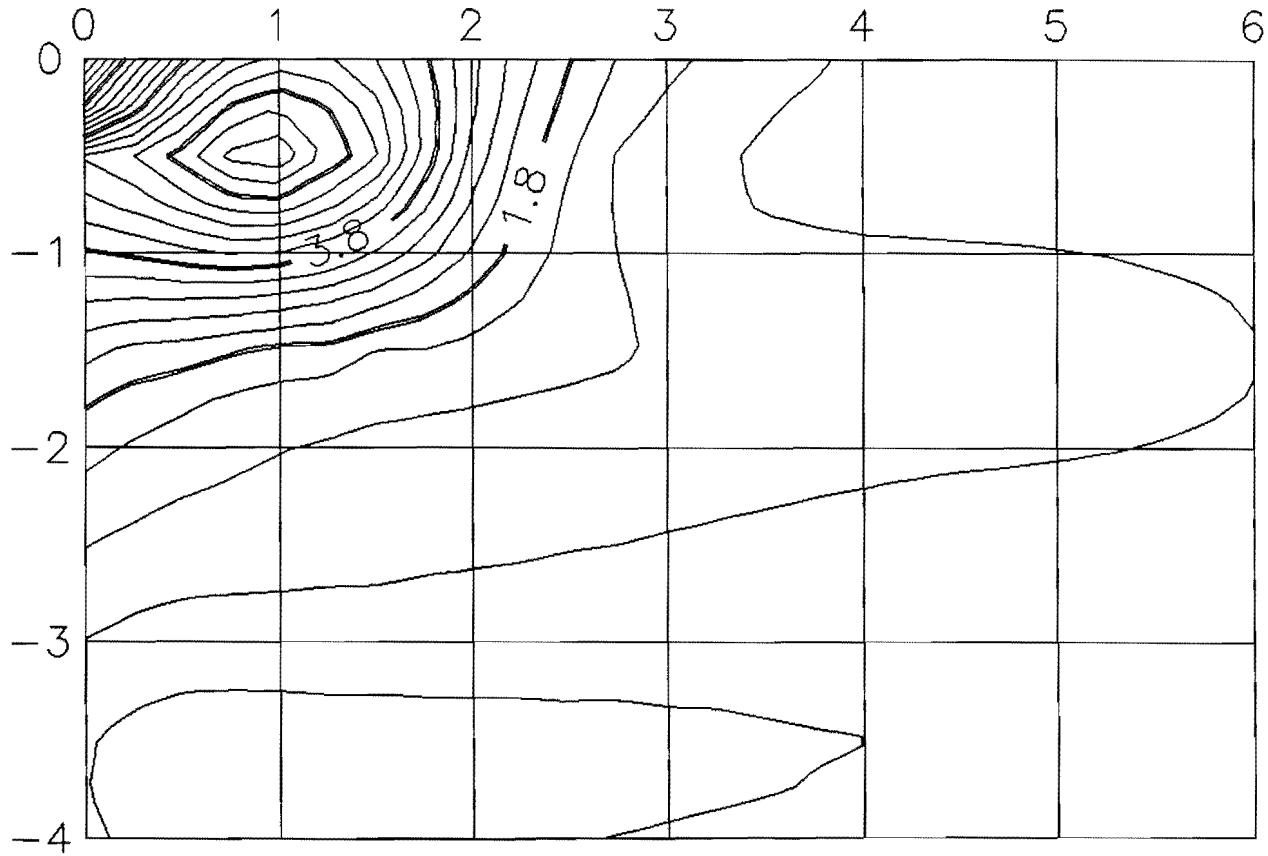
B-53

Nor. Oct. Stress (psi) - 4 in. AC/CLS Base - Hot Season - Braking Wheel - Bond



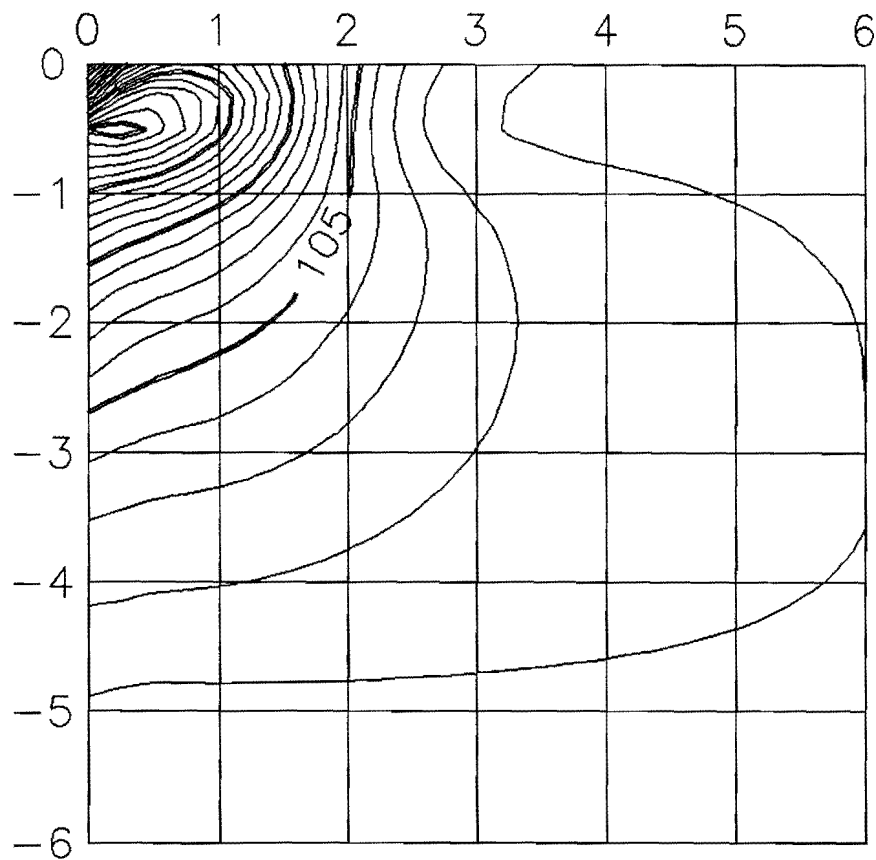
B-54

NTSR - 4 in. AC/CLS Base - Hot Season - Braking Wheel - Bond



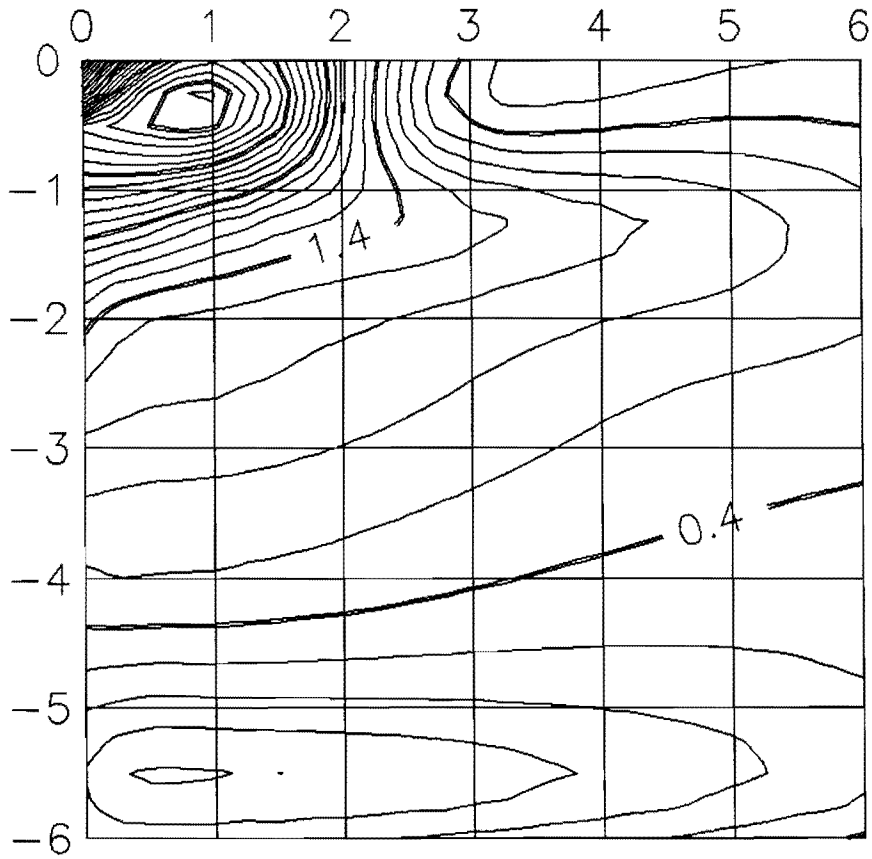
B-55

Nor. Oct. Stress (psi) - 6 in. AC/CLS Base - Hot Season - Braking Wheel - bond



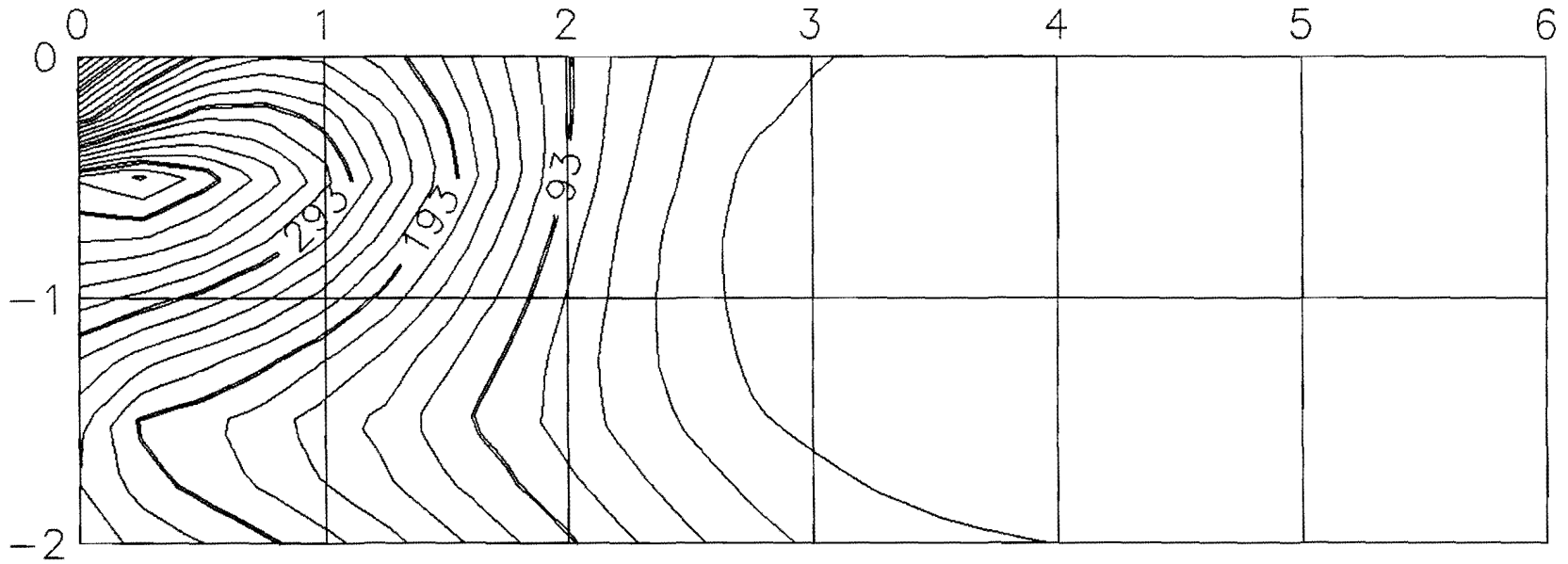
B-56

NTSR - 6 in. AC/CLS Base - Hot Season - Braking Wheel - Bond

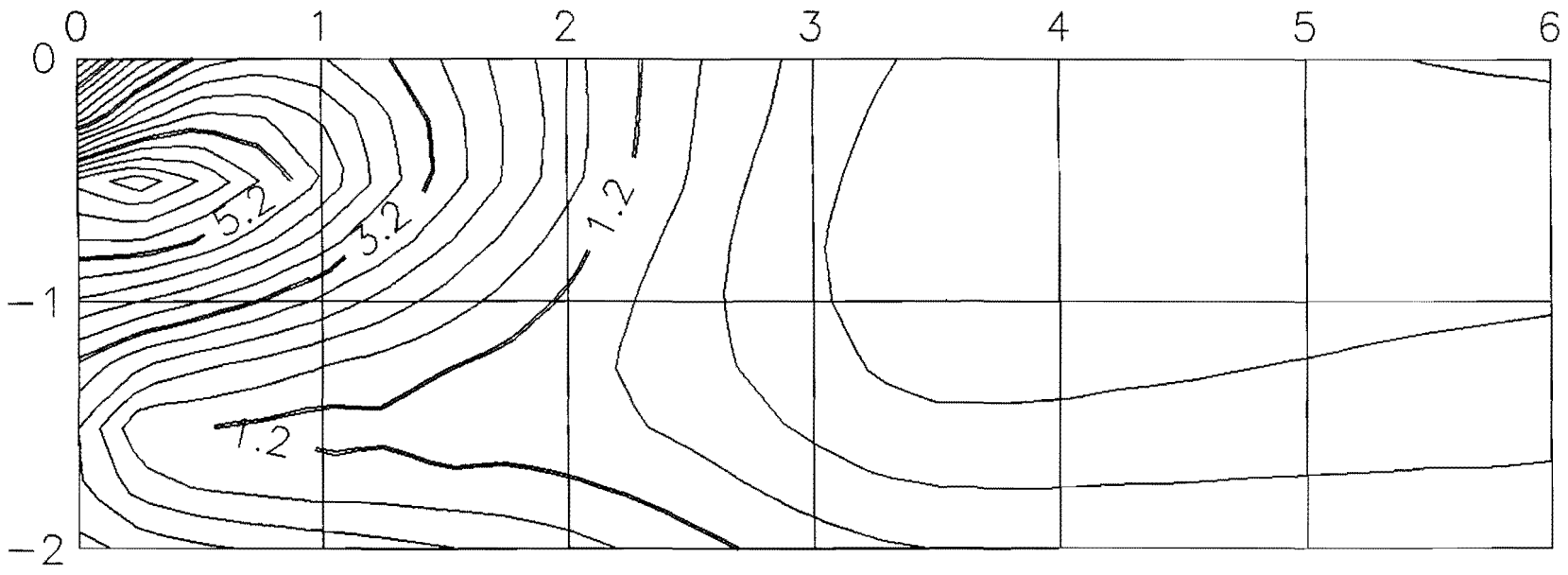


B-57

Nor. Oct. Stress (psi) - 2 in. AC/AC Base - Hot Season - Braking Wheel - Slip

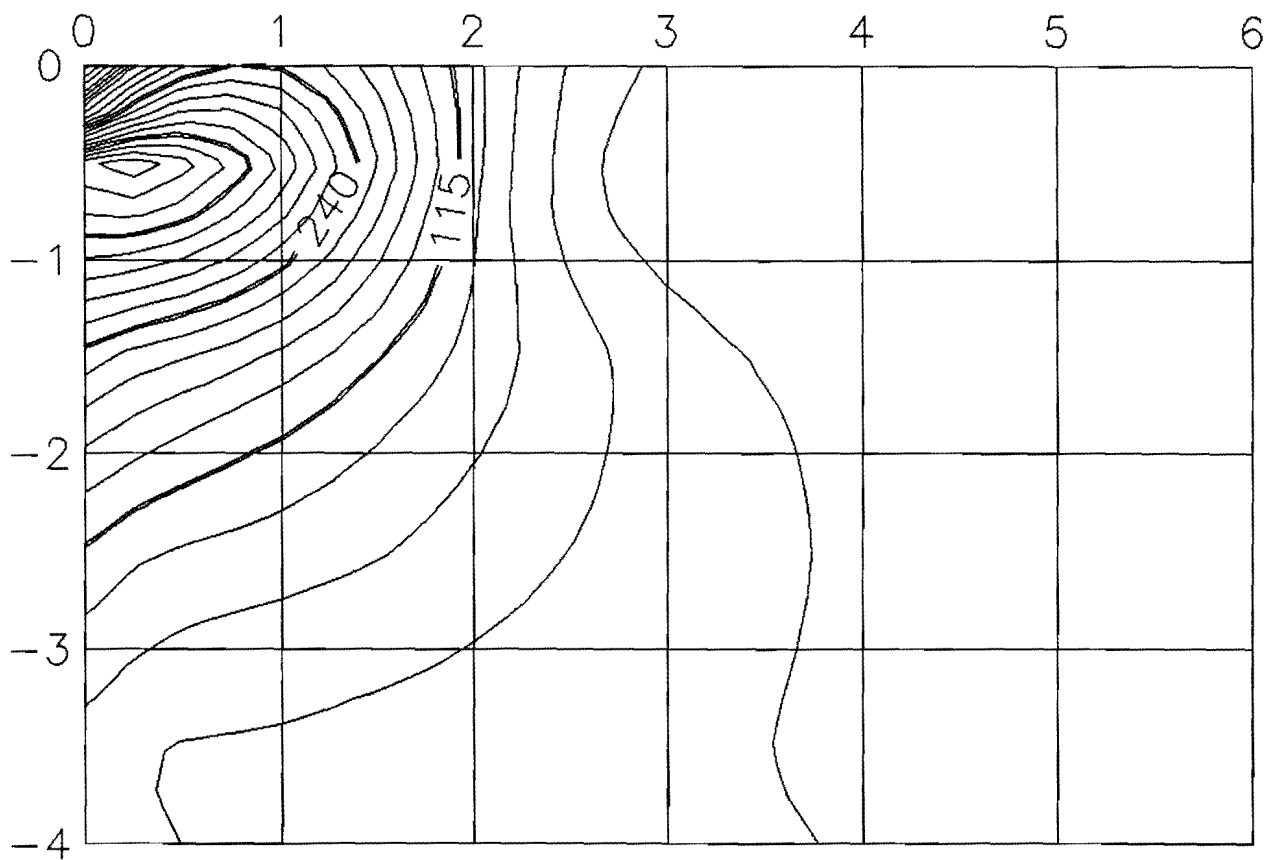


NTSR - 2 in. AC/AC Base - Hot Season - Braking Wheel - Slip



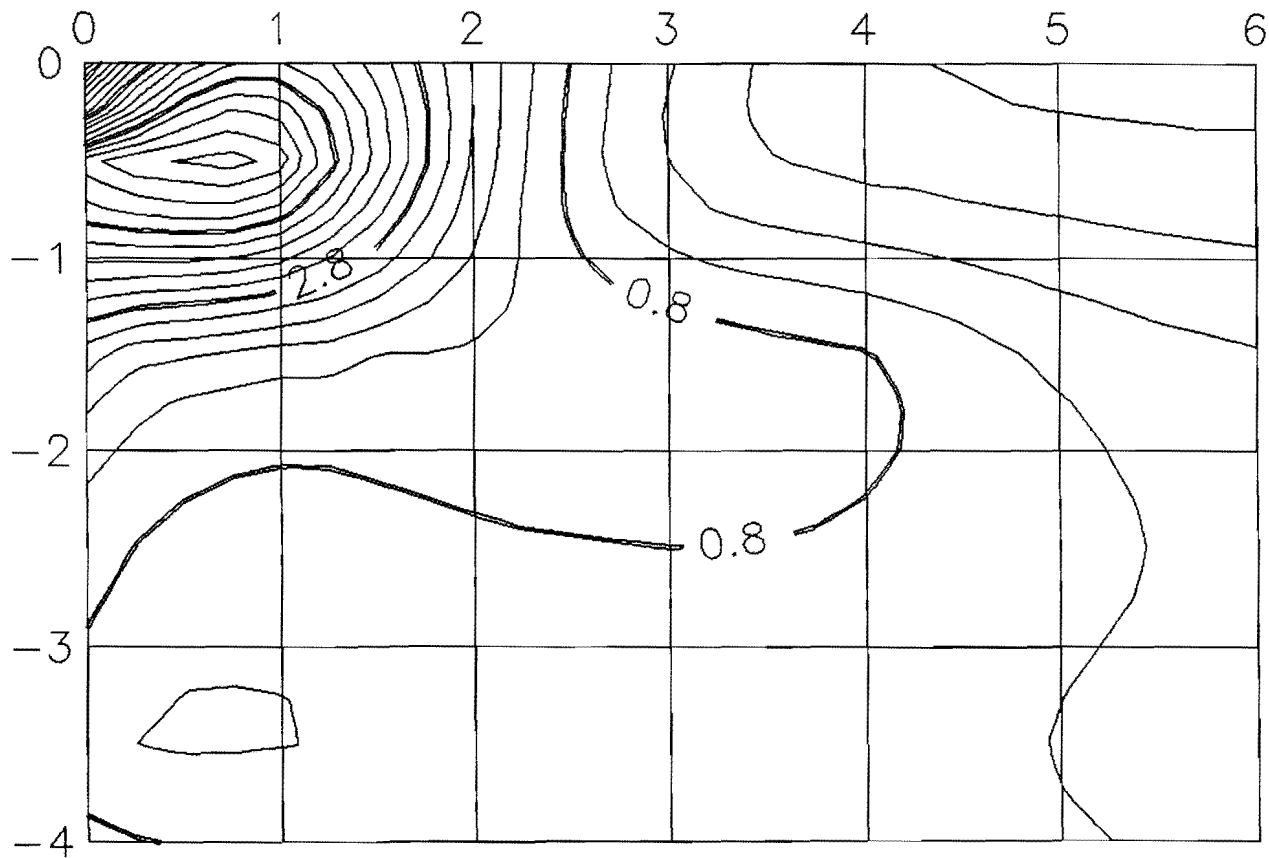
B-59

Nor. Oct. Stress - 4 in. AC/AC Base - Hot Season - Braking Wheel

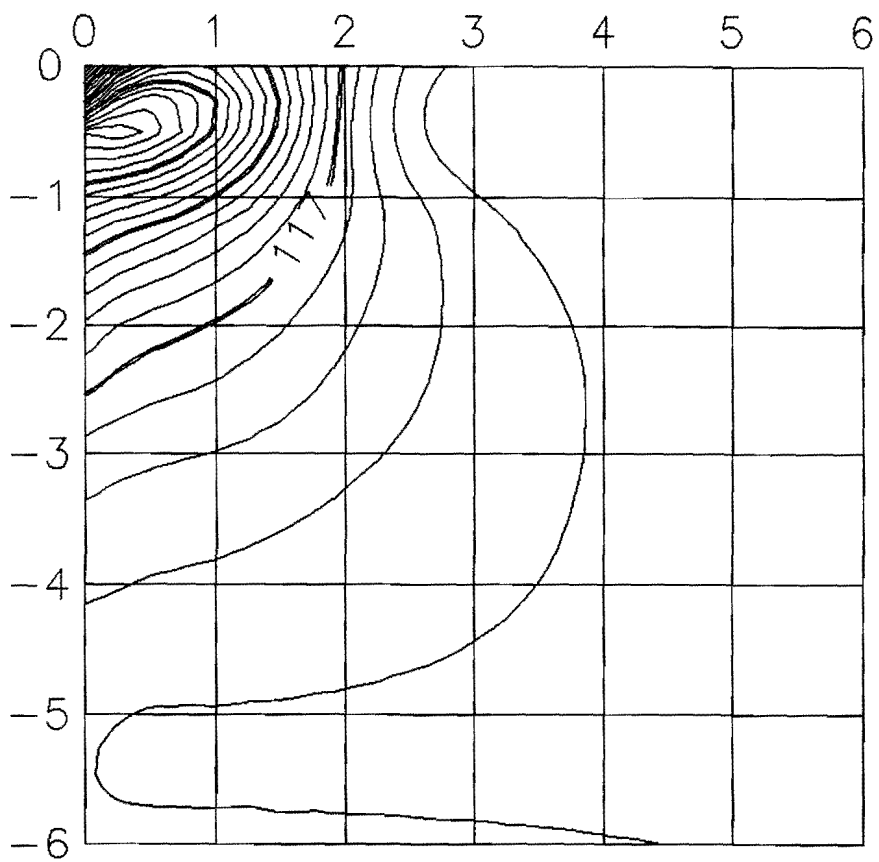


B-60

NTSR - 4 in. AC/AC Base - Hot Season - Braking Wheel slip

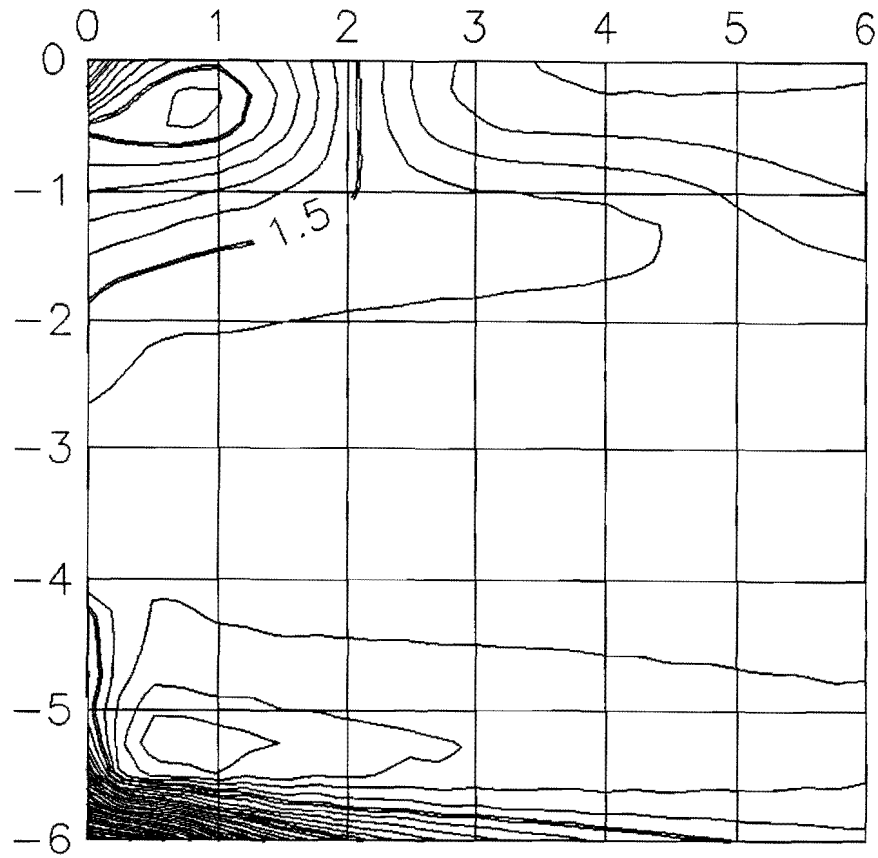


Nor. Oct. Stress (psi) - 6 in. AC/AC Base - Hot Season - Braking Wheel - Slip

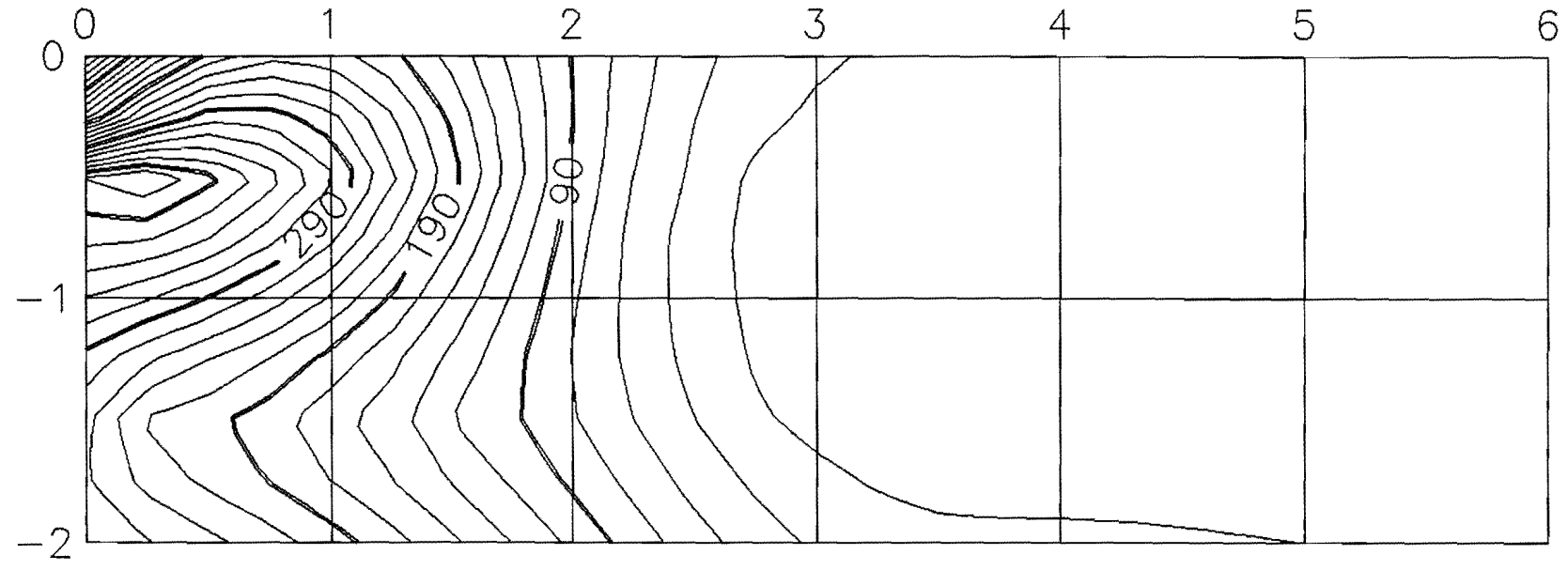


B-62

NTSR - 6 in. AC/AC Base - Hot Season - Braking Wheel - Slip

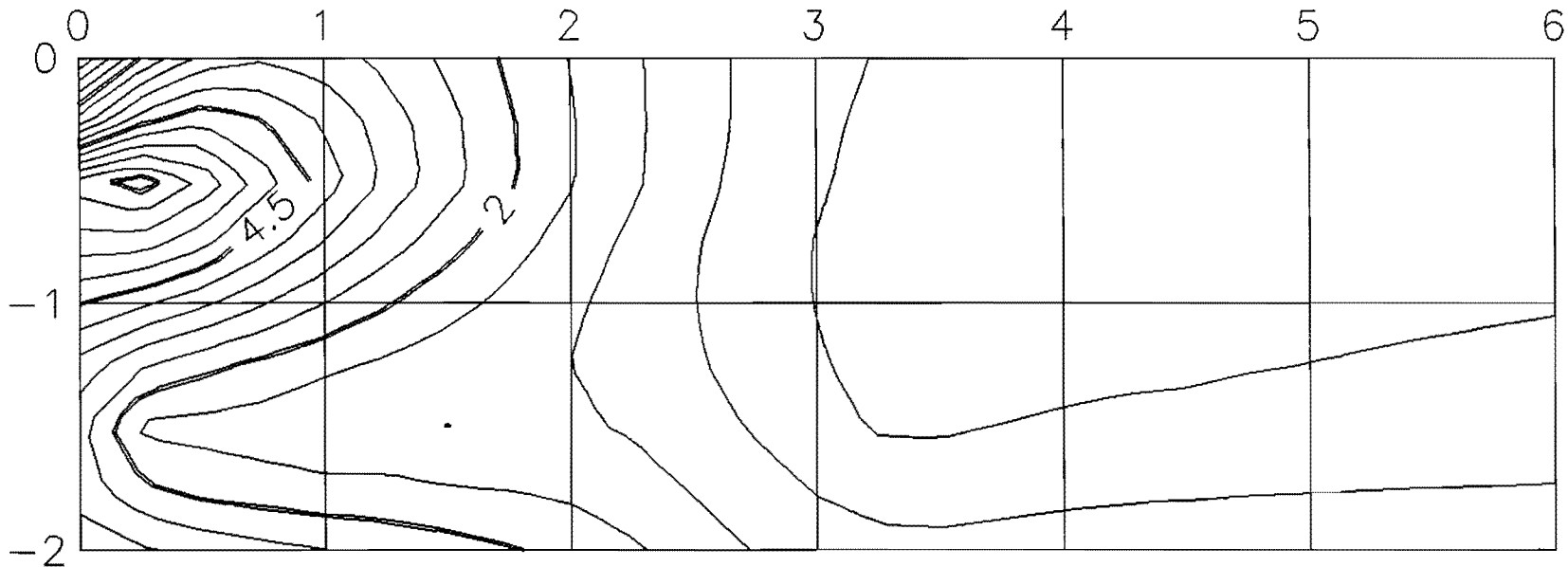


Nor. Oct. Stress (psi) - 2 in. AC/PCC Base - Hot Season - Braking wheel - Slip



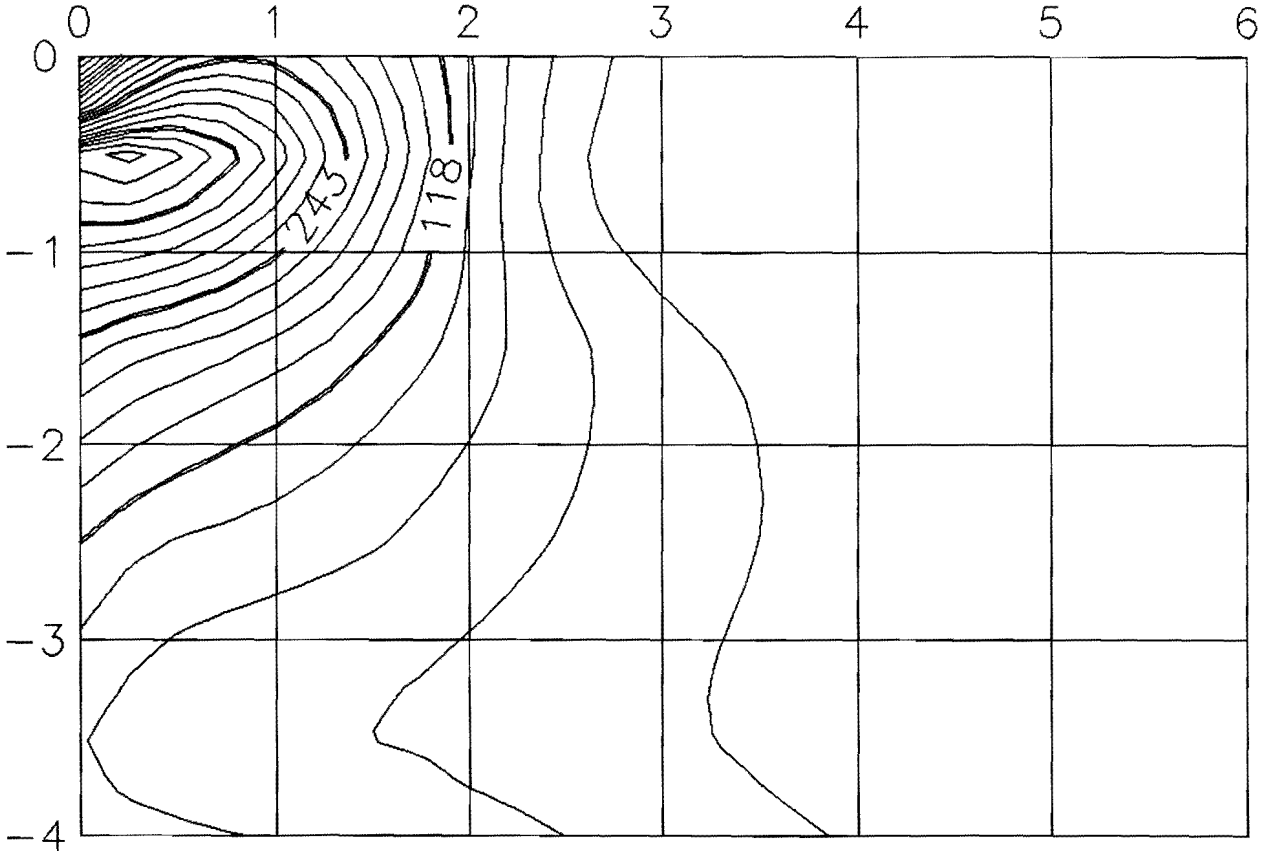
B-64

NTSR - 2 in. AC/PCC Base - Hot Season - Braking Wheel - Slip



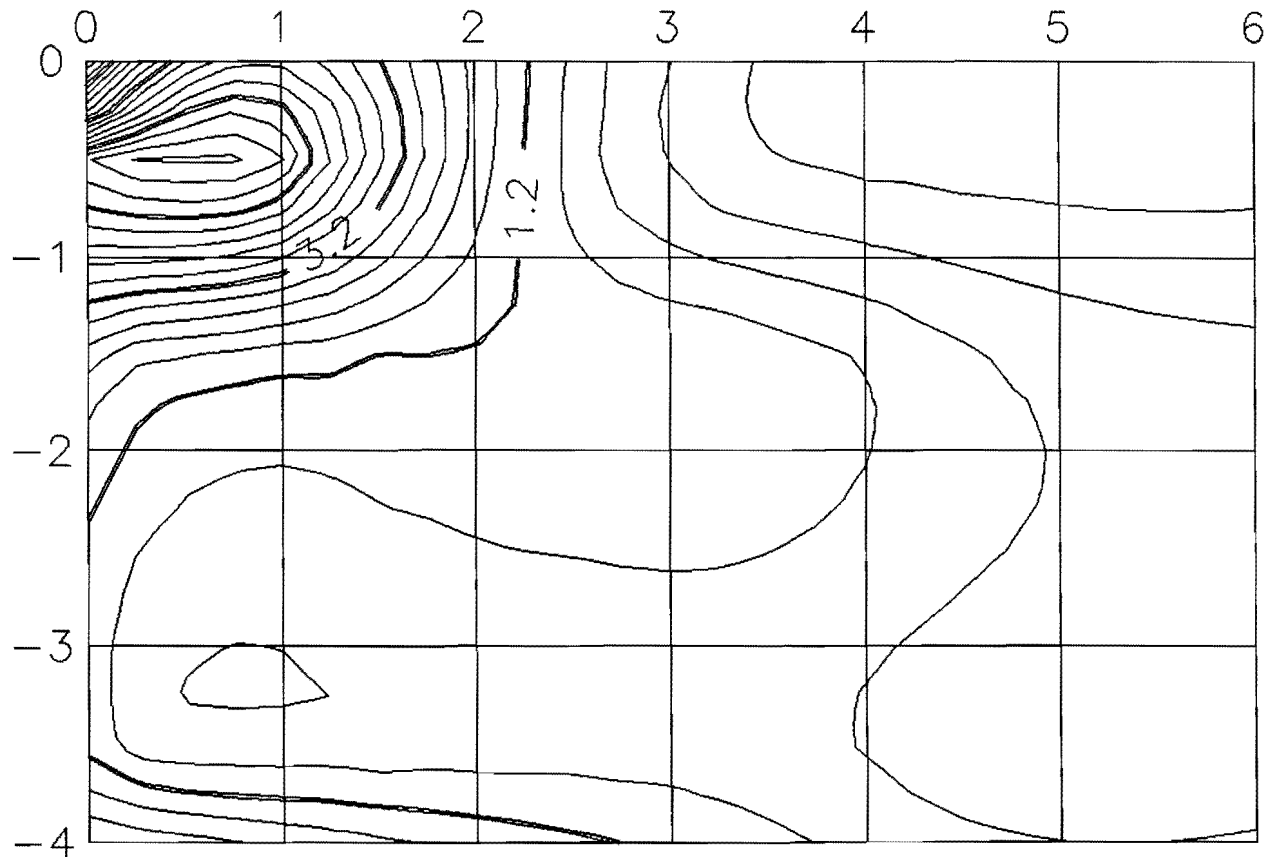
B-65

Nor. Oct. Stress (psi) - 4 in. AC/PCC Base - Hot Season - Braking wheel - Slip

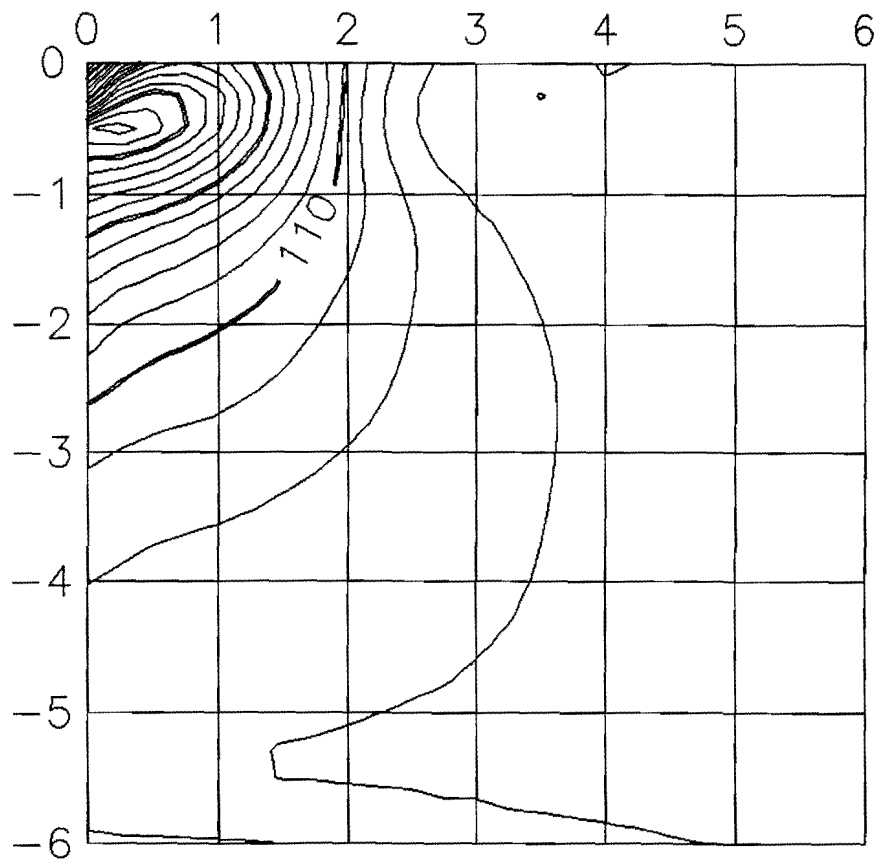


B-66

NTSR - 4 in. AC/PCC Base - Hot Season - Braking Wheel - Slip

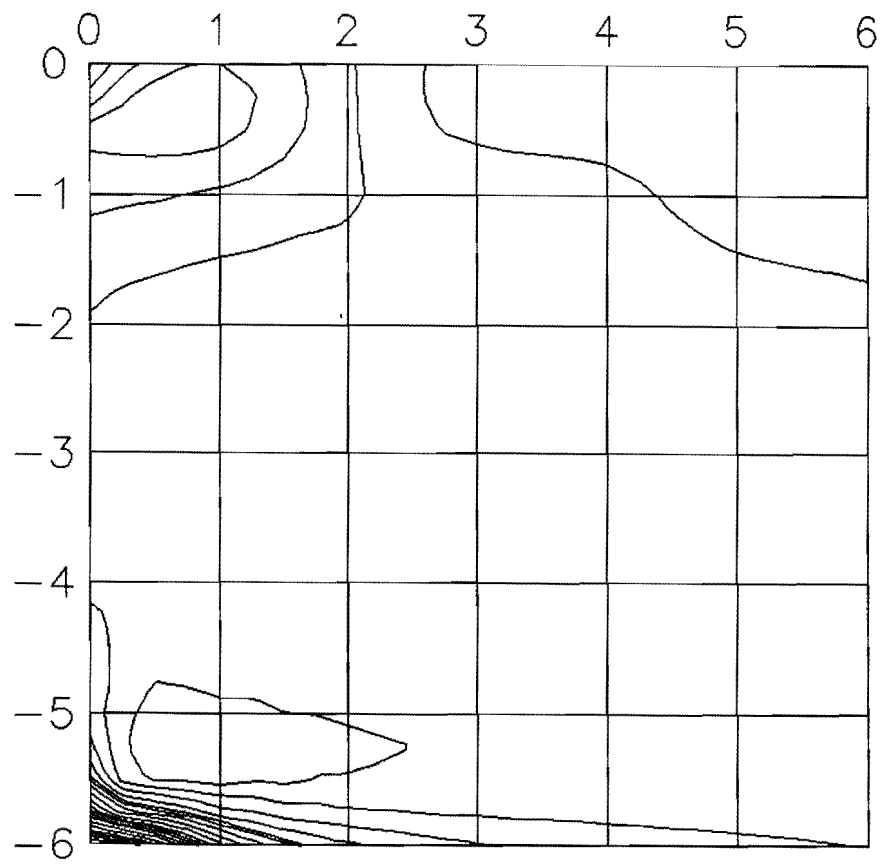


Nor. Oct. Stress (psi) - 6 in. AC/PCC Base - Hot Season - Braking Wheel - Slip



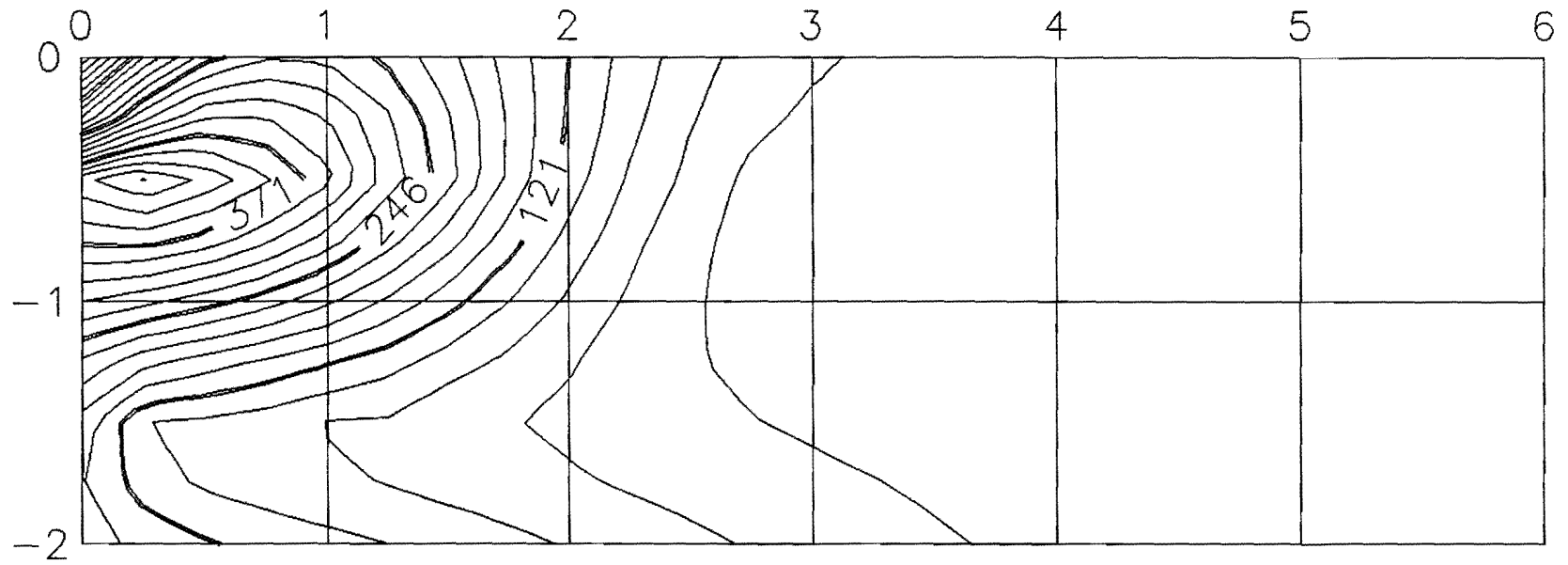
B-68

NTSR - 6 in. AC/PCC Base - Hot Season - Braking Wheel - Slip



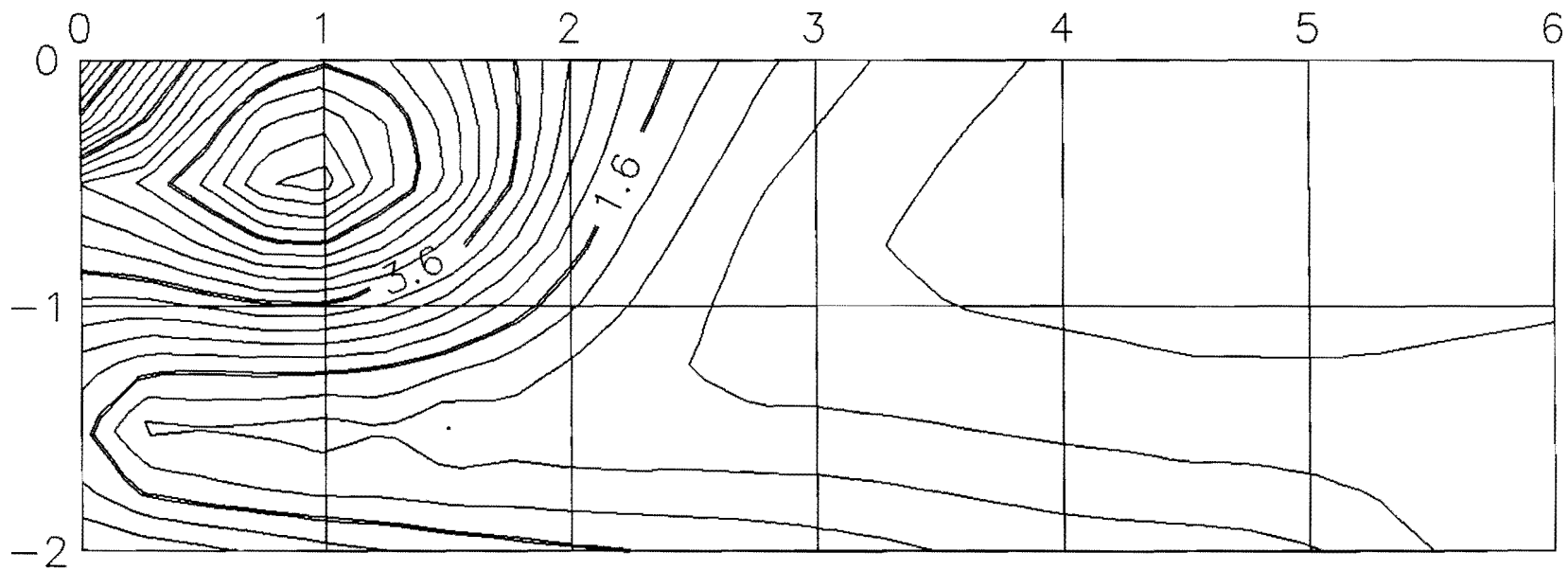
B-69

Nor. Oct. Stress (psi) - 2 in. AC/CLS Base - Hot Season - Braking Wheel - Slip

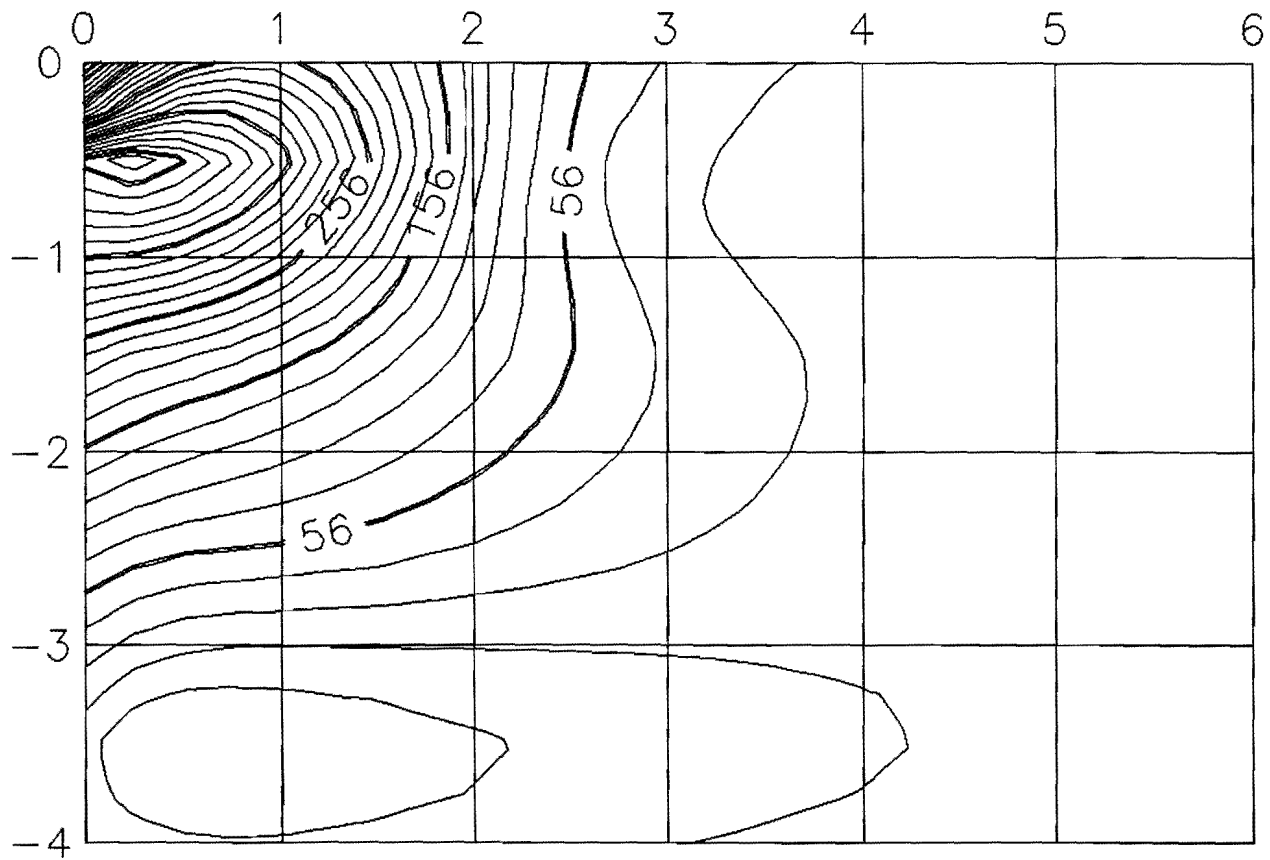


B-70

NTSR - 2 in. AC/CLS Base - Hot Season - Braking Wheel - Slip

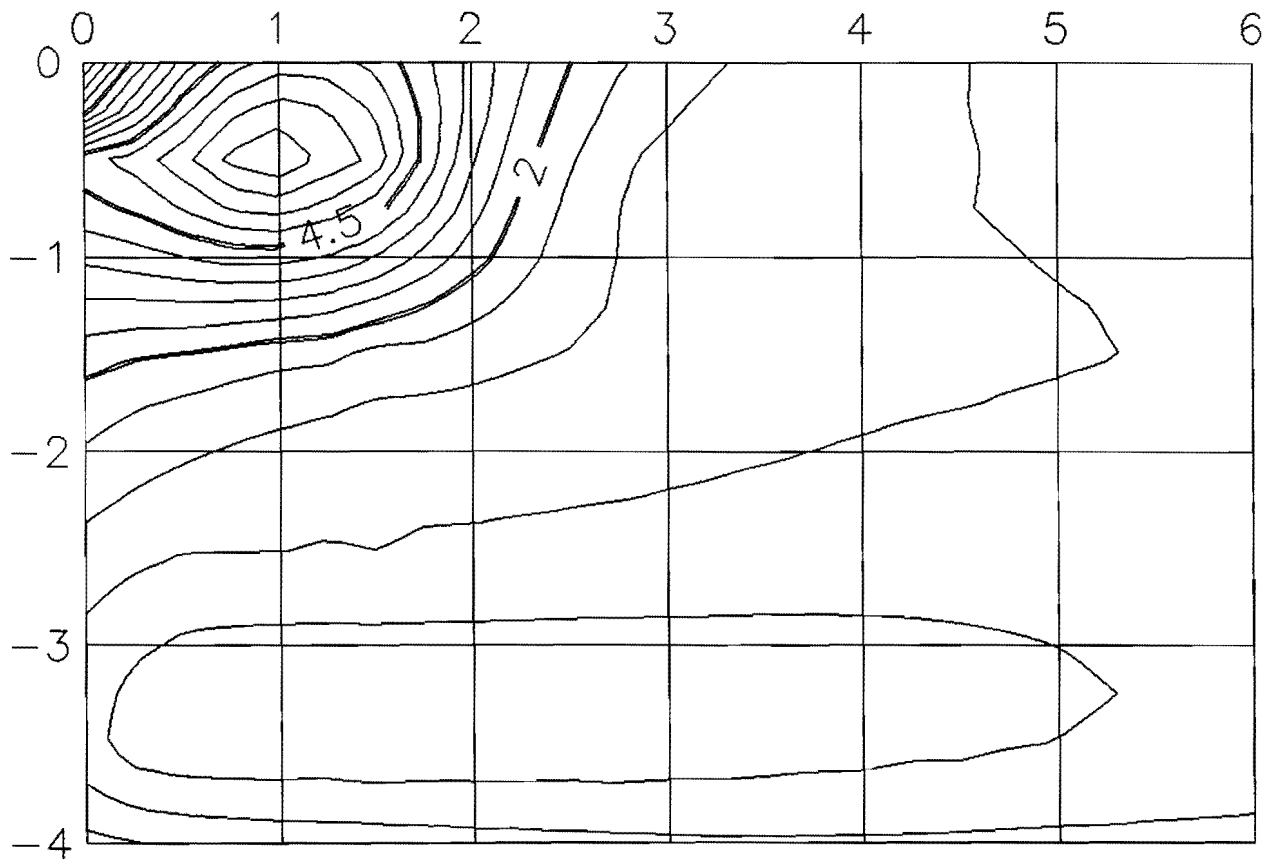


Nor. Oct. Stress (psi) - 4 in. AC/CLS Base - Hot Season - Braking Wheel - slip



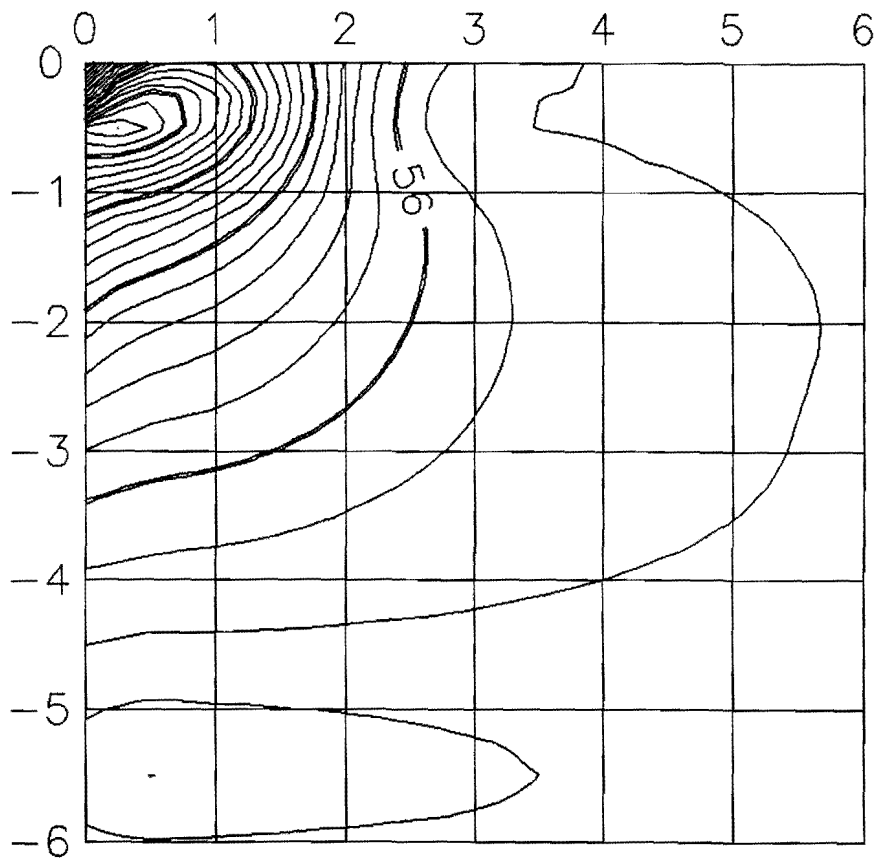
B-72

NTSR - 4 in. AC/CLS Base - Hot season - Braking Wheel - slip

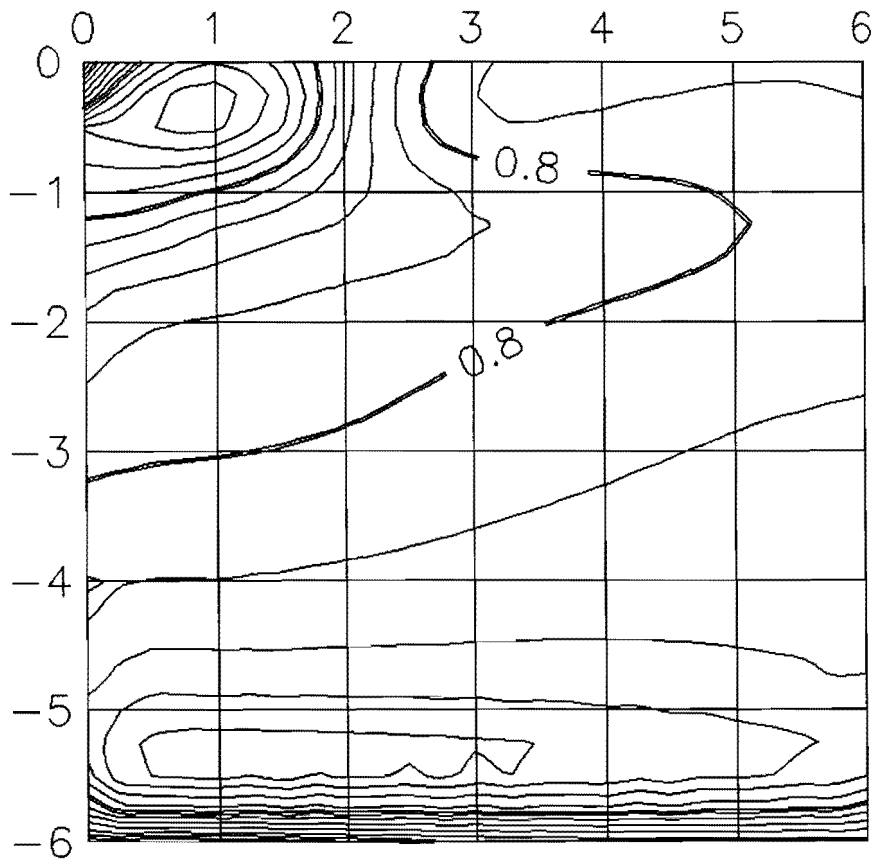


B-73

Nor. Oct. stress (psi) - 6 in. AC/CLS Base - Hot Season - Braking Wheel - Slip

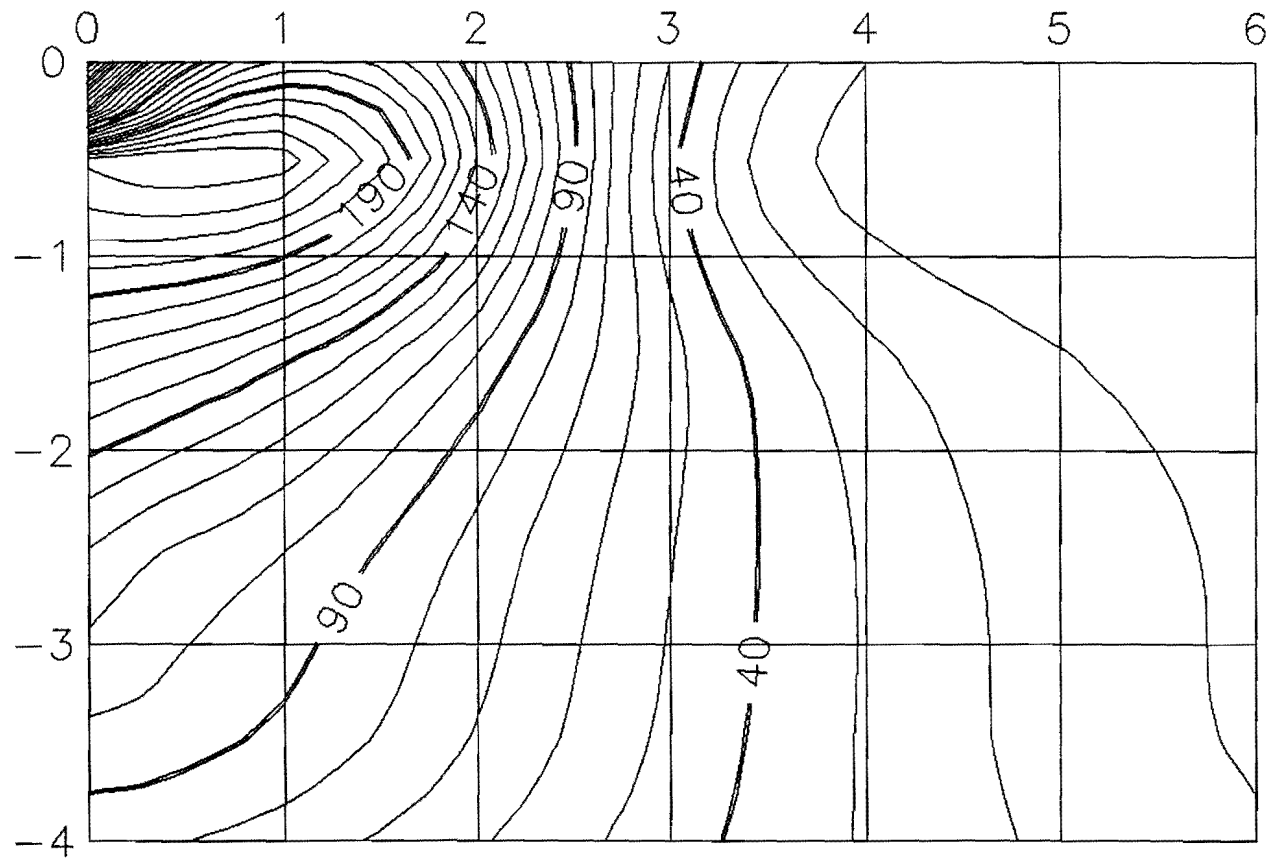


NTSR - 6 in. AC/CLS Base - Hot Season - Braking Wheel - Slip



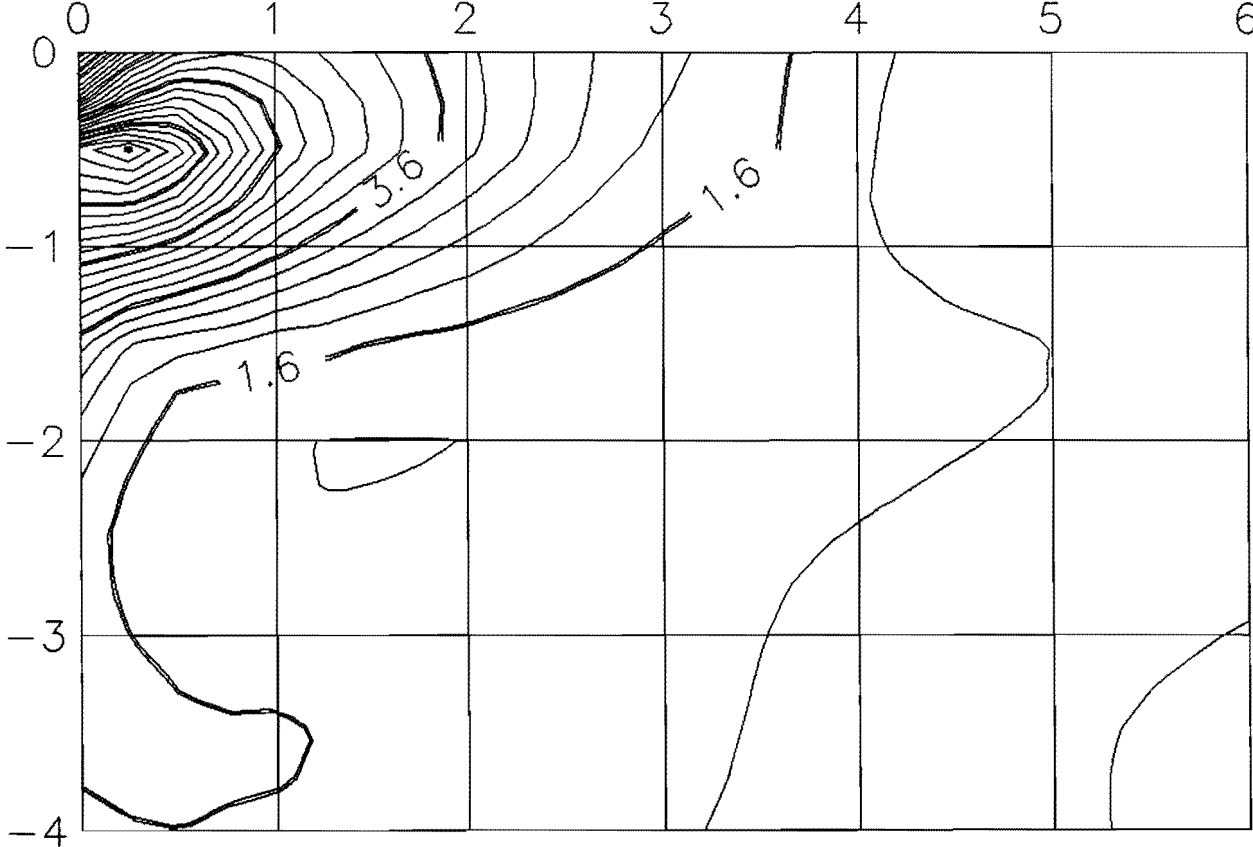
B-75

Nor. Oct. Stress (psi) - 4 in. AC/AC Base - Hot Season - Hvy. Rlg. Wheel - Bond



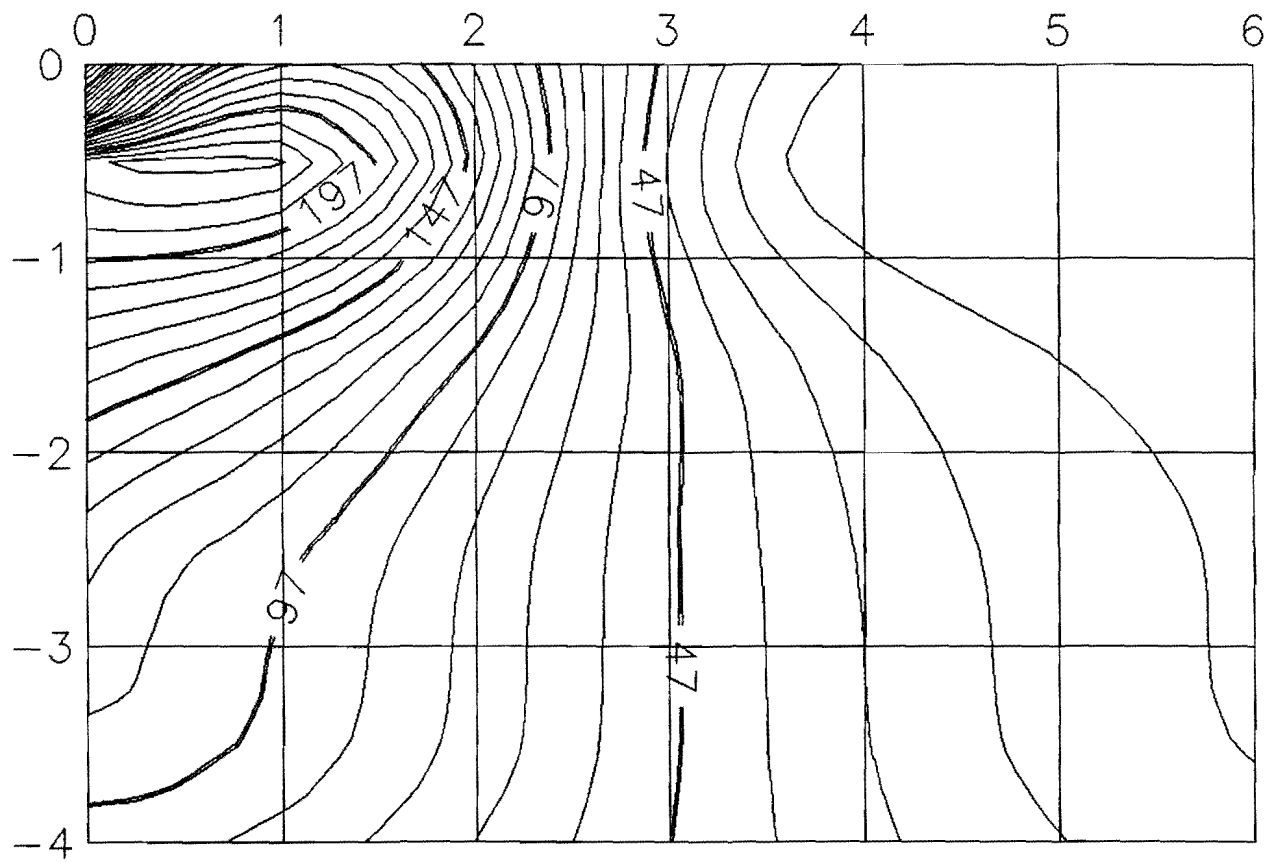
B-76

NTSR - 4 in. AC/AC Base - Hot Season - Heavy Rolling Wheel - Bond



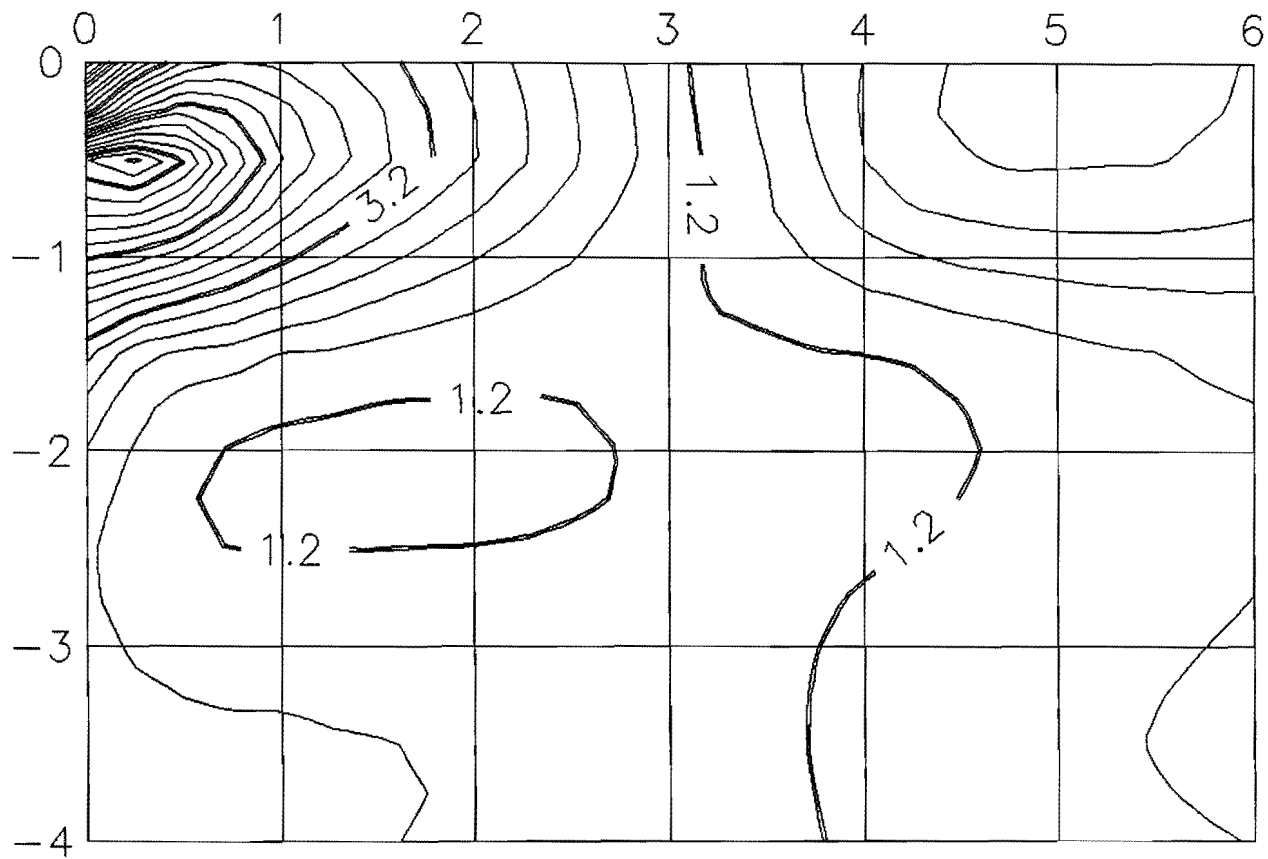
B-77

Nor. Oct. Stress (psi) - 4 in. AC/PCC Base - Hot Season - Hvy. Rlg. Wheel-Bond



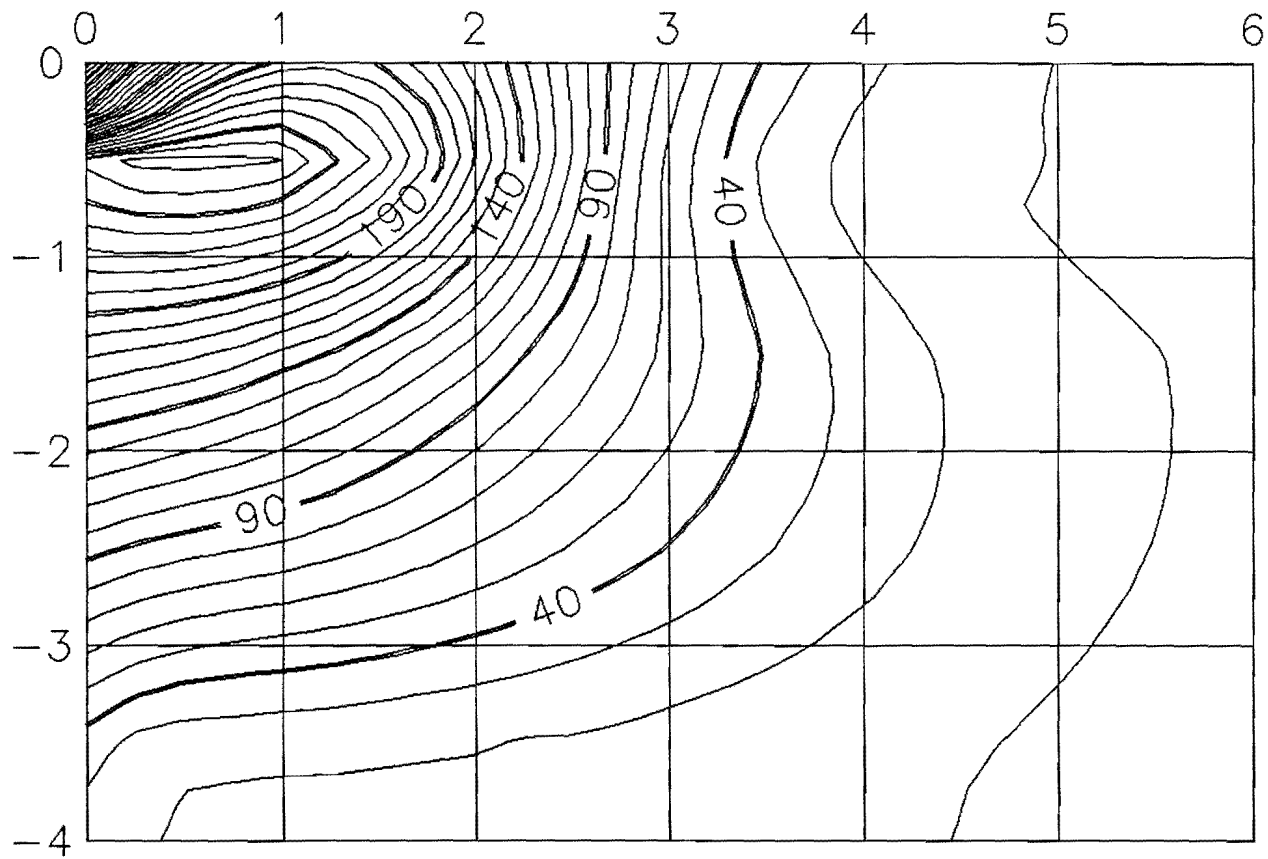
B-78

NTSR - 4 in. AC/PCC Base - Hot Season - Heavy Rolling Wheel - Bond



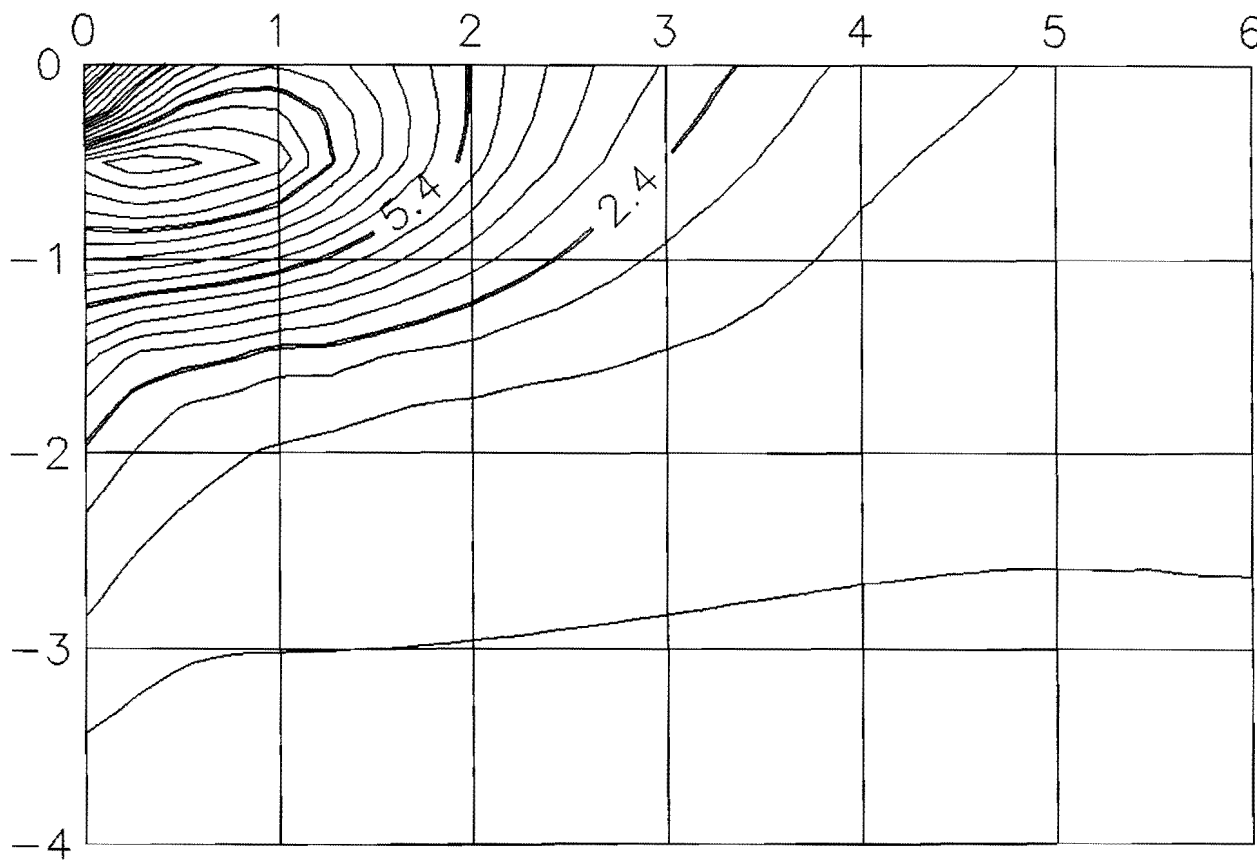
B-79

Nor. Oct. Stress (psi) - 4 in. AC/CLS Base - Hot Season - Hvy. Rlg. Wheel-Bond



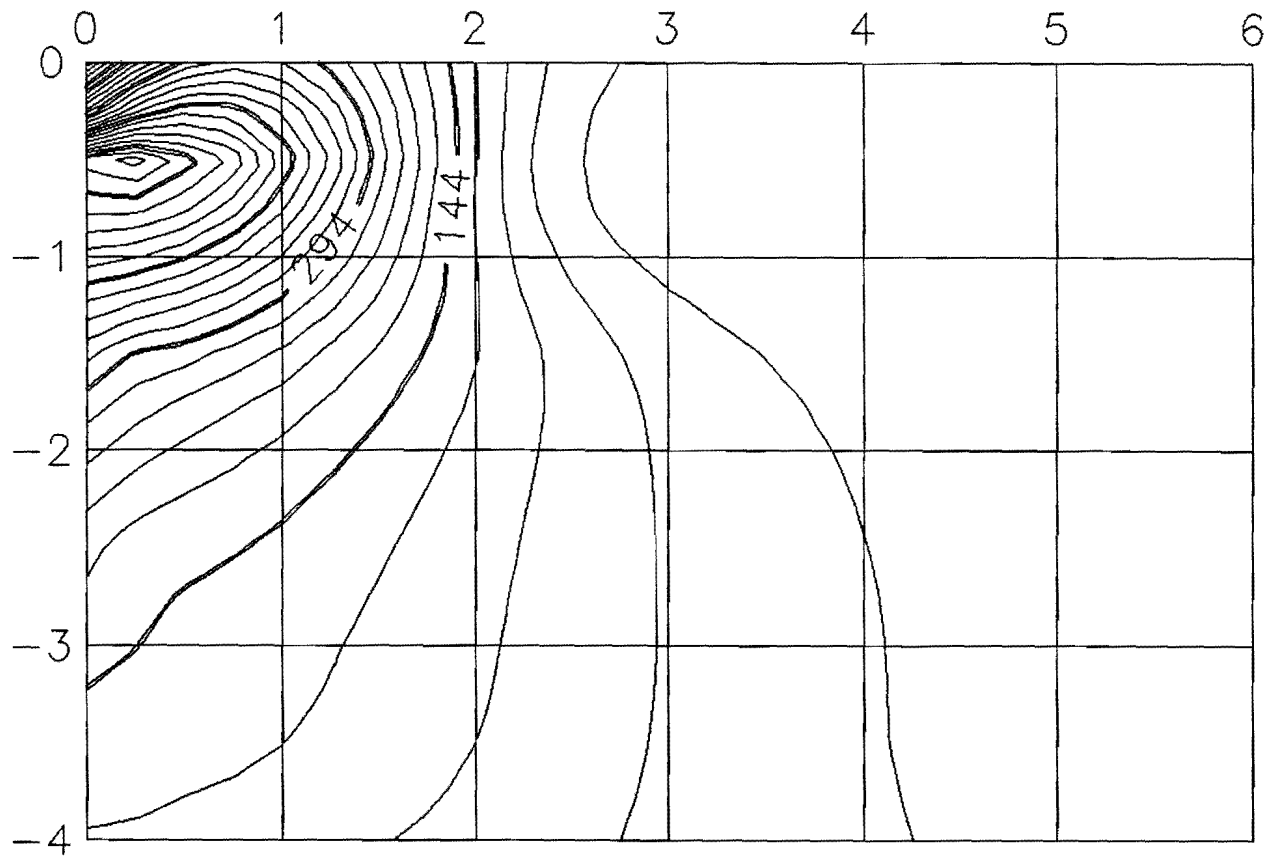
B-80

NTSR - 4 in. AC/CLS Base - Hot Season - Heavy Rolling Wheel - Bond



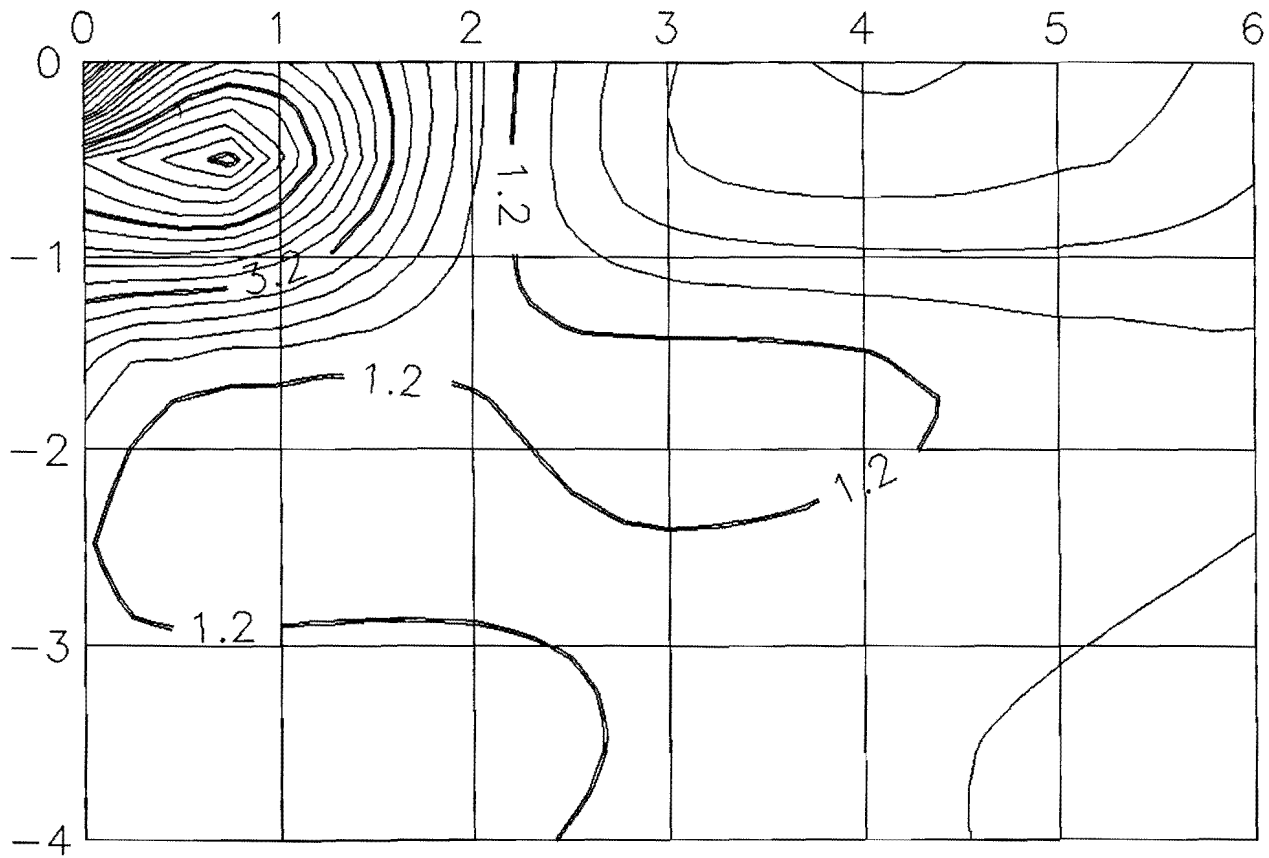
B-81

Nor. Oct. Stress (psi) - 4 in. AC/AC Base - Hot Season - Hvy. Brkg. Wheel - Bond



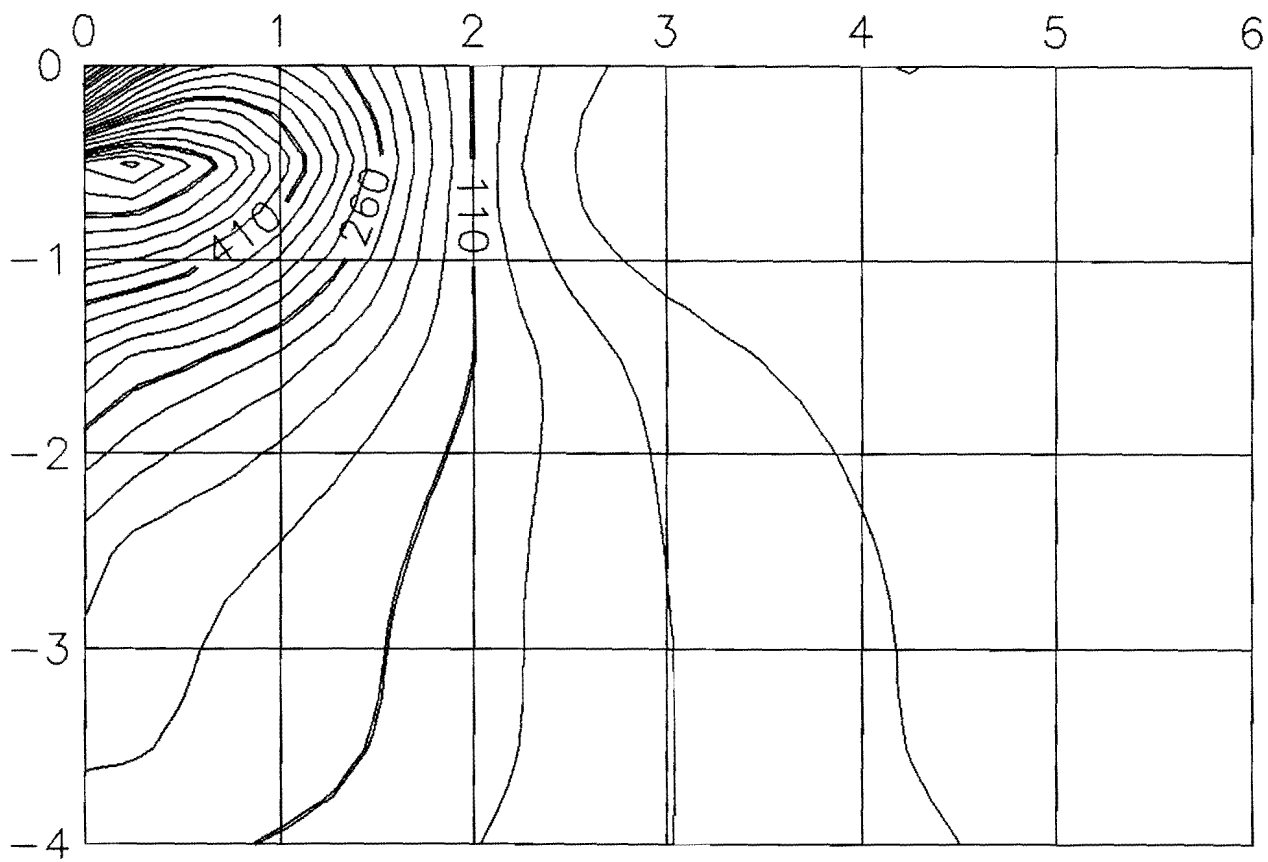
B-82

NTSR - 4 in. AC/AC Base - Hot Season - Heavy Braking Wheel - Bond



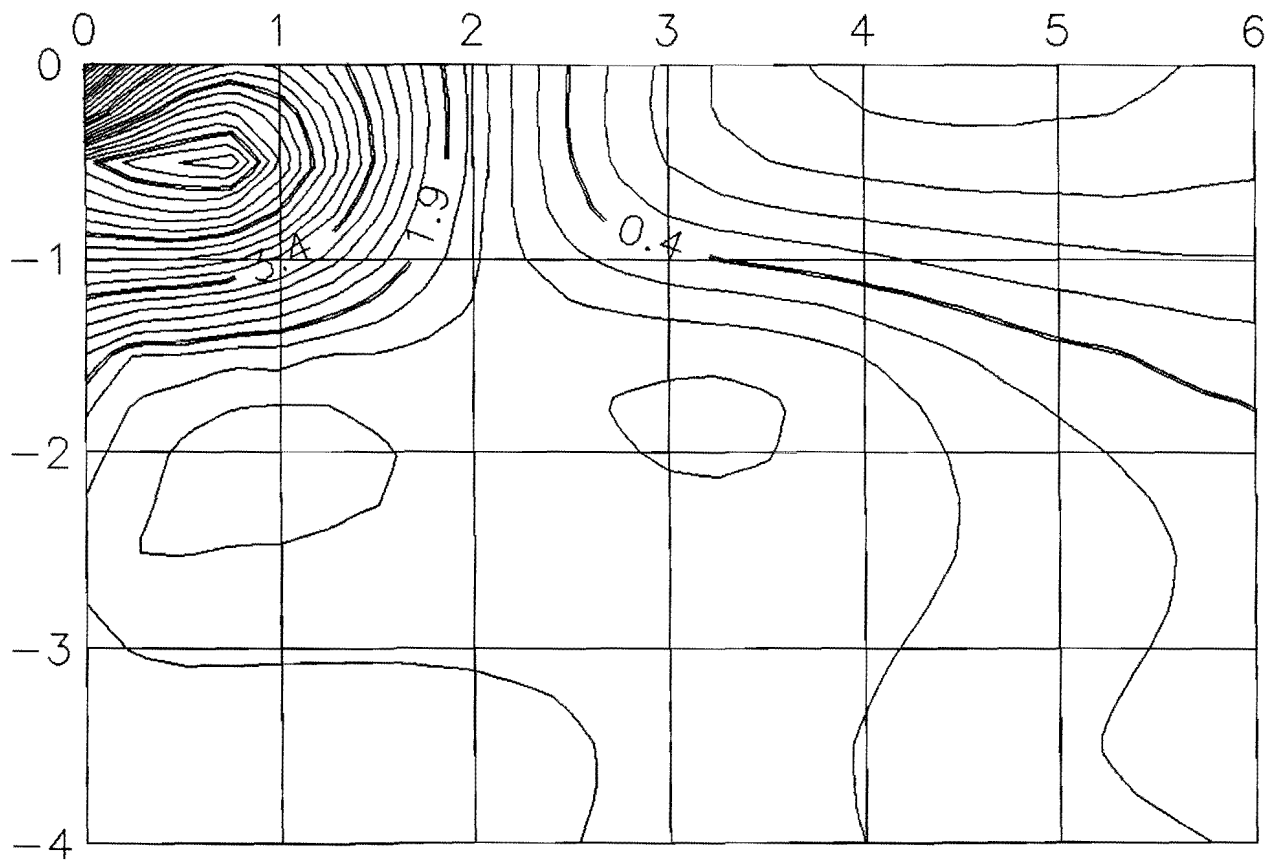
B-83

Nor.Oct. Stress (psi) - 4 in. AC/PCC Base - Hot Season - Hvy. Brkg. Wheel - Bond

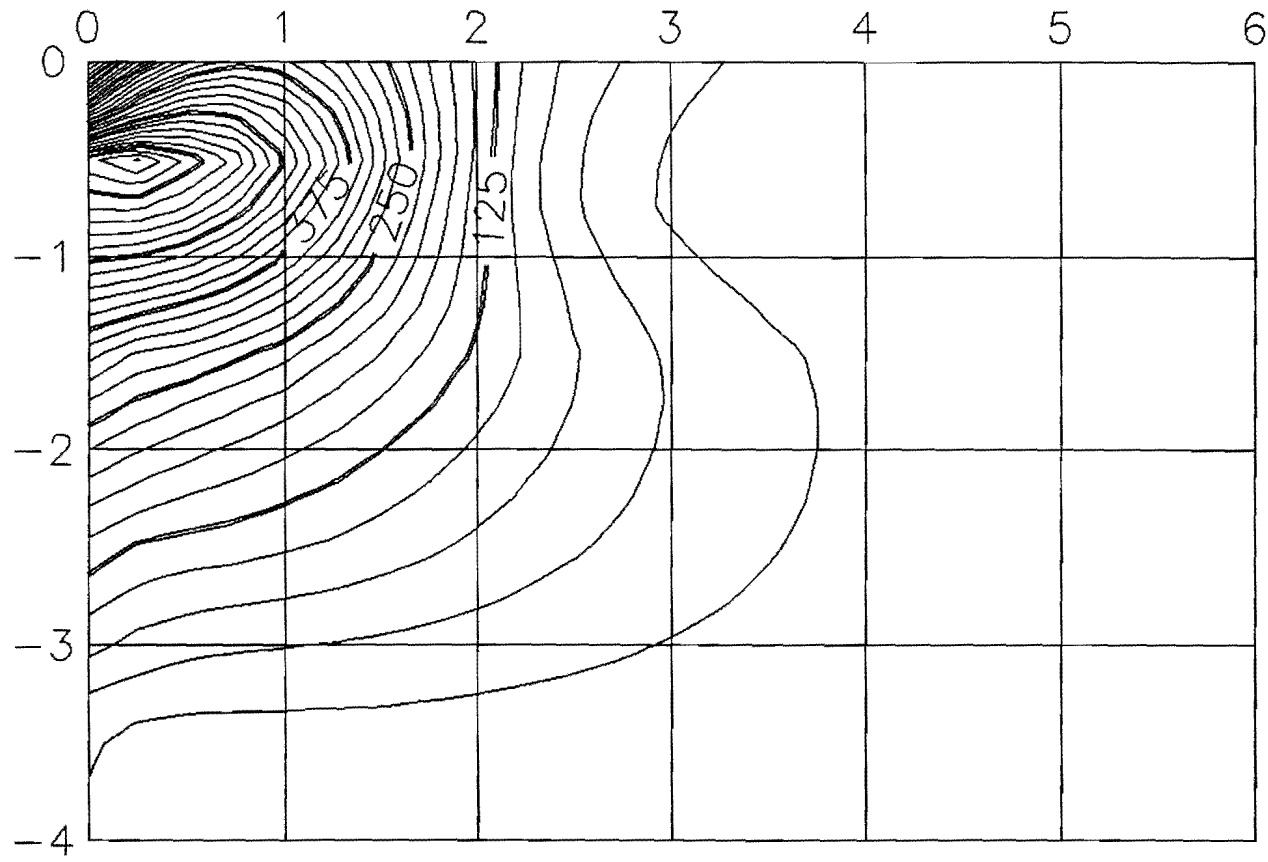


B-84

NTSR - 4 in. AC/PCC Base - Hot Season - Heavy Braking Wheel - Bond

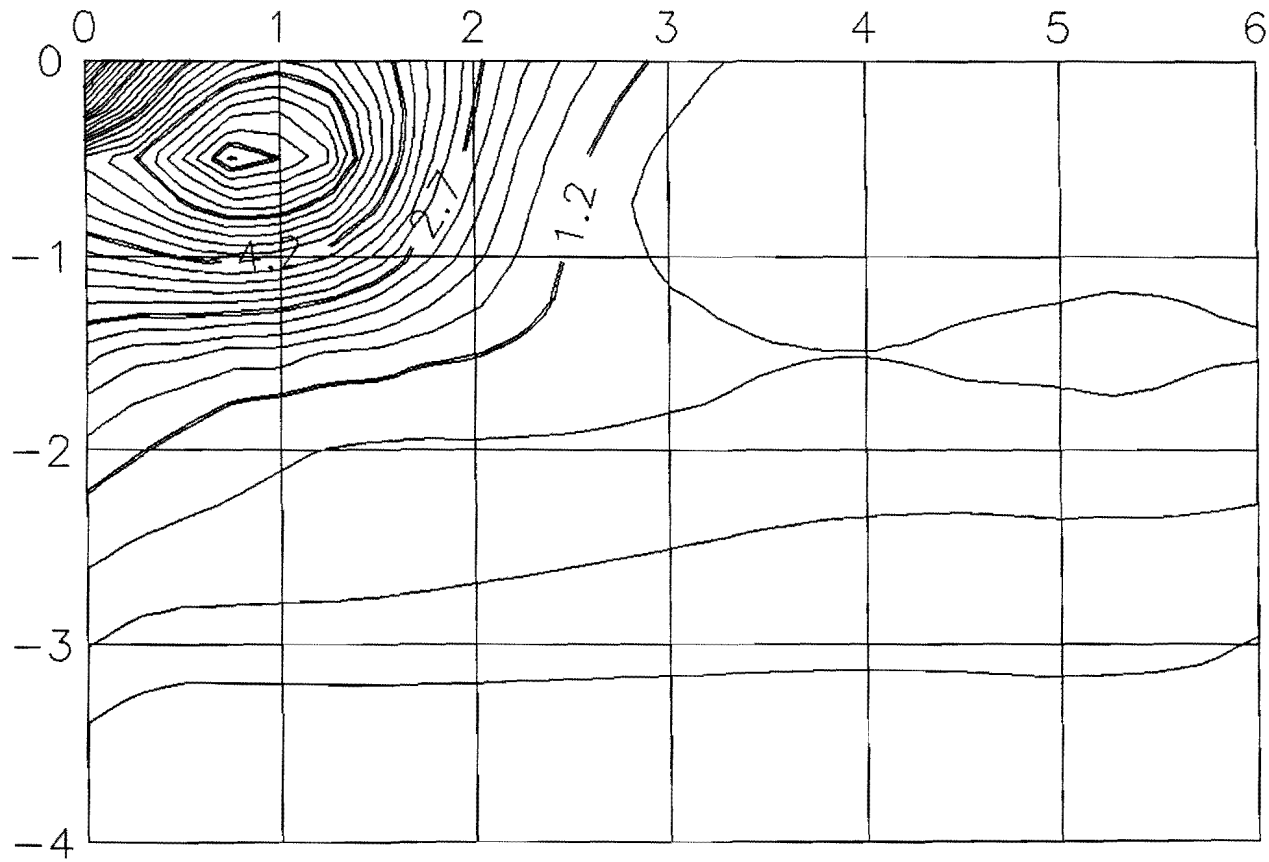


Nor. Oct. Stress (psi) - 4 in. AC/CLS Base - Hot Season - Hvy. Brkg. Wheel-Bond



B-86

NTSR - 4 in. AC/CLS Base - Hot Season - Heavy Braking Wheel - Bond



B-87

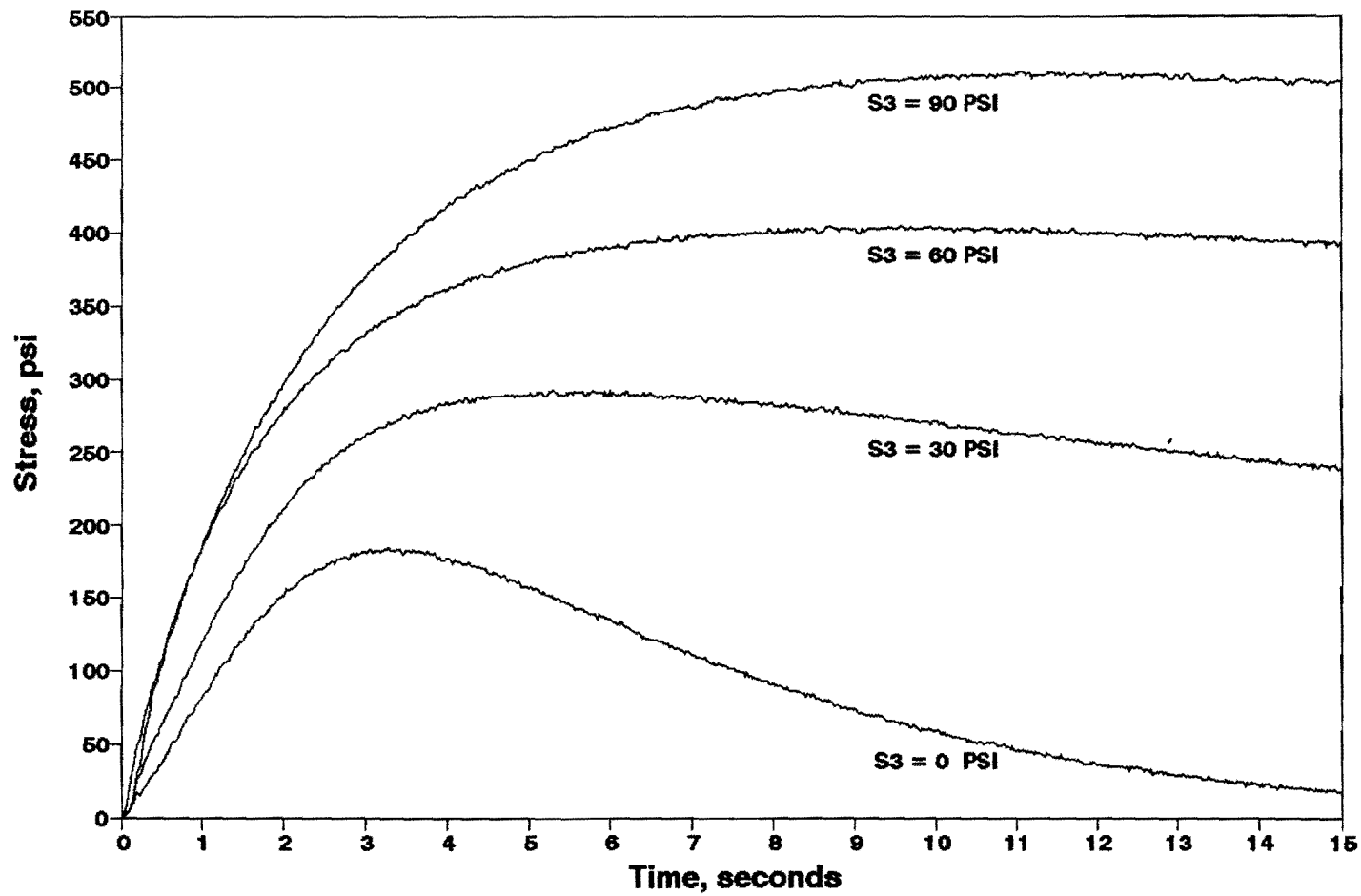


**APPENDIX C**

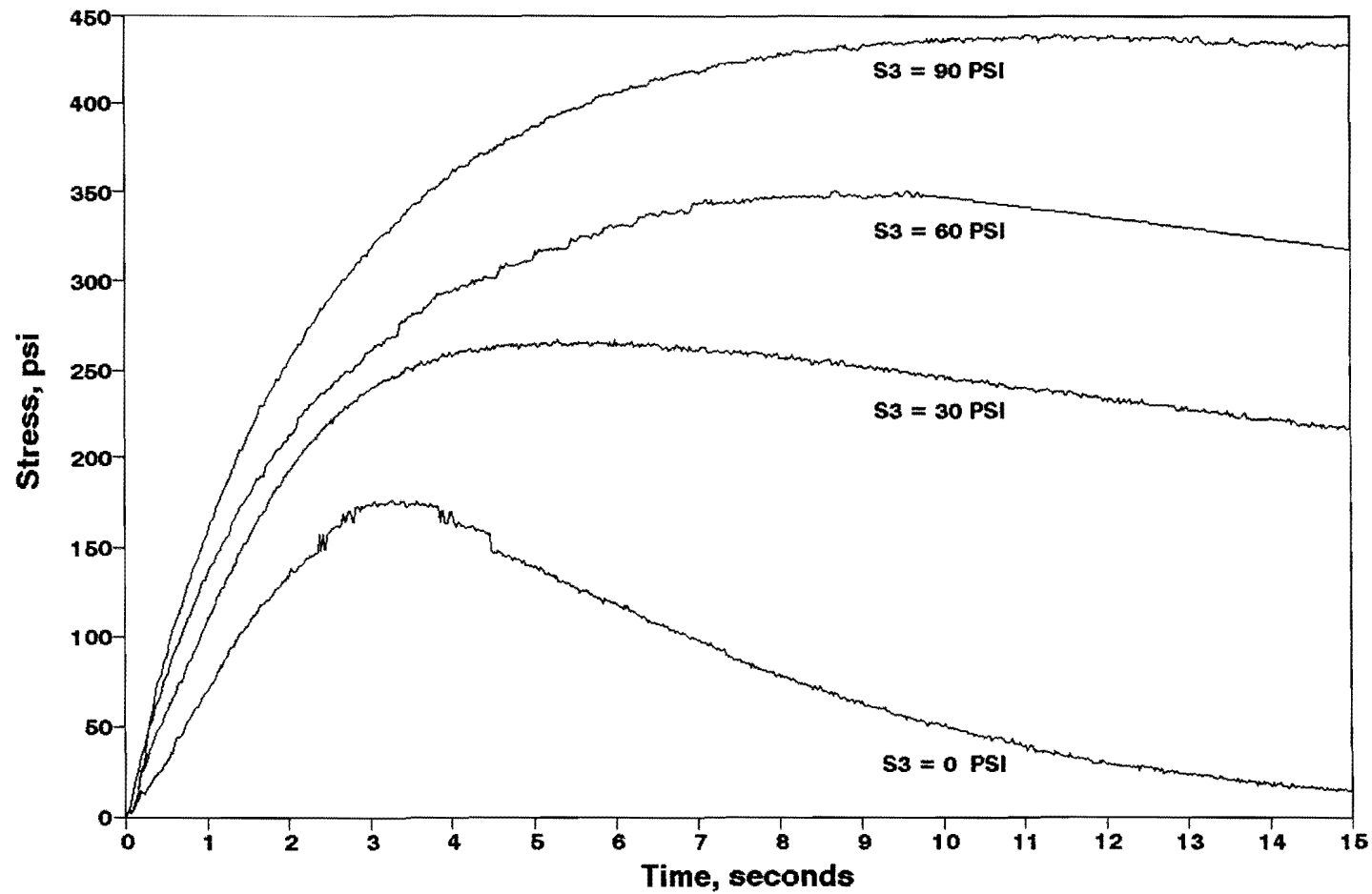
STRESS TO FAILURE VERSUS TIME OF LOADING FOR TRIAXIAL  
TESTING OF VARIOUS MIXTURES CONSIDERING THE  
EFFECTS OF THE FOLLING MIXTURE VARIABLES:

% Natural Sand  
% Air Voids  
% Binder  
Rate of Loading

NS(0%), CLS(100%), Temp.=104F, AV=(5-7%),  
AC% (opt.), Load Rate= (2in./min.)

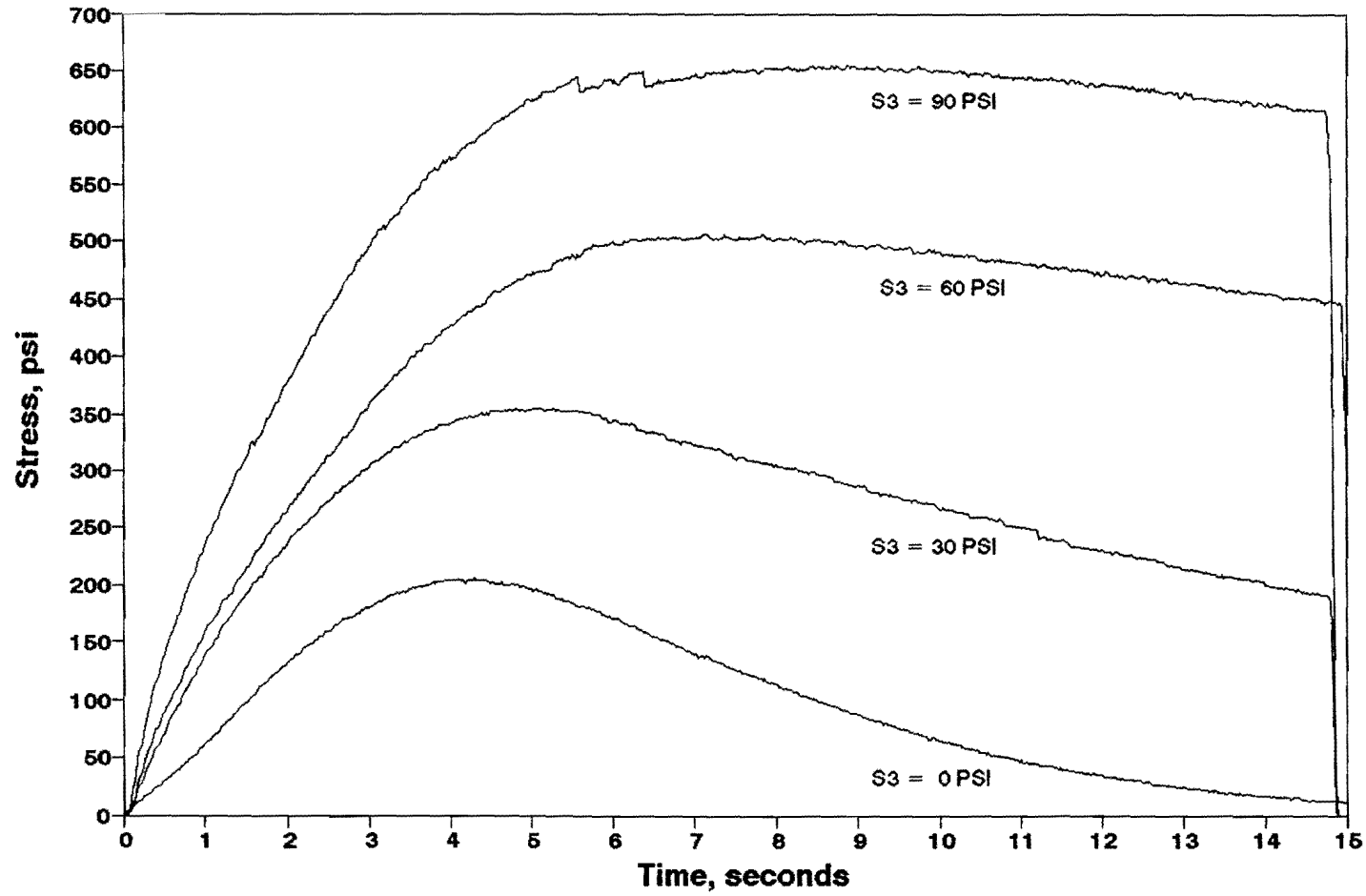


NS(0%),CLS(100%), Temp=104F, AV=(5-7%),  
AC% (opt. + 0.8), Load Rate= (2in./min.)

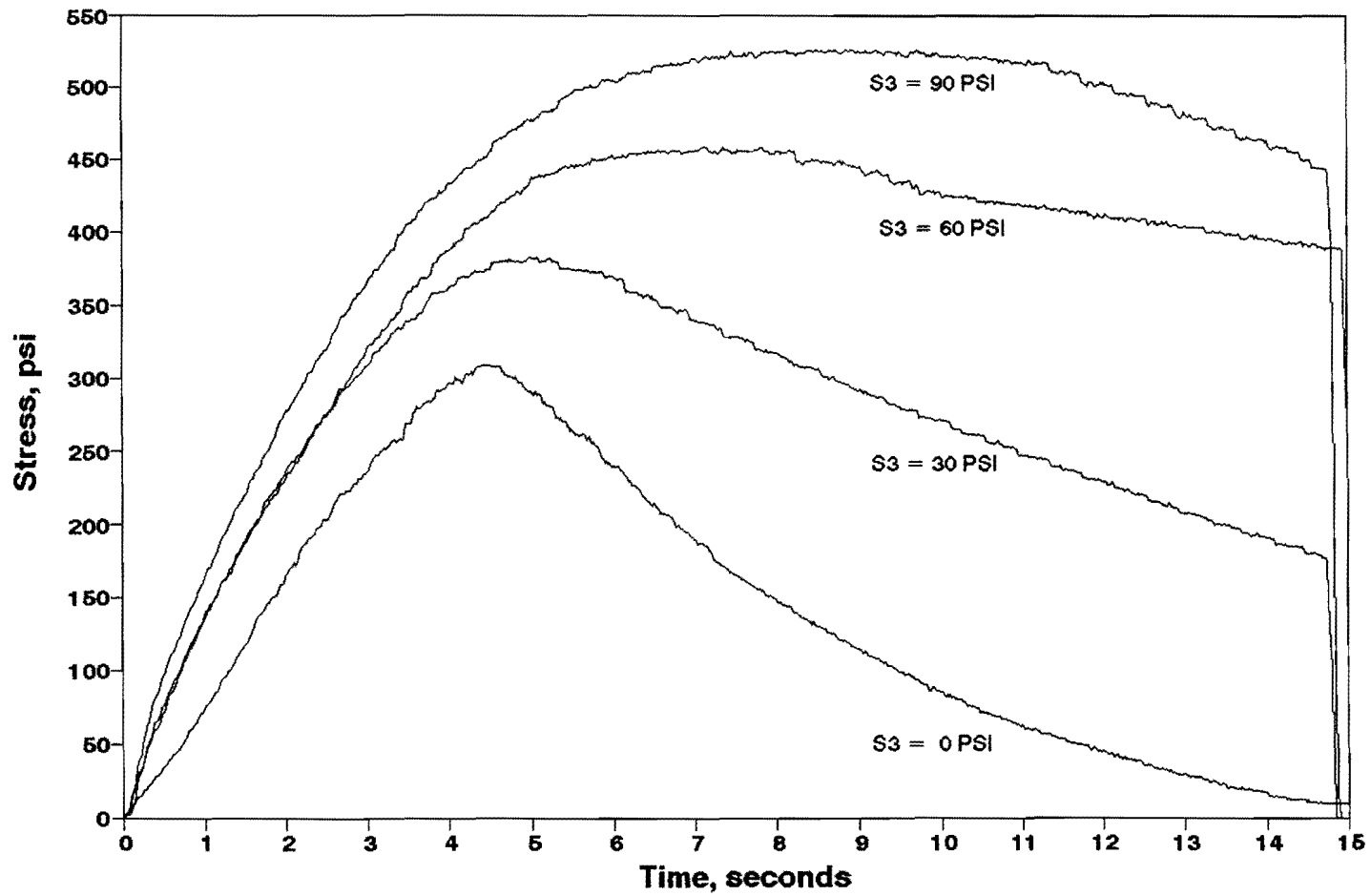


NS(0%), CLS(100%), Temp.=104F,AV=(5-7%)  
AC% (opt. - 0.8), Load Rate=(2in./min.)

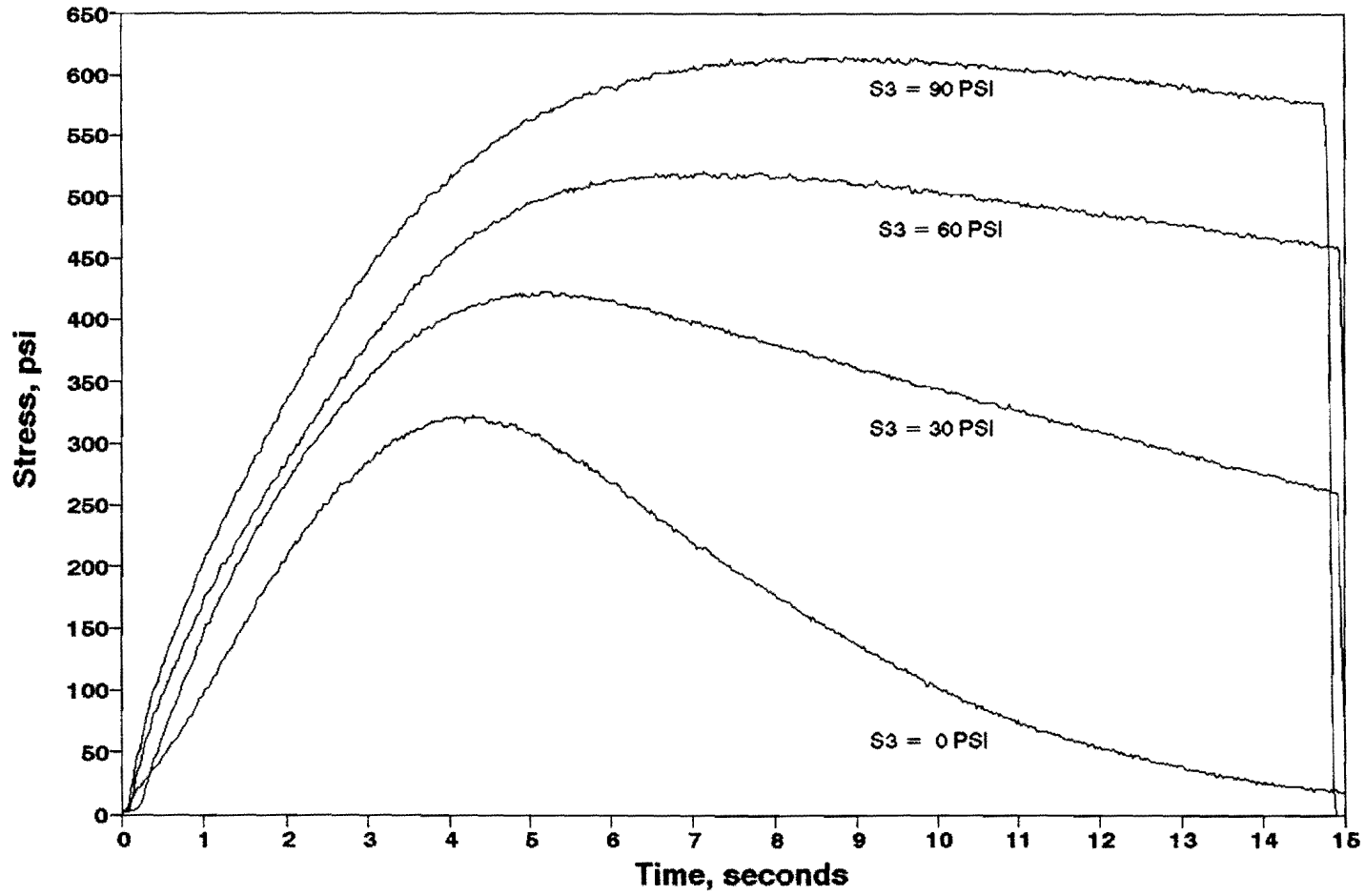
C-4



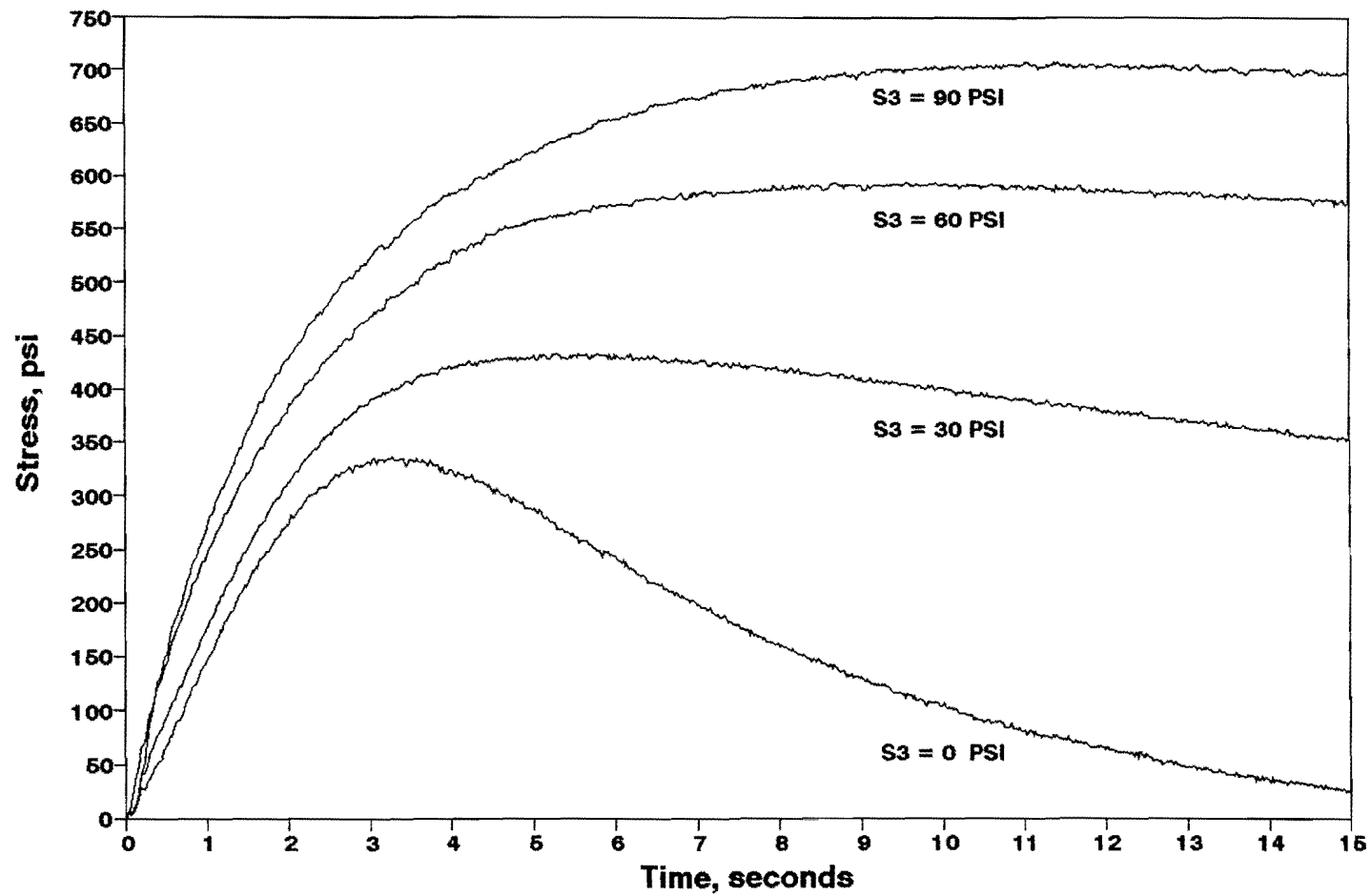
NS(0%), CLS(100%), Temp. = 104F, AV = (3-4%)  
AC% (opt + 0.8), Load Rate = (2in./min.)



NS(0%), CLS(100%), Temp.=104F,AV=(3-4%)  
AC%(opt.), Load Rate= (2in./min.)

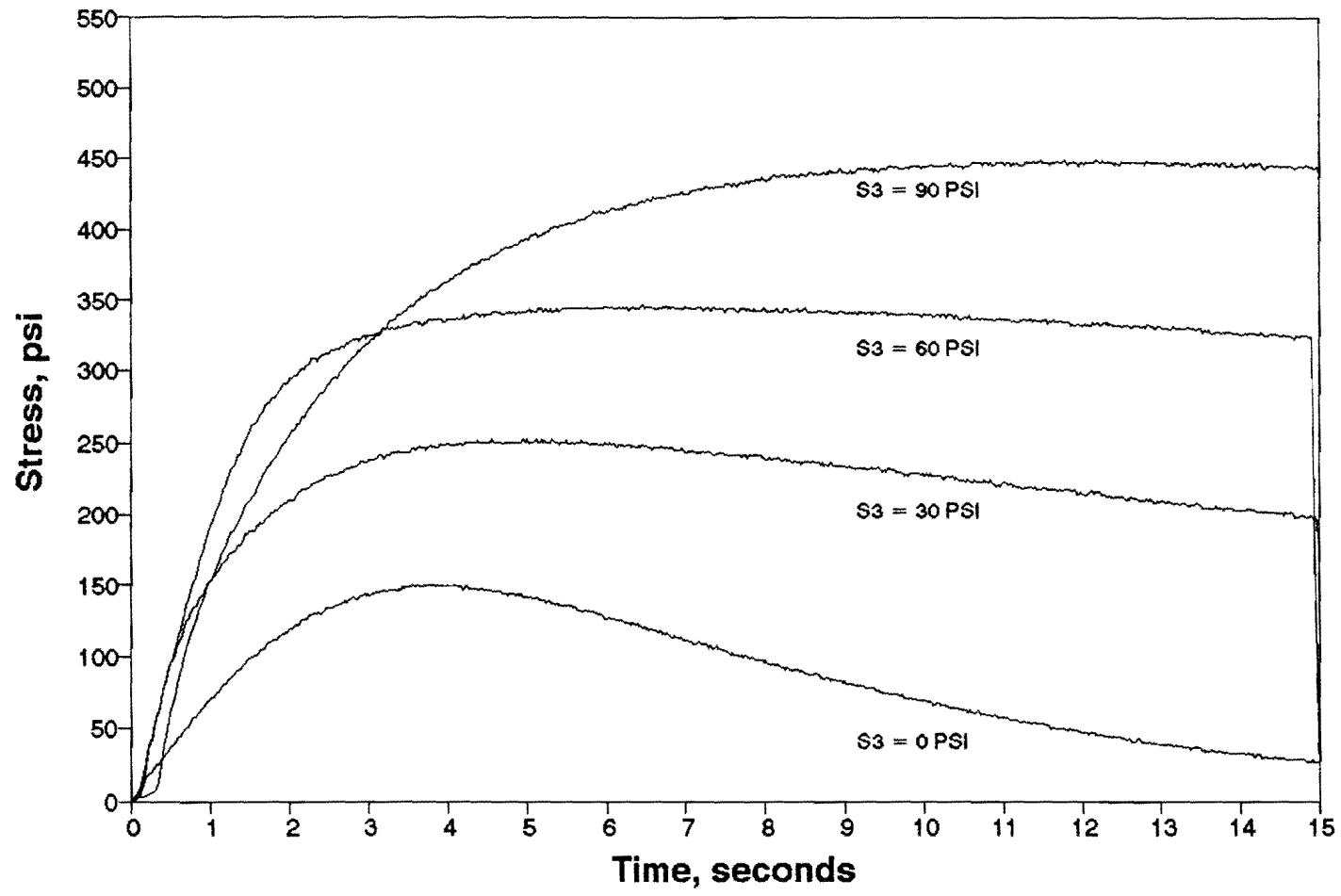


NS(0%), CLS(100%), Temp.=104F,AV=(3-5%)  
AC% (opt.-0.8%), Load Rate= (2in./min.)



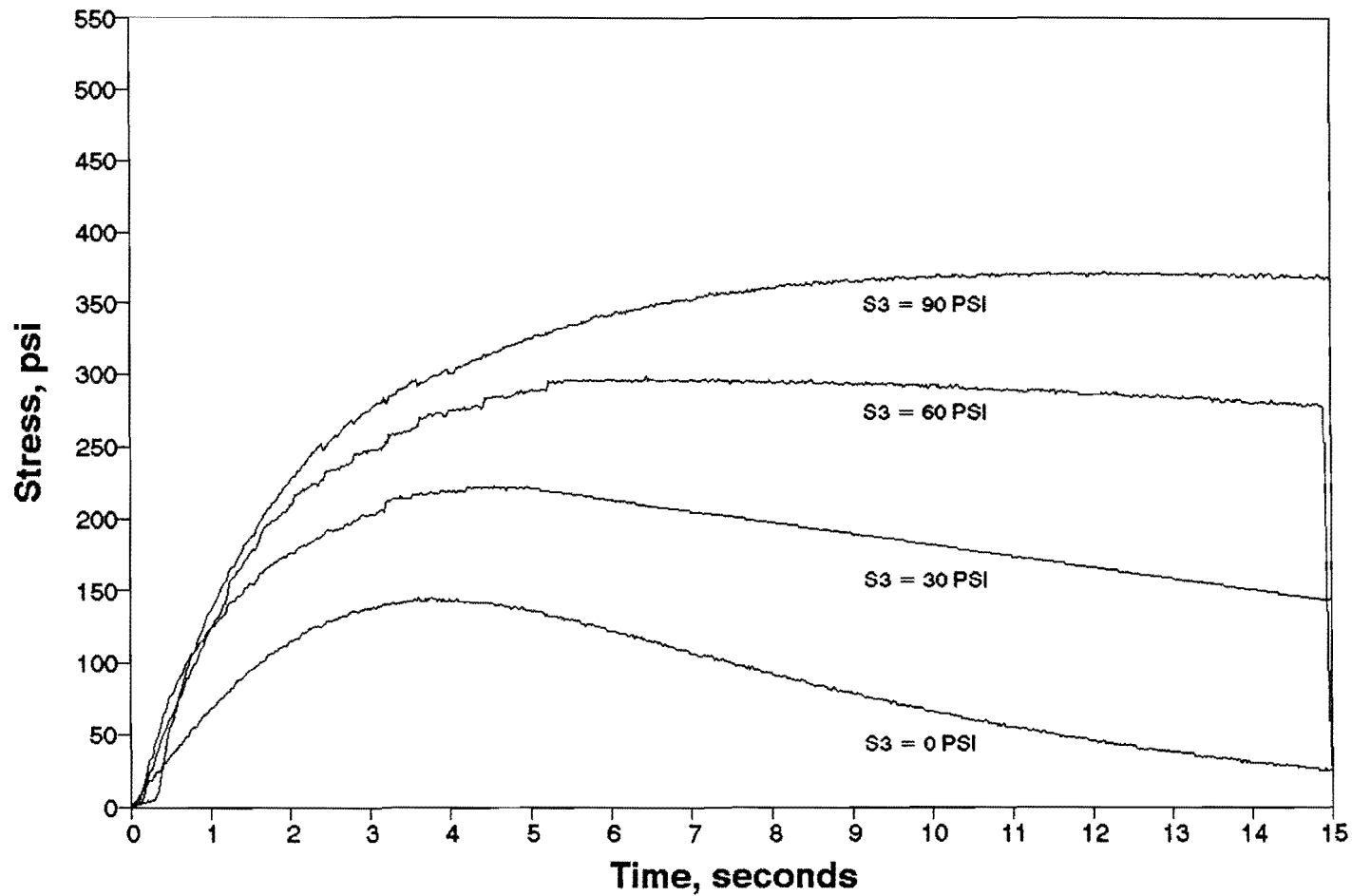
C-7

NS(10%), CLS(90%), Temp.=104F,AV=(5-7%)  
AC% (opt.), Load Rate=(2in./min.)

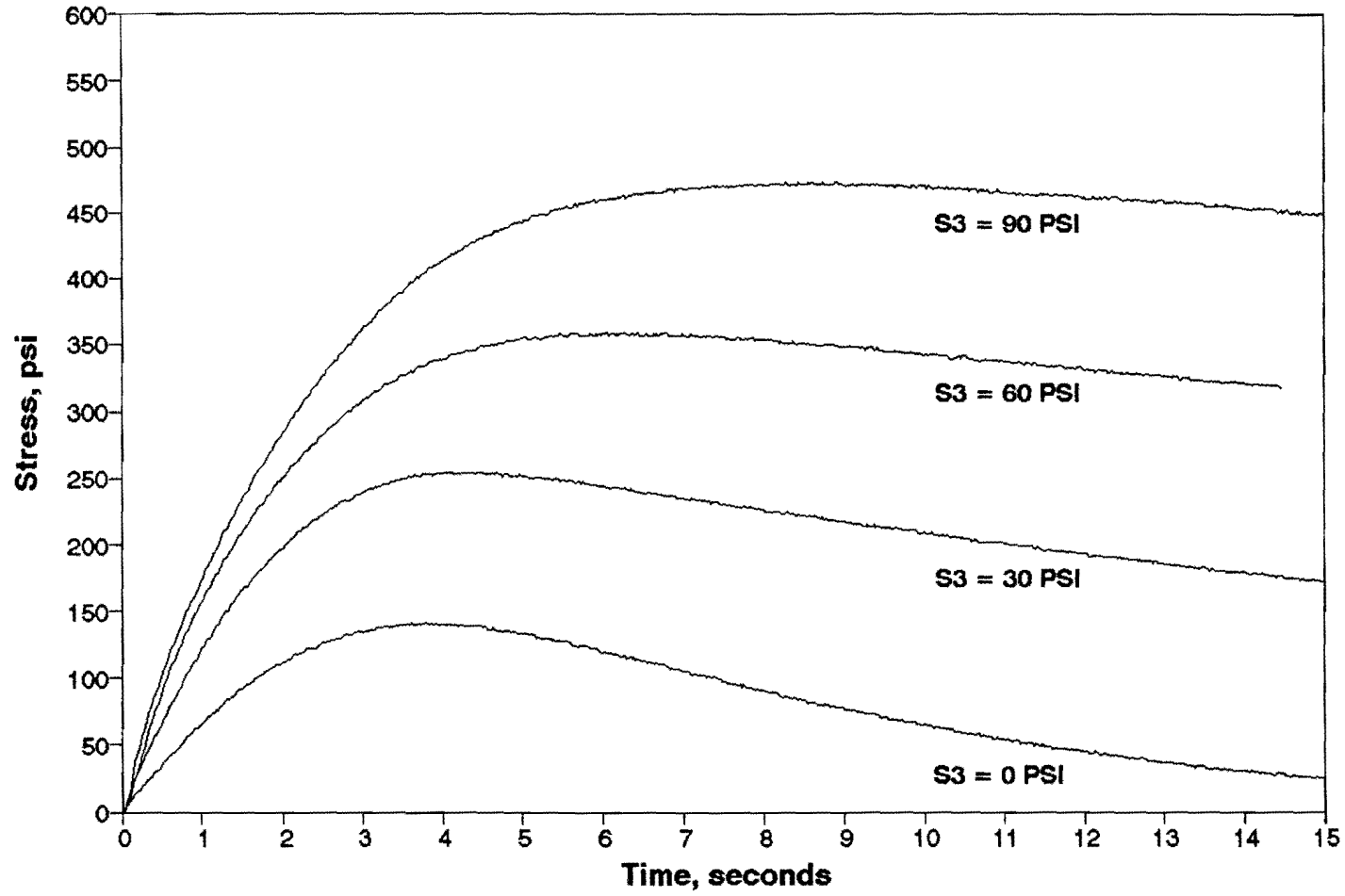


8-C

NS(10%), CLS(90%), Temp.=104F, AV=(5-7%)  
AC% (opt + 0.8), Load Rate=(2in./min.)

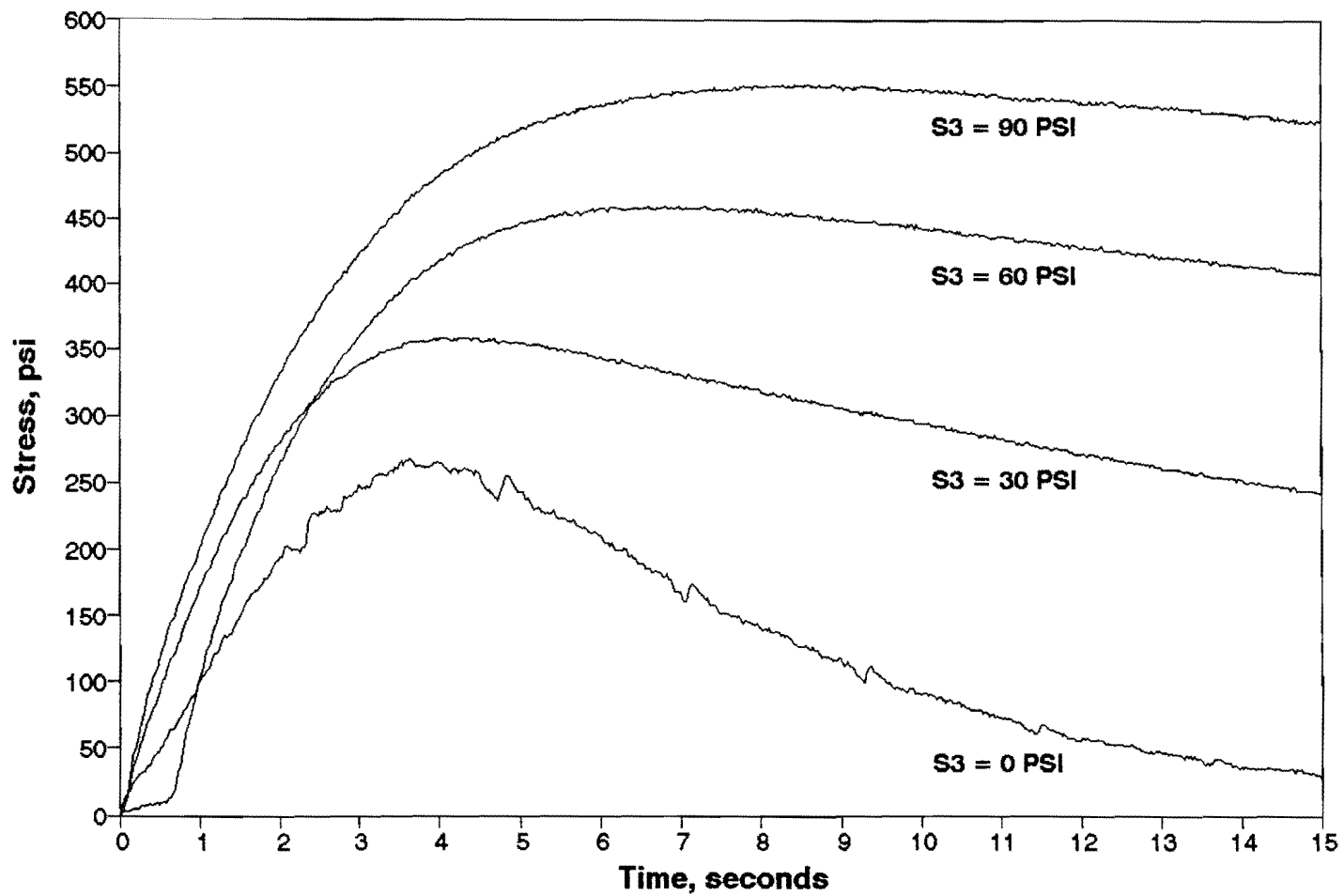


NS(10%), CLS(90%), Temp.=104F,AV=(5-7%)  
AC% (opt. - 0.8), Load Rate=(2in./min.)



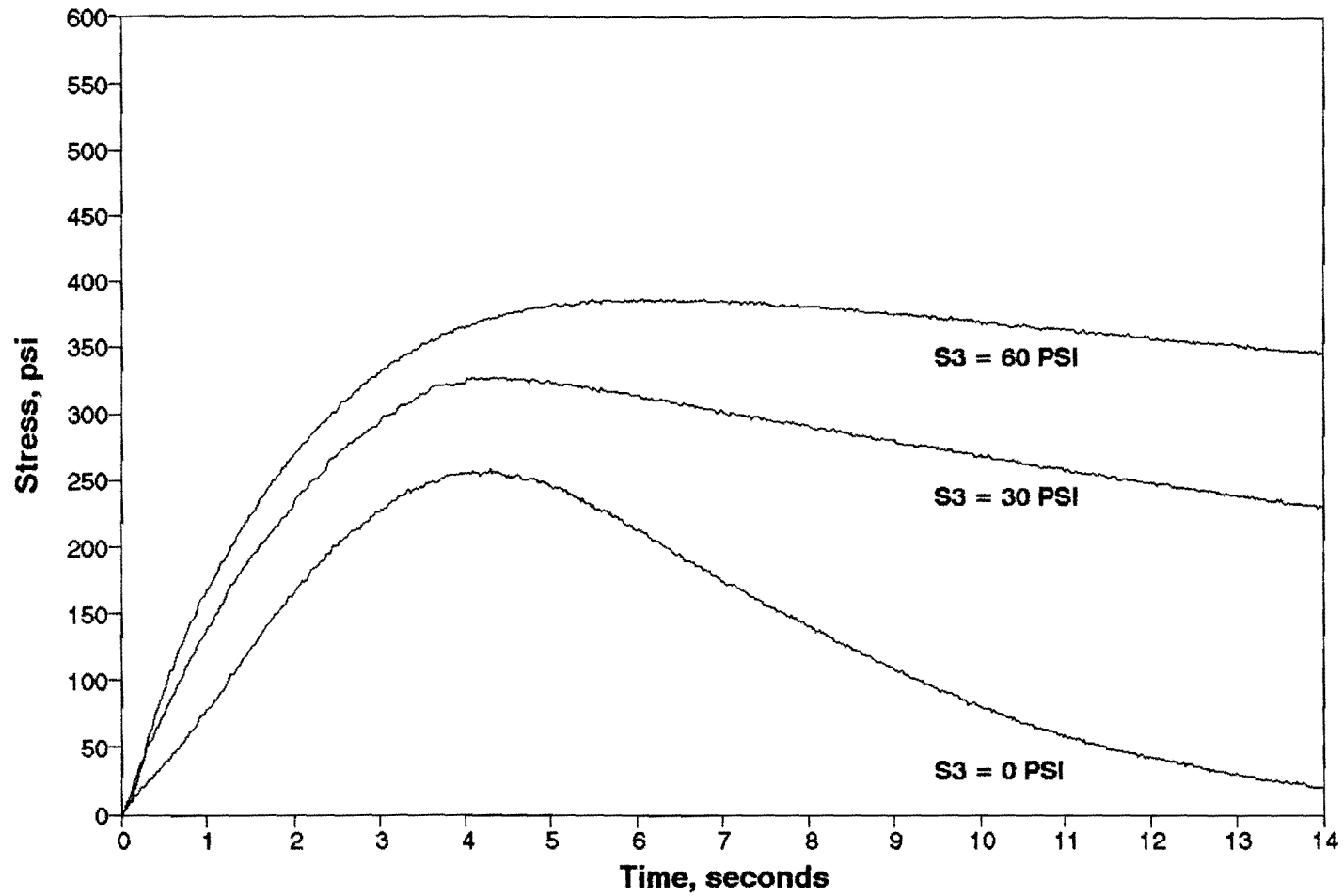
C-10

NS(10%), CLS(90%), Temp.=104F,AV=(3-4%)  
AC% (opt.), Load Rate=(2in./min.)

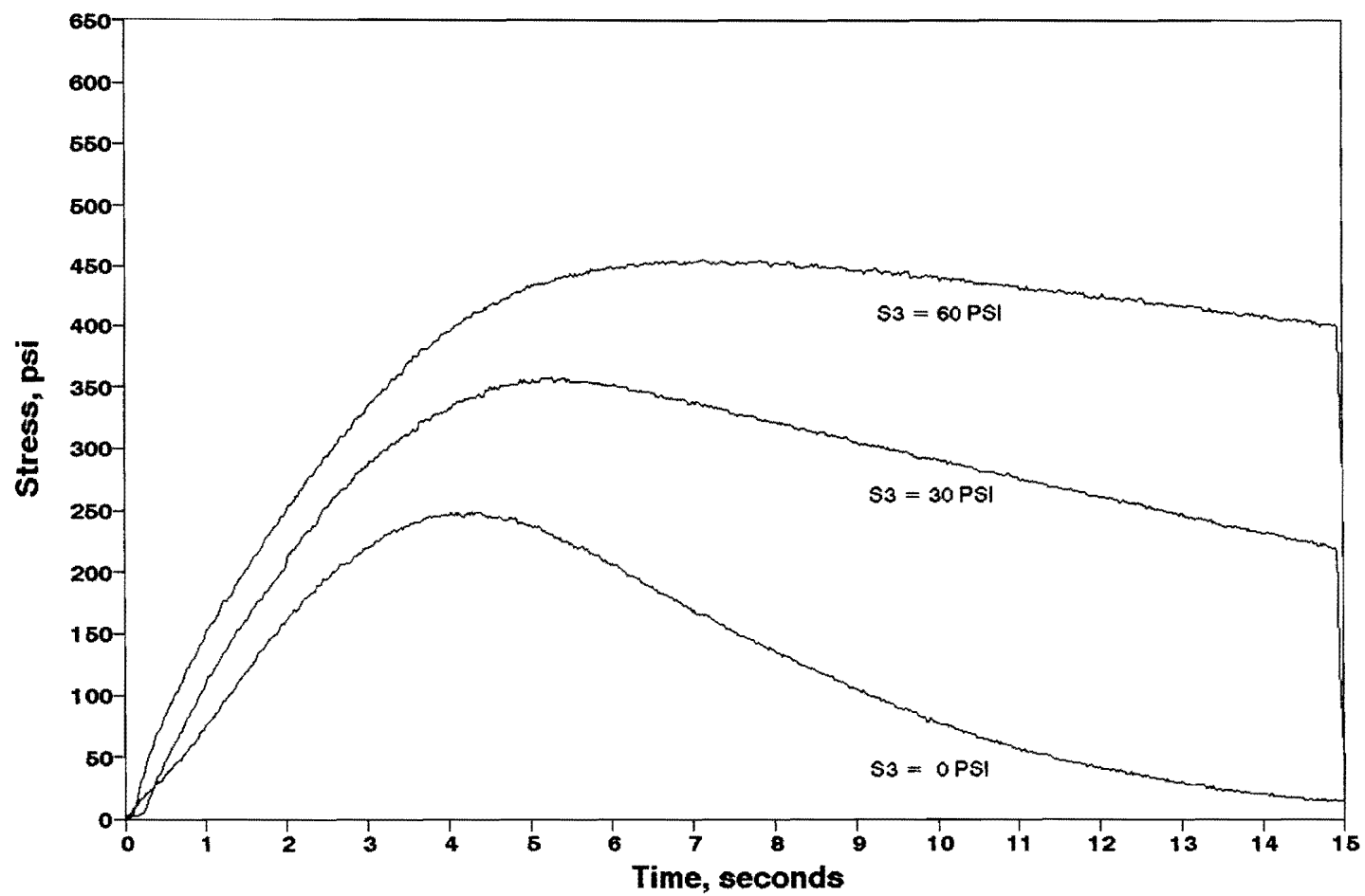


C-11

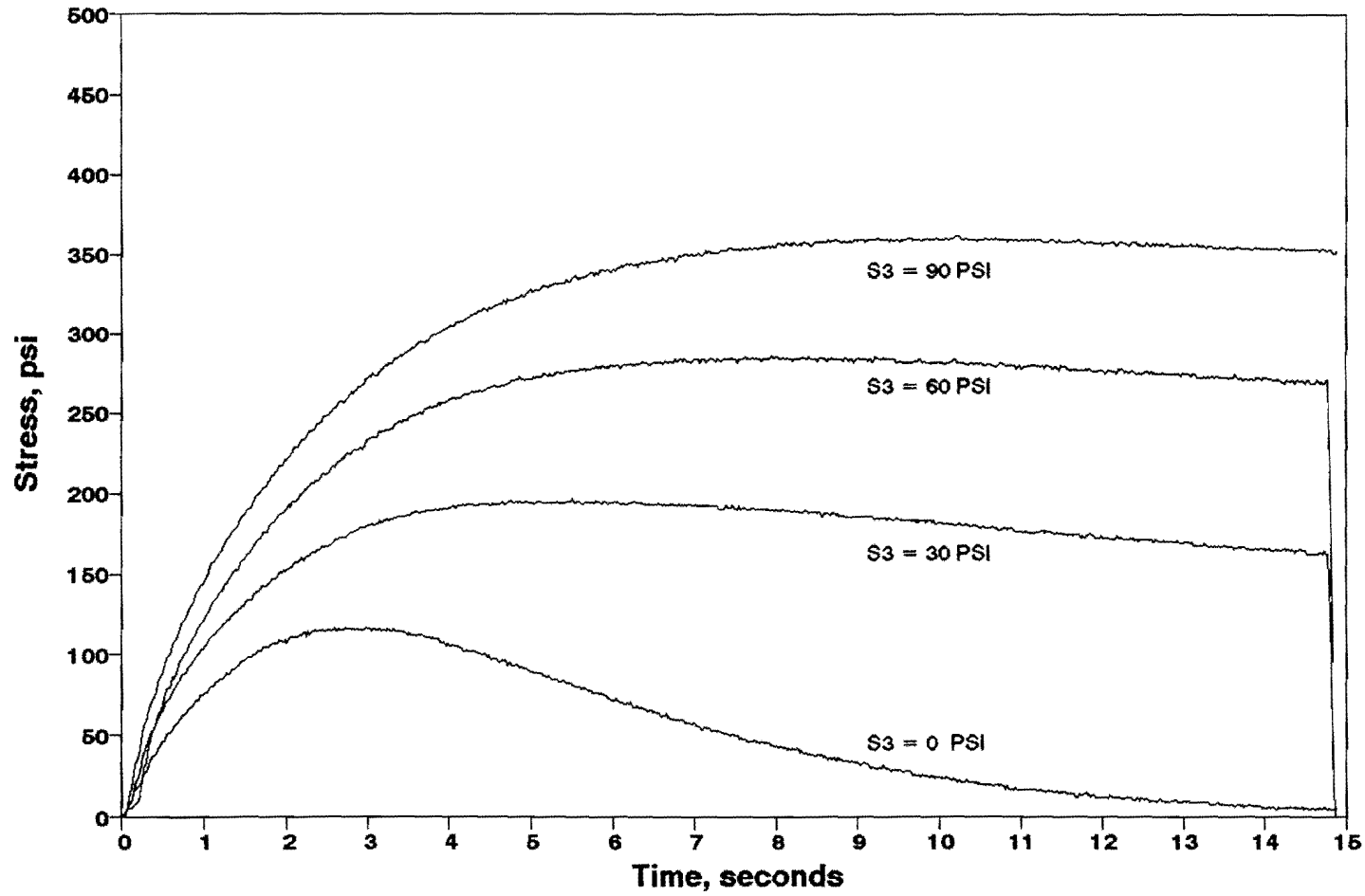
NS(10%), CLS(90%), Temp.=104F,AV=(3-4%)  
AC% (opt. + 0.8), Load Rate=(2in./min.)



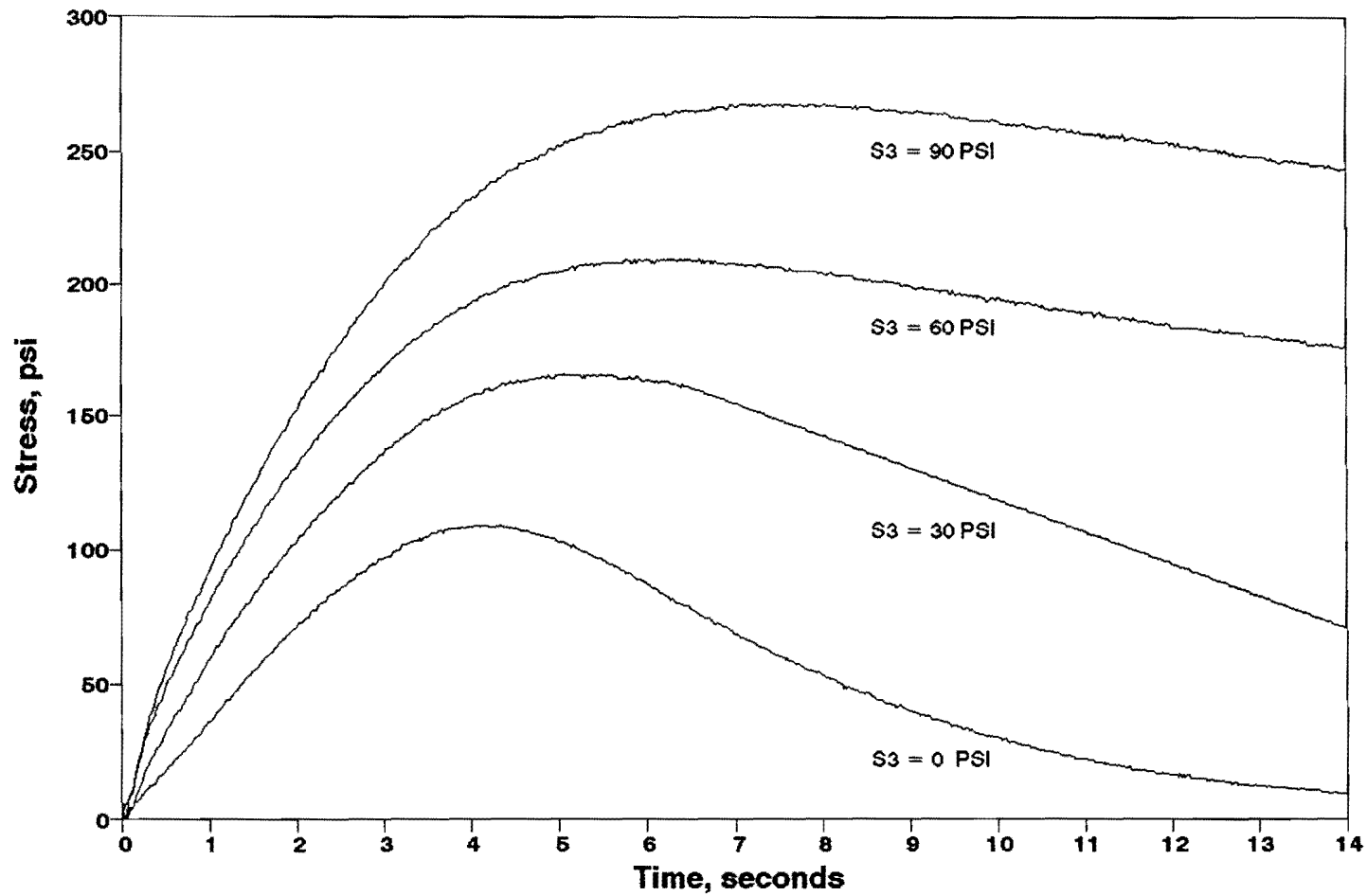
NS(10%), CLS(90%), Temp.=104F, AV=(3-4%)  
AC% (opt - 0.8), Load Rate=(2in./min.)



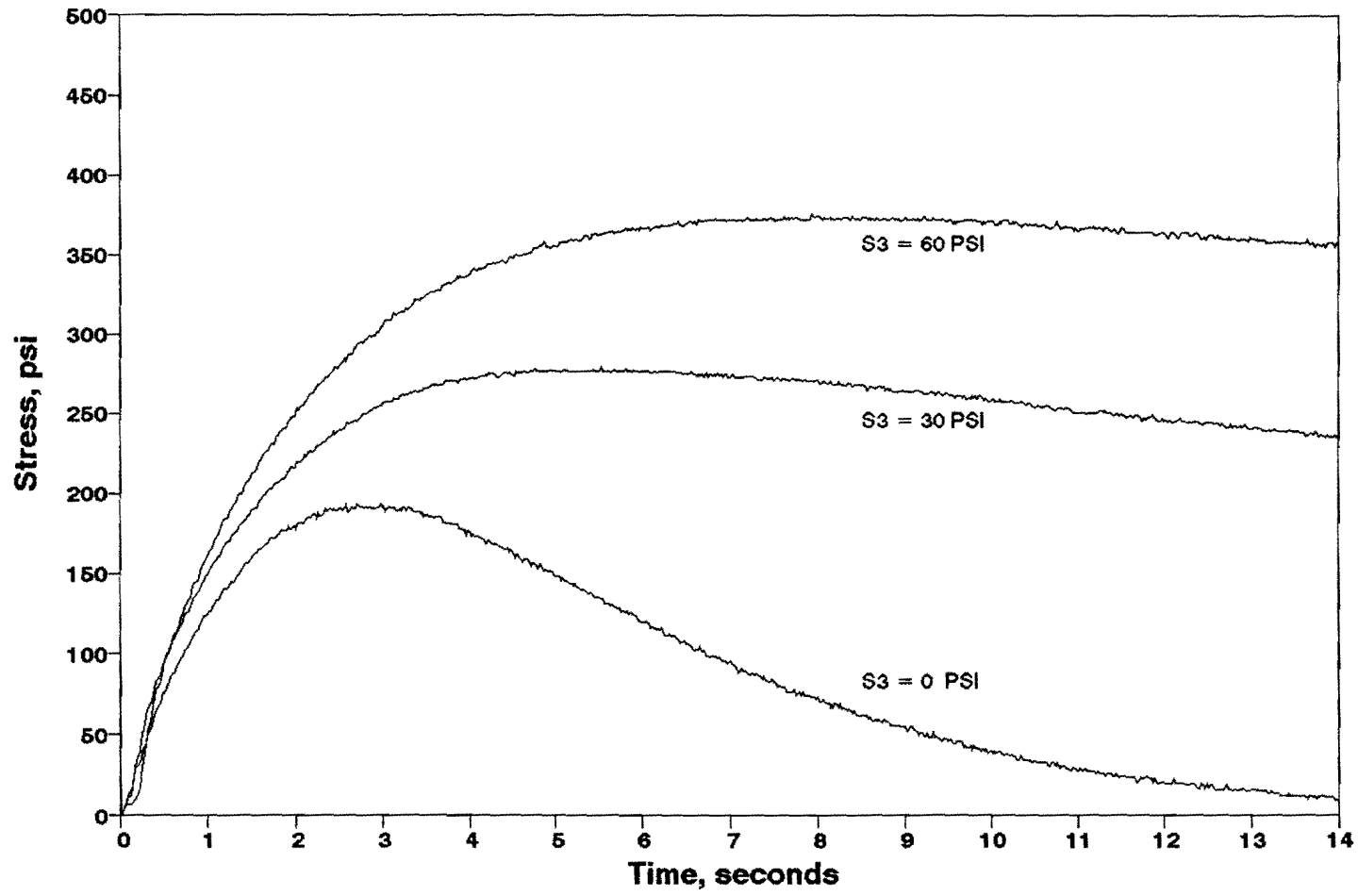
NS(20%), CLS(80%), Temp=104F, AV=(5-7%)  
AC% (opt.), Load Rate=(2in./min.)



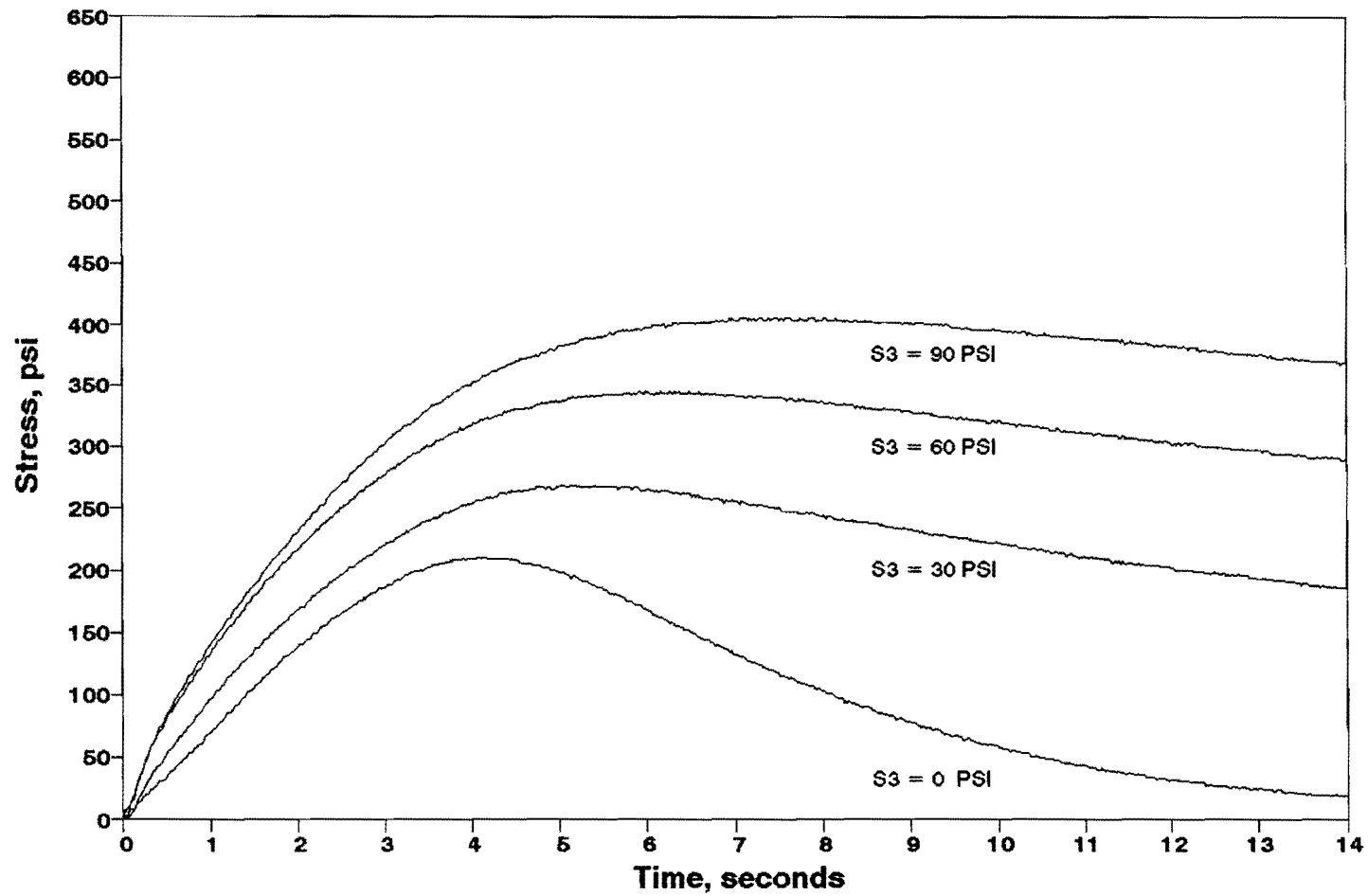
NS(20%), CLS(80%), Temp.=104F,AV=(5-7%)  
AC% (opt. + 0.8), Load Rate=(2in./min.)



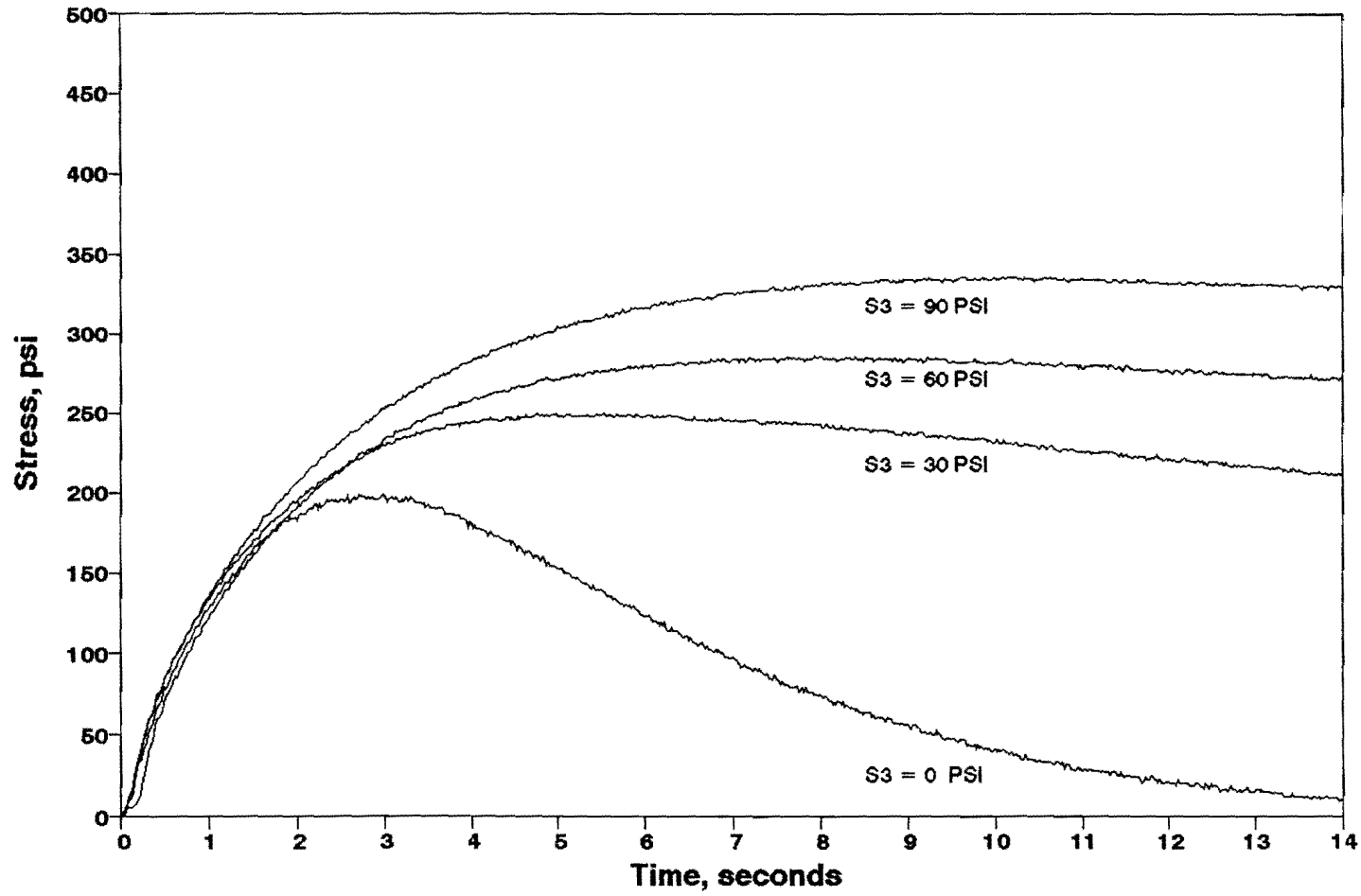
NS(20%), CLS(80%), Temp. = 104F, AV = (3-5%)  
AC% (opt. - 0.8), Load Rate = (2in./min.)



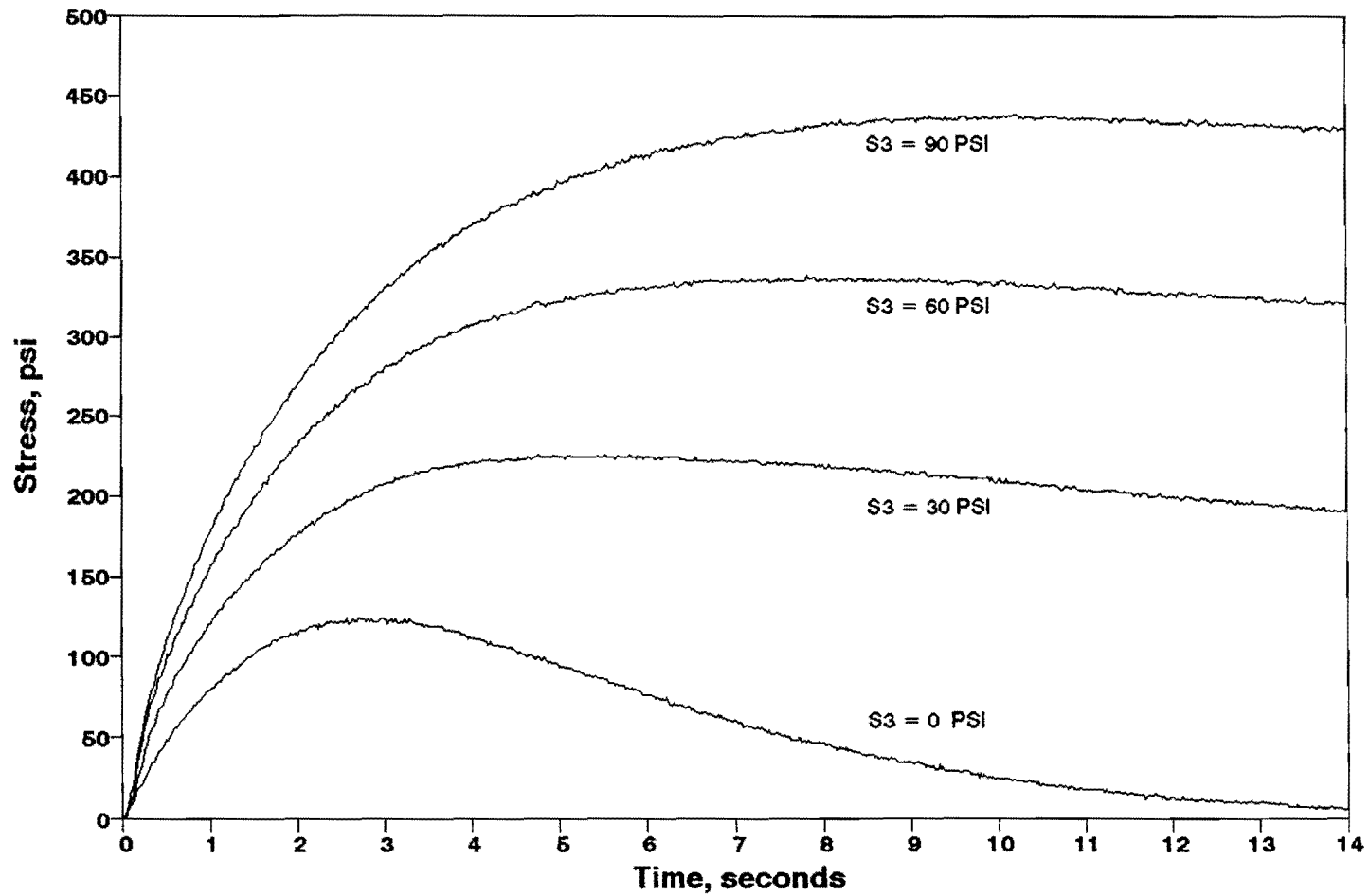
NS(20%), CLS(80%), Temp=104F, AV=(3-4%)  
AC% (opt.), Load Rate= (2in./min.)



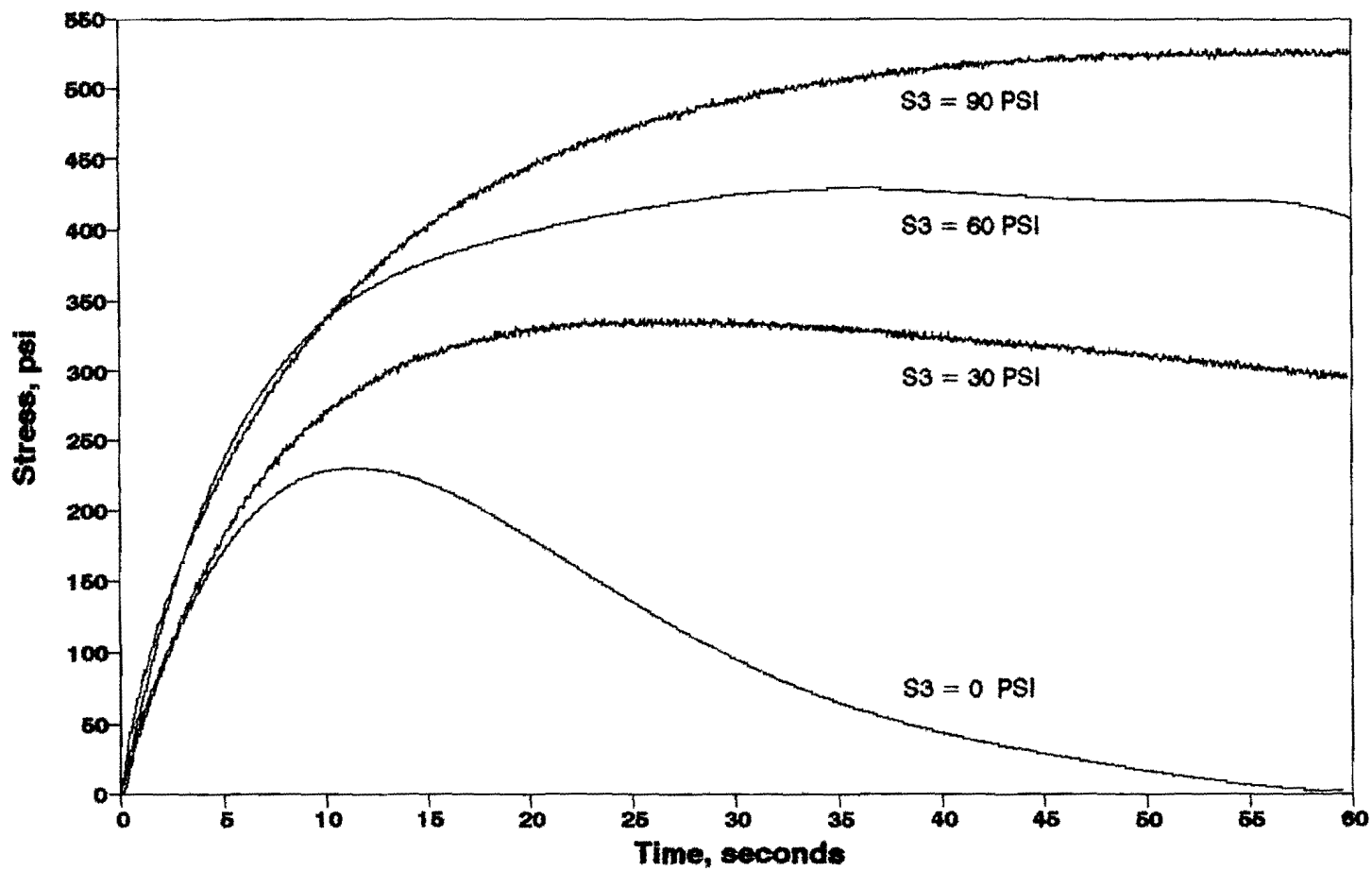
NS(20%), CLS(80%), Temp=104F, AV=(3-5%)  
AC% (opt. + 0.8), Load Rate=(2in./min.)



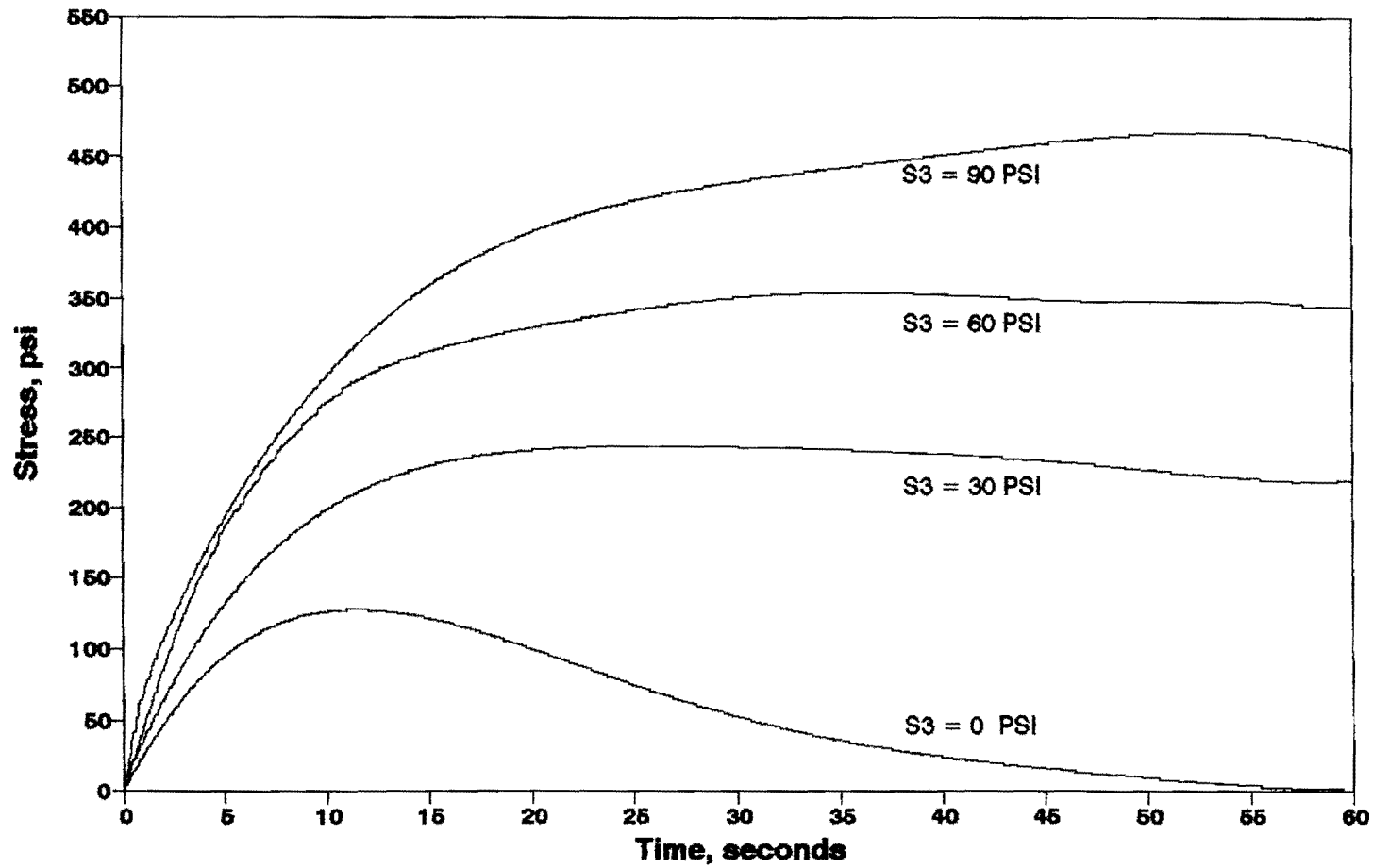
NS(20%), CLS(80%), Temp=104F, AV=(5-7%)  
AC%(opt. - 0.8), Load Rate= (2in./min.)



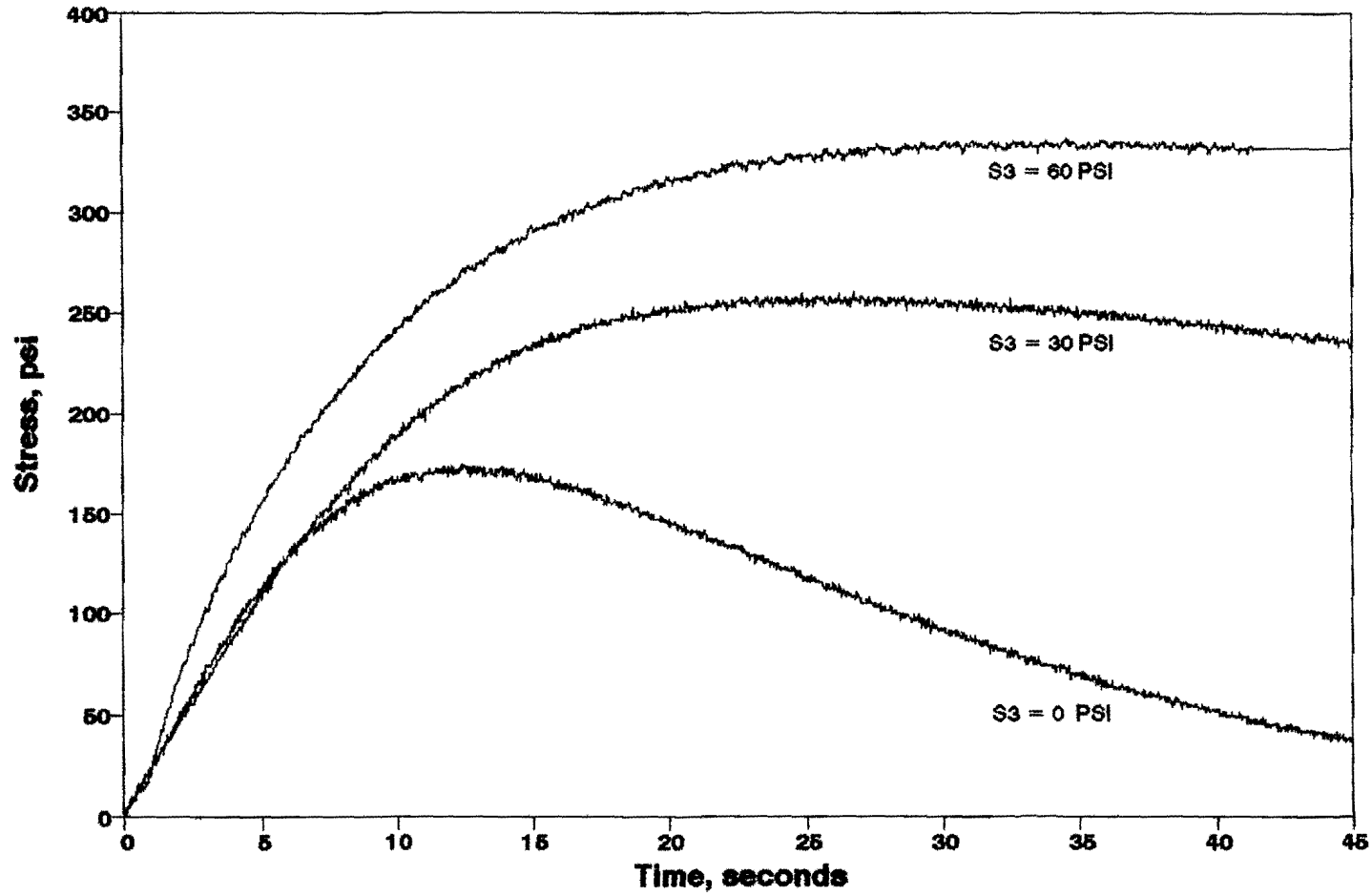
NS(0%), CLS(100%), Temp=104F, AV=(3-5%)  
AC% (opt.), Load Rate=(0.5in./min.)



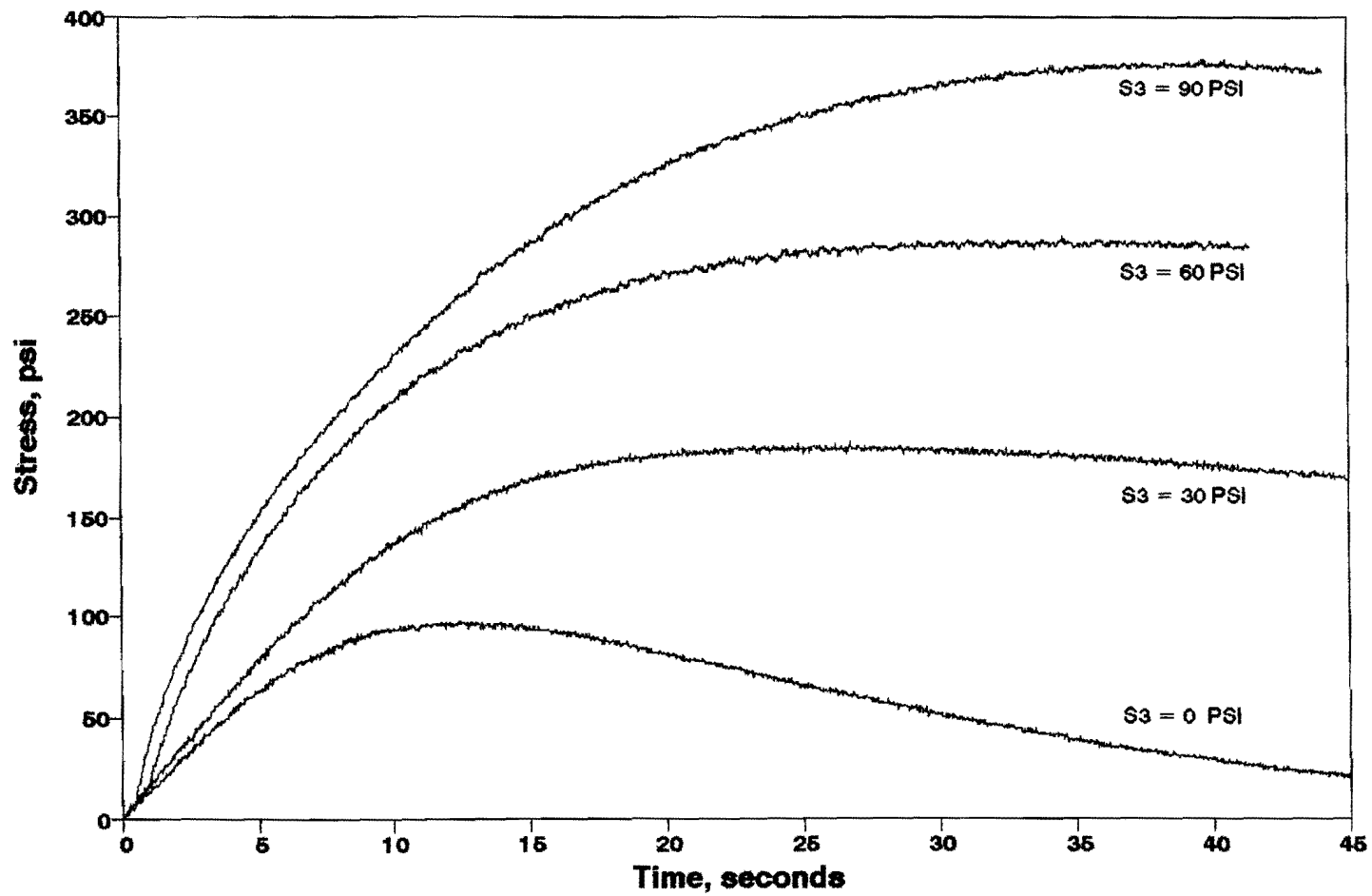
NS(0%), CLS(100%), Temp=104F, AV=(5-7%)  
AC% (opt.), Load Rate=(0.5in./min.)



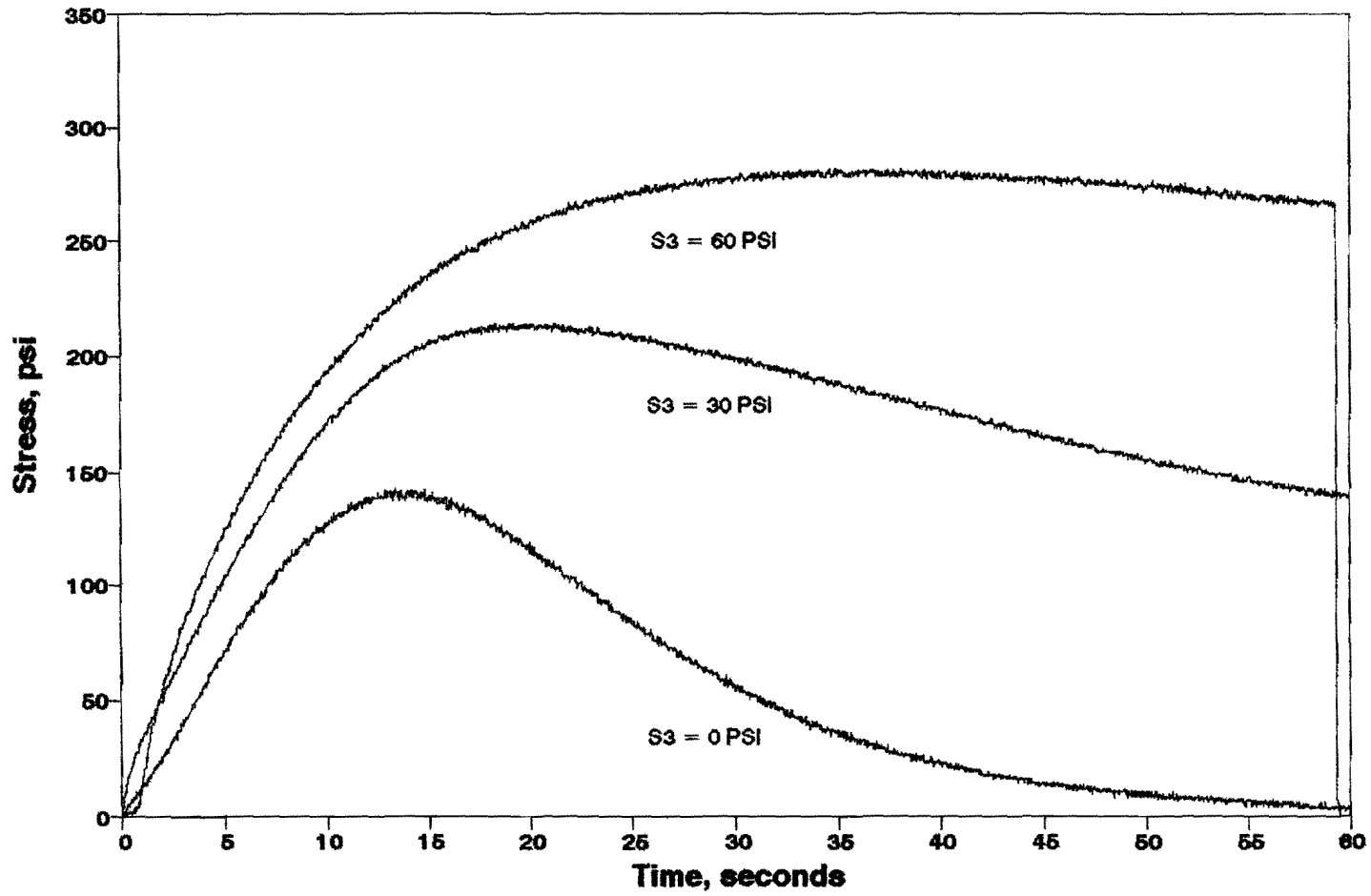
NS(10%), CLS(90%), Temp=104F, AV=(3-5%)  
AC% (opt.), Load Rate=(0.5in./min.)



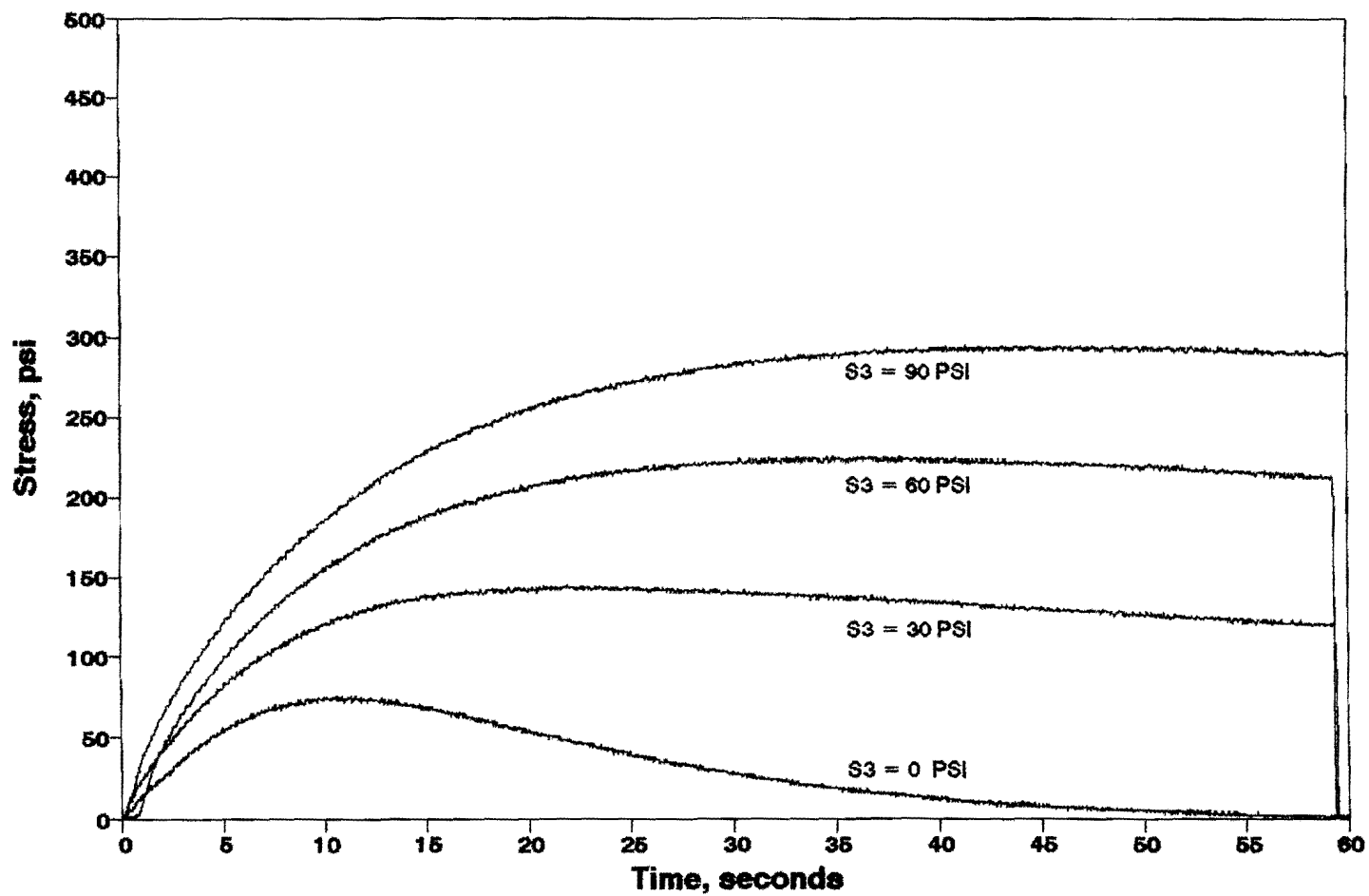
NS(10%), CLS(90%), Temp=104F, AV=(5-7%)  
AC% (opt.), Load Rate=(0.5in./min.)



NS(20%), CLS(80%), Temp=104F, AV=(3-4%)  
AC% (opt.), Load Rate=(0.5in./min.)



NS(20%), CLS(80%), Temp=104F, AV=(5-7%)  
AC% (opt.), Load Rate=(0.5in./min.)





**APPENDIX D**  
**TRIAXIAL COMPRESSION TEST**  
**FOR ASPHALT CONCRETE SPECIMENS**

**Scope**

This procedure is intended for the determination of the shearing resistance of laboratory prepared asphalt concrete cylinders. The test consists of applying an axial load until failure occurs at a specified loading rate and testing temperature. Test specimen cylinders are 4 inches in diameter and 6 or 8 inches in height. The specimens are supported by different lateral pressures.

**Apparatus**

1. Triaxial Cell, capable of holding lateral pressure up to 120 psi at temperature up to 140°F. The cell should be to house a 4 x 8 inch Cylindrical specimens.
2. Temperature Control System, capable of maintaining temperature over a range from 77°F to 140°F within  $\pm 2^\circ\text{F}$ . This system could be an environmental chamber large enough to house the triaxial cell.
3. Axial Loading System, capable of providing an axial load up to 20 ks at specified loading rates (0.05 inches/minute - 4 inches/minute). This system could be a closed-looped electrohydraulic system.
4. Air Compressor, Pressure regulator.
5. Load Measuring Device, this could be a load transducer capable of measuring the required load to an accuracy of  $\pm 1\%$  of the applied load.
6. Strain Measuring Device, this could be linear variable differential transducer (LVDT).
7. Rubber Membrane for the Cylindrical specimens.

**Procedure**

1. Laboratory specimen are prepared according to Tex-126F method using the Texas Gyrotory machine to compact the specimen. Other methods specified in AAMAS Report 338 addendum B-6 are acceptable, too.
2. The specimen is placed in the environmental chamber for at least 12

- hours to bring it to the specified test temperature. The specimen is preconditioned according to AAMAS procedure outlined in Report 338 addendum B-7.3.3. Then, specimen is placed inside the rubber membrane.
3. Test specimen is placed inside the triaxial cell and then placed in the loading apparatus.
  4. A seating load of 5-10 lbs is applied to the specimen to keep it in position while preparing the set.
  5. The air compressor is connected to the triaxial cell and the specified lateral pressure is applied.
  6. Set the time of loading and deformation for the loading system to attain the specified loading rate.
  7. The test is started and load, deformation and time are recorded until failure occurs.
  8. Test is repeated at different lateral pressures.
  9. Stresses at failure are determined for the different lateral pressures and the Mohr circles and failure envelope are constructed.

### Calculations

1. Determine the failure load for each specimen at the specified lateral pressure,  $S_3$ . This can be attained by drawing recorded load vs. recorded time or strain.
2. Calculate stress at failure,  $S_1$ .

$$S_1 = \frac{\text{load at failure}}{\text{Area of Specimen}}$$

3. Construct Mohr circles for different lateral pressures and the failure envelope.
4. Determine the intercept of the failure envelope with the Y-axis.
5. The Shear strength of the specimen equals the intercept.